IMPERIAL

Discovering and characterising the cellular regulators of influenza virus RNA replication

Amalie Boye Rasmussen

Supervised by Professor Wendy Barclay

Department of Infectious Disease

Faculty of Medicine

Imperial College London

Submitted for degree of Doctor of Philosophy

Declaration of originality

I confirm that all work presented in this thesis, except where clearly stated, is my own. Any material from other sources has been acknowledged. A license has been obtained for all figures and material from other sources where permission was required.

Copyright declaration

The copyright of this thesis rests with the author. Unless otherwise indicated, its contents are licensed under a Creative Commons Attribution-Non Commercial 4.0 International Licence (CC BY-NC). Under this licence, you may copy and redistribute the material in any medium or format. You may also create and distribute modified versions of the work. This is on the condition that: you credit the author and do not use it, or any derivative works, for a commercial purpose. When reusing or sharing this work, ensure you make the licence terms clear to others by naming the licence and linking to the licence text. Where a work has been adapted, you should indicate that the work has been changed and describe those changes. Please seek permission from the copyright holder for uses of this work that are not included in this licence or permitted under UK Copyright Law.

Acknowledgments

The biggest thank you goes to my supervisor, Wendy! Thank you for all the energy, time, and enthusiasm that you have put in to supervising me over the past four years and for all the opportunities that you have given me. I am very grateful to have had the chance to learn from such a brilliant and inspiring scientist and mentor.

A massive thank you to the rest of the Barclay Lab, both present and past members – Jie, Ksenia, Hannah K, Kyla, Kai Yi, Carol, Dorothee, JB, Joelle, Maryn, Rebecca, Hannah H, Ruthiran, Sue, Jack, Nancy, Josh, Ollie, Becky, Ada, Tom, Jess, and Liv – my PhD would not have been half as much fun without you! Thank you for always making the Barclay Lab such a supportive and exciting place to work. I am incredibly grateful for all the help, guidance, and advice that you have given me.

I also want to say thank you to Dr Laura Martin-Sancho, for all the help and advice throughout, and to my co-supervisor Prof Goedele Maertens, for always checking in and helpful discussions. Thank you to Dr Mark Skehel and Dr Fairouz Ibrahim at the Crick for all the help with the mass spectrometry.

To my family – mor, far, and Lukas, to my friends – both near and far, and to Will – thank you for your unwavering support, love, and encouragement since day one. You can make even a day of failed experiments a good day!

Finally, thank you to the MRC for funding my PhD and to Imperial College London for hosting me.

Abstract

The influenza A virus (IAV) polymerase facilitates either transcription or bidirectional replication of the viral RNA genome. These distinct activities are regulated by viral proteins and by co-opted host cell proteins that stabilise the polymerase in the different complexes required for each activity. A well-characterised example is host ANP32, which is essential for viral RNA replication. Previous proteomic screens have identified many host cell proteins that support polymerase activity, but it remains unclear which direct transcription and which replication.

In this project, we aimed to identify host proteins co-opted as either transcription- or replication-specific factors. We performed a differential interactome screen by comparing the polymerase interactome in WT cells, where both viral transcription and replication take place, to the interactome in ANP32-KO cells, where replication does not occur. The IAV polymerase was shown to interact with distinct sets of host proteins for transcription and replication. Using various gene depletion methods and experimental conditions that uncouple replication and transcription, we functionally characterised HMGB2 and RUVBL2 as replication host factors and RPAP2 as a transcription host factor. We also explored the potential use of these host factors as targets for host-directed antiviral drugs.

In addition to co-opting host cell proteins as proviral factors, IAV also evades restriction by antiviral factors, such as BTN3A3 and MxA. Both are interferon-stimulated genes that restrict avian IAVs in an NP-dependent manner. We tested the BTN3A3 and MxA sensitivity of NPs from circulating avian viruses that have caused recent widespread outbreaks in birds and mammals. We also investigated the mechanism behind BTN3A3 restriction and demonstrated that BTN3A3 inhibits the cRNA synthesis step of avian IAV RNA replication.

In summary, this project has advanced understanding of the virus-host interactions that regulate the distinct activities of the IAV polymerase, leading to insights into new antiviral strategies and host restriction.

Table of contents

DECLARATION OF ORIGINALITY **2**

COPYRIGHT DECLARATION **2**

ACKNOWLEDGMENTS **3**

ABSTRACT **4**

TABLE OF CONTENTS **5**

TABLE OF FIGURES **9**

LIST OF TABLES **11**

ACRONYMS AND ABBREVIATIONS **12**

CHAPTER 1. INTRODUCTION **14**

Section 1.1. Influenza virus **14**
Section 1.1.1. The ecology and public health burden of influenza viruses. 14
Section 1.1.2. IAV virology: virions. 16
Section 1.1.3. IAV virology: vRNPs. 17
Section 1.1.4. IAV virology: lifecycle. 18

Section 1.2. The influenza polymerase facilitates both viral transcription and replication **20**
Section 1.2.1. The influenza polymerase. 20
Section 1.2.2. The influenza nucleoprotein. 21
Section 1.2.3. Influenza polymerase activity. 22
Section 1.2.4. Mechanism of viral transcription. 26
Section 1.2.5. Mechanism of viral RNA replication. 29

Section 1.3. Host cell proteins involved in viral transcription and replication **34**
Section 1.3.1. Host cell proteins involved in viral transcription. 34
Section 1.3.2. Host cell proteins involved in viral RNA replication. 36

Section 1.4. Regulation of viral transcription and replication **43**
Section 1.4.1. Degradation of RNAP II. 44
Section 1.4.2. Viral polymerase proteins and NP. 44
Section 1.4.3. NS2. 46

Section 1.5. Interactome screens to identify host cell proteins that regulate polymerase activity **50**
Section 1.5.1. Genetic and protein-protein interaction screens. 50
Section 1.5.2. Host factors shown to support polymerase activity. 54
Section 1.5.3. Importins and CLUH. 55
Section 1.5.4. Antiviral factors. 56

Section 1.6. Adaptation of IAV to overcome host restriction **57**
Section 1.6.1. Adaptation of the polymerase to huANP32A/B. 58

Section 1.6.2. The role of the viral NS2 protein in overcoming host restriction. 63
Section 1.6.3. Adaptation of the polymerase and NP to co-opt the IMPα family. 65
Section 1.6.4. Adaptation of NP to evade restriction by BTN3A3 and MxA. 65

Section 1.7. Antiviral strategies 66

Section 1.8. Thesis aims 68

CHAPTER 2. DIFFERENTIAL INTERACTOME SCREENS TO IDENTIFY HOST PROTEINS THAT REGULATE VIRAL RNA TRANSCRIPTION AND REPLICATION 69

Section 2.1. Introduction 69

Section 2.2. Results 71
Section 2.2.1. AP-MS strategy to identify transcription-specific and replication-specific host factors. 71
Section 2.2.2. Generation and characterisation of recombinant IAV expressing an AP tag on the PB2 polymerase subunit. 72
Section 2.2.3. Optimisation of lysis buffer and wash conditions. 76
Section 2.2.4. Determining the optimal timepoint post infection and scale for interactome analysis. 80
Section 2.2.5. The PB2 interactome is different in WT and ANP32-KO cells. 82
Section 2.2.6. siRNA validation reveals host proteins with proviral and antiviral roles in IAV infection. 89
Section 2.2.7. siRNA validation reveals host proteins with proviral and antiviral roles in polymerase activity. 96
Section 2.2.8. The interactome of ANP32 is different in the presence and absence of IAV infection. 99
Section 2.2.9. PHB1 and STML2 co-precipitate with both ANP32 during infection and PB2 in WT cells. 104

Section 2.3. Discussion 107
Section 2.3.1. Differential interactome screen to identify transcription- and replication-specific host factors. 107
Section 2.3.2. Measures to study the IAV interactome in viral RNA transcription and replication. 109
Section 2.3.3. Measures to distinguish viral RNA transcription and replication. 112
Section 2.3.4. Measures to validate protein-protein interactions. 116
Section 2.3.5. Functional validation of host cell proteins. 117

CHAPTER 3. HMGB2 AND RUVBL2 SUPPORT VIRAL RNA REPLICATION AND RPAP2 SUPPORTS TRANSCRIPTION 121

Section 3.1. Introduction 121

Section 3.2. Results 122
Section 3.2.1. Generating RUVBL2-KO, HMGB2-KO, and RPAP2-KO cells using CRISPR-Cas9 genome editing. 122
Section 3.2.2. Polymerase activity is reduced in RUVBL2-KO and HMGB2-KO cells. 128
Section 3.2.3. HMGB2 and RUVBL2 promote polymerase activity of a diverse range of IAV strains. 131
Section 3.2.4. RPAP2 and HMGB2 promote polymerase activity in the context of infection. 133
Section 3.2.5. Polymerase activity in the absence of both HMGB1 and HMGB2 or both RUVBL1 and RUVBL2. 134
Section 3.2.6. Using polymerase mutants to show that HMGB2 and RUVBL2 have supportive roles in polymerase replicase activity while RPAP2 has a supportive role in polymerase transcriptase activity. 136

Section 3.2.7. Using a cRNP stabilisation assay to show that HMGB2 is a replication-specific cofactor and RPAP2 is a transcription-specific cofactor. ... 139
Section 3.2.8. Chemical inhibition of RUVBL2 ATPase activity does not inhibit polymerase activity. ... 141
Section 3.2.9. Chemical inhibition of HMGB2 inhibits virus growth and polymerase activity due to suppression of viral RNA replication. ... 143
Section 3.2.10. ICM does not improve infection outcome in a mouse model of IAV infection. ... 145

Section 3.3. Discussion ... 147
Section 3.3.1. Limitations and future work. ... 154

CHAPTER 4. CHARACTERISING THE BTN3A3 AND MXA RESISTANCE OF AVIAN INFLUENZA VIRUS ... 159

Section 4.1. Introduction ... 159

Section 4.2. Results ... 160
Section 4.2.1. Minigenome reporter assays can be used to measure BTN3A3 and MxA sensitivity of avian NPs. ... 160
Section 4.2.2. Pandemic risk assessment of zoonotic IAVs based on their sensitivity to BTN3A3 and MxA restriction. ... 161
Section 4.2.3. BTN3A3 restricts the cRNA synthesis step of RNA replication. ... 166
Section 4.2.4. BTN3A3 decreases the interaction between huANP32B and both avian and human-adapted NPs. ... 169
Section 4.2.5. NP residues that mediate NP activity and host restriction. ... 173

Section 4.3. Discussion ... 176

CHAPTER 5. DISCUSSION AND SUMMARY ... 183

Section 5.1. Discovery and characterisation of proviral regulators of viral RNA synthesis. ... 183

Section 5.2. RPAP2, HMGB2, and RUVBL2 as targets for antiviral strategies? ... 187

Section 5.3. Characterisation of antiviral regulators of viral RNA synthesis. ... 188

Section 5.4. Future work. ... 191

Section 5.5. Summary. ... 193

CHAPTER 6. MATERIALS AND METHODS ... 194

6.1. Materials ... 194
6.1.1. Cell lines ... 194
6.1.2. Viruses ... 194
6.1.3. Plasmids ... 195
6.1.4. Antibodies ... 196
6.1.5. Buffers and chemicals ... 197

6.2 Methods ... 198
6.2.1. Cell culture ... 198
6.2.2. Virology ... 198
6.2.3. Cloning ... 202
6.2.4. Co-immunoprecipitations ... 205
6.2.5. Mass spectrometry and analysis ... 206
6.2.6. Gene knockdown and knockout ... 209
6.2.7. Minigenome reporter assay ... 212

6.2.8. RT-qPCR analysis of vRNA, cRNA, and mRNA accumulation 213
6.2.9. Split luciferase assay 214
6.2.10. Western blotting, SYPRO staining, and immunofluorescence 215
6.2.11. Drug treatment 216
6.2.12. Mouse experiments 217
6.2.13. Software 217
6.2.14. Statistical analysis 218
6.2.15. Safety and biosecurity 218

REFERENCES 219

APPENDICES 242

Appendix A. 242

Appendix B. 256

Appendix C. 259

Appendix D. 260

Appendix E. 261

Table of Figures

Figure 1. The ecology of influenza viruses. 15
Figure 2. The structure of an IAV virion. 17
Figure 3. The structure of a vRNP. 18
Figure 4. The IAV lifecycle. 19
Figure 5. The structure of the IAV polymerase. 21
Figure 6. The structure of the IAV NP. 22
Figure 7. The structure of the IAV polymerase bound to host RNAP II CTD. 26
Figure 8. Overview of the mechanism of viral transcription. 28
Figure 9. Overview of the mechanism of viral RNA replication. 31
Figure 10. The IAV polymerase forms two structurally distinct dimers during viral RNA replication. .. 32
Figure 11. Current model of the proviral role of ANP32 proteins in viral RNA replication. 42
Figure 12. The temporal dynamics of vRNA, cRNA, and mRNA synthesis during infection. 44
Figure 13. Host and viral factors that regulate viral RNA transcription and replication in the early stages of infection. 49
Figure 14. Cumulative host range barriers that AIVs must overcome to initiate a pandemic in the human population. 58
Figure 15. Sequence alignment of ANP32 proteins from different species. 60
Figure 16. Paths that AIVs take to co-opt suboptimal human ANP32 proteins. 62
Figure 17. Schematic of the IAV lifecycle in ANP32-KO cells and WT cells. 72
Figure 18. Generation and characterisation of AP-tagged PR8 influenza viruses. 74
Figure 19. Optimisation of lysis buffer conditions and wash steps. 78
Figure 20. Determining the optimal timepoint and scale for interactome analysis. 81
Figure 21. Schematic of differential AP-MS strategy using PB2 as bait. 82
Figure 22. Determination of host proteins enriched above background in WT and ANP32-KO cells. . 85
Figure 23. The interactome of PB2 is different in WT and ANP32-KO cells. 86
Figure 24. PB2 co-precipitates with HMGB2 and RUVBL2 to a greater extent in WT cells than ANP32-KO cells. 89
Figure 25. Generation and characterisation of PR8 NS-ZsGreen influenza virus. 93
Figure 26. siRNA knockdown reveals host proteins with proviral and antiviral roles in IAV 95
infection. 95
Figure 27. siRNA knockdown reveals host proteins with proviral and antiviral roles in polymerase activity. 99
Figure 28. Schematic of differential AP-MS strategy using ANP32B as bait. 100
Figure 29. The interactome of ANP32B is different in the presence and absence of infection. 102
Figure 30. PHB1 and STML2 co-precipitate with both PB2 in WT cells and ANP32B during infection. 105
Figure 31. siRNA validation shows PHB1 and PHB2 to have proviral roles in polymerase activity. . 106
Figure 32. Schematic demonstrating CRISPR-Cas9 genome editing. 123
Figure 33. Generation of CRISPR-Cas9 KO cells using A549-dox-Cas9 cells. 124
Figure 34. Generation of A549 RUVBL2-KO cells using CRISPR-Cas9 genome editing. 125
Figure 35. Second round of CRISPR-Cas9 editing in RUVBL2-KO cells further reduces RUVBL2 expression. 127
Figure 36. Generation of A549 HMGB2-KO and RPAP2-KO cells using CRISPR-Cas9 genome editing. 128
Figure 37. Polymerase activity in A549 WT, RUVBL2-KO, HMGB2-KO, and RPAP2-KO cell clones. 129
Figure 38. Complementation with HMGB2 and RUVBL2 partially and fully restores polymerase activity to WT levels, respectively. 131
Figure 39. HMGB2 and RUVBL2 promote polymerase activity of a diverse range of IAV strains. 132

Figure 40. RPAP2 and HMGB2 support vRNA, cRNA, and mRNA synthesis in the context of infection. 133
Figure 41. Polymerase activity following depletion of both HMGB1 and HMGB2 or both RUVBL1 and RUVBL2. 135
Figure 42. Characterisation of replication-deficient and transcription-deficient polymerase mutants. 137
Figure 43. HMGB2 and RUVBL2 support viral RNA replication and RPAP2 supports viral RNA transcription. 138
Figure 44. Depletion of HMGB2 and RUVBL2 reduce polymerase activity of a transcription-deficient polymerase but not a replication-deficient polymerase. 139
Figure 45. HMGB2 is a replication-specific cofactor and RPAP2 is a transcription-specific cofactor. 140
Figure 46. Chemical inhibition of RUVBL2 ATPase activity has no effect on polymerase activity. ... 142
Figure 47. Chemical inhibition of HMGB2 suppresses virus growth and polymerase activity. 144
Figure 48. Chemical inhibition of HMGB2 suppresses viral RNA replication. 145
Figure 49. Determining the optimal PR8 dose for a mouse model of IAV infection. 146
Figure 50. ICM treatment did not improve disease outcome in a mouse model of IAV infection. 147
Figure 51. Domain architecture of HMGB2 and RUVBL2. 150
Figure 52. BTN3A3 and MxA restrict avian polymerase activity in an NP-dependent manner. 161
Figure 53. BTN3A3 and MxA sensitivity can be used as an indicator of pandemic risk posed by AIV NPs. 162
Figure 54. BTN3A3 and MxA sensitivity of currently circulating clade 2.3.4.4b AIV NPs. 164
Figure 55. Expression of BTN3A3, MxA-FLAG, and NP. 165
Figure 56. Approximate BTN3A3 and MxA IC50 values for each human-adapted, zoonotic, or AIV strain tested. 165
Figure 57. BTN3A3 restricts avian cRNA synthesis. 166
Figure 58. BTN3A3 restricts avian but not mammalian-adapted cRNA synthesis. 168
Figure 59. MxA restricts avian cRNA synthesis but not primary transcription. 169
Figure 60. BTN3A3 decreases the interaction between huANP32B and avian and human-adapted NP. 171
Figure 61. Mapping of residues important for NP functions onto structures of NP. 175
Figure 62. Domain architecture of BTN3A3. 181
Figure 63. Schematic demonstrating the proposed proviral roles of RPAP2, HMGB2, and RUVBL2. 185
Figure 64. Schematic demonstrating the proposed antiviral roles of BTN3A3 and MxA. 189
Figure 65. Future experiments to explore the role of host cell proteins in regulating viral RNA replication. 192

List of Tables

Table 1. Assays to measure polymerase activity. 24
Table 2. Examples of genetic screens to identify host cell proteins important for the IAV lifecycle. 51
Table 3. Examples of protein-protein interaction screens to identify host cell proteins that interact with the viral polymerase. 52
Table 4. Host proteins enriched specifically in WT cells and their host function, localisation, and role in the IAV lifecycle. 90
Table 5. Host proteins enriched in ANP32-KO cells and their host function, localisation, and role in the IAV lifecycle. 97
Table 6. Advantages and disadvantages of approaches that can be used to study the host cell interactome of IAV. 111
Table 7. Advantages and disadvantages of approaches to identify host proteins with roles specific to either viral RNA transcription or replication. 115
Table 8. Comparison of host proteins found to have a proviral or antiviral role in the IAV lifecycle in this study and the literature. 117
Table 9. Summary of novel host proteins found to have a proviral or antiviral role in the IAV lifecycle in this study. 119
Table 10. NP residues that determine BTN3A3 sensitivity. 163
Table 11. NP residues that determine MxA sensitivity. 163
Table 12. Residues important for NP interactions with RNA, viral proteins, and cellular factors. 174
Table 13. Cell lines used in this study. 194
Table 14. Virus strains used in this study. 194
Table 15. Plasmids used in this study. 195
Table 16. Primary antibodies used in this study. 196
Table 17. Secondary antibodies used in this study. 197
Table 18. Buffers used in this study. 197
Table 19. Chemicals used in this study. 198
Table 20. Primers for amplification and sequencing of PB2 and NS segment of viruses. 201
Table 21. Primers for subcloning BTN3A3 into pCAGGS. 203
Table 22. Primers for generating PB2-FLAG construct by golden gate assembly. 203
Table 23. Primers for sequencing inserts in pCAGGS and pHW2000 plasmid vectors. 205
Table 24. qPCR primers for measuring gene knockdown at the mRNA level. 210
Table 25. Primers for amplifying and sequencing CRISPR clones. 212
Table 26. Primers used for tagged RT-qPCR against PR8 HA vRNA, cRNA, and mRNA and Firefly luciferase vRNA, cRNA, and mRNA. 214

Acronyms and abbreviations

aa	amino acids
ActD	actinomycin D
AID	auxin-inducible degron
AIV	avian influenza virus
ANP32	acidic nuclear phosphoprotein 32 kDa
ANP32-KO	ANP32A/B/E-knockout
AP	affinity purification
BiFC	bimolecular fluorescence complementation
bp	base pair
BTN3A3	butyrophilin subfamily 3 member A3
BXA	baloxavir
CBD	cap-binding domain
chANP32A/B/E	chicken ANP32A/B/E
CHX	cycloheximide
CLUH	clustered mitochondria protein homolog
Co-IP	co-immunoprecipitation
CRISPR	clustered regularly interspaced short palindromic repeats
cRNA	complementary RNA
cRNP	complementary ribonucleoprotein
CTD	C-terminal domain
dox	doxycycline
DSB	double-stranded break
ECDC	European Centre for Disease Prevention and Control
ENDO	endonuclease domain
FISH	fluorescence *in situ* hybridisation
GO	gene ontology
HA	haemagglutinin
HDR	homology-directed repair
HMGB1	high-mobility group box 1
HMGB2	high-mobility group box 2
hpi	hours post infection
huANP32A/B/E	human ANP32A/B/E
huHMGB1/2	human HMGB1/2
IAV	influenza A virus
IBV	influenza B virus
ICE	inference of CRISPR edits
ICM	inflachromene
ICV	influenza C virus
IDV	influenza D virus
IF	immunofluorescence
IFN	interferon
IMPα	importin-α
Indels	insertions or deletions
ISG	interferon stimulated gene
kDa	kilo Dalton
KO	knockout
LCAR	low-complexity acidic region
LRR	leucine-rich repeat
M1	matrix 1

M2	matrix 2
MCM	minichromosome maintenance complex
MOI	multiplicity of infection
mRNA	messenger RNA
MS	mass spectrometry
muANP32A/B	murine ANP32A/B
muHMGB1/2	murine HMGB1/2
MxA	myxovirus resistance protein A
NA	neuraminidase
NanoBiT	Nano luciferase Binary Technology
NCR	non-coding region
NHBE	normal human nasal epithelial
NHEJ	non-homologous end joining
NHNE	normal human nasal epithelial
NLS	nuclear localisation signal
NP	nucleoprotein
NS1	non-structural protein 1
NS2	non-structural protein 2
NTD	N-terminal domain
nts	nucleotides
PA	polymerase acidic
PB1	polymerase basic 1
PB2	polymerase basic 2
PFU	plaque forming units
PHB	prohibitin
PLA	proximity ligation assay
$\text{Polymerase}_{(APO)}$	RNA-free polymerase
$\text{Polymerase}_{(E)}$	encapsidation-competent polymerase
$\text{Polymerase}_{(R)}$	replication-competent polymerase
$\text{Polymerase}_{(T)}$	transcription-competent polymerase
PP2A	protein phosphatase 2A
PP6	protein phosphatase 6
PROTAC	proteolysis targeting chimera
PTM	post translational modification
R2TP	Rvb1-Rvb2-Tah1-Pih1
RdRp	RNA-dependent RNA polymerase
RNAi	RNA interference
RNAP II	DNA-dependent RNA polymerase II
RPAP2	RNA polymerase II associated protein 2
RUVBL1	RuvB-like 1
RUVBL2	RuvB-like 2
SFPQ	splicing factor proline-glutamine rich
sgRNA	single guide RNA
SIM	SUMO-interacting motif
siRNA	short interfering RNA
snoRNA	small nucleolar RNA
snRNA	small nuclear RNA
svRNA	small viral RNA
vRNA	viral RNA
vRNP	viral ribonucleoprotein
WHO	World Health Organisation
WT	wildtype

Chapter 1. Introduction

Section 1.1. Influenza virus

Section 1.1.1. The ecology and public health burden of influenza viruses.

Influenza is a respiratory virus that belongs to the Orthomyxoviridae family. There are four types of influenza: influenza A virus (IAV), IBV, ICV, and IDV, which differ in their disease burden and host range (Bouvier and Palese, 2008, Krammer et al., 2018). IAV, IBV, and ICV cause disease in the human population, with IAV and IBV responsible for seasonal infections, resulting in approximately 3-5 million severe cases and 290,000-650,000 deaths annually, and ICV causing rare and typically mild infections (Krammer et al., 2018, WHO, 2025). The annual return of IAV and IBV is due to their ability to rapidly evade immunity induced by previous infection or vaccination (Paules and Subbarao, 2017). This evasion is mediated by the gradual acquisition of mutations in the main antigenic domains, namely the haemagglutinin (HA) and neuraminidase (NA) surface glycoproteins, in a process referred to as antigenic drift.

IBV and ICV mainly circulate in human hosts, IDV circulates in cattle, goat, and pigs, and IAV has a wide host range (Figure 1) (Long et al., 2019b). The natural reservoir of IAV is aquatic birds but it circulates in many avian species, including wild birds and poultry, and mammalian species, including humans, wild and domestic animals, aquatic mammals, and bats (Long et al., 2019b, Webster et al., 1992). Unlike the three other influenza types, IAV is further classified into subtypes based on antigenic differences in its HA and NA surface glycoproteins (Paules and Subbarao, 2017). There are a total of 18 different HA subtypes and 11 different NA subtypes (Figure 1). Of these only three HA (H1, H2, and H3) and two NA (N1 and N2) subtypes have established sustained lineages in the human population.

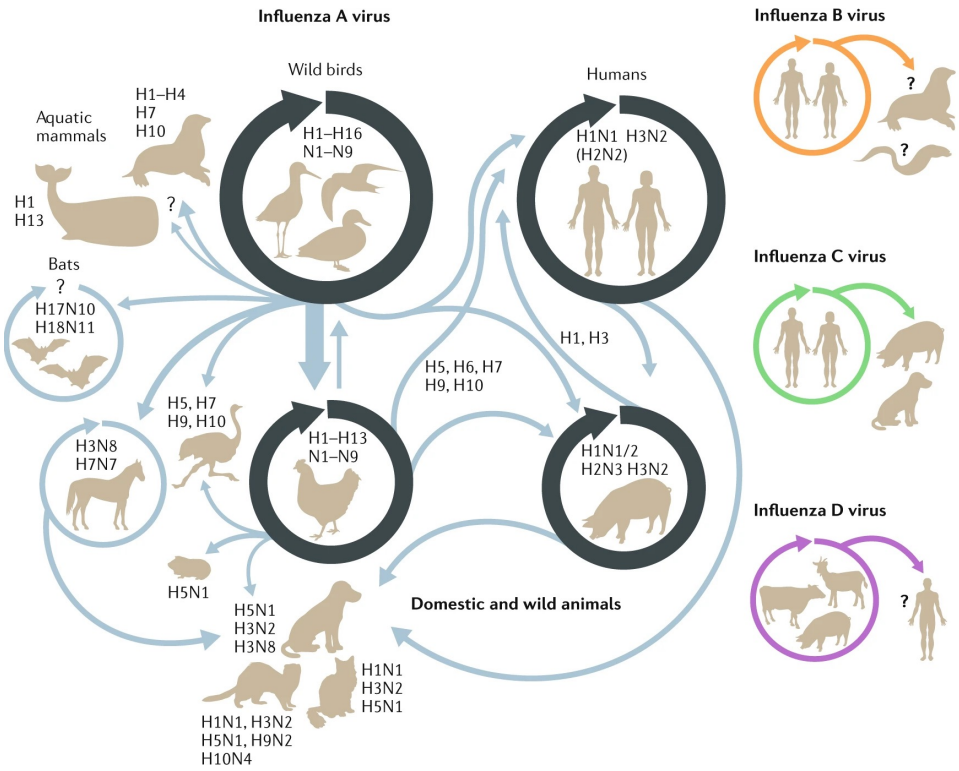

Figure 1. The ecology of influenza viruses.
Figure taken from Long et al., 2019b. Reproduced with permission from Springer Nature. Influenza A virus (IAV) HA (H) and NA (N) subtypes H1-H16 and N1-N9 circulate in wild birds. Light blue arrows show the different species that these subtypes can spill over into. Spillovers can occur directly, via adaptive mutations, or via intermediate species. Dark blue arrows show the subtypes that predominate in the given species. H1N1 and H3N2 subtypes currently circulate in humans, and H2N2 subtypes have recently circulated. The same three subtypes circulate in pigs. The H17 and H18 subtypes only circulate in bats with no spillovers into other species. Influenza B virus (IBV) circulates in humans. Influenza C virus (ICV) circulates in humans with spillover events into swine and dogs. Influenza D virus (IDV) circulates in cattle, goats, and pigs.

An important aspect of the public health burden associated with IAV is its ability to cause pandemics (reviewed in Taubenberger and Kash, 2010). The first step to pandemic emergence is a zoonotic event in which IAV spills over from the animal reservoir and causes infection in the human population. The wide host range of IAV means that there are many opportunities for such zoonoses to occur, however the actual exposure rate of humans to zoonotic infections is difficult to estimate due to limited data (Ciminski et al., 2021). H5, H6, H7, H9, and H10 avian IAVs (AIVs) have all caused zoonotic infections in the human population, but the H5 and H7 subtypes are of particular concern as they can be associated with more severe disease (Richard et al., 2014). Although usually associated with severe disease and high mortality, most zoonoses are dead-end events that do not result in onwards transmission in the human population (Long et al., 2019b, Taubenberger and Kash, 2010). This is largely due to host range barriers such as incompatibility between surface HA proteins

and host cell receptors, species-specific differences in proviral host factors, and antiviral activity imposed by restriction factors (reviewed in Long et al., 2019b). However, on some rare occasions, IAV acquires genetic changes that enable the virus to overcome the host range barrier and cause a pandemic (Long et al., 2019b, Taubenberger and Kash, 2010). Two aspects of IAV's virology make it particularly prone to pandemic emergence. First, IAV is segmented and is, therefore, able to undergo reassortment. This allows avian IAVs to rapidly acquire segments from mammalian-adapted viruses if they co-infect the same cell in either a human host or intermediate host, such as pigs. Reassortment of the HA and NA segments is termed antigenic shift. Second, IAV's error-prone polymerase allows zoonotic viruses to acquire mutations that adapt the virus to its new host.

As the human population is typically immunologically naïve to newly emerged viruses, pandemics can have devastating consequences. In the past century, there have been five IAV pandemics: the 1918 H1N1, 1957 H2N2, 1968 H3N2, 1977 H1N1, and 2009 H1N1 pandemics (Neumann et al., 2009, Scholtissek et al., 1978, Taubenberger and Morens, 2006). In recent times, the risk of pandemic emergence is heightened due to urbanisation, increased global travel, and climate-mediated changes to animal migration and land use, which increase the likelihood of human interactions with the animal IAV reservoir (Carlson et al., 2022, Harrington et al., 2021). However, efforts to predict and prepare for the next influenza pandemic, including surveillance, laboratory research to understand host range determinants, and effective antiviral strategies, may prevent its emergence or mitigate its impact (Harrington et al., 2021).

This thesis will focus on IAV, but IBV, ICV, and IDV will be mentioned throughout.

Section 1.1.2. IAV virology: virions.

IAV has a segmented negative-sense single-stranded RNA genome, consisting of eight segments that encode ten core proteins and at least seven accessory proteins (Bouvier and Palese, 2008, Pinto et al., 2021). IBV also has eight segments while ICV and IDV have seven segments. Each segment is named after the main protein that it encodes which are polymerase basic 1 (PB1), polymerase basic 2 (PB2), polymerase acidic (PA (P3 in ICV/IDV)), nucleoprotein (NP), HA, NA, matrix protein (M1), and non-structural protein (NS1) (Bouvier and Palese, 2008). IAV employs various strategies to increase its coding capacity. This includes alternative mRNA splicing of its M and NS segments to generate the M2 and NS2 core proteins, respectively (Dubois et al., 2014). Additionally, accessory proteins are generated, mainly from the PA and PB1 segments, by ribosomal frameshifts and the use of alternative translation initiation sites (Jagger et al., 2012, Wise et al., 2011).

The IAV virion is enveloped with a spherical shape, in the case of laboratory-adapted strains, and a filamentous shape, in the case of many clinical isolates (Figure 2A and B) (Calder et al., 2010, Peterl et al., 2025). The HA, NA, and M2 viral proteins are found on the

surface of the virion (Figure 2C) (Bouvier and Palese, 2008). HA and NA extend from the lipid viral envelope onto the surface of the virion where they mediate cell entry and exit of the virus. M2 ion channels cross the lipid envelope. Inside the virion, the M1 protein, which is the most abundant viral protein, forms a layer that encloses the genetic material. In each virion, the genetic material consists of one copy of each of the eight viral RNA (vRNA) segments assembled into a viral ribonucleoprotein (vRNP) complex (see Section 1.1.3) (Eisfeld et al., 2015). These vRNPs are packaged into the virion in a 7+1 arrangement (Figure 2D) (Noda et al., 2006). Importantly, some viral proteins are also contained within the virion such as NS1 and NS2 and even host cell proteins (Hutchinson et al., 2014, Shaw et al., 2008). These viral and host proteins are released together with the eight vRNPs into the infected host cell.

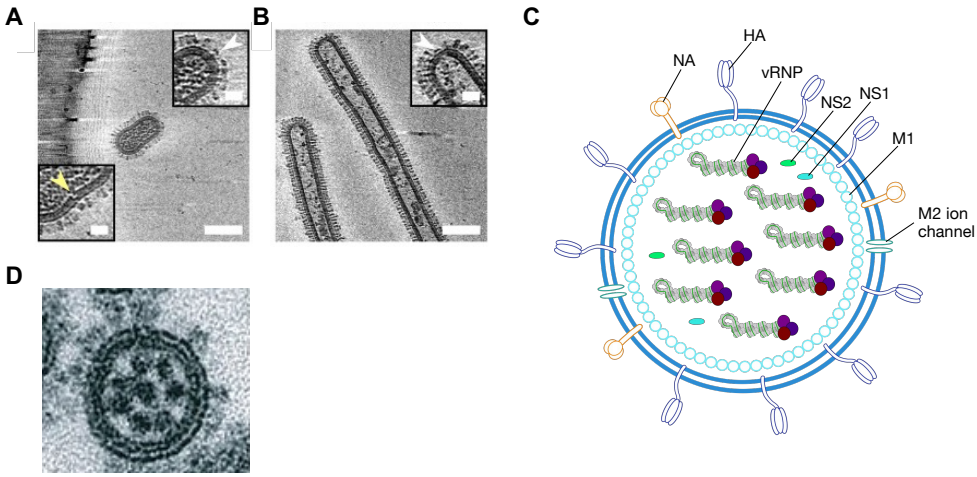

Figure 2. The structure of an IAV virion.
A and B) Cryo-electron tomogram showing a spherical (A) and filamentous (B) IAV virion. Taken from Peterl et al., 2025. C) Cartoon demonstrating an IAV virion. HA and NA glycoproteins are on the surface of the virion (Bouvier and Palese, 2008). M2 ion channels traverse the lipid viral envelope. The M1 protein forms a capsid around the core of the virion. The genetic material is contained within the core in the form of eight vRNPs each encoding one of the eight genome segments (Eisfeld et al., 2015). NS1 and NS2 viral proteins are also contained within the core. D) Electron micrograph of an IAV particle showing a 7+1 arrangement of the vRNPs. Taken from Noda et al., 2006. Reproduced with permission from Spinger Nature.

Section 1.1.3. IAV virology: vRNPs.

In vRNP complexes, the 5' and 3' termini of the vRNA, which constitute the promoter, base pair to form a double stranded structure that is bound by a single polymerase molecule (Figure 3A) (Eisfeld et al., 2015). The rest of the vRNA is bound by multiple copies of oligomeric NP. The NP molecules adopt a right-handed antiparallel double helical structure forming a loop at the opposite end of the complex than the polymerase-bound promoter (Figure 3A and B) (Arranz et al., 2012, Coloma et al., 2020, Moeller et al., 2012, Peng et al., 2025). NP does not associate evenly with the vRNA, allowing the vRNA to adopt secondary

structures which may be important for RNA-RNA interactions within and between segments and selective packaging of vRNPs into virions (Dadonaite et al., 2019).

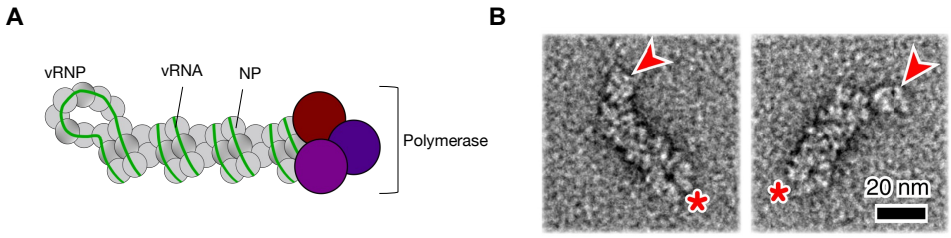

Figure 3. The structure of a vRNP.
A) Cartoon demonstrating a vRNP. The 5' and 3' ends of the vRNA form the vRNA promoter and are bound by the viral polymerase (Eisfeld et al., 2015). The polymerase is a heterotrimer composed of the subunits PB2, PB1, and PA. The rest of the vRNA is bound by NP, which adopts a double-helical arrangement and forms a loop at the opposite end of the vRNP to the polymerase. B) Negative-stain electron micrograph of the IDV vRNP. The arrow indicates the polymerase, and the asterisks indicates the loop end. Taken from Peng et al., 2025. Reproduced with permission from AAAS.

Section 1.1.4. IAV virology: lifecycle.

As an obligate intracellular parasite, IAV relies heavily on host cell proteins and pathways for all steps of its lifecycle. A schematic of the IAV lifecycle is provided in Figure 4. This thesis will focus on IAV polymerase activity and the host factors that regulate this step of the viral lifecycle.

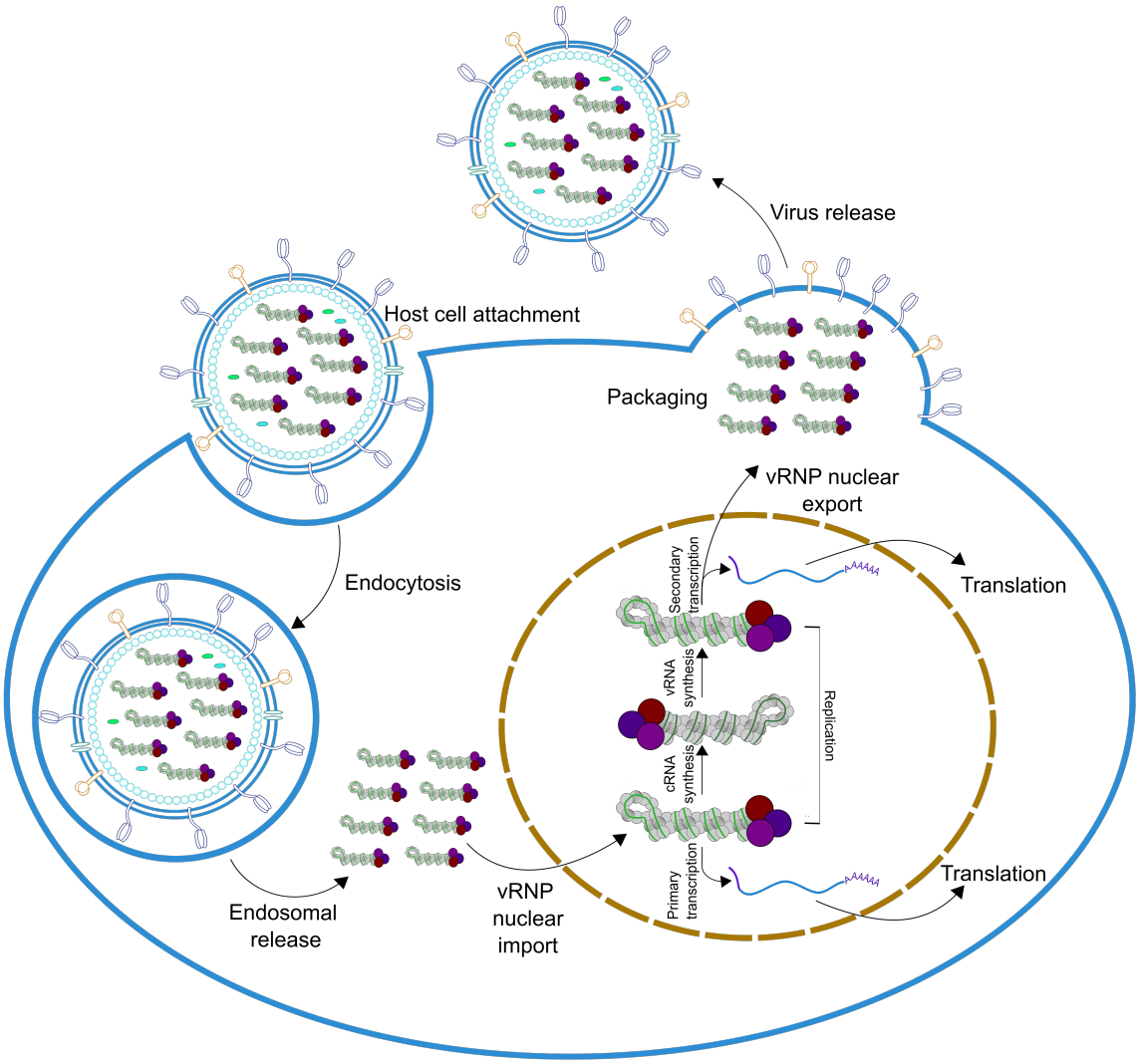

Figure 4. The IAV lifecycle.
The first step to infection is attachment of the IAV virion to the surface of the cell. This is achieved by the binding of the HA surface glycoprotein to sialic acid receptors on the cell surface (Bouvier and Palese, 2008). The virus is then internalised by endocytosis. The lower pH within the endosome triggers a conformational change in the HA, which stimulates fusion of the viral envelope and endosomal membrane (Bullough et al., 1994). This opens up a pore through which vRNPs are released into the cytoplasm. Meanwhile, the lower pH also opens the M2 ion channel, resulting in an influx of protons and potassium ions into the virion, which causes vRNPs to be dissociated from M1 and released into the cytoplasm (Stauffer et al., 2014). vRNPs are then imported into the nucleus via the IMPα/IMPß nuclear import pathway (Cros et al., 2005, O'Neill et al., 1995). Inside the nucleus, the IAV genome is transcribed and replicated by the viral polymerase. The viral mRNA is transported to the cytoplasm where it is translated by the host cell machinery. Nascent vRNPs are exported to the cytoplasm by M1 and NS2 via the CRM1 pathway (Neumann et al., 2000, O'Neill et al., 1998). This is followed by transport of the vRNPs to the cell surface where they are packaged and the viral genome is incorporated into budding virus particles (Bouvier and Palese, 2008). New virions are released by scission of the membrane by M2 and onward spread is facilitated by cleavage of the sialic acid receptors on the cell surface by NA.

Section 1.2. The influenza polymerase facilitates both viral transcription and replication

Section 1.2.1. The influenza polymerase.

The influenza polymerase is an RNA-dependent RNA polymerase (RdRp) composed of the subunits PB1, PB2, and PA. Structures of the heterotrimeric polymerase have been solved using x-ray crystallography and cryo-EM for IAV (Pflug et al., 2014, Reich et al., 2014), IBV (Reich et al., 2014, Thierry et al., 2016), ICV (Hengrung et al., 2015), and IDV (Peng et al., 2019). These structures have been solved in the absence (Hengrung et al., 2015) and presence (Peng et al., 2019, Pflug et al., 2014, Reich et al., 2014, Thierry et al., 2016) of vRNA and cRNA templates, revealing the binding site of the RNA promoter and the structural rearrangements that take place upon promoter binding.

Despite sequence differences between IAV, IBV, ICV, and IDV, the structure of the polymerase is similar across the influenza types (Pflug et al., 2017). Overall, the viral polymerase adopts a globular conformation with a core catalytic domain and flexible peripheral domains (Figure 5A). The PB1 subunit has a right-hand-like structure typical of RdRps, consisting of finger, palm, and thumb subdomains as well as a priming loop that extends from the thumb subdomain into the active site. PB1 constitutes most of the core domain and possesses the catalytic activity necessary for viral RNA synthesis (Figure 5A). The PA and PB2 subunits each contain an N-terminal domain (NTD) and C-terminal domain (CTD) which contribute both to the core domain and flexible domains of the polymerase (Figure 5A and B). The PA^{CTD} forms part of the core together with the N-terminal third of PB2. The flexible domains consist of the PA endonuclease domain (PA^{ENDO}), which is connected to the core via a flexible linker, and the $PB2^{CTD}$ (PB2 cap-binding ($PB2^{CBD}$), PB2 mid-link ($PB2^{mid\text{-}link}$), PB2 627 ($PB2^{627}$), and PB2 nuclear localisation signal (NLS) ($PB2^{NLS}$) domains). All three polymerase subunits contribute to formation of the template entry and exit channels, the nucleotide triphosphate (NTP) entry channel, and the product exit channel. Structures of the polymerase in complex with vRNA or cRNA templates show that the 5’ end of the vRNA/cRNA forms a “hook” structure that binds in a pocket between the PB1 finger subdomain and the PA^{CTD} near the template entry channel. The 3’ end of the vRNA/cRNA binds near the surface of the polymerase, with two binding sites for the vRNA 3’ end (Peng et al., 2019).

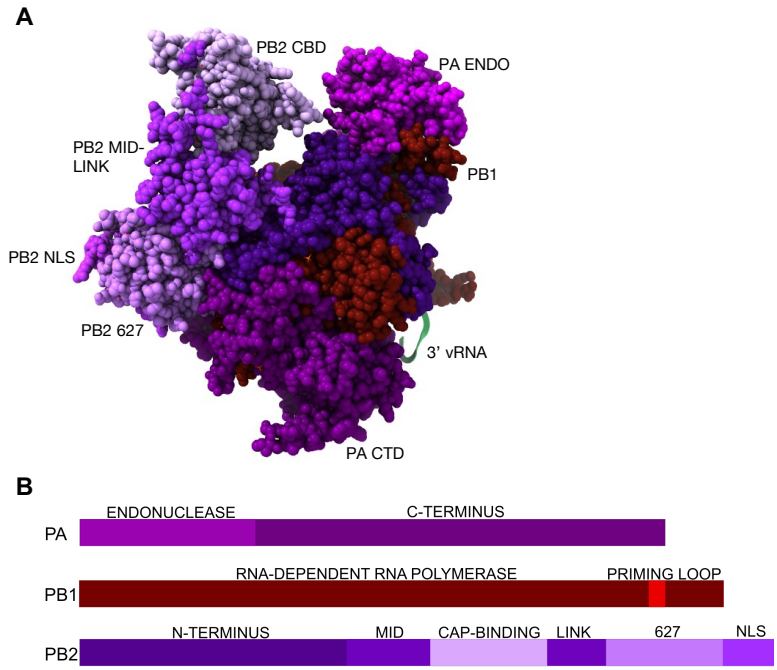

Figure 5. The structure of the IAV polymerase.
A) X-ray crystallography structure of heterotrimeric IAV (bat H17N10) polymerase bound to a vRNA promoter (PDB accession code: 4WSB) (Pflug et al., 2014). Each of the subunit domains are colour-coded as in (B). The structure was visualised using ChimeraX v.1.9. B) PB2, PB1, and PA subunit domain structures showing the names of the subdomains and the colour scheme used in (A).

More recently structural analyses have further shown that the influenza polymerase exists in distinct states and complexes as it performs the different steps of viral RNA synthesis (Arragain et al., 2024, Carrique et al., 2020, Fan et al., 2019, Kouba et al., 2019, Staller et al., 2024, Wandzik et al., 2020, Chang et al., 2015, Peng et al., 2019). Taken together, the structural data from the past decade suggests that the different conformations of the polymerase can be divided into four broad categories: RNA-free polymerase (polymerase$_{(APO)}$) likely representing the structure of a newly assembled polymerase, transcription-competent (polymerase$_{(T)}$), replication-competent (polymerase$_{(R)}$), and encapsidation-competent (polymerase$_{(E)}$), which either exist as monomers or come together to form higher order oligomers. The polymerase structures are similar in their core catalytic domains but show different arrangements of their flexible domains, particularly of the PB2^{CTD}. These diverse conformations are triggered by the binding of RNA, binding of additional polymerase heterotrimers, and interaction with host factors that stabilise the polymerase conformations.

Section 1.2.2. The influenza nucleoprotein.

Various structures of the IAV NP have been solved using x-ray crystallography and cryo-EM (Chenavas et al., 2013, Chenavier et al., 2023, Knight et al., 2021, Ng et al., 2008, Ye et al., 2006). These structures show NP in monomeric and oligomeric forms and in the

absence and presence of RNA. NP adopts a similar conformation in all structures, with a head and body domain as well as a flexible tail-loop (Figure 6A and B). The protein has two arginine-rich basic grooves located between the head and body domains to which RNA binds (Figure 6A). Each NP molecule associates with approximately 24 RNA nucleotides in a sequence-independent manner, such that NP is capable of binding both viral and cellular RNA (Ortega 2002). To begin RNA encapsidation, the initial NP is proposed to bind the viral polymerase, and indeed, NP has been shown to interact with the PB2 and PB1 subunits (Biswas et al., 1998, Newcomb et al., 2009). Subsequent NPs are then recruited by NP-NP homo-oligomerisation (Ng et al., 2008, Turrell et al., 2013, Ye et al., 2006). In this process, the tail-loop of the existing NP inserts into a groove in the body domain of the neighbouring incoming NP monomer. Although free NP self-assembles into oligomers, it needs to be in a monomeric state prior to oligomerisation on viral RNA and vRNP assembly (Chenavas et al., 2013). Consequently, NP oligomerisation is tightly regulated, and this regulation occurs in a manner that depends on its phosphorylation state, with phosphorylated NP maintained in a monomeric state (Mondal et al., 2015, Turrell et al., 2015). Host factors, such as importins (see Section 1.5.3) and UAP56 have also been implicated in this regulation and chaperoning of NP (Boulo et al., 2011, Hu et al., 2017, Momose et al., 2001, Morris et al., 2020).

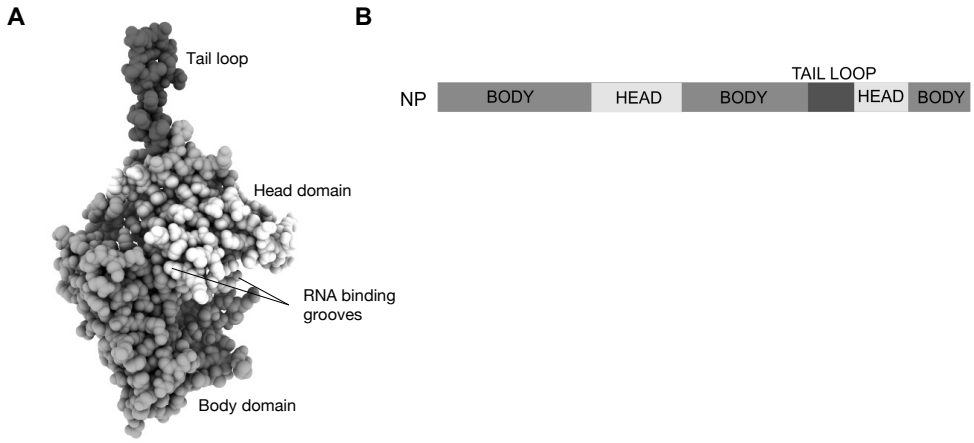

Figure 6. The structure of the IAV NP.
A) Crystal structure of monomeric IAV (H5N1) NP (PDB accession code: 2Q06) (Ng et al., 2008). Each of the domains are colour-coded as in (B). The structure was visualised using ChimeraX v.1.9. B) NP domain structure showing the head, body, and flexible tail-loop subdomains and the colour scheme used in (A).

Section 1.2.3. Influenza polymerase activity.

The influenza virus polymerase catalyses both transcription and replication of the vRNA template (Fodor and Te Velthuis, 2020). Transcription converts vRNA into viral mRNA. RNA replication occurs via a complementary RNA (cRNA) intermediate, which is then

converted back into vRNA. Consequently, polymerase activity results in the synthesis of three different viral RNAs: vRNA, cRNA, and mRNA, all of which are synthesised in the context of RNPs (Coloma et al., 2020, Moeller et al., 2012, Peng et al., 2025, Fodor and Te Velthuis, 2020). Various methods exist to measure polymerase activity both in terms of total polymerase activity and the synthesis of individual RNAs, as summarised in Table 1 (Te Velthuis et al., 2018). Firstly, polymerase activity can be measured during infection by quantifying the accumulation of vRNA, cRNA, and mRNA using primer extension or RT-qPCR methods. Additionally, *in situ* minigenome reporter assays can be used in which the polymerase proteins and NP are reconstituted in cells from cDNA clones and polymerase activity is measured by supplying a viral-like RNA template that encodes a reporter gene. The main advantage of these methods is that they consider the role of host factors, and in the case of infection assays, the role of other viral proteins not included in minigenome assays. However, as vRNA, cRNA, and mRNA synthesis are interdependent, the role of the viral polymerase in each step of viral RNA synthesis cannot be determined using these assays, unless drugs, mutants, or cellular conditions are employed that block one or more polymerase activities (Te Velthuis et al., 2018, Vreede et al., 2004). To study individual steps of viral RNA synthesis, cell-free *in vitro* biochemical assays can be used (Te Velthuis et al., 2018). These assays involve purified polymerase proteins, different RNA templates, and capped or uncapped primers. Many of the findings about the viral polymerase and the host and viral factors involved in regulating its activity described below were made using the assays summarised in Table 1.

Table 1. Assays to measure polymerase activity.

Method	Advantages	Disadvantages	References
Quantification of vRNA, cRNA, mRNA after infection. The accumulation of vRNA, cRNA, and mRNA is quantified following infection by RT-qPCR or primer extension using strand- and segment specific primers.	• Takes the role of all viral proteins into account. • Takes the role of host factors and the cellular environment into account. • Represents the actual temporal dynamics of viral RNA synthesis during infection.	• vRNA, cRNA, and mRNA synthesis are interdependent so effects on each step of viral RNA synthesis cannot be distinguished.	(Kawakami et al., 2011, Phan et al., 2021, Te Velthuis et al., 2018)
cRNP stabilisation or replication assay. Infection assays where effects on transcription and RNA replication can be distinguished. Cells are infected and treated with drugs that uncouple transcription and replication. The drugs are either: - actinomycin D (ActD), which blocks host cell transcription and consequently viral transcription, such that no mRNA synthesis can occur, or - cycloheximide (CHX), which blocks host cell translation and consequently synthesis of new viral proteins, allowing primary mRNA synthesis to occur. To stabilise cRNA and vRNA products, polymerase proteins and NP are pre-expressed prior to infection and drug treatment.	• Distinguishes vRNA, cRNA, and mRNA synthesis in the context of infection. • cRNP stabilisation assay: shows effects directly on the pioneering round of cRNA synthesis and primary mRNA synthesis (if CHX-treated). • Replication assay: shows effects on v-to-cRNA and c-to-vRNA synthesis and primary mRNA synthesis (if CHX-treated).	• Artificial assay and, therefore, might disturb normal temporal dynamics of viral RNA synthesis. • Drugs may impact virus-host interplay.	(Manz et al., 2012, Nilsson et al., 2017, Vreede et al., 2004)
Minigenome reporter assay. *In situ* assay where cells are transfected with a viral-like RNA that encodes a reporter plasmid (such as a luciferase or fluorescent protein). The viral polymerase to be studied can then either be delivered through infection or transfection of plasmids encoding the polymerase subunits and NP. The polymerase will then transcribe and replicate the reporter gene, leading to the production of a luminescent or fluorescent measurable signal.	• Takes the role of host factors and the cellular environment into account. • Relatively high throughput. • Can be performed in multiple cell types and cells from different species. The RNAP I promoter that controls expression of the reporter gene is species-specific so must be modified accordingly. • Can be used to test polymerases from different viral strains (of which isolates, or reverse genetics system may not be readily available) and different polymerase mutations. • Readout can either be expression of the reporter gene as total polymerase activity or the individual RNA species. In a minigenome setup, replication	• Polymerase proteins and NP are overexpressed and, therefore, the assay does not accurately reflect an infection. • Temporal dynamics of vRNA, cRNA, and mRNA synthesis are different in the absence of NS2.	(Neumann et al., 1994, Robb et al., 2009, Te Velthuis et al., 2018, Turrell et al., 2013)

	occurs independently of transcription but not vice versa. • Different viral-like RNA templates can be used: - Short templates (≤76nts) which are NP independent. - Templates with promoter mutants to study the individual steps of vRNA, cRNA, and mRNA synthesis (must be read out in terms of individual viral RNAs).		
***In vitro* biochemical assay.** Cell-free replication/transcription reconstitution assays where individual steps of viral RNA synthesis can be studied. Involves the use of purified polymerase proteins/RNPs, RNA template, or a capped/uncapped primer.	• Different RNA templates and/or primers can be used to study each step of viral RNA synthesis separately. • Polymerase mutants and promoter mutants can be studied. • Inclusion of purified host cell proteins allows their role in viral RNA synthesis to be determined without interference from the cellular environment.	• Does not take the role of host cell proteins or other viral proteins into account (unless directly supplied in the assay). • Does not reflect the temporal dynamics of an actual infection. • Relatively low throughput.	(Te Velthuis et al., 2018, Zhu et al., 2023a)

Section 1.2.4. Mechanism of viral transcription.

Following nuclear import of vRNPs from an incoming virion, primary transcription occurs (Fodor and Te Velthuis, 2020). Transcription is a primer-dependent one-step process in which a *cis*-acting monomeric polymerase converts negative-sense vRNA into positive-sense viral mRNA. Importantly, viral mRNAs have a 5' cap and 3' poly(A) tail and, therefore, resemble host mRNAs. This allows them to be spliced, exported, and translated by the host cell machinery (York and Fodor, 2013). Recent structures of the polymerase$_{(T)}$ throughout transcription (from a pre-initiation to a termination state), achieved by stalling the polymerase at different stages of transcription, offer great insight into the mechanism of v-to-mRNA synthesis (Kouba et al., 2019, Wandzik et al., 2020).

As the influenza polymerase is unable to synthesise and methylate its own cap structures, influenza hijacks nascent host capped RNA fragments for use as primers for transcription initiation, in a process called cap-snatching (Plotch et al., 1979). The preferred substrates for cap-snatching are small nuclear RNAs (snRNAs) or small nucleolar RNAs (snoRNAs) rather than mRNAs (Gu et al., 2015, Koppstein et al., 2015). To bring vRNPs into proximity of host capped RNAs, the polymerase binds the C-terminal domain (CTD) of the large subunit of host DNA-dependent RNA polymerase II (RNAP II), a host factor essential for viral transcription (Figure 7) (Engelhardt et al., 2005, Walker and Fodor, 2019) (see Section 1.3.1.1).

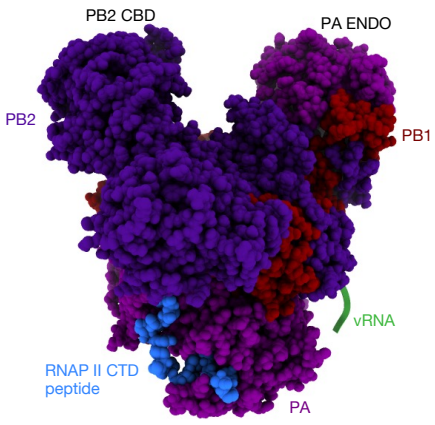

Figure 7. The structure of the IAV polymerase bound to host RNAP II CTD.
Cryo-EM structure of 1918 pandemic IAV (H1N1) polymerase bound to the host RNAP II CTD phosphorylated at Ser5 (Ser5P) and a vRNA promoter (PDB accession code: 8R65) (Keown et al., 2024). The structure was visualised using ChimeraX v.1.9.

Binding of the viral polymerase to the RNAP II CTD stabilises the viral polymerase in a polymerase$_{(T)}$ pre-initiation conformation, in which the PB2^{CBD} and PA^{ENDO} domains are well-positioned for cap-snatching (Figure 7 and 8A) (Krischuns et al., 2022, Lukarska et al., 2017,

Serna Martin et al., 2018, Keown et al., 2024). In cap-snatching, host RNAs are bound at the 5' cap by the $PB2^{CBD}$ domain and then cleaved 10-14bp downstream of the cap by the PA^{ENDO} domain (Dias et al., 2009, Guilligay et al., 2008, Yuan et al., 2009). Rotation of the $PB2^{CBD}$ domain then transfers the capped RNA primer from the PA^{ENDO} active site to the polymerase active site (Reich et al., 2014). At the same time the 3' end of the vRNA template also enters the polymerase active site where it base pairs with the snatched host primer (Figure 8B) (Kouba et al., 2019). The primer is then extended in a template-dependent manner, with NP being detached from the vRNA template before it enters the active site.

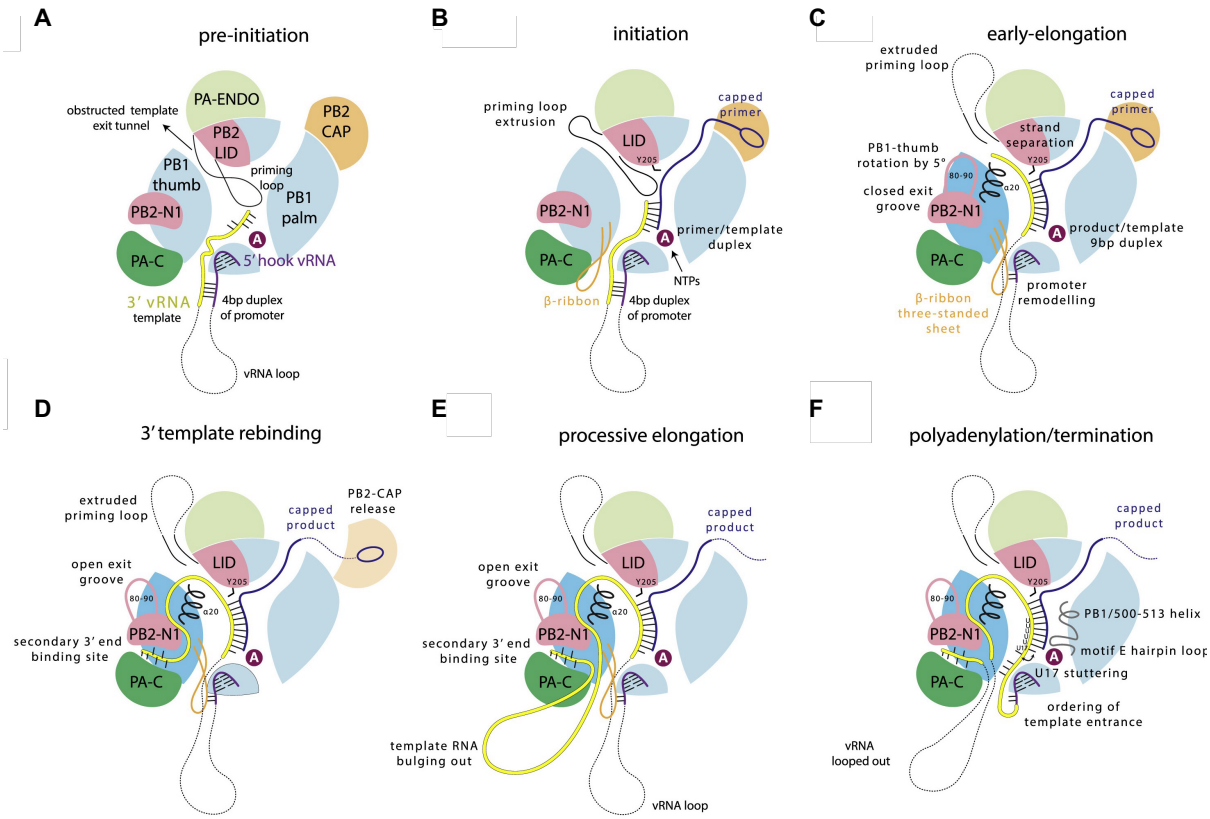

Figure 8. Overview of the mechanism of viral transcription.
Figure from Wandzik et al., 2020. Reproduced with permission from Elsevier. A) In the pre-initiation state, the 3' end of the vRNA template is bound in the active site, designated "A" (Kouba et al., 2019). The PB1 priming loop is also present in the active site where it obstructs the template exit tunnel. The polymerase binds the RNAP II CTD allowing the PB2 cap-binding domain and PA endonuclease domain to perform "cap-snatching" in order to acquire a host capped RNA primer (Engelhardt et al., 2005). B) In the initiation state, a stochastic disordering of the priming loop occurs. This allows the 3' end of the vRNA template and the host capped RNA primer to hybridise and for the first few nucleotides to be added (Kouba et al., 2019). C) In the early-elongation state the template-product duplex grows. This leads to extrusion of the PB1 priming loop which, in turn, opens the template exit channel. When the product-template duplex reaches a length of 9bp it contacts the PB2 lid domain, forcing the two strands to separate and enter their separate exit channels. D) The transcribed template moves along the template exit channel. After translocation of 24nts, the 3' end of the vRNA template is bound in a secondary 3' end binding site where it remains bound until the end of transcription (Wandzik et al., 2020). E) Further translocation forces the transcribed template to bulge out in a loop between the exit channel and the 3' vRNA binding site. The template RNA that is bulging out is in close proximity to the vRNA loop waiting to be transcribed. The short distance between the two suggests that the NP dissociated from the entering template is transferred directly to the exiting template loop. The polymerase continues transcribing in this manner until termination. F) In polyadenylation/termination the polymerase reaches a poly(U) stretch, which starts at position 17 from the 5' end of the vRNA template. At this stage, the vRNA loop is tightened and further translocation would strain the polymerase's linkage to the 5' vRNA hook. The polymerase stutters on the poly(U) stretch, due to the steric hindrance caused by the bound 5' vRNA, which results in the formation of the poly(A) tail. The viral mRNA product is released due to mismatches in the A-U rich template-product duplex.

Next, polymerase$_{(T)}$ transitions from an initiation to an elongation state (Figure 8C) (Kouba et al., 2019). This occurs as the space constraints imposed by the growing template-product duplex extrudes the PB1 priming loop from the active site (Kouba et al., 2019, Te

Velthuis and Oymans, 2018). Extrusion of the priming loop opens the template exit channel (Kouba et al., 2019). Once the template-product duplex reaches a length of 9-10bp the two strands are separated and exit via the template and product exit channels, respectively. Upon exit, the 3' end of the vRNA binds at a secondary binding site within the exit channel where it remains bound until transcription is complete (Figure 8D) (Wandzik et al., 2020). This forces the upstream exiting template to bulge out in a loop between the exit channel and the 3' vRNA binding site (Figure 8E). Given the structural proximity between the template entry and exit channels, it is likely that the NP detached from the entering template is translocated to the exit channel where it then rebinds the exiting template. This sliding movement of the polymerase along the template strand in the context of the vRNP, referred to as a processive helical track, has two benefits: 1) it ensures that the template RNA remains protected from host nucleases throughout transcription and 2) it allows the polymerase to complete transcription without having to release the 3' and 5' vRNA template ends (Coloma et al., 2020, Wandzik et al., 2020).

Transcription termination occurs once polymerase$_{(T)}$ reaches a poly(U) stretch near the 5' end of the vRNA template (Figure 8F). Steric hindrance resulting from the sustained binding of the polymerase to the 5' vRNA end causes the polymerase to stall and stutter on the poly(U) stretch, generating a poly(A) tail (Poon et al., 1999, Wandzik et al., 2020). The viral mRNA is then released and the polymerase switches back into the pre-initiation state, ready for another round of transcription (Wandzik et al., 2020).

Section 1.2.5. Mechanism of viral RNA replication.

Later in infection, viral RNA replication occurs (Fodor and Te Velthuis, 2020). Replication is a primer-independent two-step process that relies on dimerisation of the polymerase (Fodor and Te Velthuis, 2020, Zhu et al., 2023b). In the first step, a full-length positive-sense cRNA intermediate is synthesised from the vRNA template. In the second step, cRNA is used as a template to produce new vRNA genomes, which are then either exported from the nucleus or used as templates for secondary transcription. Initiation of both v-to-cRNA and c-to-vRNA synthesis is triggered by entry of the 3' end of the RNA template into the polymerase active site. However, the mechanisms of initiation differ due to differences in the vRNA and cRNA promoters, as discussed below (Deng et al., 2006, Robb et al., 2019). After initiation, elongation likely proceeds in a manner similar to in transcription, in which a conformational change in the priming loop allows nascent RNA to exit from the active site (Kouba et al., 2019). Lastly, termination of replication occurs. In termination of replication, the 5' end of the RNA template must be released from its binding pocket so that the full RNA template can be copied (Zhu et al., 2023b). This contrasts with termination of transcription where the 5' end of the vRNA remains bound causing the polymerase to stutter (Wandzik et

al., 2020). The exact mechanisms of replication elongation and termination as well as the factors that mediate the release of the 5' vRNA end remain unknown.

In v-to-cRNA synthesis, *de novo* initiation occurs via a process known as terminal initiation (Figure 9A) (Deng et al., 2006). Here, a pppApG dinucleotide is bound opposite residues U1 and C2 of the 3' vRNA template. This depends on structural support from the PB1 priming loop, which acts as a stacking platform that supports formation of the dinucleotide on the end of the template (Te Velthuis et al., 2016). Once synthesised, the nascent cRNA is assembled into a complementary ribonucleoprotein (cRNP) (Vreede et al., 2004, York et al., 2013). Similar to vRNPs, cRNPs have a double-helical arrangement in which the cRNA is bound by NP along its length and a newly synthesised polymerase heterotrimer at its promoter (York et al., 2013).

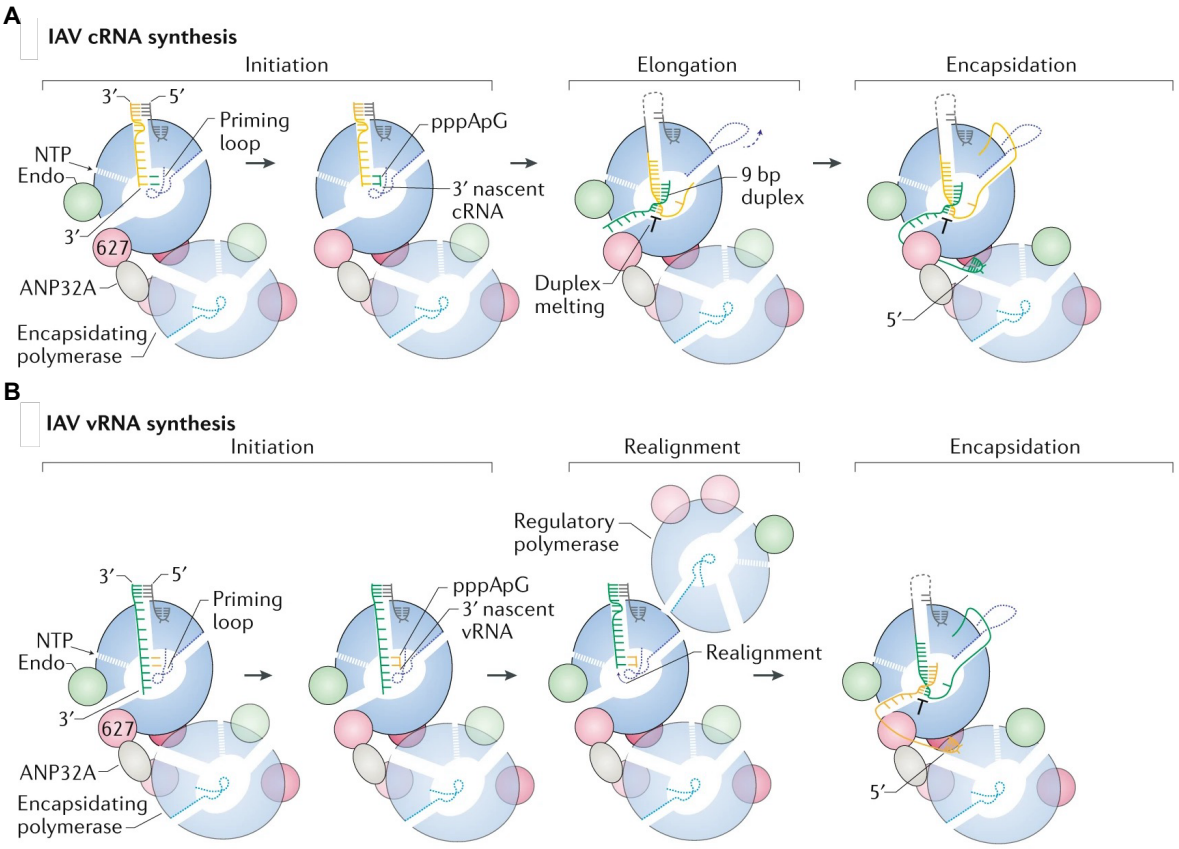

Figure 9. Overview of the mechanism of viral RNA replication.
Figure taken from Te Velthuis et al., 2021. Reproduced with permission from Springer Nature. Replication occurs in two steps. First the vRNA template is copied into a positive-sense complementary RNA (cRNA) intermediate (A), which is then used as a template for vRNA synthesis (B). A) v-cRNA synthesis. cRNA synthesis is initiated by terminal initiation. A pppApG dinucleotide is synthesised on residues U1 and C2 of the 3' vRNA template and stabilised by the PB1 priming loop (Deng et al., 2006, Te Velthuis et al., 2016). B) c-vRNA synthesis. vRNA synthesis is initiated by internal initiation. A pppApG dinucleotide is synthesised on residues U4 and C5 (Deng et al., 2006). Prior to elongation, prime realignment occurs where the dinucleotide is realigned to the start of the cRNA template. This involves a conformational change in the priming loop and the formation of a symmetric dimer between the replicating polymerase and a trans-activating polymerase (Fan et al., 2019, Oymans and Te Velthuis, 2018, York et al., 2013). In both v-cRNA synthesis (A) and c-vRNA synthesis (B), the RNA-bound replicating polymerase binds to an RNA-free encapsidating polymerase to form an asymmetric dimer that is stabilised by the proviral host factor ANP32 (Arragain et al., 2024, Carrique et al., 2020, Staller et al., 2024). The resulting replication platform is essential for the co-replicative assembly of cRNA and vRNA into cRNPs and vRNPs, respectively.

In c-to-vRNA synthesis, *de novo* initiation occurs via a process known as internal initiation (Figure 9B) (Deng et al., 2006). Here, a pppApG dinucleotide is bound opposite residues U4 and C5 of the 3' cRNA template. To allow the full-length cRNA to be copied, prime realignment occurs, in which the dinucleotide is realigned to residues U1 and C2 by backtracking of the cRNA template. This is facilitated by a conformational change in the priming loop and the binding of a second trans-activating polymerase (Jorba et al., 2009, Oymans and Te Velthuis, 2018, York et al., 2013). The unique requirement for a trans-

activating polymerase in the second step of replication was shown as only cRNPs, and not vRNPs, are dependent on additional polymerase to be active *in vitro* (York et al., 2013). Importantly, the second polymerase can be inactive, confirming that it plays a regulatory role as opposed to an enzymatic role. X-ray crystallography and cryo-EM structures show that this trans-activating polymerase forms a symmetric dimer with the cRNP bound polymerase (Figure 10A) (Fan et al., 2019). The dimer interface is largely formed by the PA^{CTD}, the PB2 N-terminus, and the PB1 thumb subdomain. While the PA^{ENDO} domain and PB2 CTD could not be fully resolved, the presence of a 3' cRNA binding site on the dimer interface suggests that this symmetric dimer is important for replication and specifically c-to-vRNA synthesis. This was confirmed as disruption of the dimer interface decreases c-to-vRNA synthesis but has no effect on v-to-cRNA synthesis. Furthermore, disruption of the dimer interface generates short, incorrectly initiated products from the cRNA template, supporting the notion that the structure promotes the prime realignment step necessary for full length vRNAs to be synthesised.

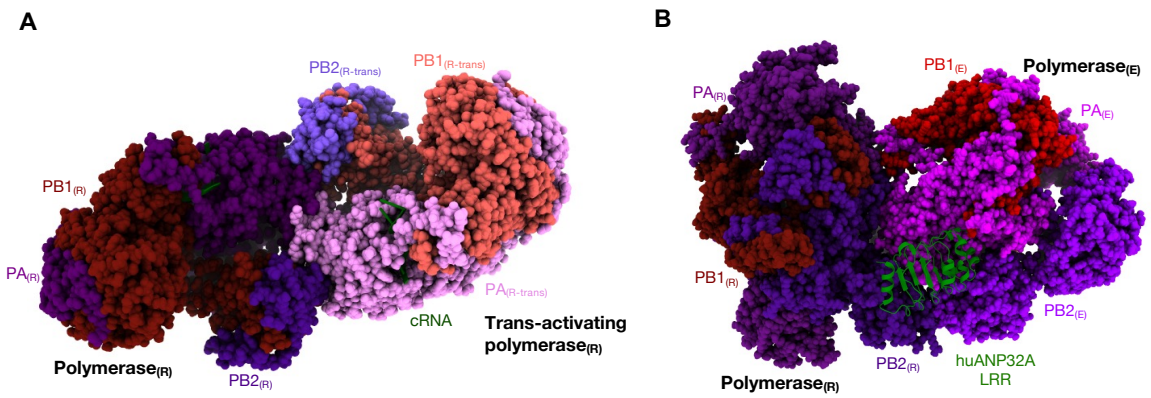

Figure 10. The IAV polymerase forms two structurally distinct dimers during viral RNA replication.
A) Cryo-EM structure of the symmetric IAV (H3N2) polymerase dimer bound to a cRNA promoter (PDB accession code: 6QX8) (Fan et al., 2019). Both polymerases adopt the same replicase structure as in (B), with one of the polymerases proposed to act as a trans-activating polymerase required for c-to-vRNA synthesis. B) Cryo-EM structure of the asymmetric IAV (H7N9) polymerase dimer stabilised by huANP32A (PDB accession code: 8RMR) (Arragain et al., 2024). One of the polymerases adopts a replicase structure and the other polymerase adopts an encapsidase structure. The structures were visualised using ChimeraX v.1.9.

In infection, both cRNA and vRNA synthesis rely on newly synthesised polymerase subunits and NP for encapsidation into cRNP and vRNP complexes, respectively (Vreede et al., 2004, Zhu et al., 2023b). These complexes are assembled as soon as the nascent RNA emerges to prevent triggering of the innate immune response and degradation of the RNA. To ensure co-replicative RNP assembly, the viral polymerase adopts an asymmetric dimer structure, in which one of the polymerases acts as a replicase ($polymerase_{(R)}$) and the other acts as an encapsidase ($polymerase_{(E)}$) (Figure 10B) (Arragain et al., 2024, Carrique et al.,

2020, Staller et al., 2024). Hereafter, polymerase subunits from the replicase will be referred to as $PB1_{(R)}$, $PB2_{(R)}$, and $PA_{(R)}$ while polymerase subunits from the encapsidase will be referred to as $PB1_{(E)}$, $PB2_{(E)}$, and $PA_{(E)}$. The dimeric replication platform is stabilised by ANP32, which is a host factor that is essential for viral RNA replication (see Sections 1.3.2.1 and 1.3.2.2). Asymmetric dimer structures have been solved for the ICV polymerase in complex with huANP32A and chANP32A (Carrique et al., 2020), H5N1 IAV polymerase in complex with huANP32B (Staller et al., 2024), H7N9 IAV polymerase in complex with huANP32A, and the IBV polymerase in complex with huANP32A (Arragain et al., 2024). The overall arrangement of the IAV, IBV, and ICV asymmetric dimers is similar with slight differences mainly in the conformation of $polymerase_{(E)}$ and the binding mode of ANP32 (see Section 1.3.2.2).

In the IAV, IBV, and ICV structures, $polymerase_{(R)}$ adopts a conformation similar to the structure of a cRNA-bound polymerase solved as a monomer and symmetric dimer (Thierry et al., 2016, Fan et al., 2019). In this conformation, the $PA_{(R)}^{ENDO}$ domain packs against the $PB2_{(R)}^{NLS}$ domain while the $PB2_{(R)}^{CBD}$ packs against the $PB1_{(R)}$ palm subdomain, rendering the polymerase transcriptionally inactive. $Polymerase_{(E)}$ adopts a more flexible conformation, distinct from the $polymerase_{(R)}$ conformation and previously solved structures. In the IAV dimer, the $PA_{(E)}^{ENDO}$ domain packs against the $PB2_{(E)}^{CBD}$ in a manner that is mediated by the $PB2_{(E)}^{LID}$. This contrasts with the ICV dimer, where the $PB2_{(E)}^{CTD}$ packs against the $P3_{(E)}^{CTD}$ and the $P3_{(E)}^{ENDO}$ domain is disordered. In both the IAV and ICV structures, the dimer interface largely consists of interactions between the PB2 subunit of $polymerase_{(R)}$ and the PA/P3 subunit of $polymerase_{(E)}$. In the IBV dimer, all three subunits of $polymerase_{(E)}$ were found to contact the PB2 subunit of $polymerase_{(R)}$. Importantly, in all structures, the two heterotrimers are arranged in such a way that $polymerase_{(E)}$ is well-positioned to capture the nascent RNA as it emerges from $polymerase_{(R)}$ (Carrique et al., 2020). The asymmetric dimer has been shown to be important for v-to-cRNA synthesis as disruption of the dimer interface resulted in a reduction in cRNA accumulation. Considering that both cRNA and vRNA synthesis involve assembly into RNPs it is likely that this replication platform is applicable to both steps of replication. The structural similarity between the vRNA-bound $polymerase_{(R)}$ and the previously determined structures of a cRNA-bound polymerase further support this (Thierry et al., 2016, Fan et al., 2019).

Fine-tuned levels of dimerisation are necessary for optimal IAV replication (Chen et al., 2019). It is unknown how $polymerase_{(R)}$ transitions from the asymmetric dimer that conducts v-to-cRNA synthesis to the structurally distinct symmetric dimer required for c-to-vRNA synthesis and how the balance between the two dimer states is maintained. Post translational modification (PTM) may play a role in coordinating formation of the two dimers. For instance, ubiquitylation of residues at the symmetric dimer interface has been shown to modulate symmetric dimer formation (Gunl et al., 2023). Host cell proteins are also likely to

play a role in maintaining the balance between the two dimers. It is also possible that the asymmetric and symmetric dimers combine to form a trimer on the cRNA template but there is no structural evidence for this yet (Arragain et al., 2024). Structures of the polymerase through initiation, elongation, and termination in both cRNA and vRNA synthesis, as has been achieved for transcription, would help elucidate these unknowns (Kouba et al., 2019, Wandzik et al., 2020). Lastly, the role of NP in formation of the replication platform and whether NP binds to polymerase$_{(E)}$ to initiate encapsidation of RNA is unknown.

Section 1.3. Host cell proteins involved in viral transcription and replication

The ability of the viral polymerase to function both as a transcriptase and a replicase is largely due to the flexibility of the polymerase proteins and their ability to adopt various conformations and complexes. Host cell proteins play an essential role in the formation and stabilisation of these polymerase structures. Accordingly, distinct sets of host proteins are co-opted by the IAV polymerase to facilitate the different steps of viral RNA synthesis (reviewed in Peacock et al., 2019). Sections 1.3.1 and 1.3.2 outline examples of host cell proteins that support either transcription or replication.

Section 1.3.1. Host cell proteins involved in viral transcription.

Section 1.3.1.1. RNAP II

RNAP II is the most well-characterised host cell protein integral to viral transcription (Krischuns et al., 2021, Walker and Fodor, 2019). The viral polymerase associates with RNAP II during the cap-snatching step of viral transcription to acquire the host capped RNA fragments that act as primers for transcription initiation. RNAP II is a 12-subunit complex, the large subunit of which (POLR2A) has a long unstructured C-terminal domain (CTD) which consists of 52 repeats of the heptad consensus sequence Tyr1-Ser2-Pro3-Thr4-Ser5-Pro6-Ser7 (Eick and Geyer, 2013, Schuller et al., 2016). Phosphorylation of the CTD (at positions Tyr1, Ser2, Thr4, Ser5, and Ser7, with phosphorylation of Ser2 (Ser2P) and Ser5 (Ser5P) being the most prevalent) determines the progression of RNAP II through the host transcription cycle. Ser5P is associated with transcription initiation and Ser2P is associated with transcription elongation (Eick and Geyer, 2013).

The IAV polymerase interacts directly with the CTD of the large POLR2A subunit when it is phosphorylated at Ser5 but not when it is unphosphorylated or phosphorylated at Ser2 (Engelhardt et al., 2005, Martinez-Alonso et al., 2016, Keown et al., 2024). The interaction occurs when the viral polymerase exists as a heterotrimer and as a vRNP, but not when individual polymerase subunits are expressed. Importantly, the CTD is sufficient for interaction, as demonstrated using CTD peptide mimics (Martinez-Alonso et al., 2016).

Considering that the Ser5P CTD is involved in the capping of nascent host RNAs, the preferential association of the IAV polymerase with this form of RNAP II provides the right spatiotemporal conditions for the IAV polymerase to steal such capped host RNAs (Walker and Fodor, 2019). More recently, the IAV polymerase has also been shown to associate with the Ser7P CTD, but to a lesser extent compared with the Ser5P CTD (Keown et al., 2024). Ser7P is also associated with transcription initiation and specifically transcription of snRNA genes, but the functional implications of its association with the viral polymerase have not been investigated (Egloff et al., 2007, Lyons et al., 2020).

Structures of the IAV, IBV, and ICV polymerases in complex with the RNAP II CTD have revealed the structural basis of their interaction (Keown et al., 2024, Krischuns et al., 2022, Lukarska et al., 2017, Serna Martin et al., 2018). Although all structures show a bipartite CTD binding site involving the PA/P3 subunit, the RNAP II CTD binding modes of the three influenza types differ. In the IAV polymerase, both binding sites are on the PA^{CTD}, with the second binding site including the PA 550 loop (Keown et al., 2024, Krischuns et al., 2022, Lukarska et al., 2017). A recent cryo-EM structure shows the RNAP II CTD to link the two binding sites (Figure 7) (Keown et al., 2024). Binding site 1 is conserved between IAV and IBV (Krischuns et al., 2022, Lukarska et al., 2017). However, in IBV, binding site 2 is unique and spans a region from the PA^{CTD} to the $PB2^{627/NLS}$ domain (Krischuns et al., 2022). Lastly, in ICV both binding sites are distinct from those on IAV and IBV, but still involve the $P3^{CTD}$ (Serna Martin et al., 2018). In all three influenza types, Ser5P residues of the CTD are accommodated by positively charged or basic pockets within the polymerase binding sites.

Most studies have focused on the role of the RNAP II CTD in viral transcription. However, a recent publication suggests that RNAP II may act as an anchor for both viral transcription and replication, such that the polymerase remains bound to the CTD while assembling into a dimeric form for replication (Krischuns et al., 2024). Disruption of the RNAP II CTD binding interface on the IAV polymerase decreases RNA replication (in addition to transcription) and reduces binding of the polymerase to the known replication host factor ANP32. A cryo-EM structure shows RNAP II to occupy the CTD binding sites on the polymerase when it is in a putative replication initiation conformation (the $PB2^{CTD}$ in a replicase-like conformation and the PA^{ENDO} domain in a transcriptase-like conformation). This suggests that CTD binding is compatible with formation of a replication complex, although further structural data is necessary to confirm this in the context of a fully replication-competent conformation (a symmetric dimer or an ANP32-bound asymmetric dimer). However, it remains unclear how this study fits with contradicting evidence in the literature. Two recent studies suggest that RNAP II and ANP32 compete for binding to the viral polymerase, implying that the polymerase does not remain bound to RNAP II during RNA replication (see Section 1.3.2.2) (Arragain et al., 2024, Staller et al., 2024).

Section 1.3.1.2. Additional examples of host proteins involved in viral transcription: the exosome complex and SFPQ

The IAV polymerase also co-opts further host cell proteins to support viral transcription (Peacock et al., 2019). Two examples are the nuclear RNA exosome complex and splicing factor proline-glutamine rich (SFPQ) (Landeras-Bueno et al., 2011, Rialdi et al., 2017). Firstly, the IAV polymerase exploits the RNA exosome during the early stages of viral transcription. The exosome is a multisubunit complex with 3'-5' exoribonuclease activity that degrades ncRNAs, aberrant transcripts, and mRNAs that have been marked for decay (Januszyk and Lima, 2014). The complex interacts with the PA subunit of the viral polymerase (Rialdi et al., 2017). This was found using affinity purification-mass spectrometry (AP-MS) screens performed using the PA subunit as bait in the context of transfection. Depletion of the catalytic or core subunits of the exosome leads to a reduction in the use of 5' ncRNAs as primers for viral transcription and a general decrease in host capped viral mRNA transcripts. This suggests that the exosome complex coordinates the activity of the viral polymerase and host RNAP II during cap-snatching of ncRNAs. Overall, this may allow the IAV polymerase to exploit cellular control mechanisms in order to acquire host capped RNA fragments that were otherwise targeted for degradation.

Secondly, SFPQ is a host cell protein co-opted by the IAV polymerase to support the late stages of viral transcription (Landeras-Bueno et al., 2011). The host protein was identified as a polymerase interactor in a proteomics screen using the PB2 polymerase subunit as bait in the context of the heterotrimeric polymerase complex (Jorba et al., 2008). SFPQ supports the polyadenylation stage of viral transcription as less polyadenylated RNAs are synthesised in the absence of SFPQ (Landeras-Bueno et al., 2011). In the host cell, SFPQ is an RNA binding protein that preferentially binds poly(U) sequences (Patton et al., 1993). Given that viral transcription termination occurs by stuttering of the viral polymerase on a poly(U) stretch on the vRNA template, it seems plausible that SFPQ interacts with both the viral polymerase and viral RNA to promote stuttering at this site, although further work is required to confirm such a mechanism.

Section 1.3.2. Host cell proteins involved in viral RNA replication.

Section 1.3.2.1. ANP32 proteins

Acidic nuclear phosphoprotein 32 kDa (ANP32) proteins are a family of evolutionarily conserved proteins that are essential for influenza virus replication (Sugiyama et al., 2015). Five family members exist in vertebrates: ANP32A-E, however ANP32C and ANP32D are thought to be pseudogenes (reviewed in Reilly et al., 2014). ANP32A, ANP32B, and ANP32E proteins are characterised by having multiple leucine-rich repeats (LRRs) at the N-terminus, a low-complexity acidic region (LCAR) at the C-terminus, and a central region that links the

LRR and the LCAR (Figure 15) (Reilly et al., 2014). The LRR has a well-defined elongated and curved structure, consisting of five LRRs (Huyton and Wolberger, 2007, Matilla and Radrizzani, 2005). In contrast the LCAR is a highly acidic disordered domain (Reilly et al., 2014). ANP32 proteins can be phosphorylated, as suggested by their name, and this PTM increases the acidity of the LCAR (Hong et al., 2004). In addition to phosphorylation, ANP32 proteins can be SUMOylated and their SUMOylation increases upon IAV infection, but the functional implication of this is unknown (Domingues et al., 2015). SUMOylation is a ubiquitin-like modification that typically occurs in the nucleus (Geiss-Friedlander and Melchior, 2007). ANP32 proteins can be nuclear as they have a NLS at their C-terminus. They can also be cytoplasmic and move from the nucleus to the cytoplasm via interaction with the nuclear export protein CRM1 through their N-terminal LRR domain (Brennan et al., 2000).

ANP32 proteins have been assigned a number of roles in the host cell, involving both the LRR and LCAR domains (Reilly et al., 2014). Firstly, all three ANP32 proteins have histone chaperone activity and thereby regulate chromatin and transcription. ANP32A binds histone tails, preferentially binding unmodified histone H3 tails (Schneider et al., 2004). Binding of ANP32A sterically blocks their acetylation, repressing transcription (Yang et al., 2018). ANP32B binds the histone dimers H3-H4 and macroH2A-H2B, facilitating their incorporation into nucleosomes (Mandemaker et al., 2023, Tochio et al., 2010). ANP32E binds the histone dimer H2A.Z-H2B and removes H2A.Z from nucleosomes (Mao et al., 2014, Obri et al., 2014). Secondly, the ANP32 proteins also inhibit protein phosphatase 2A (PP2A). ANP32A was first discovered to bind and inhibit PP2A, and more recently this was also found to be the case for ANP32B and ANP32E (Li et al., 1995, Rivero-Rodriguez et al., 2021, Shin et al., 2018). Lastly, a role has also been described for the ANP32 proteins in nuclear export of proteins through interactions with CRM1, as mentioned above (Brennan et al., 2000).

All IAV strains tested, including both mammalian adapted and avian strains, rely on ANP32 for replication (Peacock et al., 2019). This is also true for IBV and ICV as well as orthomyxoviruses from the thogotovirus genus including Bourbon virus (BRBV) (Zhang et al., 2025b) and Dhori virus (DHOV) (Andrew Mehle, personal communication, June 2025) but, interestingly, not thogotovirus (THOV) (Xue et al., 2024). Mammalian influenza hosts have two proviral ANP32 proteins (ANP32A and ANP32B), although the hosts show differences in whether ANP32A or ANP32B is the preferred cofactor (Peacock et al., 2023, Zhang et al., 2019). An exception is murine hosts in which only ANP32B (muANP32B) is proviral (Staller et al., 2019). In avian hosts, there are also three ANP32 paralogues (referred to as chicken ANP32A (chANP32A), chANP32B, and chANP32E), however only chANP32A is proviral (Long et al., 2019a). A key interaction domain of ANP32 with the IAV polymerase is residues 129/130 in the LRR, and whether an ANP32 paralogue is proviral for IAV can usually be attributed to sequence variation at these residues (see Sections 1.3.2.2 and 1.6.1, Figure 15).

Importantly, compared to huANP32A/B, chANP32A has a 33 amino acid insertion between the LRR and LCAR, which is important for its ability to support AIV replication (Figure 15) (Long et al., 2016). The third family member ANP32E is non-functional in the IAV lifecycle in mammalian and avian influenza hosts.

Since the major finding that species-specific differences in ANP32 proteins are an important host range barrier for the influenza virus polymerase (see Section 1.6.1) (Long et al., 2016), many functional and structural studies have elucidated the mechanism behind the essential proviral role of ANP32 proteins in viral RNA replication (see Section 1.3.2.2).

Section 1.3.2.2. The proviral role of ANP32 proteins

ANP32A and ANP32B serve essential but functionally redundant roles in polymerase activity (Staller et al., 2019, Zhang et al., 2019). Ablation of either protein alone has no effect on polymerase activity or virus growth, but when both proteins are ablated, no polymerase activity or virus growth can occur. In the absence of both ANP32A and ANP32B, IAV can evolve to co-opt the otherwise non-functional ANP32E by acquiring adaptive mutations in the polymerase subunits (Sheppard et al., 2023).

The ANP32 proteins interact with the polymerase when it is in a heterotrimeric form, but not with individual polymerase proteins (Baker et al., 2018, Bradel-Tretheway et al., 2011, Domingues and Hale, 2017, Mistry et al., 2020, Sugiyama et al., 2015). The interaction is increased in the presence of RNA when the polymerase is inactive but decreased when the polymerase is active (Baker et al., 2018, Mistry et al., 2020). This is the case regardless of whether the template provided is a short NP-independent RNA template or a full-length vRNA or cRNA template (Mistry et al., 2020). This suggests that ANP32 proteins are important at the early stages of viral RNA synthesis and dissociate once the polymerase becomes active. Consistent with a role for ANP32 in polymerase activity, the polymerase-ANP32 interaction occurs in the nucleus, as demonstrated by an immunofluoresence assay measuring the interaction between PB1 and ANP32A (Mistry et al., 2020). Interestingly, ANP32 has also been found to interact with individually transfected NA protein, but the functional significance of this is unknown (Watanabe et al., 2014).

ANP32 specifically supports the RNA replication step of viral RNA synthesis, but is not required for viral transcription (Nilsson-Payant et al., 2022, Staller et al., 2019, Sugiyama et al., 2015, Swann et al., 2023). The role of ANP32 in the IAV lifecycle and its role in RNA replication was first shown by Sugiyama et al. Using a cell-free *in vitro* replication assay, purified ANP32A and ANP32B were shown to stimulate replication from a cRNA template but not from a vRNA template (Sugiyama et al., 2015). This initially suggested that ANP32 only plays a role in the second step of RNA replication. More recently, ANP32 has been shown to be essential for the v-to-cRNA synthesis step of replication as well (Nilsson-Payant et al.,

2022, Swann et al., 2023). In a minigenome setup that employs vRNA and cRNA templates with mutated promoters to only permit v-to-cRNA synthesis or c-to-vRNA synthesis, ANP32 was shown to be required for both steps of replication (Nilsson-Payant et al., 2022). This was confirmed in the context of infection using a cRNP stabilisation assay, in which only v-to-cRNA synthesis can occur. In the absence of ANP32, no cRNA accumulates both when quantified by RT-qPCR and visualised using an RNA fluorescence *in situ* hybridisation (FISH) method (Swann et al., 2023).

A role for ANP32 in both cRNA and vRNA synthesis is consistent with structural analyses of ANP32 in complex with the IAV, IBV, and ICV polymerases (Arragain et al., 2024, Staller et al., 2024, Carrique et al., 2020). In these structures, the ANP32 LRR bridges the asymmetric polymerase dimer required for RNA replication (see Section 1.2.5). This implies that the ANP32 LRR stabilises the dimeric replication platform, whereby ANP32 delivers polymerase$_{(E)}$ onto the nascent RNA, ensuring co-replicative assembly of RNAs into RNPs.

The binding mode of ANP32 is similar for the IAV and IBV structures with some differences compared to the ICV structure. In all three structures, the C-terminus of the ANP32 LRR interacts with polymerase$_{(E)}$ and particularly the PA$_{(E)}^{CTD}$. For example, residues N129/D130, which are important for the ability of ANP32 to support viral replication, contact residue K635 of the PA$_{(E)}^{CTD}$ (Arragain et al., 2024, Long et al., 2019a, Staller et al., 2024). In the IAV structure, the PB2$_{(E)}^{627}$ domain also contacts the C-terminus of the LRR and the PA$_{(E)}$ 550 loop binds between the LRR and LCAR (Arragain et al., 2024, Staller et al., 2024). Meanwhile, the N-terminus of the ANP32 LRR interacts with polymerase$_{(R)}$ and particularly the PB2$_{(R)}^{627/NLS}$ domain, but this interaction is more tenuous for the IAV and IBV complexes (Arragain et al., 2024, Carrique et al., 2020, Staller et al., 2024).

The ANP32 LRR also interacts with IAV and IBV polymerase$_{(APO)}$, present either in a monomeric form (Staller et al., 2024) or symmetric dimeric form (Arragain et al., 2024). The binding of ANP32 to polymerase$_{(APO)}$ is similar to its binding to polymerase$_{(E)}$ in the asymmetric dimer. This suggests that ANP32 may perform a second role in RNA replication by acting as a chaperone that recruits polymerase$_{APO}$ (which then becomes polymerase$_{(E)}$) to the vRNP-bound polymerase$_{(R)}$. The polymerase has been shown to exist in different higher order oligomeric complexes including dimers, tetramers, and even hexamers depending on the conditions used and the presence of other viral proteins (Arragain et al., 2024, Chang et al., 2015, Sun et al., 2024a). Whether these structures are relevant in the context of an actual infection is unclear but it could be speculated that ANP32 acts as a chaperone that maintains the polymerase in a state that is compatible with asymmetric dimer formation.

The ANP32 binding site on polymerase$_{(E)}$ and polymerase$_{(APO)}$ is in a similar position to that of the host RNAP II CTD (Arragain et al., 2024, Staller et al., 2024). For instance, residue K635 of the PA$_{(E)}^{CTD}$ has previously been shown to be important for binding of the RNAP II

CTD (Lukarska et al., 2017). Moreover, the $PA_{(E)}$ 550 loop is also found in the binding site of the RNAP II CTD. This suggests that binding of RNAP II and ANP32 to the viral polymerase is mutually exclusive. Competition experiments in which ANP32 outcompeted the binding of RNAP II CTD peptide mimics to the viral polymerase in a concentration-dependent manner confirm this (Staller et al., 2024).

ANP32 also plays a further role in the co-replicative assembly of RNA into RNPs, in which the LCAR of ANP32 acts as molecular whip that recruits NP to nascent RNA (Wang et al., 2022a). The ANP32 LCAR could not be fully resolved in the asymmetric dimer structures, indicating this part of ANP32 to be highly dynamic. However, functional studies have shown the LCAR to enhance binding of ANP32 to the viral polymerase and support its ability to promote polymerase activity (Domingues and Hale, 2017, Mistry et al., 2020, Wang et al., 2022a). The importance of the LCAR is NP-dependent as the LCAR is not required for ANP32 to support replication of a short NP-independent RNA template (Wang et al., 2022a). Indeed, ANP32 interacts directly with NP in a manner that is dependent on the LCAR. The ANP32-NP binding interface involves the RNA binding grooves of NP and consequently ANP32 and RNA compete for binding, with NP showing higher affinity for RNA. This suggests a model in which the ANP32 LCAR binds free monomeric NP molecules, recruiting them to the nascent RNA. The stronger binding of NP to RNA then causes NP to dissociate from the ANP32 LCAR and associate with the nascent RNA strand instead, ensuring assembly of the RNA into RNPs. Such a role for the ANP32 LCAR is reminiscent of the role of the acidic phosphoprotein (P protein) encoded by non-segmented negative strand RNA viruses, which similarly recruits nucleoprotein (N protein) to nascent RNA products (Jamin and Yabukarski, 2017). As IAV does not encode such a protein, it makes sense that a similar function is performed by a co-opted host protein. Given that the LCAR is long enough to accommodate multiple NP monomers, an alternative model could be that ANP32 simply enhances the local density of NP, making eventual recruitment to the RNA more efficient (Wang et al., 2022a).

Taking the structural and functional data together, a mechanism can be proposed for ANP32's proviral role (Figure 11). Initially ANP32 acts as a chaperone, binding $polymerase_{(APO)}$ monomers or dimers. Binding of ANP32 prevents the polymerase from binding host RNAP II. Staller et al., propose that this has the additional benefit of preventing transcription-incompetent $polymerase_{(APO)}$ from blocking RNAP II CTDs (Staller et al., 2024). ANP32 then recruits the bound $polymerase_{(APO)}$ to a vRNP-resident polymerase and a replication platform is assembled. The ANP32-bound $polymerase_{(APO)}$ becomes $polymerase_{(E)}$ and the vRNP-bound polymerase becomes $polymerase_{(R)}$. Once the replication platform has assembled, the ANP32 LCAR recruits NP to the nascent RNA. As both cRNA and vRNA need to be encapsidated and ANP32 is important for both cRNA and vRNA synthesis, it is likely that the ANP32 LRR stabilises the replication platform and the ANP32 LCAR recruits NP in both

RNA replication steps. It is unknown whether the ANP32 LCAR is involved in the recruitment of just the first NP molecule, or all NPs required to encapsidate the RNA. Previous work showing ANP32 to dissociate once the polymerase becomes active is consistent with a model in which ANP32 is only required for the recruitment of the first NP (Baker et al., 2018, Mistry et al., 2020). It could be speculated that additional host proteins are involved in the recruitment of subsequent NPs but further work is necessary to elucidate this.

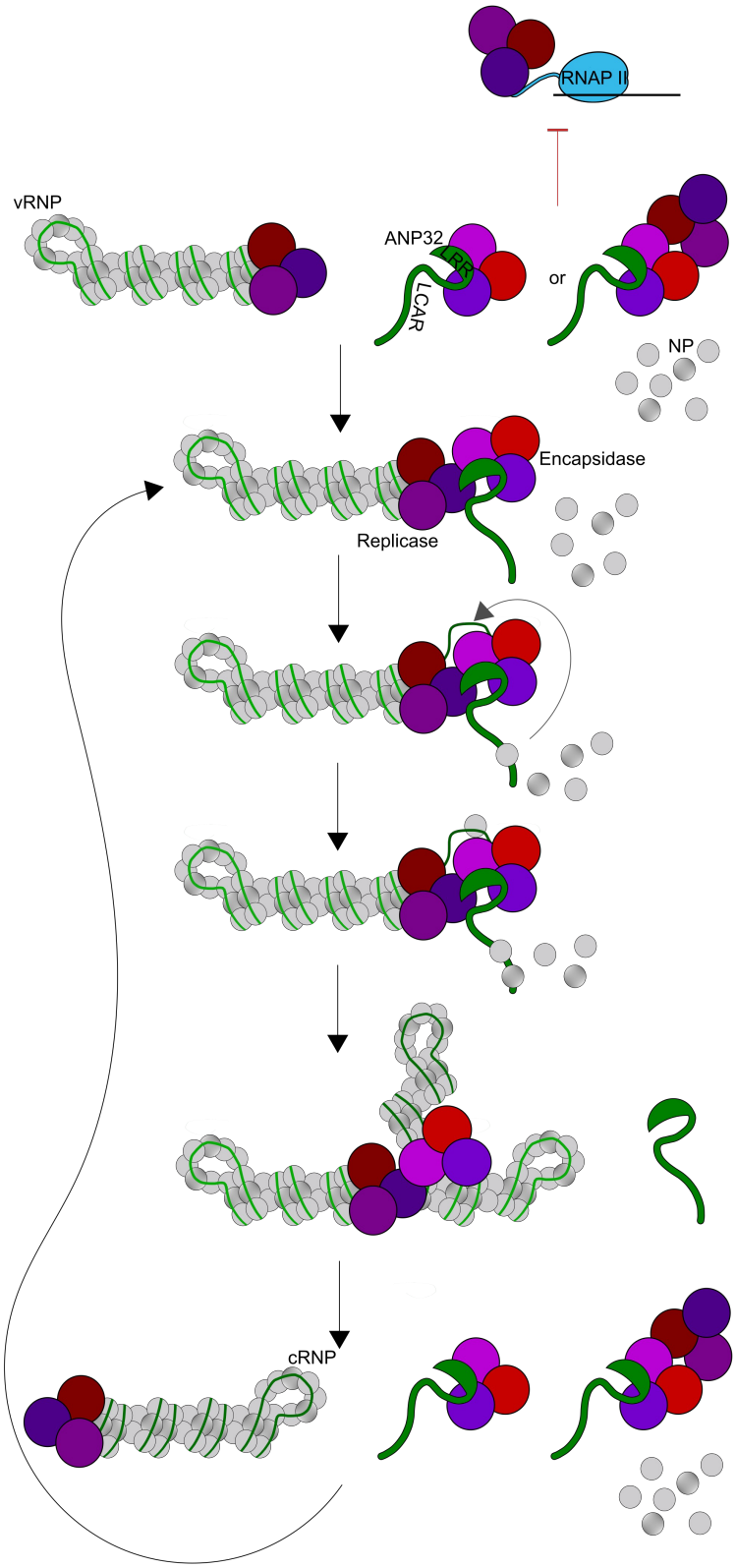

Figure 11. Current model of the proviral role of ANP32 proteins in viral RNA replication.
The ANP32 leucine-rich repeat region (LRR) binds an RNA-free polymerase either existing as a monomer or dimer (Arragain et al., 2024, Staller et al., 2024). Binding of ANP32 to the polymerase prevents binding of the polymerase to the RNAP II CTD. ANP32 then recruits the RNA-free polymerase to a vRNP-bound polymerase. This results in the formation of an asymmetric dimer, bridged by ANP32, in which the vRNP-bound polymerase is a replicase and the RNA-free polymerase is an encapsidase

(Arragain et al., 2024, Carrique et al., 2020, Staller et al., 2024). ANP32 thereby ensures that the encapsidating polymerase is loaded onto the nascent cRNA strand as it emerges from the active site of the replicating polymerase. Once RNA synthesis has begun, the ANP32 low-complexity acidic region (LCAR) acts as a molecular whip that recruits NP onto the nascent cRNA strand (Wang et al., 2022a). ANP32 then dissociates, likely when the polymerase transition from initiation to elongation. ANP32 also plays an essential role in c-to-vRNA synthesis and is believed to ensure co-replicative assembly on a cRNP template via the same mechanism. Adapted from Swann, 2023.

Section 1.3.2.3. Other host proteins that specifically support RNA replication: the MCM complex

The only other host factor shown to specifically support RNA replication is the minichromosome maintenance (MCM) complex, consisting of MCM2, 3, 4, 5, 6, and 7 (Kawaguchi and Nagata, 2007). MCM interacts with the polymerase heterotrimer and vRNPs via the PA polymerase subunit. The complex was identified as a proviral factor using a similar cell-free replication assay as the one used by Sugiyama et al., to identify ANP32A/B (Kawaguchi and Nagata, 2007, Sugiyama et al., 2015). In contrast to ANP32A/B, purified MCM proteins stimulate cRNA synthesis from a vRNA template, indicating that MCM proteins play a proviral role in the first v-to-cRNA synthesis step of RNA replication (Kawaguchi and Nagata, 2007). This is further supported as knockdown of MCM2 and MCM3 reduce cRNA synthesis but not mRNA synthesis. MCM is proposed to stabilise the transition from an initiation to an elongation state by acting as a scaffold between the nascent RNA and viral polymerase. In turn, this promotes synthesis of full length cRNA and prevents abortive replication.

Section 1.4. Regulation of viral transcription and replication

During infection, the temporal dynamics of vRNA, cRNA, and mRNA synthesis differ (Kawakami et al., 2011, Phan et al., 2021, Robb et al., 2009). In the early stages, mRNA synthesis dominates, with mRNA levels peaking at approximately four hours post infection (hpi) (Figure 12). cRNA synthesis begins shortly after mRNA synthesis and the cRNA levels remain low throughout the infection. In the late stages, vRNA synthesis dominates and continues to increase throughout infection. These dynamics suggest that a switch from viral transcription to RNA replication occurs and this switch must be properly timed and regulated to achieve a productive infection (reviewed in Deng et al., 2025). Several cellular and viral factors have been implicated in regulating such a switch, which are outlined in Sections 1.4.1-1.4.3.

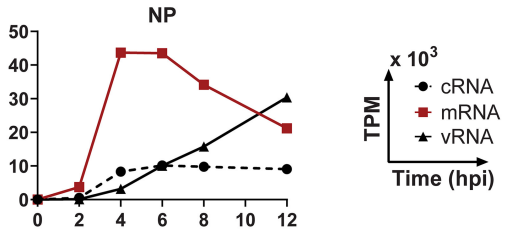

Figure 12. The temporal dynamics of vRNA, cRNA, and mRNA synthesis during infection. Taken from Phan et al., 2021. mRNA synthesis begins shortly after infection with maximum mRNA levels reached at 4 hours post infection (hpi). cRNA synthesis begins shortly after mRNA synthesis begins. The cRNA levels remain low throughout infection consistent with that they are an intermediate product produced in RNA replication. vRNA synthesis begins shortly after cRNA synthesis and continues to increase throughout infection. The vRNA, cRNA, and mRNA levels are shown for the NP segment. The data is plotted as transcripts per kilobase per million (TPM) against time (hpi).

Section 1.4.1. Degradation of RNAP II.

Host RNAP II is degraded during IAV infection, likely as a consequence of its interaction with the viral polymerase (Bauer et al., 2018, Rodriguez et al., 2007, Vreede et al., 2010). Phosphorylated RNAP II is degraded in the presence of vRNPs and polymerase heterotrimers (Vreede et al., 2010). Its degradation is proposed to occur via the proteasome pathway as IAV infection and binding of the viral polymerase induces its ubiquitylation. Alternatively, the proteolytic activity of the PA subunit may be responsible for its degradation (Rodriguez et al., 2007, Vreede et al., 2010). Regardless of the mechanism, degradation of RNAP II means that less will be available for the viral polymerase to hijack and acquire host capped RNAs from. In turn, this may contribute to the drop in viral mRNA synthesis at later stages of infection and the switch to replication (Vreede et al., 2010). Moreover, degradation of RNAP II leads to inhibition of host gene expression and may, therefore, also serve as a way for the virus to suppress activation of innate immune responses (Bauer et al., 2018, Vreede et al., 2010). Interestingly, unphosphorylated RNAP II is also degraded at later timepoints post infection. This even occurs when PA is expressed alone, perhaps suggesting that PA's proteolytic activity may be responsible for this (Rodriguez et al., 2007, Vreede et al., 2010). However, the implications of unphosphorylated RNAP II degradation aside from contributing to host cell shutoff are unclear.

Section 1.4.2. Viral polymerase proteins and NP.

An early model for the transcription to replication switch proposes that the switch is determined by the accumulation of viral polymerase proteins (Vreede et al., 2004) and NP (Beaton and Krug, 1986). Whether the polymerase proteins and NP are simply required for encapsidation of the nascent RNA or act to induce a switch in the polymerase from a transcriptase to a replicase is unresolved. Vreede et al., propose that the viral polymerase is

capable of catalysing both mRNA and cRNA synthesis in *cis*, but that in the absence of free polymerase heterotrimers and NP (in the early stages of infection), the naked cRNA is degraded by host cell nucleases (Vreede and Brownlee, 2007, Vreede et al., 2004). Such a model is supported by data from cell-free replication assays which show that low levels of v-to-cRNA synthesis can occur without addition of polymerase proteins, NP, or host cell proteins (York et al., 2013, Zhang et al., 2025a, Zhu et al., 2023a). Considering recent structures showing higher order polymerase complexes, an alternative model is that accumulation of polymerase proteins allows replication-competent polymerase complexes to form, triggering a switch from transcription to replication (Carrique et al., 2020, Fan et al., 2019, Staller et al., 2024). Such a model is supported by Olson et al., who found that addition of polymerase to a cell-free replication assay switches the polymerase from a transcriptase to a replicase (Olson et al., 2010). More recently, Zhu et al., have also found that addition of polymerase and ANP32 to a cell-free replication assay increases cRNA accumulation and decreases mRNA levels (Zhu et al., 2023a). Taken together, it is possible that a monomeric polymerase can synthesise cRNA inefficiently, but this may not be physiologically relevant. In the context of an actual infection, it appears that newly synthesised polymerase heterotrimers (and NP) play a role in the switch of the polymerase from a transcriptase to a replicase, and, most certainly, in the encapsidation of nascent RNA.

Furthermore, several lines of evidence in the literature suggest that it is also possible that NP plays a direct role in formation of the replicase complex, in addition to its role in encapsidation of RNA. Firstly, addition of NP to a cell-free replication assay increases cRNA accumulation to a greater extent than when only polymerase proteins and ANP32 are added and allows c-to-vRNA synthesis to occur as well (Zhu et al., 2023a). Additionally, NP mutants deficient in RNA binding are still partially able to support v-to-cRNA synthesis (Newcomb et al., 2009, Zhu et al., 2023a). Although the resulting cRNPs are non-functional, this suggests an additional role of NP in directly stimulating replication activity aside from RNA encapsidation. Moreover, mutant NPs have been identified that result in replication incompetent-vRNPs but replication-competent cRNPs, suggesting that NP has a specific role in the early stages of RNA replication on a vRNA template (Mena et al., 1999). Considering that NP binds PB2 and PB1, it is possible that binding of NP to the polymerase triggers a conformational change that switches the polymerase into a replication-competent state (Biswas et al., 1998, Newcomb et al., 2009). Alternatively, it is also possible that NP alters the vRNA promoter structure to allow replication to occur. For instance, NP has been implicated in the synthesis of full length cRNA templates by preventing termination at the polyadenylation site used in mRNA synthesis (Beaton and Krug, 1986, Shapiro and Krug, 1988). Overall, these findings imply a role for NP in directly stimulating a switch from mRNA to cRNA synthesis, although the mechanism remains unknown.

Section 1.4.3. NS2

The proteins produced from segment 8, NS1 and NS2, also contribute to the regulation of transcription and replication (Deng et al., 2025). NS1 is translated from the unspliced NS segment mRNA, while a weak 5' splice site results in a spliced mRNA product from which NS2 is translated (Dubois et al., 2014). The main function of NS1 is as an antagonist of the innate immune response (Garcia-Sastre et al., 1998). NS1 also interferes with cellular functions, triggering host cell shutoff (Hale et al., 2008). For instance, NS1 interacts with the cellular CPSF30 protein, which prevents 3' end cleavage and polyadenylation of host mRNAs and consequently their nuclear export (Nemeroff et al., 1998). NS2, which consists of an NTD and CTD, plays an important role in facilitating the nuclear export of vRNPs via the CRM1 pathway, in a manner that is dependent on M1 (Neumann et al., 2000, O'Neill et al., 1998). Aside from these roles, there is mounting evidence that the two proteins, and particularly NS2, ensure proper timing of vRNA, cRNA, and mRNA synthesis during infection (Robb et al., 2009, Zhang et al., 2023, Zhang et al., 2025a).

NS1 promotes transcription, consistent with its early expression during infection (Min et al., 2007, Zhang et al., 2023). This was shown by overexpression of NS1 in infected cells treated with CHX (such that only primary mRNA synthesis can occur) (Zhang et al., 2023). The effect of NS1 on transcription occurs independently of its interferon (IFN) antagonism and interaction with CPSF30. NS1 interacts with vRNPs in infected cells and this interaction occurs in RNAP II-containing chromatin fractions of the infected cells (Marion et al., 1997, Robb et al., 2011). Further work is necessary to understand whether this finding contributes to the role of NS1 in transcription and the mechanism behind its enhancement of transcription.

A role for NS2 in regulation of polymerase activity was first proposed by Robb et al., who found that the relative vRNA, cRNA, and mRNA levels in a minigenome setup (when only polymerase proteins, NP, and a viral-like RNA template are present) were different compared to in an infection (Robb et al., 2009). Addition of NS2 to the minigenome assay caused the viral RNA synthesis dynamics to resemble those of an infection. NS2 was found to have two effects on viral RNA synthesis: inhibition of transcription and promotion of RNA replication, implicating NS2 in regulating the switch between transcription and replication. NS2 also enhances overall polymerase activity, encompassing both transcription and replication, in a dose-dependant manner, suggesting that the regulatory role of NS2 ensures optimal polymerase activity (Reuther et al., 2014).

NS2 is proposed to inhibit transcription by preventing the interaction between the viral polymerase and host RNAP II (Sun et al., 2024a). This is suggested as NS2 decreases the interaction between the viral polymerase and the RNAP II CTD in a dose-dependent manner. ANP32 is also proposed to compete with the host RNAP II CTD for binding to the viral polymerase (Staller et al., 2024, Arragain et al., 2024). A scenario could be envisioned where

both are compatible if NS2 competes for binding to a vRNP-resident polymerase and ANP32 competes for binding to an RNA-free polymerase. However, further work is necessary to clarify this. The roles of NS2 in inhibition of transcription and enhancement of replication are believed to be independent as different parts of NS2 are responsible for each. The N-terminus, and particularly the first twenty amino acids (aa), are important for the role of NS2 in transcription (Zhang et al., 2023).

NS2 enhances the v-to-cRNA synthesis step of RNA replication but does not directly act on the c-to-vRNA synthesis step (Zhang et al., 2025a). This was shown using a minigenome setup with vRNA and cRNA templates mutated at the promoter to only allow v-to-cRNA or c-to-vRNA synthesis, which is the same assay that was used to show that ANP32 is important for both steps of replication (Nilsson-Payant et al., 2022, Zhang et al., 2025a). In standard minigenome assays where vRNA synthesis depends on cRNA synthesis, NS2 promotes both steps of replication (Robb et al., 2009, Zhang et al., 2023). Given that NS2 preferentially enhances cRNA synthesis, its effect on vRNA synthesis in these assays is likely a secondary effect of the increase in cRNA accumulation. NS2 promotes cRNA synthesis via interactions with the polymerase as it was found to preferentially bind a vRNA-resident polymerase compared to a cRNA-resident polymerase (Zhang et al., 2025a). Consistent with this, the replication enhancing properties of NS2 are NP-independent (Zhang et al., 2023). Interestingly, NS2 even enhances v-to-cRNA synthesis in an *in vitro* cell-free replication assay with purified polymerase and a vRNA template (Zhang et al., 2025a). This suggests that the role of NS2 in enhancing cRNA synthesis is, at least partially, due to a direct effect of NS2 on vRNPs and independent of any other host factors, such as ANP32.

The C-terminus of NS2 is sufficient for its role in RNA replication (Reuther et al., 2014). In particular, the last residue (I121) of NS2 is important as mutation of this residue abolishes NS2's ability to promote replication but has no effect on its ability to inhibit transcription (Reuther et al., 2014, Zhang et al., 2023). The importance of this residue is further shown as adaptive mutations in the PA and PB1 polymerase subunits arise upon serial passage of viruses with a mutated 121 residue (Zhang et al., 2024). These polymerase mutants restore NS2's ability to promote replication, confirming that the mutated NS2 results in a defect in replication. How residue 121 supports replication remains unclear but it is possible that this residue is important for interactions with the polymerase (or a host factor). Reuther et al., have proposed the CTD of NS2 to be the active domain, and for its activity to be regulated by the conformation of the NTD. Using a split luciferase assay, which measures protein-protein interactions, the authors show the NTD to fold back on the CTD, generating a closed conformation (Reuther et al., 2014). It is proposed that a conformational change in the NTD may open the structure, allowing the C-terminus to become active and interact with the

polymerase or a host factor and thereby enhance replication. How such a model fits with the role of the NS2 N-terminus in viral transcription remains to be studied.

Importantly, the effects of NS2 on viral RNA synthesis are concentration-dependent: low NS2 concentrations have little effect on polymerase activity and too high concentrations have an inhibitory effect (Bullido et al., 2001, Reuther et al., 2014, Zhang et al., 2025a). The role of NS2 in nuclear export is also concentration dependent, with premature export occurring at high NS2 concentrations (Chua et al., 2013). Accordingly, the amount of NS2 produced during infection is carefully controlled, with only 10-15% of NS-derived mRNA encoding NS2. It is thought that influenza uses the low efficiency splice site on segment 8 to coordinate viral replication. Specifically, the splice site may act as a molecular timer that allows NS2 to slowly accumulate, triggering the switch from transcription to replication and, in turn, nuclear export of the resulting progeny vRNPs (Chua et al., 2013).

Lastly, in addition to directly promoting cRNA synthesis, NS2 has also been implicated in the synthesis of small viral RNAs (svRNAs), which are 22-27nt long RNA fragments that correspond to the 5' end of vRNA segments (Perez et al., 2010, Perez et al., 2012). svRNA synthesis requires the polymerase, NP, and NS2. The requirement for NS2 is due to its role in promoting cRNA synthesis as svRNA synthesis is only NS2-dependent in the presence of a vRNA template but not when a cRNA template is directly supplied (Perez et al., 2012). svRNAs are proposed to specifically promote c-to-vRNA synthesis by binding an RNA binding cleft in the PA subunit. How svRNAs achieve this remains unclear but their binding is believed to induce a conformational change that makes the polymerase competent for vRNA synthesis (Perez et al., 2010, Perez et al., 2012).

The host and viral factors that regulate vRNA, cRNA, and mRNA synthesis are summarised in Figure 13.

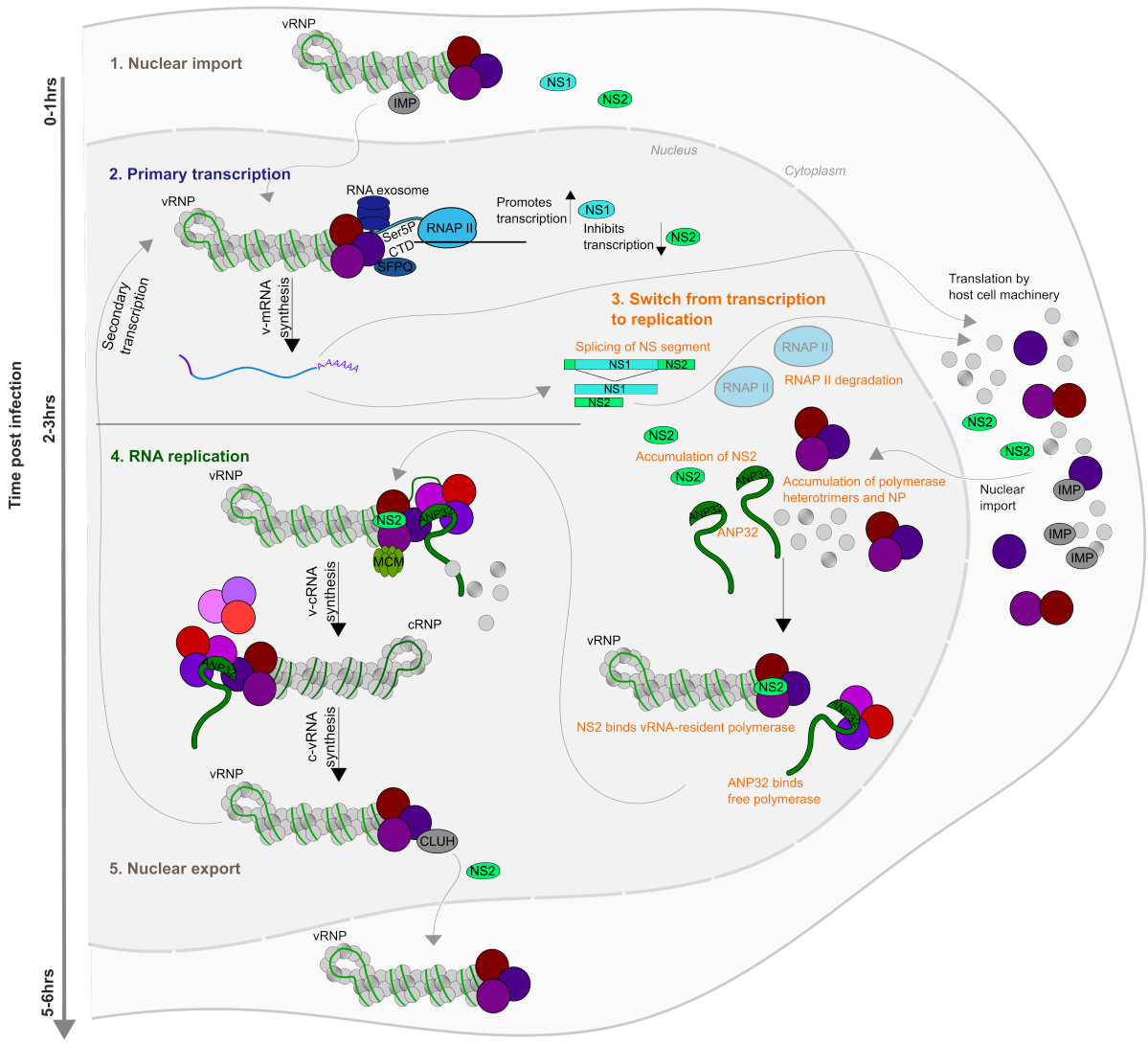

Figure 13. Host and viral factors that regulate viral RNA transcription and replication in the early stages of infection.

1. vRNPs are imported into the nucleus via NP-mediated interaction with IMPα proteins (Cros et al., 2005, O'Neill et al., 1995). 2. Primary transcription occurs. The viral polymerase interacts with the RNAP II CTD phosphorylated at Ser5 (Ser5P), adopting a transcription-competent conformation (Walker and Fodor, 2019). The RNA exosome and SFPQ also support viral transcription (Landeras-Bueno et al., 2011, Rialdi et al., 2017). Meanwhile, NS1 and NS2 viral proteins from the infecting virion upregulate and downregulate transcription, respectively (Robb et al., 2009, Zhang et al., 2023). The viral mRNA is exported to the cytoplasm where it is translated into new viral proteins. The NS segment undergoes splicing to generate mRNAs encoding NS1 and NS2, which leads to a gradual accumulation of NS2 (Chua et al., 2013). 3. The polymerase switches from transcription to replication. This occurs due to degradation of RNAP II, accumulation of newly synthesised polymerase heterotrimers and NP, and increasing amounts of NS2 (Deng et al., 2025). Newly synthesised polymerase is bound by ANP32 and recruited to a vRNA resident polymerase, triggering the formation of an asymmetric dimer competent for v-to-cRNA synthesis (Arragain et al., 2024, Carrique et al., 2020, Staller et al., 2024). NS2 binds a vRNA-resident polymerase and promotes v-to-cRNA synthesis (Zhang et al., 2025a). 4. RNA replication occurs. v-to-cRNA synthesis is supported by the MCM complex (Kawaguchi and Nagata, 2007). c-to-vRNA synthesis depends on an additional newly synthesised polymerase heterotrimer to function as a trans-activating polymerase (York et al., 2013). 5. The progeny vRNPs are then exported from the nucleus via interaction with CLUH or used as a template for secondary transcription (Ando et al., 2016).

Section 1.5. Interactome screens to identify host cell proteins that regulate polymerase activity

Section 1.5.1. Genetic and protein-protein interaction screens.

Many genetic and protein-protein interaction screens have been performed with the aim of identifying host cell proteins important for the IAV lifecycle. Indeed, these screens, which have been performed with various IAV strains and in various cell models, have generated a multitude of datasets on IAV's host cell partners. To identify hits that are relevant to multiple IAVs, recent screens have used multiple virus strains and/or multiple cell types (Rialdi et al., 2017, Haas et al., 2023). An alternative way to find proteins of significance is to take a multi-omics approach combining genetic, proteomic, and transcriptomic data (Haas et al., 2023, Martin-Sancho et al., 2021).

Most genetic screens have been performed in a loss-of-function setting, using either RNA interference (RNAi) or CRISPR-Cas9 based methods (Schaack and Mehle, 2020). Briefly, in these screens, cells are infected with influenza following gene depletion, and infection is monitored to assess the impact of loss of each gene. Details of previous RNAi and CRISPR genetic screens are provided in Table 2. Genetic screens are associated with several strengths and weaknesses. First, genome-wide libraries for both RNAi and CRISPR screens are readily available and both screen types are compatible with high throughput workflows, making it feasible to test many genes in one experiment (Schaack and Mehle, 2020). Second, depending on the dynamic range, these methods can identify both proviral and antiviral factors. In fact, a major advantage of genetic screens is that they directly indicate whether a host cell protein is proviral, antiviral, or neutral. The conditions of the screen can also be skewed towards identification of either negative or positive regulators, for example by interferon treatment prior to infection (Martin-Sancho et al., 2021). However, in most genetic screens, the readout is the impact of gene knockdown on virus replication and, therefore, such screens are not able to pinpoint the exact stage of the viral lifecycle that the host cell protein is involved in nor the viral proteins that are involved. Consequently, downstream functional validation is necessary to confirm that the identified host proteins are not false positives and to understand the mechanistic details behind their role. Furthermore, as typically only one gene is targeted per siRNA/sgRNA, host factors may be missed due to redundancy, which is perhaps why the ANP32 proteins have not been identified in these screens. Lastly, functional screens, and especially CRISPR screens, cannot be used to identify host proteins that are essential for cell viability (Puschnik et al., 2017).

Table 2. Examples of genetic screens to identify host cell proteins important for the IAV lifecycle.

Type of screen	Details	Reference
RNAi	Performed in A549 cells using the laboratory adapted WSN strain of IAV.	(Konig et al., 2010)
RNAi	Performed in A549 cells using the laboratory adapted WSN strain of IAV.	(Karlas et al., 2010)
RNAi	Performed in HBEC cells with the laboratory adapted PR8 strain of IAV.	(Shapira et al., 2009)
RNAi	Performed in U2OS cells using the laboratory adapted PR8 strain of IAV.	(Brass et al., 2009)
RNAi	Performed in macrophage-like THP-1 cells using a seasonal H3N2 strain and an avian H5N1 strain of IAV.	(Martin-Sancho et al., 2021)
CRISPR	Performed in A549 cells using the laboratory adapted PR8 strain of IAV.	(Li et al., 2020)
CRISPR	Performed in A549 cells with a human isolate of an avian H5N1 strain of IAV.	(Han et al., 2018)

Many independent RNAi screens have been performed but there is very little overlap in the host proteins identified in these screens (Table 2). Indeed, a study comparing four RNAi studies (Brass et al., 2009, Hao et al., 2008, Karlas et al., 2010, Konig et al., 2010) found that only 7% of the genes overlapped (Hao et al., 2013). This variation may be due to the discovery of both false positive and false negative hits. Off-target effects of siRNAs may lead to the identification of false positives, although such effects can be reduced by using multiple, independent siRNAs against the target gene. CRISPR is associated with less off-target effects than RNAi because it both uses a 20nt guide sequence specified by the sgRNA to bind the target DNA and requires a proteolytic adjacent motif (PAM) sequence adjacent to the target DNA site to cleave (Smith et al., 2017). Meanwhile, false negatives may arise due to various reasons including, inefficient gene knockdown, redundancy, and systematic errors. Considering that CRISPR-based screens typically use pools of sgRNAs to achieve complete gene knockout, such screens may result in the identification of fewer false negatives than RNAi screens (Puschnik et al., 2017). It is also possible that the variation in genes identified in RNAi screens is due to the use of different experimental setups and methods, including cell types, virus strains, MOIs, timepoints post infection, and thresholds for the identification of hits (Schaack and Mehle, 2020)

Screens to identify virus-host protein-protein interactions have been performed using yeast-two-hybrid and MS-based approaches (Schaack and Mehle, 2020). Details of previous physical interaction screens that have identified viral polymerase interactors are provided in Table 3. Yeast-two-hybrid screens identify pairwise protein-protein interactions using a viral protein as bait and a host protein library as prey. Although yeast-two-hybrid screens have provided valuable insight into the host cell interactome of influenza, MS-based approaches have largely replaced this type of screen. Most MS proteomic approaches involve purification of an AP-tagged viral protein followed by identification of the co-purifying host proteins by

mass spectrometry. This strategy has been used to generate a physical interactome map for all influenza virus proteins, when individually transfected (Watanabe et al., 2014) and in the context of infection (Heaton et al., 2016). AP-MS screens have also been performed to identify the interactome of the viral polymerase or vRNPs in the context of transfection (with transfection of individual polymerase proteins, different combinations of polymerase proteins, or the full heterotrimer or vRNP) or infection (Bradel-Tretheway et al., 2011, Haas et al., 2023, Hubel et al., 2019, York et al., 2014, Jorba et al., 2008, Mayer et al., 2007, Rialdi et al., 2017).

Table 3. Examples of protein-protein interaction screens to identify host cell proteins that interact with the viral polymerase.

Type of screen	Details	Reference
Yeast-two-hybrid	Each viral protein was used as bait. Laboratory-adapted PR8 strain of IAV used.	(Shapira et al., 2009)
Yeast-two-hybrid	PA subunit was used as bait.	(Huarte et al., 2001)
AP-MS	Strep-AP using NP as bait in the context of transfected vRNPs. Performed in HEK 293T cells with laboratory adapted WSN strain of IAV.	(Mayer et al., 2007)
AP-MS	TAP-AP using PB2 subunit as bait in the context of transfected polymerase. Performed in HEK 293T cells with a H5N2 strain of IAV.	(Jorba et al., 2008)
AP-MS	TAP-AP using PA as bait when transfected individually, together with PB1, or as a polymerase heterotrimer. Performed in A549 cells with H5N1 strain and two H1N1 (WSN and Cal04) strains of IAV.	(Bradel-Tretheway et al., 2011)
AP-MS	Strep-AP using PB2 polymerase subunit as bait in the context of infection. Performed in HEK 293T cells with laboratory adapted WSN strain of IAV.	(York et al., 2014)
AP-MS	FLAG-AP using each viral protein as bait when individually transfected. Performed in HEK 293T cells with laboratory adapted PR8 strain of IAV.	(Watanabe et al., 2014)
AP-MS	FLAG-AP using each viral protein as bait in the context of infection. Performed in A549 cells with laboratory adapted PR8 strain of IAV.	(Heaton et al., 2016)
AP-MS	Strep-AP using PA, PB1, and PB2 subunits as bait in the context of transfection. Performed in A549 cells with H1N1 and H3N2 IAV strains and in the presence and absence of IFN treatment.	(Rialdi et al., 2017)
AP-MS	Strep-AP using PB2 polymerase subunit as bait in the context of infection. Performed in A549 cells with laboratory adapted WSN strain of IAV.	(Hubel et al., 2019)
AP-MS	Strep-AP using each viral protein as bait when individually stably expressed. Performed in A549, NHBE, and differentiated THP-1 cells using a pandemic H1N1 strain, a seasonal H3N2 strain, and an avian H5N1 strain of IAV.	(Haas et al., 2023)

A big advantage of AP-MS based approaches is that they can be used to reveal multi-protein complexes and elucidate protein-protein interactions in an unbiased manner. This contrasts with yeast-two-hybrid screens which characterise only pairwise interactions between two known potential interaction partners (Schaack and Mehle, 2020). Another advantage of

AP-MS is that it can be used to acquire quantitative information about interactions as well as to characterise post-translational modifications of host and viral proteins as in Hutchinson et al., (Hutchinson et al., 2012). In addition, AP-MS is a well-established method that can be performed in many different cell types (Meyer and Selbach, 2015, Lum and Cristea, 2016). A large variety of AP tags also exist, many of which are small in size, limiting the risk that they interfere with the normal functions of the bait protein. This is particularly useful for the study of IAV interactomes as it allows fully infectious IAVs that encode an AP tag on a viral protein to be generated. Studying the interactome of IAV proteins, especially the polymerase proteins, in the context of live virus is important. This is because the polymerase is known to adopt different conformations depending on whether the proteins are individually expressed, as a heterotrimer, or as a vRNP (Pflug et al., 2017). Moreover, live virus captures the actual temporal dynamics of viral RNA synthesis, which may be disturbed by transfection of vRNP components, as well as the effect of other viral proteins, such as NS1 and NS2, which are known to affect the timing of viral RNA transcription and replication (Robb et al., 2009, Zhang et al., 2023). Consequently, studies that have focused on the interactome of the IAV polymerase in the context of transfection may have missed important interactors. What is more, overexpression of the bait protein in such studies may also have resulted in identification of non-physiological or artificial interactions (Meyer and Selbach, 2015). When performing AP-MS in the context of IAV infection it is important to consider the timepoint post infection for interactome analysis as early timepoints are more likely to reveal interactors involved in the early stages of the IAV lifecycle such as nuclear import and viral RNA synthesis while late timepoints are more likely to reveal interactors involved in the late stages of the IAV lifecycle such as nuclear export and packaging.

AP-MS based approaches are also associated with various limitations, including high rates of false positives and negatives as well as the need for downstream functional validation of hits. The cell lysis step causes proteins from different cellular compartments that would not normally interact to come into contact, potentially leading to the identification of false positives (Meyer and Selbach, 2015). On a similar note, proteins may non-specifically bind to the AP beads or the AP tag. To reduce non-specific binding, stringent wash steps are typically employed. However, the downside of stringent wash steps is that weak and transient interactions may be disrupted such that some important interactors may not be captured. Furthermore, AP-MS does not distinguish between direct and indirect interactors such that validation of interactions is necessary to confirm which proteins are directly involved. Considering that physical interaction does not necessarily correlate with function, downstream functional validation is also necessary to confirm that the interacting host proteins play a functional role in the IAV lifecycle and to identify their exact role.

Polymerase interactors could play a role in the polymerase replicase or transcriptase activity or the nuclear import or export of polymerases or vRNPs. Sections 1.5.2 and 1.5.3 outline examples of polymerase interactors identified in AP-MS screens, whose role in polymerase activity is unclear or that do not directly affect transcription/replication. In addition, polymerase interactors could play either a proviral or antiviral role. Examples of host proteins with antiviral activity (albeit identified in genetic screens) are provided in Section 1.5.4.

Section 1.5.2. Host factors shown to support polymerase activity.

Protein phosphatase 6 (PP6) is a host cell protein identified as a polymerase interactor in a live-virus AP-MS screen using the PB2 polymerase subunit as bait (York et al., 2014). The host protein interacts with both PB1 and PB2 individually and as part of the heterotrimeric polymerase complex. PP6 plays a proviral role in polymerase activity, supporting viral RNA synthesis. Under standard infection conditions, depletion of PP6 reduces the accumulation of all three viral RNA species. Meanwhile, in a cycloheximide (CHX)-treated infection assay, in which only primary mRNA synthesis can occur, depletion of PP6 had no effect on mRNA accumulation, suggesting that PP6 acts at a stage of the viral lifecycle downstream of primary transcription, likely in RNA replication or RNP assembly. Importantly, viral proteins are phosphorylated, and their phosphorylation state modulates their activity (Hutchinson et al., 2012). Considering that PP6 is a phosphatase, it could be speculated that PP6 dephosphorylates PB1 and/or PB2 (or another viral or host protein close to PB1 and PB2) and thereby regulates polymerase activity, however further studies are needed to confirm this (York et al., 2014).

The host protein hCLE was identified as an interactor of the PA subunit in a yeast-two-hybrid screen (Huarte et al., 2001). It interacts with all polymerase subunits in the context of infection and colocalises with vRNPs inside the nucleus (Rodriguez et al., 2011). hCLE is a proviral factor that promotes viral RNA synthesis. However, it remains unknown which stage of viral RNA synthesis is supported by hCLE. The host protein is proposed to play a role specifically in mRNA synthesis due to its host function, where it binds both phosphorylated and unphosphorylated RNAP II and promotes host transcription (Perez-Gonzalez et al., 2006). One theory is that hCLE recruits the viral polymerase to nuclear sites where capped host RNAs are being generated by RNAP II, but further experiments are needed to confirm this. Interestingly, hCLE has also been found to be incorporated into IAV virions (Rodriguez-Frandsen et al., 2016). The reason and functional consequence of this remains unknown, but the finding provides further evidence for an important role of hCLE in the viral lifecycle.

Section 1.5.3. Importins and CLUH.

It is also possible for host cell proteins to interact with the polymerase but not directly affect its activity in transcription and/or replication. Instead, some polymerase interactors may affect its nuclear import or export. For example, the importin-α (IMPα) protein family interact with PB2 and NP to facilitate their nuclear import (Figure 13) (Cros et al., 2005, Tarendeau et al., 2007, Wang et al., 1997, O'Neill et al., 1995). IMPα proteins, of which there are six (IMPα1, IMPα3, IMPα4, IMPα5, IMPα6, IMPα7), are key components of the classical IMPα/IMPß nuclear import pathway (Goldfarb et al., 2004). In this pathway, IMPα binds the NLS of a cargo protein. IMPα is then recognised by the IMPß receptor, and the ternary IMPß-IMPα-cargo protein complex is imported into the nucleus via the nuclear pore complex. IMPα proteins bind PB2 at a bipartite NLS on its C-terminus and NP at a non-classical NLS on its N-terminus (Cros et al., 2005, Tarendeau et al., 2007, Wang et al., 1997). PB2 has been shown to interact with IMPα5 in an MS screen using transfected AP-tagged PB2 as bait and NP was found to interact with IMPα1 and IMPα3 in a yeast-two-hybrid screen (Resa-Infante et al., 2008, Wang et al., 1997). Since then, PB2 and NP have been shown to interact with all members of the IMPα family (Hudjetz and Gabriel, 2012, Resa-Infante et al., 2008). Despite these interactions, IMPα1 and IMPα7 are the most important for mammalian adapted IAV replication with the remaining importins appearing to be redundant (Gabriel et al., 2011). This was shown as knockdown of IMPα1 and IMPα7 reduced virus replication but knockdown of IMPα3-α5 did not. While the PB2-IMPα interaction is believed to be important for the nuclear import of free PB2, the NP-IMPα interaction is believed to be important for both nuclear import of free NPs and vRNPs (Cros et al., 2005, Wang et al., 1997, Tarendeau et al., 2007, O'Neill et al., 1995).

The IMPα family has also been proposed to play a direct role in polymerase activity. This was first suggested by Resa Infante et al., who found the PB2-IMPα interaction to be more stable than would otherwise be expected for an IMPα-cargo protein interaction (Resa-Infante et al., 2008). The authors also found that disruption of the PB2 NLS resulted in a reduction in polymerase activity but had no effect on polymerase complex formation. Restoration of nuclear import by insertion of an alternative NLS did not rescue polymerase activity, suggesting that interaction with IMPα at the C-terminal bipartite NLS of PB2 is important for a step downstream of nuclear import. One study suggests that IMPα7 may support polymerase activity by promoting the interaction between ANP32 and the vRNP (Yu et al., 2022). The amount of IMPα7 was found to be important as both knockdown and overexpression of IMPα7 inhibits the ANP32-vRNP interaction, suggesting a regulatory role for importins in ANP32-mediated viral polymerase activity. Furthermore, IMPα5 has also been shown to bind NP and maintain it in a monomeric state (Boulo et al., 2011). Binding of IMPα5 did not affect the ability of NP to bind RNA, suggesting that importins may play a role in chaperoning NP and preventing its oligomerisation prior to RNA encapsidation.

The host cell protein clustered mitochondria protein homolog (CLUH) supports nuclear export of vRNPs (Figure 13). CLUH was identified as an interactor of PB2 in an AP-MS screen where transfected AP-tagged PB2 was used as bait (Watanabe et al., 2014). In infected cells, CLUH also interacts with PB2, PB1, NP, and M1, which together with the viral NS2 protein facilitates vRNP nuclear export via the CRM1 pathway (Ando et al., 2016). Depletion of CLUH inhibits vRNP nuclear export but has no effect on progeny vRNP assembly. CLUH is proposed to guide the subnuclear transport of vRNPs to M1-containing nuclear speckles, which leads to assembly of M1-vRNP nuclear export intermediate complexes. These complexes then translocate to nuclear export assembly sites, where they associate with NS2 to form a nuclear export complex that can be exported via the CRM1 pathway (Ando et al., 2016, Neumann et al., 2000, O'Neill et al., 1998).

Section 1.5.4. Antiviral factors.

Some host proteins identified in functional and proteomics screens play an antiviral role in the IAV lifecycle. Examples of antiviral factors that target the early stages of the viral lifecycle are butyrophilin subfamily 3 member A3 (BTN3A3) and myxovirus resistance protein A (MxA) (Petric et al., 2023). Both are IFN stimulated genes (ISGs) that are produced by the IFN response triggered by virus infection. They restrict the early stages of the lifecycle of avian IAVs more efficiently than of human-adapted IAVs, and the degree of sensitivity to BTN3A3 and MxA restriction is determined by mutations in NP (Haller and Kochs, 2020, Pinto et al., 2023, Zimmermann et al., 2011). The two restriction factors, therefore, form part of the host range barrier, preventing spread of avian IAVs in the human population (see Section 1.6.4). Despite the similarities in their antiviral activity, BTN3A3 and MxA are proposed to act independently and via different mechanisms of action.

BTN3A3, and its family member BTN3A1, were identified as antiviral factors in IAV infection in an expression screen of human and macaque ISGs against two human adapted IAVs and one avian IAV strain, where they were found to specifically restrict the avian strain (Pinto et al., 2023). BTN3A3 shows more potent restriction than BTN3A1, and their third family member, BTN3A2 has no antiviral activity. BTN3A3 interacts with NP in the context of vRNPs and is believed to act at a stage downstream of primary transcription, likely at the stage of RNA replication. This is suggested as overexpression of BTN3A3 reduces viral RNA synthesis in infected cells but has no effect on mRNA synthesis in infected cells treated with CHX (such that only primary transcription can occur). However, the exact step of RNA replication that is affected and the mechanism behind BTN3A3's antiviral role remains unknown.

MxA (or Mx1), which is a member of the large GTPases family, was originally identified as an anti-IAV restriction factor in mice (Lindenmann, 1962, Staeheli et al., 1986). Since then, MxA has appeared in many functional IAV screens aiming to identify IAV restriction factors

and is often used as a positive control in such screens (Martin-Sancho et al., 2021, Pinto et al., 2023). MxA restricts IAV at two early steps of the IAV lifecycle. First, MxA prevents primary transcription likely by restricting nuclear import of incoming vRNPs (Xiao et al., 2013). Importantly, this restriction only occurs in the presence of another, unidentified ISG. Second, MxA prevents RNA replication likely by restricting nuclear import of newly synthesised NP (Nigg and Pavlovic, 2015, Pavlovic et al., 1992). MxA oligomerises into dimers, and this oligomerisation together with its GTPase activity is necessary for its antiviral activity, however the exact mechanism is unknown (Haller et al., 2015). More recently, MxA has also been shown to be antiviral towards human-adapted IAVs at late stages of infection (McKellar et al., 2024). This inhibition occurs following nuclear export of vRNPs and works by restricting cytoplasmic trafficking of vRNPs to the plasma membrane.

Section 1.6. Adaptation of IAV to overcome host restriction

To emerge from its natural avian reservoir and cause a pandemic in the human population, AIV needs to adapt and evolve the ability to co-opt proviral factors and evade restriction by antiviral factors in its new host (Long et al., 2019b, Taubenberger and Kash, 2010). Host range barriers due to species-specific differences in host cell proteins are imposed at various stages of the virus lifecycle including host cell attachment, polymerase activity, and nuclear import of vRNPs (Figure 14) (Long et al., 2019b). One major determinant of host range is the IAV polymerase, with adaptation of the polymerase considered the first step to adaptation to a human host following a zoonotic event (Long et al., 2019b, Cauldwell et al., 2014). Sections 1.6.1-1.6.4 will focus on the adaptation of the polymerase to co-opt mammalian versions of proviral host factors, the role of the viral NS2 protein, and adaptation of NP to evade restriction by antiviral factors.

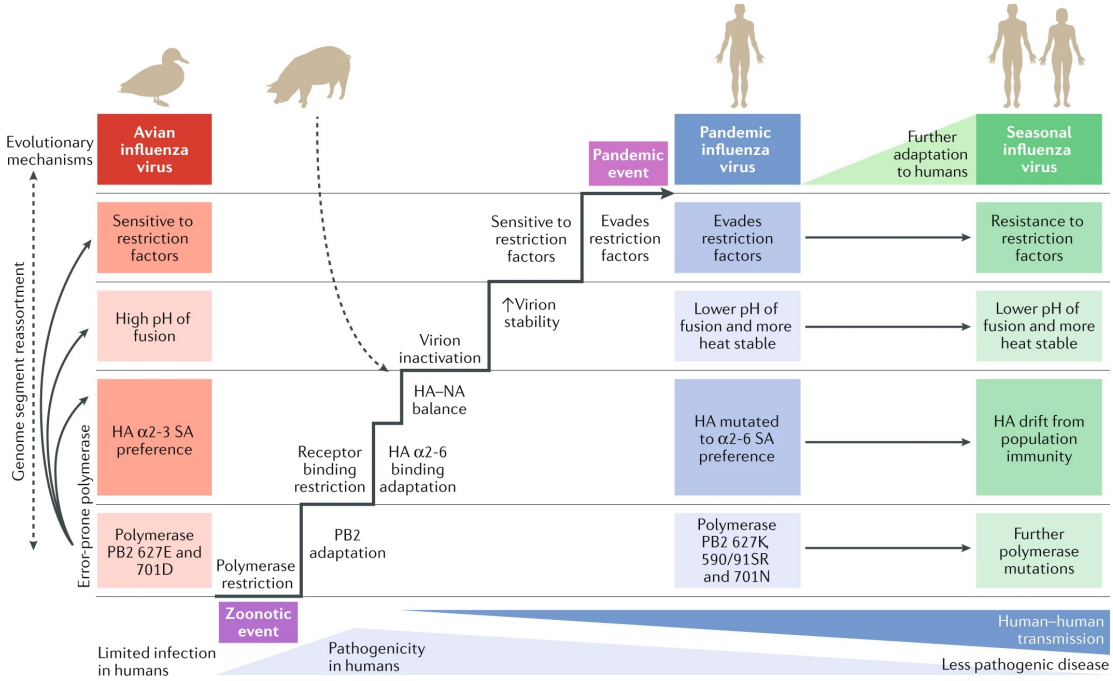

Figure 14. Cumulative host range barriers that AIVs must overcome to initiate a pandemic in the human population.
Figure taken from Long et al., 2019b. Reproduced with permission from Springer Nature. Avian influenza viruses (AIVs) (shown in red) must overcome several host range barriers for a zoonotic event to initiate a pandemic in humans (shown in blue) and eventually become seasonal (shown in green). AIVs must overcome polymerase restriction by acquiring mutations in the PB2 subunit such as E627K, Q590S, Q591R, or D701N (Cauldwell et al., 2014). AIVs must switch receptor binding preference from an α2-3 linked sialic acid to an α2-6 linked sialic acid by acquiring adaptive mutations in the HA receptor binding site (Long et al., 2019b). To be able to transmit between humans, virion stability must increase, and the HA must be able to survive the pH of the upper respiratory tract and in airborne droplets. Lastly, AIVs need to acquire the ability to evade restriction by antiviral factors such as MxA and BTN3A3 (Petric et al., 2023). This is achieved by acquiring adaptive mutations in the NP subunit. AIVs may acquire these genetic changes by reassortment, mutations resulting from the error-prone polymerase, or in intermediate species such as pigs. Generally, IAVs are found to be most pathogenic soon after the initial zoonotic event. As the virus adapts to the new human host there is a trade-off between pathogenicity and increased human-human transmission.

Section 1.6.1. Adaptation of the polymerase to huANP32A/B.

AIV polymerases are restricted in RNA replication in mammalian cells but not in transcription (Manz et al., 2012). To overcome this restriction, adaptive polymerase mutations are selected for (reviewed in Cauldwell et al., 2014), particularly in the PB2 subunit (Almond, 1977, Subbarao et al., 1993). The most common mammalian-adapting mutation is a glutamic acid to lysine mutation at position 627 (E627K) of the PB2 subunit, which enables replication of AIVs in human cells (Subbarao et al., 1993). The E627K mutation was present in all four pandemic IAVs of the 20th century (1918 H1N1 virus, 1957 H2N2 virus, 1968 H3N2 virus, 1977 H1N1 virus) and is also detected in human isolates of H5N1 and H7N9 strains (Liu et al., 2013, Long et al., 2013, Scholtissek et al., 1978, Taubenberger and Kash, 2010). In contrast, the

2009 H1N1 pandemic virus retained PB2 627E and instead acquired a pair of alternative PB2 mutations, namely G590S and Q591R, that together enable replication in human cells (Cauldwell et al., 2013, Mehle and Doudna, 2009). Other mammalian adapting PB2 mutations also exist including D701N and T271A (Bussey et al., 2010, Cauldwell et al., 2013, Gao et al., 2009). More recently, PB2 M631L has also been identified as a mammalian-adapting mutation in the ongoing outbreak of H5N1 clade 2.3.4.4b virus in dairy cattle in the USA (Dholakia et al., 2025).

Species-specific differences in ANP32 proteins account for the poor replication of avian polymerases in human cells (Long et al., 2016). Exogenous expression of chANP32A in mammalian cells restores activity of an avian polymerase harbouring PB2 627E to levels comparable to a mammalian-adapted polymerase harbouring PB2 627K. The 33aa insertion between the LRR and LCAR in chANP32A accounts for this ability of chANP32A (Figure 15). Deletion of this region abrogates the ability of chANP32A to support avian polymerase activity and insertion of the region allows human ANP32A/B (huANP32A/B) to support avian polymerase activity. chANP32A can support the activity of both avian and mammalian-adapted polymerases. All ANP32 variants bind the viral polymerase to the same extent regardless of its E/K627 signature, although chANP32A binds more strongly than huANP32A/B (Baker et al., 2018, Domingues and Hale, 2017, Mistry et al., 2020). This suggests that the species-specific differences in the proviral role of ANP32 proteins cannot be explained by differences in polymerase binding, at least when measured using co-immunoprecipitation or split luciferase methods.

The sequence identity of the 33aa insertion in chANP32A is important for its ability to support AIV polymerase activity (Long et al., 2019a). The insertion consists of a unique hexapeptide sequence, in which four of the amino acids constitute a SUMO-interacting motif (SIM)-like sequence (Figure 15) (Domingues and Hale, 2017, Long et al., 2019a). This is followed by 27 amino acids that are the result of a duplication of an upstream sequence (Baker et al., 2018, Domingues et al., 2019, Long et al., 2019a). The SIM-like sequence is important for chANP32A's ability to rescue AIV polymerase activity and contributes to the enhanced binding of chANP32A to the polymerase complex (Domingues and Hale, 2017, Baker et al., 2018, Bi et al., 2019, Domingues et al., 2019, Mistry et al., 2020). It remains unknown whether the chANP32A SIM acts by recruiting a SUMOylated host factor that stabilises the polymerase complex or indeed by binding to SUMO-modified polymerase itself (Domingues and Hale, 2017). While the 27aa insertion alone cannot support avian polymerase activity, a naturally occurring splice variant of chANP32A with a 29aa insertion that lacks the SIM is able to rescue avian polymerase activity, albeit to a lesser extent than chANP32A with the full 33aa insertion (Figure 15) (Baker et al., 2018, Bi et al., 2019, Domingues et al., 2019). chANP32B is non-functional in IAV replication as it not only lacks the 33aa insertion but also carries the N129I

and D130N mutations, which render it unable to interact with the viral polymerase (Figure 15) (Long et al., 2019a).

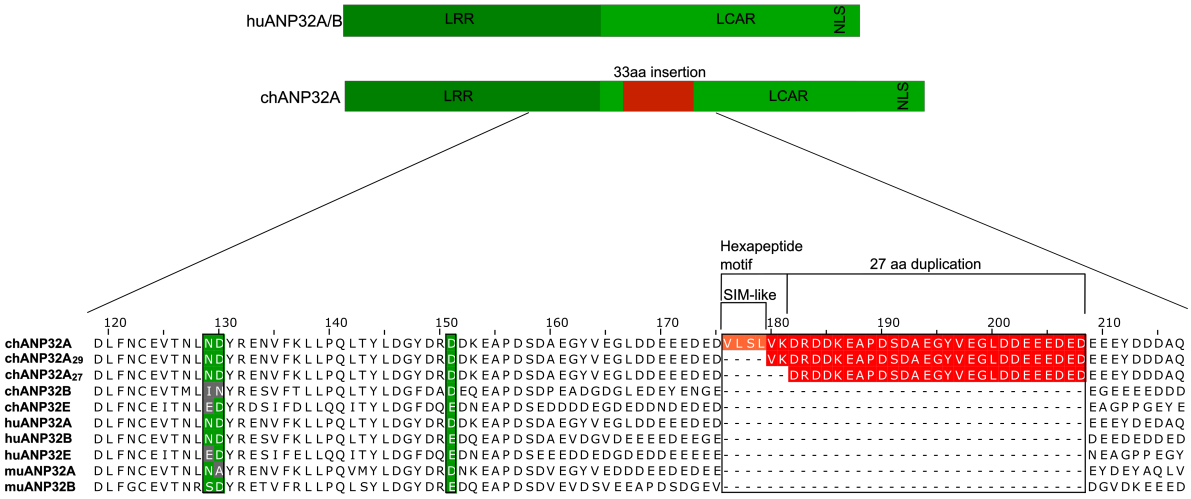

Figure 15. Sequence alignment of ANP32 proteins from different species.
ANP32 proteins have a leucine-rich repeat region (LRR) at the N-terminus and a low-complexity acidic region (LCAR) at the C-terminus which are separated by a central region (Reilly et al., 2014). Chicken ANP32A (chANP32A) is longer than human ANP32A/B (huANP32A/B) due to a 33 amino acid (aa) insertion between the LRR and LCAR (Long et al., 2016). Similar to huANP32A/B, chANP32B/E, huANP32E, and murine ANP32A/B (muANP32A/B) lack this 33aa insertion. The 33aa insertion consists of a unique hexapeptide motif, four amino acids of which constitute a SIM-like sequence (Domingues and Hale, 2017, Long et al., 2019a). This is followed by 27aa that are the result of a duplication of an upstream sequence (Long et al., 2019a, Baker et al., 2018, Domingues and Hale, 2017). chANP32A with just the 27aa insertion cannot support avian polymerase activity. However, a naturally occurring splice variant of chANP32A with a 29aa insertion is able to support avian polymerase activity (Baker et al., 2018, Bi et al., 2019, Domingues et al., 2019, Long et al., 2019a). Structures of ANP32 in complex with the viral polymerase show that residues 129/130 are an important contact point. (Arragain et al., 2024, Carrique et al., 2020, Staller et al., 2024). Sequence variation at these residues determines whether the ANP32 protein can be co-opted by IAV as a proviral replication factor. For example, chANP32B is non-functional due to mutations N129I and D130N (Long et al., 2019a). Residue 151, which is acidic in all ANP32 proteins aligned here, is also an important contact point with the IAV polymerase (Arragain et al., 2024, Staller et al., 2024). Residues are colour-coded as follows: grey, does not support polymerase activity; green, supports polymerase activity; orange/red, chANP32A specific residues. Sequence alignments were visualised using Jalview v.2.11.5.

Structures of the asymmetric polymerase dimer in complex with ANP32 have provided insights into the mechanism by which ANP32-mediated host restriction might occur (Arragain et al., 2024, Carrique et al., 2020, Staller et al., 2024). Despite the LCAR not being fully resolved in the asymmetric dimer structures, continuous density suggests that it contacts the $PB2^{627}$ domain of $polymerase_{(R)}$, where residue E/K627 sits. $PB2_{(R)}^{627}$ forms a basic groove together with $PB2_{(E)}^{NLS}$ in the IAV and IBV dimer structures and $PB2_{(E)}^{627}$ in the ICV dimer structure, which the ANP32 LCAR is proposed to pass through. Considering that the LCAR of huANP32A/B is highly acidic, the charge of the binding groove is likely important for its ability

to accommodate the LCAR. Carrique et al., propose that the E627K mutation works by eliminating the electrostatic clash between the otherwise acidic E627 residue and the acidic huANP32A/B LCAR (Carrique et al., 2020). Such electrostatic clashes do not occur with chANP32A as the 33aa insertion, which contains a mix of acidic and basic residues, displaces the acidic region. This is supported as the structure of the ICV polymerase in complex with chANP32A shows the 33aa insertion to bind in this basic groove and contact the $PB2_{(R)}^{627}$ domain (Carrique et al., 2020). The mixture of acidic and basic residues within the insertion also explains why chANP32A supports both 627E and 627K polymerase activity. Such a model is also supported by Camacho-Zarco et al., who used NMR to show that the 627K domain interacts with the huANP32A LCAR in a multivalent manner (Camacho-Zarco et al., 2020). In contrast, the 627E domain makes fewer and weaker contacts with huANP32A but is capable of strong interaction with the chANP32A LCAR and particularly its 33aa insertion. Interestingly, other PB2 residues that have been implicated in host range also line this basic groove, such as D701 and Q591 in $PB2_{(E)}^{NLS}$ (Arragain et al., 2024, Staller et al., 2024). This suggests that the mammalian adapting D701N and Q591R mutations also work by reducing the acidity of the binding groove so that huANP32 can be accommodated. Indeed, Q591R and D701N have been shown to adapt avian polymerase to use mammalian ANP32 proteins (Peacock et al., 2023).

Some mammalian-adapting mutations may perform a dual role in host adaptation by both generating a basic groove for the huANP32 LCAR to bind and also directly strengthening the interaction with the huANP32 LRR. For example, PB2 residues E627, Q591, and M631 are in the same cluster on the $PB2_{(E)}^{627/NLS}$ domain opposite the C-terminus of the ANP32 LRR (Arragain et al., 2024, Staller et al., 2024). Mutation into a basic residue allows the formation of a salt bridge with huANP32 E/D151, strengthening the interaction between the $polymerase_{(E)}$ and ANP32.

In addition, mammalian-adapting mutations have also been identified that do not directly enhance binding to huANP32 but instead indirectly allow the polymerase to use suboptimal huANP32 proteins (Sheppard et al., 2023, Idoko-Akoh et al., 2023). IAV passaged in the absence of huANP32A/B can evolve to use the otherwise non-functional huANP32E protein by acquiring two polymerase mutations: PB1 K577E and PA Q556R. These mutations sit in the symmetric dimer interface where they disrupt this dimerisation, pushing the polymerase to adopt an asymmetric dimer structure even when only a suboptimal ANP32 is present. The PA Q556R mutation likely also serves to directly enhance interaction with ANP32 as it is found in the $PA_{(E)}$ 550 loop that contacts the ANP32 LRR (Arragain et al., 2024, Staller et al., 2024). Along a similar note, AIV replicating in gene edited chickens that have been engineered to carry non-functional chANP32A proteins, also evolves adaptive mutations. These include PA E349K and PB2 M631L, which allow the polymerase to co-opt the otherwise

non-functional chANP32B and chANP32E (Idoko-Akoh et al., 2023). The PA E349K mutation acts by weakening the symmetric dimer while the PB2 M631L mutation may enhance binding of polymerase$_{(E)}$ to the ANP32 LRR and polymerase$_{(R)}$ to the LCAR. Taking these two studies together, it would seem that mutations that disrupt the symmetric dimer are typically accompanied by mutations that enhance binding of polymerase$_{(E)}$ to ANP32.

Collectively, the multiple ways that avian viruses have evolved the ability to co-opt mammalian or suboptimal ANP32 proteins demonstrate the absolute necessity of ANP32 proteins for RNA replication and virus infection (Figure 16A and B).

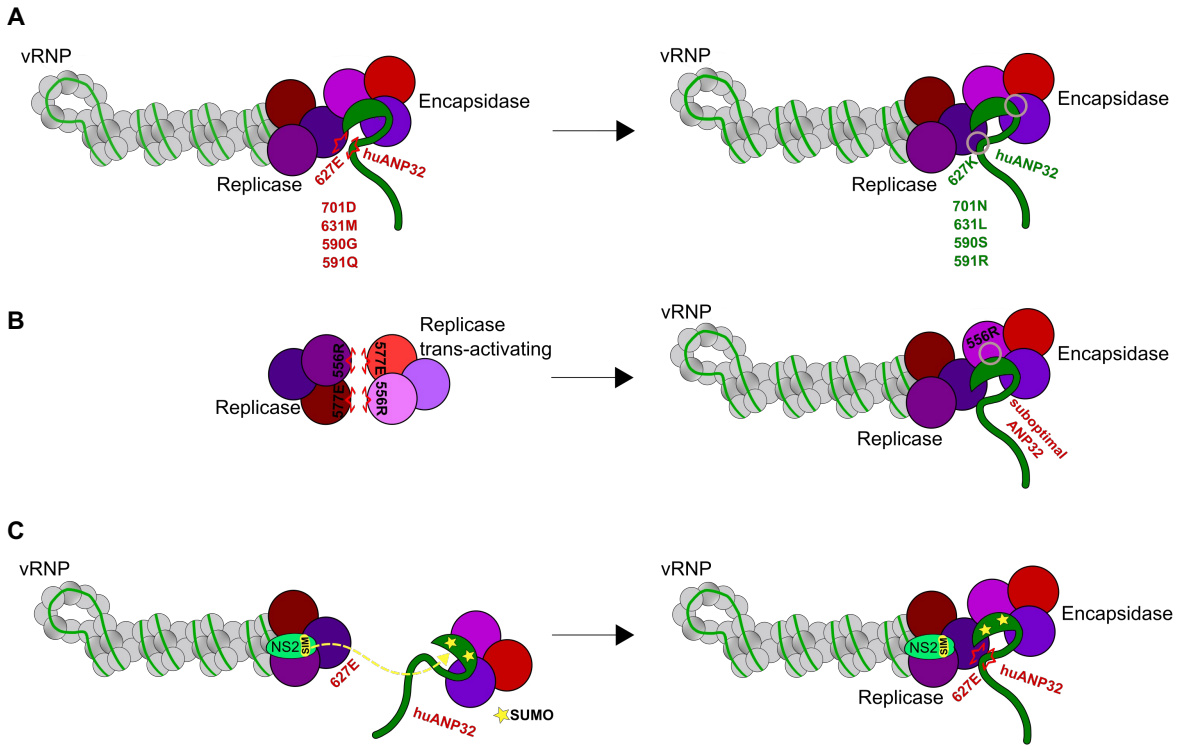

Figure 16. Paths that AIVs take to co-opt suboptimal human ANP32 proteins.
A) Avian polymerase with PB2 627E cannot co-opt huANP32 proteins due to electrostatic clashes between the huANP32 LCAR and the 627E domain of polymerase$_{(R)}$ (Arragain et al., 2024, Carrique et al., 2020, Staller et al., 2024, Camacho-Zarco et al., 2020). E627K mutation eliminates the electrostatic clashes between polymerase$_{(R)}$ and huANP32 LCAR. This mutation also enhances binding between polymerase$_{(E)}$ and the huANP32 LRR. D701N, M631L, G590S, and Q591R adaptive mutations work via similar mechanisms. B) In the absence of functional ANP32 proteins, the IAV polymerase can acquire adaptive mutations in the PA and PB1 subunits that reduce symmetric dimerisation, favouring co-option of otherwise non-functional ANP32 proteins and formation of the asymmetric dimer (Sheppard et al., 2023, Idoko-Akoh et al., 2023). Some mutations also serve to enhance binding between polymerase$_{(E)}$ and the ANP32 LRR. C) Avian NS2 may utilise its SIM to interact with SUMOylated huANP32 proteins, increasing the interaction between avian vRNPs and huANP32 (Sun et al., 2023, Sun et al., 2024b). In turn, this allows AIVs to overcome the block in RNA replication in human cells.

The structural evidence combined with the finding that ANP32 is essential for both steps of replication suggests that an avian influenza polymerase (PB2 627E) should be

restricted in both steps of replication in human cells. Surprisingly, in a cRNP stabilisation assay, in which only the pioneering round of v-to-cRNA synthesis can occur, cRNA accumulates to the same extent regardless of whether polymerase$_{(R)}$, polymerase$_{(E)}$, or both have the avian 627E signature (Swann et al., 2023). However, in a replication assay, in which both steps of RNA replication but not transcription can occur, c-to-vRNA synthesis is restricted when polymerase$_{(R)}$, but not polymerase$_{(E)}$, has the avian 627E signature. Together, this suggests that avian polymerases are restricted only in the second c-to-vRNA synthesis step in human cells. The restriction maps to ANP32 as exogenous expression of chANP32A rescues c-to-vRNA synthesis. The requirement for polymerase$_{(R)}$ to have the E627K mutation to function as a replicase for c-to-vRNA synthesis in human cells fits with the structural evidence that only the polymerase$_{(R)}$ 627 residue lines the basic groove bound by the LCAR in the IAV asymmetric dimer (Arragain et al., 2024). However, it remains unclear why this restriction would only affect vRNA synthesis and not cRNA synthesis. Interestingly, in a minigenome setup, when only polymerase proteins, NP, and a viral-like RNA template are provided, 627E polymerases are restricted in cRNA synthesis as well (Nilsson-Payant et al., 2022). This contrasts the cRNP stabilisation assay data and suggests that a viral protein, such as NS2, may play a role in overcoming host restriction at the v-to-cRNA synthesis step (see Section 1.6.2.).

Section 1.6.2. The role of the viral NS2 protein in overcoming host restriction.

The viral NS2 protein can also contribute to the ability of avian polymerases to overcome species-specific restriction in mammalian cells (Manz et al., 2012, Reuther et al., 2014, Sun et al., 2024b, Sun et al., 2023). NS2 enhances polymerase activity and virus replication of AIVs in human cells in a manner that is dependent on huANP32A/B (Sun et al., 2024b, Sun et al., 2023). This is reminiscent of its role in enhancing polymerase activity of mammalian adapted IAVs (see Section 1.4.3), but its effect on AIVs is greater. Sun et al., propose that NS2 enhances avian polymerase activity in human cells by promoting avian vRNP assembly and avian vRNP-huANP32A/B interaction (Sun et al., 2023). NS2 achieves this by using its SIM ($_{106}$LLEVE$_{110}$), which is highly conserved among NS2s of IAV strains of all hosts, to interact with SUMOylated human ANP32. The SUMOylation of ANP32 is known to increase upon infection and the NS2 SIM specifically interacts with huANP32A SUMOylated at residues K68/K153 and huANP32B SUMOylated at residues K68/K116 (Domingues et al., 2015, Sun et al., 2024b). The interaction between NS2 and huANP32A/B was confirmed to be SIM-SUMO mediated as mutation of the NS2 SIM or disruption of huANP32A/B SUMOylation prevents the interaction from occurring (Sun et al., 2024b). It remains unclear whether the supportive, but smaller, effect of NS2 on mammalian adapted polymerase activity involves similar enhanced interactions. It could be speculated that NS2 also promotes vRNP assembly

of mammalian adapted IAVs, given the finding that NS2 preferentially interacts with a vRNA-resident polymerase. However, the involvement of the NS2 SIM in enhancing avian vRNP-huANP32A/B interactions may be specific to avian IAVs, providing a way for the avian vRNP to recruit the suboptimal huANP32 for RNA replication (Figure 16C).

Considering that NS2 specifically enhances v-to-cRNA synthesis of a mammalian adapted polymerase, it is likely that NS2 enhances avian polymerase activity in human cells by also promoting avian v-to-cRNA synthesis (Zhang et al., 2025a). This would explain why 627E polymerases were restricted in cRNA synthesis in human cells in a minigenome setup but not in infection, when NS2 and other viral proteins are present as well (see Section 1.6.1) (Nilsson-Payant et al., 2022, Swann et al., 2023). However, further work is needed to confirm that the ability of 627E viruses to synthesise cRNA to the same extent as 627K viruses is due to their NS2.

In further support of a role for NS2 in determining host range, avian viruses acquire adaptive mutations in their NS2 protein that help escape host restriction of RNA replication (Manz et al., 2012, Reuther et al., 2014). This is exemplified by human H5N1 isolates which did not acquire the typical mammalian adapting E627K mutation but were still able to replicate and cause pathogenesis in humans (Manz et al., 2012). The ability of these isolates to replicate in humans was attributed to mutations in their NS2 protein, such as S7L, M16L, Y41C, and E75G, which enhance avian polymerase activity in human cells (Manz et al., 2012, Reuther et al., 2014). These mutations are outside the conserved SIM sequence and, therefore, may enhance avian polymerase activity in a manner that is independent of ANP32. One model proposes that these mutations affect regulation of the NS2 C-terminus by its N-terminus (Reuther et al., 2014). The mutation M16L reduces the interaction between the N- and C- termini, allowing the C-terminus to become active and perform its role in enhancing polymerase activity. It is possible that these NS2 mutations are selected for to adapt to the temperature change between birds and humans. Specifically, the higher temperatures in avian species may be sufficient to reduce the affinity between the N- and C-termini of NS2. However, in humans, where temperatures are lower, the affinity between the N- and C-termini of NS2 is increased such that adaptive NS2 mutations may be necessary to break the interaction.

It is interesting to note that human H5N1 virus isolates with PB2 E627K rarely also have adaptive mutations in their NS2 protein, suggesting that either PB2 E627K or adapting NS2 mutations are sufficient to sustain polymerase activity, at least in the early stages of zoonosis (Manz et al., 2012). It is unknown whether adaptive NS2 mutations are a first step for the virus to acquire the PB2 E627K mutation later in infection or whether once NS2 adaptations are acquired, the driver to select further PB2 mutations is reduced.

Section 1.6.3. Adaptation of the polymerase and NP to co-opt the IMPα family.

Both mammalian and avian IAVs rely on IMPα1 for nuclear import of their PB2 and NP proteins (Gabriel et al., 2011). However, a switch from IMPα3 to IMPα7 dependency occurs as AIVs adapt to replication in humans. The 2009 H1N1 pandemic virus is reliant on both IMPα3 and IMPα7, suggesting ongoing adaptation of this virus. The switch from IMPα3 to IMPα7 dependency is mediated by amino acid substitutions in the PB2 and NP subunits, including PB2 E627K, PB2 D701N, and NP N319K, suggesting that the E627K and D701N mutations may play additional roles in overcoming host restriction aside from adaptation to huANP32 (Gabriel et al., 2011, Hudjetz and Gabriel, 2012). The mutations also improve binding of PB2 and NP to IMPα1 in mammalian cells (Gabriel et al., 2008, Hudjetz and Gabriel, 2012). Interestingly, a higher abundance of the IMPα7 isoform is detected at the mRNA level in human nasal mucosa compared to the abundance of IMPα3 (Ninpan et al., 2016). It is, therefore, possible that this higher abundance of IMPα7 exerts the selective pressure on AIVs to adapt and acquire the ability to co-opt this more readily available IMPα isoform instead.

Section 1.6.4. Adaptation of NP to evade restriction by BTN3A3 and MxA.

To generate a pandemic strain, AIVs not only need to adapt to co-opt the mammalian version of proviral host factors but also to evade the anti-AIV activity of restriction factors (Long et al., 2019b). Two examples of human restriction factors that are particularly potent towards AIV are BTN3A3 and MxA (see Section 1.5.4) (Petric et al., 2023). To evade restriction by either of these factors, AIVs acquire adaptive mutations in their NP protein (Manz et al., 2013, Pinto et al., 2023). Despite independent mechanisms of action, the residues all sit in the same surface-exposed region of the NP head domain and some of the adaptive mutations are shared. In the case of BTN3A3, the NP mutations that mediate escape from restriction are Y52N/H, R100V, and F313Y/V, with mutations at position 52 or 313 able to confer BTN3A3 resistance on their own (Pinto et al., 2023). In both the 1918 and 2009 pandemic viruses, where novel NP gene segments were acquired, the NP was mutated at position 313. How these adaptive mutations facilitate escape is unknown. Pinto et al., found that BTN3A3 interacts with NP regardless of its signature at position 313. This suggests that differences in interaction are not responsible for the species-specific restriction (Pinto et al., 2023). BTN3 orthologues are found in other mammalian IAV hosts, such as swine, horses, and dogs, and distantly related BTN1 orthologues are found in avian species (Pinto et al., 2023). However, these orthologues do not have antiviral properties. The anti-AIV activity of human BTN3A3 is thought to have arisen in primates, which explains why humans are the only IAV hosts with this restriction mechanism.

Unlike BTN3A3 restriction where a single NP mutation can mediate escape, combinations of NP mutations are necessary to mediate escape from MxA restriction (Manz

et al., 2013). These combinations vary for different IAV lineages. For example, the combinations are R100I/V, L283P, and F313Y in the case of the 1918 pandemic virus and E53D, R100I/V, and F313Y in the case of the 2009 pandemic virus. Acquisition of MxA escape mutations results in viral growth defects owing to defective nuclear import of vRNPs (Gotz et al., 2016). It is unknown whether this is due to decreased binding of vRNPs to IMPα isoforms or another unidentified host factor that is required for vRNP nuclear import. To overcome this defect, viruses acquire further adaptive mutations, such as G16D, which restore nuclear import. MxA/Mx1 orthologues are found in many mammalian and avian species with murine, porcine, and bovine Mx1s shown to have antiviral activity (Verhelst et al., 2013). In contrast all avian Mx orthologues tested lack anti-IAV activity (Bernasconi et al., 1995).

It is unclear at what stage during mammalian adaptation such NP mutations arise. Considering that avian BTN3A3 and MxA are not restrictive, it is unlikely that there is a selective pressure in avian species to acquire such mutations. Despite this, Pinto et al., suggest that BTN3A3 resistance may arise in avian species as some avian strains were found to already carry adaptive mutations (Pinto et al., 2023). This may be unique to BTN3A3, considering that only a single mutation is necessary to confer resistance, and this mutation is not associated with a fitness cost. Monitoring the occurrence of mutations that may lead to escape from BTN3A3 and MxA escape, alongside other mammalian-adapting mutations (see Sections 1.6.1-1.6.3), is important as such mutations are a good indicator of the pandemic potential of circulating AIVs and zoonotic viruses.

Section 1.7. Antiviral strategies

Vaccination is the best method for control and prevention of influenza (Paules and Subbarao, 2017, Krammer et al., 2018). There are three classes of licensed vaccines, which are administered annually: inactivated vaccines, live-attenuated vaccines, and recombinant HA vaccines. Each vaccine is multivalent containing antigens that represent the IAV and IBV strains anticipated to be circulating during influenza season of that year. Adaptation of seasonal influenza viruses by antigenic drift mean that the vaccine needs to be updated annually, with such updates being made on recommendation by the WHO (Paules and Subbarao, 2017). The current vaccine strategy presents many challenges, which limit its efficacy (Houser and Subbarao, 2015). For instance, its long production timeline mean that strain predictions must be made months in advance, which may lead to mismatches between the vaccine strains and circulating strains. Furthermore, specificity of the vaccine for seasonal strains means that it is unlikely to provide protection in the event of a pandemic (Krammer, 2015). Consequently, efforts are ongoing to generate a universal influenza vaccine which

would be effective against all influenza strains and subtypes (Houser and Subbarao, 2015, Krammer, 2015).

Antivirals represent an alternative line of defence against influenza (Bonomini et al., 2025, Paules and Subbarao, 2017). There are four classes of antivirals: NA inhibitors, such as oseltamivir and zanamivir; polymerase inhibitors, such as baloxavir (BXA), which targets the PA endonuclease activity; adamantanes, which are M2 ion channel inhibitors; and membrane fusion inhibitors. Of these antivirals, NA and polymerase inhibitors are recommended for use in the USA and Europe (Bonomini et al., 2025). Antivirals are particularly important in response to a pandemic, where an effective vaccine may not be available, and infection often leads to severe disease (Krammer et al., 2018). Antivirals are also important for the treatment of severe seasonal influenza cases. As high levels of inflammation are associated with severe influenza disease, efforts are ongoing to improve disease outcomes by combining antiviral drugs and immunomodulatory therapies (de Jong et al., 2006, Ramos and Fernandez-Sesma, 2015). One major challenge posed by antivirals is antiviral resistance, which readily emerges due to the high mutation rate of influenza viruses (Hurt, 2014). Resistance may render antivirals ineffective as exemplified by adamantanes, which are no longer recommended for use due to widespread resistance (Bonomini et al., 2025, Hurt, 2014). To limit the emergence of resistance, combinations of antivirals with different mechanisms of action could be used (Paules and Subbarao, 2017). An alternative therapeutic option that increases the barrier to resistance is to target host proteins important for influenza replication rather than viral proteins (Watanabe et al., 2014). Currently, there are no such therapies available for the treatment of influenza. However, research to identify and characterise host factors co-opted by IAV are an important first step to developing such host-directed therapies.

In addition to strategies that aim to mitigate the impact of pandemic viruses, efforts are ongoing to develop antiviral strategies that prevent pandemic emergence altogether. AIVs circulating in poultry pose a significant pandemic threat to humans (Wang et al., 2021a). This is attributed to the proximity of farmed chickens to poultry workers and usually other farmed animals such as pigs, which are considered a “mixing vessel” for pandemic IAVs. To limit AIV infection and spread in chickens, genome-editing has been used to generate chickens with a non-functional chANP32A protein so that they cannot support viral polymerase activity (Idoko-Akoh et al., 2023). Challenge with a low AIV dose only resulted in one out of ten chickens becoming infected with no onwards transmission, demonstrating the potential of this strategy in limiting AIV infection. However, breakthrough infections occurred following challenge with a higher dose. This suggests that to generate chickens that are completely influenza-resistant, further edits are needed either in the ANP32 protein or other host proteins important for AIV

Section 1.8. Thesis aims

The IAV polymerase catalyses both transcription and replication of the vRNA genome by adopting vastly different conformations and higher order complexes. These conformations and complexes are likely facilitated and stabilised by interaction of the viral polymerase with distinct sets of host factors in transcription and replication. This thesis aims to discover and characterise host cell proteins that regulate IAV RNA transcription and replication. We are particularly interested in host proteins that regulate RNA replication. To achieve this, the thesis will firstly focus on the discovery and characterisation of proviral host factors that are co-opted to support RNA replication. Secondly, the thesis will further characterise the role of antiviral factors, focusing on the recently discovered antiviral factor, BTN3A3, which is suggested to restrict the RNA replication step. Overall, this will aid understanding of the role of host cell proteins in IAV polymerase activity and their role in promoting and restricting efficient viral RNA synthesis.

The precise aims of each results chapter are:

- Chapter 2 - Differential interactome screens to identify host proteins that regulate viral RNA transcription and replication
    - Establish a live-virus AP-MS strategy to distinguish host proteins co-opted to support either IAV transcription or replication.
    - Functionally validate a role for identified host proteins in polymerase activity and viral replication.
- Chapter 3 - HMGB2 and RUVBL2 support viral RNA replication and RPAP2 supports transcription
    - Generate cell lines knocked out for HMGB2, RUVBL2, and RPAP2 using CRISPR-Cas9 genome editing and use these cell lines to further characterise the role of the host proteins in polymerase activity.
    - Use assays that distinguish cRNA and mRNA synthesis to investigate which step of viral RNA synthesis HMGB2, RUVBL2, and RPAP2 play a role in.
    - Test the effect on polymerase activity and viral replication of drugs that inhibit the host cell activity of RUVBL2, HMGB2, and RPAP2.
- Chapter 4 - Characterising the BTN3A3 and MxA resistance of avian influenza virus
    - Use a minigenome reporter assay to test the BTN3A3 and MxA sensitivity of currently circulating clade 2.3.4.4b AIVs.
    - Use assays that distinguish cRNA and mRNA synthesis to confirm the step of viral RNA synthesis restricted by BTN3A3 and MxA.
    - Begin to unravel the mechanism by which BTN3A3 restricts AIVs.

Chapter 2. Differential interactome screens to identify host proteins that regulate viral RNA transcription and replication

Section 2.1. Introduction

The IAV genome is transcribed and replicated inside the nucleus of an infected cell (Fodor and Te Velthuis, 2020). First, primary transcription occurs in *cis* converting the incoming vRNA template into viral mRNA, which is then translated into new viral proteins. Replication is a two-step process, where the vRNA genome is copied into a positive-sense cRNA intermediate, which is then copied back into new vRNA genomes (York et al., 2013, Fodor and Te Velthuis, 2020). All steps of viral RNA synthesis (v-to-mRNA, v-to-cRNA, and c-to-vRNA) are catalysed by the IAV polymerase, which is a heterotrimer composed of the subunits PB2, PB1, and PA (Lukarska et al., 2017, Zhu et al., 2023b). This happens in the context of vRNPs, in which the vRNA is bound by NP and a polymerase heterotrimer (Eisfeld et al., 2015). The polymerase is capable of both transcription and replication due to its flexibility, ability to adopt different conformations, including various dimers, and its interaction with host cell proteins that support different stages of viral RNA synthesis (Carrique et al., 2020, Fan et al., 2019, Lukarska et al., 2017, Peacock et al., 2019, Arragain et al., 2024, Staller et al., 2024). One key example of a proviral host factor is the ANP32 family of host proteins (Sugiyama et al., 2015). Three members of the ANP32 family are expressed in human cells; ANP32A and ANP32B, which are essential but functionally redundant for viral RNA replication, and ANP32E, which is non-functional in RNA replication unless both ANP32A and ANP32B are absent and the virus has undergone mutations to enable utilisation of otherwise suboptimal ANP32 proteins (Staller et al., 2019, Sheppard et al., 2023). ANP32 supports the assembly of nascent RNA into RNPs, making it essential for both the cRNA and vRNA synthesis steps of replication but not mRNA synthesis (Carrique et al., 2020, Nilsson-Payant et al., 2022, Swann et al., 2023, Wang et al., 2022a). This means that in cells with ANP32A/B/E ablated (ANP32-KO), only primary transcription of the incoming vRNA template can occur (Swann et al., 2023). In addition to ANP32, other host factors are also co-opted to support polymerase activity (Peacock et al., 2019). Examples include RNAP II, which is essential for viral transcription as it provides access to host capped RNA fragments that act as primers for transcription initiation, and PP6, a phosphatase which interacts with the viral polymerase

complex and supports viral RNA synthesis (York et al., 2014, Engelhardt et al., 2005, Walker and Fodor, 2019).

Virus-host interactions are an important area of study because host proteins serve as good targets for the improvement or development of antiviral strategies (Idoko-Akoh et al., 2023, Watanabe et al., 2014). Many previous studies have identified host cell proteins important for the IAV lifecycle using various strategies, such as genome-wide RNAi or CRISPR screening or mass spectrometry (MS) of interacting factors resulting from affinity purification (AP) of tagged viral proteins (see Section 1.5.1, Tables 2 and 3 for examples). Most of these studies aimed to generate a global map of host proteins associated with any stage of the IAV lifecycle. The MS-based screens have been performed in the context of viral components reconstituted either after transfection or infection. Although, some of the AP-MS screens focused on the interactome of the IAV polymerase by using AP-tagged polymerase proteins as bait, such studies do not distinguish between host proteins co-opted to support viral transcription versus replication (Bradel-Tretheway et al., 2011, Haas et al., 2023, Heaton et al., 2016, Watanabe et al., 2014, York et al., 2014, Mayer et al., 2007, Hubel et al., 2019, Jorba et al., 2008, Rialdi et al., 2017). Consequently, many host cell proteins have been identified that support viral polymerase activity, but it remains unclear which direct transcription and which replication.

In this chapter, we performed a differential interactome screen to distinguish host proteins that are co-opted to support either the IAV polymerase replicase or transcriptase activity. We made use of ANP32-KO cells as a unique tool to uncouple viral transcription and replication. Particularly, we compared the interactome of PB2 during infection in WT cells, where viral transcription and replication take place, to the interactome in ANP32-KO cells, where replication does not occur. This allowed us to separate the host cell proteins that are recruited upstream of and for primary transcription (host proteins enriched in both cell types) from those that are recruited downstream of primary transcription (host proteins enriched in WT cells only). The PB2 interactome was studied in the context of live virus by using a recombinant virus that expresses an AP tag on the PB2 polymerase subunit. To capture host cell proteins involved in the early stages of the viral lifecycle, the infection and AP conditions were optimised prior to performing the interactome screen. The PB2 interactome was found to be different in WT and ANP32-KO cells. We employed siRNAs to functionally validate a role in IAV infection and polymerase activity of a subset of the host proteins uniquely co-precipitating from WT cells, potential replication-specific factors, and both WT and ANP32-KO cells, potential transcription-specific factors. Lastly, to identify replication-specific factors using an alternative approach, we performed a second differential interactome screen comparing the interactome of ANP32 in the presence and absence of infection. The role in polymerase

activity of host proteins found to co-precipitate with both ANP32 during infection and PB2 in WT cells was also assessed.

Mass spectrometry analysis of all AP samples for the differential interactome screens was performed by Dr Fairouz Ibrahim and Dr Mark Skehel of the Proteomics Science Technology Platform at the Francis Crick Institute. The tagged RT-qPCR primers targeting segment 4 were generated by this author with the help of Dr Olivia Swann (Swann et al., 2023). The PR8 NS-ZsGreen plasmid used to rescue the PR8 NS-ZsGreen virus was a kind gift from Professor Edward Hutchinson. Figures 17, 18, 20, 21, 22, 23, 24, 26, 27 and Tables 4 and 5 and the accompanying text are adapted from Rasmussen et al., 2025, manuscript in review and pre-printed on Biorxiv (Rasmussen et al., 2025).

Section 2.2. Results

Section 2.2.1. AP-MS strategy to identify transcription-specific and replication-specific host factors.

We and others have previously shown ANP32 to be an essential cofactor for viral RNA replication, but not transcription (Nilsson-Payant et al., 2022, Swann et al., 2023, Staller et al., 2019, Sugiyama et al., 2015). This means that only steps upstream of RNA replication (virus entry, nuclear import, and primary transcription) are supported in ANP32-KO cells (Figure 17). Meanwhile, all steps of the IAV lifecycle can proceed unhindered in WT cells. The main aim of this chapter was to identify host cell proteins that are co-opted by the IAV polymerase to support either viral RNA transcription or replication. To achieve this, we first used our ANP32-KO cells as a unique tool to uncouple viral transcription and replication. We reasoned that host proteins co-precipitating from WT, but not ANP32-KO cells, would include polymerase interactors with roles downstream of transcription, some of which may be specific to polymerase replicase activity. Meanwhile, proteins co-precipitating from both cell types, or from ANP32-KO cells only may have roles specific to polymerase transcriptase activity. Prior to performing our differential AP-MS screen, we generated the tools needed (Section 2.2.2) and optimised the AP protocol (Sections 2.2.3 and 2.2.4). The optimisation involved trialling different conditions in WT and ANP32-KO cells and analysing the IPs by western blot.

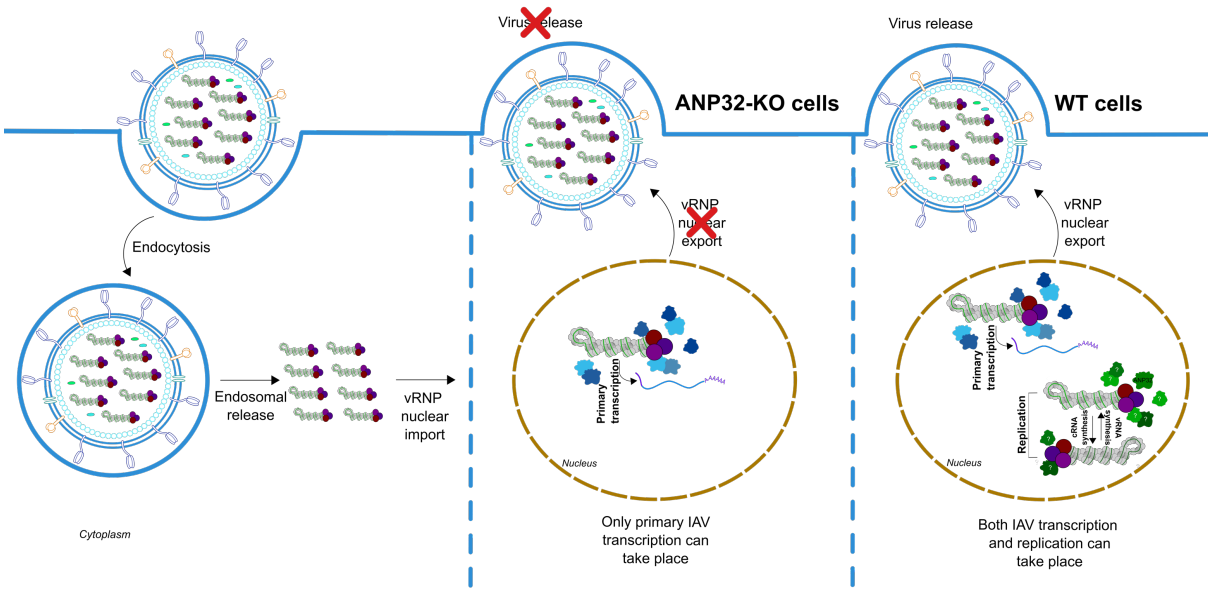

Figure 17. Schematic of the IAV lifecycle in ANP32-KO cells and WT cells.
In ANP32-KO cells only primary viral transcription and steps upstream of this (virus entry, endocytosis, and vRNP nuclear import) are supported. In WT cells, all steps of the IAV lifecycle can occur.

Section 2.2.2. Generation and characterisation of recombinant IAV expressing an AP tag on the PB2 polymerase subunit.

To study the interactome of the IAV polymerase in the context of live virus, we generated recombinant H1N1 A/Puerto Rico/8/1934 (PR8) influenza viruses that express an AP tag (FLAG or Strep) on the C-terminus of the PB2 polymerase subunit (Figure 18A). The PR8 strain was selected because it is a laboratory-adapted strain that is amenable to genetic modification. We decided to tag the PB2 protein at the C-terminus because previous studies have generated similar tagged viruses with little impact on viral fitness (Dos Santos Afonso et al., 2005, Heaton et al., 2016, Rameix-Welti et al., 2009).

To generate AP-tagged PR8 virus, we made use of a plasmid-based reverse genetics system (Hoffmann et al., 2000). This system consists of eight pHW2000 expression plasmids each encoding one of the eight viral cDNAs of the IAV genome inserted between a RNAP I and RNAP II promoter. The presence of the two promoters allows the cDNA template to be transcribed into both negative-sense viral RNA analogous to the genome and positive-sense mRNA, from which viral proteins can then be expressed. Assembly of the negative-sense viral RNAs with polymerase proteins and NP eventually leads to the production of all eight vRNPs which are packaged together to generate fully infectious virus particles.

We modified the pHW2000-PB2 plasmid so that it would produce PB2-FLAG or PB2-Strep RNA instead of PB2-WT RNA. Importantly, the packaging signals, usually consisting of non-coding regions (NCRs) and adjacent coding regions at both the 3’ and 5’ ends, on each vRNA segment must remain intact to allow all eight segments to be incorporated into viral

particles and for stable infectious virus to be generated (Li et al., 2021). In the case of PB2, the last 150nts constitute the minimum requirement for packaging (Duhaut and Dimmock, 2002, Li et al., 2021). Indeed, previous studies have successfully generated IAV with an AP-tagged PB2 segment by inserting a duplication of the last 109, 143, or 169nts of the coding region between the tag and the 5' NCR (Dos Santos Afonso et al., 2005, Heaton et al., 2016, Rameix-Welti et al., 2009). Consequently, to ensure proper packaging, we generated AP-tagged constructs with an AP tag (FLAG/Strep) inserted at the 5' end of the coding region as well as a duplication of the last 173nts of the coding region inserted between the AP tag (after the stop codon) and the 5' NCR (Figure 18A). We also included a 3x alanine linker between the PB2 coding region and the tag to minimise the risk that the tag interferes with PB2's functions as part of the heterotrimeric viral polymerase complex.

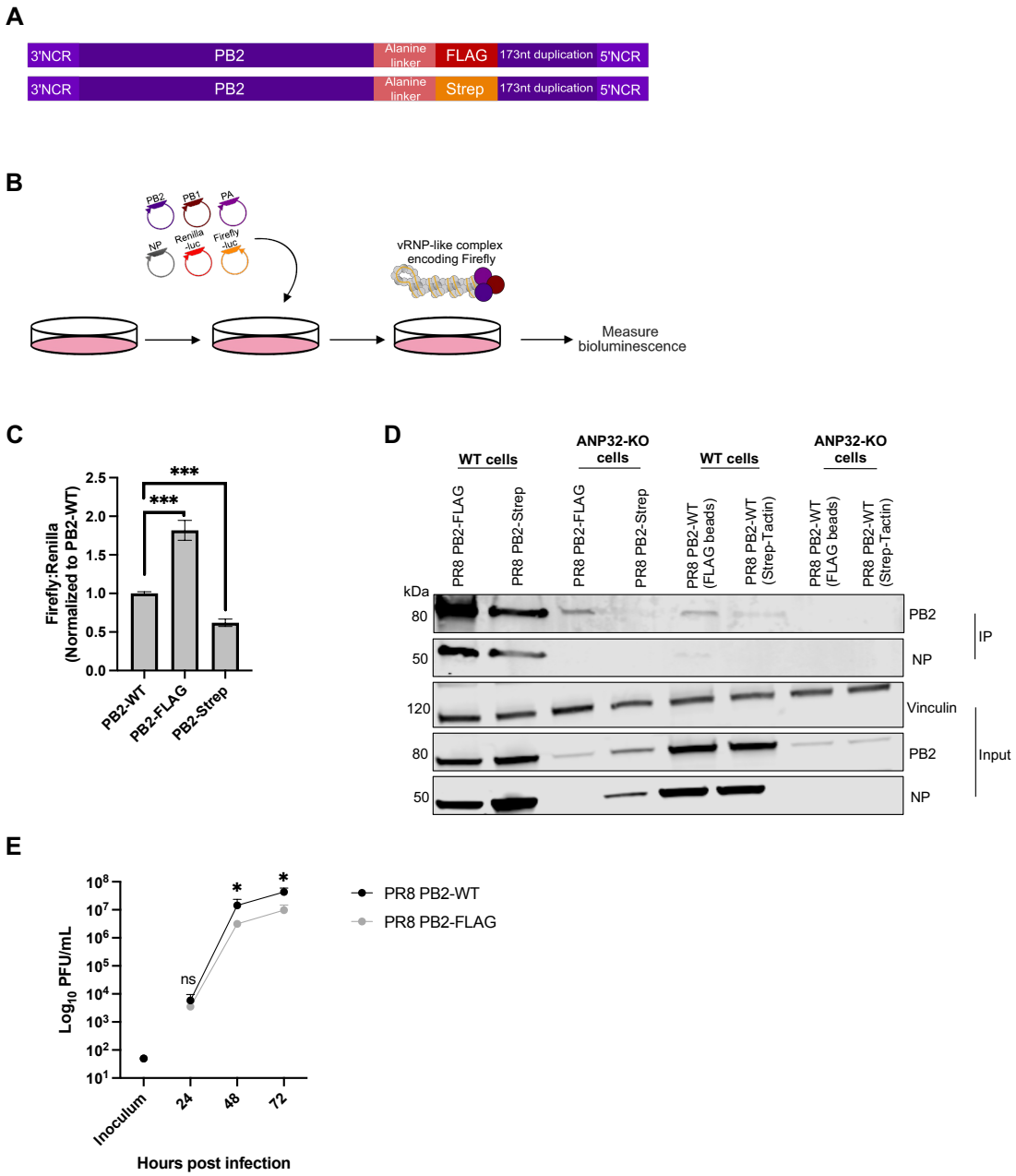

Figure 18. Generation and characterisation of AP-tagged PR8 influenza viruses.
A) Schematic showing the design of the PB2-FLAG and PB2-Strep segments. Each segment consists of a 3x alanine linker, FLAG/Strep tag, stop codon, and 173nt duplication of the packaging signal inserted between the coding region and the 5'NCR. B) Schematic of a minigenome reporter assay. Cells are transfected with plasmids encoding PB2, PB1, PA, and NP, a reporter plasmid (Firefly luciferase (Firefly)), and a Renilla luciferase (Renilla) expression plasmid. 20hrs post transfection, cells are lysed, and bioluminescence is measured. C) Minigenome reporter assay in eHAP WT cells using polymerase constellations consisting of pCAGGS PR8 PB1, PA, and NP and pHW2000 PR8 PB2-WT, PB2-FLAG, or PB2-Strep. Firefly luciferase activity relative to co-transfected Renilla luciferase levels was normalised to PB2-WT. Data is shown as mean ± SD of n=3 technical repeats, representative of n=3 biological repeats. Statistical significance was assessed compared to PB2-WT. D) Western blot of inputs and IPs from eHAP WT cells and ANP32-KO cells infected with PR8 PB2-FLAG or PR8 PB2-Strep (MOI=5). Cells were lysed at 5hpi, and IPs were performed using FLAG or Strep-tactin magnetic beads. The blots were probed for PB2, NP, and vinculin (cellular control) protein expression. E) Virus replication in eHAP WT cells infected with PR8 PB2-WT (black) or PR8 PB2-FLAG (grey) (MOI=0.001).

Supernatants were harvested at indicated timepoints post infection, and titres were determined by plaque assay on MDCK cells. Statistical significance was assessed at each timepoint. For panels C and E: Statistical significance was assessed using an unpaired *t* test. ns, not significant; *, $p<0.05$; ***, $p<0.001$.

Prior to using the PB2-FLAG and PB2-Strep constructs to generate recombinant virus, we tested whether the constructs were functional and capable of supporting polymerase activity. To achieve this, the activity of IAV polymerase reconstituted with PB2-FLAG or PB2-Strep was compared to the activity of PB2-WT in a minigenome reporter assay. This is an *in situ* assay in which a vRNP-like complex is reconstituted by co-transfecting plasmids encoding the vRNP components: PB2, PB1, PA, NP, and a viral-like RNA template (Figure 18B) (Te Velthuis et al., 2018). The viral-like RNA encodes a reporter gene, in this case a Firefly luciferase gene, flanked by the IAV NCRs and further flanked by a host cell RNAP I promoter and terminator. A Renilla luciferase expression plasmid is also transfected to control for transfection efficiency. The reporter plasmid gives a measure of total IAV polymerase activity, because transcription is necessary to express the reporter gene (and generate a luciferase signal) and replication of the reporter gene increases the number of vRNP-like complexes from which transcription can occur. Typically, all the viral proteins are expressed from a pCAGGS expression vector, but in this case PB2-FLAG, PB2-Strep, and PB2-WT were expressed from the pHW2000 vector and the remaining viral proteins from the pCAGGS vector. Interestingly, polymerase activity with PB2-FLAG was significantly higher than WT polymerase activity (Figure 18C). Conversely, polymerase activity with PB2-Strep was significantly lower than WT polymerase activity. This difference was surprising because the two tags are similar: 8 amino acids in length and about 1kDa in size. The main difference between the two is their charge; the FLAG tag is negatively charged while the Strep tag is positively charged. The lower polymerase activity with PB2-Strep could be explained if the positively charged Strep tag interferes with the ability of the polymerase to assemble into heterotrimers, RNPs, or dimers, which are known to be important for RNA replication. Nevertheless, we still proceeded to generate recombinant viruses with both the PB2-FLAG and PB2-Strep constructs.

To rescue recombinant viruses, the pHW2000-PB2-FLAG and pHW2000-PB2-Strep plasmids (substituted for pHW2000-PB2-WT) were co-transfected alongside the remaining seven pHW2000 PR8 plasmids into 293T cells, which are human cells permissive to transfection. The 293T cells were then co-cultured with Madin-Darby canine kidney (MDCK) cells, which are permissive to influenza infection and allow the generation of infectious influenza virus particles. PR8 PB2-WT (PR8 WT) was generated as a control, substituting pHW2000-PB2-WT for the AP-tagged versions. Successful rescue of the viruses was confirmed by plaque assay on MDCK cells and retention of the AP tags and duplicated

packaging signal was confirmed by Sanger sequencing after rescue and one passage (data not shown).

To check that the tags could be used in immunoprecipitations (IPs), we infected eHAP WT and ANP32-KO cells with PR8 PB2-FLAG or PR8 PB2-Strep and IPs were performed using FLAG magnetic beads or Strep-tactin beads, respectively. The inputs and IPs were then analysed by western blot probing for PB2, NP, and vinculin (Figure 18D). More PB2 and NP expression was detected in the input from WT cells than ANP32-KO cells, as expected given that no RNA replication can occur in the ANP32-KO cells. In WT cells, PB2 was immunoprecipitated with both the FLAG and Strep tags, confirming that both tags were expressed. NP co-precipitated with PB2 in both cases, confirming that PB2-FLAG and PB2-Strep can form RNPs. More PB2 and NP were detected in FLAG IPs than Strep IPs, suggesting the FLAG IPs to be more efficient than the Strep IPs. Furthermore, in ANP32-KO cells, PB2 was detected in FLAG IPs but not in Strep IPs, further suggesting the FLAG IPs to be more efficient. As a control to determine the level of non-specific binding to either set of beads, IPs were also performed from PR8 WT-infected WT and ANP32-KO cells. More non-specific binding was observed with the FLAG beads than the Strep-tactin beads. However, we reasoned that the higher non-specific binding could be reduced by improving the wash steps prior to elution. Collectively, our data showed that PR8 PB2-FLAG achieved higher levels of polymerase activity than PR8 PB2-Strep (and PR8 WT) as well as more efficient IPs. We therefore decided to use the PR8 PB2-FLAG virus in future experiments.

We next compared virus growth of PR8 PB2-FLAG to that of PR8 WT in a multi-cycle growth curve. Virus growth of PR8 PB2-FLAG was slightly attenuated compared to PR8 WT but followed the same trend (Figure 18E). Recombinant PR8 PB2-FLAG viruses have previously been reported to show slightly attenuated virus growth compared to PR8 WT (Heaton et al., 2016). We reasoned that the slightly lower viral fitness of PR8 PB2-FLAG would not be an issue as we would be comparing the PB2 interactome in two different cell types both infected with the same PR8 PB2-FLAG virus.

Section 2.2.3. Optimisation of lysis buffer and wash conditions.

We reasoned that many of the important virus-host interactions controlling transcription and replication would take place with host proteins located in the nucleus. To break down the cellular membranes, including nuclear membranes, and release host and viral proteins, the cells were lysed in lysis buffer containing NP-40 detergent. NP-40 is a non-ionic detergent which has previously been used to separate nuclear and cytoplasmic fractions when used in lysis buffers containing physiological salt concentration (<150mM NaCl) (Kamel et al., 2024). Here, we used this mild detergent in lysis buffer with high salt to achieve nuclear lysis without disrupting protein-protein interactions. The high salt concentration disrupts electrostatic

interactions between nuclear proteins and DNA, weakening the structural integrity of the nuclear envelope and causing chromatin decondensation. When combined with detergents like NP-40 that solubilise the membrane lipid bilayer, this aids nuclear lysis. In the IPs shown in Figure 18D, the cells were lysed in lysis buffer containing 0.2% NP-40 detergent and 200mM NaCl. To confirm that this detergent concentration is sufficient, we lysed WT cells infected with PR8 PB2-FLAG using lysis buffers with different NP-40 concentrations (0.1%, 0.2%, and 0.5%). We analysed the lysates by western blot, probing for lamin B1, a component of the nuclear lamin that is used as a nuclear marker, vinculin, a ubiquitously expressed cytoskeletal protein that is used as a cytoplasmic marker, and PB2 (Figure 19A). A similar level of lamin B1 was detected with all tested NP-40 concentrations, suggesting that NP-40 concentrations as low as 0.1% can lyse the nuclear membrane. Slightly more vinculin was observed with 0.5% NP-40 concentration than 0.1%. Having confirmed that 0.2% NP-40 can lyse the nuclear membrane, we decided to continue to use this concentration in future IPs. However, it is essential to note that this experiment was missing an important control, namely cells lysed with a detergent expected to achieve full nuclear lysis, such as SDS. This would indicate the amount of lamin B1 protein expected with full nuclear lysis. We, therefore, cannot conclude from our experiment the degree of nuclear lysis achieved, only that the lysis buffer composition was sufficient to achieve some nuclear lysis.

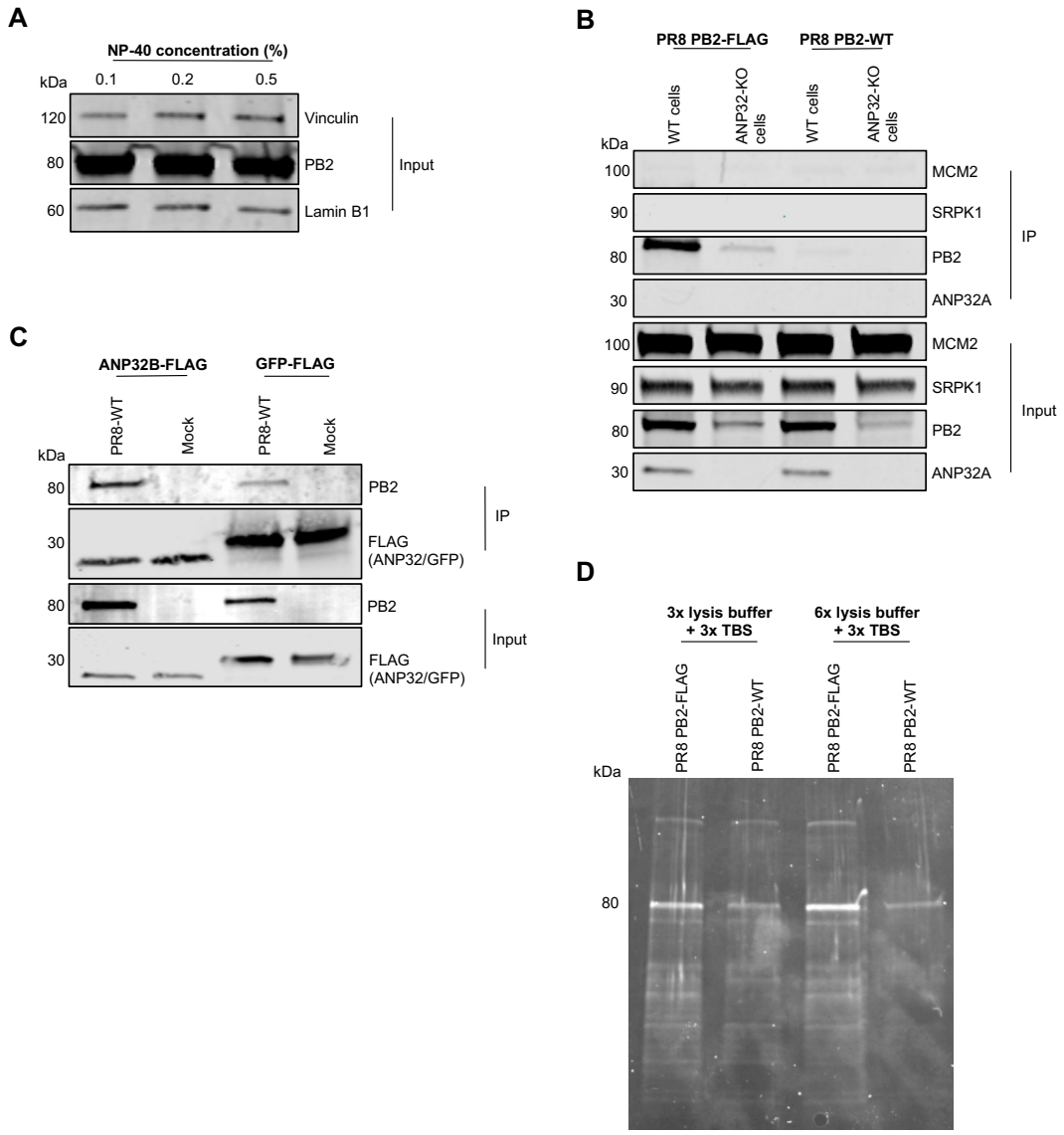

Figure 19. Optimisation of lysis buffer conditions and wash steps.
A) Western blot of lysates (input) from eHAP WT cells infected with PR8 PB2-FLAG (MOI=5). Cells were lysed at 5hpi. The blots were probed for vinculin, PB2, and lamin B1 protein expression. B) Western blot of inputs and IPs from eHAP WT and ANP32-KO cells infected with PR8 PB2-FLAG or PR8 PB2-WT (MOI=5). Cells were lysed at 5hpi. The blots were probed for MCM2, SRPK1, PB2, and ANP32A protein expression. C) Western blot of inputs and IPs from eHAP ANP32-KO cells transfected with ANP32B-FLAG or GFP-FLAG and huANP32B, and infected with PR8 WT (MOI=5) or mock-infected. Cells were lysed at 5hpi. The blots were probed for PB2 and FLAG (ANP32B/GFP) protein expression. D) SYPRO staining of IPs from eHAP WT cells infected with PR8 PB2-FLAG or PR8 PB2-WT (MOI=5), lysed at 5hpi, and washed in 3x lysis buffer and 3x TBS or 6x lysis buffer and 3x TBS.

Next, we wanted to confirm that known virus-host interactions remained intact using this detergent concentration. To achieve this, we performed IPs from WT and ANP32-KO cells infected with PR8 PB2-FLAG or PR8 WT. The inputs and IPs were then analysed by western blot probing for the co-precipitation of MCM2, which has previously been shown to interact with the polymerase and vRNPs (Kawaguchi and Nagata, 2007), SRPK1, which was reported as a polymerase interactor in a previous polymerase interactome screen using PA as bait

(Mistry, 2019), and ANP32A, which has previously been shown to interact with the polymerase and NP (Figure 19B) (Mistry et al., 2020, Wang et al., 2022a, Baker et al., 2018, Domingues and Hale, 2017, Bradel-Tretheway et al., 2011, Sugiyama et al., 2015). MCM2 and SRPK1 were expressed to a similar extent in the inputs from WT and ANP32-KO cells while ANP32A was only expressed in the WT cells, as expected. Also as expected and similar to in Figure 18D, more PB2 was expressed in WT cells than ANP32-KO cells. PB2 was immunoprecipitated from both WT and ANP32-KO cells, but none of the host proteins were found to co-precipitate with PB2. This could be because this timepoint post infection (5hpi) was not suitable for detecting these interactions. It is also possible that the detergent is disrupting virus-host interactions or that only small amounts of the host proteins interact with PB2 during infection such that the interactions were not detectable by western blot.

To test this, we performed IPs using overexpressed ANP32B-FLAG as bait. Specifically, ANP32-KO cells were transfected with ANP32B-FLAG or GFP-FLAG, as a control to eliminate proteins non-specifically binding to the FLAG tag, and infected with PR8 WT or mock-infected. The inputs and IPs were analysed by western blot probing for PB2 and FLAG (ANP32/GFP) (Figure 19C). PB2 co-precipitated with ANP32B, indicating that the lysis conditions allow the PB2-ANP32 interaction to remain intact. A small amount of PB2 also co-precipitated with GFP-FLAG. We have previously found PB2 and other proteins to non-specifically bind to GFP (data not shown), which could explain the co-precipitation of PB2 with GFP-FLAG. Nevertheless, we cannot exclude the possibility that PB2 may also be non-specifically binding to the FLAG tag, such that some of the PB2 in the ANP32B-FLAG IPs may be non-specific. Taken together our data further suggests that a 0.2% NP-40 concentration is capable of lysing the nuclear membrane and indicates that this detergent concentration allows at least some virus-host interactions, exemplified by the PB2-ANP32B interaction, to remain intact.

Prior to elution, the beads were washed in lysis buffer and TBS to remove host proteins non-specifically binding to the beads. To understand whether more stringent washes should be used to reduce non-specific binding to the FLAG beads, we performed IPs from eHAP WT cells infected with PR8 PB2-FLAG or PR8 WT and washed as previously (3x in lysis buffer and 3x in TBS) or more stringently (6x in lysis buffer and 3x in TBS). The IPs were then analysed by SYPRO staining (Figure 19D). Less non-specific binding (indicated by the IPs from PR8 WT-infected cells) was observed with more stringent washing. However, it also appeared that the amount of proteins co-precipitating with PB2 (indicated by the IPs from PR8 PB2-FLAG-infected cells) was reduced with more stringent washing. To minimise the risk that the wash steps remove specific binders as well as non-specific binders, we decided to use wash conditions more moderate than the stringent ones tested here, namely 4x in lysis buffer and 4x in TBS.

Section 2.2.4. Determining the optimal timepoint post infection and scale for interactome analysis.

To determine the optimal timepoint post infection for distinguishing replication and transcription host factors, we quantified the accumulation of segment 4 (HA) vRNA, cRNA, and mRNA in eHAP WT and ANP32-KO cells infected with PR8 PB2-FLAG virus (Figure 20A-C). The viral RNA species were quantified using a tagged RT-qPCR method developed by Kawakami et al., which uses primers specific to each of the RNA species (Kawakami et al., 2011). We have previously validated the specificity of this method for distinguishing the three viral RNA species and used this method to show that ANP32 proteins are essential for cRNA synthesis (Swann, 2023, Swann et al., 2023). The infections were performed in 10cm dishes to mimic the replication kinetics of the virus during IPs. As expected, no vRNA or cRNA products accumulated above input in the ANP32-KO cells over time (Figure 20A and B). At 2 hours post infection (hpi), mRNA levels had increased 30-fold in both cell types, after which time the amplification of vRNA in the WT cells resulted in logarithmically more transcripts (Figure 20C). Meanwhile, cRNA but not yet vRNA had accumulated by 2hpi in the WT cells, and vRNA was evident by 3hpi (Figure 20A and B). The early timepoint of 3hpi was selected for interactome analysis because at this timepoint primary transcription had taken place in both cell types and both cRNA and vRNA synthesis had occurred in the WT cells (Figure 20A-D).

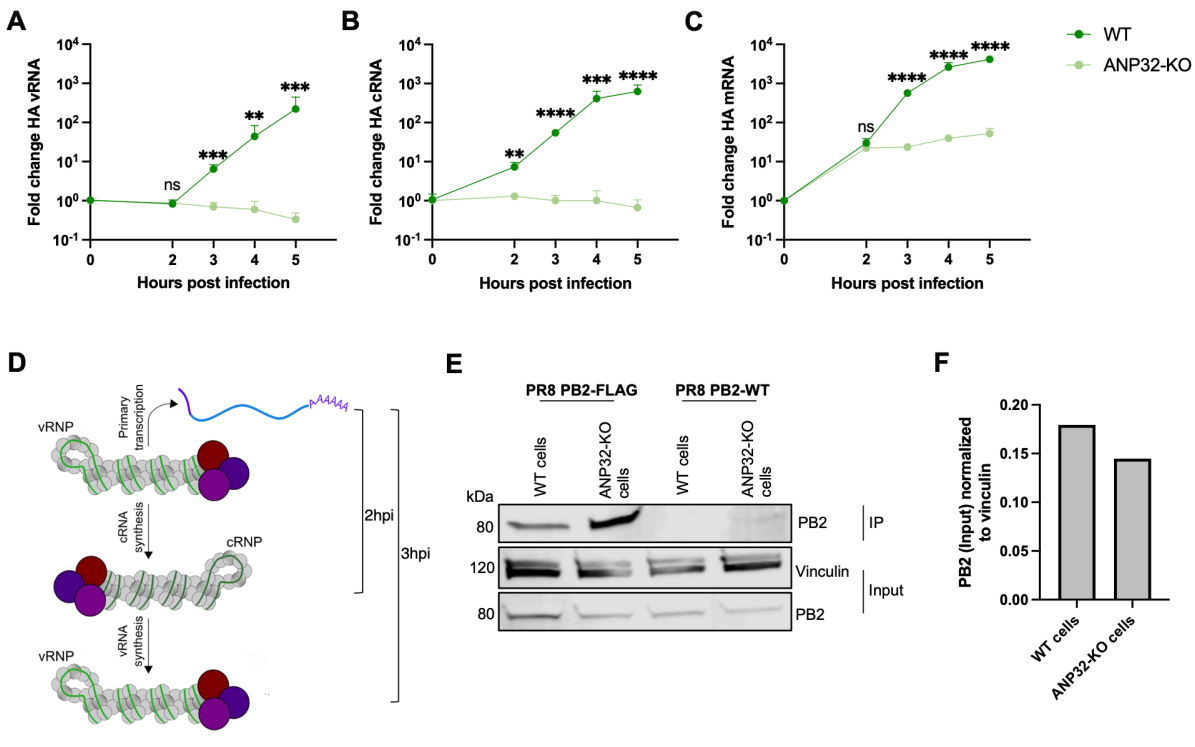

Figure 20. Determining the optimal timepoint and scale for interactome analysis.
A-C) Accumulation of segment 4 (HA) vRNA (A), cRNA (B), and mRNA (C) in eHAP WT and ANP32-KO cells infected with PR8 PB2-FLAG (MOI=5), quantified by RT-qPCR at indicated timepoints post infection. The fold change was calculated versus input (0hpi). Data is shown as mean ± SD of n=3 technical repeats, representative of n=2 biological repeats. Statistical significance was assessed using multiple unpaired *t* tests corrected for multiple comparisons using the false discovery rate, following log transformation. ns, not significant; **, p<0.01; ***, p<0.001; ****, p<0.0001. D) Schematic showing vRNA, cRNA, and mRNA synthesis at 2hpi and 3hpi in eHAP WT cells. At 3hpi, primary transcription has occurred in both WT and ANP32-KO cells and cRNA and vRNA synthesis have occurred in WT cells. E) Western blot of inputs and IPs from eHAP WT and ANP32-KO cells, infected with PR8 PB2-FLAG or PR8 PB2-WT (MOI=5), and lysed at 3hpi. IPs were performed from 3x more infected ANP32-KO cell lysate (input) than WT cell lysate. The blots were probed for PB2 and vinculin (cellular control) protein expression. F) Quantification of western blot in (E) shown as the amount of PB2 expression in the input (PR8 PB2-FLAG-infected cells) normalised to the amount of vinculin expression.

Considering that no viral RNA replication occurs in ANP32-KO cells, the amount of PB2-FLAG bait does not increase above input levels in these cells (Figure 20A and B). Meanwhile, in the WT cells, where both viral transcription and replication occur, the PB2-FLAG bait is amplified. This is evident in previous inputs and IPs analysed by western blot, where less PB2 was observed in infected lysates from ANP32-KO cells than lysates from WT cells (Figure 18D and 19B). To ensure comparable amounts of the PB2-FLAG bait in the WT and ANP32-KO cells, three times more lysate was used for the latter condition. This resulted in similar levels of PB2-FLAG bait in the WT and ANP32-KO cells, although there was still slightly less PB2-FLAG bait in the ANP32-KO cells (Figure 20E). Quantification of the bands and normalisation of the amount of bait PB2 in the input to vinculin further corroborated this (Figure 20F).

Section 2.2.5. The PB2 interactome is different in WT and ANP32-KO cells.

Based on the experiments performed in Sections 2.2.2-2.2.4 to generate the necessary tools and optimise the AP conditions, the differential AP-MS interactome screen was performed by infecting eHAP WT and ANP32-KO cells with PR8 PB2-FLAG virus at an MOI=5, harvesting the cells at 3hpi, lysing the cells in lysis buffer containing 0.2% NP-40, immunoprecipitating PB2-FLAG from three times more ANP32-KO cell lysate than WT cell lysate, washing the beads with moderate stringency, and analysing the IPs by MS (Figure 21A). As a control to eliminate proteins non-specifically binding to the FLAG beads, the same IPs were performed from WT and ANP32-KO cells infected with PR8 WT virus, which lacks a FLAG tag (Figure 21B). A similar negative background control has been employed in previous IAV polymerase interactome studies (York et al., 2014, Hubel et al., 2019). We decided to use this control instead of cells transfected with GFP-FLAG or a similar construct as we reasoned that transfecting the cells might alter the cellular environment, making the background control less comparable to the experimental samples.

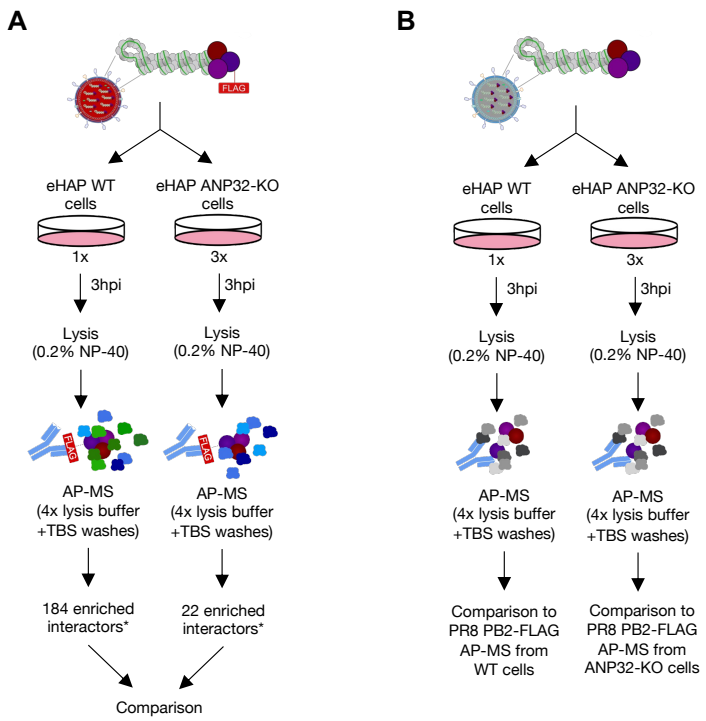

Figure 21. Schematic of differential AP-MS strategy using PB2 as bait.
A) Schematic of AP-MS strategy to compare the interactome of PB2 in WT and ANP32-KO cells in the context of infection. eHAP WT and ANP32-KO cells are infected with PR8 PB2-FLAG (MOI=5), lysed in lysis buffer containing 0.2% NP-40 detergent at 3hpi, immunoprecipitated using FLAG magnetic beads, washed in 4x lysis buffer and 4x TBS, and then analysed by MS. IPs are performed from 3x more infected ANP32-KO cell lysate than WT cell lysate. * = number of proteins enriched above background (PR8 PB2-WT-infected cells) (B) in WT and ANP32-KO cells. B) Schematic of how non-specific binding to the FLAG beads is determined. IPs are performed as in (A), but with PR8 WT infection instead.

Screens were conducted three independent times and showed good reproducibility with an average Pearson correlation coefficient of 0.86 between each screen repeat. The background levels of non-specific binding in WT and ANP32-KO cells were similar with an average coefficient of variation of 6%. All samples showed similar protein LFQ intensity distribution (Figure 22A). Principal component analysis (PCA) revealed that samples from each group mostly clustered together (Figure 22B). For instance, samples from the PR8 PB2-FLAG-infected WT cells group clustered together and separately from the PR8 PB2-FLAG-infected ANP32-KO cells group. Some variation was observed between biological repeats within each group, while technical repeats of each biological repeat clustered tightly together. Host and viral proteins were classified as interactors based on their enrichment (S_0=0.2, FDR=0.05) over negative background control in each cell type (Figure 22C and D). We also assessed the correlation between the fold change over negative background control and the LFQ intensity for each protein in each cell type (Figure 22E and F). We found that in both WT and ANP32-KO cells, most of the data points centred around a fold change value of 0 (coloured in grey for both WT and ANP32-KO cells). In both cell types, many of the proteins with a high fold change (coloured in dark green for WT cells and light green for ANP32-KO cells) also had high LFQ intensities, suggesting these proteins to be true polymerase interactors. However, some of the proteins with a high fold change had fairly low LFQ intensities, making it unclear from the AP-MS data whether the proteins are true polymerase interactors or have high fold changes due to a lower signal-to-noise ratio. The raw and processed data is provided in Appendix A. The host proteins found to be enriched above background in the WT cells were then compared to the host proteins found to be enriched above background in the ANP32-KO cells (Figure 22C, E, and G).

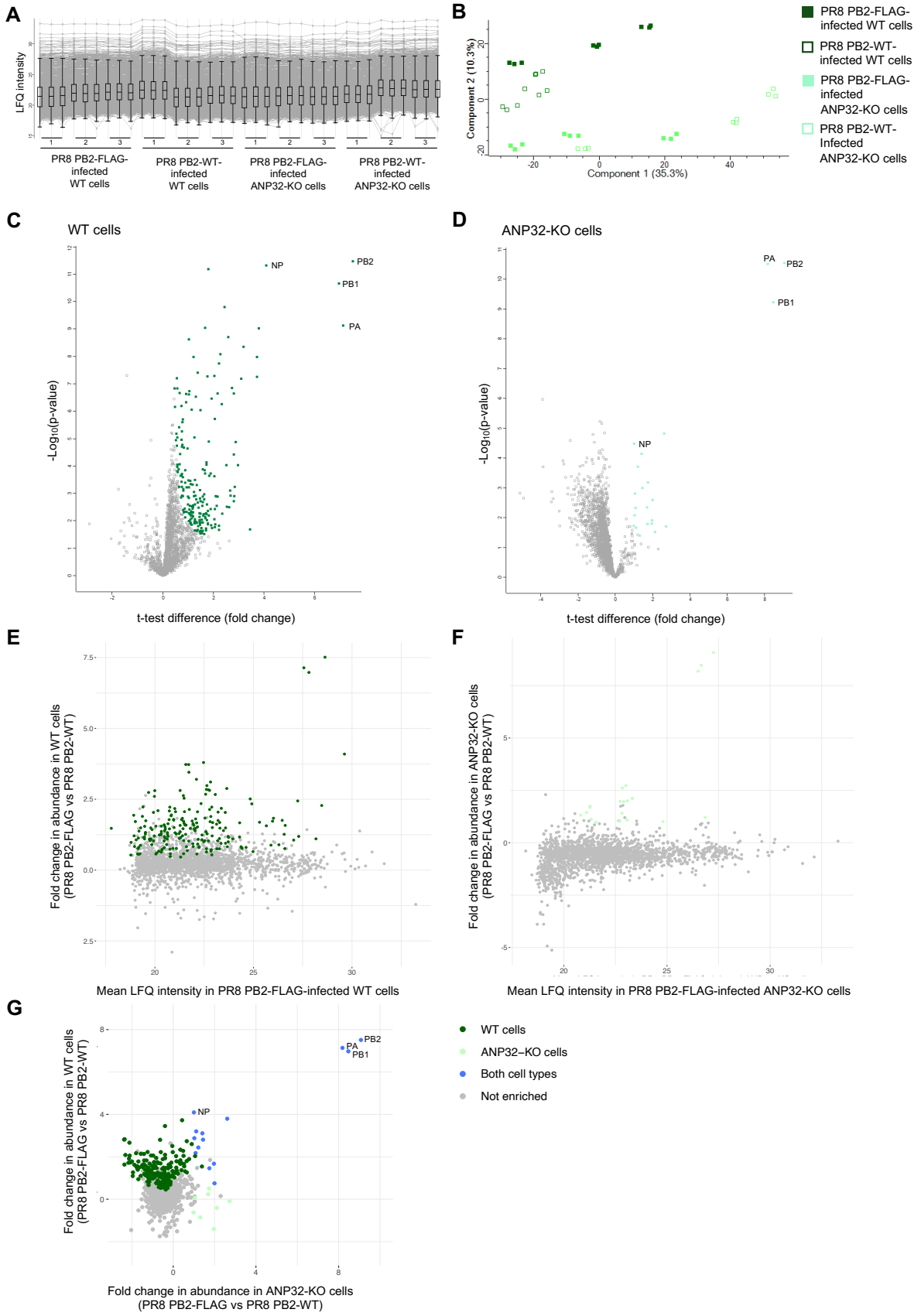
A
LFQ intensity
PR8 PB2-FLAG-infected WT cells
PR8 PB2-WT-infected WT cells
PR8 PB2-FLAG-infected ANP32-KO cells
PR8 PB2-WT-infected ANP32-KO cells
B
Component 2 (10.3%)
Component 1 (35.3%)
PR8 PB2-FLAG-infected WT cells
PR8 PB2-WT-infected WT cells
PR8 PB2-FLAG-infected ANP32-KO cells
PR8 PB2-WT-Infected ANP32-KO cells
C
WT cells
NP
PB2
PB1
PA
-Log10(p-value)
t-test difference (fold change)
D
ANP32-KO cells
PA
PB2
PB1
NP
-Log10(p-value)
t-test difference (fold change)
E
Fold change in abundance in WT cells (PR8 PB2-FLAG vs PR8 PB2-WT)
Mean LFQ intensity in PR8 PB2-FLAG-infected WT cells
F
Fold change in abundance in ANP32-KO cells (PR8 PB2-FLAG vs PR8 PB2-WT)
Mean LFQ intensity in PR8 PB2-FLAG-infected ANP32-KO cells
G
Fold change in abundance in WT cells (PR8 PB2-FLAG vs PR8 PB2-WT)
Fold change in abundance in ANP32-KO cells (PR8 PB2-FLAG vs PR8 PB2-WT)
PB2
PA
PB1
NP
WT cells
ANP32–KO cells
Both cell types
Not enriched

Figure 22. Determination of host proteins enriched above background in WT and ANP32-KO cells.
A) Box plot showing the LFQ intensity distribution of each sample. Box plot was generated using Perseus v.2.011. B) Principal component analysis of samples within each group (PR8 PB2-FLAG-infected WT cells, PR8 PB2-WT-infected WT cells, PR8 PB2-FLAG-infected ANP32-KO cells, and PR8 PB2-WT-infected ANP32-KO cells). Each data point represents a technical repeat of each sample. C and D) Volcano plot of proteins co-precipitated in WT cells (C) and ANP32-KO cells (D) infected with PR8 PB2-FLAG or PR8 PB2-WT. Proteins classified as interactors (S0=0.2, FDR=0.05) are shown in green (C) and light green (D). Volcano plots were generated using Perseus v.2.011. E and F) Mean-average plot showing the fold-change over negative background control versus the LFQ intensity of each protein in WT cells (E) and ANP32-KO cells (F). Proteins found to be enriched in PR8 PB2-FLAG-infected WT cells in (C) are coloured in dark green (E) and proteins found to be enriched in PR8 PB2-FLAG-infected ANP32-KO cells in (D) are coloured in light green (F). G) Fold change in abundance of proteins above background in WT and ANP32-KO cells. Background was determined using IPs from WT and ANP32-KO cells infected with PR8 PB2-WT. E-G) Graphs were plotted using R v.4.2.2.

Using these criteria, 170 proteins were uniquely co-precipitated from WT cells, 8 proteins from ANP32-KO cells, and 14 proteins were common to both cell types (Figure 23A). Focusing on the viral proteins, similar amounts of PB2-FLAG bait were immunoprecipitated in both WT and ANP32-KO cells, suggesting that the conditions chosen allow a fair comparison (22A-C). Overall, the PB2-FLAG, PB1, and PA polymerase subunits were the most abundant proteins in both cell types. The polymerase proteins were enriched above background to a similar extent in both WT and ANP32-KO cells, suggesting that PB2-FLAG was immunoprecipitated in its heterotrimeric form in both cell types (Figure 22A and B). In addition, NP co-precipitated with PB2-FLAG as well, suggesting that some of the polymerase heterotrimers were incorporated into their RNP form, at least in the WT cells. Less NP co-precipitated from ANP32-KO cells than WT cells, potentially because although viral proteins are synthesised from the incoming vRNP template in ANP32-KO cells, progeny vRNPs do not assemble (Figure 22A and B). Consequently, the NP co-precipitating from ANP32-KO cells is likely the result of direct PB2-NP interactions.

A

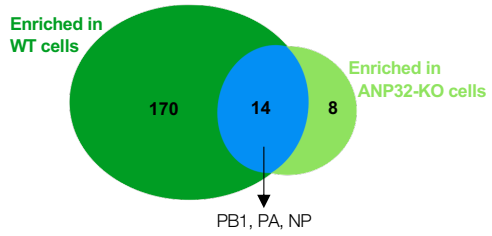

B

Category	GO term	P-value
Cellular component	Nuclear envelope	0.0227
	Nucleolus	4.3E-4
	Prohibitin complex	0.0143
	Proteasome core complex	8.05E-6
	R2TP complex	0.0438
	RNA polymerase II	1.74E-12
Biological process	ATP metabolic process	2.5E-4
	Protein folding	1.11E-8
	RIG-I signaling pathway	0.0139
	Regulation of protein ubiquitination	0.0281
	Regulation of translation initiation	0.0224
	Transcription	0.0025

C

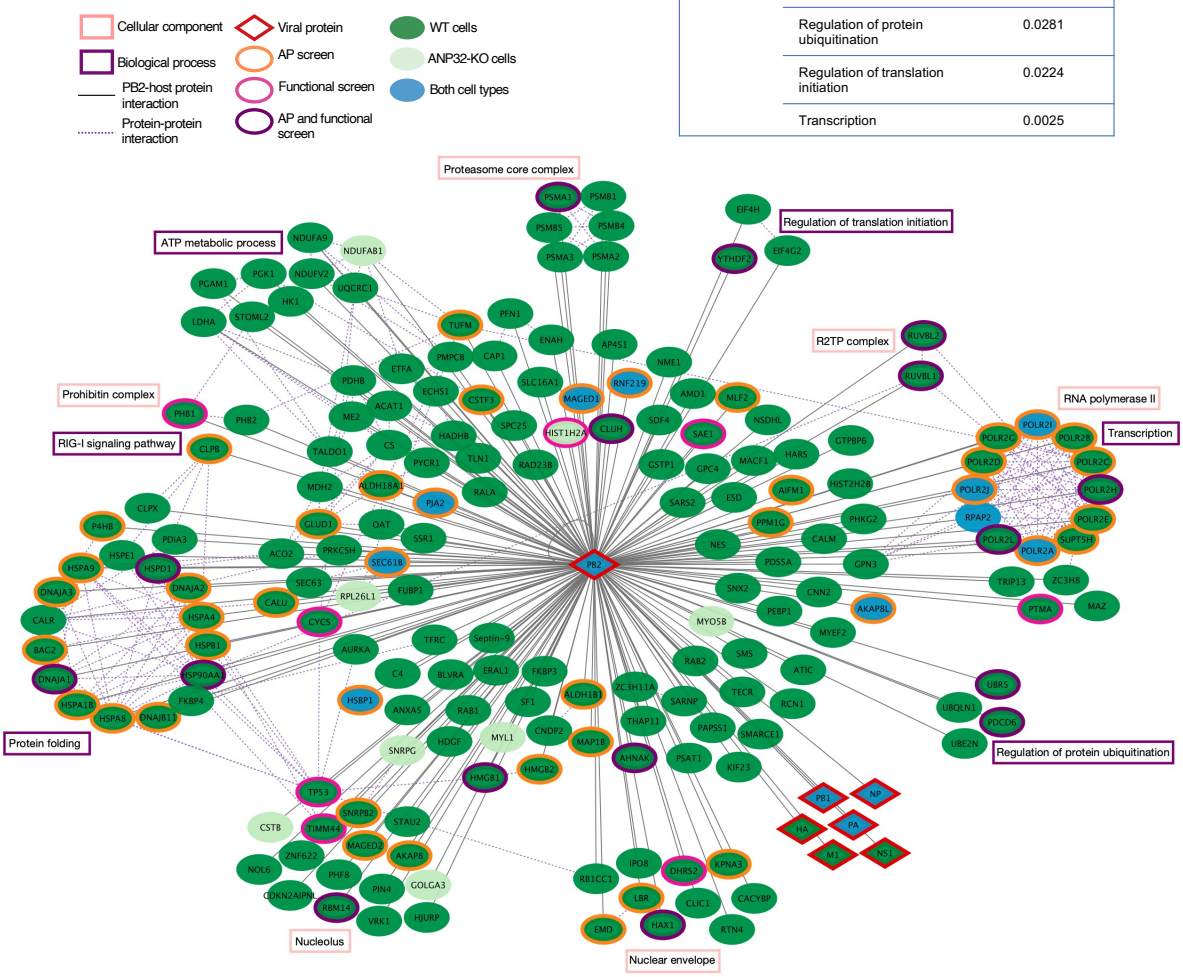

Figure 23. The interactome of PB2 is different in WT and ANP32-KO cells.
A) Venn diagram comparing the number of proteins enriched above background in WT and ANP32-KO cells. B) P-values associated with classification of host proteins based on GO cellular component and biological process terms. GO terms were determined using the StringApp in Cytoscape. C) Interaction network between PB2 (blue, filled) and 170 proteins in WT cells only (potential replication-specific factors) (green, filled), 8 proteins in ANP32-KO cells only (potential transcription-specific factors) (light green, filled), and 13 proteins in both cell types (potential transcription-specific factors) (blue, filled). The node outline indicates whether proteins were previously identified in screens, with the outline colour indicating the type of screen: AP-MS screens in orange, genetic screens in pink, and both AP-MS and genetic screens in purple. Viral proteins are diamond-shaped and outlined in red. Host protein-protein interactions (purple dotted lines) were predicted using STRING. Proteins are clustered based on GO cellular component (coral squares) or biological process (purple squares) terms. Protein interaction network was generated using Cytoscape v.3.10.2.

Focusing on the host proteins, the higher number of proteins co-precipitating from WT cells was expected, given that all steps following primary transcription (including replication and vRNP assembly and transport) can occur in the WT cells but not in the ANP32-KO cells (Figure 17 and 23A). In support of this, one of the host proteins uniquely co-precipitating from WT cells was CLUH, which has been shown to promote subnuclear transport of progeny vRNPs (Figure 23C) (Ando et al., 2016).

The host proteins found to co-precipitate with PB2 are visualised in an interactome map, with host proteins enriched specifically in WT cells (potential replication-specific factors) shown in dark green, host proteins enriched in both WT and ANP32-KO cells (potential transcription-specific factors) shown in blue, and host proteins enriched specifically in ANP32-KO (also potential transcription-specific factors) shown in light green (Figure 23C). Many of the host proteins found to uniquely co-precipitate from WT cells have previously been associated with polymerase activity or other steps of the IAV lifecycle (Figure 23C). Gene ontology (GO) cellular component and biological process terms also found these host proteins to be involved in host pathways and nuclear sites previously reported to be important for viral RNA synthesis (Figure 23B and C). To exemplify, the WT cell only interactome included the R2TP complex (RUVBL1 and RUVBL2), which was previously reported to interact with various polymerase proteins and NP, in the context of individually transfected proteins, transfected vRNPs, or infection (Haas et al., 2023, Kakugawa et al., 2009, Heaton et al., 2016, Mayer et al., 2007, Watanabe et al., 2014). Similarly, members of the HMGB protein family (HMGB1 and HMGB2) were in the WT cell only interactome. Both proteins were previously shown to interact with NP, with HMGB1 found to have a proviral role in polymerase activity and virus growth (Moisy et al., 2012). Our screen also found host proteins involved in protein folding to co-precipitate with PB2 from the infected WT cells only. Such host proteins included HSP90 and DNAJA1 which have previously been implicated in IAV polymerase activity (Cao et al., 2014, Naito et al., 2007). Additionally, GO cellular component terms revealed that many of these PB2 interactors are components of the nucleolus, which is a nuclear site believed to be important for NP assembly and, by extension, RNP formation (Miyamoto, 2022). One example is RBM14, which has also previously been shown to play a supportive role in polymerase activity (Bortz et al., 2011). Considering that these interactions all occurred specifically in the WT cells and not in the ANP32-KO cells, we expect these host factors to play roles in the IAV lifecycle downstream of primary transcription. This is consistent with the previously reported roles of the host factors outlined here.

Furthermore, in our screen we also found proteins common to both WT and ANP32-KO cells that have previously have been identified as polymerase interactors and cofactors (Figure 23C). For instance, we found that in both cells the interactome included AKAP8L, which has previously been shown to interact with PB2 (Haas et al., 2023). We also found PB2

to interact with RNAP II subunits, including the large POLR2A subunit, which is known to be essential for the cap-snatching step of viral transcription (Engelhardt et al., 2005). This is consistent with the notion that viral transcription occurs in both WT and ANP32-KO and provides further support for our hypothesis that host proteins co-precipitating from both cell types may have roles specific to transcription.

Lastly, our screen also revealed novel interactors (Figure 23C). These include the FKBP3 and FKBP4 proteins, which were enriched in the WT cells and may, therefore, play a role in the IAV lifecycle downstream of primary transcription. GO biological process terms revealed FKBP4 to be involved in protein folding, similar to HSP90 (Figure 23B and C). Another example of a novel interactor was RPAP2, which was enriched in both WT and ANP32-KO cells, suggesting that it may play a role in viral RNA transcription. Such a prediction fits well with its host function, where it supports the nuclear import of RNAP II, which is known to be important for viral transcription (Forget et al., 2013).

To validate the interaction between PB2 and host proteins identified in our screen, we performed IPs with two of the host proteins enriched in WT cells as bait: HMGB2 and RUVBL2. The biological rationale for selecting these two host proteins for validation of their interaction with PB2 is explained in the introduction of Chapter 3, where the functional significance of HMGB2 and RUVBL2 in the IAV lifecycle is investigated. We transfected eHAP WT and ANP32-KO cells with expression plasmids encoding HMGB2-FLAG and RUVBL2-FLAG, infected the cells with PR8 WT, performed IPs at 3hpi using the same conditions as for the differential interactome screen, such that three times as much cell lysate was used for the ANP32-KO cells. We analysed the inputs and IPs by western blot probing for PB2, FLAG (HMGB2/RUVBL2), and vinculin (Figure 24A-D). As expected, the higher amount of ANP32-KO cell lysate resulted in similar amounts of viral PB2 in the inputs from the two cell types, with only slightly more PB2 present in the WT cells (Figure 24A and C). The higher amount of ANP32-KO cell lysate also meant that more transfected HMGB2-FLAG and RUVBL2-FLAG were present in the ANP32-KO cell input than WT cell input. PB2 co-precipitated with both HMGB2 and RUVBL2. Consistent with the interactome data, more PB2 co-precipitated with either host protein in WT cells than in ANP32-KO cells. This occurred despite the lower amounts of HMGB2 and RUVBL2 bait in the WT cells. To take the small difference in PB2 inputs in the WT and ANP32-KO cells into account, we quantified and normalised the PB2 amount in the IP to that in the input (Figure 24B and D). This further corroborated that more PB2 co-precipitated with HMGB2 and RUVBL2 in WT cells than ANP32-KO cells. We decided to not include a GFP-FLAG negative background control, because we reasoned that the HMGB2-FLAG/RUVBL2-FLAG-transfected WT and ANP32-KO cells would serve as controls for each other since any host proteins non-specifically binding to the FLAG tag should do so in both cell types.

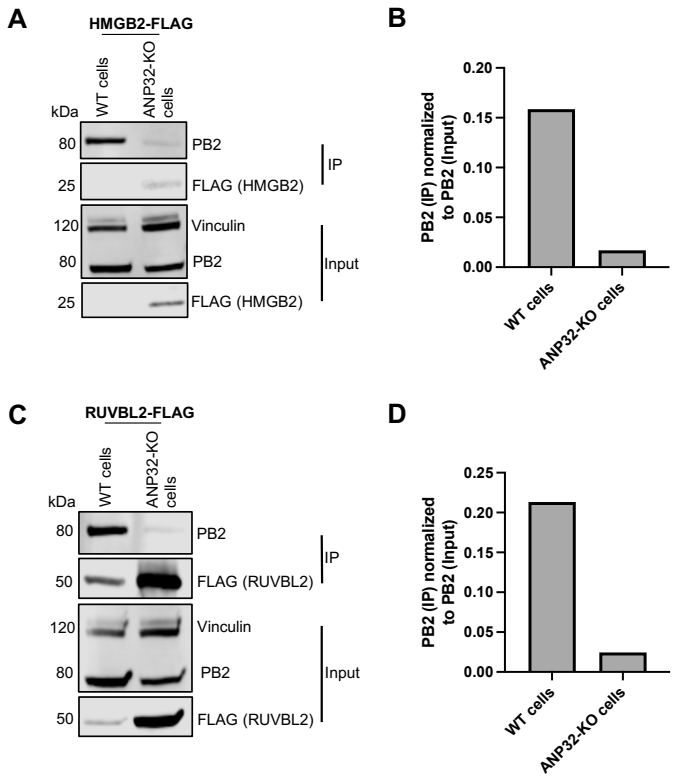

Figure 24. PB2 co-precipitates with HMGB2 and RUVBL2 to a greater extent in WT cells than ANP32-KO cells.
A and C) Western blot of inputs and FLAG IPs from eHAP WT and ANP32-KO cells transfected with HMGB2-FLAG (A) or RUVBL2-FLAG (C) and infected with PR8 WT (MOI=5). Cells were lysed at 3hpi. The blots were probed for PB2, FLAG (HMGB2/RUVBL2), and vinculin (cellular control) protein expression. B) Quantification of western blot in (A) shown as the amount of PB2 detected in the IP normalised to the amount of PB2 expression in the input. D) Quantification of western blot in (C) shown as the amount of PB2 detected in the IP normalised to the amount of PB2 expression in the input.

Section 2.2.6. siRNA validation reveals host proteins with proviral and antiviral roles in IAV infection.

We initially prioritised 13 of the 170 host proteins co-precipitating uniquely from WT cells for onwards validation based on various factors including host function, nuclear localisation, previous reports of polymerase subunit or NP interaction, or known role in the IAV lifecycle (Table 4). Considering that these host proteins were co-precipitated from WT cells but not ANP32-KO cells, we hypothesised that some of these host proteins are regulators of polymerase replicase activity.

Table 4. Host proteins enriched specifically in WT cells and their host function, localisation, and role in the IAV lifecycle.
Proteins in bold were previously identified in proteomic or genetic screens or previously shown to play a role in the IAV lifecycle. Proteins in green were selected for onwards validation as replication-specific host factors. Viral proteins are not shown.

GO term	Protein names	Role in IAV lifecycle
Biological process: ATP metabolic process	NDUFA9, NDUFV2, UQCRC1, PGAM1, STML2, HK1, PGK1, LDHA	N/A
Biological process: Regulation of protein ubiquitination	**UBR5**, UBQLN1, UBE2N, **PDCD6**	UBR5 identified as PA and PB2 interactor (Haas et al., 2023, York et al., 2014, Hubel et al., 2019, Watanabe et al., 2014). PDCD6 identified as PB2 interactor (Hubel et al., 2019). UBR5 and PDCD6 found to be proviral regulators of IAV lifecycle (Haas et al., 2023, Li et al., 2020).
Biological process: Regulation of translation initiation	**YTHDF2**, EIF4H, EIF4G2	YTHDF2 identified as PB2 interactor and proviral factor in IAV lifecycle (Courtney et al., 2017, York et al., 2014).
Biological process: RIG-I signalling pathway	**PHB1**, PHB2, **CLPB**	PHB1 shown to have a proviral role in IAV lifecycle (Watanabe et al., 2014). CLPB identified as a PB2 interactor (Hubel et al., 2019).
Biological process: Protein folding	**HSPA9**, **HSPA8**, HSPE1, **HSP90AA1**, **HSPD1**, **HSPA4**, **HSPB1**, **HSPA1B**, **DNAJA1**, **DNAJA2**, **DNAJA3**, **DNAJB11**, **BAG2**, FKBP4, CLPX, PDIA3, **P4HB**, CALR	Proteins in bold identified as polymerase interactors (Haas et al., 2023, Heaton et al., 2016, Watanabe et al., 2014, York et al., 2014, Hubel et al., 2019) or as regulators of the IAV lifecycle (Karlas et al., 2010, Konig et al., 2010, Cao et al., 2014, Naito et al., 2007). HSP90AA and DNAJA1 act as polymerase chaperones (Cao et al., 2014, Naito et al., 2007).
Biological process: Transcription	**POLR2B**, **POLR2C**, **POLR2D**, **POLR2E**, **POLR2G**, **POLR2H**, **POLR2L**, **SUPT5H**, TRIP13, ZC3H8, MAZ, **PTMA**	Proteins in bold identified as polymerase interactors (Haas et al., 2023, Heaton et al., 2016, Watanabe et al., 2014, York et al., 2014, Hubel et al., 2019) or as regulators of the IAV lifecycle (Karlas et al., 2010, Konig et al., 2010, Shapira et al., 2009). Host RNAPII is important for viral transcription (Engelhardt et al., 2005).
Cellular component: Nuclear envelope	IPO8, **DHRS2**, **KPNA3**, CACYBP, **LBR**, **EMD**, RTN4, CLIC1, **HAX1**, RB1CC1	Proteins in bold shown to be polymerase interactors (Heaton et al., 2016, York et al., 2014, Hubel et al., 2019, Hsu et al., 2013) or regulators of IAV lifecycle (Hsu et al., 2013, Karlas et al., 2010).
Cellular component: Nucleolus	NOL6, STAU2, **MAGED2**, ZNF622, PIN4, **AKAP8**, CDKN2AIPNL, HJURP, **RBM14**, VRK1, PHF8, **SNRPB2, TIMM44, TP53,** ZNF622, **SNRPB2**	Proteins in bold identified as polymerase (Heaton et al., 2016, York et al., 2014, Watanabe et al., 2014). RBM14 shown to have a proviral role in IAV polymerase activity (Bortz et al., 2011). TIMM44 and TP53 shown to be regulators of the IAV lifecycle (Karlas et al., 2010, Shapira et al., 2009).

Cellular component: Prohibitin complex	**PHB1**, PHB2	PHB1 shown to have a proviral role in IAV lifecycle (Watanabe et al., 2014).
Cellular component: Proteasome core complex	**PSMA1**, PSMA2, PSMA3, PSMB1, PSMB5, PSMB4	PSMA1 identified as PB2 interactor and proviral factor in IAV lifecycle (Karlas et al., 2010, Watanabe et al., 2014).
Cellular component: R2TP complex	**RUVBL1**, **RUVBL2**	Identified as interactors of PB2, PB1, and NP (Haas et al., 2023, Heaton et al., 2016, Kakugawa et al., 2009, Mayer et al., 2007, Watanabe et al., 2014). Shown to be regulators of IAV lifecycle (Haas et al., 2023, Kakugawa et al., 2009).
Cellular component: RNA polymerase II	**POLR2B**, **POLR2C**, **POLR2D**, **POLR2E**, **POLR2G**, **POLR2H**, **POLR2L**	Proteins in bold identified as polymerase interactors (Haas et al., 2023, Heaton et al., 2016, Watanabe et al., 2014, York et al., 2014, Hubel et al., 2019) or as regulators of the IAV lifecycle (Karlas et al., 2010).
Other	SEC63, HISTH2B, SPC25, SSR1, PRKCSH, RALA, SARS2, GPC4, **CLUH**, TLN1, HADHB, ECHS1, PYCR1, RAD23B, CAP1, SLC16A1, **CSTF3**, NME1, NSDHL, GTPBP6, ME2, **MLF2**, SDF4, **SAE1**, **PPM1G**, ZC3H11A, HARS, ESD, NES, PDS5A, GPN3, CNN2, **AIFM1**, PHKG2, CALM, PFN1, CS, MDH2, ACO2, MYEF2, PEBP1, ATIC, **ALDH18A1**, OAT, RCN1, RAB2, SMS, SNX2, SARNP, PSAT1, TECR, THAP11, **ALDH1B1**, PMPCB, **MAP1B**, PDHB, KIF23, SNRPG, **TUFM**, PAPSS1, **AHNAK**, FKBP3, CNDP2, SF1, AP4S1, ERAL1, **CALU**, SEPTIN-9, BLVRA, ACTA1, SMARCE1, RAB1, HDGF, ANXA5, TFRC, **GLUD1**, C4, ETFA, **CYCS**, FUBP1, ENAH, TALDO1, MACF1, AURKA, GSTP1, AMD1, **HMGB1, HMGB2**	Proteins in bold shown to be polymerase interactors (Haas et al., 2023, Heaton et al., 2016, Moisy et al., 2012, Watanabe et al., 2014, York et al., 2014, Hubel et al., 2019, Mayer et al., 2007) or regulators of IAV lifecycle (Konig et al., 2010, Shapira et al., 2009, Moisy et al., 2012, Karlas et al., 2010).

To functionally validate a role for these PB2 interactors in virus infection, we made use of a recombinant PR8 virus that expresses a ZsGreen fluorophore on segment 8 (PR8 NS-ZsGreen), which we generated using the pHW2000 plasmid-based reverse genetics system described in Section 2.2.2 (Figure 25A). The ZsGreen virus synthesises three proteins from segment 8: NS1, ZsGreen, and NS2. ZsGreen is a similar fluorescent protein to GFP but produces a brighter and more stable signal. A PR8 NS-ZsGreen virus, generated using the same NS-ZsGreen plasmid used here, has previously been used to study how viral antigens are transferred from conventional dendritic cells to resident dendritic cells in lymph nodes in infected mice (Pirillo et al., 2023).

Having generated the recombinant virus, we confirmed that visualising ZsGreen can be used in place of staining for NP as a measure of the success of virus infection. eHAP WT cells were infected with PR8 NS-ZsGreen, cells were fixed, stained for NP and DAPI, and imaged at 24hpi (Figure 25B). The ZsGreen signal was present in all cells positive for NP, suggesting that the PR8 NS-ZsGreen virus is a useful tool for directly determining the success of an infection without needing to fix and stain the cells. Next, we performed a multi-cycle time course with the PR8 NS-ZsGreen virus in A549 cells. As expected, the ZsGreen count increased with time (Figure 25C). We decided to use the 48hpi timepoint in future validation experiments because at this timepoint there was capacity for the ZsGreen count to decrease or increase following knockdown of proviral or antiviral factors, respectively.

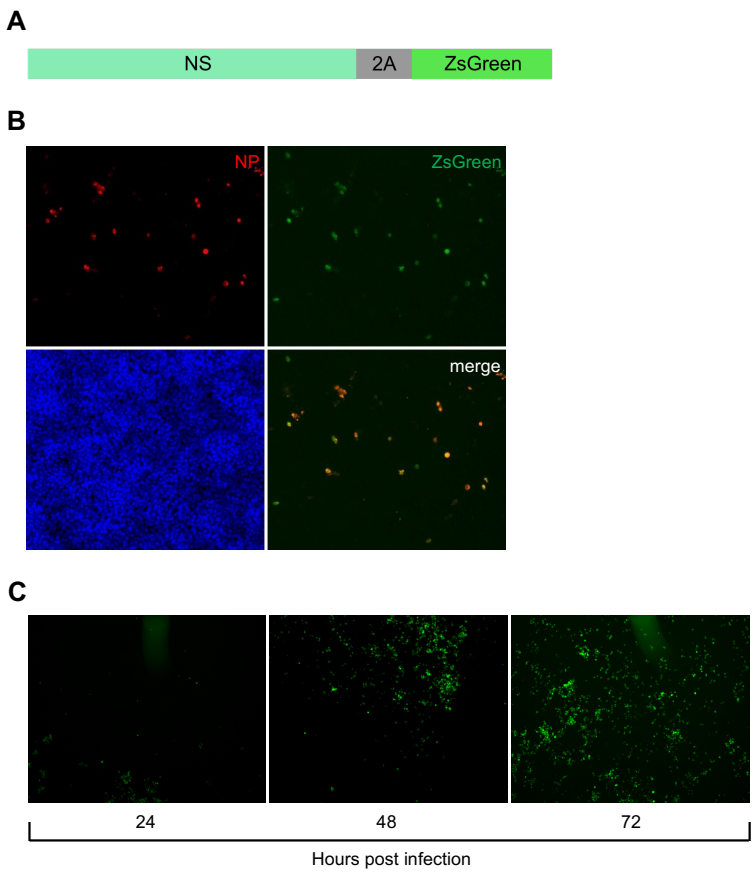

Figure 25. Generation and characterisation of PR8 NS-ZsGreen influenza virus.
A) Schematic showing the design of the PR8 NS-ZsGreen segment. ZsGreen is encoded downstream of the NS1 protein and the two are separated by a 2A linker. B) Immunofluorescence of eHAP WT cells infected with PR8 NS-ZsGreen (MOI=0.5), fixed at 24hpi, and stained for NP and DAPI. C) Immunofluorescence of A549 cells infected with PR8 NS-ZsGreen (MOI=0.1) in a multi-cycle infection and imaged at indicated timepoints post infection. B and C) Images are representative fields of view, visualised using an M5000 EVOS microscope and 10x objective (B) or 4x objective (C).

To assess the effect of knockdown of the 13 selected host proteins in IAV infection, we employed siRNA pools targeting each of the genes (Figure 26A). As a positive control for proviral host factors, two separate siRNA pools targeting both ANP32A and ANP32B were used. Targeting both ANP32A and ANP32B was necessary because the two are functionally redundant in their support for RNA replication (Staller et al., 2019, Zhang et al., 2019).

A549 cells were transfected with the siRNA pools targeting each of the selected genes, a non-targeting siRNA control (siNT), and the siRNA pools targeting both ANP32A and ANP32B (siANP32.1 and siANP32.2). The cells were then infected with PR8 NS-ZsGreen and the impact of each gene knockdown on virus growth was determined by imaging and quantification of ZsGreen at 48hpi (Figure 26A). Knockdown of ANP32A and ANP32B significantly reduced virus replication compared to siNT. Knockdown of six of the genes (FKBP4, FUBP1, HMGB2, PIN4, RBM14, and RUVBL2) also resulted in a significant reduction in virus replication compared to siNT, suggesting these host proteins to be proviral. Depletion

of most of these genes resulted in a similar decrease in virus replication as knockdown of ANP32A and ANP32B, while depletion of RBM14 reduced virus growth to an even greater extent. Knockdown of CLUH, which has previously been shown to be proviral, RUVBL1, and VRK1, also reduced virus growth, but the reduction did not reach significance compared to siNT (Ando et al., 2016). In contrast, knockdown of MAZ significantly increased virus replication, suggesting this host protein to be antiviral. Cell viability was measured using a CellTiter-Glo luminescent cell viability assay and a 70% cell viability threshold was applied. A threshold of 70% was selected as this is commonly used in siRNA screens as the cell viability cut-off (Martin-Sancho et al., 2021). Cell viability remained above 90% following each gene knockdown, confirming that the effects on virus replication were a result of gene knockdown and not toxicity (Figure 26B). The level of gene expression was determined at the mRNA level by qPCR (Figure 26C). Most siRNA pools resulted in at least 80% gene knockdown compared to siNT, except for the siRNA pools targeting AHNAK, FUBP1, RBM14, and SUPT5H, which resulted in closer to 65% gene knockdown. Collectively, our data revealed seven regulators of IAV infection, six of which were proviral, one of which was antiviral, and two of which (RUVBL2 and RBM14) have previously been shown to be regulators of the IAV lifecycle (Bortz et al., 2011, Kakugawa et al., 2009, Haas et al., 2023).

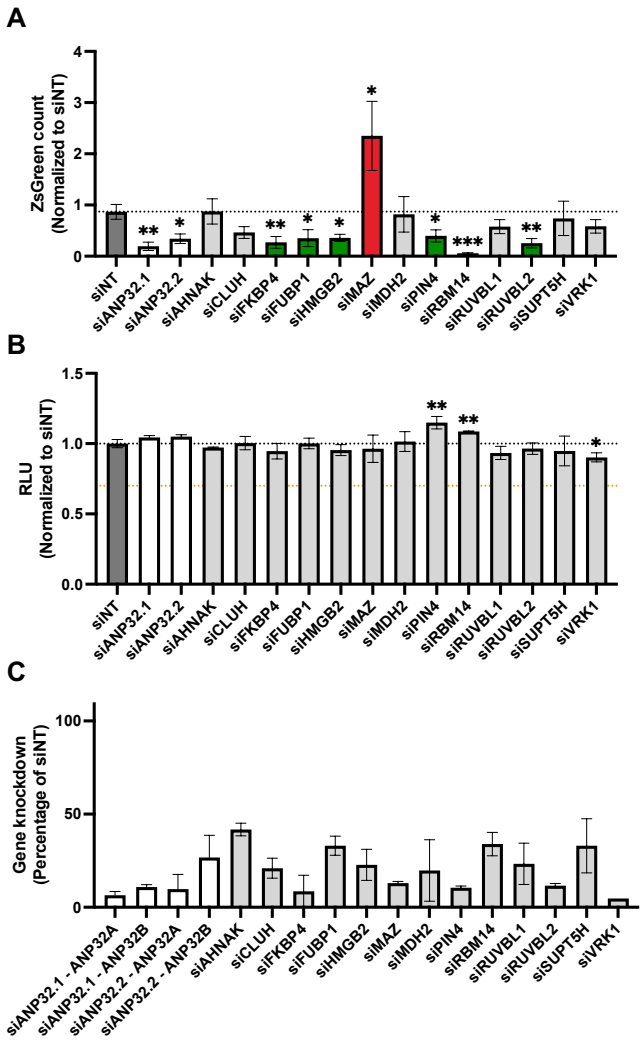

Figure 26. siRNA knockdown reveals host proteins with proviral and antiviral roles in IAV infection.

A) Virus replication in A549 cells transfected with a non-targeting siRNA (siNT), two siRNA pools targeting both ANP32A and ANP32B (siANP32.1 and siANP32.2), or siRNA pools targeting 13 genes enriched in WT cells only. Cells were infected with PR8 NS-ZsGreen (MOI=0.1) in a multi-cycle infection and entire wells were imaged at 48hpi using an M5000 EVOS microscope. The ZsGreen count was quantified using ImageJ. Proviral factors are shown in green and antiviral factors are shown in red. Data is shown as mean ± SEM of n=3 biological repeats performed in triplicate. B) Cell viability following siRNA transfection, determined using a CellTiter-Glo assay. Luciferase activity (RLU) was normalised to siNT. Black dotted line indicates cell viability of siNT-treated cells. Orange dotted line indicates 70% cell viability threshold. Data is shown as mean ± SD of n=3 technical repeats, representative of n=3 biological repeats. C) mRNA levels of target genes following siRNA transfection determined by qPCR. Data is shown as the percentage gene knockdown relative to mRNA levels in cells transfected with siNT. Data is mean ± SD of n=3 technical repeats. For panels B and C: Statistical significance was assessed compared to siNT using an unpaired *t* test. *, $p<0.05$; **, $p<0.01$; ***, $p<0.001$.

Section 2.2.7. siRNA validation reveals host proteins with proviral and antiviral roles in polymerase activity.

Our AP-MS screen was focused on the interactome of PB2, the main function of which is as part of the heterotrimeric viral polymerase complex. We, therefore, next wanted to assess whether the PB2 interactors play a role in polymerase activity. In addition to the 13 host factors functionally characterised in Figure 26, we also selected 17 more host proteins co-precipitating uniquely from WT cells for onwards validation. As mentioned previously, we hypothesised that some of these interactors would be replication-specific host factors as they were uniquely enriched in the PB2 interactome in WT cells. We also selected two host proteins enriched in both WT and ANP32-KO cells for onwards validation. We hypothesised that these interactors may be transcription-specific host factors, given that viral transcription can occur in both cell types. Again, selections were made based on host function, cellular localisation, and previous association with the IAV lifecycle (Tables 4 and 5).

Table 5. Host proteins enriched in ANP32-KO cells and their host function, localisation, and role in the IAV lifecycle.
Proteins enriched in both WT and ANP32-KO cells as well as ANP32-KO cells alone are included. Proteins in bold were previously identified in proteomic or genetic screens or previously shown to play a role in the IAV lifecycle. Proteins in blue were selected for onwards validation as transcription-specific host factors. Viral proteins are not shown.

GO term	Protein names	Role in IAV lifecycle
Biological process: Transcription	**POLR2A**, **POLR2I**, **POLR2J**, RPAP2	Proteins in bold identified as polymerase interactors (Heaton et al., 2016). Host RNAPII is important for viral transcription (Engelhardt et al., 2005).
Cellular component: RNA polymerase II	**POLR2A, POLR2I, POLR2J,** RPAP2	Proteins in bold identified as polymerase interactors (Heaton et al., 2016). Host RNAPII is important for viral transcription (Engelhardt et al., 2005).
Other	**SEC61B, PJA2**, **MAGED1**, **RNF219**, **AKAP8L**, **HSBP1**	Proteins in bold shown to be polymerase interactors (Haas et al., 2023, Watanabe et al., 2014, York et al., 2014, Hubel et al., 2019).
Biological process: ATP metabolic process	NDUFAB1	N/A
Cellular component: Nucleolus	CSTB, GOLGA3	N/A
Other	**HIST1H2A**, MYO5B, MYL1, SNRPG, RPL26L1	HIST1H2A shown to be regulator of IAV infection (Shapira et al., 2009).

To measure polymerase activity, eHAP WT cells were used instead of A549 cells as in Figure 26, because they are more amenable to plasmid transfection and therefore more reliable for minigenome reporter assays. eHAP WT cells were transfected with siNT, siANP32.1, siANP32.2, or siRNA pools targeting each of the selected genes (Figure 27A). Polymerase activity was then measured using a minigenome reporter assay (see Section 2.2.2, Figure 18B). This gives a measure of total polymerase activity as both transcription and replication of the viral-like reporter RNA is necessary to produce a luciferase signal. Knockdown of ANP32A and ANP32B significantly reduced polymerase activity compared to siNT, as expected (Figure 27A). Knockdown of ten of the genes (CLUH, FKBP4, FUBP1, HMGB2, PIN4, RBM14, RUVBL1, RUVBL2, AKAP8L, and RPAP2) also resulted in a significant loss of polymerase activity, suggesting that these host proteins play supportive roles in polymerase activity. The proviral host proteins enriched in WT cells are shown in green and proviral host proteins enriched in both cell types are shown in blue. Of these, six (FKBP4, FUBP1, HMGB2, PIN4, RBM14, and RUVBL2) had also been found to support viral infection in A549 cells using the PR8 NS-ZsGreen virus readout (Figure 26A). A role in IAV infection of AKAP8L and RPAP2 was not tested. Knockdown of five of the genes (AHNAK, MAZ, MDH2, VRK1, and SUPT5H), shown in red, increased polymerase activity, suggesting that these host proteins play restrictive roles in polymerase activity (Figure 27A). Of these, MAZ had been found to have a restrictive role in viral infection (Figure 26A). Gene knockdown did not reduce cell viability by more than 80% compared to siNT (Figure 27B). Efficient gene knockdown was confirmed by qPCR at the mRNA level (Figure 27C). Most siRNA pools resulted in at least 70% gene knockdown, compared to siNT, except for the siRNA pools targeting KPNA3 and ZNF622, which resulted in closer to 60% gene knockdown, and siRNA pools targeting AKAP8L, IPO8, and ZC3H8, which resulted in closer to 40% gene knockdown. We only measured the cell viability and gene knockdown levels with the siRNA pools not already validated in Figure 26, although this had been performed in A549 cells so we cannot exclude that there was some cell type specific cytotoxicity that we did not probe. Together, our data identified eight putative replication-specific proviral factors, two putative transcription-specific proviral factors, and five putative replication-specific antiviral factors.

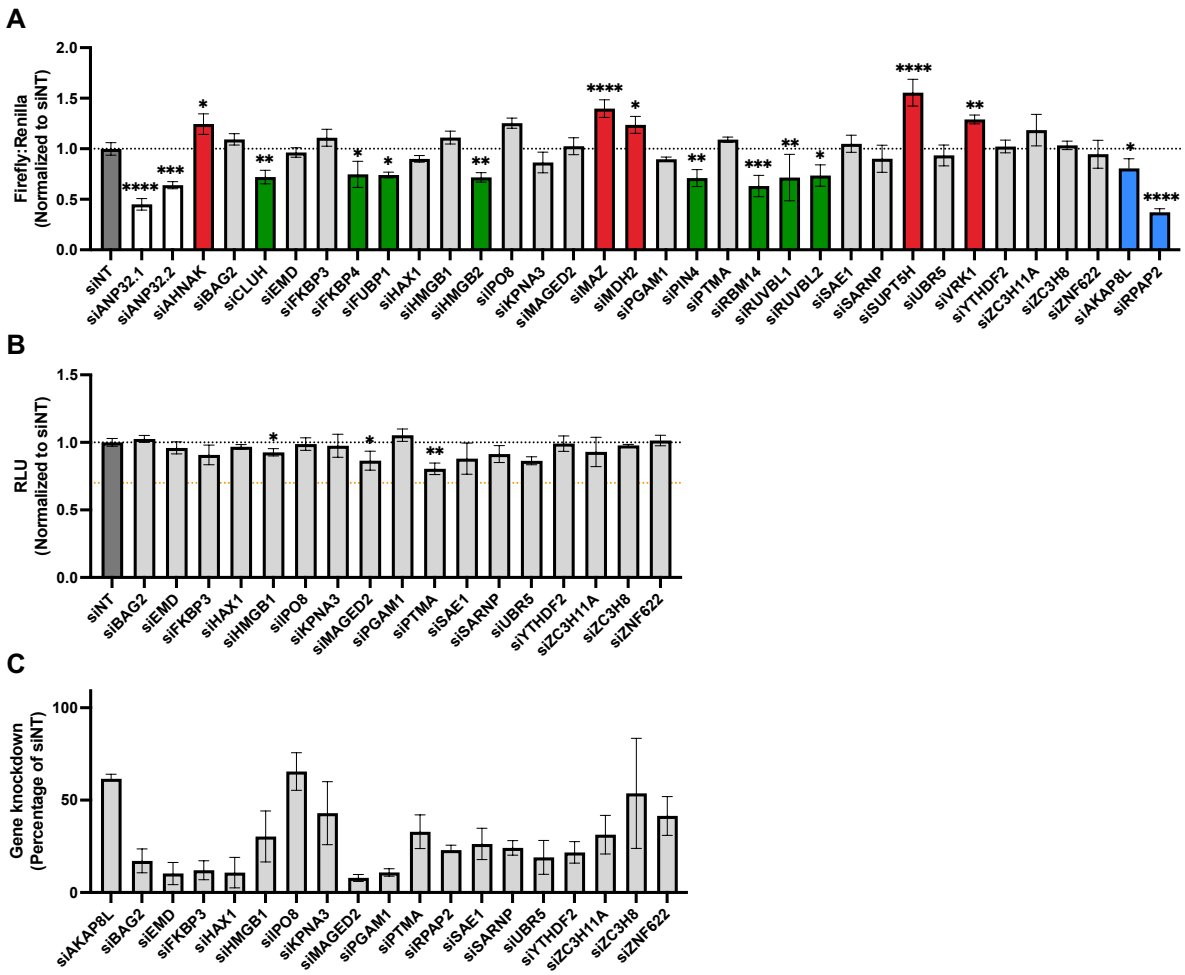

Figure 27. siRNA knockdown reveals host proteins with proviral and antiviral roles in polymerase activity.

A) Minigenome reporter assay in eHAP WT cells transfected with a non-targeting siRNA (siNT), two siRNA pools targeting both ANP32A and ANP32B (siANP32.1 and siANP32.2), or siRNA pools targeting 30 genes enriched in WT cells only or 2 genes enriched in both WT and ANP32-KO cells. Cells were transfected with expression plasmids to reconstitute PR8 polymerase activity. Firefly luciferase activity relative to co-transfected Renilla luciferase levels was normalised to siNT. Putative proviral replication factors are shown in green, proviral transcription factors in blue, and antiviral replication factors in red. Data is shown as mean ± SD of n=3 biological repeats performed in triplicate. B) Cell viability following siRNA transfection, determined using a CellTiter-Glo assay. Luciferase activity (RLU) was normalised to siNT. Black dotted line indicates cell viability of siNT-treated cells. Orange dotted line indicates 70% cell viability threshold. Data is shown as mean ± SD of n=3 technical repeats, representative of n=3 biological repeats. C) mRNA levels of target genes following siRNA transfection determined by qPCR. Data is shown as the percentage gene knockdown relative to mRNA levels in cells transfected with siNT. Data is mean ± SD of n=3 technical repeats. For panels A and B: Statistical significance was assessed compared to siNT using an unpaired *t* test. *, $p<0.05$; **, $p<0.01$; ***, $p<0.001$; ****, $p<0.0001$.

Section 2.2.8. The interactome of ANP32 is different in the presence and absence of IAV infection.

We also developed a second differential interactome screen as a complementary approach to identifying replication-specific cofactors. This screen compared the interactome

of ANP32 in the presence and absence of IAV infection. Considering that ANP32 is essential specifically for RNA replication, we hypothesised that host proteins co-precipitating with ANP32 during infection could be replication-specific cofactors that perhaps work in conjunction with ANP32 (Nilsson-Payant et al., 2022, Swann et al., 2023, Staller et al., 2019, Sugiyama et al., 2015).

eHAP ANP32-KO cells were transfected with huANP32B-FLAG or GFP-FLAG, as a control to eliminate any host proteins non-specifically binding to the FLAG tag (Figure 28A and B). The ANP32-KO cells transfected with GFP-FLAG were also transfected with untagged huANP32B to allow replication of IAV in these cells (Figure 28B). We decided to use the ANP32-KO cells because these provide a cleaner system than WT cells as no endogenous ANP32 is present. The transfected cells were then infected with PR8 WT or mock-infected, huANP32B-FLAG or GFP-FLAG were immunoprecipitated, and the co-precipitating host proteins were identified by MS (Figure 28A and B). The infection and AP conditions employed were the same as for the differential interactome screen described in Section 2.2.5 to make the two screens comparable.

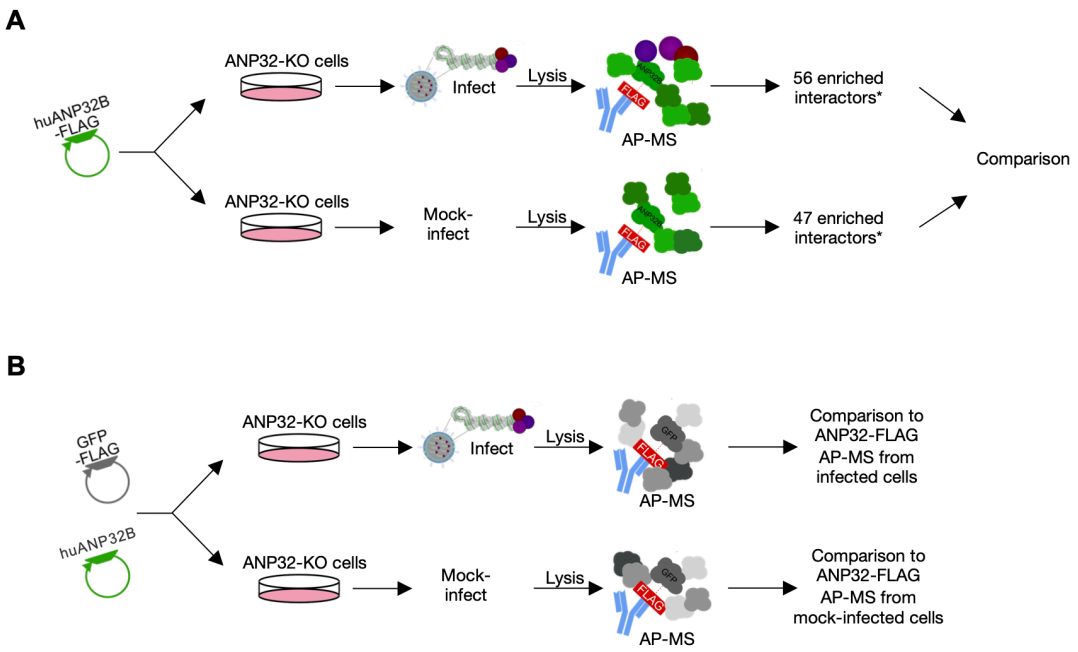

Figure 28. Schematic of differential AP-MS strategy using ANP32B as bait.
A) Schematic of AP-MS strategy to compare the interactome of ANP32B in infected and uninfected cells. eHAP ANP32-KO cells are transfected with an expression plasmid encoding FLAG-tagged human ANP32B (huANP32B-FLAG), infected with PR8 WT (MOI=5) or mock-infected, lysed in lysis buffer containing 0.2% NP-40 detergent at 3hpi, immunoprecipitated using FLAG magnetic beads, washed in 4x lysis buffer and 4x TBS, and then analysed by MS. * = number of proteins enriched above background (GFP-FLAG-transfected cells) (B) in infected and mock-infected cells. B) Schematic of how non-specific binding to the FLAG tag is determined. IPs are performed as in (A), but with transfection of a plasmid encoding GFP-FLAG instead. A plasmid encoding untagged huANP32B is co-transfected as well to allow replication of IAV in the control samples.

Screens were conducted three independent times. Overall, the relative quantities of the proteins co-precipitating with ANP32B-FLAG under infected and uninfected conditions were lower than for the differential interactome screen with PB2-FLAG as bait. This is perhaps due to low transfection efficiency of the ANP32-KO cells, such that little ANP32B-FLAG bait was available. We were, therefore, unable to analyse the dataset using the same method as previously. Instead, host and viral proteins were classified as interactors based on the fold change (FC) in their abundance in ANP32B-FLAG-transfected samples compared to GFP-FLAG transfected samples for each infected or uninfected condition. The threshold applied was FC=2, p-value=0.2. The raw and processed data is provided in Appendix B.

Using these criteria, 48 host proteins were co-precipitated in the presence of infection, 39 host proteins in the absence of infection, and 8 host proteins were common to both infected and uninfected conditions (Figure 29A). No viral proteins co-precipitated with ANP32B, which is surprising considering the known interaction between ANP32 and the polymerase heterotrimer and NP (Figure 29C) (Mistry et al., 2020, Wang et al., 2022a, Baker et al., 2018, Domingues and Hale, 2017, Sugiyama et al., 2015, Bradel-Tretheway et al., 2011). The ANP32B-PB2 interaction was also previously detected using similar IP and infection conditions in this study (see Section 2.2.3, Figure 19C). Considering that the interaction between ANP32 and viral proteins is thought to be transient, it is possible that under the exact conditions employed here, the ANP32B-PB2 interaction was missed or disrupted during the IP.

A

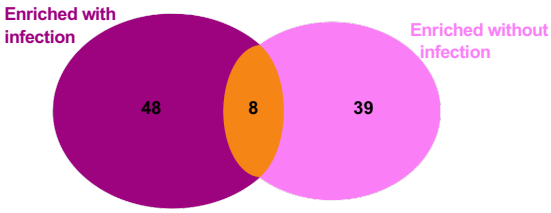

B

Category	GO term	P-value
Cellular component	Chromosome	0.0024
	Nucleolus	3.4E-4
Biological process	Chromosome organisation	0.0083
	Nucleocytoplasmic transport	7.35E-5

C

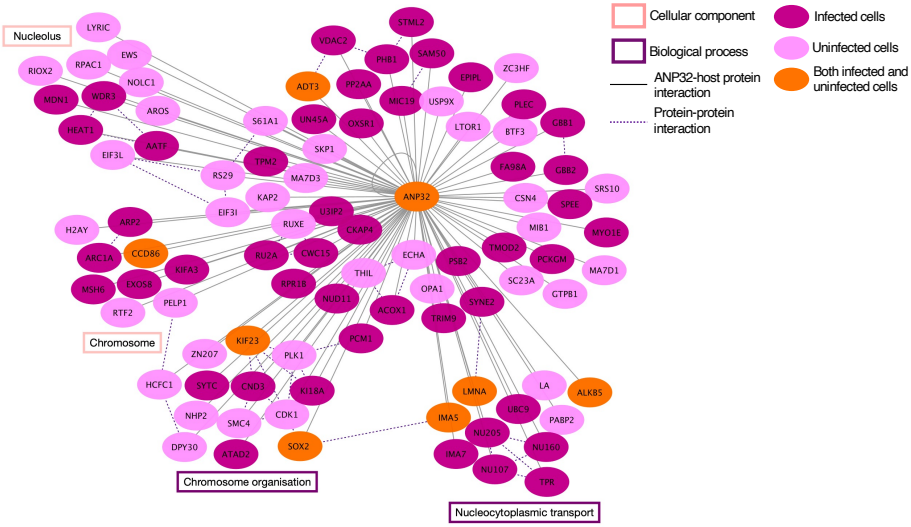

Figure 29. The interactome of ANP32B is different in the presence and absence of infection. A) Venn diagram comparing the number of proteins enriched above background in the ANP32 interactome under infected and uninfected conditions. B) P-values associated with classification of host proteins based on GO cellular component and biological process terms. GO terms were determined using the StringApp in Cytoscape. C) Interaction network between ANP32B (orange, filled) and 48 host proteins in the presence of infection (magenta, filled), 39 proteins in the absence of infection (pink, filled), and 7 proteins under both infected and uninfected conditions (orange, filled). Host protein-protein interactions (purple dotted lines) were predicted using STRING. Proteins are clustered based on GO cellular component (coral squares) or biological process (purple squares) terms. Protein interaction network was generated using Cytoscape v.3.10.2.

Additionally, the little overlap between the host proteins co-precipitating under infected and uninfected conditions was surprising (Figure 29A). There are several factors that could explain this. Firstly, it is possible that the state and proteome of the host cell was altered upon infection, making the infected and uninfected conditions difficult to compare. Secondly, it is also possible that unequal amounts of ANP32 bait were available in the infected and uninfected conditions due to variable transfection efficiency of the eHAP ANP32-KO cells. This could explain why PP2AA (PP2A) was found to co-precipitate with ANP32 only in the presence of infection (Figure 29C). ANP32B has previously been shown to interact directly with PP2A and inhibit its activity, modulating the DNA damage response in the host cell (Rivero-Rodriguez et al., 2021). This is similar to ANP32A which is a well-known PP2A inhibitor (Li et al., 1995). We would, therefore, expect the ANP32B-PP2A interaction to also occur in the

uninfected condition. Thirdly, as mentioned above, in our previous work we have found proteins to non-specifically bind to the GFP in the GFP-FLAG control, such that some real interactors may have been eliminated because they appeared in the background IPs. If time had allowed, the screen would have been repeated using a different control or more stringent washes. Alternatively, it would also be interesting to reanalyse the dataset and directly compare the interactome of ANP32 in the presence and absence of infection, without taking the GFP-FLAG background control into account. This would employ the same logic as in Figure 24, namely that the ANP32-FLAG transfected cells should serve as controls for each other since any host proteins non-specifically binding to the FLAG tag should do so in both the presence and absence of infection.

Even so, GO cellular component and biological process terms revealed that some of the ANP32 interactors in both infected and uninfected cells are associated with chromosome activities and nucleocytoplasmic transport, which fits well with the known cellular role of ANP32 in regulating chromatin architecture (Figure 29B and C) (Reilly et al., 2014). One of the chromosome-associated proteins that co-precipitated with ANP32B in the absence of infection was H2AY. This is consistent with previous reports of ANP32 proteins having histone chaperone activity (Reilly et al., 2014). In particular, a recent study showed ANP32B to be a chaperone of macroH2A histones (also known as H2AY), aiding their incorporation into chromatin (Mandemaker et al., 2023). It is possible that the IAV polymerase co-opts ANP32 away from some of its histone chaperone activities, such that the interaction with H2AY would only occur in the absence of infection.

Despite the lack of viral proteins in the ANP32 interactome, some of the host proteins enriched in the presence of infection or common to both infected and uninfected conditions, may be host proteins that work in conjunction with ANP32 to support viral RNA replication. In support of this, one of the host proteins co-precipitating with ANP32 in the presence of infection was EXOSC8 (Figure 29C). This host protein was previously shown to co-precipitate with the IAV polymerase under conditions where RNA replication is supported (PB2 672K polymerase in human cells or PB2 627E polymerase in human cells supplemented with chANP32A) but not when it was restricted (PB2 627E polymerase in human cells), suggesting that it plays a role in polymerase replicase activity (Mistry, 2019). Furthermore, members of the IMPα family also co-precipitated with ANP32 in infected cell lysates (Figure 29C). This included IMPα7, which has previously been shown to interact with ANP32 during IAV infection and support viral polymerase activity (Yu et al., 2022). IMPα5, which has been shown to interact with PB2 and NP, also co-precipitated with ANP32 under infected and uninfected conditions (Resa-Infante et al., 2008, Hudjetz and Gabriel, 2012, Tarendeau et al., 2007). Although several factors have limited the conclusions that can be drawn from the differential

ANP32 interactome, the co-precipitation of previously identified IAV cofactors lends some confidence to the dataset.

Section 2.2.9. PHB1 and STML2 co-precipitate with both ANP32 during infection and PB2 in WT cells.

To pinpoint which host proteins might be co-opted to support viral RNA replication, the host proteins enriched in the ANP32 interactome during infection were compared to the host proteins enriched in the PB2 interactome in WT cells only (Figure 30B). Host protein-protein interactions predicted using STRING revealed that many of the host proteins identified in the two screens interact with each other, potentially suggesting that similar complexes were co-precipitated with PB2 and ANP32. Moreover, GO analysis revealed that many of the proteins belong to the same GO cellular component and biological process terms (Figure 30A). For instance, many of the proteins were involved in protein folding and nuclear export processes and/or are components of the nuclear envelope and nucleolus. Host proteins PHB1 and STML2 co-precipitated with both PB2 in WT cells only and ANP32 during infection (Figure 30B). This direct overlap suggests that these two host proteins may play a role in RNA replication perhaps via a mechanism that involves ANP32.

A

Category	GO term	P-value
Cellular component	Nuclear envelope	6.64E-7
	Nucleolus	3.1E-4
	Prohibitin complex	0.0178
	Proteasome complex	3.73E-7
	RNA polymerase II	6.9E-4
Biological process	Nuclear export	1.7E-4
	Protein folding	2.01E-8

B

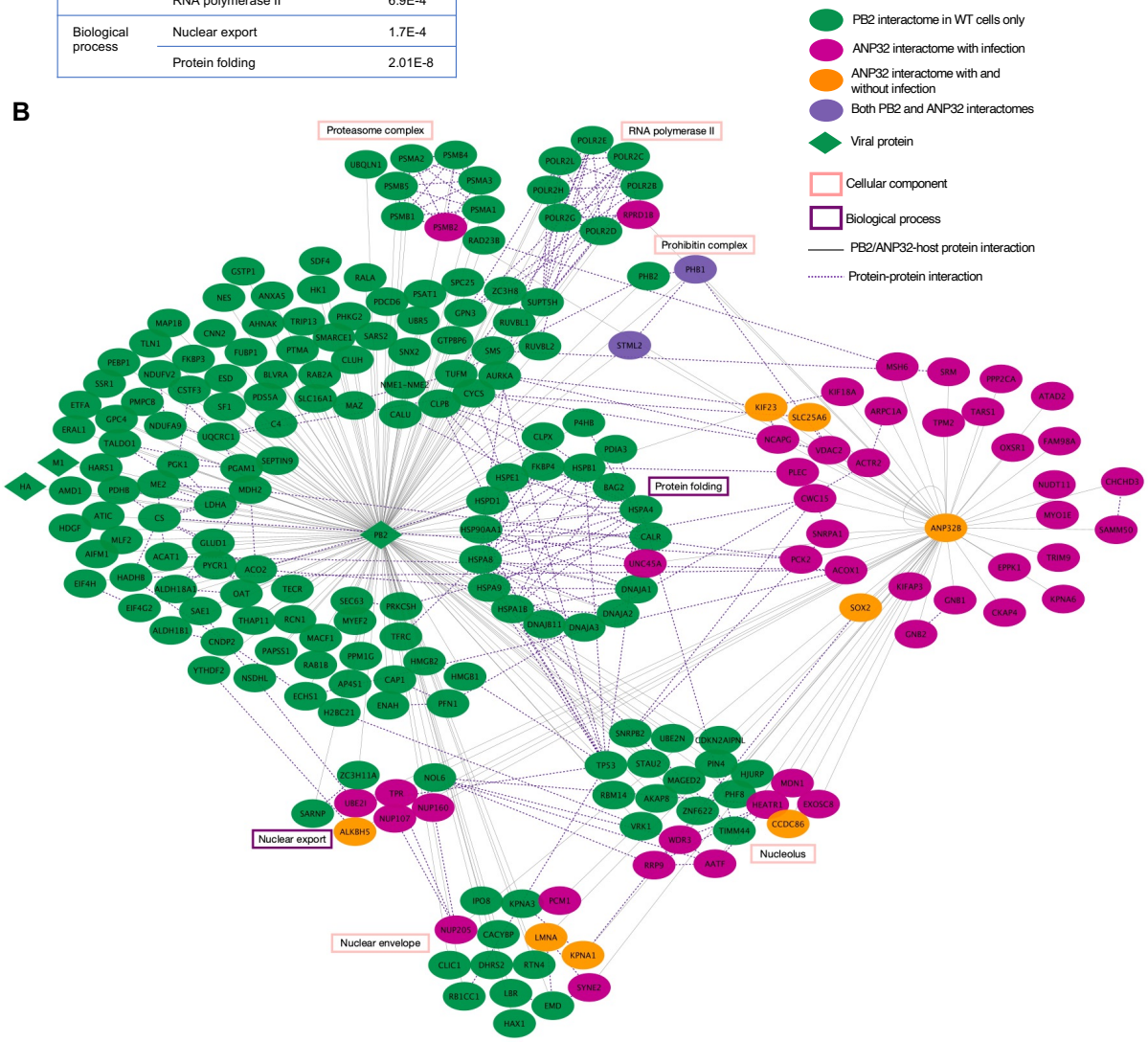

Figure 30. PHB1 and STML2 co-precipitate with both PB2 in WT cells and ANP32B during infection.

A) P-values associated with classification of host proteins based on GO cellular component and biological process terms. GO terms were determined using the StringApp in Cytoscape. B) Interaction network comparing the host proteins co-precipitating with PB2 in WT cells only and huANP32B in the presence of infection. The network shows proteins co-precipitating with PB2 in WT cells (green, filled), ANP32B in the presence of infection (magenta, filled), ANP32B in both the presence and absence of infection (orange, filled) or both PB2 and ANP32B (purple). Host protein-protein interactions (purple dotted lines) were predicted using STRING. Proteins are clustered based on GO cellular component (coral squares) or biological process (purple squares) terms. Protein interaction network was generated using Cytoscape v.3.10.2.

Next, we sought to functionally validate a role for PHB1 and STML2 in polymerase activity. PHB1 exists as a prohibitin (PHB) complex together with PHB2 in the host cell. PHB2 was not identified as an ANP32 interactor but was shown to interact with PB2 in WT cells only (Figure 23C). We, therefore, decided to also validate the role of PHB2 in polymerase activity. To achieve this, eHAP WT cells were transfected with siNT, siANP32.1, siANP32.2, an siRNA pool targeting STML2, two individual siRNAs targeting PHB1 (PHB1.1 and PHB1.2), or two individual siRNAs targeting PHB2 (PHB2.1 and PHB2.2) and polymerase activity was measured (Figure 31A). We employed individual siRNAs to target PHB1 and PHB2 because pooled siRNAs targeting each of PHB1 and PHB2 reduced the cell viability by more than 50% (data not shown). Knockdown of ANP32A and ANP32B significantly reduced polymerase activity compared to siNT, as expected (Figure 31A). Knockdown of PHB1 and PHB2 also significantly reduced polymerase activity compared to siNT. This was observed for both of the individual siRNAs targeting PHB1 or PHB2 and suggests these two host proteins to play a supportive role in polymerase activity. In contrast, depletion of STML2 had no effect on polymerase activity.

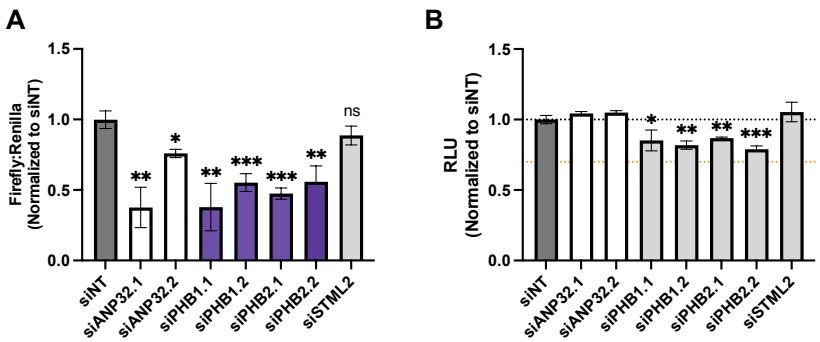

Figure 31. siRNA validation shows PHB1 and PHB2 to have proviral roles in polymerase activity. A) Minigenome reporter assay in eHAP WT cells transfected with a non-targeting siRNA (siNT), two siRNA pools targeting both ANP32A and ANP32B (siANP32.1 and siANP32.2), an siRNA pool targeting STML2, or two individual siRNAs targeting each of PHB1 (PHB1.1 and PHB1.2) and PHB2 (PHB2.1 and PHB2.2). Firefly luciferase activity relative to co-transfected Renilla luciferase levels was normalised to siNT. Data is shown as mean ± SD of n=3 biological repeats performed in triplicate. B) Cell viability following siRNA transfection, determined using a CellTiter-Glo assay. Luciferase activity (RLU) was normalised to siNT. Black dotted line indicates cell viability of siNT-treated cells. Orange dotted line indicates 70% cell viability threshold. Data is shown as mean ± SD of n=3 technical repeats, representative of n=3 biological repeats. Statistical significance was assessed compared to siNT using an unpaired *t* test. *, $p<0.05$; **, $p<0.01$; ***, $p<0.001$.

Cell viability remained above the 70% threshold following each gene knockdown but was nevertheless significantly reduced following knockdown of PHB1 and PHB2 compared to siNT (Figure 31B). As mentioned above, a threshold of 70% was selected as this is commonly used in siRNA screens as the cell viability cut-off (Martin-Sancho et al., 2021). The lower cell viability was already taken into account when measuring the impact on the polymerase activity,

because minigenome reporter assay data is shown as the Firefly luciferase activity normalised to the Renilla luciferase control, and Renilla luciferase would be impacted by any reduction in the cell viability. However, the slightly reduced cell viability may become an issue when studying the role of PHB1 and PHB2 in assays that lack a Renilla luciferase cellular control.

Section 2.3. Discussion

Section 2.3.1. Differential interactome screen to identify transcription- and replication-specific host factors.

In this chapter, we aimed to establish a differential AP-MS strategy that allows the host factors that regulate polymerase replicase versus transcriptase activity to be distinguished. To achieve this, we made use of a recombinant influenza virus that expresses a FLAG tag on PB2 to compare the polymerase interactome in two different cell types (WT and ANP32-KO cells) in the context of infection. Comparison of the PB2 interactome in the ANP32-KO cells, where only steps up to and including primary viral transcription can occur, to its interactome in the WT cells, where the IAV lifecycle can proceed unhindered, showed the PB2 interactome to be different in the two cell types. We speculate that the host proteins enriched specifically in WT cells regulate steps downstream of primary transcription, including RNA replication. Meanwhile, host proteins enriched in both WT and ANP32-KO cells may regulate steps upstream of and including primary transcription. The host proteins enriched in either cell type fits with these predictions; some of the host proteins enriched in WT cells only were previously reported to be involved in vRNP assembly and transport, while some of the host proteins enriched in both cell types were previously reported to be important for viral transcription.

We also performed a complementary differential interactome screen comparing the interactome of ANP32 in the presence and absence of IAV infection. Unexpectedly, there was little overlap between the ANP32 interactomes in the presence and absence of infection. We suspected that this could in part be due to variable transfection efficiency of the ANP32-KO cells, resulting in unequal amounts of ANP32B-FLAG bait in the two conditions. To avoid this in future experiments, cell lines transduced with ANP32B-FLAG or GFP-FLAG (or another control) could be used instead. Nevertheless, the screen identified ANP32 interactors in the presence of infection that have previously been associated with the IAV lifecycle. This provides some confidence in the dataset and suggests that with further optimisation, it may be possible to identify further replication-specific host factors by studying the infected cell interactome of ANP32 or other known proviral host factors co-opted for viral RNA replication.

To compare interactomes in the two cell types (WT and ANP32-KO) or the two conditions (infected and uninfected), we first identified the host proteins enriched above background in each cell type/condition and then compared the interactomes. As the samples

were analysed in separate MS runs, variability could have been introduced at this stage. To avoid this, samples could have been metabolically labelled using SILAC, for example, which incorporates heavy isotopes into proteins prior to sample preparation (Ong et al., 2002). Alternatively, the samples could have been labelled using isobaric tagging methods, such as iTRAQ, which covalently modifies peptides after sample preparation (Ross et al., 2004). Samples would then be pooled, analysed on the same MS run, and deconvoluted based on the labels.

Prior to AP-MS analysis, cells were lysed in lysis buffer containing 0.2% NP-40 detergent. Although the lysis buffer also contained a high salt concentration, it is unclear whether this detergent and experimental approach was sufficient to achieve full nuclear lysis. To ensure full nuclear lysis, we could have performed subcellular fractionation. This could be achieved by lysing the cells in mild lysis buffer (for example with NP-40 detergent and a low salt concentration) in order to achieve cell lysis but not nuclear lysis. Following centrifugation, the cytoplasmic supernatant could then be removed and the pelleted nuclear fraction subjected to further lysis, as has previously been described (Kamel et al., 2024, Pinto et al., 2023). Nuclear lysis could be achieved using radioimmunoprecipitation (RIPA) buffer which contains the ionic and denaturing detergent, SDS. However, there is a risk that using such a harsh detergent might disrupt protein-protein interactions. As an alternative, nuclei could be lysed using more gentle mechanical methods, such as sonication or dounce homogenisation. Using subcellular fractionation to lyse the nucleus has the added benefit of solely including nuclear proteins in the AP-MS analysis. However, full nuclear lysis could also have been achieved without subcellular fractionation by performing mechanical lysis directly on our existing whole cell lysates.

We decided to study the PB2 and ANP32 interactomes using AP-MS because of its specificity, ability to identify host proteins in stable complexes with the bait protein (through direct or indirect interactions), and the feasibility of generating recombinant influenza viruses that express an AP tag (Lum and Cristea, 2016). Using this strategy, we were able to identify host proteins with known roles in the IAV lifecycle in our PB2 interactome study, which provides confidence in our dataset. Despite this, ANP32 was not among the PB2 interactors. Furthermore, in our ANP32 screen, PB2 was also not among the ANP32 interactors in the presence of infection, nor were any of the other viral proteins. The IAV polymerase is known to interact directly with ANP32, but the interaction appears to be transient as ANP32 is rarely enriched in AP-MS screens for polymerase interactors (Mistry et al., 2020, Baker et al., 2018, Bradel-Tretheway et al., 2011, Domingues et al., 2019, Sugiyama et al., 2015). Considering this, we cannot exclude the risk that we have missed other important, but transient, interactions. To capture such interactors, UV or chemical cross-linking could be employed,

which stabilises complexes and helps preserve biologically relevant interactions during the lysis and IP steps (Piersimoni et al., 2022).

Section 2.3.2. Measures to study the IAV interactome in viral RNA transcription and replication.

In addition to AP-MS, other methods to study protein-protein interactions also exist, such as proximity labelling methods (Schaack and Mehle, 2020). These involve fusing a biotin ligase or peroxidase to a protein of interest, which then biotinylates interacting and neighbouring proteins upon the addition of a substrate. The biotinylated proteins can then be isolated and identified by MS. Several different biotin ligases and peroxidases have been developed, including BioID, TurboID, and APEX, which vary in their size (27-35kDa), labelling time (1min-18hrs), labelling radius (10-20nm), and toxicity of their substrates (Branon et al., 2018, Rhee et al., 2013, Roux et al., 2012). Considering that interacting/proximal proteins are stably covalently modified, two advantages of this method are that it allows transient and weak interactors to be identified without the need for cross-linking as well as the use of harsh lysis conditions and stringent wash steps.

However, one limitation is that, due to its large size, fusion of the biotin ligase/peroxidase gene to a polymerase subunit may interfere with polymerase functions or packaging of vRNA segments, making it difficult to generate a stable virus expressing the biotin ligase or peroxidase. Consequently, proximity labelling methods might be best suited for studying polymerase interactomes in a minigenome setup. For example, TurboID has previously been used to study the polymerase interactome of Lassa virus (LASV) in the context of functional vRNPs (Fang et al., 2022). Similar to IAV, LASV has a single-stranded RNA genome which is transcribed and replicated by its polymerase inside the nucleus of an infected cell and in the context of vRNPs. Additionally, BioID2 has been used to compare the interactome of the PB1-F2 protein from two different IAV strains (Mettier et al., 2023).

Alternatively, instead of studying protein-protein interactions, RNA-protein interactions could be studied (Ramanathan et al., 2019, Schaack and Mehle, 2020). This could be achieved by encoding an RNA aptamer in the RNA of interest and would allow the interactome of both vRNA and cRNA to be studied depending on the orientation of the RNA tag (York et al., 2013). This approach was reported by York et al., who used an RNA tag to isolate the replicative cRNP intermediate (York et al., 2013). Importantly, the authors also show that RNA tags can be incorporated into the genome of replication competent and fully infectious influenza virus when inserted into the NA gene. The RNA tag employed by the authors was a PP7 tag which was affinity purified from infected cells that express the PP7 coat protein (PP7CP), to which PP7 binds with high affinity. While the authors focused on the polymerase subunits and NP copurifying with the RNA, the copurifying host proteins could also be

analysed. Alternatively, an RNA aptamer that recruits a biotin ligase for proximity labelling of nearby proteins, as described above, could be encoded. This method, known as RaPID, has not yet been applied to IAV, but has been used to study the Zika virus interactome (Ramanathan et al., 2018).

Another way to study RNA-protein interactions could be to use RNA probes to purify specific RNAs of interest and then identify the copurifying proteins by MS (Ramanathan et al., 2019). A major advantage of this method is that it does not require genetic modification of IAV and can, therefore, be applied to any strain of interest. RNA probes have recently been used to study the interactome of NP mRNA (Dupont et al., 2024). This was achieved by UV-crosslinking IAV-infected cells, adding a NP probe bound to magnetic beads to the lysate, and then identifying the captured proteins by MS. In addition, recent work started in the Barclay Lab has applied a HyPro-MS technique, which combines RNA probes and proximity labelling, to study the interactome of IAV vRNA and cRNA (unpublished). In this technique, after cross-linking, RNA probes that bind to the RNA of interest are added to infected cell lysates. The RNA probes are then recognised by a HyPro enzyme, which biotinylates proximal proteins that can then be captured and identified by MS (Yap et al., 2022).

The techniques that can be used to study the host cell interactome of IAV alongside their advantages and disadvantages, discussed above, are summarised in Table 6.

Table 6. Advantages and disadvantages of approaches that can be used to study the host cell interactome of IAV.

Approach	Advantages	Disadvantages
Protein-protein interactions: AP-MS. An AP tag is fused to a viral protein of interest. The tagged protein is then expressed in cells, either in the context of infection or transfection, immunoprecipitated, and co-precipitating proteins are identified by MS (Lum and Cristea, 2016).	• Can be used in the context of live virus, transfected vRNPs, or transfected individual proteins. • Captures direct protein-protein interactions. • Captures proteins in stable complex with the bait protein. • Can also be used to study PTMs of proteins (Hutchinson et al., 2012).	• Requires cross-linking to capture transient/weak interactors. • Requires genetic modification of virus if used in the context of live virus. • High false-positive rates making controls necessary to identify specific interactors (Schaack and Mehle, 2020).
Protein-protein interactions: Proximity labelling. A biotin ligase (BioID or TurboID) or peroxidase (APEX) is fused to a viral protein of interest. The tagged protein is then expressed in cells, neighbouring proteins are biotinylated, isolated, and identified by MS (Schaack and Mehle, 2020).	• Does not require cross-linking to detect transient and weak interactors (Schaack and Mehle, 2020). • Allows harsh lysis conditions and stringent wash steps. • Different biotin ligases/peroxidases that vary in size and labelling radius (Branon et al., 2018, Rhee et al., 2013, Roux et al., 2012). • APEX can be used to study proteomes over time (Rhee et al., 2013).	• May be difficult to use in the context of infection due to the large size of the biotin ligase/peroxidase. • Captures neighbouring proteins such that some interactors may be non-specific.
RNA-protein interactions: RNA aptamers encoded in RNA of interest. An RNA aptamer is encoded in the RNA of interest. Cells are infected with virus that harbours a tag in the RNA. Tag is either immunoprecipitated and co-precipitating proteins are identified by MS or tag recruits biotin ligase, which biotinylates proximal proteins that can then be captured and identified by MS (Ramanathan et al., 2019).	• Can be used in the context of live virus. • Interactomes of cRNA and vRNA can be studied depending on the orientation of the tag (York et al., 2013). • Different RNA aptamers can be used (PP7 (AP-MS-based approach) or RaPID (proximity labelling-based approach)) (Ramanathan et al., 2018, York et al., 2013).	• More focused on RNA-protein interactions than protein-protein interactions. • Requires genetic modification of virus.
RNA-protein interactions: RNA probes. Cells are infected with virus and cross-linked. RNA of interest is recognised by RNA probes. The RNA is then purified and co-purifying proteins are identified by MS (Ramanathan et al., 2019).	• Can be used in the context of live virus. • Interactomes of cRNA and vRNA can be studied depending on RNA probe design. • Applied to any strain and cell type as does not require genetic modification of virus.	• More focused on RNA-protein interactions than protein-protein interactions. • Requires cross-linking.

Section 2.3.3. Measures to distinguish viral RNA transcription and replication.

To distinguish host cell proteins important for polymerase transcriptase or replicase activity, we compared the polymerase interactome in WT and ANP32-KO cells. The advantage of this approach is that it can be performed in the context of live virus and, therefore, takes the viral and host cell changes that occur during infection into account. For instance, during infection the polymerase subunits assemble into various complexes including heterotrimers, RNPs, and higher order oligomeric complexes. Additionally, the viral NS2 protein downregulates transcription and promotes replication (Zhang et al., 2025a, Robb et al., 2009, Zhang et al., 2023). One disadvantage is that more infected cell lysate for IPs from ANP32-KO cells than WT cells was necessary to equalize the amount of PB2-FLAG bait in the two cell types. Another option to directly identify host proteins involved in RNA replication could be to study the interactome of a known replication cofactor, as we attempted by studying the interactome of ANP32 in the context of infection.

Alternatively, the host proteins supportive of RNA replication could be directly identified using a recombinant virus that encodes a PP7 tag in the cRNA replicative intermediate of one of the eight viral RNAs (see Section 2.3.2). This would allow identification of host proteins involved in the c-to-vRNA synthesis step of replication. Another approach to identifying host proteins important for the c-to-vRNA synthesis step could be to study the interactome of a cRNA-resident polymerase in the context of transfection. To prevent viral RNA synthesis from the template, a catalytically dead PB1 D446Y mutant could be substituted for PB1 WT (Cauldwell et al., 2013). Previous studies have shown that NS2 preferentially interacts with a vRNA-resident polymerase using a Nano luciferase Binary Technology (NanoBiT) measuring the interaction between NS2 and PA/PB2 (Zhang et al., 2025a). Given that NS2 shows different affinity for the polymerase depending on the RNA template supplied, it could be speculated that different sets of host proteins may also be recruited to a cRNA-resident polymerase compared to a vRNA-resident polymerase.

An alternative approach to identifying host proteins important for polymerase replicase activity could be to exploit the host restriction of AIV polymerases in human cells. AIVs with a PB2 subunit harbouring a 627E residue can perform transcription and the first step of replication (v-to-cRNA synthesis) in human cells, similar to mammalian-adapted viruses with a E627K mutation (Swann et al., 2023). It is thought that avian viruses carry out cRNA synthesis in human cells with the help of the viral NS2 protein encoded by the IAV genome and the suboptimal mammalian ANP32 proteins already present in the cells, although experimental evidence for this is lacking in the literature (Sun et al., 2024b, Swann et al., 2023, Zhang et al., 2025a). AIVs are host restricted at the second step of replication (c-to-vRNA synthesis) (Swann et al., 2023). In this step, the virus needs to acquire the mammalian adapting E627K mutation to co-opt the mammalian version of ANP32 proteins (Long et al.,

2016, Swann et al., 2023). Consequently, to distinguish the host proteins that are important for the second step of replication, a differential interactome screen could be performed that compares the interactomes of a 627E virus (proteins important for steps up to and including v-to-cRNA synthesis) and a 627K virus (proteins important for all steps of the IAV lifecycle including both v-to-cRNA and c-to-vRNA synthesis) in human cells. However, this would also require more input from the PB2 627E-infected cells compared to PB2 627K-infected cells to equalise the amount of bait in the two conditions.

The interactome of avian polymerases could also be studied in the context of transfected vRNPs. This would involve a minigenome-style setup with plasmids encoding the polymerase subunits (PB1, PA and PB2 627E or 627K), NP and a viral-like RNA template. A variation of such a screen has previously been performed in the Barclay Lab, where the interactomes of PB2 627E, PB2 627K, and PB2 627E with chANP32A in human cells were compared (Mistry, 2019). This identified host proteins that co-precipitated only with a replication-competent polymerase (PB2 627K or PB2 627E with chANP32A) but not with a replication-incompetent polymerase (PB2 627E). PA and PB1 subunits were also supplied but not NP and a viral-like RNA template. It would be interesting to revisit such an interactome screen in a minigenome setup with fully reconstituted vRNPs. Another version of this screen was also recently performed in the Barclay Lab in which the interactome of PB2 627E in human cells in the presence of either NS2 or chANP32A was compared (unpublished). The aim was to identify host proteins important for the different steps of viral RNA replication (supplying NS2 is thought to allow host-restricted polymerases to perform v-to-cRNA synthesis and supplying chANP32A is known to allow both v-to-cRNA and c-to-vRNA synthesis) (Swann et al., 2023, Long et al., 2016). However, functional validation is necessary to confirm that this differential interactome screen has, indeed, identified host proteins important for the different steps of RNA replication, given that it is currently unclear whether NS2 supports avian v-to-cRNA synthesis in human cells. To ascertain that equal amounts of bait are present in the samples, a catalytically dead PB1 D446Y mutant could be substituted for PB1 WT, as mentioned above, such that the bait is not amplified (Cauldwell et al., 2013).

Another approach could be to study the interactomes of mutant polymerases that can only transcribe or replicate. One set of previously characterised transcription and replication deficient mutations in the PA subunit are D108A and E410A, respectively (Rehwinkel et al., 2010). We also characterised these mutants in this work and used them for functional validation of transcription- and replication-specific host factors (Chapter 3). Alternatively, mutation of the promoter region of the vRNA template could also be used to uncouple viral transcription and replication (te Velthuis et al., 2013). Deletion of the adenosine residue at position 10 of the 5’ end of the vRNA promoter (5’ A10) has been shown to reduce transcription without affecting replication. One disadvantage of such an approach is that these mutants can

only be used in a minigenome style assay and not with full virus, given that both transcription and replication are necessary for virus rescue.

Table 7 summarises the approaches that can be used to distinguish transcription and replication host factors, alongside their advantages and disadvantages.

Table 7. Advantages and disadvantages of approaches to identify host proteins with roles specific to either viral RNA transcription or replication.

Approach	Advantages	Disadvantages
Host protein ANP32: Interactome in WT vs ANP32-KO cells or ANP32 interactome during infection.	• Can be performed in the context of live virus. • WT cells vs ANP32-KO cells: Can be used to identify both transcription and replication factors. • ANP32 interactome: Can be used to directly identify replication factors.	• WT cells vs ANP32-KO cells: Requires more infected cell lysate for IPs from ANP32-KO cells than WT cells. • WT cells vs ANP32-KO cells: Differential interactome screen necessary as does not directly identify transcription/replication host factors.
cRNA interactome: Virus with PP7-tagged cRNA or cRNA-resident vRNP.	• Can be used in the context of live virus (PP7-tagged cRNA) (York et al., 2013). • Allows direct identification of host proteins important for c-to-vRNA synthesis.	• Requires genetic modification of virus if used in the context of live virus.
Host restriction of avian polymerase in human cells: 627E vs 627K viruses or polymerases.	• 627E vs 627K interactome can be performed in the context of infection or transfection. • Can be used to distinguish host proteins important for each step of viral RNA synthesis (v-to-mRNA, v-to-cRNA, and c-to-vRNA synthesis).	• Requires more infected cell lysate for IPs from 627E-infected cells than 627K-infected cells. • Supplementation with NS2 can only be performed in the context of transfected vRNPs and not infection. • Differential interactome screen necessary as does not directly identify transcription/replication host factors.
Transcription/replication deficient mutant polymerases.	• Allows direct identification of host proteins important for transcription or replication.	• Can only be used in the context of transfected vRNPs as generation of infectious virus requires both transcription and replication of vRNA template. • Structural understanding of mutants necessary to predict whether interactomes will be different.

Section 2.3.4. Measures to validate protein-protein interactions.

One limitation of performing our differential interactome screen using full virus is that we were unable to deduce from our dataset whether the host proteins interact directly with PB2 or indirectly via a PB2-containing complex. For example, HMGB2, and its family member HMGB1, were previously shown to interact directly with NP (Moisy et al., 2012). It is, therefore, likely that HMGB2 and HMGB1 co-precipitated with PB2 in our screen because of an indirect interaction via RNPs.

We validated the interaction between PB2 and HMGB2 and RUVBL2 by co-IP using HMGB2/RUVBL2 as bait and western blotting for the co-precipitation of PB2 following infection. We found PB2 to interact with HMGB2 and RUVBL2, and more so in the WT cells than ANP32-KO cells, which was consistent with the interactome data. However, as this was done in the context of infection, it still remains unclear whether the host proteins interact directly with PB2 or not. To understand this, similar IPs could be performed with transfection of individual viral proteins instead.

More quantitative and sensitive techniques to validate interactions also exist. For instance, a split luciferase complementation assay could have been used which measures the interaction between two proteins of interest by fusing one half of a gaussia luciferase enzyme onto each of the proteins (described in detail in Section 4.2.4) (Cassonnet et al., 2011). The enzyme then produces a measurable luminescent signal when the two proteins interact. This method has previously been used to characterise the interaction between ANP32 and viral proteins (Mistry et al., 2020, Wang et al., 2022a). The interactions could also have been validated *in situ* using assays such as a bimolecular fluorescence complementation (BiFC) assay or proximity ligation assay (PLA). Similar to a split luciferase complementation assay, in a BiFC assay two proteins of interest are each fused to one half of a Venus fluorescent protein, which produces a fluorescent signal when the two proteins interact (Hu et al., 2002). In PLA, primary antibodies specific to each protein of interest are used, which are, in turn, recognised by secondary antibodies bound to DNA strands, known as proximity ligation probes (Soderberg et al., 2006). When the proteins interact, the DNA strands hybridise, generating a circular template that can be amplified by a DNA polymerase. Fluorescently labelled oligonucleotides then bind to the amplified DNA, generating a signal that can be visualised and imaged. The benefit of *in situ* approaches is that they allow the cellular location of the interaction to be determined as well.

Section 2.3.5. Functional validation of host cell proteins.

In this chapter, we functionally validated a role in IAV infection and polymerase activity of selected host proteins identified in the PB2 differential interactome screen. To achieve this, we made use of siRNA pools targeting each of the genes selected. We also trialled the use of shRNAs, which have the benefit of generating a stable cell line in which all cells would have the gene expression reduced (data not shown). However, we chose siRNAs instead because we found them to be less time consuming and labour intensive, making it feasible to functionally validate a larger number of genes. We measured the effects in both minigenome reporter assays and in the context of virus infection using the PR8 NS-ZsGreen reporter virus, and even though these two different assays were carried out in different human cell lines, the results mostly overlapped. Overall, we found ten host proteins to have a proviral role in polymerase activity (six of which also were proviral in infection), five to have an antiviral role in polymerase activity (one of which also was antiviral in infection). Seventeen of the interactors tested appeared to have no role in polymerase activity and six interactors did not impact infection. As summarised in Table 8 our findings were partially consistent with the literature.

Table 8. Comparison of host proteins found to have a proviral or antiviral role in the IAV lifecycle in this study and the literature.
Antiviral role is shown in red, proviral role in green, no effect in grey, not tested in white.

Host protein	**This study:** Infection (Figure 26)	**This study:** Polymerase activity (Figure 27)	**Literature:** Infection	**Literature:** Polymerase activity	**References**
AHNAK					(Haas et al., 2023)
CLUH					(Ando et al., 2016, Karlas et al., 2010)
HAX1					(Hsu et al., 2013)
HMGB1					(Moisy et al., 2012)
HMGB2					(Moisy et al., 2012)
KPNA3					(Gabriel et al., 2011)
PTMA					(Konig et al., 2010)
RBM14					(Bortz et al., 2011)
RUVBL2					(Haas et al., 2023, Kakugawa et al., 2009)
SAE1					(Konig et al., 2010)
UBR5					(Haas et al., 2023)
YTHDF2					(Courtney et al., 2017)
PHB1					(Watanabe et al., 2014, Zou et al., 2023)

For instance, in agreement with our data, knockdown of RBM14 has previously been shown to reduce polymerase activity of both a mammalian-adapted and avian IAV strain (Bortz et al., 2011). We also found knockdown of CLUH to result in a significant reduction in polymerase activity as well as a trend in reduction in virus infection. This is somewhat consistent with the literature, where CLUH has been reported as proviral factor with a role in vRNP nuclear export but not in vRNA synthesis (Ando et al., 2016). It is therefore not clear why CLUH knockdown would decrease polymerase activity. In addition, we found SAE1 and PTMA to have no effect on polymerase activity. We did not test their role in IAV infection. A previous genome-wide RNAi screen has reported both as proviral factors in IAV infection but did not specify the step of the IAV lifecycle that they act at (Konig et al., 2010). Our data combined with the literature, would, therefore, suggest that SAE1 and PTMA play a role in the IAV lifecycle downstream of polymerase activity.

Although we found HAX1 to have no effect on polymerase activity, previous reports have shown shRNA-mediated knockdown of HAX1 to increase polymerase activity and virus growth, suggesting the protein to be an antiviral factor (Hsu et al., 2013). Moreover, we found HMGB1 to have no effect on polymerase activity and HMGB2 to have a proviral role. Previous reports have shown the opposite pattern; HMGB1 to have a proviral role and HMGB2 to have no significant role (Moisy et al., 2012). Such discrepancies between our data and the literature, as was the case for HAX1 and the HMGB protein family, could be due to experimental differences such as varying gene knockdown efficiencies, or use of different cell types or IAV strains. For instance, the role of the HMGB family in IAV infection was previously studied using mouse embryonic fibroblasts (MEFs) knocked out for HMGB1/HMGB2, while our experiments were performed in human cells (discussed in detail in Section 3.3) (Moisy et al., 2012).

We also functionally validated a role in polymerase activity of the two host proteins that were enriched in both the ANP32 interactome during infection and the PB2 interactome in WT cells only, STML2 and PHB1, as well as its family member PHB2. We found knockdown of PHB1 and PHB2 to reduce polymerase activity. The two proteins have not previously been associated with IAV polymerase activity, but PHB1 has been shown to play a proviral role in IAV infection (Table 8) (Watanabe et al., 2014). PHB1 has also previously been assigned a role in regulation of the antiviral innate immune response against IAV (Zou et al., 2023). PHB1 was shown to interact with IMPα1 and IMPα5, inhibiting their ability to facilitate the nuclear import of IRF3, a major regulator of IFNß production. In turn, this led to the inhibition of IFNß production and enhancement of virus replication. An IFN response should not be stimulated in our minigenome reporter assay, suggesting that the PHB proteins may support polymerase activity via another unrelated mechanism. However, the downregulation of IFNß by PHB1 could mean that it might have an even greater proviral role in the context of infection.

Functional validation of hits from our differential interactome screens also revealed novel regulators of the IAV lifecycle (Table 9). This included host factors with proviral roles in polymerase activity, including FKBP4, FUBP1, PIN4, and RPAP2 and antiviral roles in polymerase activity, including MAZ, MDH2, VRK1, and SUPT5H.

Table 9. Summary of novel host proteins found to have a proviral or antiviral role in the IAV lifecycle in this study.
Antiviral role is shown in red, proviral role in green, no effect in grey, not tested in white.

Host protein	**This study:** Infection (Figure 26)	**This study:** Polymerase activity (Figure 27)
FKBP4		
FUBP1		
MAZ		
MDH2		
PGAM1		
PIN4		
RUVBL1		
SUPT5H		
VRK1		
AKAP8L		
RPAP2		
PHB2		

For further functional characterisation we focused on the proviral factors identified in the PB2 interactome screen and selected a mix of novel host factors and host proteins previously associated with the IAV lifecycle. Particularly, as a proof-of-principle that our differential AP-MS screen can be used as a tool to distinguish host proteins important for polymerase replicase and transcriptase activity, we further characterised two of the host proteins enriched specifically in WT cells, HMGB2 and RUVBL2, as potential replication-specific factors, and one of the host proteins enriched in both WT and ANP32-KO cells, RPAP2, as a potential transcription-specific factor (Chapter 3). We selected HMGB2 and RUVBL2 because they have not previously been assigned specific roles in RNA transcription and replication but have been reported to interact with NP, which is consistent with a potential role for the host proteins in RNA replication (Kakugawa et al., 2009, Moisy et al., 2012, Mayer et al., 2007). Meanwhile, RPAP2 was selected because its potential role in viral transcription fits well with its host function, where it directly binds RNAP II and supports its nuclear import (Forget et al., 2013).

If time had allowed, it would have been interesting to further characterise the role in polymerase activity of some of the other novel host proteins identified. It would have been particularly interesting to better understand the role of some of the antiviral factors, such as MAZ, which we found to restrict both polymerase activity and virus replication. While MAZ has not previously directly been associated with the IAV lifecycle, it has recently been shown to

be required for the recruitment of STAT1 to innate immune genes and ISGs (Xiao et al., 2024). Such genes include MxA, which is known to be important for the restriction of AIV in human cells. In this study, we used siRNAs for functional validation. To understand the role of the antiviral factors in more detail, we could test the effect of overexpression of the factors on polymerase activity and accumulation of viral RNA species, similar to our experiments with BTN3A3 and MxA (Chapter 4).

In this chapter, we performed a differential interactome screen using a live-virus AP-MS strategy to identify host proteins that are exploited by either the viral transcriptase or replicase machinery. We provided functional evidence that host proteins co-precipitating from WT cells, potential replication-specific factors, or both WT and ANP32-KO cells, potential transcription-specific factors, play roles in virus replication, polymerase activity, or both. As a proof-of-principle that our differential AP-MS screen is a more targeted approach to studying the IAV polymerase interactome, in the next chapter we further characterise the roles of HMGB2 and RUVBL2, potential replication-specific cofactors, and RPAP2, a potential transcription-specific cofactor.

Chapter 3. HMGB2 and RUVBL2 support viral RNA replication and RPAP2 supports transcription

Section 3.1. Introduction

Host cell proteins are co-opted by IAV to support viral RNA synthesis (Peacock et al., 2019). The specific roles of some host proteins have been well characterised, such as ANP32 in RNA replication and RNAP II in transcription (Engelhardt et al., 2005, Nilsson-Payant et al., 2022, Staller et al., 2019, Sugiyama et al., 2015, Swann et al., 2023, Walker and Fodor, 2019). Although many other host proteins have been shown to support polymerase activity, their specific roles have not been elucidated. It therefore remains unclear whether additional host proteins are recruited as replication-specific or transcription-specific factors. Such host factors may support various stages of viral RNA synthesis such as the switch from transcription to replication, formation of the replication platform, or recruitment of NP. In the previous chapter, we performed a live-virus differential interactome screen to distinguish host proteins important for polymerase replicase or transcriptase activity using the PB2 polymerase subunit as bait. As a proof-of-principle that our differential interactome screen can be used as a targeted approach to discover host factors, in this chapter we further characterised the role of high-mobility group box 2 (HMGB2) and RuvB-like 2 (RUVBL2) as potential replication-specific host factors and RNA polymerase II associated protein 2 (RPAP2) as a potential transcription-specific host factor.

We selected these three host proteins for further characterisation for several reasons. All three proteins were previously shown to localise to the nucleus (Forget et al., 2013, Huen et al., 2010, Starkova et al., 2023). Given that the nucleus is also the site of IAV RNA transcription and replication, this fits with a role for these host proteins at these stages of the viral lifecycle. In the host cell, HMGB2 binds DNA via its highly-conserved DNA-binding HMGB domain, and remodels chromatin (Starkova et al., 2023). Interestingly, HMGB2 exists in the same so-called SET complex as ANP32A. The SET complex has six members (HMGB2, ANP32A, SET, NME1, TREX1, and APEX1), and can be both nuclear and cytoplasmic and has roles in DNA damage (Chowdhury and Lieberman, 2008). RUVBL2 is an AAA+ ATPase that has a diverse range of roles in the host cell (Huen et al., 2010). First, RUVBL2 is involved in chromatin remodelling and is a component of various chromatin remodelling complexes. RUVBL2 also forms part of the Rvb1-Rvb2-Tah1-Pih1 (R2TP) chaperone complex together with its family member RUVBL1 and is involved in the assembly of various protein and protein-RNA complexes, such as small nucleolar ribonucleoproteins (snoRNPs). RPAP2 binds and

supports the activity of host RNAP II (Forget et al., 2013). HMGB2 and RUVBL2 have not previously been assigned specific roles in RNA transcription and replication but have been reported to interact with NP, which is consistent with a potential role for the host proteins in viral RNA replication, since NP is not required to generate mRNAs (Kakugawa et al., 2009, Mayer et al., 2007, Moisy et al., 2012). Meanwhile, RPAP2 has not previously been associated with the IAV lifecycle. However, the potential role for RPAP2 in viral transcription fits well with its host function since RNAP II is known to be essential for viral transcription initiation (Engelhardt et al., 2005).

In this chapter, we used CRISPR-Cas9 genome editing to target expression of HMGB2, RUVBL2, and RPAP2 in cell lines. We showed that all three factors support polymerase activity, either using a minigenome reporter assay or strand-specific RT-qPCR in the context of virus infection. Using experimental conditions that allow cRNA and mRNA synthesis to be distinguished as well as replication- and transcription-deficient polymerase mutants, we showed that HMGB2 and RUVBL2 support cRNA synthesis while RPAP2 supports mRNA synthesis. We also tested the application of these host proteins as antiviral drug targets. Inflachromene (ICM), a previously discovered inhibitor of HMGB2, was found to inhibit virus growth by inhibiting cRNA and/or vRNA synthesis. The effect of ICM in a mouse model of IAV infection was also tested. In contrast to the antiviral effect of ICM in cell culture, we found that ICM did not improve disease outcome in IAV-infected mice.

The A549-dox-Cas9 cells used to generate HMGB2-KO, RUVBL2-KO, and RPAP2-KO cells were a kind gift from Dr Laura Martin-Sancho. Data presented in Figure 39 was collected by a BSc student, Nancy Liu, under the supervision of this author. Plasmids to express the viral polymerase constellations used in Figure 39 were generated by Dr Olivier Moncorge. Plasmids to express replication-deficient and transcription-deficient PA mutants and the catalytically dead PB1 mutant were generated by Dr Olivia Swann (Swann, 2023, Swann et al., 2023). Data presented in Figures 49 and 50 were produced by Dr Jie Zhou and Ksenia Sukhova. Data presented in Figures 35, 36, 38-40, 42, 43, 45, 47, and 48 and the accompanying text are adapted from Rasmussen et al., 2025, manuscript in review and pre-printed on Biorxiv (Rasmussen et al., 2025).

Section 3.2. Results

Section 3.2.1. Generating RUVBL2-KO, HMGB2-KO, and RPAP2-KO cells using CRISPR-Cas9 genome editing.

Clustered regularly interspaced short palindromic repeats (CRISPR)-Cas9 genome editing is a useful tool for impacting expression of genes (Ran et al., 2013). In this method, a CRISPR-Cas9 nuclease stimulates a double-stranded break (DSB) at a target genomic locus,

which is specified by a 20nt targeting sequence encoded by a single guide RNA (sgRNA) (Figure 32). After cleavage by Cas9, the target locus undergoes DNA damage repair via one of two pathways, non-homologous end joining (NHEJ) or homology-directed repair (HDR), depending on whether a repair template is provided. If the desired editing outcome is gene knockout, as in our case, no repair template is provided and the DSB will be repaired through the error prone NHEJ process. This may result in insertions or deletions (indels) within the coding exon, which in turn may lead to frameshift mutations, premature stop codons, and gene knockout. Alternatively, if the desired editing outcome is a precise and defined modification at a target locus, a repair template can be exogenously provided and the DSB will repaired by HDR.

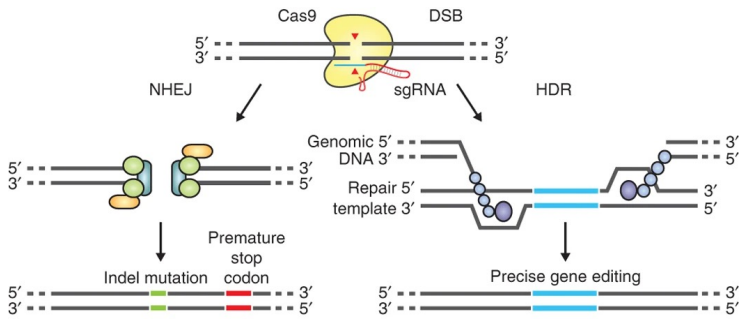

Figure 32. Schematic demonstrating CRISPR-Cas9 genome editing.
Figure taken from Ran et al., 2013. Reproduced with permission from Springer Nature. Cas9 will induce a double strand break (DSB) at a DNA region specified by the single guide RNA (sgRNA). If no repair template is provided, the DSB will be repaired by error prone non-homologous end joining (NHEJ), which may result in indel mutation, premature stop codon formation, and in turn gene knockout. If a repair template is provided, the DSB will be repaired by homology-directed repair (HDR) and a defined modification will be made within the target locus.

Here, we made use of the CRISPR-Cas9 technology to generate A549 cells knocked out for three of the genes identified in the differential interactome screen described in Chapter 2: HMGB2, RUVBL2, and RPAP2. A549 cells are a hypotriploid human cell line with a modal chromosome count of 66. This means that the cell line on average has more than the diploid number of chromosomes (46) but less than the triploid number (69), such that each chromosome may have 2, 3, or even more copies. The RUVBL2 gene is located on chromosome 19, HMGB2 on chromosome 4, and RPAP2 on chromosome 1 (Perez et al., 2025). A549 cells have at least two copies of chromosomes 19 and 4 and three copies of chromosome 1 (Park et al., 2001). However, the exact number of each of these chromosomes is unclear from the literature, and variations in cell culture conditions may also cause differences in the number of chromosomes (Isaka et al., 2003, Park et al., 2001, Peng et al., 2010). To achieve complete knockout, all alleles of the RUVBL2, HMGB2, and RPAP2 genes need to be targeted.

Pools of sgRNAs targeting an early exon of each gene were designed by and obtained from Synthego. Alignment of the sgRNA sequences to the HMGB2, RUVBL2, and RPAP2 genes is shown in Appendix C. To achieve gene editing, we made use of A549 cells expressing Cas9 under control of a doxycycline (dox) inducible promoter (A549-dox-Cas9). This cell line has previously been used to generate cells knocked out for TBC1D5 to study the role of this protein in restricting IAV (Martin-Sancho et al., 2021). The advantage of using this cell line is that the cells only need to be transfected with the sgRNAs and not also the Cas9 protein, increasing the transfection efficiency. First, we confirmed that the A549-dox-Cas9 cells express Cas9 upon dox treatment (Figure 33A). Cas9 protein expression was visible at 48hrs post dox treatment and its expression was found to increase with increasing duration of dox treatment.

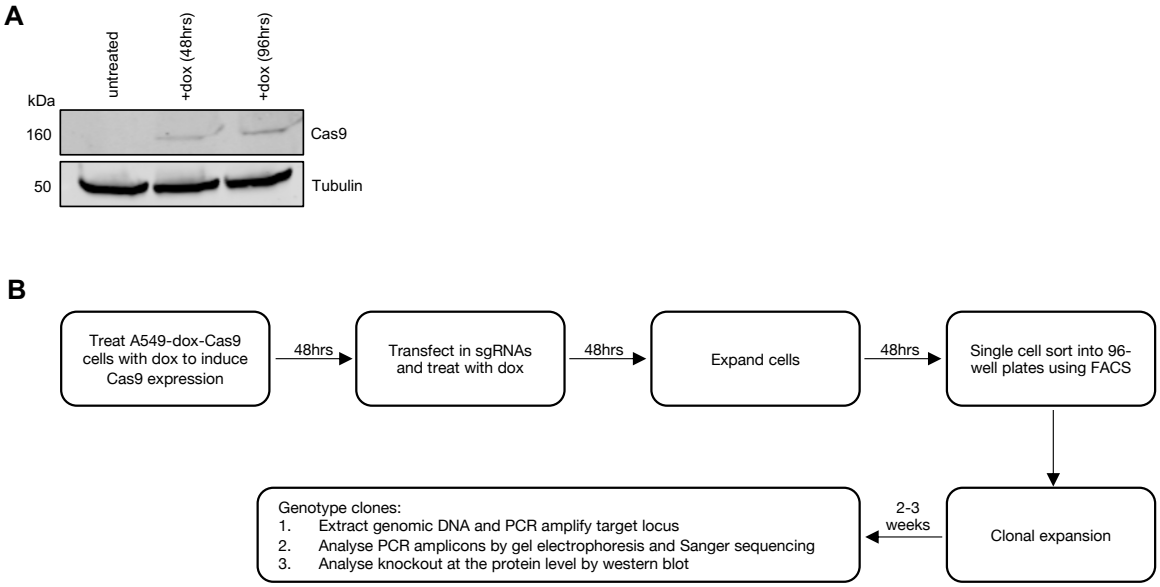

Figure 33. Generation of CRISPR-Cas9 KO cells using A549-dox-Cas9 cells.
A) Western blot showing Cas9 and tubulin (cellular control) protein expression in A549-dox-Cas9 cells that were untreated, treated with dox for 48hrs, and treated with dox for 96hrs. B) Schematic of the CRISPR-Cas9 genome editing protocol. A549-dox-Cas9 cells are treated with dox, transfected with sgRNAs, expanded, single-cell sorted, clonally expanded, and genotyped.

Next, we performed an initial round of CRISPR using pooled sgRNAs targeting RUVBL2 (Figure 33B). To achieve this, we treated A549-dox-Cas9 cells with dox for 48hrs and transfected the cells with pools of sgRNAs targeting RUVBL2. Clonal populations were then obtained by single cell sorting into 96-well plates using a fluorescence-activated cell sorter (FACS). A control cell line (WT) was generated simultaneously by transfecting cells with a non-targeting sgRNA.

We tested clonal populations for knockout of RUVBL2 by extracting the genomic DNA, PCR amplifying the region of interest, and analysing the PCR amplicons by gel electrophoresis

and Sanger sequencing (Figure 34A and B). A single band of the expected size (500bp) was observed for the WT PCR amplicon (Figure 34A). We observed multiple bands for PCR amplicons from individual clones RUVBL2-KO C1, C5, C7, C9, C10, and C11, suggesting that CRISPR editing resulted in indels within the target locus within the different chromosomes in each clone. For example, two bands were observed for the C11 amplicon: one at 500bp, presumably amplified from a chromosome still unedited, and a second lower band presumably indicating a deletion in one strand of the DNA.

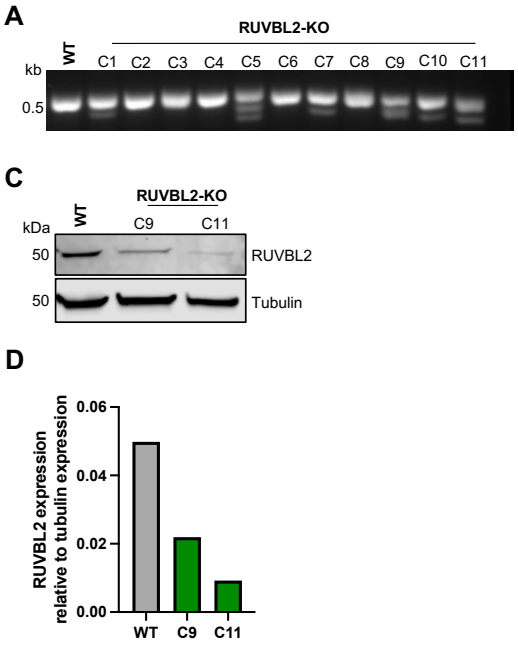

B

RUVBL2-KO clone	Indel %	KO score	R^2
C1	49	49	0.93
C2	17	17	1
C3	32	0	0.98
C4	18	18	0.99
C5	80	58	0.86
C6	0	0	1
C7	30	30	0.84
C8	8	8	0.98
C9	97	96	0.93
C10	51	51	0.92
C11	100	99	0.94

Figure 34. Generation of A549 RUVBL2-KO cells using CRISPR-Cas9 genome editing.
A) Gel electrophoresis analysis of the PCR amplified target locus of WT clonal cells and RUVBL2-KO clonal cells. B) ICE analysis of Sanger sequencing of the PCR amplicons from (A) indicating the indel percentage, KO score, and R^2 value. The KO score is a value between 0 and 100. The higher the KO score, the higher the percentage of sequences within the sample that are likely to lead to KO. C) Western blot showing RUVBL2 and tubulin (cellular control) protein expression in WT cells and RUVBL2-KO C9 and C11 cell clones. D) Quantification of western blot in (C) shown as the amount of RUVBL2 expression relative to the amount of tubulin expression.

Sanger sequences of the PCR amplicons were analysed using an inference of CRISPR edits (ICE) tool developed by Synthego. This tool produces quantitative analysis of CRISPR editing based on a provided control chromatogram (WT), edited chromatogram, and sgRNA sequences. The output includes an indel percentage, which indicates the percentage of the sample with edited sequence compared to the control, KO score, which indicates the proportion of the sample with a frameshift or 21+ bp indel, and an R^2 value, which indicates the confidence in the KO score. Consistent with the gel electrophoresis analysis of the PCR amplicons, clones that appeared to have indels by gel electrophoresis also had the highest

indel percentages and KO scores (Figure 34B). C9 and C11 clones showed the greatest indel percentage, KO score, and R^2 value. We, therefore, decided to analyse these clones by western blot to assess the level of knockout at the protein level.

Western blotting showed that RUVBL2 protein expression was reduced in the C9 and C11 clones compared to WT, but not completely ablated (Figure 34C). Quantification of RUVBL2 expression in the WT and KO clones relative to tubulin expression revealed that RUVBL2 protein expression was 81% lower in the C11 clone and 56% lower in the C9 clone compared to the WT clone (Figure 34D).

To improve editing efficiency, we attempted another round of CRISPR in the RUVBL2-KO C11 clone using the same pooled sgRNAs. We followed the same protocol as described previously and assessed editing efficiency of the single-cell clones by PCR, Sanger sequencing, and western blotting (Figure 33B and 35A-D). Analysis of the PCR amplicons by gel electrophoresis revealed two bands for all clones (C1-C8) in comparison to a single band of the expected size (500bp) for the WT PCR amplicon (Figure 35A). Sanger sequencing of the PCR amplicons and ICE analysis revealed that most of the clones, except C6, had an indel percentage of 100% and a KO score of 90-97 (Figure 35B). This suggests that the second round of CRISPR editing in the C11 clone further reduced RUVBL2 expression. To confirm this at the protein level, we analysed the clones by western blot probing for RUVBL2 and tubulin (Figure 35C). RUVBL2 protein expression was reduced in the KO clones compared to in the WT clone, but still not completed ablated. Quantification of RUVBL2 expression relative to tubulin expression for each clone revealed that clone C7 had the highest reduction in RUVBL2 expression of 90% compared to the WT clone (Figure 35D). Clones C2 and C3 also had a high reduction in RUVBL2 expression of 89%. RUVBL2 expression remained similar in the remaining clones compared to the original clone C11. We decided to take clones C2 and C7 as well as our initial clones C9 and C11 forward for further experiments.

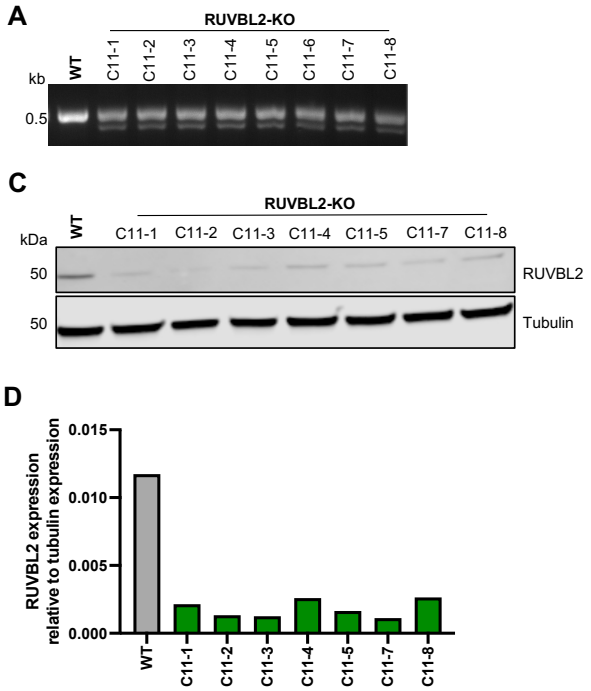

B

RUVBL2-KO clone	Indel %	KO score	R^2
C11-1	100	90	0.91
C11-2	100	91	0.92
C11-3	100	91	0.91
C11-4	100	90	0.91
C11-5	100	90	0.92
C11-6	86	73	0.88
C11-7	100	97	0.93
C11-8	100	90	0.92

Figure 35. Second round of CRISPR-Cas9 editing in RUVBL2-KO cells further reduces RUVBL2 expression.
A) Gel electrophoresis analysis of the PCR amplified target locus of WT clonal cells and RUVBL2-KO C11 clonal cells transfected with sgRNAs targeting RUVBL2. B) ICE analysis of Sanger sequencing of the PCR amplicons from (A) indicating the indel percentage, KO score, and R^2 value. The KO score is a value between 0 and 100. The higher the KO score, the higher the percentage of sequences within the sample that are likely to lead to KO. C) Western blot showing RUVBL2 and tubulin (cellular control) protein expression in WT cells and RUVBL2-KO C1, C2, C3, C4, C5, C7, C8 cell clones. D) Quantification of western blot in (C) shown as the amount of RUVBL2 expression relative to the amount of tubulin expression.

We next applied the same protocol to generate A549 HMGB2-KO and RPAP2-KO cell lines using pooled sgRNAs targeting HMGB2 or RPAP2, respectively (Figure 33B). We observed multiple bands for HMGB2-KO C1, C6, C8, C14, and C17 PCR amplicons compared to a single band for the WT PCR amplicon, suggesting that CRISPR editing had resulted in indels with the target locus of these clones (Figure 36A). We next confirmed this at the protein level by analysing HMGB2-KO clones C8 and C14 by western blot probing for HMGB2 and tubulin, which showed HMGB2 protein expression to be reduced in both KO clones, but not completely ablated (Figure 36B). Quantification of HMGB2 expression relative to tubulin expression revealed that HMGB2 protein expression was approximately 60% lower in both the C8 and C14 clones (Figure 36C). In the case of the RPAP2-KO clones, we observed multiple bands for C2, C22, and C27 PCR amplicons in comparison to the single band observed for the WT PCR amplicon (Figure 35D). Sanger sequencing of these PCR amplicons revealed that C2 followed by C22 had the highest indel percentage and KO score. We were unable to detect RPAP2 by western blot and so were unable to confirm knockout at the protein

level. Two different RPAP2 primary antibodies were tested, both of which showed no bands corresponding to RPAP2 despite clear bands for the tubulin cellular control (Appendix D).

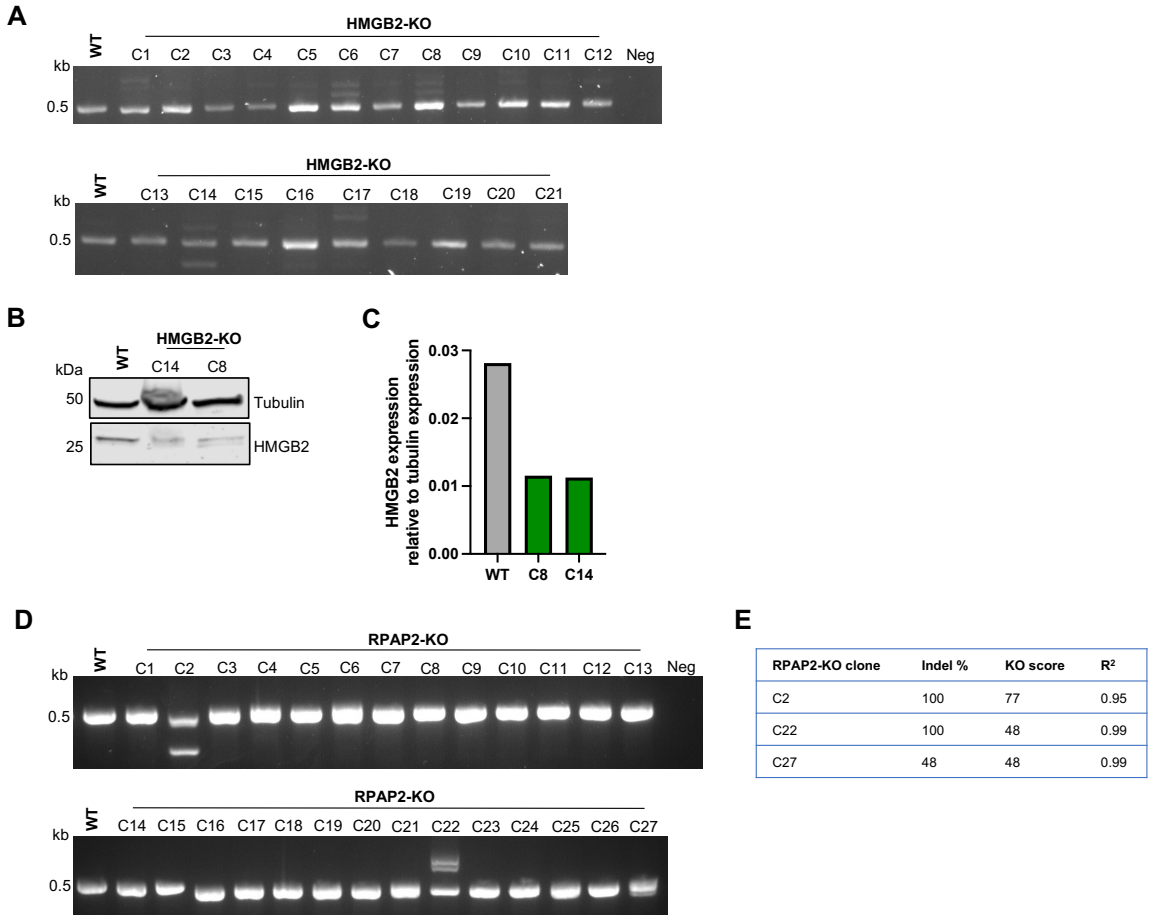

RPAP2-KO clone	Indel %	KO score	R^2
C2	100	77	0.95
C22	100	48	0.99
C27	48	48	0.99

Figure 36. Generation of A549 HMGB2-KO and RPAP2-KO cells using CRISPR-Cas9 genome editing.
A) Gel electrophoresis analysis of the PCR amplified target locus of WT clonal cells and HMGB2-KO clonal cells. B) Western blot showing HMGB2 and tubulin (cellular control) protein expression in WT cells and HMGB2-KO C8 and C14 cell clones. C) Quantification of western blot in (B) shown as the amount of HMGB2 relative to the amount of tubulin. D) Gel electrophoresis analysis of the PCR amplified target locus of WT clonal cells and RPAP2-KO clonal cells. E) ICE analysis of Sanger sequencing of the PCR amplicons from (D) indicating the indel percentage, KO score, and R^2 value. The KO score is a value between 0 and 100. The higher the KO score, the higher the percentage of sequences within the sample that are likely to lead to KO.

We did not attempt a second round of CRISPR in the HMGB2-KO and RPAP2-KO clones in the interest of time. Instead, we took HMGB2-KO clones C8 and C14 and RPAP2-KO clones C2 and C22 forward for further experiments.

Section 3.2.2. Polymerase activity is reduced in RUVBL2-KO and HMGB2-KO cells.

Next, we tested PR8 polymerase activity in the selected RUVBL2-KO (C2, C7, C9, and C11), HMGB2-KO (C8 and C14), and RPAP2-KO (C2 and C22) cell clones using a

minigenome reporter assay (see Section 2.2.2, Figure 18B). As explained, polymerase activity is measured by the signal produced by a Firefly luciferase reporter, which is then normalised to a Renilla luciferase signal to control for transfection efficiency. To ascertain that our minigenome reporter assay worked as expected in the KO cell clones, we analysed the average Firefly and Renilla values separately as well as the Firefly:Renilla ratios (Figure 37A-I).

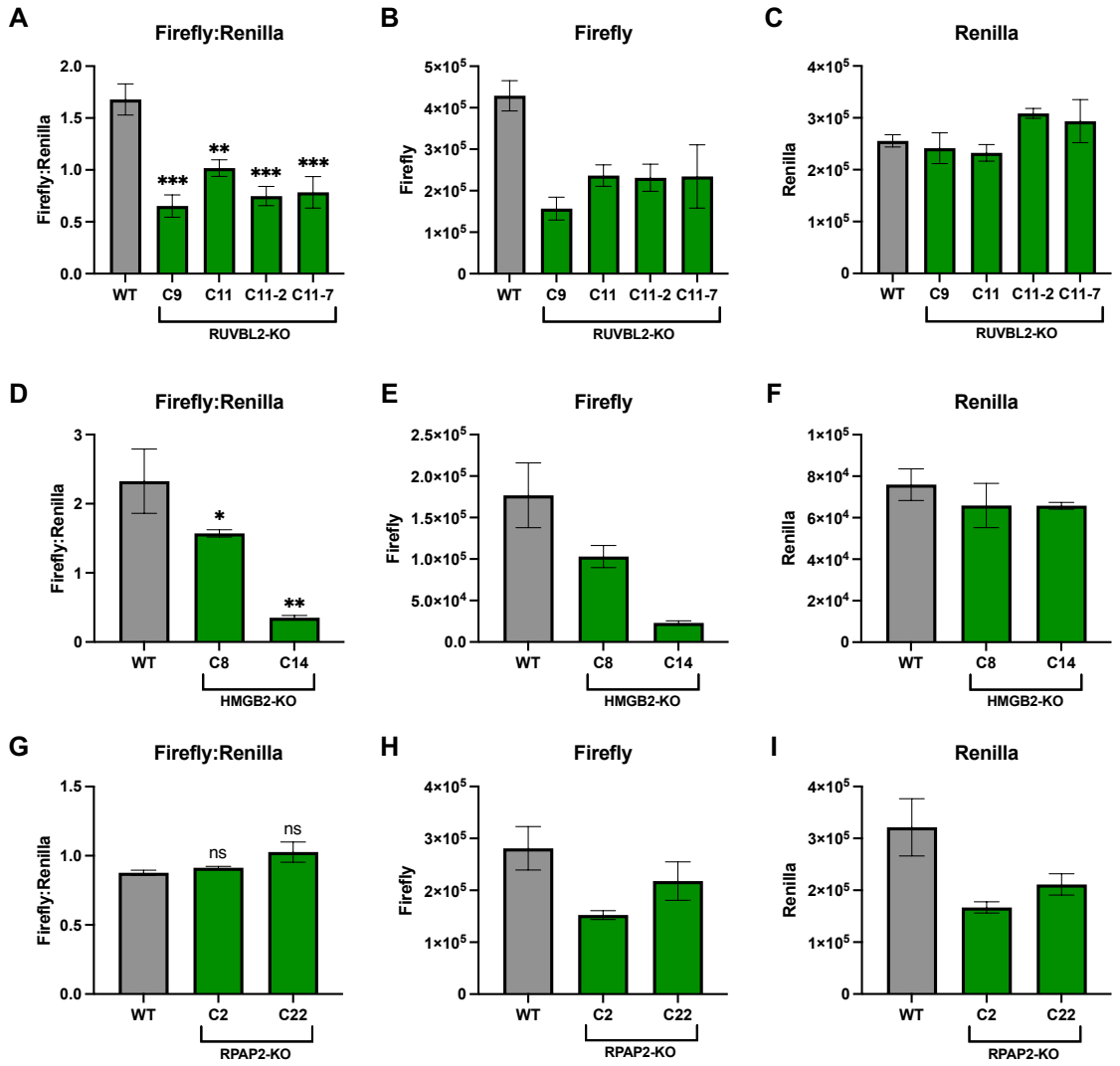

Figure 37. Polymerase activity in A549 WT, RUVBL2-KO, HMGB2-KO, and RPAP2-KO cell clones. A-I) Minigenome reporter assay in A549 WT, RUVBL2-KO (A-C), HMGB2-KO (D-F), and RPAP2-KO (G-I) cells using a PR8 polymerase constellation. Data is shown as Firefly luciferase activity relative to co-transfected Renilla luciferase levels (Firefly:Renilla) (A, D, G), Firefly luciferase activity (B, E, H), or Renilla luciferase activity (C, F, I). Data is shown as mean ± SD of n=3 technical repeats, representative of n=3 biological repeats. Statistical significance compared to WT was assessed using an unpaired *t* test. ns, not significant; *, $p<0.05$; **, $p<0.01$; ***, $p<0.001$.

Polymerase activity, indicated by the Firefly:Renilla ratio, was reduced in all RUVBL2-KO and HMGB2-KO cell clones compared to in the WT cells (Figure 37A and D). Analysis of

the Firefly and Renilla values separately showed that Firefly activity was reduced in all RUVBL2-KO and HMGB2-KO clones compared to in the WT clone while the Renilla values remained similar between the two (Figure 37B, C, E, and F). This suggests that KO of RUVBL2 and HMGB2 had no effect on the transfectability of the A549 cells nor their ability to express exogenous proteins and confirms the reduced polymerase activity to be a result of reduced amplification of the minigenome in the absence of HMGB2 or RUVBL2. Polymerase activity was lowest in RUVBL2-KO C9, C2, and C7 clones and the HMGB2-KO C14 clone compared to in the WT cells. We, therefore, decided to use the RUVBL2-KO C7 cells and HMGB2-KO C14 cells (hereafter referred to as RUVBL2-KO and HMGB2-KO, respectively) in future experiments.

Despite reduced Firefly activity in the RPAP2-KO cell clones, no difference in the Firefly:Renilla ratio was observed between the RPAP2-KO and WT clones (Figure 37G and H). The unchanged Firefly:Renilla ratios can be explained by the reduced Renilla levels in the RPAP2-KO cells as well (Figure 37I). Considering that Renilla expression is controlled by a RNAP II promoter and RPAP2 has a host function important for RNAP II cellular transcription activity, a likely explanation for the reduction in Renilla is that depletion of RPAP2 interferes with Renilla expression (Forget et al., 2013). This in turn implies that any effect on expression from the minigenome could be due to decreased expression of the viral polymerase proteins rather than an impact on actual activity of the enzyme. We decided to not report any further minigenome reporter assay data from these cells. Nevertheless, we decided to use the RPAP2-KO C2 cells (hereafter referred to as RPAP2-KO) in future experiments that would employ virus infection rather than plasmid transfections. We chose this clone because knockout of RPAP2 appeared to have been more successful in this clone than the C22 clone (Figure 36D and E).

Overall, these data show polymerase activity to be reduced in the absence of RUVBL2 and HMGB2 in multiple KO cell clones derived from A549 cells. This is consistent with the reduction in polymerase activity observed following siRNA-mediated knockdown of the genes in eHAP WT cells (see Section 2.2.7, Figure 27A) and corroborates that RUVBL2 and HMGB2 have supportive roles in polymerase activity.

To confirm that the reduction in polymerase activity in HMGB2-KO and RUVBL2-KO cells was due to depletion of the genes and not off-target effects, we provided the HMGB2-KO and RUVBL2-KO cells with exogenously expressed codon-optimised HMGB2 and RUVBL2 and tested for complementation by performing minigenome assays (Figure 38A-D). To test for gradual rescue of polymerase activity, we expressed increasing amounts of the two proteins. Polymerase activity was only partially restored with HMGB2 expression (Figure 38A). Polymerase activity was restored to the greatest extent when HMGB2 expression was similar to WT HMGB2 levels (40ng HMGB2) as determined by western blotting (Figure 38A and B).

This suggests that the IAV polymerase is only supported when HMGB2 is expressed at endogenous levels and that too high amounts of HMGB2 may exert an inhibitory effect. Meanwhile, complementation with RUVBL2 fully restored polymerase activity to WT levels and this occurred in a dose-dependent manner (Figure 38C and D).

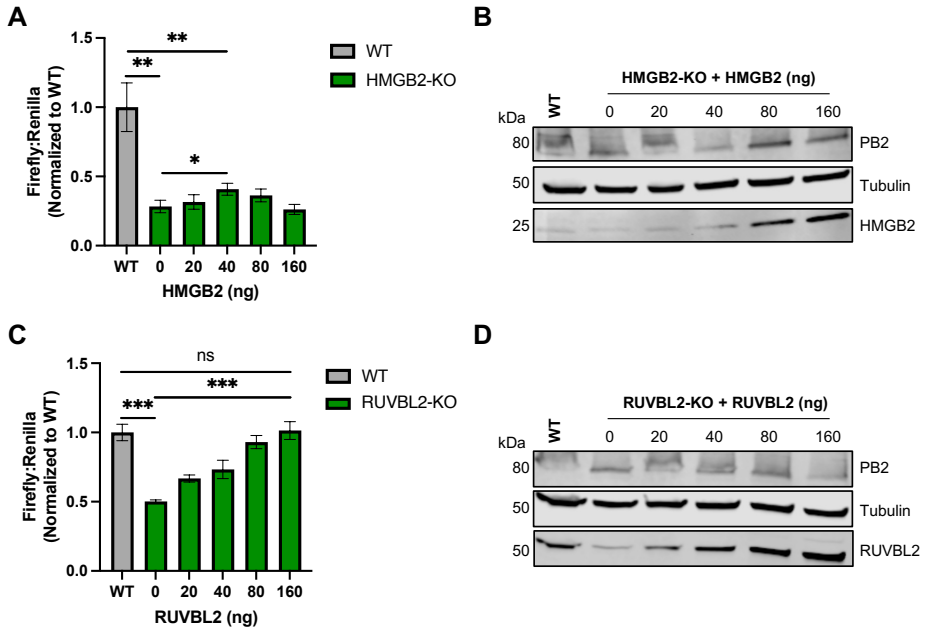

Figure 38. Complementation with HMGB2 and RUVBL2 partially and fully restores polymerase activity to WT levels, respectively.
A and C) Minigenome reporter assay in A549 WT and HMGB2-KO cells (A) or A549 WT and RUVBL2-KO cells (C). Polymerase constellation used was PR8. Plasmids expressing codon-optimised HMGB2 (A) and RUVBL2 (C) were co-transfected as annotated. Firefly luciferase activity relative to co-transfected Renilla luciferase levels was normalised to WT. Data is shown as mean ± SD of n=3 technical repeats, representative of n=3 biological repeats. Statistical significance was assessed compared to WT or 0ng HMGB2/RUVBL2, as indicated, using an unpaired *t* test. ns, not significant; *, $p<0.05$; **, $p<0.01$; ***, $p<0.001$. Accompanying western blots show HMGB2 (B), RUVBL2 (D), PB2, and tubulin (cellular control) protein expression for each condition.

Section 3.2.3. HMGB2 and RUVBL2 promote polymerase activity of a diverse range of IAV strains.

Having determined that HMGB2 and RUVBL2 support polymerase activity of the laboratory adapted PR8 strain, we wanted to understand whether this proviral role of the two proteins was conserved across IAV strains. To achieve this, we measured the activity of polymerase constellations from a seasonal H3N2 A/Victoria/3/75 (Vic75) strain, a pandemic H1N1 A/England/195/2009 (Eng195), and an avian H5N1 A/turkey/Turkey/05/2005 (Tky05) strain that harboured the mammalian-adapting PB2 E627K mutation (Figure 39B-D and F-H). We also included the PR8 polymerase constellation as a positive control (Figure 39A and E). Activity of all the viral polymerases tested was significantly reduced in the HMGB2-KO and

RUVBL2-KO cells compared to in the WT cells (Figure 39A-H). Polymerase activity of all strains tested was reduced to a similar extent in both HMGB2-KO and RUVBL2-KO cells, except for Eng195, the activity of which was less reduced in the HMGB2-KO cells. We showed that the level of PB2 expression remained similar in WT and HMGB2-KO or RUVBL2-KO cells for all strains by western blotting for PB2 expression in each cell type (Figure 39I and J). In some cases, PB2 expression was higher in the KO cells than WT cells, but nevertheless there was a reduction in polymerase activity. This confirms that the reduction in polymerase activity in the KO cells compared to WT cells can be attributed to gene depletion and not differences in transfection efficiency or reduced expression of the polymerase proteins. Overall, these data suggest that HMGB2 and RUVBL2 promote polymerase activity of a diverse range of IAV strains.

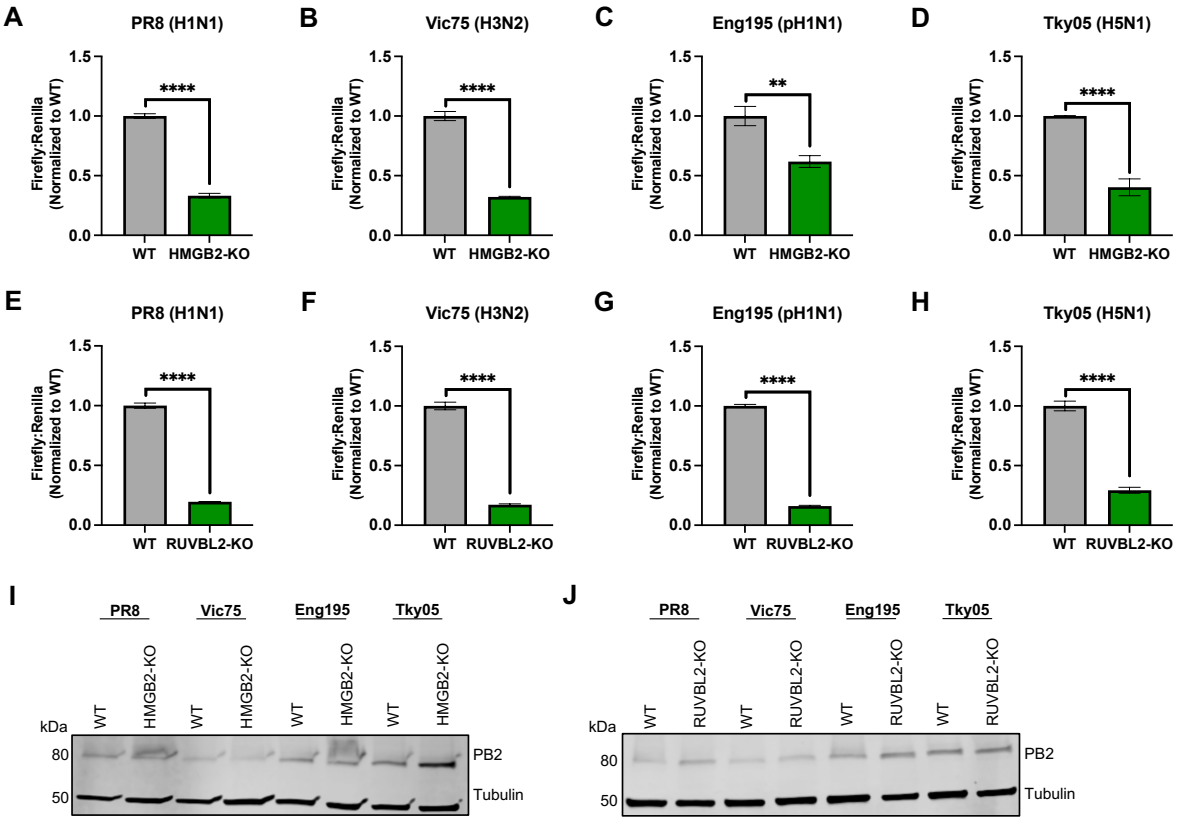

Figure 39. HMGB2 and RUVBL2 promote polymerase activity of a diverse range of IAV strains. A-H) Minigenome reporter assay in A549 WT and HMGB2-KO cells (A-D) or A549 WT and RUVBL2-KO cells (E-H) using PR8 (A and E), Vic75 (B and F), Eng195 (C and G), and Tky05 (D and H) polymerase constellations. Firefly luciferase activity relative to co-transfected Renilla luciferase levels was normalised to WT. Data is shown as mean ± SD of n=3 technical repeats, representative of n=3 biological repeats. Statistical significance was compared to WT using an unpaired *t* test. **, $p<0.01$; ****, $p<0.0001$. I and J) Western blots showing PR8, Vic75, Eng195, and Tky05 PB2 and tubulin (cellular control) protein expression in A549 WT and HMGB2-KO cells (I) or A549 WT and RUVBL2-KO cells (J).

Section 3.2.4. RPAP2 and HMGB2 promote polymerase activity in the context of infection.

As we were unable to reliably measure polymerase activity in the RPAP2-KO cells using a minigenome reporter assay, we instead investigated the role of RPAP2 in supporting viral polymerase activity by using a tagged RT-qPCR method to quantify the accumulation of segment 4 (HA) vRNA, cRNA, and mRNA following infection in WT and RPAP2-KO cells (see Section 2.2.4) (Figure 40A-C). At 2hpi, a significant reduction in mRNA synthesis was observed in the RPAP2-KO cells compared to in WT cells, while no difference was observed yet in vRNA and cRNA synthesis. At 5hpi, a significant reduction in the accumulation of all three viral RNA species was observed in the RPAP2-KO cells. This suggests that RPAP2 is important for robust polymerase activity in the context of infection.

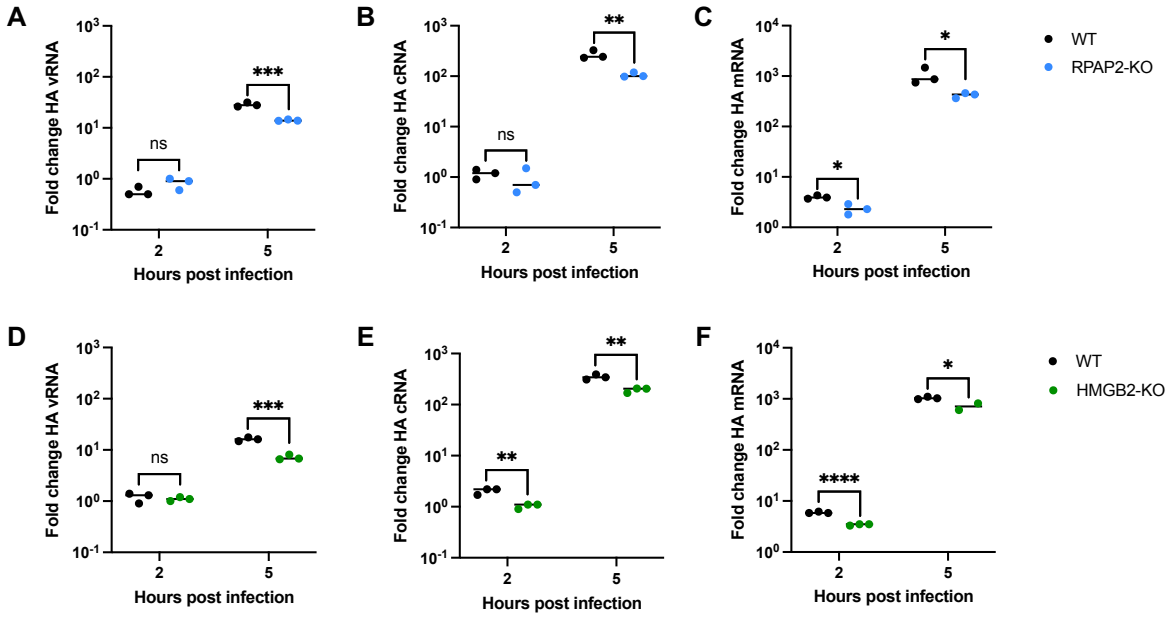

Figure 40. RPAP2 and HMGB2 support vRNA, cRNA, and mRNA synthesis in the context of infection.
A-F) Accumulation of segment 4 (HA) vRNA (A and D), cRNA (B and E), and mRNA (C and F) in A549 WT and RPAP2-KO cells (A-C) or A549 WT and HMGB2-KO cells (D-F) infected with PR8 (MOI=3), quantified by RT-qPCR at indicated timepoints post infection. The fold change was calculated versus input (0hpi). Data is shown as mean of n=3 technical repeats, representative of n=3 biological repeats. Statistical significance compared to WT was assessed at each timepoint using an unpaired *t* test, following log transformation. ns, not significant; *, p<0.05; **, p<0.01; ***, p<0.001; ****, p<0.0001.

We also compared the accumulation of vRNA, cRNA, and mRNA in WT and HMGB2-KO cells to confirm that HMGB2 plays a role in polymerase activity in the context of infection (Figure 40D-F). At 2hpi, a significant reduction in cRNA and mRNA accumulation was observed in HMGB2-KO cells compared to in WT cells (Figure 40E and F). Similar to in the RPAP2-KO cells, at 5hpi, a significant reduction in the accumulation of vRNA, cRNA, and

mRNA was observed in the HMGB2-KO cells (Figure 40D-F). This is consistent with our minigenome data and provides evidence that HMGB2 plays a proviral role in viral RNA synthesis in the context of infection.

Taken together, the data presented in this section, Section 3.2.3, and Chapter 2, show HMGB2, RUVBL2, and RPAP2 to be proviral host factors that support polymerase activity. This was shown in two different cell types (eHAPs and A549s) and using two gene depletion methods (siRNA and CRISPR-Cas9) as well as two methods of measuring polymerase activity (minigenome reporter assay and RT-qPCR).

Section 3.2.5. Polymerase activity in the absence of both HMGB1 and HMGB2 or both RUVBL1 and RUVBL2.

In addition to HMGB2, we had found its family member HMGB1 to co-precipitate from WT cells but not ANP32-KO cells in our differential interactome screen (see Section 2.2.5, Figure 23C). However, siRNA-mediated knockdown of HMGB1 had no effect on polymerase activity (see Section 2.2.7, Figure 27A). Considering that two of the ANP32 family members, ANP32A and ANP32B, are redundant in their support for polymerase activity, we next sought to investigate whether knockdown of both HMGB1 and HMGB2 further reduced polymerase activity and whether the two might perform functionally redundant roles (Staller et al., 2019, Zhang et al., 2019). First, we measured polymerase activity in eHAP WT cells following transfection with siNT or siRNA pools targeting HMGB1 (siHMGB1), HMGB2 (siHMGB2), or both HMGB1 and HMGB2 (siHMGB1+2) (Figure 41A). Knockdown of HMGB1 alone had no effect on polymerase activity, as expected. Knockdown of HMGB1+2 reduced polymerase activity to a slightly greater extent than knockdown of HMGB2 alone, although the difference was not significant. To further corroborate this, we tested the effect on polymerase activity of knockdown of HMGB1 in the A549 HMGB2-KO cells (Figure 41B). As expected, polymerase activity was reduced in HMGB2-KO cells treated with siNT compared to WT cells. Consistent with our data from eHAP WT cells, polymerase activity was slightly lower in HMGB2-KO cells treated with siHMGB1 than siNT, but again the difference was not significant. It is possible that knockdown of HMGB1 further decreased expression of HMGB2, and this is the reason behind the slightly reduced polymerase activity when both HMGB family members were targeted. However, western blots were not performed and, therefore, this cannot be said for certain. Together, our data suggests that HMGB2, but not HMGB1 is a cofactor for the IAV polymerase in human cells.

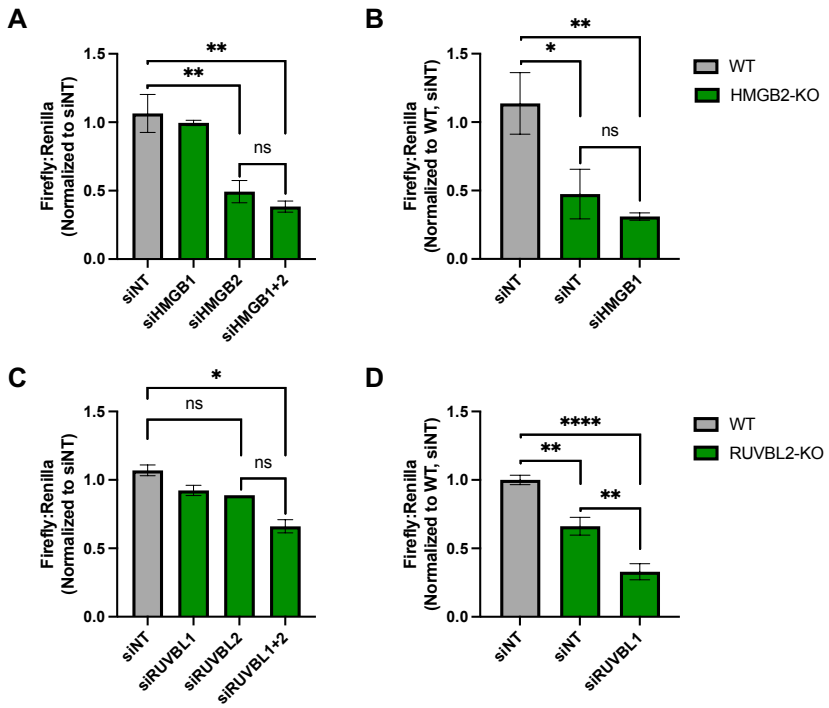

Figure 41. Polymerase activity following depletion of both HMGB1 and HMGB2 or both RUVBL1 and RUVBL2.
A and C) Minigenome reporter assay in eHAP WT cells transfected with a non-targeting siRNA (siNT) and siRNA pools targeting HMGB1, HMGB2, or HMGB1 and HMGB2 (A) or siRNA pools targeting RUVBL1, RUVBL2, or RUVBL1 and RUVBL2 (C). B and D) Minigenome reporter assay in A549 WT and HMGB2-KO cells transfected with siNT and an siRNA pool targeting HMGB1 (B) or A549 WT and RUVBL2-KO cells transfected with siNT and an siRNA pool targeting RUVBL1 (D). A-D) Polymerase constellation used was PR8. Firefly luciferase activity relative to co-transfected Renilla luciferase levels was normalised to siNT (A and C) or siNT-treated WT cells (B and D). Data is shown as mean ± SD of n=3 technical repeats, representative of n=2 biological repeats. Statistical significance was assessed compared to siNT (A and C) or siNT-treated WT cells (B and D) using an unpaired *t* test. ns, not significant; *, $p<0.05$; **, $p<0.01$; ****, $p<0.0001$.

Similarly, in addition to RUVBL2, we also found its family member, RUVBL1, to co-precipitate from WT cells but not ANP32-KO cells in our differential interactome screen (see Section 2.2.5, Figure 23C). siRNA-mediated knockdown of RUVBL1 reduced polymerase activity and virus replication, although the latter did not reach significance (see Sections 2.2.6 and 2.2.7, Figures 26A and 27A). We therefore decided to also test the effect on polymerase activity of depletion of both RUVBL1 and RUVBL2 in eHAP WT cells and A549 RUVBL2-KO cells, as we did for HMGB1 and HMGB2 (Figure 41C and D). In eHAP WT cells, knockdown of both RUVBL1 and RUVBL2 (siRUVBL1+2) significantly reduced polymerase activity whereas knockdown of RUVBL1 (siRUVBL1) or RUVBL2 (siRUVBL2) alone did not (Figure 41C). We have previously observed a significant reduction in polymerase activity following individual knockdown of either RUVBL1 or RUVBL2 (Chapter 2, Figure 27). The lack of effect of their individual knockdown observed here was, therefore, unexpected but could be explained if siRNA transfection was less efficient in this experiment. A greater reduction in

polymerase activity was observed in A549 RUVBL2-KO cells treated with siRUVBL1 than RUVBL2-KO cells treated with siNT (Figure 41D). Overall, this shows that knockdown of both RUVBL1 and RUVBL2 further reduces polymerase activity but cannot distinguish whether their roles are different or redundant.

Section 3.2.6. Using polymerase mutants to show that HMGB2 and RUVBL2 have supportive roles in polymerase replicase activity while RPAP2 has a supportive role in polymerase transcriptase activity.

So far, we measured polymerase activity using a minigenome reporter assay, which is a measure of bulk polymerase activity as both transcription and replication of the viral-like RNA template are necessary to generate a Firefly luciferase signal. We also measured polymerase activity by quantifying the accumulation of the three viral RNA species in the context of infection. In that assay, vRNA, cRNA, and mRNA synthesis are interdependent, meaning that effects on RNA transcription and replication cannot be distinguished. However, the unique strategy of our AP-MS screen was designed to discover host proteins important for either polymerase replicase or transcriptase activity. Specifically, based on the comparative interactomes obtained in WT and ANP32-KO cells, we hypothesised that HMGB2 and RUVBL2 would be replication-specific factors, and RPAP2 would be a transcription-specific factor. To provide functional evidence that this is the case, we next employed assays that allow cRNA and mRNA synthesis to be distinguished.

Although the outcome of a minigenome reporter assay is usually read out as a Firefly luciferase signal, it can also be measured in terms of individual viral RNAs (vRNA, cRNA, and mRNA). This can be achieved using the tagged RT-qPCR method with primers that target the vRNA, cRNA, and mRNA of the viral-like RNA template supplied, in this case Firefly luciferase. Alternatively, the viral-like RNA template could be generated from a plasmid expressing a viral gene, under the control of a RNAP I promoter. For example, a pPolI-HA plasmid and products detected using the RT-qPCR primers used in Figure 40. Importantly, unlike in infection, where vRNA, cRNA, and mRNA synthesis are interdependent, in a minigenome setup, cRNA and vRNA synthesis occur independently of mRNA synthesis. This is because encapsidation of the replication products and trans-activation of c-to-vRNA synthesis are dependent on the transfected polymerase subunits and NP which are expressed independently of viral polymerase activity.

As controls for measuring vRNA, cRNA, and mRNA accumulation in a minigenome setup, we made use of previously established replication-deficient (PA E410A) or transcription-deficient (PA D108A) mutant polymerases (Rehwinkel et al., 2010). The replication-deficient polymerase generated less vRNA and cRNA compared to the WT polymerase, but near WT levels of mRNA (Figure 42A-C). Conversely, the transcription-

deficient polymerase generated similar vRNA and cRNA levels compared to WT polymerase, but lower mRNA levels.

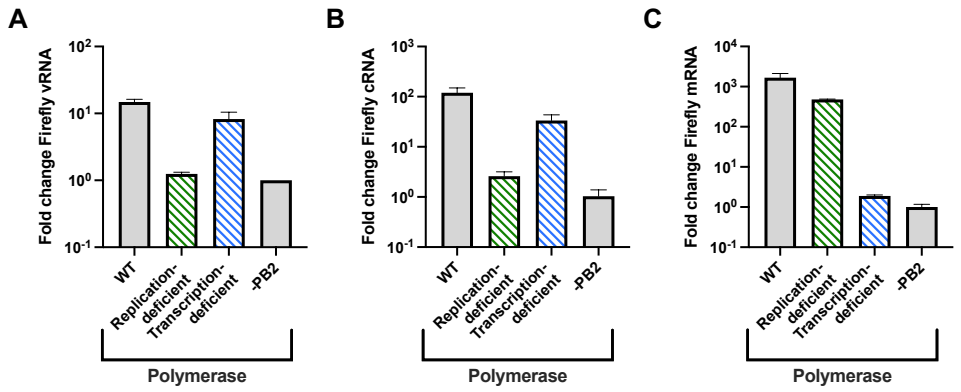

Figure 42. Characterisation of replication-deficient and transcription-deficient polymerase mutants.
A-C) Accumulation of Firefly luciferase vRNA (A), cRNA (B), and mRNA (C) in a minigenome reporter assay in eHAP WT cells, quantified by RT-qPCR. Cells were transfected with plasmids to reconstitute PR8 WT polymerase, replication-deficient polymerase (PA E410A), and transcription-deficient polymerase (PA D108A). vRNA template provided was a pPolI-Firefly luciferase plasmid. Empty plasmid was substituted for PB2 as a negative control. Data is shown as mean ± SD of n=3 technical repeats, representative of n=3 biological repeats.

We then assessed the effect of knockdown of HMGB2, RUVBL2, and RPAP2 on the accumulation of viral RNA species in a minigenome setup (Figure 43A-C). We compared the cRNA:vRNA ratio following knockdown of HMGB2, RUVBL2, and RPAP2 to that of the transcription-deficient polymerase in WT cells and the mRNA:vRNA ratio to that of the replication-deficient polymerase in WT cells (Figure 43A-C). We also included siRNA pools targeting both ANP32A and ANP32B (siANP32.1 and siANP32.2) as a positive control for replication-specific host factors. Knockdown of ANP32A and ANP32B resulted in a significant decrease in the cRNA:vRNA ratio compared to siNT (Figure 43B). As expected, given that vRNA also acts as a template for mRNA synthesis in the minigenome assay, the mRNA:vRNA ratio also decreased following knockdown of ANP32A and ANP32B (Figure 43C). Similar to knockdown of ANP32, both the cRNA:vRNA and mRNA:vRNA ratios were reduced following knockdown of HMGB2 and RUVBL2 (Figure 43B and C). In contrast, knockdown of RPAP2 had no effect on the cRNA:vRNA ratio but significantly reduced the mRNA:vRNA ratio. Overall, this shows that HMGB2 and RUVBL2 support RNA replication and RPAP2 supports RNA transcription, as predicted based on the differential AP-MS interactome screen (Chapter 2).

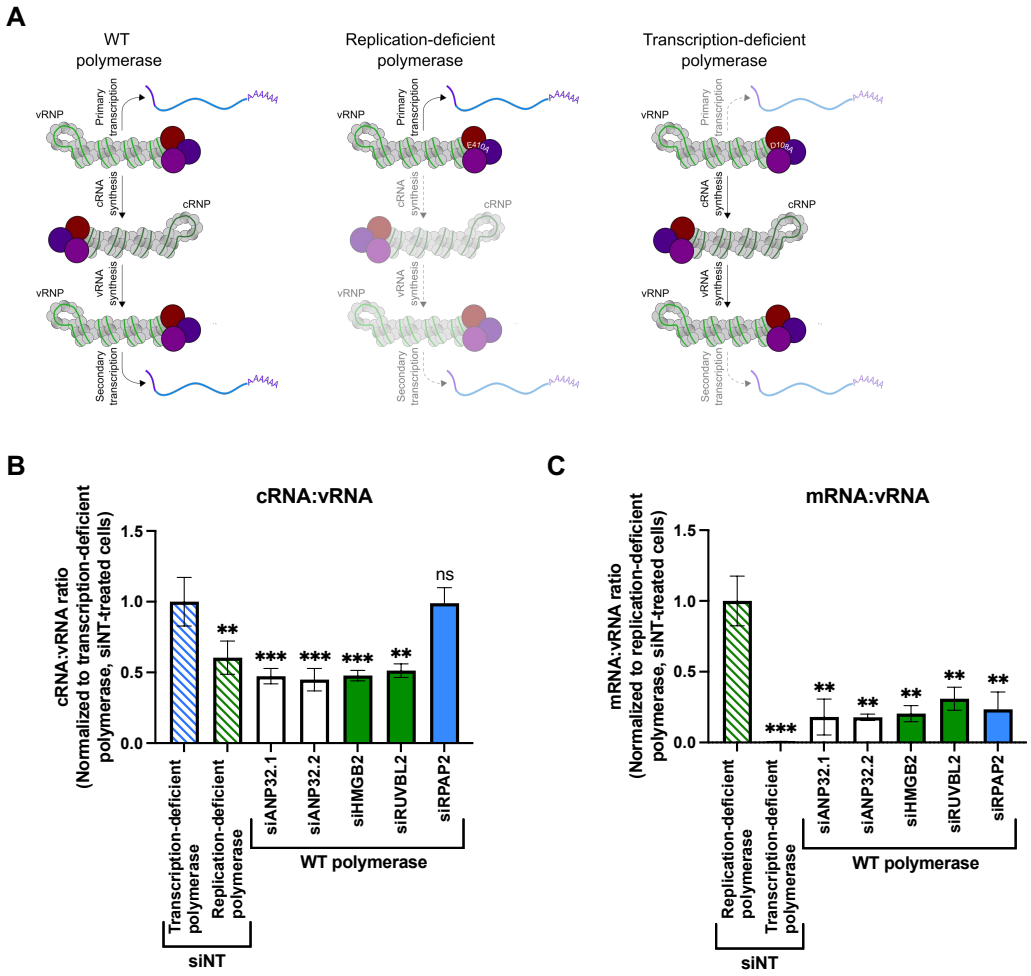

Figure 43. HMGB2 and RUVBL2 support viral RNA replication and RPAP2 supports viral RNA transcription.
A) Schematic showing vRNA, cRNA, and mRNA synthesis in a minigenome reporter assay with a WT, replication-deficient (PA E410A), or transcription-deficient (PA D108A) polymerase. B) cRNA:vRNA ratio and C) mRNA:vRNA ratio produced by a PR8 WT polymerase following transient knockdown of ANP32 (siANP32.1 and siANP32.2), HMGB2, RUVBL2, or RPAP2. cRNA:vRNA ratios were normalised to the ratio produced by a transcription-deficient polymerase in siNT-treated cells. mRNA:vRNA ratios were normalised to the ratio produced by a replication-deficient polymerase in siNT-treated cells. vRNA template provided was a pPolI-Firefly luciferase plasmid. Data is shown as mean ± SD of n=3 biological repeats performed in triplicate. Statistical significance was assessed compared to replication-deficient/transcription-deficient polymerases using an unpaired *t* test. ns, not significant; **, p<0.01; ***, p<0.001.

To provide further evidence that support from RUVBL2 and HMGB2 is replication-specific, we made use of the same replication-deficient and transcription-deficient mutants to bias the minigenome reporter assay luciferase readout towards transcription or replication, respectively (Figure 44A and B). Based on the characterisation of the mutants in Figure 42, the low but measurable bulk Firefly luciferase signal obtained with the replication-deficient mutant will largely be due to the polymerase transcriptase activity while the signal provided by the transcription-deficient mutant will largely be due to the polymerase replicase activity. In

both the HMGB2-KO and RUVBL2-KO cells, the replicase activity was significantly reduced compared to in the WT cells (Figure 44A and B). While the transcriptase activity remained the same between the HMGB2-KO and WT cells, it was slightly reduced in the RUVBL2-KO cells, although not significantly compared to WT. Together, this further corroborates that HMGB2 and RUVBL2 play supportive roles in RNA replication.

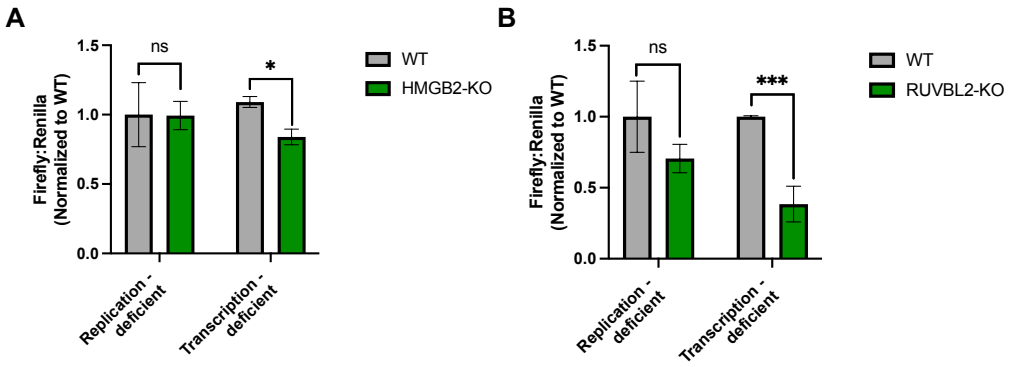

Figure 44. Depletion of HMGB2 and RUVBL2 reduce polymerase activity of a transcription-deficient polymerase but not a replication-deficient polymerase.
Minigenome reporter assay in A549 WT and HMGB2-KO cells (A) or A549 WT and RUVBL2-KO cells (B) using a replication-deficient (PA E410A) or transcription-deficient (PA D108A) PR8 polymerase constellation. Firefly luciferase activity relative to co-transfected Renilla luciferase levels was normalised to WT cells. Data is shown as mean ± SD of n=3 technical repeats, representative of n=3 biological repeats. Statistical significance was compared to WT using an unpaired *t* test. ns, not significant; *,p<0.05; ***, p<0.001.

Section 3.2.7. Using a cRNP stabilisation assay to show that HMGB2 is a replication-specific cofactor and RPAP2 is a transcription-specific cofactor.

To confirm using a different approach that HMGB2 is a replication-specific factor and RPAP2 is a transcription-specific factor, we made use of a previously established cRNP stabilisation assay (Swann et al., 2023, Vreede et al., 2004). In this assay, cells are infected with IAV to supply a vRNP template, after pre-expression of a catalytically dead PB1 mutant (PB1 D446Y), PA, PB2, and NP (Figure 45A). Pre-expression of this inactive polymerase allows stabilisation of the cRNA but not onwards replication. To prevent translation of WT replication competent PB1 from the infecting vRNA template, cells are treated with cycloheximide (CHX), which blocks translation of any new proteins. This means that only the pioneering round of cRNA synthesis and primary mRNA synthesis can occur. We have previously used this assay to demonstrate that ANP32 proteins play a direct role in cRNA synthesis but not mRNA synthesis (Swann et al., 2023).

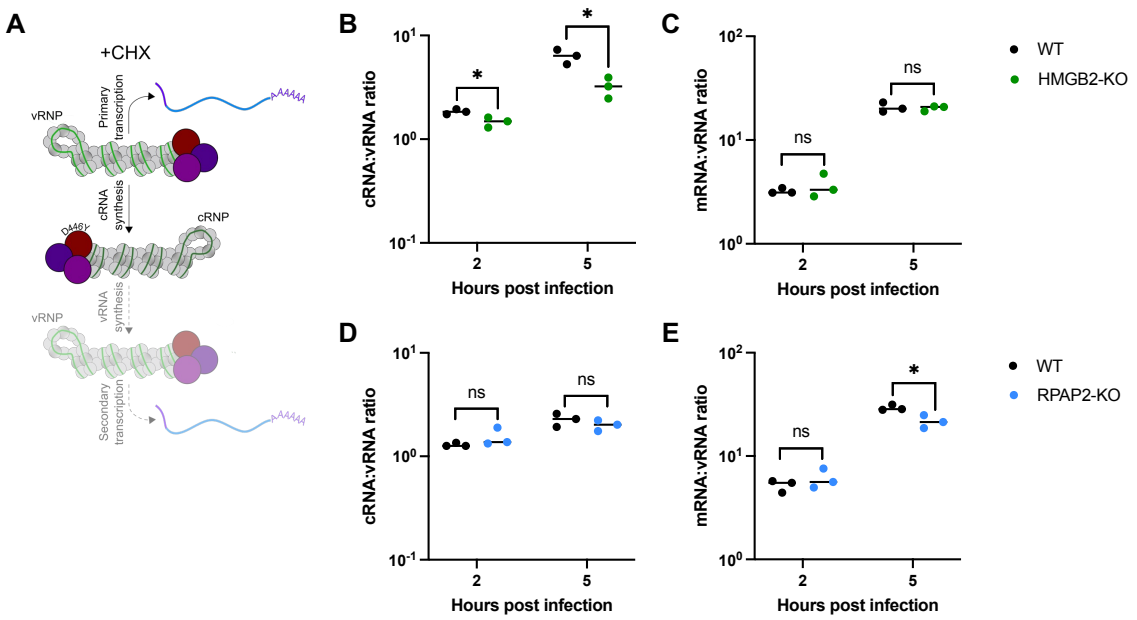

Figure 45. HMGB2 is a replication-specific cofactor and RPAP2 is a transcription-specific cofactor.
A) Schematic illustrating vRNA, cRNA, and mRNA synthesis under conditions of a cRNP stabilisation assay with cycloheximide (CHX) treatment. B-E) cRNP stabilisation assay with CHX treatment in A549 WT and HMGB2-KO cells (B and C) or WT and RPAP2-KO cells (D and E). Cells were infected with PR8 (MOI=3). Accumulation of segment 4 (HA) vRNA, cRNA, and mRNA was quantified by RT-qPCR at indicated timepoints post infection. Data is shown as fold change in cRNA:vRNA ratio (B and D) and mRNA:vRNA ratio (C and E) versus input (0hpi). Data is shown as mean of n=3 technical repeats, representative of n=3 biological repeats. Statistical significance was determined compared to WT at each timepoint using an unpaired *t* test, following log transformation. ns, not significant; *, $p<0.05$.

We compared segment 4 (HA) cRNA:vRNA and mRNA:vRNA ratios, measured using the tagged RT-qPCR method, in a cRNP stabilisation assay in WT and HMGB2-KO cells or WT and RPAP2-KO cells (Figure 45B-E). A significant decrease in cRNA accumulation was observed in HMGB2-KO cells compared to WT cells at 2 and 5hpi (Figure 45B). Meanwhile, no difference in mRNA synthesis was observed between the two cell types (Figure 45C). This demonstrates that HMGB2 has a direct role in cRNA synthesis, confirming it as a replication-specific cofactor. In contrast, the opposite pattern was observed in RPAP2-KO cells; less mRNA accumulated in RPAP2-KO cells than in WT cells at 5hpi and no difference in cRNA accumulation was observed between the two cell types (Figure 45D and E). This corroborates that RPAP2 has a direct role in mRNA synthesis. Taken together, these data provide further evidence that HMGB2 and RPAP2 are important host factors supporting IAV polymerase replicase and transcriptase activity, respectively, and confirm that the differential AP-MS screen can be used as a tool to identify replication- and transcription-specific host factors.

Section 3.2.8. Chemical inhibition of RUVBL2 ATPase activity does not inhibit polymerase activity.

Having shown that HMGB2, RUVBL2, and RPAP2 promote polymerase activity, we next sought to investigate whether the host factors can be used as antiviral drug targets. We performed a literature search to find previously discovered inhibitors of RUVBL2, HMGB2, or RPAP2. We found two inhibitors of RUVBL2 (Sorafenib and CB-6644), investigated in this section, and one inhibitor of HMGB2 (Inflachromene (ICM)), investigated in Section 3.2.9 (Assimon et al., 2019, Lee et al., 2014, Nano et al., 2020). Our literature search did not identify any inhibitors of RPAP2.

Both Sorafenib and CB-6644 allosterically inhibit the ATPase activity of RUVBL2, which is essential for the role of the RUVBL1/2 proteins in cancer progression (Assimon et al., 2019, Nano et al., 2020). While binding of Sorafenib to RUVBL2 results in a conformational change that is thought to either prevent ATP binding or ADP release, CB-6644 locks RUVBL2 in an ATP-bound state that prevents ATP hydrolysis. Sorafenib was originally shown to be a multikinase inhibitor and has been approved by the FDA for the treatment of various cancers including liver and kidney cancer (Wilhelm et al., 2006).

First, we tested the maximum concentrations of Sorafenib and CB-6644 that were tolerated by 293T cells (Figure 46A and B). We found that only low Sorafenib concentrations of up to 1.6μM had no effect on cell viability (Figure 46A). A Sorafenib concentration of 3.2μM reduced cell viability compared to the DMSO-treated control, although not significantly. All CB-6644 concentrations tested reduced cell viability, but this reduction did not reach significance compared to the DMSO-treated control (Figure 46B).

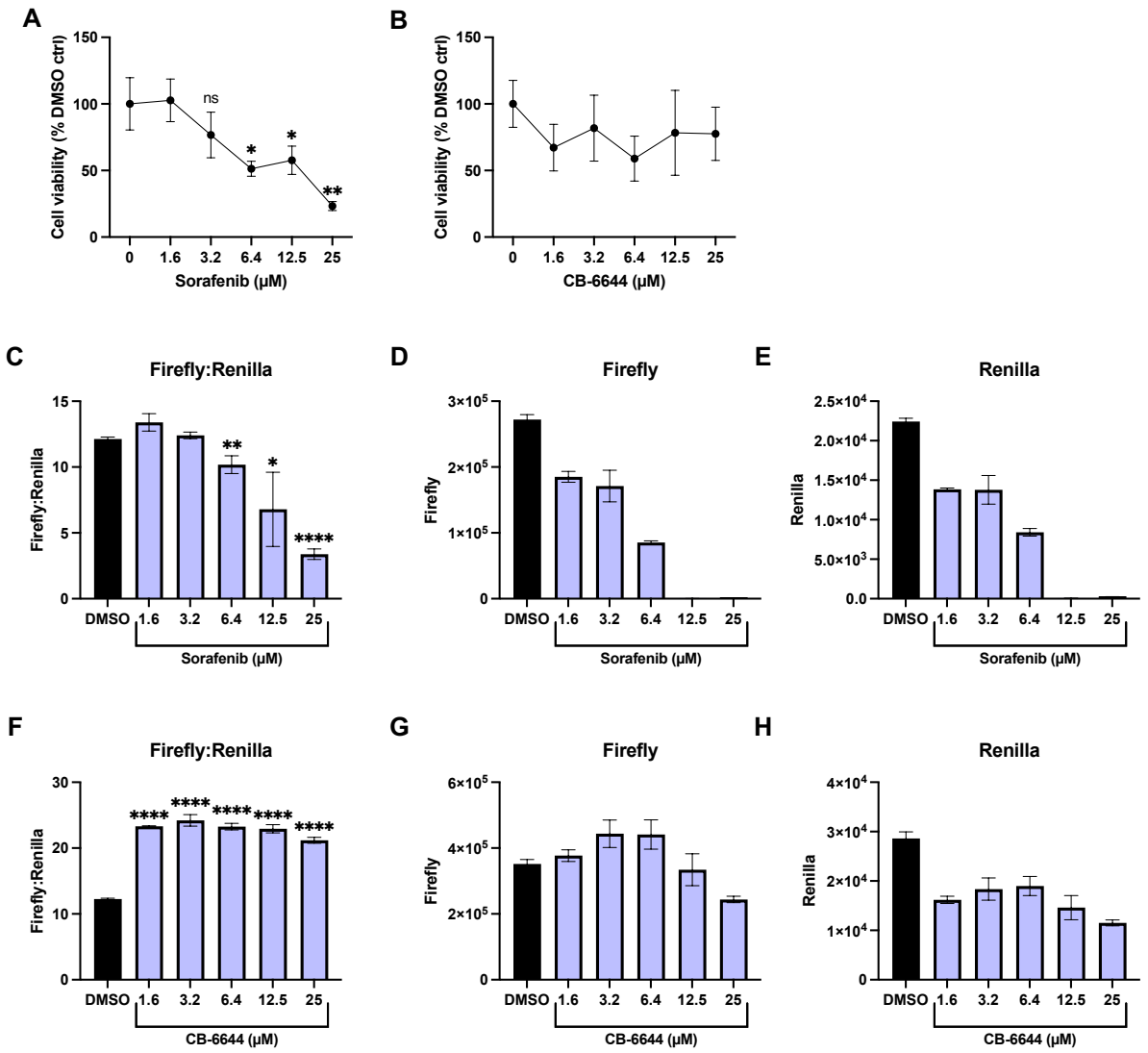

Figure 46. Chemical inhibition of RUVBL2 ATPase activity has no effect on polymerase activity. A and B) MTS assay of Sorafenib (0-25μM) (A) and CB-6644 (0-25μM) (B) in 293T cells. Cell viability is shown as percentage of DMSO control. Data is shown as mean ± SD of n=3 technical repeats. C-H) Minigenome reporter assay in 293T cells treated with Sorafenib (0-25μM) (C-E) or CB-6644 (0-25μM) (F-H) using a PR8 polymerase constellation. Data is shown as Firefly luciferase activity relative to co-transfected Renilla luciferase levels (Firefly:Renilla) (C and F), Firefly luciferase activity (D and G), and Renilla luciferase activity (E and H). Data is shown as mean ± SD of n=3 technical repeats, representative of n=2 biological repeats. For A-C and F: Statistical significance was assessed compared to DMSO-treated control using an unpaired *t* test. *, $p<0.05$; **, $p<0.001$; ****, $p<0.0001$.

Next, we tested the effect of Sorafenib and CB-6644 on polymerase activity of PR8 (Figure 46C-H). Considering the reduced cell viability observed with most concentrations of the drugs, we analysed the Firefly and Renilla (which also gives a measure of cell viability) values separately in addition to the Firefly:Renilla ratio, as in Figure 37. Sorafenib treatment reduced the Firefly values in a dose-dependent manner (Figure 46D). The Renilla values were also reduced in a dose-dependent manner, consistent with the MTS assay data (Figure 46A and E). The Firefly:Renilla values decreased with increasing Sorafenib dose but it is unclear

whether this decrease can be attributed to a reduction in polymerase activity given the reduced cell viability and reduced Renilla signals observed at these concentrations (Figure 46A, C-E). Meanwhile, CB-6644 treatment had little effect on the Firefly values but reduced the Renilla values (Figure 46G and H). The Firefly:Renilla values increased with CB-6644 treatment compared to the DMSO-treated control (Figure 46F). This increase is likely due to the unchanged Firefly values being normalised to the lower Renilla values and is, therefore, not a reflection of CB-6644 increasing polymerase activity.

Overall, we found that Sorafenib reduced polymerase activity, but it is likely that this was an indirect effect due to reduced cell viability. CB-6644 had no effect on polymerase activity.

Section 3.2.9. Chemical inhibition of HMGB2 inhibits virus growth and polymerase activity due to suppression of viral RNA replication.

ICM is a small molecule inhibitor of HMGB2 and its family member HMGB1 (Lee et al., 2014). ICM binds and prevents post-translational modification of the HMGB proteins. The drug was previously discovered as a therapeutic for the treatment of neuroinflammatory disease. We first determined the highest concentration of ICM tolerated by eHAP WT cells using an MTS assay (Figure 47A). We found that ICM concentrations up to 20uM had no effect on the cell viability of eHAP WT cells compared to the DMSO-treated control. We, therefore, used this ICM concentration or lower in further experiments.

To assess the effect of ICM on viral replication, we infected eHAP WT cells with PR8 virus and treated the cells with ICM (20uM) or DMSO. Virus released into supernatant was assayed at 24, 48, and 72hpi. ICM reduced virus titres at all timepoints compared to the DMSO-treated control (Figure 47B). Next, we tested the effect of ICM on polymerase activity of three different IAV strains; PR8, Eng195 and an avian H5N1 A/turkey/England/50-92/1991 (5092) strain bearing the mammalian-adapting E627K mutation to allow robust replication of the polymerase in mammalian cells (Figure 47C-E). ICM treatment resulted in a decrease in polymerase activity of all three strains in a dose-dependent manner.

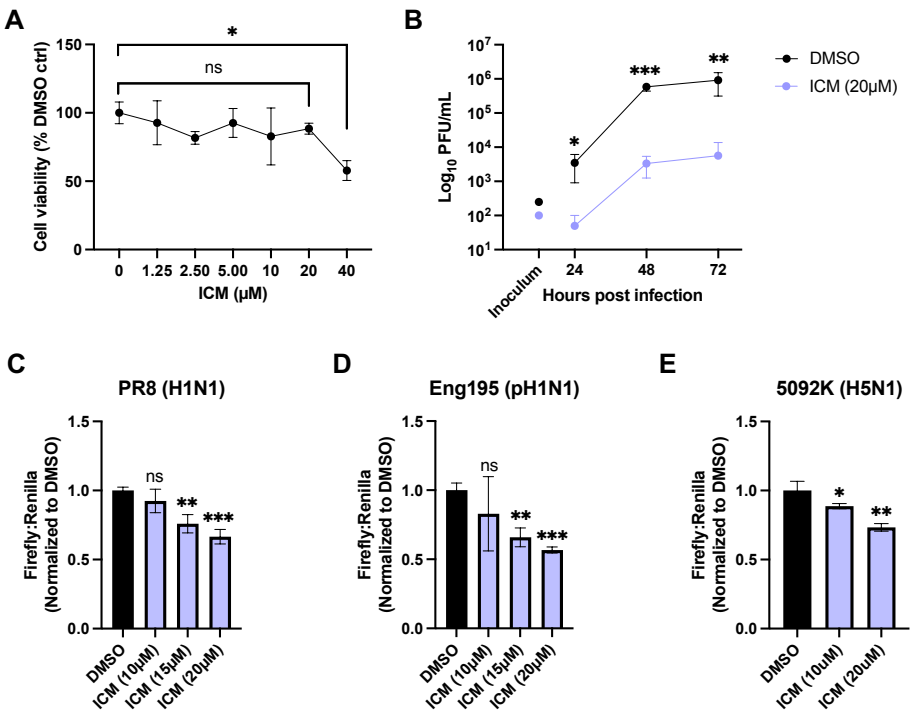

Figure 47. Chemical inhibition of HMGB2 suppresses virus growth and polymerase activity. A) MTS assay of ICM (0-40uM) in eHAP WT cells. Cell viability is shown as percentage of DMSO control. B) Virus replication in eHAP WT cells infected with PR8 (MOI=0.001) and treated with ICM (20uM) or DMSO. Supernatants were harvested at indicated timepoints post infection, and titres were determined by plaque assay on MDCK cells. C-E) Minigenome reporter assay in eHAP WT cells treated with ICM (10, 15, 20uM) or DMSO. Polymerase constellations used were PR8 (C), Eng195 (D), and 5092 bearing the mammalian adapting E627K mutation (5092K) (E). Firefly luciferase activity relative to co-transfected Renilla luciferase levels was normalised to DMSO-treated controls. For all panels: data is shown as mean ± SD of n=3 technical repeats, representative of n=3 biological repeats. Statistical significance was compared to DMSO-treated control using an unpaired *t* test. ns, not significant; *,p<0.05; **, p<0.001; ***, p<0.001.

To validate that ICM phenocopies the knockout of HMGB2, we compared the accumulation of segment 4 (HA) vRNA, cRNA, and mRNA in eHAP WT and ANP32-KO cells infected with PR8 and treated with ICM (20uM) or DMSO (Figure 48A-F). In eHAP WT cells treated with DMSO, the accumulation of vRNA, cRNA, and mRNA increased over time, as expected (Figure 48A-C). ICM treatment reduced the accumulation of cRNA and mRNA synthesis at 2hpi and the accumulation of all three viral RNA species at 5hpi. This was similar to the reduced viral RNA synthesis observed in HMGB2-KO cells under standard infection conditions (Figure 40D-F). To understand whether ICM directly inhibits vRNA and cRNA synthesis or indirectly via inhibition of mRNA synthesis, we tested the effect of ICM on the accumulation of the viral RNA species in ANP32-KO cells (Figure 48D-F). In both the ICM- and DMSO-treated ANP32-KO cells, the vRNA and cRNA levels did not increase above input, as expected (Figure 48D and E). mRNA accumulation increased over time, confirming that only mRNA synthesis is supported in these cells (Figure 48F). No difference in the mRNA

levels was observed in the ICM- and DMSO-treated cells, implying that ICM has no effect on viral transcription and therefore must specifically inhibit the cRNA and/or vRNA synthesis steps of replication in the WT cells. Overall, these data corroborate a direct role for HMGB2 in RNA replication, considering that ICM is an inhibitor of HMGB2, and suggest ICM to be a novel antiviral compound that warrants further investigation.

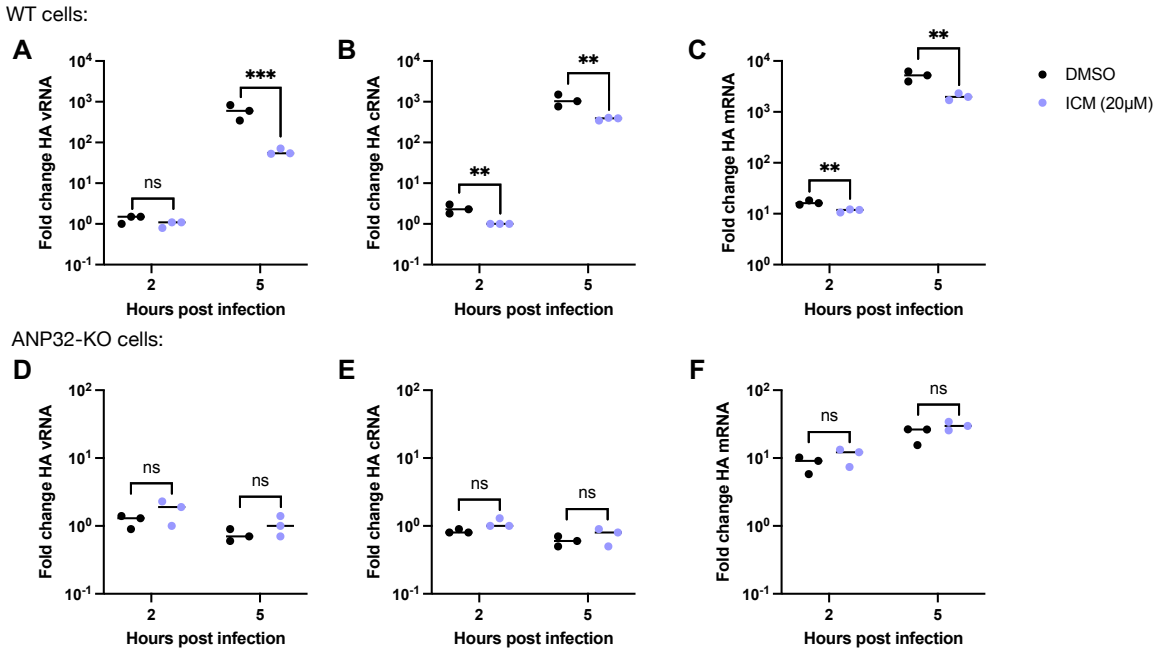

Figure 48. Chemical inhibition of HMGB2 suppresses viral RNA replication.
A-F) Accumulation of segment 4 (HA) vRNA (A and D), cRNA (B and E), and mRNA (C and F) in eHAP WT cells (A-C) or ANP32-KO cells (D-F) following infection with PR8 (MOI=3) and treatment with ICM (20um) or DMSO, quantified by RT-qPCR at indicated timepoints. Data is shown as the fold change over input (0hpi). Data is shown as mean of n=3 technical repeats, representative of n=3 biological repeats. Statistical significance compared to DMSO-treated control was assessed at each timepoint using an unpaired *t* test, following log transformation. ns, not significant; **, p<0.001; ***, p<0.001.

Section 3.2.10. ICM does not improve infection outcome in a mouse model of IAV infection.

Having demonstrated that ICM inhibits virus growth by suppressing viral RNA replication, we next wanted to assess whether ICM also shows efficacy in a mouse model of IAV infection. We employed the PR8 strain, because this strain is well-adapted to replication in mice, and we had found this strain to be inhibited by ICM in cell culture (Figures 47 and 48).

First, the optimal PR8 dose for infection of mice was determined. BALB/c mice (n=3) were infected with PR8 at four different doses (10, 100, 1000, 10,000 plaque forming units (PFU)) (Figure 49A-C). Weight, measured daily, was used as a measure of disease burden in the mice (Figure 49A). The three highest doses tested, 100PFU, 1000PFU, and 10,000PFU, resulted in high weight loss at early timepoints post infection and a low probability of survival

of 3 or 4 days (Figure 49A and B). Viral titres in the lungs were also measured (Figure 49C). As expected, the three highest doses resulted in the highest viral titres in the lung. In contrast, the lowest dose tested of 10PFU only resulted in limited weight loss by 7 days post inoculation (dpi) and low viral titres in the lung (Figure 49A and C). We, therefore, decided to use a PR8 dose intermediate between 10 and 100PFU, namely 30PFU, in future experiments.

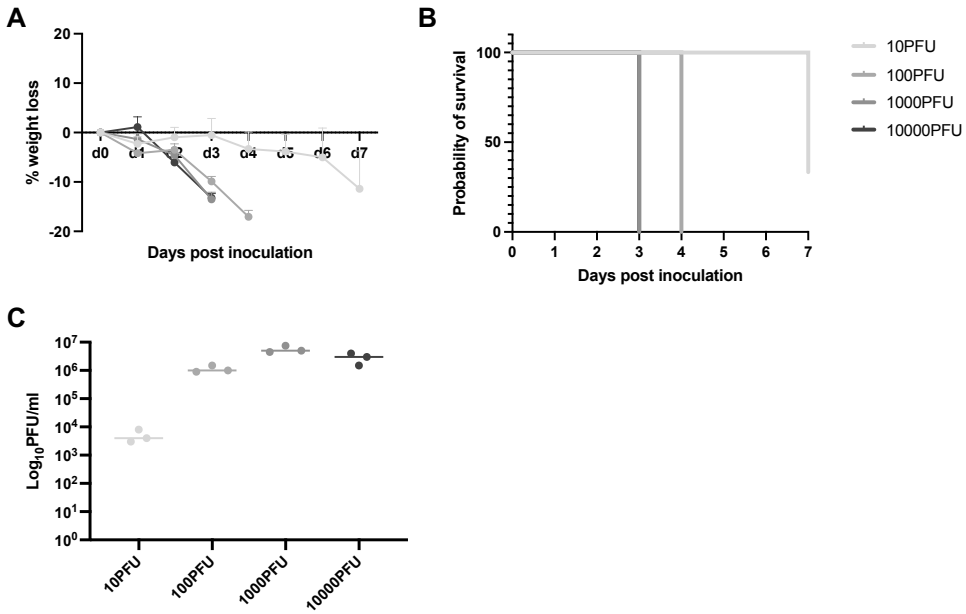

Figure 49. Determining the optimal PR8 dose for a mouse model of IAV infection.
BALB/c mice (n=3) were inoculated intranasally with 10, 100, 1000, 10000PFU of PR8. A) Percentage weight loss measured daily post inoculation relative to 0 days post inoculation (dpi). B) The probability of survival with each dose. C) Viral titres in the lungs of mice, harvested and homogenised 7dpi (10PFU), 4dpi (100PFU), or 3dpi (1000 and 10000PFU). Viral titres were determined by plaque assay on MDCK cells.

Next, we tested the effect of ICM in mice infected with PR8. BALB/c mice were mock-infected (n=10), PR8-infected and treated with a vehicle control (n=10), or PR8-infected and treated with ICM (n=10) (Figure 50A-C). Mice were treated with the vehicle control and ICM at inoculation and daily post inoculation. As expected, the mock-infected mice did not lose any weight over the course of the experiment and all survived (Figure 50A and B). Weight loss in the ICM-treated group followed a similar trend as the vehicle-treated group until 3dpi (Figure 50A). At this timepoint, the viral titres in the lung were also similar between the ICM-treated and vehicle-treated groups (Figure 50C). However, by 6dpi, ICM treatment resulted in more weight loss than vehicle treatment (Figure 50A). At this timepoint, viral titres in the lungs of ICM-treated mice were also unexpectedly higher than viral titres in the lungs of vehicle-treated mice (Figure 50C). This suggests that, in contrast to our results obtained in cell culture, ICM treatment exacerbates IAV infection in mice.

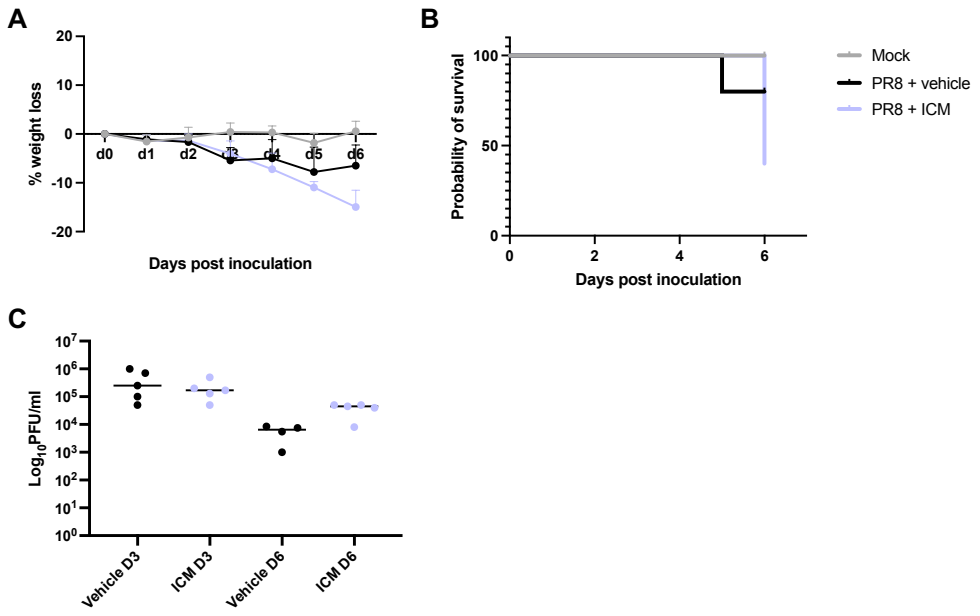

Figure 50. ICM treatment did not improve disease outcome in a mouse model of IAV infection. Mice (n=10) were mock-infected, PR8-infected and treated with a vehicle control, or PR8-infected and treated with ICM. (A) Percentage weight loss measured daily post inoculation relative to 0 days post inoculation (dpi). B) The probability of survival for each condition. C) Viral titres in the lungs of mice, harvested and homogenised 3dpi or 6dpi. Viral titres were determined by plaque assay on MDCK cells.

It is important to note that we did not include a control group of mice that were mock-infected and treated with ICM. We, therefore, cannot determine from our data whether the higher weight loss of ICM-treated mice was due solely to a proviral effect of ICM on viral infection or also to toxicity of the drug. Furthermore, the drug was administered intraperitoneally, and it is, therefore, not certain that the drug reached the lungs, which is the primary site of influenza virus replication in mice. Although if the drug did not reach the lungs, then it is unclear how viral lung titres were affected. Even so, in future experiments, a different route of administration, such as intranasal, could be tested.

Section 3.3. Discussion

In this chapter, HMGB2 and RUVBL2 were shown to support polymerase replicase activity and RPAP2 was shown to support polymerase transcriptase activity. This was demonstrated using various gene depletion methods (CRISPR-Cas9 and siRNA), polymerase mutants that can only perform transcription or replication, and assays that allow cRNA and mRNA synthesis to be distinguished. Overall, the data presented in this chapter serves as a proof-of-principle that the differential interactome screen performed in Chapter 2 can be used as a more targeted approach to discovering host proteins important for polymerase replicase or transcriptase activity.

RPAP2 supports IAV RNA transcription

We identified RPAP2 as a transcription-specific host factor. We showed that depletion of RPAP2 reduced mRNA accumulation but not cRNA accumulation in a minigenome setup and in a cRNP stabilisation assay. RPAP2 has not previously been implicated in the IAV lifecycle, but such a proviral role for RPAP2 fits with its host function where it binds RNAP II and supports its nuclear import (Forget et al., 2013). Host RNAP II is known to be essential for viral transcription, providing access to host capped RNA fragments that serve as primers for viral transcription initiation (Engelhardt et al., 2005). Interestingly, RPAP2 has also been found to play an additional, more specific role in host transcription, binding the RNAP II CTD phosphorylated at Ser7 and promoting transcription of snRNA genes (Egloff et al., 2007, Egloff et al., 2012). Considering that snRNA genes are the preferred target for viral cap-snatching, we speculate that RPAP2 plays a direct role in the cap-snatching step of transcription initiation, perhaps by bringing the IAV polymerase into proximity with host RNAP IIs transcribing snRNA genes (Gu et al., 2015, Koppstein et al., 2015). However, it is also possible that the effect of RPAP2 on viral transcription is indirect; loss of RPAP2 reduces nuclear accumulation of RNAP II such that less RNAP II is available to support viral transcription.

RUVBL2 supports IAV RNA replication

We demonstrated that RUVBL2 plays a supportive role in viral RNA replication as depletion of RUVBL2 reduced the cRNA:vRNA ratio in a minigenome setup as well as the activity of a mutant polymerase that can only replicate. RUVBL2 has previously been implicated in the IAV lifecycle. It was identified as a polymerase and NP interactor in various interactome screens and shown to interact with PB1, PB2, and NP in co-IP or BiFC assays (Haas et al., 2023, Heaton et al., 2016, Kakugawa et al., 2009, Mayer et al., 2007, Watanabe et al., 2014). However, the functional role of RUVBL2 in IAV infection remains unclear from the literature. A truncated version of quail RUVBL2 was shown to enhance avian (PB2 627E) polymerase activity in human cells (Kakugawa et al., 2009). However, full length quail and human RUVBL2 were found to reduce polymerase activity when overexpressed and increase polymerase activity when depleted, suggesting the host factor to play an antiviral role in viral RNA synthesis. More recent work has shown knockdown of human RUVBL2 to decrease virus replication, suggesting RUVBL2 to be a proviral factor in IAV infection (Haas et al., 2023). Our data is consistent with this latter study, and we further show that this proviral role of RUVBL2 is, at least in part, due to its support at the RNA replication stage.

We cannot exclude that RUVBL2 may also play an additional role in viral RNA transcription given that depletion of RUVBL2 not only reduced the cRNA:vRNA but also the mRNA:vRNA ratio in a minigenome setup. While this may be an indirect effect due to the dependency of transcription on replication to amplify the vRNA template, we also found that

depletion of RUVBL2 slightly reduced the activity of a mutant polymerase that can only transcribe, although this did not reach significance. In the host cell, RUVBL2 has been shown to bind the RNAP II CTD and promote RNAP II clustering and transcription initiation (Wang et al., 2022b). Given the known role of host RNAP II in viral transcription, this could further implicate RUVBL2 in supporting viral transcription. Interestingly, it is not resolved whether IAV remains associated with or dissociates from host RNAP II during RNA replication. Recent reports have suggested that binding of the RNAP II CTD and ANP32 to the viral polymerase is mutually exclusive (Arragain et al., 2024, Staller et al., 2024). Given the known role of ANP32 in cRNA and vRNA synthesis, this implies that the polymerase does not remain bound to RNAP II for RNA replication. However, another report has suggested host RNAP II to act as anchor for the IAV polymerase and that the two remain associated during both transcription and replication (Krischuns et al., 2024). Further work is needed to understand whether RUVBL2 supports viral transcription as well as RNA replication and whether its association with host RNAP II has an impact.

Aside from acting as a transcriptional activator by promoting RNAP II clustering, RUVBL2 is known to have a diverse range of additional functions in the host cell. Such functions include chromatin remodelling, chaperone activity as part of the R2TP complex, and DNA helicase activity (Huen et al., 2010). RUVBL2 exists either as a homo-hexameric ring consisting of RUVBL2 monomers or a hetero-hexomeric ring consisting of alternating RUVBL2 and RUVBL1 monomers (Figure 51A and B) (Gorynia et al., 2011, Silva et al., 2018). The center of the ring is formed by RUVBL2's AAA+ domain and contains nucleotide binding pockets as well as the catalytic residues necessary for ATP hydrolysis (Silva et al., 2018). RUVBL2 (and RUVBL1) also has an insertion domain that extends from the AAA+ core and acts as a scaffold which recruits various proteins (Figure 51A and B) (Dauden et al., 2021). The insertion domain has an external part, which is important for protein-protein interactions, and an internal part, which is connected to the AAA+ core. This domain is responsible for RUVBL2's (and RUVBL1's) interactions with components of the R2TP complex, components of chromatin remodelling complexes, as well as various transcription factors, perhaps including RNAP II (Dauden et al., 2021). Monomeric RUVBL2 is also capable of directly binding single-stranded DNA (Silva et al., 2018). Interestingly, DNA binding causes RUVBL2 to assemble into hexameric rings around the DNA. This suggests a mechanism for RUVBL2's helicase activity whereby RUVBL2 oligomerises around a single-stranded DNA overhang and then subsequently facilitates unwinding of the upstream double-stranded DNA in an ATP-dependent manner. The insertion domain is also thought to be involved in binding of DNA, but its exact role remains unclear (Lopez-Perrote et al., 2012). Considering the known role of the insertion domain in protein-protein interactions, it could be speculated that this domain is also involved in interactions with IAV vRNP components.

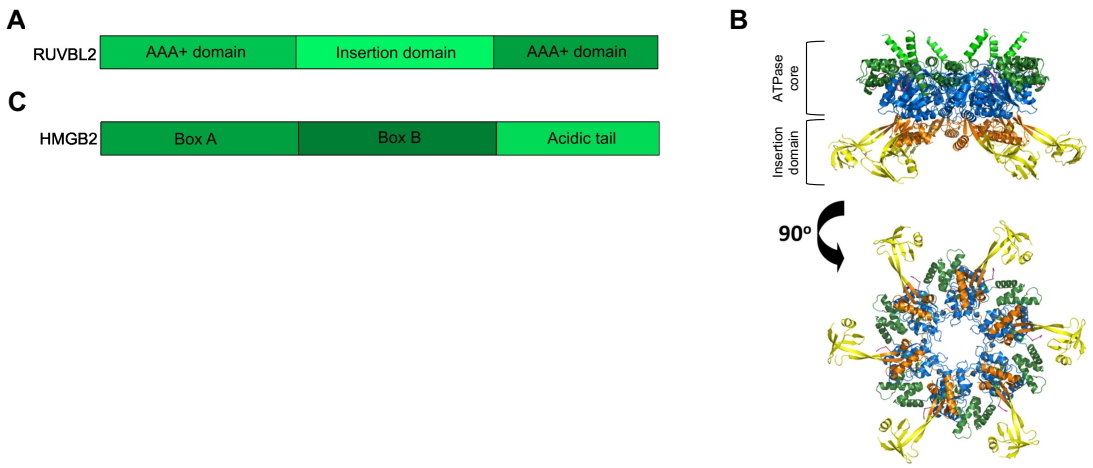

Figure 51. Domain architecture of HMGB2 and RUVBL2.
A and B) Domain structures of HMGB2 (A) and RUVBL2 (B). Cartton of the x-ray crystallography structure of homo-hexameric human RUVBL2. Taken from Silva et al., 2018.

RUVBL2 has also been shown to interact with the viral NS1 protein and contribute to the regulation of apoptosis in infected cells (Wang et al., 2021b). Interestingly, NS1 has also been shown to play a supportive role in polymerase activity by enhancing transcription (Zhang et al., 2023, Min et al., 2007). It is possible that RUVBL2 is involved in this role of NS1, although further work is necessary to test this.

<u>HMGB2 supports IAV RNA replication</u>

We propose that HMGB2 is a replication-specific host factor. We showed that depletion of HMGB2 reduced the cRNA:vRNA and mRNA:vRNA ratios in a minigenome setup. We confirmed that the reduction in mRNA levels in this assay was an indirect effect, by using a cRNP stabilisation assay to show that only cRNA and not mRNA accumulation was reduced in HMGB2-KO cells. Furthermore, depletion of HMGB2 reduced activity of a mutant polymerase that can only replicate but not the activity of a mutant polymerase that can only transcribe. While complementation with RUVBL2 fully restored polymerase activity in RUVBL2-KO cells, complementation with HMGB2 did not. At the highest HMGB2 plasmid amounts tested, the supportive role of HMGB2 in polymerase activity was even reduced. This suggests that there is an optimal HMGB2 amount for its proviral role, beyond which the host factor is no longer proviral and becomes inhibitory. Such a concept of an optimal amount has been observed with other host factors as well. Notably, ANP32 has been found to have an inhibitory effect on polymerase activity when highly expressed (Bi et al., 2019, Long et al., 2016, Staller et al., 2019, Zhang et al., 2019). The same has been observed with IMPα7 as well (Yu et al., 2022).

In the host cell, HMGB2 and its family member HMGB1 play roles in modulating nucleosome and chromatin structure and recruiting transcription factors. The two HMGB

proteins share 80% amino acid sequence identity and structural motifs: two HMG box domains (box A and box B) and a C-terminal acidic tail (Figure 51C) (Zheng et al., 2023). The main role of the box A and box B HMGB domains, which are rich in positively charged residues, is to bind DNA in a sequence-independent manner. The two domains bind to the minor groove of DNA, introducing a bend in the DNA, and also recognise already distorted DNA structures such as kinks, bends, and junctions (Agresti and Bianchi, 2003). HMGB proteins are proposed to modulate nucleosome assembly by binding DNA at nucleosome entries/exits, loosening the DNA, and enhancing accessibility of chromatin remodelling complexes (Travers, 2003). In addition, HMGB proteins are believed to recruit transcription factors by acting as transient chaperones that bind both DNA and protein and then dissociate from the resulting ternary complex once the protein is stably bound to the DNA (Starkova et al., 2023).

In contrast to the N-terminal HMGB DNA-binding domains, the C-terminal region of the HMGB proteins is highly acidic and negatively charged. The C-terminal region has been shown to bind both core histones and linker histones, potentially displacing these from their binding sites on DNA and further facilitating nucleosome remodelling (Cato et al., 2008). The C-terminal domain also regulates the activity of the N-terminal HMGB domains by adopting either a collapsed or extended conformation (Stott et al., 2010). In its collapsed conformation, the C-terminal domain inserts between the box A and box B domains, rendering the protein functionally inactive. In the active state, these interactions are disrupted, and the C-terminal domain exists in an extended conformation.

Although HMGB2 (and HMGB1) are typically found in the nucleus where they carry out their roles in transcriptional regulation described above, the two proteins have also been shown to localise to the cytoplasm and the extracellular space (Starkova et al., 2023). The cellular localisation of the HMGB proteins is modulated by their post-translational modification, which occurs at residues near their NLS and DNA-binding domains. The HMGB proteins undergo phosphorylation, acetylation, and methylation all of which induce cytoplasmic accumulation of the two proteins. In activated immune cells, the HMGB proteins can be released from the cytoplasm into the extracellular space, where they function as pro-inflammatory cytokines (Zhang et al., 2020). Specifically, the HMGB proteins interact with pattern recognition receptors (PRRs) on the cell surface, which leads to the activation of inflammatory signaling pathways, including the NF-kB pathway, and activation of the immune response.

In the context of IAV, HMGB2, and its family member HMGB1, have previously been shown to interact with NP both when present as a vRNP and as a free NP (Moisy et al., 2012). The box A domain of either protein was found to be sufficient for NP binding (Moisy et al., 2012). In fact, the C-terminal domain of the HMGB proteins was found to reduce NP binding. This could be explained by the finding that in its collapsed conformation, the C-terminal domain

causes the HMGB proteins to become inactive (Stott et al., 2010). Considering that the HMGB proteins act as chaperones in the host cell and recruit proteins to DNA targets, it could be speculated that HMGB2 similarly aids in the recruitment of the viral NP protein to viral RNA during replication.

Aside from its interaction with NP, HMGB2 has not previously been shown to play a functional role in the IAV lifecycle. Specifically, in contrast to our data, Moisy et al., found knockout of HMGB2 to have no significant effect on viral replication in MEFs, whereas knockout of HMGB1 did (Moisy et al., 2012). Considering that our data was acquired from human cells, the contradiction between the findings could be because of differences in the roles of HMGB1 and HMGB2 in mice and humans (discussed in more detail below).

RUVBL2 and HMGB2 as antiviral drug targets

In this chapter, we also tested whether RUVBL2 and HMGB2 could be feasible antiviral drug targets. Firstly, we tested two drugs, Sorafenib and CB-6644, which both inhibit RUVBL2 ATPase activity and were previously developed as anti-cancer drugs (Assimon et al., 2019, Nano et al., 2020). We concluded that neither drug inhibited polymerase activity at non-cytotoxic concentrations. This is in line with a previous report suggesting that the ATPase activity of RUVBL2 is not important for its role in IAV infection (Kakugawa et al., 2009). The authors showed a RUVBL2 mutant lacking ATPase activity to have the same effect on polymerase activity and virus growth as WT RUVBL2. Taken together with our data, this suggests that future antivirals targeting RUVBL2 should interfere with a different function than its ATPase activity.

Secondly, we tested the efficacy of ICM, a previously discovered inhibitor of HMGB2 and HMGB1, against IAV infection (Lee et al., 2014). We found ICM to be a promising antiviral in cell culture, suppressing virus growth by inhibiting viral RNA replication. ICM prevents phosphorylation and acetylation of the HMGB proteins at sites near their NLS, which induces accumulation of the proteins in the nucleus. It is, therefore, possible that the inhibitory effect of ICM on viral RNA replication is due to the drug altering the availability of HMGB2 inside the nucleus. It could also be speculated that the high amounts of HMGB2 inside the nucleus upon ICM treatment may be inhibitory to IAV polymerase activity, considering that we found too high amounts of overexpressed HMGB2 to be inhibitory in a minigenome reporter assay. ICM is predicted to bind at the DNA-binding domain of Box A, which is near the NLS. Given that previous studies have shown this part of HMGB2 to be important for NP binding, it is also possible that ICM directly prevents HMGB2 from interacting with NP (Moisy et al., 2012).

We showed ICM to suppress polymerase activity of three different IAV strains, including a H5N1 strain. Considering the pandemic potential of avian strains of the H5N1 subtype, this finding suggests that ICM may be an effective antiviral in the event of a pandemic.

To confirm this, the efficacy of ICM against further H5N1 strains should be tested, including the H5N1 strains responsible for the current IAV outbreak in dairy cattle in the USA (Caserta et al., 2024). Importantly, ICM also has anti-inflammatory properties as it inhibits the post-translational modification of HMGB2, leading to its nuclear accumulation and preventing its release into the extracellular space (Lee et al., 2014). In turn, this suppresses HMGB2's role in activating the inflammatory response and the NF-kB pathway. This anti-inflammatory property of ICM may make the drug even more suited for use in a pandemic where infections often result in overexuberant inflammation, which can lead to severe disease (de Jong et al., 2006).

We also tested the efficacy of ICM in a mouse model of IAV infection. In contrast to the antiviral properties of ICM in cell culture in human cells, we found that ICM had a proviral effect on IAV infection in mice. Specifically, ICM treatment resulted in greater weight loss and higher viral titres in the lungs of IAV-infected mice than vehicle treatment. As mentioned previously, the role of murine HMGB proteins in IAV infection has previously been studied using MEFs derived from HMGB1- or HMGB2-deficient mice (Moisy et al., 2012). Virus growth of a mammalian-adapted IAV strain was impaired in HMGB1-KO MEFs but not in HMGB2-KO MEFs. In fact, virus growth appeared to be slightly enhanced in HMGB2-KO MEFs compared to WT MEFs. Murine HMGB1 (muHMGB1) was further shown to support polymerase activity. This suggests that in mice, muHMGB1 plays a proviral role in IAV infection while muHMGB2 may perhaps play an antiviral role, in contrast to the proviral role of human HMGB2 (huHMGB2) shown in this study. Considering that ICM inhibits both HMGB1 and HMGB2, its proviral effect in mice could be explained if muHMGB2 is in fact antiviral and the drug inhibits HMGB2 to a greater extent than HMGB1 or if muHMGB2's potential antiviral role is more dominant than muHMGB1's proviral role in mice (Lee et al., 2014). We could test whether the proviral effect of ICM in mice is due to species-specific differences in the roles of HMGB proteins by directly comparing the efficacy of ICM against IAV infection in human and mouse cells. Alternatively, it may be that the anti-inflammatory properties of ICM reduced activation of the immune response in the mice and, consequently, allowed greater IAV replication (Lee et al., 2014).

It is also possible that the drug was cytotoxic in mice at the concentration we used. We cannot conclude this from our data as a control group of mock-infected mice treated with ICM was omitted. If the experiment is repeated, such a control should be included. ICM has previously been shown to protect against disease progression in a mouse model of neuroinflammation (Lee et al., 2014). This study used the same dose of ICM as in our experiment but did not report weight loss data. We, therefore, cannot conclude whether ICM was cytotoxic in their mouse model either. Finally, ICM was administered intraperitoneally, and it is possible that ICM therefore did not reach the lungs, which is the site of IAV infection

and replication. If we were to repeat this experiment, it would be interesting to try an intranasal route of administration where there is a higher chance of the drug reaching the lungs. Despite the unprobed potential cytotoxicity and potentially suboptimal route of administration, we still observed an increase in viral lung titres upon ICM treatment compared to vehicle treatment at day 6 post inoculation. This cannot be explained by these two potential limitations, suggesting involvement of another factor, such as species differences in the proviral roles of HMGB proteins, as discussed above.

Overall, antivirals that target host factors may reduce the risk that IAV evolves antiviral resistance. This contrasts with current anti-IAV drugs that target viral proteins and whose long-term effectiveness is limited as resistance to such drugs readily emerges (Hurt, 2014). Understanding the exact stage of the viral lifecycle that host factors targeted by antivirals are involved in is important. This is because it allows multiple drugs that block different stages of the viral lifecycle to be used together, further reducing the risk that antiviral resistance arises. For instance, ICM, which we found to block RNA replication, could be used together with BXA, which blocks viral transcription (Noshi et al., 2018).

Section 3.3.1. Limitations and future work.

To study the role of HMGB2, RUVBL2, and RPAP2 in viral RNA synthesis, we made cell lines with depleted expression of each of the three genes using CRISPR-Cas9 genome editing. Expression of HMGB2 and RUVBL2 was found to be reduced in the HMGB2-KO and RUVBL2-KO cells, but not completely ablated. There are two main factors that could be the reason for the cells not being complete knockouts, namely the hypotriploid-nature of the A549 cells and the essentiality of some of the genes. Although unconfirmed as we were unable to detect RPAP2 by western blot, it is unlikely that we achieved complete knockout of RPAP2 expression in the RPAP2-KO cells because this protein is essential for cell survival (Arafeh et al., 2025, DepMap, 2025).

The incomplete knockout of HMGB2, which is not an essential gene, was likely due to A549 cells being hypotriploid (Arafeh et al., 2025, DepMap, 2025). This means that these cells have more than two sets of chromosomes, making gene knockout difficult as all alleles of the genes need to be targeted by the sgRNAs. If time had allowed, we would have tried another round of CRISPR using the same sgRNAs in the most successful HMGB2-KO cell clone. We attempted this in a RUVBL2-KO clone and found that a second round of CRISPR further reduced protein expression. Alternatively, we could use a different cell line that is more amenable to genetic manipulation such as eHAP cells, which are a haploid cell line and have previously been used in the Barclay Lab to make cell lines with ANP32 ablated (Staller et al., 2019, Sheppard et al., 2023). To use the same method of genome editing as in the A549-dox-Cas9 cells, we would first need to engineer the eHAP cell line to express Cas9 under the

control of a dox-inducible promoter. An advantage of using eHAP cells instead is that this would allow direct comparison of IAV phenotypes in the HMGB2-KO and ANP32-KO cells.

The incomplete knockout of RUVBL2 and RPAP2 was more likely due to the essentiality of the genes (Arafeh et al., 2025, DepMap, 2025). Further rounds of CRISPR or switching to a haploid cell line may not lead to complete knockout of these proteins. To circumvent this, we could engineer conditional or inducible knockout cells instead. One approach to achieve inducible gene knockout is an inducible degron system, in which the protein of interest is fused to a degron tag resulting in its degradation in the presence of a defined ligand (Ma, 2021). An example of such a degron system is the auxin-inducible degron (AID) system (Natsume et al., 2016, Nishimura et al., 2009). In this system, an AID tag is fused to the protein of interest by CRISPR-Cas9 genome editing. This tag will target the protein for degradation when auxin is supplied in cells that are engineered to express the plant-specific auxin receptor TIR1. The protein is degraded via the ubiquitin proteasome pathway as the plant TIR1 receptor forms a SCF E3 ligase complex together with endogenous mammalian proteins. One major advantage of this method is that protein degradation occurs quickly (20-40min), such that there is little time for the cells to compensate or adapt to the protein of interest being depleted. Another advantage is that the auxin-mediated degradation can be reversed by growing the cells in auxin-free media.

Alternatively, proteolysis targeting chimeras (PROTACs) are another method to achieve protein knockout (Schneekloth et al., 2004). PROTACs are heterobifunctional compounds with one part specific to the protein of interest and a second part that binds and recruits an E3 ligase. Recruitment of the E3 ligase ubiquitinates the protein of interest, targeting it for degradation. Two advantages of using PROTACs are that the method does not require genetic modification of the protein of interest and the method is reversible. However, a drawback of this method is that the structure of the target protein needs to be well defined to allow PROTACs that bind to a specific binding site on the target protein to be designed. This is important because the PROTAC needs to stably bind the target protein to recruit the E3 ligase to it and to minimise off-target effects.

Our existing A549 HMGB2-KO, RUVBL2-KO, and RPAP2-KO cells or improved versions could be used in the future to better understand the mechanism behind the proviral roles of the host proteins in RNA replication and transcription proposed in this chapter. Firstly, HMGB2 and RUVBL2 were shown to promote v-to-cRNA synthesis, but it is unknown whether they also support c-to-vRNA synthesis. In addition, it is unknown whether RUVBL2 promotes mRNA synthesis as well. To test this, in the future we could:

- Perform a cRNP stabilisation assay in WT and RUVBL2-KO cells to understand whether RUVBL2 plays a direct role in both cRNA and mRNA synthesis.

- As previously demonstrated by Nilsson-Payant et al., promoter mutations in the RNA templates could be used to separate cRNA and vRNA synthesis (Nilsson-Payant et al., 2022). A G5U mutation in the 5' vRNA promoter prevents internal initiation on the resulting cRNA product such that v-to-cRNA synthesis (and v-to-mRNA synthesis) can occur but not subsequent c-to-vRNA synthesis. Meanwhile, a 2C9G mutation in the 5' cRNA promoter prevents terminal initiation on the resulting vRNA product such that c-to-vRNA synthesis can occur but not further v-to-cRNA synthesis. The mutants must be used in a minigenome reporter assay setup as both cRNA and vRNA synthesis are necessary during viral infection. Furthermore, the assay must be read out using strand-specific RT-qPCR primers as both steps of replication are necessary to amplify the Firefly template and generate a luminescent signal. Such promoter mutants have previously been used to show that ANP32 supports both cRNA and vRNA synthesis steps of RNA replication and that NS2 specifically promotes the cRNA synthesis step of replication (Nilsson-Payant et al., 2022, Zhang et al., 2025a).

Secondly, both HMGB2 and RUVBL2 have previously been shown to interact with NP. Consequently, it is conceivable that the two host proteins play roles in NP recruitment to the replication platform or RNP assembly. If this is the case, it is likely that HMGB2 and RUVBL2 will support both the cRNA and vRNA synthesis steps of replication. To elucidate whether the mechanism behind the proviral roles of HMGB2 and RUVBL2 is NP-dependent, we could:

- Perform minigenome reporter assays in WT, HMGB2-KO, and RUVBL2-KO cells in the presence of a 76nt vRNA template instead of a full-length template. Replication of short vRNA templates (76nts or less) has previously been shown to occur in the absence of NP (Resa-Infante et al., 2010, Turrell et al., 2013). So, if support from HMGB2 and/or RUVBL2 is NP-dependent then polymerase activity should not be affected in the HMGB2-KO/RUVBL2-KO cells when a short vRNA template is supplied.

In addition, it is unknown whether RUVBL2 and HMGB2 work independently or in conjunction with ANP32. As mentioned above, HMGB2 and ANP32 exist in the same complex in the host cell nucleus and it could, therefore, be speculated that the two work together to support IAV replication. To test this, in the future we could:

- Perform co-IP experiments using ANP32 as bait and test whether HMGB2 or RUVBL2 co-precipitate with the host factor. This could be done in the absence and presence of infection. In the ANP32 interactome described in Section 2.2.8, Figure 29, HMGB2 and RUVBL2 were not among the ANP32 interactors in neither the absence nor presence of infection. However, as previously discussed, it is possible that these interactions are transient, such that cross-linking may be necessary to capture them. Alternatively, a

PLA method could be used to detect endogenous interactions between ANP32 and HMGB2/RUVBL2 in the presence and absence of IAV infection.

- Perform split luciferase complementation assays measuring the interaction between ANP32B and NP in HMGB2-KO and RUVBL2-KO cells to understand whether HMGB2 and/or RUVBL2 help facilitate the interaction (described in Section 4.2.4). The interaction between ANP32B and NP has previously been measured using a split luciferase assay (Mistry, 2019, Wang et al., 2022a).

Moreover, the mechanism behind RPAP2's proviral role in viral transcription is unknown. We speculated that its role might involve host RNAP II, given the known association between the two in the host cell. Several experiments could be performed to test this:

- A split luciferase complementation assay has previously been used to measure the interaction between the CTD of the large RNAP II subunit (POLR2A) and the IAV polymerase (Krischuns et al., 2024, Morel et al., 2022). This same assay could be used in WT and RPAP2-KO cells to test whether RPAP2 plays a role in the RNAP II CTD-polymerase interaction. In addition, this assay could also be performed in WT and RUVBL2-KO cells to understand whether RUVBL2 plays a role in the formation of the RNAP II-polymerase complex, given its known association with the host RNAP II CTD as well.
- Considering that RPAP2 has previously been shown to support nuclear import of RNAP II (Forget et al., 2013), we could compare the cellular localisation of RNAP II by immunofluorescence (IF) in the WT and RPAP2-KO cells to assess whether nuclear accumulation of RNAP II is reduced in the absence of RPAP2. This may begin to answer whether the mechanism behind RPAP2's role in viral transcription involves reducing the availability of RNAP II inside the nucleus.

Lastly, it would be interesting to determine the intracellular localisation of HMGB2, RUVBL2, and RPAP2 during infection. This could be achieved by detecting the host proteins by IF in the absence and presence of infection. We could also use this method to look at the colocalisation of the host proteins with viral proteins. What is more, we have previously established a RNAscope FISH assay for detecting negative-sense RNAs (vRNA) and positive-sense RNAs (mRNA and cRNA) (Swann et al., 2023). This assay can be performed under conditions of a cRNP stabilisation assay (treated with actinomycin D (ActD) instead of CHX, to block primary transcription) to specifically visualise cRNA accumulation. We have previously used this assay to show that ANP32 plays a direct role in cRNA synthesis (Swann et al., 2023). It would be interesting to use the RNAscope assay to detect viral RNAs in the HMGB2-KO, RUVBL2-KO, and RPAP2-KO cells to confirm the findings shown in this chapter.

To conclude, in this chapter we further characterised the roles of HMGB2, RUVBL2, and RPAP2 in viral RNA synthesis. We showed that HMGB2 and RUVBL2 support viral RNA replication and RPAP2 supports viral transcription. This was consistent with their predicted roles from our differential interactome screen, suggesting that comparative proteomics can be used as a targeted approach to uncover virus-host interactions that regulate specific stages of the viral lifecycle. We also demonstrated the application of this work in the identification of host-directed antivirals by showing that ICM, an inhibitor of HMGB2, suppresses virus growth by inhibiting RNA replication.

Chapter 4. Characterising the BTN3A3 and MxA resistance of avian influenza virus

Section 4.1. Introduction

Spillover of IAV from its natural avian reservoir into the human population sporadically occurs. Although such zoonoses may cause severe or lethal disease, they rarely result in a pandemic because of the intrinsically poor replication and transmission of AIVs in humans (de Jong et al., 2006, Taubenberger and Kash, 2010). To overcome the species barrier and establish a new lineage in the human population, AIVs must adapt to their new host (Long et al., 2019b). First, this includes acquiring the ability to exploit human cellular factors. For instance, the AIV polymerase needs to evolve adaptive mutations that enable it to co-opt human versions of the host factors necessary to support viral RNA replication. An E to K mutation at position 627 of the PB2 subunit is the most common example, which allows AIV polymerase to co-opt mammalian ANP32 proteins (Long et al., 2016, Subbarao et al., 1993). Second, AIVs also need to acquire the ability to evade restriction by antiviral factors (Long et al., 2019b). The IFN response is a major component of the host innate immune response to viral infection, with many ISGs being antiviral against both avian and mammalian-adapted IAVs (Petric et al., 2023). However, two ISGs that act as a host range barrier by preferentially blocking AIVs are BTN3A3 and MxA. BTN3A3 was recently discovered as an ISG that interferes with avian RNA replication in human cells (Pinto et al., 2023). MxA is an IFN-inducible GTPase that restricts AIV at an early stage of the viral lifecycle (Haller et al., 2015). Variations in NP sequence have been shown to be the main determinant of both BTN3A3 and MxA restriction and, to generate a pandemic strain, AIVs must acquire adapting NP mutations that reduce sensitivity to these restriction factors (Petric et al., 2023, Pinto et al., 2023, Zimmermann et al., 2011). The BTN3A3 and MxA resistance of avian and zoonotic IAV strains has, therefore, been proposed to be a strong indicator for their pandemic potential. While BTN3A3 and MxA have been reported to act independently, the mechanism behind their restriction of AIV polymerase activity remains unclear.

In this chapter, we aimed to further characterise the BTN3A3 and MxA sensitivity of IAV strains. To achieve this, we first showed that BTN3A3 and MxA restriction of AIV strains can be measured using a minigenome reporter assay and restriction occurs in an NP-dependent manner. We demonstrated that IAV strains become less sensitive to BTN3A3 and MxA restriction as the virus evolves from being an avian strain to a pandemic strain, using NPs from representative avian, zoonotic, and pandemic strains. Next, we assessed the

BTN3A3 and MxA sensitivity of panzootic clade 2.3.4.4b viruses that have caused recent widespread outbreaks in birds and mammals. We concluded that these strains may pose an increased pandemic risk as they were found to be less sensitive to BTN3A3 restriction than pre-panzootic H5N1 avian strains. Finally, we further characterised the mechanism behind BTN3A3 restriction and confirm that it specifically interferes with RNA replication by inhibiting the cRNA synthesis step.

Plasmids to express the NPs tested in Figures 53 and 54 were generated by Jessica Quantrill and Dr Thomas Peacock. The sequence alignments summarised in Tables 10 and 11 were performed by this author with the help of Dr Thomas Peacock. The tagged RT-qPCR primers targeting segment 4 were generated by this author with the help of Dr Olivia Swann (Swann et al., 2023). The split luciferase constructs used in Figure 60 were generated by Dr Bhakti Mistry and Dr Carol Sheppard (Mistry, 2019, Wang et al., 2022a).

Section 4.2. Results

Section 4.2.1. Minigenome reporter assays can be used to measure BTN3A3 and MxA sensitivity of avian NPs.

To confirm that BTN3A3 restriction is specific to AIVs, we tested the effect of exogenously expressed human BTN3A3 on polymerase activity of PR8, a laboratory- and mammalian-adapted H1N1 strain, and 5092, a highly pathogenic avian H5N1 strain, using a minigenome reporter assay (Figure 52A). The PB2 of the 5092 strain was mutated to carry the mammalian-adapting E627K mutation to allow robust replication in human cells. The polymerase activity of 5092 was inhibited by human BTN3A3, while PR8 polymerase activity was not (Figure 52A). This suggests that typical avian influenza strains are sensitive to BTN3A3 restriction, consistent with the literature (Pinto et al., 2023). To verify that the BTN3A3 sensitivity of 5092 was due to its NP, we tested the effect of BTN3A3 on polymerase activity reconstituted with PR8 polymerase subunits and 5092 NP. 5092 NP conferred similar sensitivity to the PR8 polymerase background as it did to the full 5092, confirming that NP is the main determinant of BTN3A3 sensitivity.

Next, we performed similar experiments with human MxA (Figure 52B). As expected, 5092 NP in a PR8 background showed similar sensitivity to MxA and MxA-FLAG as full 5092. PR8 NP was poorly restricted by MxA or MxA-FLAG, confirming that avian, but not mammalian-adapted, NPs are sensitive to MxA restriction (Figure 52B). This is consistent with previous reports showing that MxA restricts AIVs in an NP-dependent manner (Zimmermann et al., 2011). We decided to use MxA-FLAG in future experiments because it makes detection of exogenous MxA by western blot more feasible but has little impact on the antiviral activity of the protein. Overall, the data shows that we can use a minigenome reporter assay to

measure BTN3A3 and MxA sensitivity of polymerase constellations consisting of a PR8 background (PB2, PB1, and PA) with different NPs of interest. However, it is important to note that western blots were not included and, therefore, we cannot exclude the possibility that the differences were partly due to differences in NP expression.

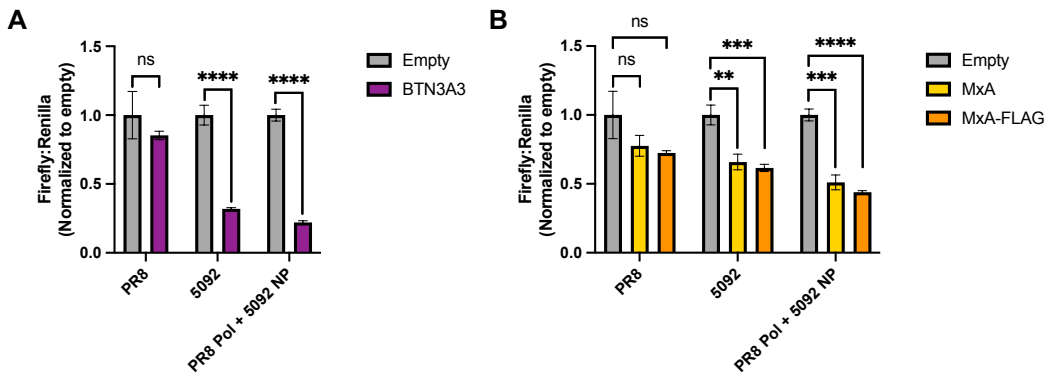

Figure 52. BTN3A3 and MxA restrict avian polymerase activity in an NP-dependent manner. A and B) Minigenome reporter assay in 293T cells using a polymerase constellation consisting of full PR8, full 5092, or PR8 polymerase subunits (PB2, PB1, and PA) and 5092 NP. 5092 PB2 was engineered to carry the mammalian adapting PB2 E627K mutation. Plasmids expressing BTN3A3 (100ng) (A) or MxA (100ng) and MxA-FLAG (100ng) (B) were co-transfected as annotated. Firefly luciferase activity relative to co-transfected Renilla luciferase levels was normalised to empty. Data is shown as mean ± SD of n=3 technical repeats, representative of n=3 biological repeats. Statistical significance compared to empty was assessed using an unpaired *t* test. ns, not significant; **, p<0.01; ***, p<0.001; ****, p<0.0001.

Section 4.2.2. Pandemic risk assessment of zoonotic IAVs based on their sensitivity to BTN3A3 and MxA restriction.

Aside from mammalian-adapting mutations in the polymerase subunits (such as PB2 E627K), a key characteristic of all human IAVs is reduced sensitivity to restriction by BTN3A3 and MxA (Long et al., 2019b, Petric et al., 2023). As a result, zoonotic IAV strains that have acquired the ability to evade BTN3A3 and MxA restriction are suggested to be more likely to cause a pandemic in the human population. To assess whether BTN3A3 and MxA sensitivity measured using our minigenome reporter assay can be used as an indicator of pandemic risk, we tested the sensitivity of NPs derived from PR8, Eng195, a human pandemic pH1N1 strain, or 5092, an avian strain that has not been associated with any spillover events into the human population. We also included NPs from two zoonotic IAVs; Anhui, which is a H7N9 virus with H9N2-origin internal genes, or from Tky05, which is a H5N1 virus of the goose/Guandong (gs/Gd) lineage (Kilpatrick et al., 2006, Pu et al., 2015). Both Anhui and Tky05 led to widespread outbreaks in birds and caused many zoonotic infections, some of which were fatal (Philippon et al., 2020). As expected, Eng195 NP was not restricted by BTN3A3 or MxA (Figure 53A and B). While PR8 NP was not restricted by BTN3A3, it did show some sensitivity

to MxA at the highest concentration tested (Figure 53A and B). Slight restriction of mammalian-adapted NPs at high MxA concentrations has previously been observed in the literature as well (Zimmermann et al., 2011). 5092 and Tky05 NPs were restricted by BTN3A3 and MxA, both showing higher sensitivity to BTN3A3 at the same plasmid concentration. Anhui NP was restricted by MxA but not BTN3A3.

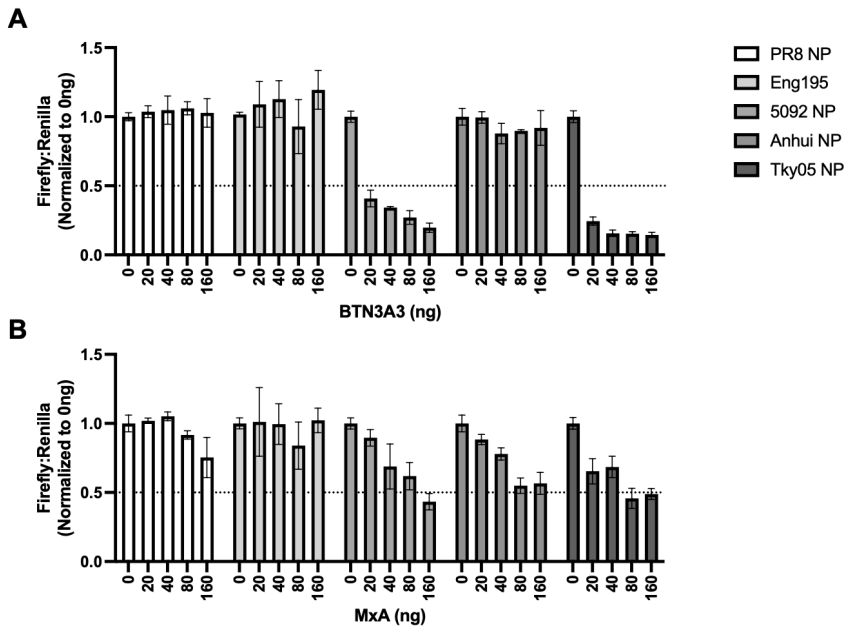

Figure 53. BTN3A3 and MxA sensitivity can be used as an indicator of pandemic risk posed by AIV NPs.
A and B) Minigenome reporter assay in 293T cells using polymerase constellations consisting of PR8 polymerase subunits (PB2, PB1, and PA) and PR8, Eng195, 5092, Anhui, or Tky05 NP. Plasmids expressing BTN3A3 (A) or MxA-FLAG (B) were co-transfected as annotated. Firefly luciferase activity relative to co-transfected Renilla luciferase levels was normalised to 0ng BTN3A3/MxA for each polymerase constellation. Data is shown as mean ± SD of n=3 biological repeats performed in triplicate.

The NP amino acid substitutions that mediate BTN3A3 and MxA escape have previously been identified and are summarised in Tables 10 and 11 (Manz et al., 2013, Pinto et al., 2023). Out of the three NP mutations that can mediate BTN3A3 escape, only one of Y52N/H or F313Y/V is necessary (Table 10) (Pinto et al., 2023). In contrast, combinations of amino acid substitutions are needed to confer MxA resistance (R100I/V, L283P, and F313Y in the case of the 1918 H1N1 pandemic strain (from which PR8 is derived) and E53D, R100I/V, and F313V in the case of the 2009 pH1N1 pandemic strain (Eng195)) (Table 11) (Manz et al., 2013). The remaining amino acid substitutions shown in Table 11 also contribute to MxA resistance. The patterns of BTN3A3 and MxA sensitivity observed using our minigenome reporter assay are consistent with the presence of known NP adapting mutations (Figure 53A and B, Tables 10 and 11). This suggests that the minigenome reporter assay can be used as a reliable measure of BTN3A3 and MxA sensitivity of IAV NPs.

Table 10. NP residues that determine BTN3A3 sensitivity.

		NP residue			
Strain	**Full strain name**	**52**	**100**	**313**	**Overall**
PR8	A/Puerto Rico/8/1934 (H1N1)	Y	V	Y	
Eng195	A/England/195/2009 (pH1N1)	Y	V	V	
5092	A/turkey/England/50-92/1991 (H5N1)	Y	R	F	
Anhui	A/Anhui/1/2013 (H7N9)	N	R	F	
Tky05	A/turkey/Turkey/1/2005 (H5N1)	Y	R	F	
H5N8	A/chicken/England/030786/2020 (H5N8)	Y	R	F	
AIV07	A/chicken/England/053052/2021 (H5N1)	H	R	F	
APS	A/pheasant/Scotland/000348/2021 (H5N1)	H	R	F	
AIV09	A/chicken/Scotland/054477/2021 (H5N1)	Y	R	F	
AIV48	A/chicken/England/085598/2022 (H5N1)	N	R	F	

	Sensitive to BTN3A3
	Less sensitive to BTN3A3
	Resistant to BTN3A3

Table 11. NP residues that determine MxA sensitivity.

Strain	**16**	**53**	**100**	**283**	**289**	**305**	**313**	**316**	**350**	**351**	**353**	**357**	**Overall**
PR8	D	E	V	P	Y	R	Y	I	T	K	V	K	
Eng195	G	D	V	L	H	K	V	M	K	K	I	K	
5092	G	E	R	L	Y	R	F	I	T	R	V	Q	
Anhui	G	E	R	L	Y	R	F	I	T	R	V	Q	
Tky05		E	R	L	Y	R	F	I	T	R	V	Q	
H5N8	G	E	R	L	Y	R	F	I	T	R	V	Q	
AIV07	G	E	R	L	Y	R	F	I	T	R	V	Q	
APS	G	E	R	L	Y	R	F	I	T	R	V	Q	
AIV09	G	E	R	L	Y	R	F	I	T	R	V	Q	
AIV48	G	E	R	L	Y	R	F	I	T	R	L	Q	

	Sensitive to MxA
	Resistant to MxA
	Unknown

Since 2020, there has been an ongoing outbreak of a highly pathogenic H5N1 clade 2.3.4.4b virus in wild birds and mammals (Byrne et al., 2023). This outbreak has resulted in frequent incursions into domestic poultry, fatal incursions into wild and domestic mammals, and worryingly, some human infections (Aguero et al., 2023, Plaza et al., 2024, Pulit-Penaloza et al., 2024, Puryear et al., 2023). It remains unclear whether these AIV strains are restricted by BTN3A3 and MxA and, consequently, the pandemic risk posed by these strains.

To assess the pandemic potential of these emerging AIV strains, we determined the BTN3A3 and MxA sensitivity of NPs derived from a H5N8 strain, which was the clade 2.3.4.4b precursor to the currently circulating viruses, or from AIV07, APS, AIV09, or AIV48, all examples of circulating clade 2.3.4.4b strains from the UK between 2021-2022 (Byrne et al., 2023) (Figure 54A and B). First, we performed sequence alignments to check for the presence of NP amino acid substitutions that might alter the sensitivity of the strains to BTN3A3 and

MxA restriction (Tables 10 and 11). This revealed that AIV07, APS, and AIV48 NPs have acquired Y52N/H mutations, which should make them resistant to BTN3A3 restriction. No NP amino acid mutations that have previously been associated with escape from MxA restriction were identified. To confirm this experimentally, we next applied our minigenome reporter assay to measure the BTN3A3 and MxA sensitivity of polymerase constellations consisting of PR8 polymerase subunits and PR8, H5N8, AIV07, APS, AIV09, or AIV48 NPs (Figure 54A and B). H5N8 NP was sensitive to both BTN3A3 and MxA restriction. In contrast, all circulating strains, except AIV09, were resistant to BTN3A3 restriction (Figure 54A). AIV09 showed an intermediate phenotype where for any given dose of BTN3A3 plasmid, the degree of inhibition was less than for H5N8. AIV07, APS, and AIV09 NPs all remained sensitive to MxA restriction (Figure 54B). Surprisingly, AIV48 showed similar resistance to MxA restriction as PR8 NP, despite its only NP amino acid change being V353L, which has not previously been described as a determinant of MxA restriction alone.

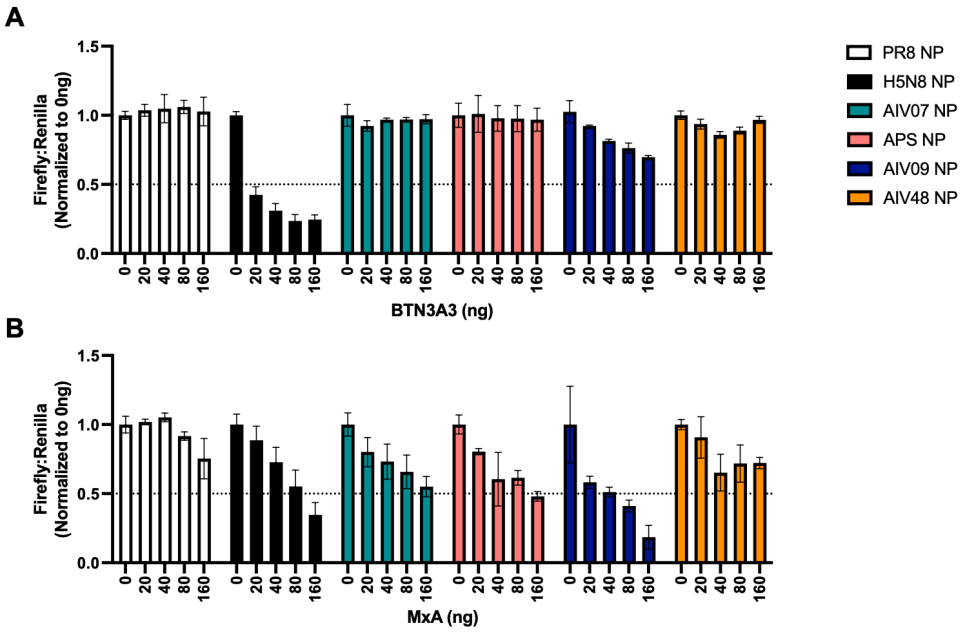

Figure 54. BTN3A3 and MxA sensitivity of currently circulating clade 2.3.4.4b AIV NPs.
A and B) Minigenome reporter assay in 293T cells using polymerase constellations consisting of PR8 polymerase subunits (PB2, PB1, and PA) and PR8, H5N8, AIV07, APS, AIV09, or AIV48 NP. Plasmids expressing BTN3A3 (A) and MxA-FLAG (B) were co-transfected as annotated. Firefly luciferase activity relative to co-transfected Renilla luciferase levels was normalised to 0ng BTN3A3/MxA for each polymerase constellation. Data is shown as mean ± SD of n=3 biological repeats performed in triplicate.

Increasing BTN3A3 and MxA protein expression and similar NP expression across all IAV strains tested was confirmed by western blotting (Figure 55A-C). Taken together, our data suggests that the currently circulating strains, except AIV09, have evolved to become more BTN3A3 resistant than their H5N8 precursor, perhaps indicating that they present an

increased pandemic risk. Meanwhile, further adaptive mutations are required to facilitate MxA escape of all strains tested, apart from AIV48.

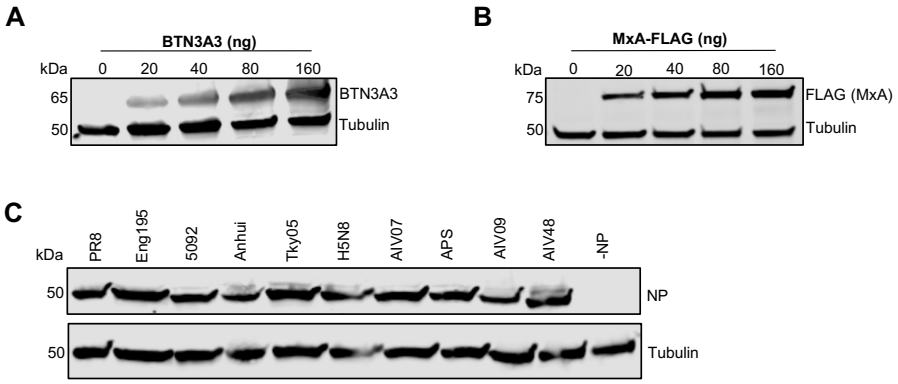

Figure 55. Expression of BTN3A3, MxA-FLAG, and NP.
A-C) Western blots showing BTN3A3 (A), MxA-FLAG (B), NP (C), and tubulin (cellular control) protein expression. The western blots accompany the minigenome reporter assays shown in Figures 53 and 54.

Lastly, we determined the approximate BTN3A3 and MxA IC50 values for each strain tested. We found that strains that were sensitive to BTN3A3 restriction, were also sensitive to MxA restriction (Figure 56). Nevertheless, there were subtle differences in the degrees of sensitivity to BTN3A3 and MxA restriction of the NPs tested. Overall, BTN3A3 restriction appeared to be more potent with low BTN3A3 plasmid amounts (20ng) achieving 50% inhibition. Meanwhile, at least a four times higher quantity of MxA plasmid was typically required to achieve the same degree of inhibition. These differences perhaps hint at different mechanisms of action of BTN3A3 and MxA, despite similar NP residues determining sensitivity to the two antiviral factors.

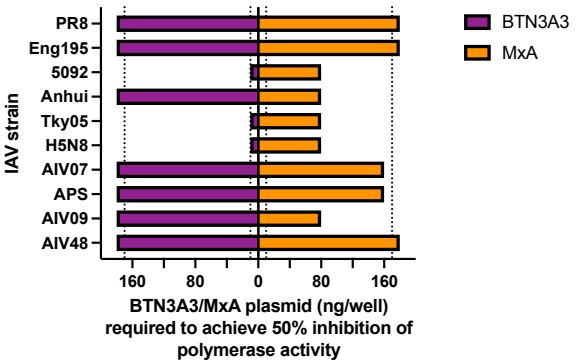

Figure 56. Approximate BTN3A3 and MxA IC50 values for each human-adapted, zoonotic, or AIV strain tested.
The IC50 values were determined from the data presented in Figures 53 and 54.

Section 4.2.3. BTN3A3 restricts the cRNA synthesis step of RNA replication.

To confirm that BTN3A3 directly restricts RNA replication, we made use of an ActD-treated cRNP stabilisation assay (Figure 57A). As for a CHX-treated cRNP stabilisation assay, a catalytically dead PB1 mutant (PB1 D446Y) was pre-expressed alongside PA, PB2, and NP prior to infection. This allows stabilisation of cRNA products but not onwards replication. ActD treatment inhibits host cell transcription and, therefore, indirectly viral transcription, such that only the pioneering round of cRNA synthesis can occur. We quantified the accumulation of viral RNA species of the avian 5092 virus, engineered to carry the mammalian adapting PB2 E627K mutation (5092K) to allow replication in human cells. As expected, no accumulation of vRNA or mRNA occurred over time (Figure 57B and D). A significant decrease in cRNA accumulation was observed over time in the presence of BTN3A3 compared to in its absence, reaching a 7-fold difference by 5hpi (Figure 57C). This suggests a direct antiviral role for BTN3A3 in cRNA synthesis.

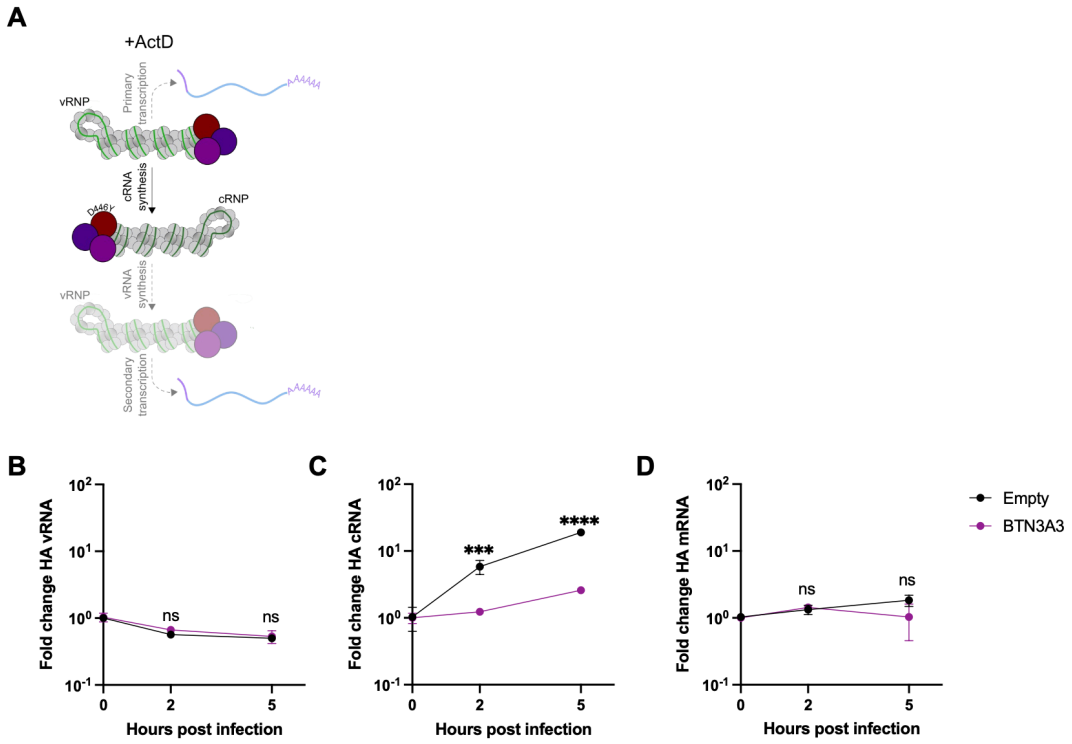

Figure 57. BTN3A3 restricts avian cRNA synthesis.
A) Schematic illustrating vRNA, cRNA, and mRNA synthesis under conditions of a cRNP stabilisation assay with actinomycin D (ActD) treatment. B-D) ActD-treated cRNP stabilisation assay in 293T cells in the absence (empty) and presence (BTN3A3) of BTN3A3. Cells were infected with 5092 bearing the mammalian adapting PB2 E627K mutation (5092K) (MOI=3). Accumulation of segment 4 (HA) vRNA (B), cRNA (C), and mRNA (D) was quantified by RT-qPCR at indicated timepoints post infection. The fold change was calculated versus input (0hpi). Data is shown as mean ± SD of n=3 technical repeats. Statistical significance compared to empty was assessed using multiple unpaired *t* tests corrected for multiple comparisons using the false discovery rate, following log transformation. ns, not significant; ***, p<0.001; ****, p<0.0001.

To understand whether BTN3A3 restriction is specific to RNA replication, we next performed a CHX-treated cRNP stabilisation assay with the 5092K virus (Figure 58A-D). As previously described, CHX inhibits host cell translation and, therefore, in this version of the assay both the pioneering round of cRNA synthesis and primary mRNA synthesis can occur (Figure 58A). As expected, no accumulation of vRNA occurred over time (Figure 58B). Less cRNA accumulation was observed in the presence of BTN3A3, consistent with the ActD-treated cRNP stabilisation assay (Figure 58C and 57C). No difference in mRNA synthesis was observed in the presence and absence of BTN3A3 (Figure 58D). Together, this indicates that BTN3A3 restricts the pioneering round of cRNA synthesis but not primary mRNA synthesis. To confirm that this mechanism of BTN3A3 restriction is specific to AIVs, we next performed a CHX-treated cRNP stabilisation assay with the mammalian-adapted PR8 virus (Figure 58E-G). No difference in cRNA or mRNA accumulation was observed in the presence and absence of BTN3A3 over time (Figure 58F and G). Taken together, these data confirm a direct role for BTN3A3 in the restriction of avian cRNA synthesis and corroborate that primary transcription and human-adapted cRNA synthesis are not restricted by BTN3A3.

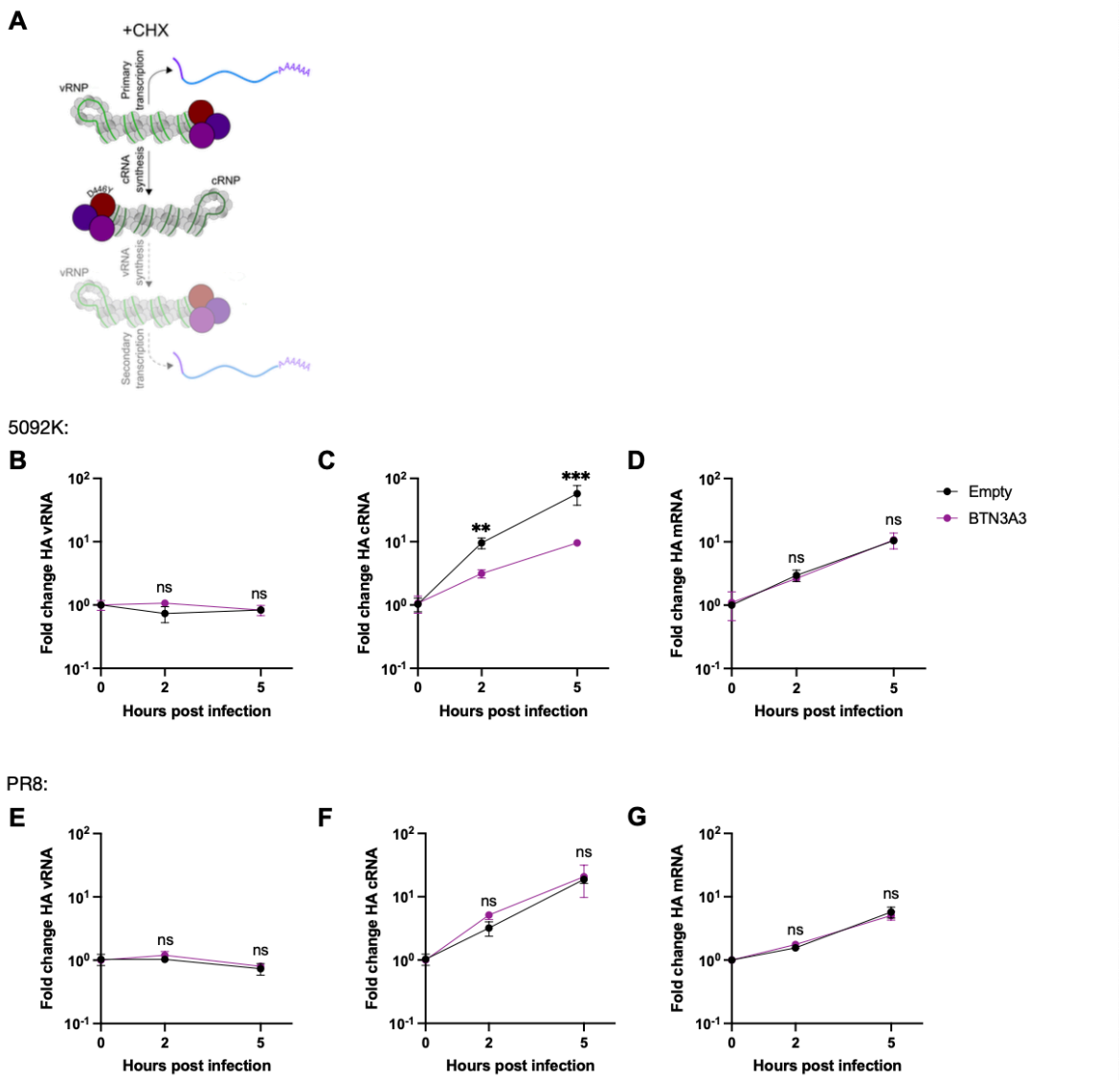

Figure 58. BTN3A3 restricts avian but not mammalian-adapted cRNA synthesis.
A) Schematic illustrating vRNA, cRNA, and mRNA synthesis under conditions of a cRNP stabilisation assay with cycloheximide (CHX) treatment. B-G) CHX-treated cRNP stabilisation assay in 293T cells in the absence (empty) and presence (BTN3A3) of BTN3A3. Cells were infected with 5092 bearing the mammalian-adapting PB2 E627K mutation (5092K) (MOI=3) (B-D) or PR8 (MOI=3) (E-G). Accumulation of segment 4 (HA) vRNA (B and E), cRNA (C and F), and mRNA (D and G) was quantified by RT-qPCR at indicated timepoints post infection. The fold change was calculated versus input (0hpi). Data is shown as mean ± SD of n=3 technical repeats, representative of n=2 biological repeats. Statistical significance compared to empty was assessed using multiple unpaired *t* tests corrected for multiple comparisons using the false discovery rate, following log transformation. ns, not significant; **, $p<0.01$; ***, $p<0.001$.

We also applied the CHX-treated cRNP stabilisation assay to study the effect of MxA overexpression on cRNA and mRNA synthesis of 5092K (Figure 59A-C). A nearly 10-fold decrease in cRNA accumulation was observed at 5hpi in the presence of MxA (Figure 59B). No difference in mRNA synthesis was observed in the presence and absence of MxA (Figure 59C). This suggests that MxA restricts cRNA synthesis but not primary transcription, similar

to BTN3A3. This is consistent with previous reports suggesting that overexpressed MxA restricts IAV at a step downstream of primary transcription (Nigg and Pavlovic, 2015, Pavlovic et al., 1992).

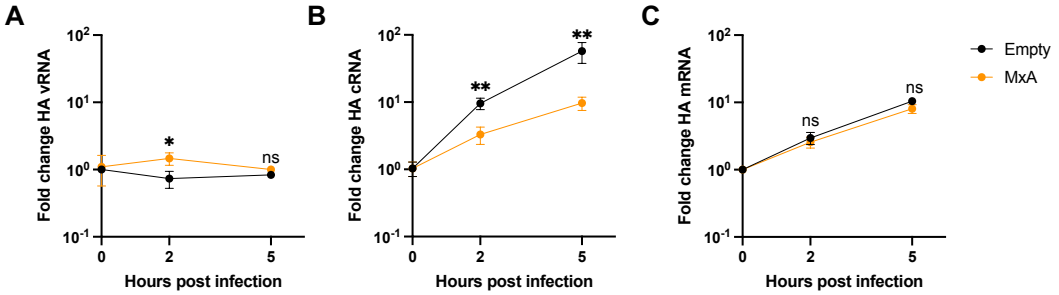

Figure 59. MxA restricts avian cRNA synthesis but not primary transcription.
A-C) CHX-treated cRNP stabilisation assay in 293T cells in the absence (empty) and presence (MxA) of MxA-FLAG. Cells were infected with 5092 bearing the mammalian adapting PB2 E627K mutation (5092K) (MOI=3). Accumulation of segment 4 (HA) vRNA (A), cRNA (B), and mRNA (C) was quantified by RT-qPCR at indicated timepoints post infection. The fold change was calculated versus input (0hpi). Data is shown as mean ± SD of n=3 technical repeats, representative of n=2 biological repeats. Statistical significance compared to empty was assessed using multiple unpaired *t* tests corrected for multiple comparisons using the false discovery rate, following log transformation. ns, not significant; *, $p<0.05$; **, $p<0.01$.

Section 4.2.4. BTN3A3 decreases the interaction between huANP32B and both avian and human-adapted NPs.

So far, our data has shown that BTN3A3 directly restricts cRNA synthesis of avian strains and this restriction occurs via a mechanism involving NP. Using the same CHX-treated cRNP stabilisation assay, we have previously shown ANP32 to be essential for the same step of replication (Swann et al., 2023). One way that ANP32 supports RNA replication is by recruiting NP for encapsidation of nascent RNA (Wang et al., 2022a). Given that BTN3A3 restricts avian cRNA synthesis and ANP32 supports cRNA synthesis, both via mechanisms that involve NP, we hypothesised that BTN3A3 inhibits AIV replication by preventing human ANP32 from recruiting avian NP. To test this, we made use of a previously established split luciferase complementation assay, which measures NP-huANP32B interactions (Mistry, 2019, Wang et al., 2022a). Specifically, in this assay, the N-terminal half of gaussia luciferase (gluc1) is fused to the C-terminus of Vic75 (human-adapted) or 5092 (avian) NP and the C-terminal half of gaussia luciferase (gluc2) is fused to the C-terminus of huANP32B (Figure 60B). The gaussia luciferase enzyme is then reconstituted upon NP-huANP32B interaction, producing a measurable luminescent signal.

First, we assessed the sensitivity of Vic75 NP to BTN3A3 restriction. Vic75 NP contains residues 52Y, 100R, and 313F, and was, therefore, expected to be resistant to BTN3A3 restriction. This was confirmed using a minigenome reporter assay (Figure 60A). We then

performed split luciferase assays with Vic75/5092 NP_{gluc1} and $huANP32B_{gluc2}$ in the absence and presence of BTN3A3. In the absence of BTN3A3, a signal was observed with both NP strains, indicating that huANP32B can interact with both human-adapted and avian NPs (Figure 60C and D). In the presence of BTN3A3, the interaction between huANP32B and Vic75 or 5092 NP both decreased (Figure 60C and D).

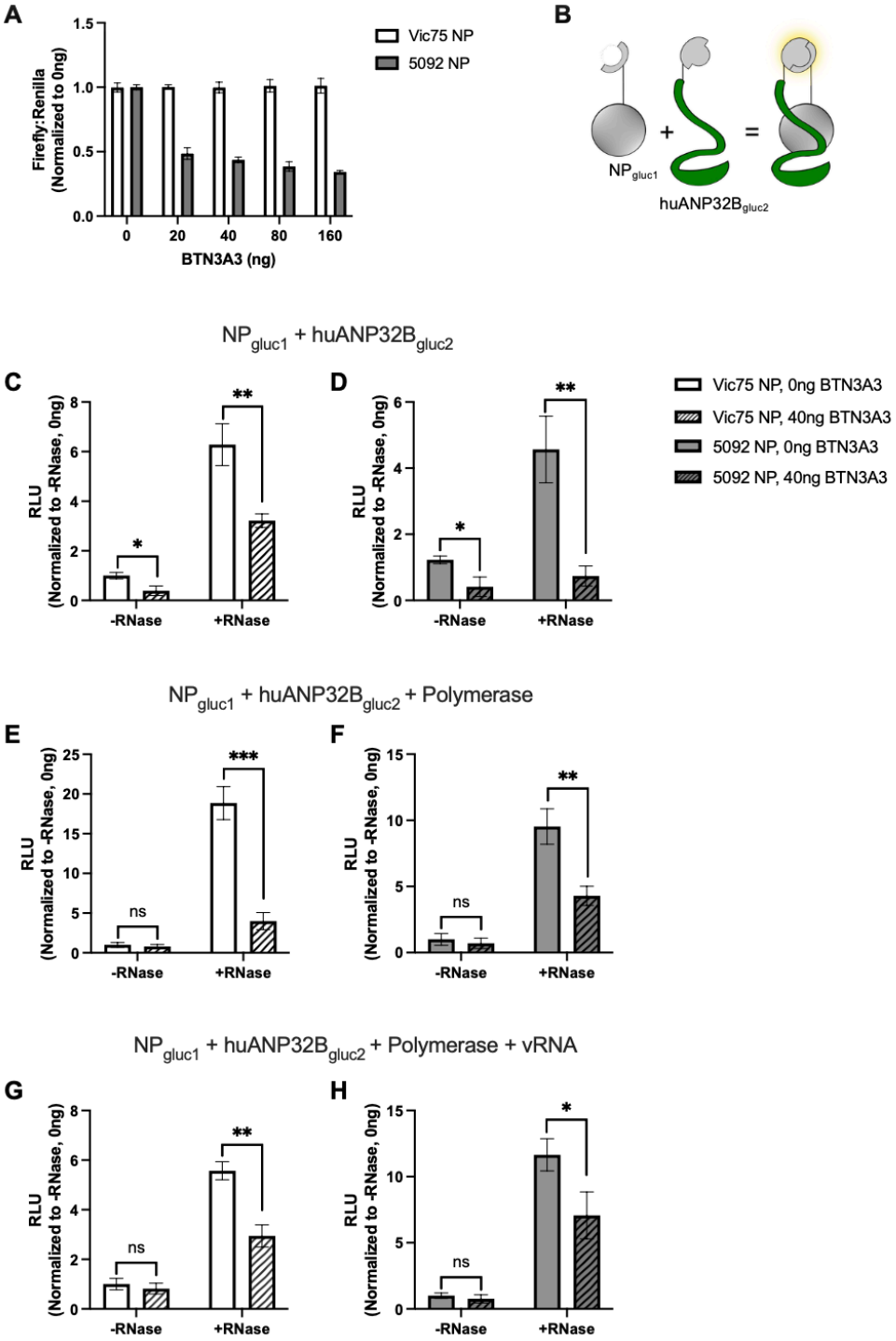

Figure 60. BTN3A3 decreases the interaction between huANP32B and avian and human-adapted NP.

A) Minigenome reporter assay in 293T cells using polymerase constellations consisting of PR8 polymerase subunits (PB2, PB1, and PA) and Vic75 or 5092 NP. A plasmid expressing BTN3A3 was co-transfected as annotated. Firefly luciferase activity relative to co-transfected Renilla luciferase levels was normalised to 0ng BTN3A3 for each polymerase constellation. Data is shown as mean ± SD of n=3 technical repeats, representative of n=2 biological repeats. B) Schematic of split luciferase complementation assay with N-terminal half of gaussia luciferase (gluc1) fused to the C-terminus of Vic75 or 5092 NP (NP_{gluc1}) and the C-terminal half of gaussia luciferase (gluc2) fused to the C-terminus of human ANP32B ($huANP32B_{gluc2}$). C-H) Split luciferase complementation assay in 293T cells measuring the interaction between Vic75 or 5092 NP_{gluc1} and $huANP32B_{gluc2}$ (C and D), in the presence

of polymerase subunits (E and F), or in the presence of polymerase subunits and a vRNA template (G and H). BTN3A3 (40ng) was co-transfected as annotated. Each combination was performed with and without RNaseA treatment. Data is shown as mean ± SD of n=3 technical repeats, representative of n=2 biological repeats. Statistical significance relative to no transfected BTN3A3 (0ng) was assessed using an unpaired *t* test. ns, not significant; *, $p<0.05$; **, $p<0.01$; ***, $p<0.001$.

Split luciferase assays were also performed with RNaseA treatment (Figure 60C and D). RNaseA degrades RNA, which otherwise binds NP in its RNA-binding groove (Ye et al., 2006). Consistent with previous reports showing that binding of ANP32 and RNA to NP is mutually exclusive (Wang et al., 2022a), the NP-huANP32B interaction increased following degradation of RNA (Figure 60C and D). BTN3A3 also decreased NP-huANP32B interactions of both strains under these conditions.

To make the conditions truer to an actual infection, we performed the same split luciferase assays in the presence of polymerase subunits (Figure 60E and F) as well as polymerase subunits and a vRNA template (Figure 60G and H). Without RNaseA treatment, we observed a small decrease in the interaction between huANP32B and Vic75 or 5092 NP in the presence of BTN3A3, but this decrease did not reach significance (Figure 60E-H). The smaller decrease could be because ANP32 is also known to bind the polymerase subunits, making less ANP32 available to bind NP. In fact, previous data from the Barclay Lab has shown that ANP32 preferentially binds the viral polymerase compared to NP, although this was determined using a split luciferase assay where the strength of interactions may be influenced by the location of the tag (Mistry, 2019). With RNaseA treatment, BTN3A3 resulted in a significant decrease in the NP-huANP32B interaction of both strains and for all conditions (Figure 60E-H).

Taken together, these data show that BTN3A3 decreases the interaction between huANP32B and both human-adapted and avian NP. We observed this to varying degrees with and without RNaseA treatment and in the absence and presence of polymerase subunits and a vRNA template. This suggests that preventing huANP32B and avian NP interaction is not the mechanism behind BTN3A3's restriction of avian cRNA synthesis as we had hypothesised.

A major caveat of these experiments is that we did not include a control for BTN3A3 overexpression. Including a condition with overexpression of a protein that should not affect the NP-ANP32 interaction would confirm that the decreased interaction is not just due to transfection of an additional protein. Furthermore, we also did not run the matched western blots and so cannot be certain that the results are not due to variable transfection efficiencies or protein expression levels.

Section 4.2.5. NP residues that mediate NP activity and host restriction.

Having concluded that BTN3A3 does not impact the interaction between human ANP32 and avian NP, we next studied structures of NP to predict what other NP functions BTN3A3 might be interfering with. Various structures of H1N1, H3N2, and H5N1 NPs in monomeric or oligomeric forms and in the absence or presence of RNA have been solved (Chenavas et al., 2013, Chenavier et al., 2023, Knight et al., 2021, Ng et al., 2008, Ye et al., 2006). In all structures, NP consists of a body domain, head domain, and flexible tail loop. The tail loop is important for oligomerisation, where it inserts into the body domain of a neighbouring NP protein (Ye et al., 2006). RNA binds in an arginine-rich basic groove between the head and body domains (Ye et al., 2006). We mapped residues determining BTN3A3 (52, 100, 313) and MxA (53, 100, 283, and 313) sensitivity onto two of the solved structures: H5N1 NP with no RNA (PDB: 2Q06) and oligomeric H1N1 NP with a 12nt RNA fragment bound (PDB: 8PZQ) (Chenavier et al., 2023, Ng et al., 2008) (Figure 61A-E). The residues determining BTN3A3 and MxA sensitivity were found to be in the same region, on a surface-exposed part of the NP body domain. To predict which other roles of NP BTN3A3 might be inhibiting, we also mapped residues important for NP's other functions and interactions. These residues are summarised in Table 12.

Table 12. Residues important for NP interactions with RNA, viral proteins, and cellular factors.

Residue	Colour in Figure. 60	NP domain	NP function	Notes
G1 (R74, R75, R174, R175) and G2 (R150, R152, R156, and R162) (Ye et al., 2006).		Head and body domains	Basic groove, binds RNA	ANP32 LCAR and UAP56 also bind in the basic groove (Morris et al., 2020, Wang et al., 2022a).
R416, E339		Tail loop, body domain	Oligomerisation	R416A, E339K disrupt oligomerisation.
N319		Body domain	Important for IMPα1 binding	N319K enhances binding of avian NP to human IMPα1 (Gabriel et al., 2008).
Amino acids 1-160, and 255-465 (Biswas et al., 1998).	Not highlighted	Head and body domains, tail loop (Biswas et al., 1998).	Important for PB2 and PB1 binding	NP fragment with only amino acids 160-255 was unable to interact with PB2.
K90, K31, S165, S407, S413, K77, K229, K184 (Hu et al., 2020).		Head and body domains, tail loop	Post-translationally modified	Modifications include acetylation, deubiquitination, and phosphorylation (Hu et al., 2020, Hutchinson et al., 2012).
Y52 (Pinto et al., 2023).		Body domain	Determines sensitivity to BTN3A3 restriction	Y52N/H evades BTN3A3 restriction.
R100, F313 (Manz et al., 2013, Pinto et al., 2023).		Body domain	Determines sensitivity to BTN3A3 and MxA restriction	R100V, F313Y evades BTN3A3 and MxA restriction.
E53, L283 (Manz et al., 2013).		Body domain	Determines sensitivity to MxA restriction	E53D, L283P evades MxA restriction.

In both the monomeric and oligomeric structures, the residues mediating BTN3A3 and MxA sensitivity were not on the same side of the body domain as regions important for oligomerisation or near the RNA binding groove (Figure 61A-E). Based on these structures, it is, therefore, not immediately clear how BTN3A3 might be interfering with these NP functions or its interactions with ANP32 and UAP56, which have been shown to bind in the RNA-binding groove (Morris et al., 2020, Wang et al., 2022a, Momose et al., 2001). UAP56 is a host factor that acts as an NP chaperone and promotes NP-RNA interactions (Morris et al., 2020, Momose et al., 2001, Hu et al., 2017). It is also not clear how BTN3A3 might be impacting the post-translational modification of NP as most of the sites known to be post-translationally modified are on the opposite side of NP or in the tail loop (Figure 61A-E). However, residue 319, important for IMPα1 binding, is close to the residues mediating BTN3A3 (and MxA) resistance (Gabriel et al., 2008) (Figure 61A and E). It could, therefore, be that BTN3A3 somehow interferes with IMPα1 binding. Furthermore, large regions across NP, encompassing both the head and body domains, are involved in interactions with PB2 and

PB1 (Biswas et al., 1998). Considering that the NP interface required for PB2/PB1 interactions includes the residues determining BTN3A3 sensitivity, it is also possible that BTN3A3 disrupts the NP-PB2/PB1 interaction.

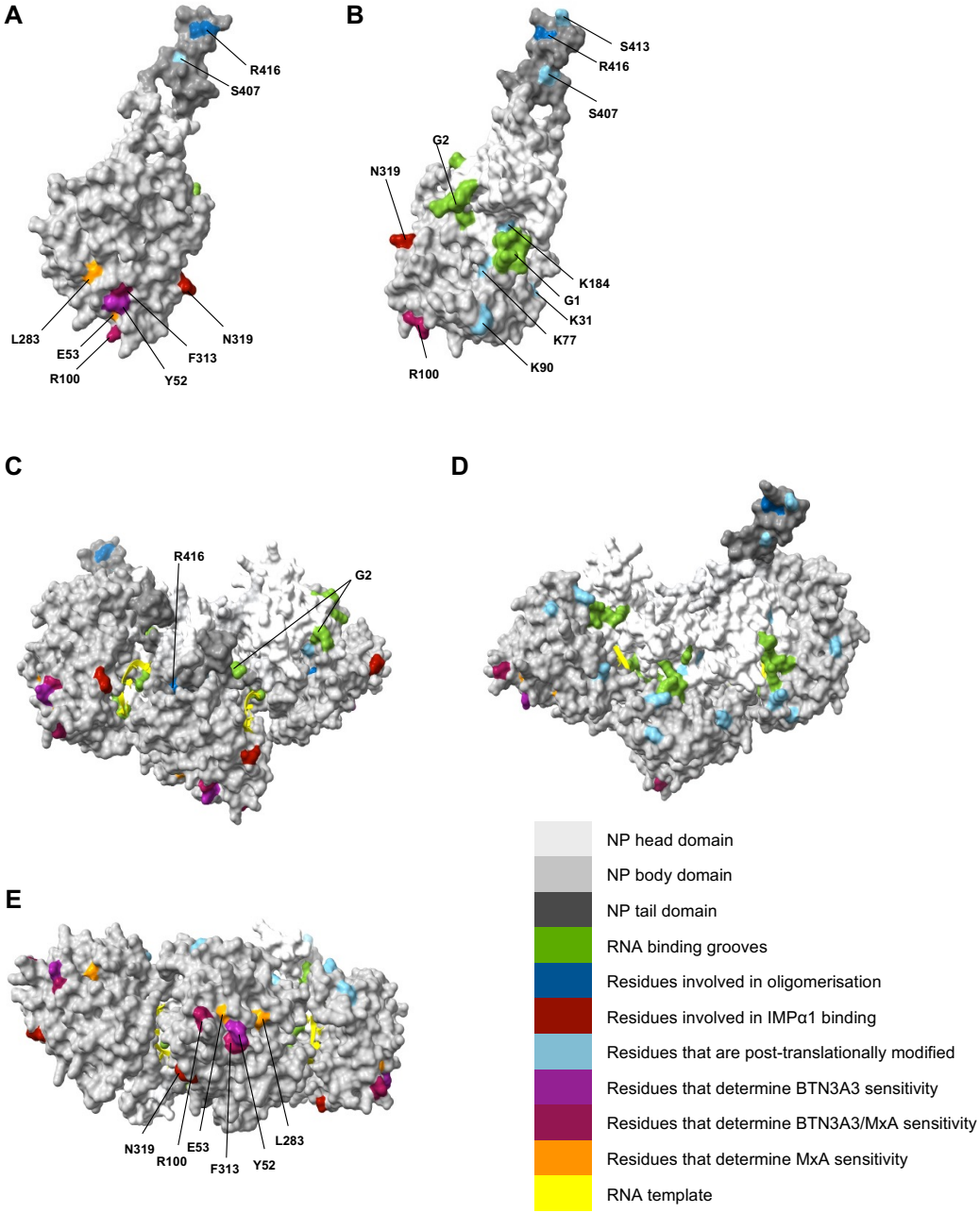

Figure 61. Mapping of residues important for NP functions onto structures of NP.
A and B) Crystal structure of monomeric IAV (H5N1) NP with no RNA (PDB accession code: 2Q06) (Ng et al., 2008). C-E) Cryo-EM structure of trimeric IAV (H1N1) NP with 12nt RNA fragment (PDB accession code: 8PZQ) (Chenavier et al., 2023). Residues of interest summarised in Table 12 are highlighted and colour coded as in Table 12. The structures were visualised using ChimeraX v.1.9.

Section 4.3. Discussion

In this chapter, we investigated the BTN3A3 and MxA restriction of AIV polymerase activity in human cells. We adapted a minigenome reporter assay to measure activity of polymerase constellations consisting of a PR8 background (polymerase subunits) and different NPs of interest in the presence and absence of BTN3A3 or MxA. A similar minigenome setup has previously been employed by Manz et al., to identify NP residues in pandemic IAV strains that confer MxA resistance (Manz et al., 2013). Our data shows that BTN3A3 and MxA restrict AIV strains in an NP-dependent manner, which agrees with previous reports (Pinto et al., 2023, Zimmermann et al., 2011). We tested the BTN3A3 and MxA sensitivity of NPs from a range of IAV strains including mammalian-adapted and pandemic strains (PR8, Eng195), zoonotic strains (Tky05 and Anhui), and a fully avian strain (5092). Comparing the pattern of BTN3A3 and MxA sensitivity of these IAV strains to their NP sequences showed that their sensitivity to BTN3A3/MxA restriction correlated with the presence of adaptive NP mutations identified in previous studies (Manz et al., 2013, Pinto et al., 2023). This pattern also correlated with the host range and actual outbreaks caused by the viruses. Overall, our data provides further support that BTN3A3 and MxA sensitivity should be monitored and built into a framework for assessing the pandemic risk of emerging IAV strains.

We assessed the pandemic potential of current panzootic clade 2.3.4.4b AIV strains by measuring the sensitivity of their NPs to BTN3A3 and MxA restriction. Most of the strains were found to have acquired BTN3A3 but not yet MxA resistance. Our findings suggest that these current strains pose an increased pandemic risk but have not completely overcome the host range barrier posed by avian-specific restriction factors. This is consistent with a recent study showing MxA to restrict clade 2.3.4.4b viruses isolated from various mammals including white mink and cats (Ankerhold et al., 2025). However, we found AIV48 NP to be somewhat resistant to both BTN3A3 and MxA. Only one NP adapting mutation was identified that could explain its reduced sensitivity to MxA (V353L), although this specific amino acid change has not previously been described in this context. Thus, position 353 alone could be a novel determinant of MxA sensitivity. Alternatively, it is possible that further residues that determine MxA sensitivity are present in the AIV48 NP gene, which were not considered in this study. Since our experiments were performed, the clade 2.3.4.4b virus has spread to the American continent where it has reassorted, creating numerous genotypes including two (genotypes B3.13 and D1.1) that have caused widespread outbreaks in dairy cattle in the USA and some human infections (Caserta et al., 2024, Garg et al., 2025). NP sequence alignments show that the NP gene in genotype B3.13 virus has not acquired further known adaptive mutations and therefore we expect this strain to be resistant to BTN3A3 and sensitive to MxA. If time had allowed, this could also have been confirmed experimentally.

It is important to note that evasion of restriction factors is only one of multiple host range barriers that AIVs must overcome to initiate a pandemic (Long et al., 2019b). Other barriers include adaptation of the polymerase (for example PB2 E627K and D701N) and changing receptor binding preference of the HA surface glycoprotein (from α2-3 to α2-6 sialic acid preference). To assess the pandemic risk posed by zoonotic IAV strains, their ability to evade restriction factors must, therefore, be considered alongside these other barriers. The importance of this is exemplified by AIV48, which has acquired resistance to antiviral factors but has not yet evolved polymerase or HA adapting mutations and is therefore still not capable of sustaining replication and transmission in the human population. The AIV48 strain is still circulating in birds, mostly in gulls, and considering that it has already overcome the host range barrier posed by restriction factors, it should be monitored closely for further human-adapting mutations.

Most of the zoonotic strains tested remained sensitive to MxA restriction (Anhui, Tky05, AIV07, APS, AIV09) and some to BTN3A3 restriction (Tky05 and AIV09), but these strains have nevertheless caused spillover events into mammalian species. This suggests that acquiring BTN3A3 and MxA restriction is not a prerequisite for zoonosis, only for establishing a new pandemic lineage in the human population. Furthermore, the finding that the strains have overcome BTN3A3 resistance but not yet MxA resistance agrees with previous reports suggesting that AIVs may more readily acquire BTN3A3 resistance (Petric et al., 2023). This is perhaps because only one adaptive NP mutation is necessary to escape BTN3A3 restriction, and this mutation does not affect viral fitness (Pinto et al., 2023). Not only are combinations of NP mutations required to confer MxA resistance, but these mutations are also associated with a fitness cost due to defective vRNP nuclear import. This means that compensatory mutations (for example G16D) are necessary as well (Gotz et al., 2016).

Subtle differences in the patterns of BTN3A3 and MxA IC50 values for some of the strains tested suggest that the two restriction factors act via different mechanisms of action. BTN3A3 was previously shown to act independently of MxA as silencing of MxA had no effect on the ability of BTN3A3 to restrict AIV (Pinto et al., 2023). Furthermore, the BTN3A3 and MxA literature suggests that both act at an early stage of the IAV lifecycle, but at slightly different steps and via different mechanisms. BTN3A3 was reported to restrict RNA replication of AIVs in human cells (Pinto et al., 2023). MxA was reported to act at two distinct stages, depending on its cellular localisation and the presence of other IFN-induced factors (Haller and Kochs, 2020). First, MxA, which is predominantly cytoplasmic, was shown to inhibit IAV at a stage downstream of primary transcription, perhaps by preventing the nuclear import of newly synthesised NP (Pavlovic et al., 1992, Nigg and Pavlovic, 2015). Second, together with an unidentified IFN-induced factor(s), MxA was found to prevent nuclear import of vRNPs, inhibiting primary transcription (Xiao et al., 2013). A similar role was reported for a variant of

MxA carrying a foreign NLS as well as murine Mx1, which is predominantly nuclear (Pavlovic et al., 1992, Zurcher et al., 1992). Interestingly, the antiviral activity of BTN3A3 is specific to AIVs, while MxA has antiviral activity against many different viruses, including both RNA and DNA viruses (Haller et al., 2015, Pinto et al., 2023). Generally, MxA appears to bind viral components that enter the cell upon infection or that are produced shortly after infection, restricting early steps in the viral lifecycle (Haller et al., 2015). This further suggests inherently different antiviral properties of BTN3A3 and MxA and different mechanisms of action. Although more is known about MxA than BTN3A3, the mechanisms behind both their antiviral activities against AIV remain unclear. Nevertheless, in this work, we mainly focused on elucidating the mechanism behind BTN3A3 restriction.

The specific effect of BTN3A3 on replication was previously shown by comparing the accumulation of vRNA, cRNA, and mRNA following infection with a WT avian strain or an avian strain with the desensitising F313Y NP mutation in the absence and presence of BTN3A3 and CHX treatment (Pinto et al., 2023). With CHX treatment, BTN3A3 had no effect on mRNA synthesis. Without CHX-treatment, BTN3A3 reduced the accumulation of all three viral RNA species. This suggests that BTN3A3 does not impact transcription and instead acts at the RNA replication stage. However, from this data it remains unclear which of the two steps of viral RNA replication are affected by BTN3A3. Here, we used cRNP stabilisation assays to directly measure the effect of BTN3A3 on cRNA and mRNA synthesis and unambiguously confirm that BTN3A3 inhibits the cRNA synthesis step of avian RNA replication.

An essential role for NP in the replication of full length vRNA templates is encapsidation of the cRNA replicative intermediate into cRNPs (York et al., 2013). As part of this process, the host factor ANP32 recruits NP to the site of RNA replication (Wang et al., 2022a). We hypothesised that BTN3A3 specifically restricts avian cRNA synthesis by preventing human ANP32 from recruiting avian NP. However, split luciferase complementation assays measuring NP-ANP32 interactions in the absence and presence of BTN3A3 showed BTN3A3 to decrease the interaction between ANP32 and both avian and human-adapted NPs. This suggests that disrupting NP-ANP32 interactions is not the mechanism behind BTN3A3's specific restriction of AIV. Pinto et al., showed that BTN3A3 interacts to the same extent with both mammalian- and avian-signature NP (determined by the residue at position 313) (Pinto et al., 2023). The decrease in NP-ANP32 interaction for both strains observed in this study could, therefore, be because BTN3A3 is capable of binding both avian and mammalian-adapted NP, making less NP available to bind huANP32 in both cases.

It is important to note that the split luciferase experiments should be repeated with overexpression of a factor that is known to not affect NP-ANP32 interactions. Moreover, the split luciferase assay requires lysis of the cells before bioluminescence is measured, which could affect interactions and result in mixing of proteins that were otherwise in separate

compartments before lysis. To eliminate the need for cell lysis and to visualise interactions *in situ*, a BiFC assay or PLA could be employed instead. These assays are described in more detail in Section 2.3.4. Such assays could also be used to study the interaction between BTN3A3 and NP, which to date has only been studied using a co-IP method (that also requires cell lysis) (Pinto et al., 2023). A major advantage of the BiFC assay or PLA is that these assays also allow the cellular localisation (nuclear or cytoplasmic) of the interaction to be determined as well.

Many other aspects of NP's role are important for cRNA synthesis and could be targeted by BTN3A3. For example, one model for RNA encapsidation suggests that the initial NP interacts directly with the PB2 and PB1 subunits of the polymerase bound to the nascent RNA (Biswas et al., 1998, Turrell et al., 2013). Subsequent NPs are then suggested to be recruited by NP-NP oligomerisation in which the tail loop of the incoming NP inserts into a groove on the resident NP (Turrell et al., 2013, Ye et al., 2006, Ng et al., 2008). NP also binds RNA in a sequence-independent manner via its RNA-binding groove (Turrell et al., 2013, Ye et al., 2006). Additionally, NP is imported into the nucleus via its interaction with IMPαs and chaperoned by various host factors, such as UAP56 (Gabriel et al., 2008, Morris et al., 2020, Momose et al., 2001). Finally, post-translational modifiers also bind to NP, altering its acetylation, ubiquitination, and phosphorylation states (Hu et al., 2020, Hutchinson et al., 2012). Mapping of the residues important for such interactions onto available NP structures hinted that BTN3A3 could be inhibiting avian NP activity by preventing NP-IMPα1 interactions or NP-PB2/PB1 interactions. Interestingly, previous reports have shown mouse Mx1 to disrupt the NP-PB2 interaction in a dose-dependent manner (Verhelst et al., 2012). It is possible that BTN3A3 indirectly disrupts other NP interactions through steric hindrance, but this is difficult to predict without structures of NP in complex with BTN3A3 (or MxA). In the future, to test whether BTN3A3 prevents NP-IMPα1 or NP-PB2/PB1 interactions or any of the other NP interactions mentioned (for instance NP-NP interactions), we plan to generate split luciferase or BiFC constructs that would allow us to measure such interactions in the absence and presence of BTN3A3.

A potential explanation for BTN3A3's inhibitory effect on the pioneering round of cRNA synthesis could be that it restricts nuclear import of newly synthesised NP. Considering that the residues determining BTN3A3 sensitivity (e.g., 313) are near residues important for IMPα1 binding (e.g., 319) and these residues map closely to each other on solved NP structures, it could be speculated that BTN3A3 interferes with IMPα1-mediated nuclear import of NP (Gabriel et al., 2008). Pinto et al., showed that BTN3A3 does not affect vRNP nuclear import (Pinto et al., 2023). Our data agrees with this finding as no effect of BTN3A3 on primary transcription was observed, which would otherwise be expected if vRNPs were blocked from entering the nucleus. However, Pinto et al., did not directly address whether BTN3A3 affects

nuclear import of newly synthesised NP, which occurs after primary transcription. They show that constitutively expressed BTN3A3 localises to the nucleus in hBEC3-KT cells and that overall NP accumulation is reduced with high nuclear BTN3A3 expression (Pinto et al., 2023). Investigating BTN3A3-NP interactions *in situ*, for example using the BiFC assay or PLA described above, would help elucidate whether BTN3A3 blocks the nuclear import of free NP. Alternatively, this could be studied using a nuclear localisation IF experiment with staining for BTN3A3 and NP. Such experiments could be performed with expression of NP alone or in the context of vRNPs to compare the effect of BTN3A3 on the cellular localisation of free NP and vRNP-bound NP.

We also demonstrated that MxA restricts avian cRNA synthesis but has no effect on primary transcription. This is consistent with previous reports suggesting that cytoplasmic MxA suppresses RNA replication, potentially by interfering with the nuclear import of newly synthesised NP (Pavlovic et al., 1992). While the exact mechanism behind MxA restriction remains unclear, one proposed mechanism is that dimeric MxA associates with newly synthesised NP, sequestering it from nuclear replication sites (Nigg and Pavlovic, 2015). No other ISGs apart from MxA were induced in our cRNP stabilisation assay. Our data, therefore, provides further support that MxA only restricts vRNP nuclear import (and consequently primary transcription) when another, as yet unidentified, ISG is also present (Xiao et al., 2013). It remains to be tested whether the same is true for BTN3A3 and, specifically, whether BTN3A3 would also reduce vRNP nuclear import (and primary transcription) if other ISGs were present as well.

While the NP residues that determine BTN3A3 sensitivity are known, it remains unclear which part of BTN3A3 is responsible for its antiviral activity. BTN3A3 is one of three family members; BTN3A1 shows slight antiviral activity and BTN3A2 has no antiviral activity (Pinto et al., 2023). All three family members contain two extracellular domains at their N-terminus, namely an immunoglobulin variable-like (IgV) domain and an immunoglobulin constant-like (IgC) domain, as well as a transmembrane domain, which anchors the protein in the plasma membrane (Figure 62) (Rhodes et al., 2001). The main difference between the three family members is that BTN3A3 and BTN3A1 have an intracellular tail containing a conserved PRYSPRY domain, while BTN3A2 does not. This suggests that the antiviral activity of BTN3A3 (and BTN3A1) is mediated through this domain.

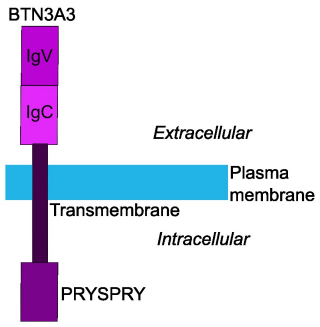

Figure 62. Domain architecture of BTN3A3.
Domain structure of BTN3A3 demonstrating its extracellular, transmembrane, and intracellular parts.

A PRYSPRY domain is approximately 170 amino acids in length and is found in BTN3A1/3 and 33 of the human tripartite motif (TRIM) proteins, most of which are involved in the innate immune response to virus infection or other pathogens (Rhodes et al., 2005). In the case of some of these TRIM proteins, their antiviral activity has been shown to be mediated by their C-terminal PRYSPRY domain. For instance, TRIM5α restricts replication of retroviruses such as HIV-1 after cell entry by binding the viral capsid in a manner that is mediated by its PRYSPRY domain (Stremlau et al., 2004, Stremlau et al., 2005). In addition, TRIM25, an E3 ubiquitin ligase, interacts with RIG-I via its PRYSPRY domain resulting in ubiquitination of RIG-I and activation of RIG-I signalling (Gack et al., 2007). TRIM25 also has RNA binding activity, which is important for its antiviral activity. Interestingly, the ability of TRIM25 to bind RNA was recently found to be mediated by its RPYSPRY domain (Alvarez et al., 2024, Choudhury et al., 2017). To elucidate whether BTN3A3's PRYSPRY domain is similarly important for its antiviral activity, we could generate variations of BTN3A3 with and without the PRYSPRY domain. We could then test whether these constructs restrict avian polymerase activity in minigenome reporter assays and interact with NP in split luciferase assays. Understanding which region of BTN3A3 possesses antiviral activity may be important for designing future antiviral therapeutics.

It remains unclear whether the antiviral effects of BTN3A3 are mediated through BTN3A3 localised to the nucleus or the cytoplasm. It is intriguing that BTN3A3 is classified as a type I transmembrane protein, with its transmembrane domain anchoring it to the plasma membrane such that the N-terminus is extracellular, and C-terminus is intracellular, yet Pinto et al., observed nuclear accumulation of BTN3A3 (Pinto et al., 2023, Rhodes et al., 2001). It could be speculated that the intracellular C-terminus of BTN3A3 is cleaved, allowing it to relocate to the nucleus and exert its antiviral effects. Testing the effect on avian RNA replication of a truncated version of BTN3A3 only containing the C-terminal PRYSPRY domain would elucidate whether this domain is sufficient for BTN3A3's antiviral activity. In addition,

inserting an NLS into this version of BTN3A3 may also elucidate whether nuclear or cytoplasmic BTN3A3 is responsible for its antiviral activity.

Finally, to gain a more comprehensive insight into the restriction of AIVs by ISGs, it would be interesting to perform a study similar to that by Hubel et al., (Hubel et al., 2019). The authors investigate the cellular cofactors that associate with both ISGs and vRNPs and find that ISGs may recruit cellular factors that are not IFN-regulated to exert their antiviral effects. For instance, they find that TCF7L2, an ISG that specifically restricts IAV, interacts with ANP32. They performed their study with a mammalian-adapted IAV strain (WSN). Performing a similar interactome study with an AIV strain would allow a better understanding of BTN3A3's antiviral activity and whether additional cellular factors are involved.

In summary, we have used two different assays that measure polymerase activity (minigenome reporter assay and RT-qPCR) to further investigate BTN3A3 and MxA restriction of AIV strains. We have demonstrated that restriction occurs in an NP-dependent manner and at the cRNA synthesis step of RNA replication, consistent with previous reports. Further work is required to understand what step of the NP lifecycle is targeted, whether additional cellular factors are involved, and how specifically avian but not mammalian-adapted IAVs are inhibited.

Chapter 5. Discussion and summary

IAV is an important pathogen to study because it is associated with a high public health and economic burden (Paules and Subbarao, 2017, Krammer et al., 2018). In the human population, IAV is responsible for both seasonal epidemics and occasional pandemics that result in significant morbidity and mortality. What is more, IAV circulating in avian species not only poses a pandemic risk but also impacts food security and animal welfare and biodiversity (Koopmans et al., 2024). The development of strategies that can mitigate the impact of IAV, in both the human and bird population, is therefore of high importance and urgency. As an obligate intracellular parasite, IAV is heavily reliant on host cell proteins for all steps of its lifecycle. Consequently, studying the virus from the perspective of virus-host interactions may lead to great insight into both IAV biology and new targets for antiviral strategies.

The subject of this thesis was the IAV polymerase, which is responsible for both transcription and replication of the IAV genome (Fodor and Te Velthuis, 2020). Many host cell proteins are hijacked by IAV to support the polymerase in its different activities (Peacock et al., 2019). At the same time, polymerase activity is also restricted by mismatches to both proviral and antiviral host proteins, and the viral polymerase and NP proteins must evolve to evade this restriction to achieve efficient replication in human cells (Long et al., 2019b). To understand how IAV polymerase activity is regulated by host cell proteins, this work was divided into two parts, with a particular focus on viral RNA replication. First, discovery and characterisation of novel proviral regulators of viral RNA synthesis (Chapters 2 and 3) and second, characterisation of known antiviral regulators of viral RNA synthesis (Chapter 4).

Section 5.1. Discovery and characterisation of proviral regulators of viral RNA synthesis.

The host cell interactome of the IAV polymerase has been extensively studied in the past, yielding insight into the virus-host interactions that support polymerase activity (Bradel-Tretheway et al., 2011, Haas et al., 2023, Heaton et al., 2016, Hubel et al., 2019, Jorba et al., 2008, Mayer et al., 2007, Rialdi et al., 2017, Watanabe et al., 2014, York et al., 2014). However, these studies often do not distinguish between the host cell proteins required for viral transcription and replication. In this work, we set out to identify host proteins that are co-opted by IAV as either transcription- or replication-specific factors, building on a decade of work from the Barclay Lab and others to characterise the role of the essential replication cofactor ANP32. To achieve this, we performed a differential interactome screen comparing the polymerase interactome in eHAP WT cells and ANP32-KO cells in the context of live-virus.

This allowed us to identify 1) host proteins recruited upstream of and for primary transcription and 2) host proteins recruited downstream of primary transcription including for RNA replication (Chapter 2). We performed a targeted siRNA screen of a subset of the host cell proteins identified in each category to investigate their functional role in polymerase activity, measured using a minigenome reporter assay, and virus replication, measured using a ZsGreen reporter virus. Using this strategy, RPAP2, HMGB2, and RUVBL2 host cell proteins were identified as proviral factors for IAV and taken forward for further characterisation.

We used siRNA-mediated gene knockdown and CRISPR-Cas9-mediated gene knockout methods to further investigate the role of RPAP2, HMGB2, and RUVBL2 in polymerase activity (Chapter 3). By combining these gene depletion methods with assays that allow cRNA and mRNA synthesis to be distinguished, we were able to identify the step of viral RNA synthesis that RPAP2, HMGB2, and RUVBL2 promote. RPAP2 was shown to be a transcription-specific cofactor, HMGB2 a replication-specific cofactor, and RUVBL2 a replication cofactor. This fits with their predicted roles from the interactome screen and serves as a proof-of-principle that differential interactomes can be used as a targeted approach to discovering host factors (Chapter 2).

While our work has identified which polymerase activity RPAP2, HMGB2, and RUVBL2 promote, further work is necessary to understand the mechanism behind their proviral roles. RPAP2 was shown to support the primary round of mRNA synthesis and given its known association with host RNAP II, likely acts at the initiation stage of viral transcription (Figure 63A) (Forget et al., 2013). HMGB2 was shown to promote the pioneering round of v-to-cRNA synthesis. It is unknown whether HMGB2 also plays a role in the second c-to-vRNA synthesis step and whether its role in RNA replication involves its known interaction with NP (Moisy et al., 2012). Considering that ANP32 is thought to dissociate once the polymerase becomes active, and thereby only be involved in the recruitment of the first NP to the nascent RNA strand, it could be speculated that HMGB2 is involved in the recruitment of subsequent NPs (Figure 63B) (Baker et al., 2018, Mistry et al., 2020, Wang et al., 2022a). It is also possible that HMGB2's role is not only NP-mediated but also involves the polymerase. While HMGB2 does not interact directly with individual polymerase proteins, it is untested whether HMGB2 interacts with the polymerase proteins when they exist as a heterotrimer (Moisy et al., 2012). Other potential mechanisms behind HMGB2's proviral role in cRNA synthesis are suggested in Section 5.4. RUVBL2 was found to support RNA replication but at which step and whether it also plays a role in mRNA synthesis is unknown. Its role in RNA replication likely involves its previously established interaction with NP and/or the PB2 and PB1 polymerase subunits (Haas et al., 2023, Heaton et al., 2016, Kakugawa et al., 2009, Mayer et al., 2007, Watanabe et al., 2014). Potential mechanisms behind its proviral role in RNA replication are also suggested in Section 5.4.

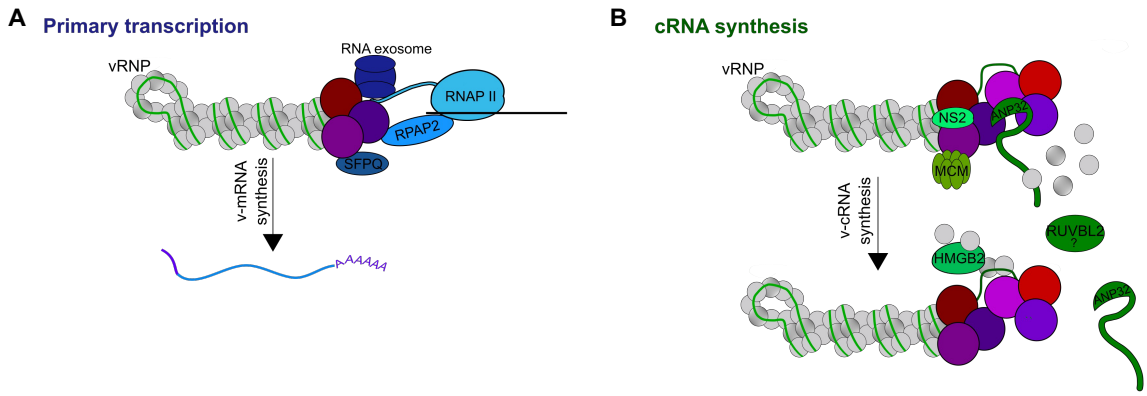

Figure 63. Schematic demonstrating the proposed proviral roles of RPAP2, HMGB2, and RUVBL2.
A) RPAP2 promotes primary mRNA synthesis. RPAP2 may play a role in the initiation of viral transcription as it has previously been shown to interact with host RNAP II, the CTD of which is essential for the cap-snatching step that initiates viral transcription (Forget et al., 2013, Engelhardt et al., 2005). B) HMGB2 promotes cRNA synthesis. In cRNA synthesis, the ANP32 LRR facilitates the formation of an asymmetric dimer, important for co-replicative assembly of RNA into RNPs, while the ANP32 LCAR recruits NP to the nascent RNA strand. Once ANP32 dissociates, likely as the polymerase begins to replicate, HMGB2 may play a role in the recruitment of subsequent NPs to the nascent RNA strand, given its known interaction with NP (Moisy et al., 2012). RUVBL2 supports RNA replication but whether it plays a direct role in cRNA synthesis remains unresolved.

The work presented in Chapters 2 and 3 has focused on the roles of human RPAP2, HMGB2, and RUVBL2 proteins. We have shown that human HMGB2 and RUVBL2 are proviral for multiple IAV strains, including an avian H5N1 strain. Future work may elucidate whether RPAP2 is proviral for multiple IAV strains and whether polymerase activity of the seasonal IBV strain is also supported by these host proteins. Considering the natural avian reservoir of influenza, in the future, we are interested in exploring the role of avian orthologues of RPAP2, HMGB2, and RUVBL2 in the IAV lifecycle. We have already identified avian orthologues of all three proteins and have performed sequence alignments to determine how similar they are to the human version. We found that the avian and human orthologues share 56% sequence identity in the case of RPAP2, 92% in the case of HMGB2, and 90% in the case of RUVBL2. It now remains to be tested whether these avian orthologues are proviral for AIV. This could be done by testing whether the avian orthologues can rescue polymerase activity of avian strains in the A549 KO cells generated in Chapter 3 or by directly testing polymerase activity in chicken cells knocked out for the proteins. Within species there may also be multiple paralogues of RPAP2, HMGB2, and RUVBL2 and these proteins may differ in their proviral activity, given the known species-specific differences in the proviral activity of ANP32 proteins. The huANP32A and huANP32B paralogues are functionally redundant while chANP32A and muANP32B are the only proviral paralogues in their respective species (Long et al., 2019a, Staller et al., 2019, Zhang et al., 2019). Additionally, this study taken together with published work suggests that there may also be species-specific differences in the

proviral roles of HMGB proteins. We found huHMGB2 to be proviral, while Moisy et al., have found muHMGB1 to be proviral (Moisy et al., 2012). It will, therefore, also be important to determine whether paralogues of RPAP2, HMGB2, and RUVBL2 exist in avian species and whether they differ in their proviral activity.

Mechanistic details of the roles of RPAP2, HMGB2, and RUVBL2 in the lifecycles of other viruses may lead to insights into their roles in IAV polymerase activity. RPAP2 is not implicated in the lifecycle of other viruses, but RUVBL2 is proviral for Ebola virus (EBOV), which is a negative-sense single-stranded RNA virus, and HMGB2 is proviral for Epstein-Barr virus (EBV), which is a double-stranded DNA virus. Firstly, RUVBL2 (and its family member RUVBL1) have been shown to interact with EBOV NP, which protects viral RNA from degradation and immune sensing, similar to IAV NP (Morwitzer et al., 2019). The implication of this interaction remains unknown, but it is reminiscent of previous work showing RUVBL2 to interact directly with IAV NP and, thus, may further suggest that RUVBL2's proviral role in IAV replication is NP-mediated (Morwitzer et al., 2019, Kakugawa et al., 2009). Secondly, EBV persists in latently infected cells as the viral EBV nuclear antigen 1 (EBNA1) protein tethers EBV episomes, which contain the genetic material, to the host chromosome during mitosis (Kang and Kieff, 2015). HMGB2 has been implicated in this function of EBNA1 as it was shown to associate with EBNA1 on chromosomes during both interphase and mitosis (Jourdan et al., 2012). Meanwhile, the closely related HMGB1 protein has been implicated in the lifecycle of bornaviruses, which are negative-sense RNA viruses that transcribe and replicate in the nucleus of an infected cell (Matsumoto et al., 2012). HMGB1 stabilises bornavirus RNPs on chromatin through interaction with the viral phosphoprotein. Whether HMGB2 plays a similar role in IAV RNA replication recruiting vRNPs to chromatin and whether IAV RNA replication even occurs on chromatin remains unknown.

Indeed, while the site of viral transcription is thought to be transcriptionally active euchromatin, given the importance of the RNAP II Ser5P CTD, it is unknown whether RNA replication occurs within another, distinct site in the nucleus (Engelhardt et al., 2005). To address this question, ongoing work aims to visualise vRNA and cRNA *in situ* using an RNA FISH approach that is compatible with correlative light electron microscopy (CLEM) (Swann, 2023). This allows RNA replication to be visualised in the context of the nuclear ultrastructure. Co-localisation with host factors such as the RNAP II Ser5P CTD and ANP32 can be used to distinguish transcription and replication factories and reveal further details about the subcellular localisation of the different steps of viral RNA synthesis. However, extensive, and diffuse staining of the host factors makes co-localisation difficult to confirm. Staining for RPAP2 and HMGB2 instead could make this more feasible if their expression levels inside the nucleus are lower. In addition to elucidating the site of viral RNA replication inside the nucleus, another long-term goal of *in situ* visualisation of RNPs is to determine an *in situ* cryo-electron

tomography (cryo-ET) structure of an actively replicating RNP in association with replication-specific cofactors, such as ANP32 or HMGB2.

Section 5.2. RPAP2, HMGB2, and RUVBL2 as targets for antiviral strategies?

In addition to vaccines, current antiviral strategies include anti-IAV therapeutics, which may mitigate the impact of seasonal and pandemic IAV, and gene-edited farmed animals to make them IAV-resistant, which may reduce the overall risk that a pandemic emerges (Idoko-Akoh et al., 2023, Bonomini et al., 2025). A major problem with current antiviral drugs that target viral proteins is that IAV rapidly evolves escape mutations (Hurt, 2014). Targeting host proteins instead may increase the barrier for antiviral resistance to emerge (Watanabe et al., 2014). In this work, we have demonstrated that HMGB2 can be used as an antiviral drug target using ICM, an inhibitor of the HMGB proteins (Lee et al., 2014) (Chapter 3). We showed that ICM is a promising antiviral in cell culture, inhibiting IAV infection by restricting RNA replication. To identify further anti-IAV drugs that target the proviral role of HMGB2, RUVBL2, or RPAP2, a drug screen could be performed. Such a screen could take the form of a split luciferase-based assay that measures the interaction between the host cell proteins and the viral polymerase or NP. Approved drugs could be tested for their ability to disrupt these virus-host interactions and thereby their suitability for being repurposed as anti-IAV drugs. Alternatively, small molecule inhibitors or compounds could be tested for their ability to disrupt these interactions and then subsequently further developed for use as anti-IAV drugs.

Understanding the exact stage of the viral lifecycle that host proteins are involved is important because it allows multiple host proteins that act at different stages to be targeted together. In turn, this may reduce the risk that antiviral resistance arises. The potential need for such multifaceted antiviral strategies was demonstrated by Idoko-Akoh et al., who generated chickens with their chANP32A protein edited to make it non-functional in its proviral role (Idoko-Akoh et al., 2023). However, the authors found that IAV was able to acquire escape mutations, making further edits necessary either in the ANP32 protein or in other host proteins to prevent IAV escape and to make the chickens IAV-resistant. RPAP2 could be a good candidate for this, considering its role in viral transcription, as well as HMGB2 and RUVBL2, especially if future work shows that they act at a different stage of RNA replication than ANP32. This is also dependent on future work identifying proviral avian orthologues of these host proteins. Similar logic could be applied to host-directed therapies: drugs that are known to block different stages of the viral lifecycle could be used in combination to increase the barrier to resistance. For instance, ICM, which we found to inhibit RNA replication, could be used together with BXA, which inhibits the PA endonuclease activity essential for viral transcription (Noshi et al., 2018).

To test whether targeting multiple host proteins with different mechanisms of proviral activity is in fact a more effective long-term antiviral strategy than targeting a single host protein, various experimental evolution studies could be performed. Firstly, the effectiveness of targeting further host proteins in addition to ANP32 in gene-edited chickens could be tested by passaging IAV in ANP32A-KO cells that are also depleted for RPAP2, HMGB2, or RUVBL2. The virus could then be monitored for the emergence of escape mutations, elucidating whether such mutations arise more slowly or perhaps not at all when multiple host proteins are targeted. Secondly, to test the effectiveness of combination therapies, IAV could be passaged in the presence of ICM, BXA, or both, and monitored for the emergence of resistance mutations, as has previously been done with Favipiravir (a nucleoside analogue that inhibits viral polymerase activity) and IAV (Goldhill et al., 2018).

Lastly, to target HMGB2, RUVBL2, and RPAP2 in antiviral strategies, it will be important to determine which parts of the host proteins are necessary for their proviral activity. This is so that precise gene edits can be made without disrupting their host functions. This may also allow small molecule inhibitors to be designed that specifically target the proviral part of the proteins. In the absence of structures of HMGB2, RUVBL2, and RPAP2 in complex with the viral polymerase or vRNPs, structure prediction tools such as AlphaFold3 could be used to model how the host and viral proteins interact with each other (Abramson et al., 2024).

Section 5.3. Characterisation of antiviral regulators of viral RNA synthesis.

BTN3A3 and MxA are human restriction factors that preferentially target AIVs and, therefore, contribute to the IAV host range barrier (Haller et al., 2015, Pinto et al., 2023). Here, we further characterised the molecular details behind the antiviral activity of BTN3A3 and MxA (Chapter 4). To achieve this, we made use of the same assays that uncouple cRNA and mRNA synthesis employed in Chapter 3. However, instead of performing these assays in cells with genes of interest depleted, BTN3A3 and MxA were overexpressed. Overexpression of either factor decreased avian cRNA synthesis but not primary mRNA synthesis in the context of infection (Figure 64). BTN3A3 was found to have no effect on viral RNA synthesis of a mammalian-adapted IAV strain. This confirms previous findings in the literature (Nigg and Pavlovic, 2015, Pavlovic et al., 1992, Pinto et al., 2023). Pinto et al., have previously shown that BTN3A3 does not restrict transcription and instead acts at the level of RNA replication (Pinto et al., 2023). This was shown by quantifying the accumulation of vRNA, cRNA, and mRNA in the absence and presence of BTN3A3 and CHX treatment. In this study, we performed a different version of the assay in which the cRNA intermediate was stabilised (cRNP stabilisation assay). Using this assay, we were able to unambiguously show that BTN3A3 restricts v-to-cRNA synthesis, which remained unclear from the literature.

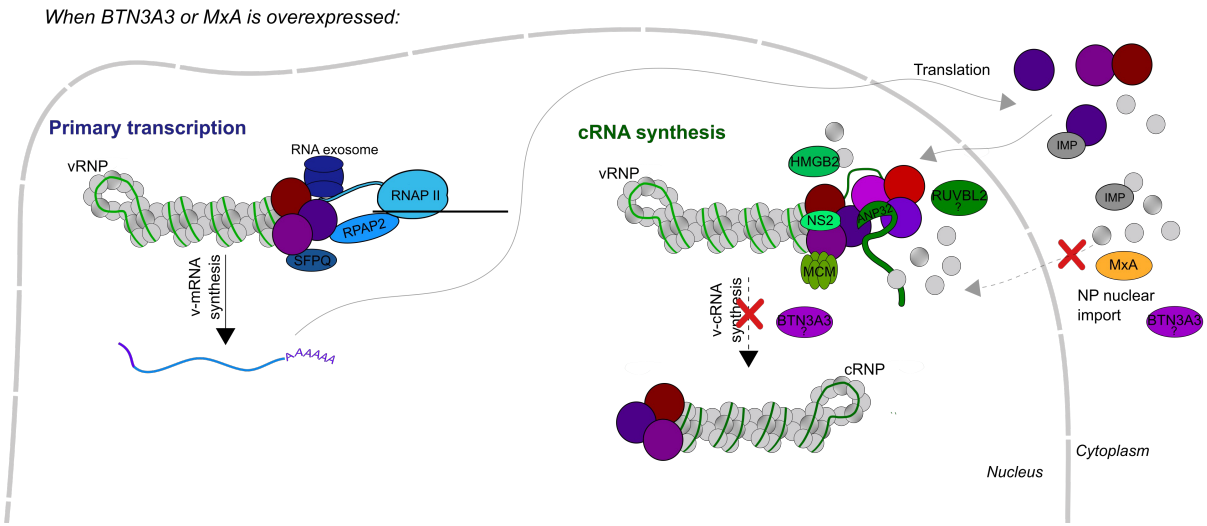

Figure 64. Schematic demonstrating the proposed antiviral roles of BTN3A3 and MxA. When BTN3A3 or MxA is overexpressed, avian cRNA synthesis is inhibited but not primary mRNA synthesis. MxA has been shown to block nuclear import of newly synthesised NP (Pavlovic et al., 1992, Nigg and Pavlovic, 2015). How BTN3A3 restricts cRNA synthesis is unknown. We hypothesise that BTN3A3 either exerts its antiviral effects by acting directly on cRNA synthesis or cRNP assembly inside the nucleus of the infected cell or by restricting nuclear import of NP.

While overexpressed MxA is thought to restrict cRNA synthesis by blocking nuclear import of newly synthesised NP, the mechanism behind BTN3A3's antiviral role is unknown (Figure 64) (Nigg and Pavlovic, 2015, Pavlovic et al., 1992). We hypothesise that BTN3A3's role could either be direct; targeting cRNA synthesis or cRNP assembly in the nucleus of the infected cell, or indirect; restricting nuclear import of newly synthesised NP (similar to MxA). Hubel et al., have shown that ISGs may associate with vRNPs through host factors that support virus replication (Hubel et al., 2019). It is possible that BTN3A3 works in this way and exerts its antiviral activity via a proviral host factor important for polymerase replicase activity. We have made a start at testing whether such a host factor could be ANP32, by testing whether BTN3A3 inhibits the interaction between NP and ANP32 in split luciferase assays. We found that overexpression of BTN3A3 reduced the interaction between huANP32B and both avian and human-adapted NPs. Given that BTN3A3 preferentially restricts avian NPs, we concluded that the mechanism behind BTN3A3 restriction is not reducing the interaction between ANP32 and NP. Instead, this reduced interaction may be a consequence of the known BTN3A3-NP interaction decreasing the amount of NP that was available to interact with ANP32. However, many other potential host factors that may play a role in the antiviral activity of BTN3A3 exist, such as IMPα, which could be investigated in the future. If BTN3A3 is found to act via a host factor specific to IAV, this could explain why BTN3A3 is active only against IAV and not any other viruses (in contrast to MxA).

In this work, we also confirmed that the NP protein is the main determinant of BTN3A3 and MxA restriction. We demonstrated that minigenome reporter assays can be used to measure the BTN3A3 and MxA sensitivity of NPs and that the measured sensitivity correlates with the presence of adaptive NP mutations previously identified in the literature (Manz et al., 2013, Pinto et al., 2023). Using this strategy, we measured the BTN3A3 and MxA sensitivity of panzootic clade 2.3.4.4b NPs and found that most of these NPs have acquired BTN3A3 resistance but not yet MxA resistance. Although it will be important to confirm these findings in the context of live virus, initial characterisation of emerging IAVs in minigenome reporter assays has several benefits. These include the fact that data can be quickly obtained, and polymerases of highly pathogenic AIV strains can be studied without the need for high containment facilities. Current frameworks for assessing the pandemic risk of influenza, such as the World Health Organisation's (WHO) tool for influenza pandemic risk assessment (TIPRA) and the European Centre for Disease Prevention and Control's (ECDC) assessment tool for influenza preparedness, rely on the use of live virus and animal models to measure transmission. Our work suggests that monitoring avian and zoonotic IAV strains for BTN3A3 and MxA resistance in minigenome reporter assays is a good indicator of their ability to overcome host restriction. This method could be built into frameworks, such as TIPRA, as an additional, more high throughput way to assess the pandemic risk of IAV strains.

It remains unknown how adaptive mutations in the NP protein mediate escape from BTN3A3 (and MxA) restriction. It is puzzling that co-IPs show BTN3A3 to interact with NP regardless of whether it harbours the avian or human-adapted signature at position 313 (Pinto et al., 2023). This is reminiscent of early work showing ANP32 to interact to the same extent with PB2 regardless of its E/K signature at position 627 by co-IP and split luciferase assays (Baker et al., 2018, Domingues and Hale, 2017, Mistry et al., 2020). Differences in the interaction between the huANP32 LCAR and the PB2 E/K627 domain were only detected recently using sensitive NMR techniques (Camacho-Zarco et al., 2020). Similar sensitive techniques could also be applied to determine whether BTN3A3 indeed interacts with both avian and mammalian-adapted NPs. Furthermore, structures of ANP32 in complex with the viral polymerase have been instrumental in understanding how the PB2 E627K mutation adapts the polymerase to be able to utilise human ANP32 proteins (Arragain et al., 2024, Carrique et al., 2020, Staller et al., 2024). Solving the structure of BTN3A3 (or MxA) in complex with NP or RNPs may lead to similar insights into the mechanism behind the NP adaptive mutations. As discussed above, in the absence of such structures, the AlphaFold3 structure prediction tool could be used (Abramson et al., 2024).

Section 5.4. Future work.

Many outstanding questions remain regarding the role of host cell proteins in regulating polymerase replicase activity, which would be interesting to address in the future. Some of the questions that remain about proviral factors are outlined below. Experiments that could be performed to explore these questions are suggested in Figure 65A and are also discussed in Chapter 3.

- In the early stages of infection, a switch from transcription to replication occurs which is tightly regulated by viral proteins and the availability of host cell proteins. The viral NS2 protein, accumulation of polymerase proteins and NP, binding of ANP32, and degradation of RNAP II have all been implicated in triggering the switch of the polymerase from a transcriptase to a replicase (reviewed in Deng et al., 2025). Are additional host cell proteins co-opted to regulate the switch to replication?
- During RNA replication, the polymerase adopts an asymmetric dimer structure stabilised by ANP32, which ensures co-replicative assembly of nascent RNA into RNPs (Arragain et al., 2024, Carrique et al., 2020, Staller et al., 2024). Are further host cell proteins involved in stabilising this replication complex?
- In addition to the asymmetric dimer, the polymerase also adopts a structurally distinct symmetric dimer structure, which is required for the second c-to-vRNA synthesis step to ensure prime realignment on the cRNA template (Fan et al., 2019). How is the balance between the asymmetric and symmetric dimer states maintained? Do the two dimers combine to form a trimer on the cRNA template? Do host cell proteins play a role in maintaining this balance or stabilising a potential trimer?
- ANP32 is known to recruit the NP that encapsidates the nascent RNA strand, but whether ANP32 is only involved in the recruitment of the first NP, or all NPs is unclear (Wang et al., 2022a). If ANP32 is only involved in the recruitment of the first NP, what is the mechanism behind the recruitment of the subsequent NPs and are host cell proteins involved?

It is possible that some of these suggested roles are carried out by HMGB2 or RUVBL2 (Figure 65A). Future work may also elucidate whether these roles are fulfilled by any of the remaining host cell proteins that were suggested in this thesis to be replication-specific based on the differential interactome screen and shown to support polymerase activity, but not further characterised (Chapter 2).

In addition, key questions that remain about the antiviral activity of BTN3A3 are summarised below. Experiments that could be performed to explore these questions are suggested in Figure 65B and discussed in Chapter 4.

- AIV cRNA synthesis is restricted by human BTN3A3. What is the mechanism behind this restriction? How do adaptive NP mutations mediate escape from BTN3A3 restriction?

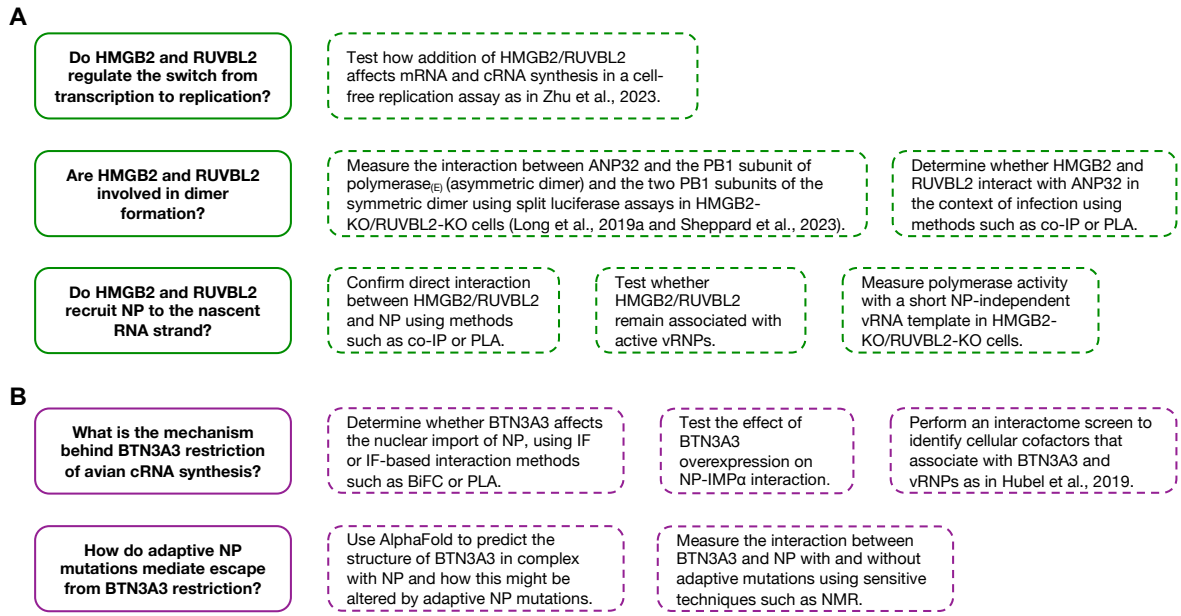

Figure 65. Future experiments to explore the role of host cell proteins in regulating viral RNA replication.
A) Remaining questions regarding the proviral role of host factors in viral RNA replication (solid boxes) and suggested experiments that could be performed to explore these questions (dashed boxes). HMGB2 and RUVBL2 were used as example host proteins. B) Remaining question regarding the antiviral role of BTN3A3 in viral RNA replication (solid boxes) and suggested experiments that could be performed to explore these questions (dashed boxes).

Lastly, the role of host cell proteins in polymerase activity was explored in this thesis using immortalised cell lines. While immortalised cell lines allow virus-host interactions to be readily studied due to their ease of use and homogeneity, they do not recapitulate the physiological state of the human airway, which is the primary site for influenza replication and transmission *in vivo*. It therefore remains unknown whether the dependency of IAV on such host factors is physiologically relevant. To investigate this, primary human airway epithelial cells, which contain a mixture of cells representative of those in the human respiratory tract such as ciliated, secretory, goblet, club, and basal cells, could be used. Normal human nasal epithelial (NHNE) cells, which simulate the upper airway, and normal human bronchial epithelial (NHBE) cells, which simulate the lower airway, are two types of airway epithelial cell cultures that are infected by IAV but that differ in their cell type composition and in the genes that they express (Matrosovich et al., 2004).

Firstly, the effect of ICM on IAV infection in airway epithelial cells could be tested. Considering that the antiviral effects of ICM on IAV infection in immortalised cell lines were

not recapitulated in a mouse model of IAV infection, perhaps due to species differences in the use of HMGB proteins, testing the effect of ICM in airway epithelial cells could be an alternative approach to testing the efficacy of ICM in a more physiologically relevant model.

It would be interesting to use RNA sequencing (RNAseq) and proteomics approaches to investigate whether proviral host factors such as ANP32, HMGB2, RUVBL2, and RPAP2 are expressed differently across the upper and lower airway and whether their expression differs in the different epithelial cell types (ciliated, secretory, basal, etc). Equally, it would also be interesting to elucidate whether antiviral factors are differentially expressed in the different epithelia and cell types upon IFN induction. Although IAV infects many different cell types, ciliated cells have been shown to be the main producers of new virions (Roach et al., 2024). It could be speculated that this difference is due to higher expression of proviral factors or lower expression of antiviral factors in ciliated cells, which could be probed using such RNAseq and proteomics datasets. For instance, if ANP32 or HMGB2 is expressed to a greater extent in ciliated cells than the other epithelial cell types, this could perhaps explain why infection of these cells is more productive.

To assess the importance of these host cell proteins in airway epithelial cells, shRNA-mediated gene knockdown or CRISPR-Cas-mediated gene knockout methods could be developed in these cell models. Virus growth could then be compared in the WT and KO cells. It would be very informative if these gene depletion methods could be further applied to target gene expression in specific epithelial cell types. This would allow us to explore whether depletion of ANP32 or HMGB2 in ciliated cells has a greater impact on virus growth than depletion of the host proteins in secretory cells, for example.

Section 5.5. Summary.

To summarise, in this thesis we have investigated the host cellular landscape that the IAV polymerase and NP navigate to perform efficient viral RNA synthesis. We have developed a differential AP-MS interactome strategy that can be used to discover host cell proteins that interact with either the viral transcriptase or the replicase. Using this strategy, HMGB2 and RUVBL2 were discovered to be proviral replication host factors and RPAP2 was found to be a proviral transcription factor. We also confirmed that viral RNA replication is restricted by the antiviral factors BTN3A3 and MxA, and this restriction is mediated by adaptive mutations in the NP protein. Altogether, this study has provided insight into the virus-host interactions that regulate viral RNA replication, furthering our understanding of IAV polymerase activity and biology.

Chapter 6. Materials and Methods

6.1. Materials

6.1.1. Cell lines

Table 13. Cell lines used in this study.

Cell line	Description	Source	Reference
eHAP WT	Completely haploid human HAP1 cells (eHAP). eHAP WT cells used in this thesis were treated with a non-targeting control sgRNA.	Horizon Discovery/ Barclay Lab	Staller et al., 2019
eHAP ANP32-KO	eHAP cells with ANP32A, ANP32B, and ANP32E ablated by CRISPR-Cas9 genome editing.	Barclay/Fodor Lab	Sheppard et al., 2023
HEK 293T (293T)	Human embryonic kidney cells that contain the SV40 T-antigen (HEK 293T).	ATCC	N/A
MDCK	Madin-Darby canine kidney (MDCK) cells.	ATCC	N/A
A549-dox-Cas9	Adenocarcinomic human alveolar basal epithelial (A549) cells that were engineered to express Cas9 under control by a dox-inducible promoter.	Martin-Sancho Lab	Martin-Sancho et al., 2021
A549-WT	A549-dox-Cas9 cells treated with a non-targeting control sgRNA.	This study	Rasmussen et al., under review
A549 RUVBL2-KO	A549-dox-Cas9 cells with RUVBL2 knocked out by CRISPR-Cas9 genome editing.	This study	Rasmussen et al., under review
A549 HMGB2-KO	A549-dox-Cas9 cells with HMGB2 knocked out by CRISPR-Cas9 genome editing.	This study	Rasmussen et al., under review
A549 RPAP2-KO	A549-dox-Cas9 cells with RPAP2 knocked out by CRISPR-Cas9 genome editing.	This study	Rasmussen et al., under review

6.1.2. Viruses

Table 14. Virus strains used in this study.

Virus	Full strain name	Description	Source
PR8 WT	A/Puerto Rico/8/1934 (H1N1) (PR8)	Full PR8	This study
PR8 PB2-FLAG	A/Puerto Rico/8/1934 (H1N1) (PR8)	PR8 virus with PB2 segment expressing a FLAG tag on the C-terminus.	This study
PR8 PB2-Strep	A/Puerto Rico/8/1934 (H1N1) (PR8)	PR8 virus with PB2 segment expressing a Strep tag on the C-terminus.	This study
PR8 NS-ZsGreen	A/Puerto Rico/8/1934 (H1N1) (PR8)	PR8 virus with NS segment expressing a ZsGreen tag.	This study
5092 E627K:PR8 5:3	A/turkey/England/50-92/1991 (H5N1) (5092K)	Virus with 5092 internal segments (PB2, PB1, PA, NP, and NS) and PR8 external segments (HA, NA, and M). The PB2 segment was engineered to carry the mammalian-adapting E627K mutation.	Thomas Peacock (Barclay Lab)

6.1.3. Plasmids

Table 15. Plasmids used in this study.

Plasmid	Extra notes	Source
pHW2000-PR8-PB2-FLAG	pHW2000 plasmid encoding PR8 PB2 with a FLAG tag on the C-terminus and duplication of the packaging signal	This study
pHW2000-PR8-PB2-Strep	pHW2000 plasmid encoding PR8 PB2 with a Strep tag on the C-terminus and duplication of the packaging signal	This study
pHW2000-PR8-NS-ZsGreen	pHW2000 plasmid encoding PR8 NS with a ZsGreen tag	Edward Hutchinson (University of Glasgow)
pCAGGS-PR8-PB2	Expression plasmids encoding PR8 polymerase subunits and NP	Barclay Lab
pCAGGS-PR8-PB1		
pCAGGS-PR8-PA		
pCAGGS-PR8-NP		
pCAGGS-PR8-PA E410A	Expression plasmid encoding replication-deficient PR8 PA mutant	Olivia Swann (Barclay Lab)
pCAGGS-PR8-PA D108A	Expression plasmid encoding transcription-deficient PR8 PA mutant	
pCAGGS-PR8-PB1 D446Y	Expression plasmid encoding catalytically dead PR8 PB1 mutant	
pCAGGS-Vic75-PB2	Expression plasmids encoding Vic75 polymerase subunits and NP	Olivier Moncorge (Barclay Lab)
pCAGGS-Vic75-PB1		
pCAGGS-Vic75-PA		
pCAGGS-Vic75-NP		
pCAGGS-Eng195-PB2	Expression plasmids encoding Eng195 polymerase subunits and NP	Olivier Moncorge (Barclay Lab)
pCAGGS-Eng195-PB1		
pCAGGS-Eng195-PA		
pCAGGS-Eng195-NP		
pCAGGS-Tky05-PB2	Expression plasmids encoding Tky05 polymerase subunits and NP	Olivier Moncorge (Barclay Lab)
pCAGGS-Tky05-PB1		
pCAGGS-Tky05-PA		
pCAGGS-Tky05-NP		
pCAGGS-5092-PB2 E627K	Expression plasmid encoding 5092 PB2 with mammalian-adapting E627K mutation	Barclay Lab
pCAGGS-5092-PB1	Expression plasmids encoding 5092 PB1, PA, and NP	
pCAGGS-5092-PA		
pCAGGS-5092-NP		
pCAGGS-5092-PB1 D446Y	Expression plasmid encoding catalytically dead 5092 PB1 mutant	Anna Cauldwell (Barclay Lab)
pCAGGS-Anhui-NP	Expression plasmid encoding Anhui NP	Barclay Lab
pCAGGS-H5N8-NP	Expression plasmid encoding H5N8 NP	Barclay Lab
pCAGGS-AIV07-NP	Expression plasmid encoding AIV07 NP	Jessica Quantrill (Barclay Lab)
pCAGGS-APS-NP	Expression plasmid encoding APS NP	
pCAGGS-AIV09-NP	Expression plasmid encoding AIV09 NP	
pCAGGS-AIV48-NP	Expression plasmid encoding AIV48 NP	
pCAGGS-Renilla	Expression plasmid encoding Renilla luciferase	Barclay Lab
pPolI-Firefly	pPolI plasmid encoding negative-sense Firefly luciferase	Olivier Moncorge (Barclay Lab)
pCAGGS-huANP32B-FLAG	Expression plasmid encoding huANP32B with a FLAG tag on the C-terminus	Jason Long (Barclay Lab)
pCAGGS-huANP32B	Expression plasmid encoding huANP32B	

pCAGGS-HMGB2	Expression plasmid encoding codon-optimised HMGB2	This study
pCAGGS-RUVBL2	Expression plasmid encoding codon-optimised RUVBL2	
pCAGGS-HMGB2-FLAG	Expression plasmid encoding HMGB2 with a FLAG tag on the C-terminus	
pCAGGS-RUVBL2-FLAG	Expression plasmid encoding RUVBL2 with a FLAG tag on the C-terminus	
pCAGGS-GFP-FLAG	Expression plasmid encoding GFP with a FLAG tag on the C-terminus	Barclay Lab
pCAGGS-BTN3A3	Expression plasmid encoding BTN3A3	This study
pCAGGS-MxA-FLAG	Expression plasmid encoding MxA with a FLAG tag on the C-terminus	Olivier Moncorge (Barclay Lab)
pCAGGS-MxA	Expression plasmid encoding MxA	
pCAGGS-5092-NP-Gluc1	Expression plasmid encoding 5092 NP with the N-terminal half of gaussia luciferase (Gluc1) on its C-terminus	Carol Sheppard (Barclay Lab)
pCAGGS-Vic75-NP-Gluc1	Expression plasmid encoding Vic75 NP with the N-terminal half of gaussia luciferase (Gluc1) on its C-terminus	Bhakti Mistry (Barclay Lab)
pCAGGS-huANP32B-Gluc2	Expression plasmid encoding huANP32B with the C-terminal half of gaussia luciferase (Gluc2) on its C-terminus	
pCAGGS-Gluc1	Expression plasmid encoding N-terminal half of gaussia luciferase (Gluc1)	
pCAGGS-Gluc2	Expression plasmid encoding C-terminal half of gaussia luciferase (Gluc2)	

6.1.4. Antibodies

Table 16. Primary antibodies used in this study.

Antibody	Details	Source	Catalogue number	Use and dilution:
α-IAV PB2	Rabbit polyclonal	Genetex	GTX125926	WB: 1:500
α-FLAG M2	Mouse monoclonal	Sigma	F1804	WB: 1:500
α-Strep	Rabbit polyclonal	Abcam	Ab76949	WB: 1:1000
α-MCM2	Mouse monoclonal	Abcam	Ab108935	WB: 1:1000
α-SRPK1	Mouse monoclonal	BD Biosciences	BD611072	WB: 1:1500
α-ANP32A	Rabbit polyclonal	Sigma-Aldric	AV40203	WB: 1:250
α-HMGB2	Rabbit monoclonal	Abcam	EPR6301	WB: 1:1000
α-RUVBL2	Rabbit polyclonal	Proteintech	10195-1-AP	WB: 1:500
α-RPAP2	Rabbit polyclonal	Invitrogen	PA5-61244	WB: 1:500
α-RPAP2	Rabbit polyclonal	Proteintech	17401-AP	WB: 1:500
α-BTN3A3	Rabbit polyclonal	Abcam	Ab251692	WB: 1:1000
α-IAV NP	Rabbit polyclonal	Invitrogen	PA5-32242	WB: 1:2000
α-IAV NP	Mouse monoclonal	Abcam	Ab128193	IF: 1:200
α-CRISPR Cas9	Mouse monoclonal	Abcam	Ab191468	WB: 1:1000
α-Lamin B1	Rabbit polyclonal	Abcam	Ab16048	WB: 1:500
α-Vinculin	Rabbit polyclonal	Abcam	Ab129002	WB: 1:1000
α-Tubulin	Mouse monoclonal	Abcam	Ab7291	WB: 1:2500

Table 17. Secondary antibodies used in this study.

Antibody	Details	Source	Catalogue number	Use and dilution:
Alexa Fluor 680	Goat anti-mouse IgG	Abcam	AB175775	WB: 1:10,000
Alexa Fluor 800	Goat anti-rabbit IgG	Abcam	No longer available	WB: 1:10,000
IRDye 800CW	Goat anti-rabbit IgG	Licor Biosciences	926-32211	WB: 1:10,000
Alexa Fluor 488	Donkey anti-mouse IgG	Invitrogen	A21202	IF: 1:10,000

6.1.5. Buffers and chemicals

Table 18. Buffers used in this study.

Buffer	Composition or source
Co-IP lysis buffer	50mM Tris-Cl (pH8.0), 200mM NaCl, 1mM EDTA (Fisher Scientific), 0.2% NP40 (ITW reagents)
Radioimmunoprecipitation assay (RIPA) buffer	50mM Tris (pH 7.4), 150 mM NaCl, 1% NP-40, 0.5% sodium deoxycholate, 0.1% sodium dodecyl sulfate
Buffer W (strep-tactin wash buffer)	10x buffer W (IBA lifesciences), diluted to 1x with purified water.
Buffer BXT (strep-tactin elution buffer)	10x buffer BXT (IBA lifesciences), diluted to 1x with purified water.
Tris acetate EDTA (TAE)	25x tris acetate EDTA (TAE; Sigma-Aldrich), diluted to 0.5x with purified water.
Tris Glycine SDS (TGS) running buffer	10x tris glycine SDS (TGS; Invitrogen) running buffer, diluted to 1x with purified water.
Tris Glycine Methanol (TGM) transfer buffer	25x tris glycine (TG; Invitrogen) transfer buffer, diluted to 1x with purified water, 10% methanol.
Tris-buffered saline (TBS) wash buffer	10x tris buffered saline (TBS; Sigma-Aldrich), diluted to 1x with purified water.
Tris-buffered saline with 0.1% tween-20 (TBS-T) wash buffer	1x TBS with 0.1% tween-20 (Sigma-Aldrich).
Permeabilisation solution for IF	1x PBS with 0.2% triton X-100 (Sigma-Aldrich).
Blocking solution for IF	1x PBS with 2% bovine serum albumin (BSA; Sigma-Aldrich) and 0.1% tween-20.
Phosphate buffered saline-tween (PBS-T)	1x PBS with 0.1% tween-20.
FACS buffer	1x PBS with 1% BSA and 2mM EDTA (Fisher Scientific) filtered using a 0.2µm filter.
Plaque assay overlay	100mL 10x minimal essential media (MEM; Gibco), 28mL BSA fraction V (Invitrogen), 5mL 1% diethylaminoethyl dextran (DEAE; Sigma-Aldrich), 10mL HEPES (Invitrogen), 10mL penicillin-streptomycin (pen-strep; Gibco), 10mL L-Glutamine (Gibco), 20mL sodium bicarbonate (Invitrogen) made up to 700mL with sterile purified water. Overlay media was supplemented with 2% agarose and 1µg/mL TPCK trypsin (Worthington Biochemical).
Crystal violet	5% crystal violet (Sigma-Aldrich) and 15% ethanol in purified water.

Table 19. Chemicals used in this study.

Chemical	Notes
Doxycycline	Doxycycline (dox; Sigma-Aldrich) was obtained as a powder and dissolved in sterile DMSO to a concentration of 10mg/mL. Aliquots were stored at -20°C. Diluted 1:10000 in DMSO to a working concentration of 1µg/mL.
Cycloheximide	Cycloheximide (CHX; Sigma-Aldrich) was obtained as a powder and dissolved in sterile DMSO to a concentration of 100mg/mL. Aliquots were stored at -20°C. Diluted 1:1000 in DMSO to a working concentration of 100µg/mL.
Actinomycin D	Actinomycin D (ActD; Gibco) was obtained as a powder and dissolved in sterile DMSO to a concentration of 5mg/mL. Aliquots were stored at -20°C. Diluted 1:500 in DMSO to a working concentration of 10µg/mL.
Sorafenib	Sorafenib (Sigma-Aldrich) was obtained as a powder and dissolved in sterile DMSO to a concentration of 5mg/mL. Aliquots were stored at -20°C. Diluted in DMSO to working concentrations indicated in Figure and Figure legend (1.6-25µM).
CB-6644	CB-6644 (Cayman Chemical) was obtained as a powder and dissolved in sterile DMSO to a concentration of 5mg/mL. Aliquots were stored at -20°C. Diluted in DMSO to working concentrations indicated in Figure and Figure legend (1.6-25µM).
Inflachromene	Inflachromene (ICM; Cayman Chemical) was obtained as a powder and dissolved in sterile DMSO to a concentration of 5mg/mL. Aliquots were stored at -20°C. Diluted in DMSO to working concentrations indicated in Figures and Figure legends (1.25-40µM).

6.2 Methods

6.2.1. Cell culture

Cell lines used in this project are described in Table 13. eHAP WT and eHAP ANP32-KO cells were maintained in Iscove's Modified Dulbecco's Medium (IMDM; Gibco; catalogue number: 12440053) supplemented with 10% fetal bovine serum (FBS; Labtech), 1% non-essential amino acids (MEM NEAA; Gibco; catalogue number: 11140050), and 1% penicillin-streptomycin (pen-strep; Gibco; catalogue number: 15140122). A549, A549-dox-Cas9, 293T, and MDCK cells were maintained in Dulbecco's Modified Eagle Medium (DMEM; Gibco; catalogue number: 11995065) supplemented with 10% FBS (Gibco), 1% NEAA, and 1% pen-strep. When siRNA-transfected, eHAP and A549 cells were maintained in IMDM or DMEM, respectively, supplemented with 20% FBS and 1% NEAA. Similarly, prior to and during dox treatment, A549-dox-Cas9 cells were maintained in DMEM supplemented with 20% FBS and 1% NEAA. All cells were cultured at 37°C and 5% CO_2.

Unless otherwise stated, cells were seeded to 70-80% confluency for use in experiments.

6.2.2. Virology

Viruses used in this study are described in Table 14.

<u>Virus rescue</u>

IAV PR8 WT, PR8 PB2-FLAG, PR8 PB2-Strep, and PR8 NS-ZsGreen viruses were generated by reverse genetics using the 8-plasmid pHW2000 reverse genetics system

(Hoffmann et al., 2000). 293T cells were seeded in a 12-well plate. Media was replaced with 1x optiMEM (Gibco) and incubated at 37°C for 1hr prior to transfection. A plasmid mix consisting of 1µg of pHW2000-NP and 500ng of pHW2000 plasmids encoding the cDNA of each of the remaining 7 viral segments (PB2 (PB2-WT, PB2-FLAG, or PB2-Strep), PB1, PA, HA, NA, M, and NS (NS-WT or NS-ZsGreen)) was generated alongside a negative control plasmid mix, lacking the PB2 plasmid. Transfections were then performed using Xtreme-gene9 transfection reagent (Roche), according to the manufacturer's instructions. In brief, 20µL of transfection reagent was added to 250µL 1x optiMEM, swirled to mix, and equilibrated for 5min at room temperature (RT). Plasmid mixes were then added to the Xtreme-gene9/optiMEM mix, swirled to mix, and incubated at RT for 20min. Next, the transfection mix was added to the 293T cells dropwise and the transfected cells were incubated at 37°C overnight (O/N). The transfected 293T cells were then co-cultured with MDCK cells. Briefly, MDCK cells were trypsinised, washed by centrifugation, and then resuspended in media. 4mL of the resuspended MDCK cells were aliquoted into T25 flasks. The transfected 293T cells were then gently washed in phosphate-buffered saline (PBS; Gibco). 1mL of the remaining MDCK suspension was used to dislodge the 293T cells by scraping and pipetting. The 293T-MDCK mix was then added to the prepared T25 flask containing 4mL of MDCKs. The cells were left to adhere to the bottom of the flask for 4-5hrs at 37°C. The media was then removed, and the cells were washed gently in serum-free (SF) media (media supplemented with 1% NEAA, 1% pen-strep). SF media supplemented with 1µg/mL of TPCK trypsin (Worthington Biochemical) was then added. The virus rescues were incubated at 37°C for 3-7 days until cytopathic effect (CPE) was observed. The supernatants were then harvested, clarified by centrifugation at 1000RCF for 5min, aliquoted, and stored at -80°C. The resulting rescued viruses were titred by plaque assay, sequenced by Sanger sequencing, and used to grow up higher titre stocks, as described below.

Growing viral stocks

To grow viral stocks on MDCK cells (PR8 WT), MDCKs were grown in a T175 flask or more as needed. The virus was diluted in SF media to MOI=0.0001. The MDCKs were washed in PBS, followed by a wash in SF media. The diluted viral inoculum was added, and the infected cells were incubated at 37°C for 1hr. The viral inoculum was then replaced with SF media supplemented with 1µg/mL of TPCK trypsin. Following incubation at 37°C for 48hrs, the supernatants were harvested, clarified by centrifugation at 1000RCF for 5min, aliquoted, and stored at -80°C. Virus stocks were titred by plaque assay and sequenced by Sanger sequencing, as described below.

To grow viral stocks in eggs (PR8 WT, PR8 PB2-FLAG, PR8 PB2-Strep, PR8 NS-ZsGreen), chicken eggs (Medeggs) were used. After 8 days of incubation, eggs were candled

to determine if the eggs were fertile or infertile, with fertile eggs showing thin blood vessels that lead to a chicken embryo. After 10 days of incubation, eggs were infected, as described in (Brauer and Chen, 2015). In brief, viral inoculum was prepared by diluting virus rescue or stock to 10^3 PFU/mL in PBS. The air space of the egg was marked, and the eggs were placed in an egg carton with the air space facing upwards. A sterile needle was used to make two holes in the eggshell over the air sac, one at the top and one on the side. Eggs were inoculated with 200uL of inoculum injected into the hole on the side of the shell. The hole was sealed with tape and the eggs were incubated at 37°C for 48hrs. Prior to harvest, eggs were incubated at 4°C O/N to kill the embryo and constrict the blood vessels. Sterile scissors were then used to cut open the eggshell above the air sac. The chorioallantoic membrane was opened and the allantoic fluid was collected using a 1mL pipette, taking care not to rupture the yolk. As much allantoic fluid as possible was collected and combined in a falcon tube. The collected virus was then clarified by centrifugation at 1000RCF for 5min at 4°C. The supernatant was aliquoted and stored at -80°C. The virus stocks were titred by plaque assay and sequenced by Sanger sequencing, as described below.

Sequencing viruses

Viral RNA was extracted from the rescued virus or virus stock using a QIAamp viral RNA mini kit (Qiagen), according to the manufacturer's instructions. The RNA segment to be sequenced (PB2 in the case of PR8 PB2-FLAG and PR8 PB2-Strep viruses and NS in the case of PR8 NS-ZsGreen) was reverse transcribed and PCR amplified in one step using a SuperScript III One-Step RT-PCR kit (Invitrogen) in a 25µL reaction, according to the manufacturer's instructions. Primers specific to each segment were used (Table 20). The SuperScript III One-Step RT-PCR cycling conditions used were:

Step	Temperature	Time
cDNA synthesis and pre-denaturation	55°C	30min
	94°C	2min
Amplification (40 cycles)	94°C	15s
	60°C	30s
	68°C	1min
Final extension	68°C	5min
Hold	10°C	Indefinitely

The PCR products were Sanger sequenced (Source Bioscience) using primers in Table 20.

Table 20. Primers for amplification and sequencing of PB2 and NS segment of viruses.
Primers are the Hoffman primers (Hoffmann et al., 2001).

Primer details	Primer sequence
Forward primer for amplification and sequencing of PB2	TATTGGTCTCCAGGGAGCGAAAGCAGGTC
Reverse primer for amplification and sequencing of PB2	ATATGGTCTCGTATTAGTAGAAACAAGGTCGTTT
Forward primer for amplification and sequencing of NS	TATTCGTCTCAGGGAGCAAAAGCAGGGTG
Reverse primer for amplification and sequencing of NS	ATATCGTCTCGTATTAGTAGAAACAAGGGTGTTTT

Plaque assays

Viral titres were determined by plaque assay on MDCK cells. MDCK cells were seeded to 100% confluency in 12-well plates. Viruses were serially diluted in SF media in a 10-fold dilution to 10^{-6}. MDCK cells were washed in PBS and infected with 200µL of each dilution at 37°C for 1hr, with occasional tipping to ensure the cells did not dry out. Inoculum was removed and replaced with 1mL overlay media containing 2% agarose and 1µg/mL TPCK trypsin. Overlay media was left to settle at RT and then the plates were incubated upside down at 37°C for 72hrs. Overlay was removed, and the cells were stained using crystal violet solution for at least 1hr at RT. Crystal violet was removed and the plaques were counted at the lowest dilution where individual plaques could be counted. The viral titres were then calculated based on the amount of inoculum added (200µL) to convert viral titres into PFU/mL.

Multi-cycle and single-cycle infections

Virus was diluted in SF media to the correct MOI (PFU/cell) as indicated in Figure legends.

For multi-cycle infections, cells were seeded in 12-well plates, unless otherwise stated below. Cells were washed in PBS, infected with viral inoculum, and incubated at 37°C for 1hr. Inoculum was replaced with prewarmed SF media supplemented with 1µg/mL TPCK trypsin and infected cells were incubated at 37°C. This timepoint was considered as timepoint 0. At the appropriate timepoint post infection, cells were imaged by IF, as described below, or supernatants were harvested for analysis by plaque assay.

Single-cycle infections were performed as for multi-cycle infections, but the inoculum was replaced with prewarmed full media without TPCK trypsin. At the appropriate timepoint, cells were harvested for co-IP analysis or fixed and stained for IF analysis.

For synchronised single-cycle infections, cells were seeded in 24-well plates. Prior to infection, cells were incubated at 4°C for 15min and then washed in cold PBS. Viral inoculum was added to the cells, followed by incubation at 4°C for 45min. The inoculum was then replaced with prewarmed full media and infected cells were incubated at 37°C. This timepoint was considered as timepoint 0. At the appropriate timepoint post infection, cells were lysed in

buffer RLT (Qiagen) supplemented with 10% β-mercaptoethanol (BME; Sigma-Aldrich) for analysis by RT-qPCR.

cRNP stabilisation assay

Cells were seeded in 24-well plates. Cells were then transfected with pCAGGS expression plasmids encoding PB2, PB1 D446Y (catalytically dead), PA, and NP in a 2:2:1:4 (PB2:PB1:PA:NP) ratio, where 1=20ng. Transfections were performed using Lipofectamine 3000 (Invitrogen), according to the manufacturer's instructions and as described below. 20hrs post transfection, media was replaced with prewarmed full media supplemented with either ActD (10µg/mL), CHX (100µg/mL), or DMSO, followed by incubation at 37°C for 1hr. Synchronised single cycle-infections were then performed as described above but with addition of ActD (10µg/mL), CHX (100µg/mL), or DMSO to viral inoculums and subsequent prewarmed full media. At the appropriate timepoint post infection, cells were lysed in buffer RLT supplemented with 10% BME for analysis by RT-qPCR.

6.2.3. Cloning

Gel electrophoresis

DNA was separated by gel electrophoresis. Gels were prepared with 1% agarose (to analyse PCR products ≥750bp) or 2% agarose (to analyse PCR products ≤750bp) in 0.5x TAE buffer supplemented with GelRed (Biotium) to visualise the DNA. 6x loading dye (NEB) was added to DNA in a 1:6 dye:DNA ratio. DNA was loaded onto gels alongside a 1kb or 100bp ladder (NEB). Gels were run at 100V for 30-60min in 0.5x TAE buffer and then visualised using a gel doc XR+ imaging system (Bio-Rad).

Plasmid insert design and digestions

Inserts were subcloned into the pCAGGS expression vector using NotI and XhoI restriction sites. HMGB2-FLAG, RUVBL2-FLAG, codon-optimised HMGB2, and codon-optimised RUVBL2 were synthesised by gene synthesis (GeneArt; ThermoFisher Scientific). The inserts were synthesised with a NotI restriction site and Kozak sequence at the N-terminus and an extra stop codon and XhoI restriction site at the C-terminus.

BTN3A3 was subcloned from human BTN3A3 cDNA (Horizon Discovery). The cDNA was PCR amplified using KOD Hot Start DNA polymerase (Sigma-Aldrich) in a 25µL reaction, according to the manufacturer's instructions. Primers used were designed to add a NotI restriction and Kozak sequence at the N-terminus and an extra stop codon and XhoI restriction site at the C-terminus (Table 21).

Table 21. Primers for subcloning BTN3A3 into pCAGGS.

Primer details	Primer sequence
Forward primer for cloning BTN3A3 into pCAGGS	TATATATAGCGGCCGCGCCACCATGAAAATGGCAAGTTCC
Reverse primer for cloning BTN3A3 into pCAGGS	TTAATTAACTCGAGTTAGTAAAGTGCTTCAGTGCGTGC

The KOD Hot Start DNA polymerase cycling conditions used were:

Step	Temperature	Time
Hot start	95°C	2min
Amplification (35 cycles)	95°C	20s
	55°C	10s
	70°C	1min
Final extension	70°C	2min
Hold	10°C	Indefinitely

The PCR product was run on a 1% agarose gel, as described above, and gel extracted using a Monarch DNA gel extraction kit (NEB), according to the manufacturer's instructions.

All inserts were digested with NotI-HF and XhoI (NEB) restriction enzymes, according to the manufacturer's instructions. In brief, 1µg or less DNA was incubated with 1µL of each enzyme and 1x rCutSmart buffer (NEB) at 37°C for 1hr. PCR products were also DpnI (NEB) digested in the same manner. Digested inserts were run on a 1% agarose gel and then gel extracted. This was followed by ligation into digested pCAGGS plasmid, described below.

Generating AP-tagged PB2 constructs

The pHW2000-PR8 PB2-FLAG construct with a 173nt duplication of the packaging signal was generated by golden gate assembly (Engler et al., 2008). Two fragments were generated using the pHW2000-PR8 PB2 plasmid as a backbone and the primers in Table 22. Fragment 1 has a BsaI restriction site, N-terminal NCR, PB2 coding region, a 3x alanine linker, the FLAG tag, 2x stop codon, and another BsaI restriction site. Fragment 2 has a BsaI restriction site, duplicated packaging signal, C-terminal NCR, and another BsaI restriction site.

Table 22. Primers for generating PB2-FLAG construct by golden gate assembly.

Primer details	Primer sequence
PB2 forward primer that introduces N-terminal BsaI restriction site (Hoffman primer) (Fragment 1)	TATTGGTCTCCAGGGAGCGAAAGCAGGTC
PB2 reverse primer that introduces C-terminal 3x alanine linker, FLAG tag, 2x stop codon and BsaI restriction site (Fragment 1)	GGTCTCGGAGACTACTACTTGTCGTCGTCGTCCTTGTAGTCGGCGGCGGCATTGATGGCCATCCGAATTCTTTTGG
PB2 forward primer that introduces a BsaI restriction site and amplifies 173nt of packaging signal before the C-terminal non-coding region (Fragment 2)	GGTCTCCAGAGATATGGGCCAGCACTAAGC
PB2 reverse primer that introduces C-terminal BsaI restriction site (Hoffman primer) (Fragment 2)	ATATGGTCTCGTATTAGTAGAAACAAGGTCGTTT

PCR reactions were set up to generate each of the two fragments using KOD Hot start DNA polymerase in a 50uL reaction, according to the manufacturer's instructions. Cycling conditions were the same as shown above. PCR products were analysed by gel electrophoresis on a 1% agarose gel and gel extracted. The gel extracted PCR products were then digested with a BsaI (NEB) restriction enzyme, according to the manufacturer's instructions. In brief, PCR products were incubated with 1µL BsaI enzyme and 1x rCutSmart buffer (NEB) at 37°C for 1hr. Products were also DpnI digested. The digested products were PCR purified using a Monarch PCR and DNA cleanup kit (NEB), according to the manufacturer's instructions. The two fragments were then ligated together into digested pHW2000 plasmid, described below.

The PR8 PB2-Strep construct was synthesised by gene synthesis (GeneArt; ThermoFisher Scientific). The insert was synthesised with BsaI restriction sites on the N-terminus and the C-terminus.

Plasmid vector digestions

pCAGGS plasmid was double digested using NotI-HF and XhoI restriction enzymes. pHW2000 plasmid was digested using the BsaI restriction enzyme. In brief, 1µg of plasmid vector was incubated with 1µL of each enzyme as appropriate and 1x rCutSmart buffer for 1hr at 37°C. The digested plasmid was run on a 1% agarose gel and the correct sized band was gel extracted. To ensure complete digest, the gel extracted product was digested again, in the same manner as described above. The digested product was then dephosphorylated by addition of 1µL antarctic phosphatase (NEB) and 1x antarctic phosphatase buffer (NEB) with incubation at 37°C for 1hr. The digested- and dephosphorylated-vector was PCR purified and then used in ligations, described below.

Ligations

Ligations between inserts and vector were performed using T4 DNA ligase (NEB). For ligation into pCAGGS, a 3:1 insert:vector ratio was used based on the insert and vector sizes. For double ligation into pHW2000, a 2:1 insert:vector ratio was used based on the insert and vector sizes. The appropriate amounts of digested vector and insert were incubated with 1µL T4 DNA ligase and 1x T4 DNA ligase buffer in a 20µL reaction. Ligations were incubated at RT for 10min, followed by incubation at 16°C O/N. 5uL ligation product was then used for transformation, as described below.

Transformations

Transformations into competent 5α E. coli cells (NEB) were performed using heat shock. High efficiency 5α cells were used for ligations and subcloning efficiency 5α cells were used for retransformations of plasmids. 5µL of ligation or 10ng of plasmid DNA was added to

5α cells and incubated on ice for 30min. The DNA-bacteria mixes were then heat-shocked by incubation at 42°C for 1min followed by incubation on ice for 5min. 500µL of SOC outgrowth medium (NEB) was then added, followed by incubation at 37°C shaking for 1hr. The bacteria were then centrifuged at 13000RCF for 2min, the pellets were resuspended in 50µL of supernatant, and then spread on prewarmed LB agar plates with 100µg/mL ampicillin. The plates were incubated upside down at 37°C O/N.

Preparation of plasmids

Minipreps were performed using a Monarch miniprep kit (NEB), according to the manufacturer's instructions. DNA was eluted in 40µL nuclease-free water and correct insertion of the insert was confirmed by Sanger sequencing. Maxipreps were performed using a Qiagen HiSpeed plasmid kit (Qiagen), according to the manufacturer's instructions. Plasmid sequences were confirmed using whole-plasmid sequencing (Full Circle Labs). Plasmid concentrations were measured using a Nanodrop Lite spectrophotometer (ThermoFisher Scientific).

Sequencing plasmids

Sanger sequencing of plasmids was performed by Source Bioscience. Plasmids were mixed with appropriate primers prior to shipment (Table 23). Whole plasmid sequencing was performed by Full Circle Labs. Sequences were analysed using Geneious Prime v.2019.2.3 software.

Table 23. Primers for sequencing inserts in pCAGGS and pHW2000 plasmid vectors.

Primer details	Primer sequence
Forward primer for sequencing inserts in pCAGGS	GCTAACCATGTTCATGCCTTC
Reverse primer for sequencing inserts in pCAGGS	GGTATTTGTGAGCCAGGGCATTG
Forward primer for sequencing inserts in pHW2000	TAATACGACTCACTATAGGG
Reverse primer for sequencing inserts in pHW2000	TAGAAGGCACAGTCGAGG

6.2.4. Co-immunoprecipitations

FLAG tag co-IP

For co-IPs comparing interactomes in eHAP WT and ANP32-KO cells, the eHAP WT cells were cultured in 1x 15cm and 1x 10cm dishes and eHAP ANP32-KO cells were cultured in 4x 15cm dishes. For MS analysis, cells were single-cycle infected with PR8 PB2-FLAG or PR8 WT, as described above. For western blot analysis, cells were transfected with pCAGGS plasmids encoding HMGB2-FLAG (10µg) or RUVBL2-FLAG (5µg) using Lipofectamine 3000, according to the manufacturer's instructions and as described below. 20hrs later, transfected

cells were single-cycle infected with PR8 WT. For co-IPs comparing the ANP32 interactome in infected and uninfected conditions, ANP32-KO cells were seeded in 2x 15cm dishes and transfected with pCAGGS plasmids encoding ANP32B-FLAG (5µg) or GFP-FLAG (0.5µg). 20hrs post transfection, cells were single-cycle infected with PR8 WT or mock-infected. In all co-IPs, cells were harvested at 3hpi, washed 3x in ice-cold PBS, and lysed in co-IP lysis buffer supplemented with EDTA-free protease inhibitor cocktail tablet (Roche) on a rotating wheel at 4°C for 30min. Lysates were centrifuged at 13000RCF for 10min. The supernatants were then incubated with anti-FLAG magnetic beads (ThermoFisher Scientific), equilibrated in TBS, on a rotating wheel at 4°C O/N. For MS analysis, beads were washed 4x in co-IP lysis buffer, 4x in TBS, and 7x in 50mM ammonium bicarbonate and then stored in 50mM ammonium bicarbonate at 4°C until analysis by MS, described below. For western blot analysis, prior to incubation with the magnetic beads, a small proportion of the supernatant was saved for use as western blot input. Beads were washed 4x in co-IP lysis buffer and 4x in TBS prior to elution by competition with 3xFLAG peptide (ThermoFisher Scientific) on a rotating wheel for 30min at RT. Supernatants were harvested and stored at -20°C until western blot analysis. For co-IP optimisation experiments, cells were seeded in 2x 10cm dishes and the remaining conditions (MOI, timepoint, lysis buffer composition) are provided in the Figure legends.

Strep tag co-IP

eHAP WT and ANP32-KO cells were seeded in 2x 10cm dishes. Cells were single-cycle infected with PR8 PB2-Strep or PR8 PB2-WT, as described above. Cells were harvested at 5hpi, washed 3x in ice-cold PBS, and lysed in co-IP lysis buffer supplemented with EDTA-free protease inhibitor cocktail tablet on a rotating wheel at 4°C for 30min. Lysates were centrifuged at 13000RCF for 10min. The supernatants were then incubated with MagStrep "type 3" XT (strep-tactin) magnetic beads (IBA lifesciences), equilibrated in 1x buffer W (IBA lifesciences), for 30min on ice, vortexing every 10min to ensure the beads remain suspended. Prior to incubation with the beads, a small proportion of the supernatant was saved for use as western blot input. Beads were washed 3x in 1x buffer W. Proteins were then eluted by incubating the beads with 1x buffer BXT (IBA lifesciences) for 10min at RT. Supernatants were harvested and stored at -20°C until western blot analysis.

6.2.5. Mass spectrometry and analysis

Mass spectrometry

Bead-bound proteins were prepared for mass spectrometric analysis by in solution enzymatic digestion. Briefly, bead-bound proteins in 50mM ammonium bicarbonate were reduced in 10mM DTT and then alkylated with 55mM iodoacetamide. 0.5µg of Trypsin (ThermoFisher Scientific) was added, and the proteins digested at 37°C for 1hr, shaking at

800rpm. Following this initial digestion, a further 0.5µg of Trypsin was added, and digestion continued O/N at 37°C. 1µl of formic acid was added and the beads centrifuged for 60s at 2000RCF, before placing them in a magnetic rack. The supernatant was then removed into a fresh tube. The resulting peptides were analysed by nano-scale capillary LC-MS/MS using an Ultimate U3000 HPLC (ThermoScientific Dionex) to deliver a flow of approximately 250nL/min. A C18 Acclaim PepMap100 5µm, 75µm x 20mm nanoViper (ThermoScientific Dionex), trapped the peptides prior to separation on a C18 Acclaim PepMap RSLC 3µm, 75µm x 500mm nanoViper (ThermoScientific Dionex). Peptides were eluted with a 90min gradient of acetonitrile (2%v/v to 80%v/v). The analytical column outlet was directly interfaced via a nano-flow electrospray ionisation source, with a hybrid dual pressure linear ion trap mass spectrometer (Orbitrap Lumos; ThermoScientific). Data dependent analysis was carried out, using a resolution of 120,000 for the full MS spectrum, followed by ten MS/MS spectra in the linear ion trap. MS spectra were collected over a m/z range of 300-1500. MS/MS scans were collected with the standard AGC target, dynamic maximum injection time mode, isolation window at 1.2 m/z and 32% normalised HCD collision energy. All raw files were processed with MaxQuant 2.4.9.0 (Cox and Mann, 2008) using standard settings and searched against a UniProt Human Reviewed KB/Influenza concatenated database with the Trypsin/ Andromeda search engine (Cox et al., 2011) integrated into the MaxQuant software suite. Enzyme search specificity was P for both endoproteinases. Up to two missed cleavages for each peptide were allowed. Carbamidomethylation of cysteines was set as fixed modification with oxidized methionine and protein N-acetylation considered as variable modifications. The search was performed with an initial mass tolerance of 6ppm for the precursor ion and 0.5Da for MS/MS spectra. The false discovery rate was fixed at 1% at the peptide and protein level.

Analysis of samples by mass spectrometry was performed by Dr Mark Skehel and Dr Fairouz Ibrahim, Francis Crick Institute. Description of the analysis was carried out by Dr Mark Skehel.

Analysis of mass spectrometry data

Prior to statistical analysis, peptides mapped to known contaminants, reverse hits, and protein groups only identified by site were removed in the Perseus module (v2.0.11) of MaxQuant (Tyanova et al., 2016). Only protein groups identified with at least two peptides, one of which was unique, and two quantitation events were considered for data analysis.

For IPs with PB2-FLAG as bait, statistical analysis was carried out using the Perseus module v.2.0.11 of MaxQuant (Tyanova et al., 2016). Missing values were imputed using normal distribution, with SD of 30% and the mean offset by -1.8 SD. Non-specific background binders were eliminated by determining the significance of the protein enrichment in experimental samples (IPs with PB2-FLAG as bait) versus control samples (IPs from cells

infected with WT virus (no FLAG tag)) for each cell type using a *t* test (two-sided, equal variance, s_0=0.2) and corrected for multiple hypotheses using FDR (FDR=0.05). A similar method of determining protein enrichment was described in (Hubel et al., 2019). Proteins identified in the FLAG CRAPome (Mellacheruvu et al., 2013) were manually removed. Proteins enriched in WT cells were then compared to the proteins enriched in ANP32-KO cells.

For IPs with ANP32B-FLAG as bait, missing values were replaced with a 0 value. Statistical analysis was carried out using R v.4.2.2. Non-specific background binders were eliminated by determining the fold change (FC) in protein enrichment in experimental samples (IPs with ANP32B-FLAG as bait) versus control samples (IPs with GFP-FLAG as bait) for each infected/uninfected condition. The significance of the protein enrichment was determined using a *t* test (two-sided, equal variance). The thresholds applied were FC=2, p-value=0.2. Proteins identified in the FLAG CRAPome (Mellacheruvu et al., 2013) were manually removed. Proteins enriched in infected cells were compared to the proteins enriched in uninfected cells.

Analysis of mass spectrometry data was performed and described with the help of Dr Mark Skehel and Dr Fairouz Ibrahim, Francis Crick Institute.

Interaction network and gene ontology

The protein interaction network was visualised in Cytoscape v.3.10.2 (Shannon et al., 2003). Host protein-protein interactions were predicted using STRING with high confidence (score >0.9) (Szklarczyk et al., 2023). The PB2 and ANP32 interactors were analysed for pathway and gene set enrichment using gene ontology (GO) biological process and GO cellular component terms determined using the StringApp. The GO terms were investigated and manually curated based on published literature. Genes that were part of enriched biological process or cellular component terms were manually clustered together and labelled. For the PB2 interactome, the cell type (WT cells, ANP32-KO cells, or both cell types) that the virus-host protein interaction occurred in was reported by the node fill colour. The PB2 interactors were compared to host proteins identified in previous AP-MS screens. A range of AP-MS screens using either PB2, PB1, or PA as bait in the context of transfection (Watanabe et al., 2014, Haas et al., 2023) or infection (York et al., 2014, Heaton et al., 2016, Hubel et al., 2019) were selected for comparison. To investigate the functional relevance of the PB2 interactors, comparisons were also made to functional screens (Konig et al., 2010, Karlas et al., 2010, Shapira et al., 2009, Li et al., 2020) and studies (Naito et al., 2007, Cao et al., 2014, Kakugawa et al., 2009, Bortz et al., 2011, Moisy et al., 2012, Courtney et al., 2017, Hsu et al., 2013). The shared interactors were reported based on node outline colour. For the ANP32B interactome, the cell condition (infected cells, uninfected cells, or both infected and uninfected cells) that the protein-protein interaction occurred in was reported by the node fill colour.

6.2.6. Gene knockdown and knockout

Gene knockdown by siRNA

For siRNA mediated gene knockdown, A549 or eHAP WT cells were reverse transfected with siRNA pools (siGENOME SMARTpool siRNA, Dharmacon) targeting human genes of interest or a non-targeting siRNA control. siRNA pools targeting both ANP32A and ANP32B were generated by combining individual siRNAs (siGENOME, Dharmacon) targeting ANP32A and ANP32B. Similarly, siRNA pools targeting both HMGB1 and HMGB2 or RUVBL1 and RUVBL2 were generated by combining individual siRNAs (siGENOME, Dharmacon) targeting each of HMGB1 and HMGB2 or RUVBL1 and RUVBL2. In addition, two separate individual siRNAs (siGENOME, Dharmacon) targeting PHB1 and PHB2 were used. All siRNAs were diluted to 20μM using 1x siRNA buffer (Dharmacon) prior to use. Transfections were performed in 96-well plates for RT-qPCR analysis, cell viability assays, and infection assays, and 48-well plates for minigenome reporter assays using Lipofectamine RNAiMAX (Invitrogen), according to the manufacturer's instructions. In brief, per reaction in a 96-well plate (3x for 48-well plate), 0.1μL siRNA (at 20μM) was diluted in 24.9uL 1x optiMEM and 25uL was spotted into a well. 0.3μL RNAiMAX was mixed with 24.7μL 1x optiMEM and incubated for 5min at RT. 25uL was spotted on top of the siRNA mix, followed by incubation for 20min at RT. 50μL of cells at a concentration of $1x10^5$ cells/mL was then added. The siRNA-transfected cells were incubated at 37°C for 48hrs. At this point, infection assays (IF readout) and minigenome reporter assays (luciferase and RT-qPCR readouts) were performed, as described below.

Gene knockdown at the mRNA level and cell viability was also determined at this point. Total RNA was extracted using a RNeasy RNA extraction kit (Qiagen), according to the manufacturer's instructions, with 30min DNase I (Qiagen) digestion at RT. mRNA levels were then determined by RT-qPCR using primers specific to each gene (Table 24) and a QuantiNova SYBR green kit (Qiagen), according to the manufacturer's instructions. RT-qPCRs were performed on a QuantStudio 7 Flex PCR system (Life Technologies), with β-actin as a cellular control. Cell viability following each gene knockdown was assessed using a CellTiter-Glo luminescent viability assay (Promega), according to the manufacturer's instructions. In brief, the plate to be analysed was equilibrated at RT for 30min prior to addition of 100μL CellTiter-Glo reagent and shaking on an orbital shaker for 2min. The plate was incubated at RT for 10min to stabilise the luminescent signal and the luminescence was then measured on a FLUOstar Omega plate reader (BMG Labtech).

Table 24. qPCR primers for measuring gene knockdown at the mRNA level.

Gene	Forward primer	Reverse primer
β-Actin	TGACGTGGACATCCGCAAAG	CTGGAAGGTGGACAGCGAGG
ANP32A	CTGGACAACAGTCGGTCGAA	GTTTGCGATTGAGGTGAGGC
ANP32B	CTGACTCAGATGCCGAGGTG	CACCATCCTCATCGTCCTCG
AHNAK	TGAACACACCACAGCCATCA	GCATTTGGGGTGGAGACTGA
AKAP8L	GCAGTCCAAGAAGTCCTCCC	TGTCGGTGAAAGGGTTCTCG
BAG2	GAGGCAGATCAGTGACGGAG	CTTGCTGCTGGGGGTTTCTA
CLUH	GCATCAACATGCGCTACCTG	GCGGGTGATGAGTTCTCCAA
DNAJA1	GGACCTGGAATGGTTCAGCA	TCTTCCTTCCGTTGCAGCTT
EMD	TTCCCAGATGCTGACGCTTT	GCGTTCCCTATCCTTGCACT
FKBP3	TTCTGCAGGAACACGGTTCA	TGTTAGCTGTCTTGGCCACA
FKBP4	ACCTGGCCATGTGTCATCTG	AGAGGCCCTTCTCGTTGTTG
FUBP1	CCAGGGATGGGGAAATGCAT	GCGTAATAAGCAGCCCAAGC
GAPDH	AATCCCATCACCATCTTCCA	TGGACTCCACGACGTACTCA
HAX1	AGTAACCCGACACGAAGCAG	GGAACCAACGTCCCAGGAAT
HMGB1	ATCCCAATGCACCCAAGAGG	GACAGGCCAGGATGTTCTCC
HMGB2	TGCTCTGAACATCGCCCAAA	GCTGACTGCTCAGACCACAT
IPO8	ACAATGTGTCTCCGTGCCAT	AGCTTGCACTGCTCTGTGAT
KPNA3	CCCTTTCTTGTGCCCCTTCT	TGAGAACAACCTGGGTCTGC
MAGED2	AAATCGGTCCAGTGAGGCTG	GAGCTTCTTCACGTCCCCAA
MAZ	GACACGAGGAGAAAGTGCCA	CACAGACATGGTGAGGACCC
MDH2	GCATGGAGTGTACAACCCCA	CGAGCTGGATCCAAACCCTT
PGAM1	CAGAAGAGAGCGATCCGGAC	GTTAGACCCCCATAGTGCCG
PHB1	GCAGAGAGGGCCAGATTTGT	AGTTGGCAATCAGCTCAGCT
PHB2	AGTGTGGTGGCCAAGTTCAA	ATGAGGCTGAAGTCCTTGGC
PIN4	CCGCCCAAAGGAAAAAGTGG	TACTGCATTGCCACCACCTT
PTMA	AAATGGAAGAGACGCCCCTG	TTCCTCCCCACCTTCTTCCT
RBM14	TCAGAGTCGCAGCTTTCGTT	TAATCGGAATGGGCATCGGG
RUVBL1	CTTGCCAAAAGGGGATGTGC	GCGCATTAGCCACATCCAAG
RUVBL2	TCCTGATCATGGCCACCAAC	GTCTATGGGGATGCCGTGAG
RPAP2	TGTCTGAAACCCGAAGCCTC	TCTGAGATTCCCTCCAGGCA
SAE1	ACTGACCATGCTGGATCACG	TCGCTCCAAAGAGGCTTCAG
SARNP	ACTGTTGATGTGGCAGCAGA	ATCGTTCAGCCCTCTTCTGC
STOML2	CGCTGCCTCCGTTATGAGAT	TAGAACTGTGGCCCGTTTCC
SUPT5H	TACCAGTTCACAGACACGCC	GCCTCCACGTAGATGTAGCC
UBR5	ATCGAGGGTCTGGGCTTTTG	GGCCTGTGAAATCAGCTCCT
VRK1	GTTGGCAGTGATGCACCTTG	CTGGTTTTGCAGCTCGTTGG
YTHDF2	GGCAGTGGGTTCGGTCATAA	GGACCGAAGCTTCTCCAACA

ZC3H11A	CTGTTGTCCCGCTTGTCTCT	AGGCAGCACAAGACTGTCTC
ZC3H8	AGATACCCCACAGGCTGCTA	TCCTTTGTTTCCAGGGCCAG
ZNF622	AAAGGAGGCCAGGAATGTCG	GCCTGCTGTTCAAACCACTG

Gene knockout by CRISPR-Cas9 genome editing

For CRISPR-Cas9 mediated gene knockout, commercial multi-guide sgRNAs targeting HMGB2, RUVBL2, and RPAP2 (Synthego) and non-targeting sgRNA (Synthego) were used. The sgRNAs were designed by Synthego. To induce Cas9 expression, A549-dox-Cas9 cells were treated with 1ug/mL dox for 48hrs before transfection. The cells were then reverse transfected with gRNAs using Lipofectamine RNAiMAX, according to the manufacturer's instructions. In brief, per well in a 6-well plate, 4µL gRNA (at 100µM) was diluted in 496µL 1x optiMEM and, in a separate tube, 4µL RNAiMAX was mixed with 496µL 1x optiMEM. The gRNA and RNAiMAX mixes were combined in one well of a 6-well plate and incubated for 20min at RT. 1mL of cells at a concentration of $1x10^5$ cells/mL in media supplemented with 1µg/mL dox was added. The cells were incubated at 37°C for 48hrs and then transferred to a T25 flask. Once confluent the cells were harvested by trypsinisation, washed in PBS, resuspended in fluorescence-activated cell sorter (FACS) buffer, and filtered with a 40µM filter. The cells were then single cell sorted using a FACS Aria III (BD Biosciences) with a 100µM nozzle into 96-well plates. FACS sorting was performed by Isabel Correa-Otero at the FACS facility at Imperial College London. Clonal populations were grown over 14-21 days. Once confluent, clonal populations were expanded into 6-well plates for genotyping.

Genomic DNA was extracted using a genomic DNA purification kit (ThermoFisher Scientific). Genetic loci targeted by the sgRNAs were amplified by PCR using AmpliTaq Gold 360 Master Mix (Qiagen), according to the manufacturer's instructions. The primers used are shown in Table 25. The amplified regions were then analysed by gel electrophoresis on a 2% agarose gel, as described above, and Sanger sequenced. The sequencing primers used are shown in Table 25. Sanger sequencing data was analysed using Inference of CRISPR Edits (ICE; Synthego), a software that analyses CRISPR edits and assesses editing efficiency. Gene knockout of successful clonal populations was then confirmed by western blotting, described below.

Table 25. Primers for amplifying and sequencing CRISPR clones.

Primer details	Primer sequence
Forward primer for amplifying HMGB2 target locus	ACTGGGGTGGCAAAGTTGAA
Reverse primer for amplifying HMGB2 target locus	CAGGAAAGGCGTTTTGAGGG
Forward primer for amplifying RUVBL2 target locus	TGGGTGACAGAGCGAGATCT
Reverse primer for amplifying RUVBL2 target locus	CCCCAAATGGCCTACCTCTAG
Forward primer for amplifying RPAP2 target locus	AGAGTTCTTCAAATAGCACTTTGCC
Reverse primer for amplifying RPAP2 target locus	GGCAGTGGTTTAATGGCTGT
Primer for sequencing HMGB2 target locus	CAAAGTTGAAGCTCATGAGTTGCCTACTAC
Primer for sequencing RUVBL2 target locus	CTTTTCCTAGAAGTCCCAGCTAGTAATGTC
Primer for sequencing RPAP2 target locus	CTGAAAGATTAAAAGCGTCAGAAAATTCTG

6.2.7. Minigenome reporter assay

293T or eHAP cells were seeded in 48-well plates if siRNA treated before transfection (described above), 24-well plates, or 6-well plates if used for western blot analysis of protein expression (described below). Plasmid mixes were made consisting of pCAGGS expression plasmids encoding PB2, PB1, PA, and NP (strains indicated in Figure legends). A pPolI-Firefly luciferase viral reporter (Firefly) plasmid and a pCAGGS-Renilla luciferase (Renilla) plasmid were also transfected. Renilla was used as a transfection efficiency control. The plasmids were transfected in a 2:2:1:4:4:2 (PB2:PB1:PA:NP:Firefly:Renilla) ratio, where 1=10ng, 20ng, or 80ng in a 48-well plate, 24-well plate, or 6-well plate, respectively. For complementation or overexpression experiments, pCAGGS expression plasmids encoding HMGB2, RUVBL2, MxA-FLAG, MxA, or BTN3A3 (20-160ng) were also transfected, as indicated in Figures and Figure legends. Transfection of empty pCAGGS was used to ensure equal amounts of DNA in all conditions. As a technical control, a plasmid mix lacking PB2 was also included. Transfections were performed using Lipofectamine 3000, according to the manufacturer's instructions. In brief, 1x optiMEM was added to plasmid mixes followed by P3000 in a 2:1 ratio based on the total amount of DNA. L3000 reagent was then added to 1x optiMEM in a 3:1 ratio based on the total amount of DNA. The L3000/optiMEM mix was added to the P3000/DNA mix. Following incubation at RT for 15min, the transfection mix was added to cells dropwise.

For luciferase readout, cells were lysed in 100µL passive lysis buffer (Promega) 20hrs post transfection. Cells were shaken at 400rpm for 1hr at RT. 20µL of lysate was transferred to a white 96-well plate and bioluminescence was measured using a dual-luciferase assay kit (Promega) on a FLUOstar Omega plate reader. Firefly luciferase activity and Renilla luciferase activity were averaged, and the average Firefly luciferase activity was normalised to the average Renilla luciferase activity.

For RT-qPCR readout, the pCAGGS Renilla luciferase plasmid was omitted from the plasmid transfection mix. Cells were lysed in buffer RLT supplemented with 10% BME.

For western blot analysis, cells were harvested by trypsinisation and centrifugation. Cells were then lysed by resuspending the pellets in RIPA buffer supplemented with EDTA-free protease inhibitor cocktail tablet. Lysates were centrifuged at 13000RCF for 10min, and supernatants were stored at -20°C until western blot analysis.

6.2.8. RT-qPCR analysis of vRNA, cRNA, and mRNA accumulation

Following infection or transfection, cell lysis in buffer RLT, and freezing at -80°C, total RNA was extracted using a RNeasy RNA extraction kit, according to the manufacturer's instructions, with 30min DNase I digestion at RT. A549 cells were homogenized with QIAshredder columns (Qiagen) prior to RNA extraction.

Segment 4 (HA) (infection setup) or Firefly (minigenome setup) vRNA, cRNA, and mRNA accumulation was quantified using a tagged RT-qPCR method, developed by Kawakami et al., 2011. vRNA, cRNA, mRNA, and GAPDH (internal control) cDNA was synthesised using RevertAid H Minus Reverse Transcriptase (ThermoFisher Scientific) according to the manufacturer's instructions. For each reaction, 200ng RNA and tagged primers targeting vRNA or cRNA, tagged poly(dT) (mRNA), or untagged poly(dT) (GAPDH) was used. Tagged cDNA was then quantified in triplicate using Fast SYBR green master mix (ThermoFisher Scientific) on a QuantStudio 7 Flex PCR system (Life Technologies). Primers used for cDNA and qPCR reactions are shown in Table 26. The $2^{-\Delta\Delta CT}$ method with GAPDH expression as internal control was used to calculate the fold change in vRNA, cRNA, and mRNA accumulation relative to input (0hpi) (infection setup) or -PB2 control (minigenome setup).

Table 26. Primers used for tagged RT-qPCR against PR8 HA vRNA, cRNA, and mRNA and Firefly luciferase vRNA, cRNA, and mRNA.

Primers for strand-specific RT-qPCR	Description	Sequence
cDNA synthesis primers	HA tagged vRNA cDNA	GGCCGTCATGGTGGCGAATGGAGAGTGCCCAAAATACGT
	HA tagged cRNA cDNA	GCTAGCTTCAGCTAGGCATCAGTAGAAACAAGGGTGTT
	HA tagged mRNA cDNA	CCAGATCGTTCGAGTCGTTTTTTTTTTTTTTTTTT
	Luciferase tagged vRNA cDNA	GGCCGTCATGGTGGCGAATTTGCCAAGAGGTTCCATCTG
	Luciferase tagged cRNA cDNA	GCTAGCTTCAGCTAGGCATCAGTAGAAACAAGGGTGTT
	Luciferase tagged mRNA cDNA	CCAGATCGTTCGAGTCGTTTTTTTTTTTTTTTTTT
qPCR primers	HA vRNA qRT-PCR Forward	GGCCGTCATGGTGGCGAAT
	HA vRNA qRT-PCR Reverse	CATACCATCCATCTATCATTCC
	HA cRNA qRT-PCR Forward	GCTAGCTTCAGCTAGGCATC
	HA cRNA qRT-PCR Reverse	GGGGGCAATCAGTTTCTG
	HA tagged mRNA qRT-PCR Forward	CCAGATCGTTCGAGTCG
	HA tagged mRNA qRT-PCR Reverse	GATTCTGGCGATCTACTCAACTGTC
	Luciferase vRNA qRT-PCR Forward	GGCCGTCATGGTGGCGAAT
	Luciferase vRNA qRT-PCR Reverse	AGATCCACAACCTTCGCTTC
	Luciferase cRNA qRT-PCR Forward	GCTAGCTTCAGCTAGGCATC
	Luciferase cRNA qRT-PCR Reverse	AAGTACCGAAAGGTCTTACC
	Luciferase mRNA qRT-PCR Forward	CCAGATCGTTCGAGTCG

6.2.9. Split luciferase assay

293T cells were seeded in 48-well plates. Plasmid mixes were made consisting of pCAGGS expression plasmids encoding NP_{gluc1} (20ng) and huANP32B_{gluc2} (20ng) as well as PB2 (10ng), PB1 (10ng), PA (5ng), and pPolI-Firefly (10ng), as indicated in Figure legend. A pCAGGS expression plasmid encoding BTN3A3 (40ng) or empty pCAGGS was also included, as indicated in Figure and Figure legend. Transfection mixes substituting pCAGGS-Gluc1 for pCAGGS-NP_{gluc1} and pCAGGS-Gluc2 for pCAGGS-huANP32B_{gluc2} were used as controls. Transfections were performed using Lipofectamine 3000, according to the manufacturer's instructions and as described above. 20hrs post transfection, cells were lysed in 60uL Renilla lysis buffer (Promega) shaking at 400rpm for 1hr at RT. 20uL of lysate was transferred to a

white 96-well plate and gaussia luciferase activity was measured using a Renilla luciferase kit (Promega) on a FLUOstar Omega plate reader. Normalised luminescence ratios were calculated by dividing the luminescence measured from the two interaction partners (NP and huANP32B) by the sum of the interaction measured from the two controls (Gluc1 and Gluc2) for each sample (Cassonnet et al., 2011).

6.2.10. Western blotting, SYPRO staining, and immunofluorescence

Western blotting

Lysates were mixed with 4x Laemmli sample buffer (Bio-Rad) with 10% BME in a 3:1 ratio. Proteins were denatured by incubation at 80°C for 10min. Proteins were then separated by SDS-PAGE on mini protean TGX precast gels 4-20% (Bio-Rad) alongside a precision plus protein standard dual colour ladder (Bio-Rad). This was followed by semi-dry transfer onto PVDF membranes (low fluorescence 0.2µM; Amersham). Membranes were blocked by incubation in 5% milk (Sigma-Aldrich) in 1x TBS for 1hr at RT followed by incubation with primary antibodies diluted in 2% milk in TBS-T at 4°C O/N. Primary antibody dilutions are shown in Table 16. Following 4x washes in TBS-T, membranes were incubated with secondary antibodies diluted in 2% milk in TBS-T. Secondary antibody dilutions are shown in Table 17. After a further 4x washes in TBS-T and 1x wash in TBS, membranes were visualised using an Odyssey imaging system (LiCor Biosciences) and processed using the Empiria Studio software.

SYPRO staining

Lysates were mixed with 4x Laemmli sample buffer with 10% BME in a 3:1 ratio. Proteins were denatured by incubation at 80°C for 10min. Proteins were separated by SDS-PAGE on mini protean TGX precast gels 4-20% alongside a precision plus protein standard dual colour ladder. The gel was fixed in 50% methanol and 7% acetic acid for 30min at RT, stained with SYPRO Ruby protein gel stain (Promega) for 3hrs at RT, washed in 10% methanol and 7% acetic acid for 1hr, and subsequently washed in purified water. The SYPRO-stained gel was then imaged using a gel doc XR+ imaging system.

Immunofluorescence

For visualisation of ZsGreen without fixation and staining, cells were transfected with siRNAs and multi-cycle infected with PR8 NS-ZsGreen, as described above. At 48hpi, cells were imaged on an M5000 EVOS microscope. Entire wells were imaged using the GFP (470/525 nm) light cube, 4x objective, and the automated focus function. ZsGreen count was quantified using ImageJ (Schneider et al., 2012). Briefly, images were converted to greyscale, the threshold was set, and the virus particle count was quantified using the “analyse particle”

tool. The parameters were set to the size and shape of the virus particles. The same thresholds and parameters were used for all images.

For visualisation of ZsGreen with fixation and staining, cells were seeded in 96-well plates and single-cycle infected with PR8 NS-ZsGreen, as described above. At 24hpi, cells were washed in PBS and fixed in 4% paraformaldehyde (PFA) for 30min, followed by 3x washes in PBS. Cells were permeabilised by incubation in permeabilisation solution for 10min followed by 3x washes in PBS. Cells were then blocked in blocking solution for 1hr at RT. This was followed by incubation with primary antibodies diluted in blocking solution for at least 2hrs at RT. Primary antibody dilutions are shown in Table 16. Cells were then washed 3x in PBS and incubated with secondary antibodies and DAPI (Roche) diluted in 2% BSA in PBS for 1hr at RT. Secondary antibody dilutions are shown in Table 17. This was followed by 3x washes in PBS. Cells were then imaged using the GFP (482/524nm) light cube, Texas Red (585/628nm) light cube, DAPI (357/447nm) light cube, and 10x objective. Images were processed using ImageJ (Schneider et al., 2012).

6.2.11. Drug treatment

MTS assay

Maximum sorafenib concentration (0-25μM), CB-6644 concentration (0-25μM), ICM concentration (0-40μM) tolerated by eHAP WT or 293T cells compared to DMSO was determined using an MTS cell proliferation kit (Abcam), according to the manufacturer's instructions. In brief, cells were seeded in a 96-well plate and then incubated with titrations of each drug or DMSO for 24hrs. MTS reagent was added to each well followed by incubation for 1hr at 37°C. The absorbance was then measured on a FLUOstar Omega plate reader at OD=490nm.

Drug assays

For minigenome reporter assays, eHAP WT or 293T cells were treated with sorafenib, CB-6644, ICM, or DMSO immediately prior to plasmid transfection (concentrations indicated in Figures). Transfections were performed as described above for minigenome reporter assays.

For multi-cycle infections, ICM (20μM) or DMSO was added to viral inoculums, and subsequent prewarmed SF media. Infections were then performed as described above. At the appropriate timepoint supernatants were harvested and infectious titres were determined by plaque assay on MDCK cells.

For synchronised single-cycle infections, eHAP WT and ANP32-KO cells were seeded in 24-well plates. Synchronised single-cycle infections were performed as described above but with addition of ICM (20μM) or DMSO to the viral inoculums and subsequent prewarmed

full media. At the appropriate timepoint, cells were lysed in buffer RLT (Qiagen) supplemented with 10% BME for analysis by RT-qPCR, described above.

6.2.12. Mouse experiments

PR8 titrations

Six-week-old female BALB/c mice, weighing 18-22g, were purchased from Charles River UK Ltd. Mice were randomly assigned to three groups. Group 1, 3 mice were inoculated with 10PFU of PR8, group 2, 3 mice were inoculated with 100PFU of PR8, group 3, 3 mice were inoculated with 1000PFU of PR8, and group 4, 3 mice were inoculated with 10000PFU of PR8. Symptoms and weight change were monitored daily. Lungs were harvested on day 7 post inoculation or when weight loss dropped below 85% of the original weight on day 0. Lungs were suspended in 1ml of PBS and homogenized using 1.3mm beads, homogenates were frozen at -80°C before virus titration by plaque assay on MDCK cells. Mouse experiments were performed by Dr Jie Zhou and Ksenia Sukhova. Description of methods was carried out with the help of Dr Jie Zhou.

ICM treatment

Six-week-old female BALB/c mice, weighing 18-22g, were purchased from Charles River UK Ltd. Mice were randomly assigned to four groups. Group 1, 10 mice were inoculated with PBS and no treatment, group 2, 10 mice were inoculated with 30PFU of PR8 and administrated vehicle daily via intraperitoneal route, group 3, 10 mice were inoculated with 30PFU of PR8 and administrated with ICM daily via intraperitoneal route. Symptoms and weight change were monitored daily. Lungs were harvested on day 3 and 8 post inoculation (5 mice per day), or when weight loss dropped below 85% of the original weight on day 0. Lungs were suspended in 1ml of PBS and homogenized using 1.3mm beads, homogenates were frozen at -80°C before virus titration by plaque assay on MDCK cells. Mouse experiments were performed by Dr Jie Zhou and Ksenia Sukhova. Description of methods was carried out with the help of Dr Jie Zhou.

6.2.13. Software

ChimeraX v.1.9 was used to visualise and analyse structures (Pettersen et al., 2021). Jalview v.2.11.5 was used to perform sequence alignments (Waterhouse et al., 2009). Schematics were generated using inkscape. The use of other software for data analysis and visualisation is described above and below where appropriate.

6.2.14. Statistical analysis

Statistical analysis was performed using Prism software v.10.2.1 (GraphPad). Statistical tests used are indicated in Figure legends. Differences were considered significant at p-values at or below 0.05, as indicated in Figure legends. Error bars indicate SD from triplicate experiments, unless otherwise stated in Figure legends. Further information about n numbers and statistical tests is presented in Figure legends.

6.2.15. Safety and biosecurity

All influenza virus work was performed at Biosafety level 2 facilities, as approved by the Health and Safety Executive of the United Kingdom and in accordance with local rules at St Mary's Hospital and the Sir Alexander Fleming building, Section of Virology, Imperial College London.

References

Abramson, J., Adler, J., Dunger, J., Evans, R., Green, T., Pritzel, A., Ronneberger, O., Willmore, L., Ballard, A. J., Bambrick, J., Bodenstein, S. W., Evans, D. A., Hung, C. C., O'neill, M., Reiman, D., Tunyasuvunakool, K., Wu, Z., Zemgulyte, A., Arvaniti, E., Beattie, C., Bertolli, O., Bridgland, A., Cherepanov, A., Congreve, M., Cowen-Rivers, A. I., Cowie, A., Figurnov, M., Fuchs, F. B., Gladman, H., Jain, R., Khan, Y. A., Low, C. M. R., Perlin, K., Potapenko, A., Savy, P., Singh, S., Stecula, A., Thillaisundaram, A., Tong, C., Yakneen, S., Zhong, E. D., Zielinski, M., Zidek, A., Bapst, V., Kohli, P., Jaderberg, M., Hassabis, D. & Jumper, J. M. 2024. Accurate structure prediction of biomolecular interactions with AlphaFold 3. *Nature,* 630**,** 493-500. 10.1038/s41586-024-07487-w

Agresti, A. & Bianchi, M. E. 2003. HMGB proteins and gene expression. *Curr Opin Genet Dev,* 13**,** 170-8. 10.1016/s0959-437x(03)00023-6

Aguero, M., Monne, I., Sanchez, A., Zecchin, B., Fusaro, A., Ruano, M. J., Del Valle Arrojo, M., Fernandez-Antonio, R., Souto, A. M., Tordable, P., Canas, J., Bonfante, F., Giussani, E., Terregino, C. & Orejas, J. J. 2023. Highly pathogenic avian influenza A(H5N1) virus infection in farmed minks, Spain, October 2022. *Euro Surveill,* 28. 10.2807/1560-7917.ES.2023.28.3.2300001

Almond, J. W. 1977. A single gene determines the host range of influenza virus. *Nature,* 270**,** 617-8. 10.1038/270617a0

Alvarez, L., Haubrich, K., Iselin, L., Gillioz, L., Ruscica, V., Lapouge, K., Augsten, S., Huppertz, I., Choudhury, N. R., Simon, B., Masiewicz, P., Lethier, M., Cusack, S., Rittinger, K., Gabel, F., Leitner, A., Michlewski, G., Hentze, M. W., Allain, F. H. T., Castello, A. & Hennig, J. 2024. The molecular dissection of TRIM25's RNA-binding mechanism provides key insights into its antiviral activity. *Nat Commun,* 15**,** 8485. 10.1038/s41467-024-52918-x

Ando, T., Yamayoshi, S., Tomita, Y., Watanabe, S., Watanabe, T. & Kawaoka, Y. 2016. The host protein CLUH participates in the subnuclear transport of influenza virus ribonucleoprotein complexes. *Nat Microbiol,* 1**,** 16062. 10.1038/nmicrobiol.2016.62

Ankerhold, J., Kessler, S., Beer, M., Schwemmle, M. & Ciminski, K. 2025. Replication Restriction of Influenza A(H5N1) Clade 2.3.4.4b Viruses by Human Immune Factor, 2023-2024. *Emerg Infect Dis,* 31**,** 199-202. 10.3201/eid3101.241236

Arafeh, R., Shibue, T., Dempster, J. M., Hahn, W. C. & Vazquez, F. 2025. The present and future of the Cancer Dependency Map. *Nat Rev Cancer,* 25**,** 59-73. 10.1038/s41568-024-00763-x

Arragain, B., Krischuns, T., Pelosse, M., Drncova, P., Blackledge, M., Naffakh, N. & Cusack, S. 2024. Structures of influenza A and B replication complexes give insight into avian to human host adaptation and reveal a role of ANP32 as an electrostatic chaperone for the apo-polymerase. *Nat Commun,* 15**,** 6910. 10.1038/s41467-024-51007-3

Arranz, R., Coloma, R., Chichon, F. J., Conesa, J. J., Carrascosa, J. L., Valpuesta, J. M., Ortin, J. & Martin-Benito, J. 2012. The structure of native influenza virion ribonucleoproteins. *Science,* 338**,** 1634-7. 10.1126/science.1228172

Assimon, V. A., Tang, Y., Vargas, J. D., Lee, G. J., Wu, Z. Y., Lou, K., Yao, B., Menon, M. K., Pios, A., Perez, K. C., Madriaga, A., Buchowiecki, P. K., Rolfe, M., Shawver, L., Jiao, X., Le Moigne, R., Zhou, H. J. & Anderson, D. J. 2019. CB-6644 Is a Selective Inhibitor of the RUVBL1/2 Complex with Anticancer Activity. *ACS Chem Biol,* 14**,** 236-244. 10.1021/acschembio.8b00904

Baker, S. F., Ledwith, M. P. & Mehle, A. 2018. Differential Splicing of ANP32A in Birds Alters Its Ability to Stimulate RNA Synthesis by Restricted Influenza Polymerase. *Cell Rep,* 24**,** 2581-2588 e4. 10.1016/j.celrep.2018.08.012

Bauer, D. L. V., Tellier, M., Martinez-Alonso, M., Nojima, T., Proudfoot, N. J., Murphy, S. & Fodor, E. 2018. Influenza Virus Mounts a Two-Pronged Attack on Host RNA

Polymerase II Transcription. *Cell Rep,* 23**,** 2119-2129 e3. 10.1016/j.celrep.2018.04.047
Beaton, A. R. & Krug, R. M. 1986. Transcription antitermination during influenza viral template RNA synthesis requires the nucleocapsid protein and the absence of a 5' capped end. *Proc Natl Acad Sci U S A,* 83**,** 6282-6. 10.1073/pnas.83.17.6282
Bernasconi, D., Schultz, U. & Staeheli, P. 1995. The interferon-induced Mx protein of chickens lacks antiviral activity. *J Interferon Cytokine Res,* 15**,** 47-53. 10.1089/jir.1995.15.47
Bi, Z., Ye, H., Wang, X., Fang, A., Yu, T., Yan, L. & Zhou, J. 2019. Insights into species-specific regulation of ANP32A on the mammalian-restricted influenza virus polymerase activity. *Emerg Microbes Infect,* 8**,** 1465-1478. 10.1080/22221751.2019.1676625
Biswas, S. K., Boutz, P. L. & Nayak, D. P. 1998. Influenza virus nucleoprotein interacts with influenza virus polymerase proteins. *J Virol,* 72**,** 5493-501. 10.1128/JVI.72.7.5493-5501.1998
Bonomini, A., Mercorelli, B. & Loregian, A. 2025. Antiviral strategies against influenza virus: an update on approved and innovative therapeutic approaches. *Cell Mol Life Sci,* 82**,** 75. 10.1007/s00018-025-05611-1
Bortz, E., Westera, L., Maamary, J., Steel, J., Albrecht, R. A., Manicassamy, B., Chase, G., Martinez-Sobrido, L., Schwemmle, M. & Garcia-Sastre, A. 2011. Host- and strain-specific regulation of influenza virus polymerase activity by interacting cellular proteins. *mBio,* 2. 10.1128/mBio.00151-11
Boulo, S., Akarsu, H., Lotteau, V., Muller, C. W., Ruigrok, R. W. & Baudin, F. 2011. Human importin alpha and RNA do not compete for binding to influenza A virus nucleoprotein. *Virology,* 409**,** 84-90. 10.1016/j.virol.2010.10.001
Bouvier, N. M. & Palese, P. 2008. The biology of influenza viruses. *Vaccine,* 26 Suppl 4**,** D49-53. 10.1016/j.vaccine.2008.07.039
Bradel-Tretheway, B. G., Mattiacio, J. L., Krasnoselsky, A., Stevenson, C., Purdy, D., Dewhurst, S. & Katze, M. G. 2011. Comprehensive proteomic analysis of influenza virus polymerase complex reveals a novel association with mitochondrial proteins and RNA polymerase accessory factors. *J Virol,* 85**,** 8569-81. 10.1128/JVI.00496-11
Branon, T. C., Bosch, J. A., Sanchez, A. D., Udeshi, N. D., Svinkina, T., Carr, S. A., Feldman, J. L., Perrimon, N. & Ting, A. Y. 2018. Efficient proximity labeling in living cells and organisms with TurboID. *Nat Biotechnol,* 36**,** 880-887. 10.1038/nbt.4201
Brass, A. L., Huang, I. C., Benita, Y., John, S. P., Krishnan, M. N., Feeley, E. M., Ryan, B. J., Weyer, J. L., Van Der Weyden, L., Fikrig, E., Adams, D. J., Xavier, R. J., Farzan, M. & Elledge, S. J. 2009. The IFITM proteins mediate cellular resistance to influenza A H1N1 virus, West Nile virus, and dengue virus. *Cell,* 139**,** 1243-54. 10.1016/j.cell.2009.12.017
Brauer, R. & Chen, P. 2015. Influenza virus propagation in embryonated chicken eggs. *J Vis Exp*. 10.3791/52421
Brennan, C. M., Gallouzi, I. E. & Steitz, J. A. 2000. Protein ligands to HuR modulate its interaction with target mRNAs in vivo. *J Cell Biol,* 151**,** 1-14. 10.1083/jcb.151.1.1
Bullido, R., Gomez-Puertas, P., Saiz, M. J. & Portela, A. 2001. Influenza A virus NEP (NS2 protein) downregulates RNA synthesis of model template RNAs. *J Virol,* 75**,** 4912-7. 10.1128/JVI.75.10.4912-4917.2001
Bullough, P. A., Hughson, F. M., Skehel, J. J. & Wiley, D. C. 1994. Structure of influenza haemagglutinin at the pH of membrane fusion. *Nature,* 371**,** 37-43. 10.1038/371037a0
Bussey, K. A., Bousse, T. L., Desmet, E. A., Kim, B. & Takimoto, T. 2010. PB2 residue 271 plays a key role in enhanced polymerase activity of influenza A viruses in mammalian host cells. *J Virol,* 84**,** 4395-406. 10.1128/JVI.02642-09
Byrne, A. M. P., James, J., Mollett, B. C., Meyer, S. M., Lewis, T., Czepiel, M., Seekings, A. H., Mahmood, S., Thomas, S. S., Ross, C. S., Byrne, D. J. F., Mcmenamy, M. J., Bailie, V., Lemon, K., Hansen, R. D. E., Falchieri, M., Lewis, N. S., Reid, S. M.,

Brown, I. H. & Banyard, A. C. 2023. Investigating the Genetic Diversity of H5 Avian Influenza Viruses in the United Kingdom from 2020-2022. *Microbiol Spectr,* 11**,** e0477622. 10.1128/spectrum.04776-22

Calder, L. J., Wasilewski, S., Berriman, J. A. & Rosenthal, P. B. 2010. Structural organization of a filamentous influenza A virus. *Proc Natl Acad Sci U S A,* 107**,** 10685-90. 10.1073/pnas.1002123107

Camacho-Zarco, A. R., Kalayil, S., Maurin, D., Salvi, N., Delaforge, E., Milles, S., Jensen, M. R., Hart, D. J., Cusack, S. & Blackledge, M. 2020. Molecular basis of host-adaptation interactions between influenza virus polymerase PB2 subunit and ANP32A. *Nat Commun,* 11**,** 3656. 10.1038/s41467-020-17407-x

Cao, M., Wei, C., Zhao, L., Wang, J., Jia, Q., Wang, X., Jin, Q. & Deng, T. 2014. DnaJA1/Hsp40 is co-opted by influenza A virus to enhance its viral RNA polymerase activity. *J Virol,* 88**,** 14078-89. 10.1128/JVI.02475-14

Carlson, C. J., Albery, G. F., Merow, C., Trisos, C. H., Zipfel, C. M., Eskew, E. A., Olival, K. J., Ross, N. & Bansal, S. 2022. Climate change increases cross-species viral transmission risk. *Nature,* 607**,** 555-562. 10.1038/s41586-022-04788-w

Carrique, L., Fan, H., Walker, A. P., Keown, J. R., Sharps, J., Staller, E., Barclay, W. S., Fodor, E. & Grimes, J. M. 2020. Host ANP32A mediates the assembly of the influenza virus replicase. *Nature,* 587**,** 638-643. 10.1038/s41586-020-2927-z

Caserta, L. C., Frye, E. A., Butt, S. L., Laverack, M., Nooruzzaman, M., Covaleda, L. M., Thompson, A. C., Koscielny, M. P., Cronk, B., Johnson, A., Kleinhenz, K., Edwards, E. E., Gomez, G., Hitchener, G., Martins, M., Kapczynski, D. R., Suarez, D. L., Alexander Morris, E. R., Hensley, T., Beeby, J. S., Lejeune, M., Swinford, A. K., Elvinger, F., Dimitrov, K. M. & Diel, D. G. 2024. Spillover of highly pathogenic avian influenza H5N1 virus to dairy cattle. *Nature,* 634**,** 669-676. 10.1038/s41586-024-07849-4

Cassonnet, P., Rolloy, C., Neveu, G., Vidalain, P. O., Chantier, T., Pellet, J., Jones, L., Muller, M., Demeret, C., Gaud, G., Vuillier, F., Lotteau, V., Tangy, F., Favre, M. & Jacob, Y. 2011. Benchmarking a luciferase complementation assay for detecting protein complexes. *Nat Methods,* 8**,** 990-2. 10.1038/nmeth.1773

Cato, L., Stott, K., Watson, M. & Thomas, J. O. 2008. The interaction of HMGB1 and linker histones occurs through their acidic and basic tails. *J Mol Biol,* 384**,** 1262-72. 10.1016/j.jmb.2008.10.001

Cauldwell, A. V., Long, J. S., Moncorge, O. & Barclay, W. S. 2014. Viral determinants of influenza A virus host range. *J Gen Virol,* 95**,** 1193-1210. 10.1099/vir.0.062836-0

Cauldwell, A. V., Moncorge, O. & Barclay, W. S. 2013. Unstable polymerase-nucleoprotein interaction is not responsible for avian influenza virus polymerase restriction in human cells. *J Virol,* 87**,** 1278-84. 10.1128/JVI.02597-12

Chang, S., Sun, D., Liang, H., Wang, J., Li, J., Guo, L., Wang, X., Guan, C., Boruah, B. M., Yuan, L., Feng, F., Yang, M., Wang, L., Wang, Y., Wojdyla, J., Li, L., Wang, J., Wang, M., Cheng, G., Wang, H. W. & Liu, Y. 2015. Cryo-EM structure of influenza virus RNA polymerase complex at 4.3 A resolution. *Mol Cell,* 57**,** 925-935. 10.1016/j.molcel.2014.12.031

Chen, K. Y., Santos Afonso, E. D., Enouf, V., Isel, C. & Naffakh, N. 2019. Influenza virus polymerase subunits co-evolve to ensure proper levels of dimerization of the heterotrimer. *PLoS Pathog,* 15**,** e1008034. 10.1371/journal.ppat.1008034

Chenavas, S., Estrozi, L. F., Slama-Schwok, A., Delmas, B., Di Primo, C., Baudin, F., Li, X., Crepin, T. & Ruigrok, R. W. 2013. Monomeric nucleoprotein of influenza A virus. *PLoS Pathog,* 9**,** e1003275. 10.1371/journal.ppat.1003275

Chenavier, F., Estrozi, L. F., Teulon, J. M., Zarkadas, E., Freslon, L. L., Pellequer, J. L., Ruigrok, R. W. H., Schoehn, G., Ballandras-Colas, A. & Crepin, T. 2023. Cryo-EM structure of influenza helical nucleocapsid reveals NP-NP and NP-RNA interactions as a model for the genome encapsidation. *Sci Adv,* 9**,** eadj9974. 10.1126/sciadv.adj9974

Choudhury, N. R., Heikel, G., Trubitsyna, M., Kubik, P., Nowak, J. S., Webb, S., Granneman, S., Spanos, C., Rappsilber, J., Castello, A. & Michlewski, G. 2017. RNA-binding activity of TRIM25 is mediated by its PRY/SPRY domain and is required for ubiquitination. *BMC Biol,* 15**,** 105. 10.1186/s12915-017-0444-9

Chowdhury, D. & Lieberman, J. 2008. Death by a thousand cuts: granzyme pathways of programmed cell death. *Annu Rev Immunol,* 26**,** 389-420. 10.1146/annurev.immunol.26.021607.090404

Chua, M. A., Schmid, S., Perez, J. T., Langlois, R. A. & Tenoever, B. R. 2013. Influenza A virus utilizes suboptimal splicing to coordinate the timing of infection. *Cell Rep,* 3**,** 23-9. 10.1016/j.celrep.2012.12.010

Ciminski, K., Chase, G. P., Beer, M. & Schwemmle, M. 2021. Influenza A Viruses: Understanding Human Host Determinants. *Trends Mol Med,* 27**,** 104-112. 10.1016/j.molmed.2020.09.014

Coloma, R., Arranz, R., De La Rosa-Trevin, J. M., Sorzano, C. O. S., Munier, S., Carlero, D., Naffakh, N., Ortin, J. & Martin-Benito, J. 2020. Structural insights into influenza A virus ribonucleoproteins reveal a processive helical track as transcription mechanism. *Nat Microbiol,* 5**,** 727-734. 10.1038/s41564-020-0675-3

Courtney, D. G., Kennedy, E. M., Dumm, R. E., Bogerd, H. P., Tsai, K., Heaton, N. S. & Cullen, B. R. 2017. Epitranscriptomic Enhancement of Influenza A Virus Gene Expression and Replication. *Cell Host Microbe,* 22**,** 377-386 e5. 10.1016/j.chom.2017.08.004

Cox, J. & Mann, M. 2008. MaxQuant enables high peptide identification rates, individualized p.p.b.-range mass accuracies and proteome-wide protein quantification. *Nat Biotechnol,* 26**,** 1367-72. 10.1038/nbt.1511

Cox, J., Neuhauser, N., Michalski, A., Scheltema, R. A., Olsen, J. V. & Mann, M. 2011. Andromeda: a peptide search engine integrated into the MaxQuant environment. *J Proteome Res,* 10**,** 1794-805. 10.1021/pr101065j

Cros, J. F., Garcia-Sastre, A. & Palese, P. 2005. An unconventional NLS is critical for the nuclear import of the influenza A virus nucleoprotein and ribonucleoprotein. *Traffic,* 6**,** 205-13. 10.1111/j.1600-0854.2005.00263.x

Dadonaite, B., Gilbertson, B., Knight, M. L., Trifkovic, S., Rockman, S., Laederach, A., Brown, L. E., Fodor, E. & Bauer, D. L. V. 2019. The structure of the influenza A virus genome. *Nat Microbiol,* 4**,** 1781-1789. 10.1038/s41564-019-0513-7

Dauden, M. I., Lopez-Perrote, A. & Llorca, O. 2021. RUVBL1-RUVBL2 AAA-ATPase: a versatile scaffold for multiple complexes and functions. *Curr Opin Struct Biol,* 67**,** 78-85. 10.1016/j.sbi.2020.08.010

De Jong, M. D., Simmons, C. P., Thanh, T. T., Hien, V. M., Smith, G. J., Chau, T. N., Hoang, D. M., Chau, N. V., Khanh, T. H., Dong, V. C., Qui, P. T., Cam, B. V., Ha Do, Q., Guan, Y., Peiris, J. S., Chinh, N. T., Hien, T. T. & Farrar, J. 2006. Fatal outcome of human influenza A (H5N1) is associated with high viral load and hypercytokinemia. *Nat Med,* 12**,** 1203-7. 10.1038/nm1477

Deng, T., Vreede, F. T. & Brownlee, G. G. 2006. Different de novo initiation strategies are used by influenza virus RNA polymerase on its cRNA and viral RNA promoters during viral RNA replication. *J Virol,* 80**,** 2337-48. 10.1128/JVI.80.5.2337-2348.2006

Deng, T., Zhang, L., Shi, Y. & Gao, G. F. 2025. In Transition: How Influenza Virus Switches from Transcription to Genome Replication. *Annu Rev Virol*. 10.1146/annurev-virology-092623-095030

Depmap 2025. DepMap Public 25Q2. *In:* BROAD (ed.).

Dholakia, V., Quantrill, J. L., Richardson, S., Pankaew, N., Brown, M. D., Yang, J., Capelastegui, F., Masonou, T., Case, K.-M., Ajeian, J., Woodall, M. N. J., Magill, C., Freimanis, G., Mccarron, A., Staller, E., Sheppard, C. M., Brown, I. H., Murcia, P. R., Smith, C. M., Iqbal, M., Digard, P., Barclay, W. S., Pinto, R. M., Peacock, T. P. & Goldhill, D. H. 2025. Polymerase mutations underlie early adaptation of H5N1 influenza virus to dairy cattle and other mammals. *bioRxiv***,** 2025.01.06.631435. 10.1101/2025.01.06.631435

Dias, A., Bouvier, D., Crepin, T., Mccarthy, A. A., Hart, D. J., Baudin, F., Cusack, S. & Ruigrok, R. W. 2009. The cap-snatching endonuclease of influenza virus polymerase resides in the PA subunit. *Nature,* 458**,** 914-8. 10.1038/nature07745

Domingues, P., Eletto, D., Magnus, C., Turkington, H. L., Schmutz, S., Zagordi, O., Lenk, M., Beer, M., Stertz, S. & Hale, B. G. 2019. Profiling host ANP32A splicing landscapes to predict influenza A virus polymerase adaptation. *Nat Commun,* 10**,** 3396. 10.1038/s41467-019-11388-2

Domingues, P., Golebiowski, F., Tatham, M. H., Lopes, A. M., Taggart, A., Hay, R. T. & Hale, B. G. 2015. Global Reprogramming of Host SUMOylation during Influenza Virus Infection. *Cell Rep,* 13**,** 1467-1480. 10.1016/j.celrep.2015.10.001

Domingues, P. & Hale, B. G. 2017. Functional Insights into ANP32A-Dependent Influenza A Virus Polymerase Host Restriction. *Cell Rep,* 20**,** 2538-2546. 10.1016/j.celrep.2017.08.061

Dos Santos Afonso, E., Escriou, N., Leclercq, I., Van Der Werf, S. & Naffakh, N. 2005. The generation of recombinant influenza A viruses expressing a PB2 fusion protein requires the conservation of a packaging signal overlapping the coding and noncoding regions at the 5' end of the PB2 segment. *Virology,* 341**,** 34-46. 10.1016/j.virol.2005.06.040

Dubois, J., Terrier, O. & Rosa-Calatrava, M. 2014. Influenza viruses and mRNA splicing: doing more with less. *mBio,* 5**,** e00070-14. 10.1128/mBio.00070-14

Duhaut, S. D. & Dimmock, N. J. 2002. Defective segment 1 RNAs that interfere with production of infectious influenza A virus require at least 150 nucleotides of 5' sequence: evidence from a plasmid-driven system. *J Gen Virol,* 83**,** 403-411. 10.1099/0022-1317-83-2-403

Dupont, M., Krischuns, T., Gianetto, Q. G., Paisant, S., Bonazza, S., Brault, J. B., Douche, T., Arragain, B., Florez-Prada, A., Perez-Perri, J. I., Hentze, M. W., Cusack, S., Matondo, M., Isel, C., Courtney, D. G. & Naffakh, N. 2024. The RBPome of influenza A virus NP-mRNA reveals a role for TDP-43 in viral replication. *Nucleic Acids Res,* 52**,** 7188-7210. 10.1093/nar/gkae291

Egloff, S., O'reilly, D., Chapman, R. D., Taylor, A., Tanzhaus, K., Pitts, L., Eick, D. & Murphy, S. 2007. Serine-7 of the RNA polymerase II CTD is specifically required for snRNA gene expression. *Science,* 318**,** 1777-9. 10.1126/science.1145989

Egloff, S., Zaborowska, J., Laitem, C., Kiss, T. & Murphy, S. 2012. Ser7 phosphorylation of the CTD recruits the RPAP2 Ser5 phosphatase to snRNA genes. *Mol Cell,* 45**,** 111-22. 10.1016/j.molcel.2011.11.006

Eick, D. & Geyer, M. 2013. The RNA polymerase II carboxy-terminal domain (CTD) code. *Chem Rev,* 113**,** 8456-90. 10.1021/cr400071f

Eisfeld, A. J., Neumann, G. & Kawaoka, Y. 2015. At the centre: influenza A virus ribonucleoproteins. *Nat Rev Microbiol,* 13**,** 28-41. 10.1038/nrmicro3367

Engelhardt, O. G., Smith, M. & Fodor, E. 2005. Association of the influenza A virus RNA-dependent RNA polymerase with cellular RNA polymerase II. *J Virol,* 79**,** 5812-8. 10.1128/JVI.79.9.5812-5818.2005

Engler, C., Kandzia, R. & Marillonnet, S. 2008. A one pot, one step, precision cloning method with high throughput capability. *PLoS One,* 3**,** e3647. 10.1371/journal.pone.0003647

Fan, H., Walker, A. P., Carrique, L., Keown, J. R., Serna Martin, I., Karia, D., Sharps, J., Hengrung, N., Pardon, E., Steyaert, J., Grimes, J. M. & Fodor, E. 2019. Structures of influenza A virus RNA polymerase offer insight into viral genome replication. *Nature,* 573**,** 287-290. 10.1038/s41586-019-1530-7

Fang, J., Pietzsch, C., Witwit, H., Tsaprailis, G., Crynen, G., Cho, K. F., Ting, A. Y., Bukreyev, A., Saphire, E. O. & De La Torre, J. C. 2022. Proximity interactome analysis of Lassa polymerase reveals eRF3a/GSPT1 as a druggable target for host-directed antivirals. *Proc Natl Acad Sci U S A,* 119**,** e2201208119. 10.1073/pnas.2201208119

Fodor, E. & Te Velthuis, A. J. W. 2020. Structure and Function of the Influenza Virus Transcription and Replication Machinery. *Cold Spring Harb Perspect Med,* 10. 10.1101/cshperspect.a038398

Forget, D., Lacombe, A. A., Cloutier, P., Lavallee-Adam, M., Blanchette, M. & Coulombe, B. 2013. Nuclear import of RNA polymerase II is coupled with nucleocytoplasmic shuttling of the RNA polymerase II-associated protein 2. *Nucleic Acids Res,* 41**,** 6881-91. 10.1093/nar/gkt455

Gabriel, G., Herwig, A. & Klenk, H. D. 2008. Interaction of polymerase subunit PB2 and NP with importin alpha1 is a determinant of host range of influenza A virus. *PLoS Pathog,* 4**,** e11. 10.1371/journal.ppat.0040011

Gabriel, G., Klingel, K., Otte, A., Thiele, S., Hudjetz, B., Arman-Kalcek, G., Sauter, M., Shmidt, T., Rother, F., Baumgarte, S., Keiner, B., Hartmann, E., Bader, M., Brownlee, G. G., Fodor, E. & Klenk, H. D. 2011. Differential use of importin-alpha isoforms governs cell tropism and host adaptation of influenza virus. *Nat Commun,* 2**,** 156. 10.1038/ncomms1158

Gack, M. U., Shin, Y. C., Joo, C. H., Urano, T., Liang, C., Sun, L., Takeuchi, O., Akira, S., Chen, Z., Inoue, S. & Jung, J. U. 2007. TRIM25 RING-finger E3 ubiquitin ligase is essential for RIG-I-mediated antiviral activity. *Nature,* 446**,** 916-920. 10.1038/nature05732

Gao, Y., Zhang, Y., Shinya, K., Deng, G., Jiang, Y., Li, Z., Guan, Y., Tian, G., Li, Y., Shi, J., Liu, L., Zeng, X., Bu, Z., Xia, X., Kawaoka, Y. & Chen, H. 2009. Identification of amino acids in HA and PB2 critical for the transmission of H5N1 avian influenza viruses in a mammalian host. *PLoS Pathog,* 5**,** e1000709. 10.1371/journal.ppat.1000709

Garcia-Sastre, A., Egorov, A., Matassov, D., Brandt, S., Levy, D. E., Durbin, J. E., Palese, P. & Muster, T. 1998. Influenza A virus lacking the NS1 gene replicates in interferon-deficient systems. *Virology,* 252**,** 324-30. 10.1006/viro.1998.9508

Garg, S., Reinhart, K., Couture, A., Kniss, K., Davis, C. T., Kirby, M. K., Murray, E. L., Zhu, S., Kraushaar, V., Wadford, D. A., Drehoff, C., Kohnen, A., Owen, M., Morse, J., Eckel, S., Goswitz, J., Turabelidze, G., Krager, S., Unutzer, A., Gonzales, E. R., Abdul Hamid, C., Ellington, S., Mellis, A. M., Budd, A., Barnes, J. R., Biggerstaff, M., Jhung, M. A., Richmond-Crum, M., Burns, E., Shimabukuro, T. T., Uyeki, T. M., Dugan, V. G., Reed, C. & Olsen, S. J. 2025. Highly Pathogenic Avian Influenza A(H5N1) Virus Infections in Humans. *N Engl J Med,* 392**,** 843-854. 10.1056/NEJMoa2414610

Geiss-Friedlander, R. & Melchior, F. 2007. Concepts in sumoylation: a decade on. *Nat Rev Mol Cell Biol,* 8**,** 947-56. 10.1038/nrm2293

Goldfarb, D. S., Corbett, A. H., Mason, D. A., Harreman, M. T. & Adam, S. A. 2004. Importin alpha: a multipurpose nuclear-transport receptor. *Trends Cell Biol,* 14**,** 505-14. 10.1016/j.tcb.2004.07.016

Goldhill, D. H., Te Velthuis, A. J. W., Fletcher, R. A., Langat, P., Zambon, M., Lackenby, A. & Barclay, W. S. 2018. The mechanism of resistance to favipiravir in influenza. *Proc Natl Acad Sci U S A,* 115**,** 11613-11618. 10.1073/pnas.1811345115

Gorynia, S., Bandeiras, T. M., Pinho, F. G., Mcvey, C. E., Vonrhein, C., Round, A., Svergun, D. I., Donner, P., Matias, P. M. & Carrondo, M. A. 2011. Structural and functional insights into a dodecameric molecular machine - the RuvBL1/RuvBL2 complex. *J Struct Biol,* 176**,** 279-91. 10.1016/j.jsb.2011.09.001

Gotz, V., Magar, L., Dornfeld, D., Giese, S., Pohlmann, A., Hoper, D., Kong, B. W., Jans, D. A., Beer, M., Haller, O. & Schwemmle, M. 2016. Influenza A viruses escape from MxA restriction at the expense of efficient nuclear vRNP import. *Sci Rep,* 6**,** 23138. 10.1038/srep23138

Gu, W., Gallagher, G. R., Dai, W., Liu, P., Li, R., Trombly, M. I., Gammon, D. B., Mello, C. C., Wang, J. P. & Finberg, R. W. 2015. Influenza A virus preferentially snatches noncoding RNA caps. *RNA,* 21**,** 2067-75. 10.1261/rna.054221.115

Guilligay, D., Tarendeau, F., Resa-Infante, P., Coloma, R., Crepin, T., Sehr, P., Lewis, J., Ruigrok, R. W., Ortin, J., Hart, D. J. & Cusack, S. 2008. The structural basis for cap binding by influenza virus polymerase subunit PB2. *Nat Struct Mol Biol,* 15**,** 500-6. 10.1038/nsmb.1421

Gunl, F., Krischuns, T., Schreiber, J. A., Henschel, L., Wahrenburg, M., Drexler, H. C. A., Leidel, S. A., Cojocaru, V., Seebohm, G., Mellmann, A., Schwemmle, M., Ludwig, S. & Brunotte, L. 2023. The ubiquitination landscape of the influenza A virus polymerase. *Nat Commun,* 14**,** 787. 10.1038/s41467-023-36389-0

Haas, K. M., Mcgregor, M. J., Bouhaddou, M., Polacco, B. J., Kim, E. Y., Nguyen, T. T., Newton, B. W., Urbanowski, M., Kim, H., Williams, M. a. P., Rezelj, V. V., Hardy, A., Fossati, A., Stevenson, E. J., Sukerman, E., Kim, T., Penugonda, S., Moreno, E., Braberg, H., Zhou, Y., Metreveli, G., Harjai, B., Tummino, T. A., Melnyk, J. E., Soucheray, M., Batra, J., Pache, L., Martin-Sancho, L., Carlson-Stevermer, J., Jureka, A. S., Basler, C. F., Shokat, K. M., Shoichet, B. K., Shriver, L. P., Johnson, J. R., Shaw, M. L., Chanda, S. K., Roden, D. M., Carter, T. C., Kottyan, L. C., Chisholm, R. L., Pacheco, J. A., Smith, M. E., Schrodi, S. J., Albrecht, R. A., Vignuzzi, M., Zuliani-Alvarez, L., Swaney, D. L., Eckhardt, M., Wolinsky, S. M., White, K. M., Hultquist, J. F., Kaake, R. M., Garcia-Sastre, A. & Krogan, N. J. 2023. Proteomic and genetic analyses of influenza A viruses identify pan-viral host targets. *Nat Commun,* 14**,** 6030. 10.1038/s41467-023-41442-z

Hale, B. G., Randall, R. E., Ortin, J. & Jackson, D. 2008. The multifunctional NS1 protein of influenza A viruses. *J Gen Virol,* 89**,** 2359-2376. 10.1099/vir.0.2008/004606-0

Haller, O. & Kochs, G. 2020. Mx genes: host determinants controlling influenza virus infection and trans-species transmission. *Hum Genet,* 139**,** 695-705. 10.1007/s00439-019-02092-8

Haller, O., Staeheli, P., Schwemmle, M. & Kochs, G. 2015. Mx GTPases: dynamin-like antiviral machines of innate immunity. *Trends Microbiol,* 23**,** 154-63. 10.1016/j.tim.2014.12.003

Han, J., Perez, J. T., Chen, C., Li, Y., Benitez, A., Kandasamy, M., Lee, Y., Andrade, J., Tenoever, B. & Manicassamy, B. 2018. Genome-wide CRISPR/Cas9 Screen Identifies Host Factors Essential for Influenza Virus Replication. *Cell Rep,* 23**,** 596-607. 10.1016/j.celrep.2018.03.045

Hao, L., He, Q., Wang, Z., Craven, M., Newton, M. A. & Ahlquist, P. 2013. Limited agreement of independent RNAi screens for virus-required host genes owes more to false-negative than false-positive factors. *PLoS Comput Biol,* 9**,** e1003235. 10.1371/journal.pcbi.1003235

Hao, L., Sakurai, A., Watanabe, T., Sorensen, E., Nidom, C. A., Newton, M. A., Ahlquist, P. & Kawaoka, Y. 2008. Drosophila RNAi screen identifies host genes important for influenza virus replication. *Nature,* 454**,** 890-3. 10.1038/nature07151

Harrington, W. N., Kackos, C. M. & Webby, R. J. 2021. The evolution and future of influenza pandemic preparedness. *Exp Mol Med,* 53**,** 737-749. 10.1038/s12276-021-00603-0

Heaton, N. S., Moshkina, N., Fenouil, R., Gardner, T. J., Aguirre, S., Shah, P. S., Zhao, N., Manganaro, L., Hultquist, J. F., Noel, J., Sachs, D., Hamilton, J., Leon, P. E., Chawdury, A., Tripathi, S., Melegari, C., Campisi, L., Hai, R., Metreveli, G., Gamarnik, A. V., Garcia-Sastre, A., Greenbaum, B., Simon, V., Fernandez-Sesma, A., Krogan, N. J., Mulder, L. C. F., Van Bakel, H., Tortorella, D., Taunton, J., Palese, P. & Marazzi, I. 2016. Targeting Viral Proteostasis Limits Influenza Virus, HIV, and Dengue Virus Infection. *Immunity,* 44**,** 46-58. 10.1016/j.immuni.2015.12.017

Hengrung, N., El Omari, K., Serna Martin, I., Vreede, F. T., Cusack, S., Rambo, R. P., Vonrhein, C., Bricogne, G., Stuart, D. I., Grimes, J. M. & Fodor, E. 2015. Crystal structure of the RNA-dependent RNA polymerase from influenza C virus. *Nature,* 527**,** 114-7. 10.1038/nature15525

Hoffmann, E., Neumann, G., Kawaoka, Y., Hobom, G. & Webster, R. G. 2000. A DNA transfection system for generation of influenza A virus from eight plasmids. *Proc Natl Acad Sci U S A,* 97**,** 6108-13. 10.1073/pnas.100133697

Hoffmann, E., Stech, J., Guan, Y., Webster, R. G. & Perez, D. R. 2001. Universal primer set for the full-length amplification of all influenza A viruses. *Arch Virol,* 146**,** 2275-89. 10.1007/s007050170002

Hong, R., Macfarlan, T., Kutney, S. N., Seo, S. B., Mukai, Y., Yelin, F., Pasternack, G. R. & Chakravarti, D. 2004. The identification of phosphorylation sites of pp32 and biochemical purification of a cellular pp32-kinase. *Biochemistry,* 43**,** 10157-65. 10.1021/bi0493968

Houser, K. & Subbarao, K. 2015. Influenza vaccines: challenges and solutions. *Cell Host Microbe,* 17**,** 295-300. 10.1016/j.chom.2015.02.012

Hsu, W. B., Shih, J. L., Shih, J. R., Du, J. L., Teng, S. C., Huang, L. M. & Wang, W. B. 2013. Cellular protein HAX1 interacts with the influenza A virus PA polymerase subunit and impedes its nuclear translocation. *J Virol,* 87**,** 110-23. 10.1128/JVI.00939-12

Hu, C. D., Chinenov, Y. & Kerppola, T. K. 2002. Visualization of interactions among bZIP and Rel family proteins in living cells using bimolecular fluorescence complementation. *Mol Cell,* 9**,** 789-98. 10.1016/s1097-2765(02)00496-3

Hu, J., Zhang, L. & Liu, X. 2020. Role of Post-translational Modifications in Influenza A Virus Life Cycle and Host Innate Immune Response. *Front Microbiol,* 11**,** 517461. 10.3389/fmicb.2020.517461

Hu, Y., Gor, V., Morikawa, K., Nagata, K. & Kawaguchi, A. 2017. Cellular splicing factor UAP56 stimulates trimeric NP formation for assembly of functional influenza viral ribonucleoprotein complexes. *Sci Rep,* 7**,** 14053. 10.1038/s41598-017-13784-4

Huarte, M., Sanz-Ezquerro, J. J., Roncal, F., Ortin, J. & Nieto, A. 2001. PA subunit from influenza virus polymerase complex interacts with a cellular protein with homology to a family of transcriptional activators. *J Virol,* 75**,** 8597-604. 10.1128/jvi.75.18.8597-8604.2001

Hubel, P., Urban, C., Bergant, V., Schneider, W. M., Knauer, B., Stukalov, A., Scaturro, P., Mann, A., Brunotte, L., Hoffmann, H. H., Schoggins, J. W., Schwemmle, M., Mann, M., Rice, C. M. & Pichlmair, A. 2019. A protein-interaction network of interferon-stimulated genes extends the innate immune system landscape. *Nat Immunol,* 20**,** 493-502. 10.1038/s41590-019-0323-3

Hudjetz, B. & Gabriel, G. 2012. Human-like PB2 627K influenza virus polymerase activity is regulated by importin-alpha1 and -alpha7. *PLoS Pathog,* 8**,** e1002488. 10.1371/journal.ppat.1002488

Huen, J., Kakihara, Y., Ugwu, F., Cheung, K. L., Ortega, J. & Houry, W. A. 2010. Rvb1-Rvb2: essential ATP-dependent helicases for critical complexes. *Biochem Cell Biol,* 88**,** 29-40. 10.1139/o09-122

Hurt, A. C. 2014. The epidemiology and spread of drug resistant human influenza viruses. *Curr Opin Virol,* 8**,** 22-9. 10.1016/j.coviro.2014.04.009

Hutchinson, E. C., Charles, P. D., Hester, S. S., Thomas, B., Trudgian, D., Martinez-Alonso, M. & Fodor, E. 2014. Conserved and host-specific features of influenza virion architecture. *Nat Commun,* 5**,** 4816. 10.1038/ncomms5816

Hutchinson, E. C., Denham, E. M., Thomas, B., Trudgian, D. C., Hester, S. S., Ridlova, G., York, A., Turrell, L. & Fodor, E. 2012. Mapping the phosphoproteome of influenza A and B viruses by mass spectrometry. *PLoS Pathog,* 8**,** e1002993. 10.1371/journal.ppat.1002993

Huyton, T. & Wolberger, C. 2007. The crystal structure of the tumor suppressor protein pp32 (Anp32a): structural insights into Anp32 family of proteins. *Protein Sci,* 16**,** 1308-15. 10.1110/ps.072803507

Idoko-Akoh, A., Goldhill, D. H., Sheppard, C. M., Bialy, D., Quantrill, J. L., Sukhova, K., Brown, J. C., Richardson, S., Campbell, C., Taylor, L., Sherman, A., Nazki, S., Long, J. S., Skinner, M. A., Shelton, H., Sang, H. M., Barclay, W. S. & Mcgrew, M. J. 2023. Creating resistance to avian influenza infection through genome editing of the ANP32 gene family. *Nat Commun,* 14**,** 6136. 10.1038/s41467-023-41476-3

Isaka, T., Nestor, A. L., Takada, T. & Allison, D. C. 2003. Chromosomal variations within aneuploid cancer lines. *J Histochem Cytochem,* 51**,** 1343-53. 10.1177/002215540305101011

Jagger, B. W., Wise, H. M., Kash, J. C., Walters, K. A., Wills, N. M., Xiao, Y. L., Dunfee, R. L., Schwartzman, L. M., Ozinsky, A., Bell, G. L., Dalton, R. M., Lo, A., Efstathiou, S., Atkins, J. F., Firth, A. E., Taubenberger, J. K. & Digard, P. 2012. An overlapping protein-coding region in influenza A virus segment 3 modulates the host response. *Science,* 337**,** 199-204. 10.1126/science.1222213

Jamin, M. & Yabukarski, F. 2017. Nonsegmented Negative-Sense RNA Viruses-Structural Data Bring New Insights Into Nucleocapsid Assembly. *Adv Virus Res,* 97**,** 143-185. 10.1016/bs.aivir.2016.09.001

Januszyk, K. & Lima, C. D. 2014. The eukaryotic RNA exosome. *Curr Opin Struct Biol,* 24**,** 132-40. 10.1016/j.sbi.2014.01.011

Jorba, N., Coloma, R. & Ortin, J. 2009. Genetic trans-complementation establishes a new model for influenza virus RNA transcription and replication. *PLoS Pathog,* 5**,** e1000462. 10.1371/journal.ppat.1000462

Jorba, N., Juarez, S., Torreira, E., Gastaminza, P., Zamarreno, N., Albar, J. P. & Ortin, J. 2008. Analysis of the interaction of influenza virus polymerase complex with human cell factors. *Proteomics,* 8**,** 2077-88. 10.1002/pmic.200700508

Jourdan, N., Jobart-Malfait, A., Dos Reis, G., Quignon, F., Piolot, T., Klein, C., Tramier, M., Coppey-Moisan, M. & Marechal, V. 2012. Live-cell imaging reveals multiple interactions between Epstein-Barr virus nuclear antigen 1 and cellular chromatin during interphase and mitosis. *J Virol,* 86**,** 5314-29. 10.1128/JVI.06303-11

Kakugawa, S., Shimojima, M., Neumann, G., Goto, H. & Kawaoka, Y. 2009. RuvB-like protein 2 is a suppressor of influenza A virus polymerases. *J Virol,* 83**,** 6429-34. 10.1128/JVI.00293-09

Kamel, W., Ruscica, V., Embarc-Buh, A., De Laurent, Z. R., Garcia-Moreno, M., Demyanenko, Y., Orton, R. J., Noerenberg, M., Madhusudhan, M., Iselin, L., Jarvelin, A. I., Hannan, M., Kitano, E., Moore, S., Merits, A., Davis, I., Mohammed, S. & Castello, A. 2024. Alphavirus infection triggers selective cytoplasmic translocation of nuclear RBPs with moonlighting antiviral roles. *Mol Cell,* 84**,** 4896-4911 e7. 10.1016/j.molcel.2024.11.015

Kang, M. S. & Kieff, E. 2015. Epstein-Barr virus latent genes. *Exp Mol Med,* 47**,** e131. 10.1038/emm.2014.84

Karlas, A., Machuy, N., Shin, Y., Pleissner, K. P., Artarini, A., Heuer, D., Becker, D., Khalil, H., Ogilvie, L. A., Hess, S., Maurer, A. P., Muller, E., Wolff, T., Rudel, T. & Meyer, T. F. 2010. Genome-wide RNAi screen identifies human host factors crucial for influenza virus replication. *Nature,* 463**,** 818-22. 10.1038/nature08760

Kawaguchi, A. & Nagata, K. 2007. De novo replication of the influenza virus RNA genome is regulated by DNA replicative helicase, MCM. *EMBO J,* 26**,** 4566-75. 10.1038/sj.emboj.7601881

Kawakami, E., Watanabe, T., Fujii, K., Goto, H., Watanabe, S., Noda, T. & Kawaoka, Y. 2011. Strand-specific real-time RT-PCR for distinguishing influenza vRNA, cRNA, and mRNA. *J Virol Methods,* 173**,** 1-6. 10.1016/j.jviromet.2010.12.014

Keown, J., Baazaoui, A., Sebesta, M., Stefl, R., Carrique, L., Fodor, E. & Grimes, J. M. 2024. Structural and functional characterization of the interaction between the influenza A virus RNA polymerase and the CTD of host RNA polymerase II. *J Virol,* 98**,** e0013824. 10.1128/jvi.00138-24

Kilpatrick, A. M., Chmura, A. A., Gibbons, D. W., Fleischer, R. C., Marra, P. P. & Daszak, P. 2006. Predicting the global spread of H5N1 avian influenza. *Proc Natl Acad Sci U S A,* 103**,** 19368-73. 10.1073/pnas.0609227103

Knight, M. L., Fan, H., Bauer, D. L. V., Grimes, J. M., Fodor, E. & Keown, J. R. 2021. Structure of an H3N2 influenza virus nucleoprotein. *Acta Crystallogr F Struct Biol Commun,* 77**,** 208-214. 10.1107/S2053230X2100635X

Konig, R., Stertz, S., Zhou, Y., Inoue, A., Hoffmann, H. H., Bhattacharyya, S., Alamares, J. G., Tscherne, D. M., Ortigoza, M. B., Liang, Y., Gao, Q., Andrews, S. E., Bandyopadhyay, S., De Jesus, P., Tu, B. P., Pache, L., Shih, C., Orth, A., Bonamy, G., Miraglia, L., Ideker, T., Garcia-Sastre, A., Young, J. A., Palese, P., Shaw, M. L. & Chanda, S. K. 2010. Human host factors required for influenza virus replication. *Nature,* 463**,** 813-7. 10.1038/nature08699

Koopmans, M. P. G., Barton Behravesh, C., Cunningham, A. A., Adisasmito, W. B., Almuhairi, S., Bilivogui, P., Bukachi, S. A., Casas, N., Cediel Becerra, N., Charron, D. F., Chaudhary, A., Ciacci Zanella, J. R., Dar, O., Debnath, N., Dungu, B., Farag, E., Gao, G. F., Khaitsa, M., Machalaba, C., Mackenzie, J. S., Markotter, W., Mettenleiter, T. C., Morand, S., Smolenskiy, V., Zhou, L., Hayman, D. T. S. & One Health High-Level Expert, P. 2024. The panzootic spread of highly pathogenic avian influenza H5N1 sublineage 2.3.4.4b: a critical appraisal of One Health preparedness and prevention. *Lancet Infect Dis,* 24**,** e774-e781. 10.1016/S1473-3099(24)00438-9

Koppstein, D., Ashour, J. & Bartel, D. P. 2015. Sequencing the cap-snatching repertoire of H1N1 influenza provides insight into the mechanism of viral transcription initiation. *Nucleic Acids Res,* 43**,** 5052-64. 10.1093/nar/gkv333

Kouba, T., Drncova, P. & Cusack, S. 2019. Structural snapshots of actively transcribing influenza polymerase. *Nat Struct Mol Biol,* 26**,** 460-470. 10.1038/s41594-019-0232-z

Krammer, F. 2015. Emerging influenza viruses and the prospect of a universal influenza virus vaccine. *Biotechnol J,* 10**,** 690-701. 10.1002/biot.201400393

Krammer, F., Smith, G. J. D., Fouchier, R. a. M., Peiris, M., Kedzierska, K., Doherty, P. C., Palese, P., Shaw, M. L., Treanor, J., Webster, R. G. & Garcia-Sastre, A. 2018. Influenza. *Nat Rev Dis Primers,* 4**,** 3. 10.1038/s41572-018-0002-y

Krischuns, T., Arragain, B., Isel, C., Paisant, S., Budt, M., Wolff, T., Cusack, S. & Naffakh, N. 2024. The host RNA polymerase II C-terminal domain is the anchor for replication of the influenza virus genome. *Nat Commun,* 15**,** 1064. 10.1038/s41467-024-45205-2

Krischuns, T., Isel, C., Drncova, P., Lukarska, M., Pflug, A., Paisant, S., Navratil, V., Cusack, S. & Naffakh, N. 2022. Type B and type A influenza polymerases have evolved distinct binding interfaces to recruit the RNA polymerase II CTD. *PLoS Pathog,* 18**,** e1010328. 10.1371/journal.ppat.1010328

Krischuns, T., Lukarska, M., Naffakh, N. & Cusack, S. 2021. Influenza Virus RNA-Dependent RNA Polymerase and the Host Transcriptional Apparatus. *Annu Rev Biochem,* 90**,** 321-348. 10.1146/annurev-biochem-072820-100645

Landeras-Bueno, S., Jorba, N., Perez-Cidoncha, M. & Ortin, J. 2011. The splicing factor proline-glutamine rich (SFPQ/PSF) is involved in influenza virus transcription. *PLoS Pathog,* 7**,** e1002397. 10.1371/journal.ppat.1002397

Lee, S., Nam, Y., Koo, J. Y., Lim, D., Park, J., Ock, J., Kim, J., Suk, K. & Park, S. B. 2014. A small molecule binding HMGB1 and HMGB2 inhibits microglia-mediated neuroinflammation. *Nat Chem Biol,* 10**,** 1055-60. 10.1038/nchembio.1669

Li, B., Clohisey, S. M., Chia, B. S., Wang, B., Cui, A., Eisenhaure, T., Schweitzer, L. D., Hoover, P., Parkinson, N. J., Nachshon, A., Smith, N., Regan, T., Farr, D., Gutmann, M. U., Bukhari, S. I., Law, A., Sangesland, M., Gat-Viks, I., Digard, P., Vasudevan, S., Lingwood, D., Dockrell, D. H., Doench, J. G., Baillie, J. K. & Hacohen, N. 2020. Genome-wide CRISPR screen identifies host dependency factors for influenza A virus infection. *Nat Commun,* 11**,** 164. 10.1038/s41467-019-13965-x

Li, M., Guo, H. & Damuni, Z. 1995. Purification and characterization of two potent heat-stable protein inhibitors of protein phosphatase 2A from bovine kidney. *Biochemistry,* 34**,** 1988-96. 10.1021/bi00006a020

Li, X., Gu, M., Zheng, Q., Gao, R. & Liu, X. 2021. Packaging signal of influenza A virus. *Virol J,* 18**,** 36. 10.1186/s12985-021-01504-4

Lindenmann, J. 1962. Resistance of mice to mouse-adapted influenza A virus. *Virology,* 16**,** 203-4. 10.1016/0042-6822(62)90297-0

Liu, Q., Lu, L., Sun, Z., Chen, G. W., Wen, Y. & Jiang, S. 2013. Genomic signature and protein sequence analysis of a novel influenza A (H7N9) virus that causes an

outbreak in humans in China. *Microbes Infect,* 15**,** 432-9. 10.1016/j.micinf.2013.04.004
Long, J. S., Giotis, E. S., Moncorge, O., Frise, R., Mistry, B., James, J., Morisson, M., Iqbal, M., Vignal, A., Skinner, M. A. & Barclay, W. S. 2016. Species difference in ANP32A underlies influenza A virus polymerase host restriction. *Nature,* 529**,** 101-4. 10.1038/nature16474
Long, J. S., Howard, W. A., Nunez, A., Moncorge, O., Lycett, S., Banks, J. & Barclay, W. S. 2013. The effect of the PB2 mutation 627K on highly pathogenic H5N1 avian influenza virus is dependent on the virus lineage. *J Virol,* 87**,** 9983-96. 10.1128/JVI.01399-13
Long, J. S., Idoko-Akoh, A., Mistry, B., Goldhill, D., Staller, E., Schreyer, J., Ross, C., Goodbourn, S., Shelton, H., Skinner, M. A., Sang, H., Mcgrew, M. J. & Barclay, W. 2019a. Species specific differences in use of ANP32 proteins by influenza A virus. *Elife,* 8. 10.7554/eLife.45066
Long, J. S., Mistry, B., Haslam, S. M. & Barclay, W. S. 2019b. Host and viral determinants of influenza A virus species specificity. *Nat Rev Microbiol,* 17**,** 67-81. 10.1038/s41579-018-0115-z
Lopez-Perrote, A., Munoz-Hernandez, H., Gil, D. & Llorca, O. 2012. Conformational transitions regulate the exposure of a DNA-binding domain in the RuvBL1-RuvBL2 complex. *Nucleic Acids Res,* 40**,** 11086-99. 10.1093/nar/gks871
Lukarska, M., Fournier, G., Pflug, A., Resa-Infante, P., Reich, S., Naffakh, N. & Cusack, S. 2017. Structural basis of an essential interaction between influenza polymerase and Pol II CTD. *Nature,* 541**,** 117-121. 10.1038/nature20594
Lum, K. K. & Cristea, I. M. 2016. Proteomic approaches to uncovering virus-host protein interactions during the progression of viral infection. *Expert Rev Proteomics,* 13**,** 325-40. 10.1586/14789450.2016.1147353
Lyons, D. E., Mcmahon, S. & Ott, M. 2020. A combinatorial view of old and new RNA polymerase II modifications. *Transcription,* 11**,** 66-82. 10.1080/21541264.2020.1762468
Ma, H. T. 2021. The Conditional Knockout Analogous System: CRISPR-Mediated Knockout Together with Inducible Degron and Transcription-Controlled Expression. *Methods Mol Biol,* 2329**,** 323-335. 10.1007/978-1-0716-1538-6_23
Mandemaker, I. K., Fessler, E., Corujo, D., Kotthoff, C., Wegerer, A., Rouillon, C., Buschbeck, M., Jae, L. T., Mattiroli, F. & Ladurner, A. G. 2023. The histone chaperone ANP32B regulates chromatin incorporation of the atypical human histone variant macroH2A. *Cell Rep,* 42**,** 113300. 10.1016/j.celrep.2023.113300
Manz, B., Brunotte, L., Reuther, P. & Schwemmle, M. 2012. Adaptive mutations in NEP compensate for defective H5N1 RNA replication in cultured human cells. *Nat Commun,* 3**,** 802. 10.1038/ncomms1804
Manz, B., Dornfeld, D., Gotz, V., Zell, R., Zimmermann, P., Haller, O., Kochs, G. & Schwemmle, M. 2013. Pandemic influenza A viruses escape from restriction by human MxA through adaptive mutations in the nucleoprotein. *PLoS Pathog,* 9**,** e1003279. 10.1371/journal.ppat.1003279
Mao, Z., Pan, L., Wang, W., Sun, J., Shan, S., Dong, Q., Liang, X., Dai, L., Ding, X., Chen, S., Zhang, Z., Zhu, B. & Zhou, Z. 2014. Anp32e, a higher eukaryotic histone chaperone directs preferential recognition for H2A.Z. *Cell Res,* 24**,** 389-99. 10.1038/cr.2014.30
Marion, R. M., Zurcher, T., De La Luna, S. & Ortin, J. 1997. Influenza virus NS1 protein interacts with viral transcription-replication complexes in vivo. *J Gen Virol,* 78 (Pt 10)**,** 2447-51. 10.1099/0022-1317-78-10-2447
Martin-Sancho, L., Tripathi, S., Rodriguez-Frandsen, A., Pache, L., Sanchez-Aparicio, M., Mcgregor, M. J., Haas, K. M., Swaney, D. L., Nguyen, T. T., Mamede, J. I., Churas, C., Pratt, D., Rosenthal, S. B., Riva, L., Nguyen, C., Beltran-Raygoza, N., Soonthornvacharin, S., Wang, G., Jimenez-Morales, D., De Jesus, P. D., Moulton, H. M., Stein, D. A., Chang, M. W., Benner, C., Ideker, T., Albrecht, R. A., Hultquist, J. F.,

Krogan, N. J., Garcia-Sastre, A. & Chanda, S. K. 2021. Restriction factor compendium for influenza A virus reveals a mechanism for evasion of autophagy. *Nat Microbiol,* 6**,** 1319-1333. 10.1038/s41564-021-00964-2

Martinez-Alonso, M., Hengrung, N. & Fodor, E. 2016. RNA-Free and Ribonucleoprotein-Associated Influenza Virus Polymerases Directly Bind the Serine-5-Phosphorylated Carboxyl-Terminal Domain of Host RNA Polymerase II. *J Virol,* 90**,** 6014-6021. 10.1128/JVI.00494-16

Matilla, A. & Radrizzani, M. 2005. The Anp32 family of proteins containing leucine-rich repeats. *Cerebellum,* 4**,** 7-18. 10.1080/14734220410019020

Matrosovich, M. N., Matrosovich, T. Y., Gray, T., Roberts, N. A. & Klenk, H. D. 2004. Human and avian influenza viruses target different cell types in cultures of human airway epithelium. *Proc Natl Acad Sci U S A,* 101**,** 4620-4. 10.1073/pnas.0308001101

Matsumoto, Y., Hayashi, Y., Omori, H., Honda, T., Daito, T., Horie, M., Ikuta, K., Fujino, K., Nakamura, S., Schneider, U., Chase, G., Yoshimori, T., Schwemmle, M. & Tomonaga, K. 2012. Bornavirus closely associates and segregates with host chromosomes to ensure persistent intranuclear infection. *Cell Host Microbe,* 11**,** 492-503. 10.1016/j.chom.2012.04.009

Mayer, D., Molawi, K., Martinez-Sobrido, L., Ghanem, A., Thomas, S., Baginsky, S., Grossmann, J., Garcia-Sastre, A. & Schwemmle, M. 2007. Identification of cellular interaction partners of the influenza virus ribonucleoprotein complex and polymerase complex using proteomic-based approaches. *J Proteome Res,* 6**,** 672-82. 10.1021/pr060432u

Mckellar, J., García De Gracia, F., Aubé, C., Chaves Valadão, A. L., Tauziet, M., Arnaud-Arnould, M., Rebendenne, A., Neyret, A., Labaronne, E., Ricci, E., Delaval, B., Gaudin, R., Naffakh, N., Gallois-Montbrun, S., Moncorgé, O. & Goujon, C. 2024. Human MX1 induces the cytoplasmic sequestration of neo-synthesized influenza A virus vRNPs. *bioRxiv***,** 2024.02.22.581565. 10.1101/2024.02.22.581565

Mehle, A. & Doudna, J. A. 2009. Adaptive strategies of the influenza virus polymerase for replication in humans. *Proc Natl Acad Sci U S A,* 106**,** 21312-6. 10.1073/pnas.0911915106

Mellacheruvu, D., Wright, Z., Couzens, A. L., Lambert, J. P., St-Denis, N. A., Li, T., Miteva, Y. V., Hauri, S., Sardiu, M. E., Low, T. Y., Halim, V. A., Bagshaw, R. D., Hubner, N. C., Al-Hakim, A., Bouchard, A., Faubert, D., Fermin, D., Dunham, W. H., Goudreault, M., Lin, Z. Y., Badillo, B. G., Pawson, T., Durocher, D., Coulombe, B., Aebersold, R., Superti-Furga, G., Colinge, J., Heck, A. J., Choi, H., Gstaiger, M., Mohammed, S., Cristea, I. M., Bennett, K. L., Washburn, M. P., Raught, B., Ewing, R. M., Gingras, A. C. & Nesvizhskii, A. I. 2013. The CRAPome: a contaminant repository for affinity purification-mass spectrometry data. *Nat Methods,* 10**,** 730-6. 10.1038/nmeth.2557

Mena, I., Jambrina, E., Albo, C., Perales, B., Ortin, J., Arrese, M., Vallejo, D. & Portela, A. 1999. Mutational analysis of influenza A virus nucleoprotein: identification of mutations that affect RNA replication. *J Virol,* 73**,** 1186-94. 10.1128/JVI.73.2.1186-1194.1999

Mettier, J., Prompt, C., Bruder, E., Da Costa, B., Chevalier, C. & Le Goffic, R. 2023. Comparison of PB1-F2 Proximity Interactomes Reveals Functional Differences between a Human and an Avian Influenza Virus. *Viruses,* 15. 10.3390/v15020328

Meyer, K. & Selbach, M. 2015. Quantitative affinity purification mass spectrometry: a versatile technology to study protein-protein interactions. *Front Genet,* 6**,** 237. 10.3389/fgene.2015.00237

Min, J. Y., Li, S., Sen, G. C. & Krug, R. M. 2007. A site on the influenza A virus NS1 protein mediates both inhibition of PKR activation and temporal regulation of viral RNA synthesis. *Virology,* 363**,** 236-43. 10.1016/j.virol.2007.01.038

Mistry, B. 2019. *The mechanisms by which ANP32 proteins support the influenza polymerase.* Doctor of Philosophy, Imperial College London.

Mistry, B., Long, J. S., Schreyer, J., Staller, E., Sanchez-David, R. Y. & Barclay, W. S. 2020. Elucidating the Interactions between Influenza Virus Polymerase and Host Factor ANP32A. *J Virol,* 94. 10.1128/JVI.01353-19

Miyamoto, S. N., M.; Morikawa, T.; Hirabayashi, A.; Tamura, R.; Fujita-Fujiharu, Y.; Hirose, N.; Muramoto, Y.; Noda, T. 2022. Migration of Influenza Virus Nucleoprotein into the Nucleolus Is Essential for Ribonucleoprotein Complex Formation. *mBio,* 4**,** e03315-21. 10.1128/mbio.03315-21

Moeller, A., Kirchdoerfer, R. N., Potter, C. S., Carragher, B. & Wilson, I. A. 2012. Organization of the influenza virus replication machinery. *Science,* 338**,** 1631-4. 10.1126/science.1227270

Moisy, D., Avilov, S. V., Jacob, Y., Laoide, B. M., Ge, X., Baudin, F., Naffakh, N. & Jestin, J. L. 2012. HMGB1 protein binds to influenza virus nucleoprotein and promotes viral replication. *J Virol,* 86**,** 9122-33. 10.1128/JVI.00789-12

Momose, F., Basler, C. F., O'neill, R. E., Iwamatsu, A., Palese, P. & Nagata, K. 2001. Cellular splicing factor RAF-2p48/NPI-5/BAT1/UAP56 interacts with the influenza virus nucleoprotein and enhances viral RNA synthesis. *J Virol,* 75**,** 1899-908. 10.1128/JVI.75.4.1899-1908.2001

Mondal, A., Potts, G. K., Dawson, A. R., Coon, J. J. & Mehle, A. 2015. Phosphorylation at the homotypic interface regulates nucleoprotein oligomerization and assembly of the influenza virus replication machinery. *PLoS Pathog,* 11**,** e1004826. 10.1371/journal.ppat.1004826

Morel, J., Sedano, L., Lejal, N., Da Costa, B., Batsche, E., Muchardt, C. & Delmas, B. 2022. The Influenza Virus RNA-Polymerase and the Host RNA-Polymerase II: RPB4 Is Targeted by a PB2 Domain That Is Involved in Viral Transcription. *Viruses,* 14. 10.3390/v14030518

Morris, A. K., Wang, Z., Ivey, A. L., Xie, Y., Hill, P. S., Schey, K. L. & Ren, Y. 2020. Cellular mRNA export factor UAP56 recognizes nucleic acid binding site of influenza virus NP protein. *Biochem Biophys Res Commun,* 525**,** 259-264. 10.1016/j.bbrc.2020.02.059

Morwitzer, M. J., Tritsch, S. R., Cazares, L. H., Ward, M. D., Nuss, J. E., Bavari, S. & Reid, S. P. 2019. Identification of RUVBL1 and RUVBL2 as Novel Cellular Interactors of the Ebola Virus Nucleoprotein. *Viruses,* 11. 10.3390/v11040372

Naito, T., Momose, F., Kawaguchi, A. & Nagata, K. 2007. Involvement of Hsp90 in assembly and nuclear import of influenza virus RNA polymerase subunits. *J Virol,* 81**,** 1339-49. 10.1128/JVI.01917-06

Nano, N., Ugwu, F., Seraphim, T. V., Li, T., Azer, G., Isaac, M., Prakesch, M., Barbosa, L. R. S., Ramos, C. H. I., Datti, A. & Houry, W. A. 2020. Sorafenib as an Inhibitor of RUVBL2. *Biomolecules,* 10. 10.3390/biom10040605

Natsume, T., Kiyomitsu, T., Saga, Y. & Kanemaki, M. T. 2016. Rapid Protein Depletion in Human Cells by Auxin-Inducible Degron Tagging with Short Homology Donors. *Cell Rep,* 15**,** 210-218. 10.1016/j.celrep.2016.03.001

Nemeroff, M. E., Barabino, S. M., Li, Y., Keller, W. & Krug, R. M. 1998. Influenza virus NS1 protein interacts with the cellular 30 kDa subunit of CPSF and inhibits 3'end formation of cellular pre-mRNAs. *Mol Cell,* 1**,** 991-1000. 10.1016/s1097-2765(00)80099-4

Neumann, G., Hughes, M. T. & Kawaoka, Y. 2000. Influenza A virus NS2 protein mediates vRNP nuclear export through NES-independent interaction with hCRM1. *EMBO J,* 19**,** 6751-8. 10.1093/emboj/19.24.6751

Neumann, G., Noda, T. & Kawaoka, Y. 2009. Emergence and pandemic potential of swine-origin H1N1 influenza virus. *Nature,* 459**,** 931-9. 10.1038/nature08157

Neumann, G., Zobel, A. & Hobom, G. 1994. RNA polymerase I-mediated expression of influenza viral RNA molecules. *Virology,* 202**,** 477-9. 10.1006/viro.1994.1365

Newcomb, L. L., Kuo, R. L., Ye, Q., Jiang, Y., Tao, Y. J. & Krug, R. M. 2009. Interaction of the influenza a virus nucleocapsid protein with the viral RNA polymerase potentiates unprimed viral RNA replication. *J Virol,* 83**,** 29-36. 10.1128/JVI.02293-07

Ng, A. K., Zhang, H., Tan, K., Li, Z., Liu, J. H., Chan, P. K., Li, S. M., Chan, W. Y., Au, S. W., Joachimiak, A., Walz, T., Wang, J. H. & Shaw, P. C. 2008. Structure of the influenza virus A H5N1 nucleoprotein: implications for RNA binding, oligomerization, and vaccine design. *FASEB J,* 22**,** 3638-47. 10.1096/fj.08-112110

Nigg, P. E. & Pavlovic, J. 2015. Oligomerization and GTP-binding Requirements of MxA for Viral Target Recognition and Antiviral Activity against Influenza A Virus. *J Biol Chem,* 290**,** 29893-906. 10.1074/jbc.M115.681494

Nilsson, B. E., Te Velthuis, A. J. W. & Fodor, E. 2017. Role of the PB2 627 Domain in Influenza A Virus Polymerase Function. *J Virol,* 91. 10.1128/JVI.02467-16

Nilsson-Payant, B. E., Tenoever, B. R. & Te Velthuis, A. J. W. 2022. The Host Factor ANP32A Is Required for Influenza A Virus vRNA and cRNA Synthesis. *J Virol,* 96**,** e0209221. 10.1128/jvi.02092-21

Ninpan, K., Suptawiwat, O., Boonarkart, C., Phuangphung, P., Sathirareuangchai, S., Uiprasertkul, M. & Auewarakul, P. 2016. Expression of importin-alpha isoforms in human nasal mucosa: implication for adaptation of avian influenza A viruses to human host. *Virol J,* 13**,** 90. 10.1186/s12985-016-0546-y

Nishimura, K., Fukagawa, T., Takisawa, H., Kakimoto, T. & Kanemaki, M. 2009. An auxin-based degron system for the rapid depletion of proteins in nonplant cells. *Nat Methods,* 6**,** 917-22. 10.1038/nmeth.1401

Noda, T., Sagara, H., Yen, A., Takada, A., Kida, H., Cheng, R. H. & Kawaoka, Y. 2006. Architecture of ribonucleoprotein complexes in influenza A virus particles. *Nature,* 439**,** 490-2. 10.1038/nature04378

Noshi, T., Kitano, M., Taniguchi, K., Yamamoto, A., Omoto, S., Baba, K., Hashimoto, T., Ishida, K., Kushima, Y., Hattori, K., Kawai, M., Yoshida, R., Kobayashi, M., Yoshinaga, T., Sato, A., Okamatsu, M., Sakoda, Y., Kida, H., Shishido, T. & Naito, A. 2018. In vitro characterization of baloxavir acid, a first-in-class cap-dependent endonuclease inhibitor of the influenza virus polymerase PA subunit. *Antiviral Res,* 160**,** 109-117. 10.1016/j.antiviral.2018.10.008

O'neill, R. E., Jaskunas, R., Blobel, G., Palese, P. & Moroianu, J. 1995. Nuclear import of influenza virus RNA can be mediated by viral nucleoprotein and transport factors required for protein import. *J Biol Chem,* 270**,** 22701-4. 10.1074/jbc.270.39.22701

O'neill, R. E., Talon, J. & Palese, P. 1998. The influenza virus NEP (NS2 protein) mediates the nuclear export of viral ribonucleoproteins. *EMBO J,* 17**,** 288-96. 10.1093/emboj/17.1.288

Obri, A., Ouararhni, K., Papin, C., Diebold, M. L., Padmanabhan, K., Marek, M., Stoll, I., Roy, L., Reilly, P. T., Mak, T. W., Dimitrov, S., Romier, C. & Hamiche, A. 2014. ANP32E is a histone chaperone that removes H2A.Z from chromatin. *Nature,* 505**,** 648-53. 10.1038/nature12922

Olson, A. C., Rosenblum, E. & Kuchta, R. D. 2010. Regulation of influenza RNA polymerase activity and the switch between replication and transcription by the concentrations of the vRNA 5' end, the cap source, and the polymerase. *Biochemistry,* 49**,** 10208-15. 10.1021/bi101011j

Ong, S. E., Blagoev, B., Kratchmarova, I., Kristensen, D. B., Steen, H., Pandey, A. & Mann, M. 2002. Stable isotope labeling by amino acids in cell culture, SILAC, as a simple and accurate approach to expression proteomics. *Mol Cell Proteomics,* 1**,** 376-86. 10.1074/mcp.m200025-mcp200

Oymans, J. & Te Velthuis, A. J. W. 2018. A Mechanism for Priming and Realignment during Influenza A Virus Replication. *J Virol,* 92. 10.1128/JVI.01773-17

Park, S. Y., Choi, H. C., Chun, Y. H., Kim, H. & Park, S. H. 2001. Characterization of chromosomal aberrations in lung cancer cell lines by cross-species color banding. *Cancer Genet Cytogenet,* 124**,** 62-70. 10.1016/s0165-4608(00)00329-0

Patton, J. G., Porro, E. B., Galceran, J., Tempst, P. & Nadal-Ginard, B. 1993. Cloning and characterization of PSF, a novel pre-mRNA splicing factor. *Genes Dev,* 7**,** 393-406. 10.1101/gad.7.3.393

Paules, C. & Subbarao, K. 2017. Influenza. *Lancet,* 390**,** 697-708. 10.1016/S0140-6736(17)30129-0

Pavlovic, J., Haller, O. & Staeheli, P. 1992. Human and mouse Mx proteins inhibit different steps of the influenza virus multiplication cycle. *J Virol,* 66**,** 2564-9. 10.1128/JVI.66.4.2564-2569.1992

Peacock, T. P., Sheppard, C. M., Lister, M. G., Staller, E., Frise, R., Swann, O. C., Goldhill, D. H., Long, J. S. & Barclay, W. S. 2023. Mammalian ANP32A and ANP32B Proteins Drive Differential Polymerase Adaptations in Avian Influenza Virus. *J Virol,* 97**,** e0021323. 10.1128/jvi.00213-23

Peacock, T. P., Sheppard, C. M., Staller, E. & Barclay, W. S. 2019. Host Determinants of Influenza RNA Synthesis. *Annu Rev Virol,* 6**,** 215-233. 10.1146/annurev-virology-092917-043339

Peng, K. J., Wang, J. H., Su, W. T., Wang, X. C., Yang, F. T. & Nie, W. H. 2010. Characterization of two human lung adenocarcinoma cell lines by reciprocal chromosome painting. *Dongwuxue Yanjiu,* 31**,** 113-21. 10.3724/SP.J.1141.2010.02113

Peng, Q., Liu, Y., Peng, R., Wang, M., Yang, W., Song, H., Chen, Y., Liu, S., Han, M., Zhang, X., Wang, P., Yan, J., Zhang, B., Qi, J., Deng, T., Gao, G. F. & Shi, Y. 2019. Structural insight into RNA synthesis by influenza D polymerase. *Nat Microbiol,* 4**,** 1750-1759. 10.1038/s41564-019-0487-5

Peng, R., Xu, X., Nepal, B., Gong, Y., Li, F., Ferretti, M. B., Zhou, M., Lynch, K. W., Burslem, G. M., Kortagere, S., Marmorstein, R. & Chang, Y. W. 2025. Molecular basis of influenza ribonucleoprotein complex assembly and processive RNA synthesis. *Science,* 388**,** eadq7597. 10.1126/science.adq7597

Perez, G., Barber, G. P., Benet-Pages, A., Casper, J., Clawson, H., Diekhans, M., Fischer, C., Gonzalez, J. N., Hinrichs, A. S., Lee, C. M., Nassar, L. R., Raney, B. J., Speir, M. L., Van Baren, M. J., Vaske, C. J., Haussler, D., Kent, W. J. & Haeussler, M. 2025. The UCSC Genome Browser database: 2025 update. *Nucleic Acids Res,* 53**,** D1243-D1249. 10.1093/nar/gkae974

Perez, J. T., Varble, A., Sachidanandam, R., Zlatev, I., Manoharan, M., Garcia-Sastre, A. & Tenoever, B. R. 2010. Influenza A virus-generated small RNAs regulate the switch from transcription to replication. *Proc Natl Acad Sci U S A,* 107**,** 11525-30. 10.1073/pnas.1001984107

Perez, J. T., Zlatev, I., Aggarwal, S., Subramanian, S., Sachidanandam, R., Kim, B., Manoharan, M. & Tenoever, B. R. 2012. A small-RNA enhancer of viral polymerase activity. *J Virol,* 86**,** 13475-85. 10.1128/JVI.02295-12

Perez-Gonzalez, A., Rodriguez, A., Huarte, M., Salanueva, I. J. & Nieto, A. 2006. hCLE/CGI-99, a human protein that interacts with the influenza virus polymerase, is a mRNA transcription modulator. *J Mol Biol,* 362**,** 887-900. 10.1016/j.jmb.2006.07.085

Peterl, S., Lahr, C. M., Schneider, C. N., Meyer, J., Podlipensky, X., Lechner, V., Villiou, M., Eis, L., Klein, S., Funaya, C., Cavalcanti-Adam, E. A., Graw, F., Selhuber-Unkel, C., Rohr, K. & Chlanda, P. 2025. Morphology-dependent entry kinetics and spread of influenza A virus. *EMBO J,* 44**,** 3959-3982. 10.1038/s44318-025-00481-6

Petric, P. P., Schwemmle, M. & Graf, L. 2023. Anti-influenza A virus restriction factors that shape the human species barrier and virus evolution. *PLoS Pathog,* 19**,** e1011450. 10.1371/journal.ppat.1011450

Pettersen, E. F., Goddard, T. D., Huang, C. C., Meng, E. C., Couch, G. S., Croll, T. I., Morris, J. H. & Ferrin, T. E. 2021. UCSF ChimeraX: Structure visualization for researchers, educators, and developers. *Protein Sci,* 30**,** 70-82. 10.1002/pro.3943

Pflug, A., Guilligay, D., Reich, S. & Cusack, S. 2014. Structure of influenza A polymerase bound to the viral RNA promoter. *Nature,* 516**,** 355-60. 10.1038/nature14008

Pflug, A., Lukarska, M., Resa-Infante, P., Reich, S. & Cusack, S. 2017. Structural insights into RNA synthesis by the influenza virus transcription-replication machine. *Virus Res,* 234**,** 103-117. 10.1016/j.virusres.2017.01.013

Phan, T., Fay, E. J., Lee, Z., Aron, S., Hu, W. S. & Langlois, R. A. 2021. Segment-specific kinetics of mRNA, cRNA and vRNA accumulation during influenza infection. *J Virol,* 95. 10.1128/JVI.02102-20

Philippon, D. a. M., Wu, P., Cowling, B. J. & Lau, E. H. Y. 2020. Avian Influenza Human Infections at the Human-Animal Interface. *J Infect Dis,* 222**,** 528-537. 10.1093/infdis/jiaa105

Piersimoni, L., Kastritis, P. L., Arlt, C. & Sinz, A. 2022. Cross-Linking Mass Spectrometry for Investigating Protein Conformations and Protein-Protein Interactions horizontal line A Method for All Seasons. *Chem Rev,* 122**,** 7500-7531. 10.1021/acs.chemrev.1c00786

Pinto, R. M., Bakshi, S., Lytras, S., Zakaria, M. K., Swingler, S., Worrell, J. C., Herder, V., Hargrave, K. E., Varjak, M., Cameron-Ruiz, N., Collados Rodriguez, M., Varela, M., Wickenhagen, A., Loney, C., Pei, Y., Hughes, J., Valette, E., Turnbull, M. L., Furnon, W., Gu, Q., Orr, L., Taggart, A., Diebold, O., Davis, C., Boutell, C., Grey, F., Hutchinson, E., Digard, P., Monne, I., Wootton, S. K., Macleod, M. K. L., Wilson, S. J. & Palmarini, M. 2023. BTN3A3 evasion promotes the zoonotic potential of influenza A viruses. *Nature,* 619**,** 338-347. 10.1038/s41586-023-06261-8

Pinto, R. M., Lycett, S., Gaunt, E. & Digard, P. 2021. Accessory Gene Products of Influenza A Virus. *Cold Spring Harb Perspect Med,* 11. 10.1101/cshperspect.a038380

Pirillo, C., Al Khalidi, S., Sims, A., Devlin, R., Zhao, H., Pinto, R., Jasim, S., Shearer, P. A., Shergold, A. L., Donnelly, H., Bravo-Blas, A., Loney, C., Perona-Wright, G., Hutchinson, E. & Roberts, E. W. 2023. Cotransfer of antigen and contextual information harmonizes peripheral and lymph node conventional dendritic cell activation. *Sci Immunol,* 8**,** eadg8249. 10.1126/sciimmunol.adg8249

Plaza, P. I., Gamarra-Toledo, V., Rodriguez Eugui, J., Rosciano, N. & Lambertucci, S. A. 2024. Pacific and Atlantic sea lion mortality caused by highly pathogenic Avian Influenza A(H5N1) in South America. *Travel Med Infect Dis,* 59**,** 102712. 10.1016/j.tmaid.2024.102712

Plotch, S. J., Bouloy, M. & Krug, R. M. 1979. Transfer of 5'-terminal cap of globin mRNA to influenza viral complementary RNA during transcription in vitro. *Proc Natl Acad Sci U S A,* 76**,** 1618-22. 10.1073/pnas.76.4.1618

Poon, L. L., Pritlove, D. C., Fodor, E. & Brownlee, G. G. 1999. Direct evidence that the poly(A) tail of influenza A virus mRNA is synthesized by reiterative copying of a U track in the virion RNA template. *J Virol,* 73**,** 3473-6. 10.1128/JVI.73.4.3473-3476.1999

Pu, J., Wang, S., Yin, Y., Zhang, G., Carter, R. A., Wang, J., Xu, G., Sun, H., Wang, M., Wen, C., Wei, Y., Wang, D., Zhu, B., Lemmon, G., Jiao, Y., Duan, S., Wang, Q., Du, Q., Sun, M., Bao, J., Sun, Y., Zhao, J., Zhang, H., Wu, G., Liu, J. & Webster, R. G. 2015. Evolution of the H9N2 influenza genotype that facilitated the genesis of the novel H7N9 virus. *Proc Natl Acad Sci U S A,* 112**,** 548-53. 10.1073/pnas.1422456112

Pulit-Penaloza, J. A., Brock, N., Belser, J. A., Sun, X., Pappas, C., Kieran, T. J., Basu Thakur, P., Zeng, H., Cui, D., Frederick, J., Fasce, R., Tumpey, T. M. & Maines, T. R. 2024. Highly pathogenic avian influenza A(H5N1) virus of clade 2.3.4.4b isolated from a human case in Chile causes fatal disease and transmits between co-housed ferrets. *Emerg Microbes Infect,* 13**,** 2332667. 10.1080/22221751.2024.2332667

Puryear, W., Sawatzki, K., Hill, N., Foss, A., Stone, J. J., Doughty, L., Walk, D., Gilbert, K., Murray, M., Cox, E., Patel, P., Mertz, Z., Ellis, S., Taylor, J., Fauquier, D., Smith, A., Digiovanni, R. A., Jr., Van De Guchte, A., Gonzalez-Reiche, A. S., Khalil, Z., Van Bakel, H., Torchetti, M. K., Lantz, K., Lenoch, J. B. & Runstadler, J. 2023. Highly Pathogenic Avian Influenza A(H5N1) Virus Outbreak in New England Seals, United States. *Emerg Infect Dis,* 29**,** 786-791. 10.3201/eid2904.221538

Puschnik, A. S., Majzoub, K., Ooi, Y. S. & Carette, J. E. 2017. A CRISPR toolbox to study virus-host interactions. *Nat Rev Microbiol,* 15**,** 351-364. 10.1038/nrmicro.2017.29

Ramanathan, M., Majzoub, K., Rao, D. S., Neela, P. H., Zarnegar, B. J., Mondal, S., Roth, J. G., Gai, H., Kovalski, J. R., Siprashvili, Z., Palmer, T. D., Carette, J. E. & Khavari, P.

A. 2018. RNA-protein interaction detection in living cells. *Nat Methods,* 15**,** 207-212. 10.1038/nmeth.4601
Ramanathan, M., Porter, D. F. & Khavari, P. A. 2019. Methods to study RNA-protein interactions. *Nat Methods,* 16**,** 225-234. 10.1038/s41592-019-0330-1
Rameix-Welti, M. A., Tomoiu, A., Dos Santos Afonso, E., Van Der Werf, S. & Naffakh, N. 2009. Avian Influenza A virus polymerase association with nucleoprotein, but not polymerase assembly, is impaired in human cells during the course of infection. *J Virol,* 83**,** 1320-31. 10.1128/JVI.00977-08
Ramos, I. & Fernandez-Sesma, A. 2015. Modulating the Innate Immune Response to Influenza A Virus: Potential Therapeutic Use of Anti-Inflammatory Drugs. *Front Immunol,* 6**,** 361. 10.3389/fimmu.2015.00361
Ran, F. A., Hsu, P. D., Wright, J., Agarwala, V., Scott, D. A. & Zhang, F. 2013. Genome engineering using the CRISPR-Cas9 system. *Nat Protoc,* 8**,** 2281-2308. 10.1038/nprot.2013.143
Rasmussen, A. B., Swann, O. C., Sukhova, K., Liu, N., Brown, M. D., Martin-Sancho, L., Sheppard, C. M. & Barclay, W. S. 2025. Influenza A virus polymerase co-opts distinct sets of host proteins for RNA transcription or replication. *bioRxiv***,** 2025.06.06.658254. 10.1101/2025.06.06.658254
Rehwinkel, J., Tan, C. P., Goubau, D., Schulz, O., Pichlmair, A., Bier, K., Robb, N., Vreede, F., Barclay, W., Fodor, E. & Reis E Sousa, C. 2010. RIG-I detects viral genomic RNA during negative-strand RNA virus infection. *Cell,* 140**,** 397-408. 10.1016/j.cell.2010.01.020
Reich, S., Guilligay, D., Pflug, A., Malet, H., Berger, I., Crepin, T., Hart, D., Lunardi, T., Nanao, M., Ruigrok, R. W. & Cusack, S. 2014. Structural insight into cap-snatching and RNA synthesis by influenza polymerase. *Nature,* 516**,** 361-6. 10.1038/nature14009
Reilly, P. T., Yu, Y., Hamiche, A. & Wang, L. 2014. Cracking the ANP32 whips: important functions, unequal requirement, and hints at disease implications. *Bioessays,* 36**,** 1062-71. 10.1002/bies.201400058
Resa-Infante, P., Jorba, N., Zamarreno, N., Fernandez, Y., Juarez, S. & Ortin, J. 2008. The host-dependent interaction of alpha-importins with influenza PB2 polymerase subunit is required for virus RNA replication. *PLoS One,* 3**,** e3904. 10.1371/journal.pone.0003904
Resa-Infante, P., Recuero-Checa, M. A., Zamarreno, N., Llorca, O. & Ortin, J. 2010. Structural and functional characterization of an influenza virus RNA polymerase-genomic RNA complex. *J Virol,* 84**,** 10477-87. 10.1128/JVI.01115-10
Reuther, P., Giese, S., Gotz, V., Kilb, N., Manz, B., Brunotte, L. & Schwemmle, M. 2014. Adaptive mutations in the nuclear export protein of human-derived H5N1 strains facilitate a polymerase activity-enhancing conformation. *J Virol,* 88**,** 263-71. 10.1128/JVI.01495-13
Rhee, H. W., Zou, P., Udeshi, N. D., Martell, J. D., Mootha, V. K., Carr, S. A. & Ting, A. Y. 2013. Proteomic mapping of mitochondria in living cells via spatially restricted enzymatic tagging. *Science,* 339**,** 1328-1331. 10.1126/science.1230593
Rhodes, D. A., De Bono, B. & Trowsdale, J. 2005. Relationship between SPRY and B30.2 protein domains. Evolution of a component of immune defence? *Immunology,* 116**,** 411-7. 10.1111/j.1365-2567.2005.02248.x
Rhodes, D. A., Stammers, M., Malcherek, G., Beck, S. & Trowsdale, J. 2001. The cluster of BTN genes in the extended major histocompatibility complex. *Genomics,* 71**,** 351-62. 10.1006/geno.2000.6406
Rialdi, A., Hultquist, J., Jimenez-Morales, D., Peralta, Z., Campisi, L., Fenouil, R., Moshkina, N., Wang, Z. Z., Laffleur, B., Kaake, R. M., Mcgregor, M. J., Haas, K., Pefanis, E., Albrecht, R. A., Pache, L., Chanda, S., Jen, J., Ochando, J., Byun, M., Basu, U., Garcia-Sastre, A., Krogan, N., Van Bakel, H. & Marazzi, I. 2017. The RNA Exosome Syncs IAV-RNAPII Transcription to Promote Viral Ribogenesis and Infectivity. *Cell,* 169**,** 679-692 e14. 10.1016/j.cell.2017.04.021

Richard, M., De Graaf, M. & Herfst, S. 2014. Avian influenza A viruses: from zoonosis to pandemic. *Future Virol,* 9**,** 513-524. 10.2217/fvl.14.30

Rivero-Rodriguez, F., Diaz-Quintana, A., Velazquez-Cruz, A., Gonzalez-Arzola, K., Gavilan, M. P., Velazquez-Campoy, A., Rios, R. M., De La Rosa, M. A. & Diaz-Moreno, I. 2021. Inhibition of the PP2A activity by the histone chaperone ANP32B is long-range allosterically regulated by respiratory cytochrome c. *Redox Biol,* 43**,** 101967. 10.1016/j.redox.2021.101967

Roach, S. N., Shepherd, F. K., Mickelson, C. K., Fiege, J. K., Thielen, B. K., Pross, L. M., Sanders, A. E., Mitchell, J. S., Robertson, M., Fife, B. T. & Langlois, R. A. 2024. Tropism for ciliated cells is the dominant driver of influenza viral burst size in the human airway. *Proc Natl Acad Sci U S A,* 121**,** e2320303121. 10.1073/pnas.2320303121

Robb, N. C., Chase, G., Bier, K., Vreede, F. T., Shaw, P. C., Naffakh, N., Schwemmle, M. & Fodor, E. 2011. The influenza A virus NS1 protein interacts with the nucleoprotein of viral ribonucleoprotein complexes. *J Virol,* 85**,** 5228-31. 10.1128/JVI.02562-10

Robb, N. C., Smith, M., Vreede, F. T. & Fodor, E. 2009. NS2/NEP protein regulates transcription and replication of the influenza virus RNA genome. *J Gen Virol,* 90**,** 1398-1407. 10.1099/vir.0.009639-0

Robb, N. C., Te Velthuis, A. J. W., Fodor, E. & Kapanidis, A. N. 2019. Real-time analysis of single influenza virus replication complexes reveals large promoter-dependent differences in initiation dynamics. *Nucleic Acids Res,* 47**,** 6466-6477. 10.1093/nar/gkz313

Rodriguez, A., Perez-Gonzalez, A. & Nieto, A. 2007. Influenza virus infection causes specific degradation of the largest subunit of cellular RNA polymerase II. *J Virol,* 81**,** 5315-24. 10.1128/JVI.02129-06

Rodriguez, A., Perez-Gonzalez, A. & Nieto, A. 2011. Cellular human CLE/C14orf166 protein interacts with influenza virus polymerase and is required for viral replication. *J Virol,* 85**,** 12062-6. 10.1128/JVI.00684-11

Rodriguez-Frandsen, A., De Lucas, S., Perez-Gonzalez, A., Perez-Cidoncha, M., Roldan-Gomendio, A., Pazo, A., Marcos-Villar, L., Landeras-Bueno, S., Ortin, J. & Nieto, A. 2016. hCLE/C14orf166, a cellular protein required for viral replication, is incorporated into influenza virus particles. *Sci Rep,* 6**,** 20744. 10.1038/srep20744

Ross, P. L., Huang, Y. N., Marchese, J. N., Williamson, B., Parker, K., Hattan, S., Khainovski, N., Pillai, S., Dey, S., Daniels, S., Purkayastha, S., Juhasz, P., Martin, S., Bartlet-Jones, M., He, F., Jacobson, A. & Pappin, D. J. 2004. Multiplexed protein quantitation in Saccharomyces cerevisiae using amine-reactive isobaric tagging reagents. *Mol Cell Proteomics,* 3**,** 1154-69. 10.1074/mcp.M400129-MCP200

Roux, K. J., Kim, D. I., Raida, M. & Burke, B. 2012. A promiscuous biotin ligase fusion protein identifies proximal and interacting proteins in mammalian cells. *J Cell Biol,* 196**,** 801-10. 10.1083/jcb.201112098

Schaack, G. A. & Mehle, A. 2020. Experimental Approaches to Identify Host Factors Important for Influenza Virus. *Cold Spring Harb Perspect Med,* 10. 10.1101/cshperspect.a038521

Schneekloth, J. S., Jr., Fonseca, F. N., Koldobskiy, M., Mandal, A., Deshaies, R., Sakamoto, K. & Crews, C. M. 2004. Chemical genetic control of protein levels: selective in vivo targeted degradation. *J Am Chem Soc,* 126**,** 3748-54. 10.1021/ja039025z

Schneider, C. A., Rasband, W. S. & Eliceiri, K. W. 2012. NIH Image to ImageJ: 25 years of image analysis. *Nat Methods,* 9**,** 671-5. 10.1038/nmeth.2089

Schneider, R., Bannister, A. J., Weise, C. & Kouzarides, T. 2004. Direct binding of INHAT to H3 tails disrupted by modifications. *J Biol Chem,* 279**,** 23859-62. 10.1074/jbc.C400151200

Scholtissek, C., Rohde, W., Von Hoyningen, V. & Rott, R. 1978. On the origin of the human influenza virus subtypes H2N2 and H3N2. *Virology,* 87**,** 13-20. 10.1016/0042-6822(78)90153-8

Schuller, R., Forne, I., Straub, T., Schreieck, A., Texier, Y., Shah, N., Decker, T. M., Cramer, P., Imhof, A. & Eick, D. 2016. Heptad-Specific Phosphorylation of RNA Polymerase II CTD. *Mol Cell,* 61**,** 305-14. 10.1016/j.molcel.2015.12.003

Serna Martin, I., Hengrung, N., Renner, M., Sharps, J., Martinez-Alonso, M., Masiulis, S., Grimes, J. M. & Fodor, E. 2018. A Mechanism for the Activation of the Influenza Virus Transcriptase. *Mol Cell,* 72**,** 396. 10.1016/j.molcel.2018.10.005

Shannon, P., Markiel, A., Ozier, O., Baliga, N. S., Wang, J. T., Ramage, D., Amin, N., Schwikowski, B. & Ideker, T. 2003. Cytoscape: a software environment for integrated models of biomolecular interaction networks. *Genome Res,* 13**,** 2498-504. 10.1101/gr.1239303

Shapira, S. D., Gat-Viks, I., Shum, B. O., Dricot, A., De Grace, M. M., Wu, L., Gupta, P. B., Hao, T., Silver, S. J., Root, D. E., Hill, D. E., Regev, A. & Hacohen, N. 2009. A physical and regulatory map of host-influenza interactions reveals pathways in H1N1 infection. *Cell,* 139**,** 1255-67. 10.1016/j.cell.2009.12.018

Shapiro, G. I. & Krug, R. M. 1988. Influenza virus RNA replication in vitro: synthesis of viral template RNAs and virion RNAs in the absence of an added primer. *J Virol,* 62**,** 2285-90. 10.1128/JVI.62.7.2285-2290.1988

Shaw, M. L., Stone, K. L., Colangelo, C. M., Gulcicek, E. E. & Palese, P. 2008. Cellular proteins in influenza virus particles. *PLoS Pathog,* 4**,** e1000085. 10.1371/journal.ppat.1000085

Sheppard, C. M., Goldhill, D. H., Swann, O. C., Staller, E., Penn, R., Platt, O. K., Sukhova, K., Baillon, L., Frise, R., Peacock, T. P., Fodor, E. & Barclay, W. S. 2023. An Influenza A virus can evolve to use human ANP32E through altering polymerase dimerization. *Nat Commun,* 14**,** 6135. 10.1038/s41467-023-41308-4

Shin, H., He, M., Yang, Z., Jeon, Y. H., Pfleger, J., Sayed, D. & Abdellatif, M. 2018. Transcriptional regulation mediated by H2A.Z via ANP32e-dependent inhibition of protein phosphatase 2A. *Biochim Biophys Acta Gene Regul Mech,* 1861**,** 481-496. 10.1016/j.bbagrm.2018.03.002

Silva, S. T. N., Brito, J. A., Arranz, R., Sorzano, C. O. S., Ebel, C., Doutch, J., Tully, M. D., Carazo, J. M., Carrascosa, J. L., Matias, P. M. & Bandeiras, T. M. 2018. X-ray structure of full-length human RuvB-Like 2 - mechanistic insights into coupling between ATP binding and mechanical action. *Sci Rep,* 8**,** 13726. 10.1038/s41598-018-31997-z

Smith, I., Greenside, P. G., Natoli, T., Lahr, D. L., Wadden, D., Tirosh, I., Narayan, R., Root, D. E., Golub, T. R., Subramanian, A. & Doench, J. G. 2017. Evaluation of RNAi and CRISPR technologies by large-scale gene expression profiling in the Connectivity Map. *PLoS Biol,* 15**,** e2003213. 10.1371/journal.pbio.2003213

Soderberg, O., Gullberg, M., Jarvius, M., Ridderstrale, K., Leuchowius, K. J., Jarvius, J., Wester, K., Hydbring, P., Bahram, F., Larsson, L. G. & Landegren, U. 2006. Direct observation of individual endogenous protein complexes in situ by proximity ligation. *Nat Methods,* 3**,** 995-1000. 10.1038/nmeth947

Staeheli, P., Haller, O., Boll, W., Lindenmann, J. & Weissmann, C. 1986. Mx protein: constitutive expression in 3T3 cells transformed with cloned Mx cDNA confers selective resistance to influenza virus. *Cell,* 44**,** 147-58. 10.1016/0092-8674(86)90493-9

Staller, E., Carrique, L., Swann, O. C., Fan, H., Keown, J. R., Sheppard, C. M., Barclay, W. S., Grimes, J. M. & Fodor, E. 2024. Structures of H5N1 influenza polymerase with ANP32B reveal mechanisms of genome replication and host adaptation. *Nat Commun,* 15**,** 4123. 10.1038/s41467-024-48470-3

Staller, E., Sheppard, C. M., Neasham, P. J., Mistry, B., Peacock, T. P., Goldhill, D. H., Long, J. S. & Barclay, W. S. 2019. ANP32 Proteins Are Essential for Influenza Virus Replication in Human Cells. *J Virol,* 93. 10.1128/JVI.00217-19

Starkova, T., Polyanichko, A., Tomilin, A. N. & Chikhirzhina, E. 2023. Structure and Functions of HMGB2 Protein. *Int J Mol Sci,* 24. 10.3390/ijms24098334

Stauffer, S., Feng, Y., Nebioglu, F., Heilig, R., Picotti, P. & Helenius, A. 2014. Stepwise priming by acidic pH and a high K+ concentration is required for efficient uncoating of influenza A virus cores after penetration. *J Virol,* 88**,** 13029-46. 10.1128/JVI.01430-14

Stott, K., Watson, M., Howe, F. S., Grossmann, J. G. & Thomas, J. O. 2010. Tail-mediated collapse of HMGB1 is dynamic and occurs via differential binding of the acidic tail to the A and B domains. *J Mol Biol,* 403**,** 706-22. 10.1016/j.jmb.2010.07.045

Stremlau, M., Owens, C. M., Perron, M. J., Kiessling, M., Autissier, P. & Sodroski, J. 2004. The cytoplasmic body component TRIM5alpha restricts HIV-1 infection in Old World monkeys. *Nature,* 427**,** 848-53. 10.1038/nature02343

Stremlau, M., Perron, M., Welikala, S. & Sodroski, J. 2005. Species-specific variation in the B30.2(SPRY) domain of TRIM5alpha determines the potency of human immunodeficiency virus restriction. *J Virol,* 79**,** 3139-45. 10.1128/JVI.79.5.3139-3145.2005

Subbarao, E. K., London, W. & Murphy, B. R. 1993. A single amino acid in the PB2 gene of influenza A virus is a determinant of host range. *J Virol,* 67**,** 1761-4. 10.1128/JVI.67.4.1761-1764.1993

Sugiyama, K., Kawaguchi, A., Okuwaki, M. & Nagata, K. 2015. pp32 and APRIL are host cell-derived regulators of influenza virus RNA synthesis from cRNA. *Elife,* 4. 10.7554/eLife.08939

Sun, J., Kuai, L., Zhang, L., Xie, Y., Zhang, Y., Li, Y., Peng, Q., Shao, Y., Yang, Q., Tian, W. X., Zhu, J., Qi, J., Shi, Y., Deng, T. & Gao, G. F. 2024a. NS2 induces an influenza A RNA polymerase hexamer and acts as a transcription to replication switch. *EMBO Rep,* 25**,** 4708-4727. 10.1038/s44319-024-00208-4

Sun, L., Guo, X., Yu, M., Wang, X. F., Ren, H. & Wang, X. 2024b. Human ANP32A/B are SUMOylated and utilized by avian influenza virus NS2 protein to overcome species-specific restriction. *Nat Commun,* 15**,** 10805. 10.1038/s41467-024-55034-y

Sun, L., Kong, H., Yu, M., Zhang, Z., Zhang, H., Na, L., Qu, Y., Zhang, Y., Chen, H. & Wang, X. 2023. The SUMO-interacting motif in NS2 promotes adaptation of avian influenza virus to mammals. *Sci Adv,* 9**,** eadg5175. 10.1126/sciadv.adg5175

Swann, O. C. 2023. *Visualising and quantifying the RNA products of influenza A virus polymerase for insights into regulation and host restriction.* PhD, Imperial College London.

Swann, O. C., Rasmussen, A. B., Peacock, T. P., Sheppard, C. M. & Barclay, W. S. 2023. Avian Influenza A Virus Polymerase Can Utilize Human ANP32 Proteins To Support cRNA but Not vRNA Synthesis. *mBio,* 14**,** e0339922. 10.1128/mbio.03399-22

Szklarczyk, D., Kirsch, R., Koutrouli, M., Nastou, K., Mehryary, F., Hachilif, R., Gable, A. L., Fang, T., Doncheva, N. T., Pyysalo, S., Bork, P., Jensen, L. J. & Von Mering, C. 2023. The STRING database in 2023: protein-protein association networks and functional enrichment analyses for any sequenced genome of interest. *Nucleic Acids Res,* 51**,** D638-D646. 10.1093/nar/gkac1000

Tarendeau, F., Boudet, J., Guilligay, D., Mas, P. J., Bougault, C. M., Boulo, S., Baudin, F., Ruigrok, R. W., Daigle, N., Ellenberg, J., Cusack, S., Simorre, J. P. & Hart, D. J. 2007. Structure and nuclear import function of the C-terminal domain of influenza virus polymerase PB2 subunit. *Nat Struct Mol Biol,* 14**,** 229-33. 10.1038/nsmb1212

Taubenberger, J. K. & Kash, J. C. 2010. Influenza virus evolution, host adaptation, and pandemic formation. *Cell Host Microbe,* 7**,** 440-51. 10.1016/j.chom.2010.05.009

Taubenberger, J. K. & Morens, D. M. 2006. 1918 Influenza: the mother of all pandemics. *Emerg Infect Dis,* 12**,** 15-22. 10.3201/eid1201.050979

Te Velthuis, A. J., Robb, N. C., Kapanidis, A. N. & Fodor, E. 2016. The role of the priming loop in Influenza A virus RNA synthesis. *Nat Microbiol,* 1. 10.1038/nmicrobiol.2016.29

Te Velthuis, A. J., Turrell, L., Vreede, F. T. & Fodor, E. 2013. Uncoupling of influenza A virus transcription and replication through mutation of the unpaired adenosine in the viral RNA promoter. *J Virol,* 87**,** 10381-4. 10.1128/JVI.00636-13

Te Velthuis, A. J. W., Long, J. S. & Barclay, W. S. 2018. Assays to Measure the Activity of Influenza Virus Polymerase. *Methods Mol Biol,* 1836**,** 343-374. 10.1007/978-1-4939-8678-1_17
Te Velthuis, A. J. W. & Oymans, J. 2018. Initiation, Elongation, and Realignment during Influenza Virus mRNA Synthesis. *J Virol,* 92. 10.1128/JVI.01775-17
Thierry, E., Guilligay, D., Kosinski, J., Bock, T., Gaudon, S., Round, A., Pflug, A., Hengrung, N., El Omari, K., Baudin, F., Hart, D. J., Beck, M. & Cusack, S. 2016. Influenza Polymerase Can Adopt an Alternative Configuration Involving a Radical Repacking of PB2 Domains. *Mol Cell,* 61**,** 125-37. 10.1016/j.molcel.2015.11.016
Tochio, N., Umehara, T., Munemasa, Y., Suzuki, T., Sato, S., Tsuda, K., Koshiba, S., Kigawa, T., Nagai, R. & Yokoyama, S. 2010. Solution structure of histone chaperone ANP32B: interaction with core histones H3-H4 through its acidic concave domain. *J Mol Biol,* 401**,** 97-114. 10.1016/j.jmb.2010.06.005
Travers, A. A. 2003. Priming the nucleosome: a role for HMGB proteins? *EMBO Rep,* 4**,** 131-6. 10.1038/sj.embor.embor741
Turrell, L., Hutchinson, E. C., Vreede, F. T. & Fodor, E. 2015. Regulation of influenza A virus nucleoprotein oligomerization by phosphorylation. *J Virol,* 89**,** 1452-5. 10.1128/JVI.02332-14
Turrell, L., Lyall, J. W., Tiley, L. S., Fodor, E. & Vreede, F. T. 2013. The role and assembly mechanism of nucleoprotein in influenza A virus ribonucleoprotein complexes. *Nat Commun,* 4**,** 1591. 10.1038/ncomms2589
Tyanova, S., Temu, T., Sinitcyn, P., Carlson, A., Hein, M. Y., Geiger, T., Mann, M. & Cox, J. 2016. The Perseus computational platform for comprehensive analysis of (prote)omics data. *Nat Methods,* 13**,** 731-40. 10.1038/nmeth.3901
Verhelst, J., Hulpiau, P. & Saelens, X. 2013. Mx proteins: antiviral gatekeepers that restrain the uninvited. *Microbiol Mol Biol Rev,* 77**,** 551-66. 10.1128/MMBR.00024-13
Verhelst, J., Parthoens, E., Schepens, B., Fiers, W. & Saelens, X. 2012. Interferon-inducible protein Mx1 inhibits influenza virus by interfering with functional viral ribonucleoprotein complex assembly. *J Virol,* 86**,** 13445-55. 10.1128/JVI.01682-12
Vreede, F. T. & Brownlee, G. G. 2007. Influenza virion-derived viral ribonucleoproteins synthesize both mRNA and cRNA in vitro. *J Virol,* 81**,** 2196-204. 10.1128/JVI.02187-06
Vreede, F. T., Chan, A. Y., Sharps, J. & Fodor, E. 2010. Mechanisms and functional implications of the degradation of host RNA polymerase II in influenza virus infected cells. *Virology,* 396**,** 125-34. 10.1016/j.virol.2009.10.003
Vreede, F. T., Jung, T. E. & Brownlee, G. G. 2004. Model suggesting that replication of influenza virus is regulated by stabilization of replicative intermediates. *J Virol,* 78**,** 9568-72. 10.1128/JVI.78.17.9568-9572.2004
Walker, A. P. & Fodor, E. 2019. Interplay between Influenza Virus and the Host RNA Polymerase II Transcriptional Machinery. *Trends Microbiol,* 27**,** 398-407. 10.1016/j.tim.2018.12.013
Wandzik, J. M., Kouba, T., Karuppasamy, M., Pflug, A., Drncova, P., Provaznik, J., Azevedo, N. & Cusack, S. 2020. A Structure-Based Model for the Complete Transcription Cycle of Influenza Polymerase. *Cell,* 181**,** 877-893 e21. 10.1016/j.cell.2020.03.061
Wang, D., Zhu, W., Yang, L. & Shu, Y. 2021a. The Epidemiology, Virology, and Pathogenicity of Human Infections with Avian Influenza Viruses. *Cold Spring Harb Perspect Med,* 11. 10.1101/cshperspect.a038620
Wang, F., Sheppard, C. M., Mistry, B., Staller, E., Barclay, W. S., Grimes, J. M., Fodor, E. & Fan, H. 2022a. The C-terminal LCAR of host ANP32 proteins interacts with the influenza A virus nucleoprotein to promote the replication of the viral RNA genome. *Nucleic Acids Res,* 50**,** 5713-5725. 10.1093/nar/gkac410
Wang, H., Li, B., Zuo, L., Wang, B., Yan, Y., Tian, K., Zhou, R., Wang, C., Chen, X., Jiang, Y., Zheng, H., Qin, F., Zhang, B., Yu, Y., Liu, C. P., Xu, Y., Gao, J., Qi, Z., Deng, W. & Ji, X. 2022b. The transcriptional coactivator RUVBL2 regulates Pol II clustering

with diverse transcription factors. *Nat Commun,* 13**,** 5703. 10.1038/s41467-022-33433-3
Wang, P., Palese, P. & O'neill, R. E. 1997. The NPI-1/NPI-3 (karyopherin alpha) binding site on the influenza a virus nucleoprotein NP is a nonconventional nuclear localization signal. *J Virol,* 71**,** 1850-6. 10.1128/JVI.71.3.1850-1856.1997
Wang, Y., Zhou, J., Mackintosh, S. G. & Du, Y. 2021b. RuvB-Like Protein 2 Interacts with the NS1 Protein of Influenza A Virus and Affects Apoptosis That Is Counterbalanced by Type I Interferons. *Viruses,* 13. 10.3390/v13061038
Watanabe, T., Kawakami, E., Shoemaker, J. E., Lopes, T. J., Matsuoka, Y., Tomita, Y., Kozuka-Hata, H., Gorai, T., Kuwahara, T., Takeda, E., Nagata, A., Takano, R., Kiso, M., Yamashita, M., Sakai-Tagawa, Y., Katsura, H., Nonaka, N., Fujii, H., Fujii, K., Sugita, Y., Noda, T., Goto, H., Fukuyama, S., Watanabe, S., Neumann, G., Oyama, M., Kitano, H. & Kawaoka, Y. 2014. Influenza virus-host interactome screen as a platform for antiviral drug development. *Cell Host Microbe,* 16**,** 795-805. 10.1016/j.chom.2014.11.002
Waterhouse, A. M., Procter, J. B., Martin, D. M., Clamp, M. & Barton, G. J. 2009. Jalview Version 2--a multiple sequence alignment editor and analysis workbench. *Bioinformatics,* 25**,** 1189-91. 10.1093/bioinformatics/btp033
Webster, R. G., Bean, W. J., Gorman, O. T., Chambers, T. M. & Kawaoka, Y. 1992. Evolution and ecology of influenza A viruses. *Microbiol Rev,* 56**,** 152-79. 10.1128/mr.56.1.152-179.1992
Who. 2025. *Influenza (seasonal)* [Online]. [Accessed 10/08/2025].
Wilhelm, S., Carter, C., Lynch, M., Lowinger, T., Dumas, J., Smith, R. A., Schwartz, B., Simantov, R. & Kelley, S. 2006. Discovery and development of sorafenib: a multikinase inhibitor for treating cancer. *Nat Rev Drug Discov,* 5**,** 835-44. 10.1038/nrd2130
Wise, H. M., Barbezange, C., Jagger, B. W., Dalton, R. M., Gog, J. R., Curran, M. D., Taubenberger, J. K., Anderson, E. C. & Digard, P. 2011. Overlapping signals for translational regulation and packaging of influenza A virus segment 2. *Nucleic Acids Res,* 39**,** 7775-90. 10.1093/nar/gkr487
Xiao, H., Killip, M. J., Staeheli, P., Randall, R. E. & Jackson, D. 2013. The human interferon-induced MxA protein inhibits early stages of influenza A virus infection by retaining the incoming viral genome in the cytoplasm. *J Virol,* 87**,** 13053-8. 10.1128/JVI.02220-13
Xiao, T., Li, X. & Felsenfeld, G. 2024. The Myc-associated zinc finger protein epigenetically controls expression of interferon-gamma-stimulated genes by recruiting STAT1 to chromatin. *Proc Natl Acad Sci U S A,* 121**,** e2320938121. 10.1073/pnas.2320938121
Xue, L., Chang, T., Li, Z., Wang, C., Zhao, H., Li, M., Tang, P., Wen, X., Yu, M., Wu, J., Bao, X., Wang, X., Gong, P., He, J., Chen, X. & Xiong, X. 2024. Cryo-EM structures of Thogoto virus polymerase reveal unique RNA transcription and replication mechanisms among orthomyxoviruses. *Nat Commun,* 15**,** 4620. 10.1038/s41467-024-48848-3
Yang, X., Lu, B., Sun, X., Han, C., Fu, C., Xu, K., Wang, M., Li, D., Chen, Z., Opal, P., Wen, Q., Crispino, J. D., Wang, Q. F. & Huang, Z. 2018. ANP32A regulates histone H3 acetylation and promotes leukemogenesis. *Leukemia,* 32**,** 1587-1597. 10.1038/s41375-018-0010-7
Yap, K., Chung, T. H. & Makeyev, E. V. 2022. Hybridization-proximity labeling reveals spatially ordered interactions of nuclear RNA compartments. *Mol Cell,* 82**,** 463-478 e11. 10.1016/j.molcel.2021.10.009
Ye, Q., Krug, R. M. & Tao, Y. J. 2006. The mechanism by which influenza A virus nucleoprotein forms oligomers and binds RNA. *Nature,* 444**,** 1078-82. 10.1038/nature05379
York, A. & Fodor, E. 2013. Biogenesis, assembly, and export of viral messenger ribonucleoproteins in the influenza A virus infected cell. *RNA Biol,* 10**,** 1274-82. 10.4161/rna.25356

York, A., Hengrung, N., Vreede, F. T., Huiskonen, J. T. & Fodor, E. 2013. Isolation and characterization of the positive-sense replicative intermediate of a negative-strand RNA virus. *Proc Natl Acad Sci U S A,* 110**,** E4238-45. 10.1073/pnas.1315068110

York, A., Hutchinson, E. C. & Fodor, E. 2014. Interactome analysis of the influenza A virus transcription/replication machinery identifies protein phosphatase 6 as a cellular factor required for efficient virus replication. *J Virol,* 88**,** 13284-99. 10.1128/JVI.01813-14

Yu, M., Sun, L., Zhang, Z., Zhang, Y., Zhang, H., Na, L. & Wang, X. 2022. KPNA6 is a Cofactor of ANP32A/B in Supporting Influenza Virus Polymerase Activity. *Microbiol Spectr,* 10**,** e0207321. 10.1128/spectrum.02073-21

Yuan, P., Bartlam, M., Lou, Z., Chen, S., Zhou, J., He, X., Lv, Z., Ge, R., Li, X., Deng, T., Fodor, E., Rao, Z. & Liu, Y. 2009. Crystal structure of an avian influenza polymerase PA(N) reveals an endonuclease active site. *Nature,* 458**,** 909-13. 10.1038/nature07720

Zhang, H., Zhang, Z., Wang, Y., Wang, M., Wang, X., Zhang, X., Ji, S., Du, C., Chen, H. & Wang, X. 2019. Fundamental Contribution and Host Range Determination of ANP32A and ANP32B in Influenza A Virus Polymerase Activity. *J Virol,* 93. 10.1128/JVI.00174-19

Zhang, L., Shao, Y., Wang, Y., Yang, Q., Guo, J., Gao, G. F. & Deng, T. 2024. Twenty natural amino acid substitution screening at the last residue 121 of influenza A virus NS2 protein reveals the critical role of NS2 in promoting virus genome replication by coordinating with viral polymerase. *J Virol,* 98**,** e0116623. 10.1128/jvi.01166-23

Zhang, L., Wang, Y., Shao, Y., Guo, J., Gao, G. F. & Deng, T. 2023. Fine Regulation of Influenza Virus RNA Transcription and Replication by Stoichiometric Changes in Viral NS1 and NS2 Proteins. *J Virol,* 97**,** e0033723. 10.1128/jvi.00337-23

Zhang, L., Yang, Q., Shao, Y., Ding, S., Guo, J., Gao, G. F. & Deng, T. 2025a. Influenza A virus NS2 protein acts on vRNA-resident polymerase to drive the transcription to replication switch. *Nucleic Acids Res,* 53. 10.1093/nar/gkaf027

Zhang, T., Zhang, X., Sun, Z., Liu, G., Hou, X. & Wei, L. 2020. Duck HMGB2 Mediates Signaling Pathways in the Innate Immunity of Hosts Against Viral Infections. *Front Immunol,* 11**,** 572289. 10.3389/fimmu.2020.572289

Zhang, Z., Aziati, I. D., Nipper, T., Boon, A. C. M. & Mehle, A. 2025b. ANP32 proteins from ticks and vertebrates are key host factors for replication of Bourbon virus across species. *J Virol,* 99**,** e0052225. 10.1128/jvi.00522-25

Zheng, X., Lu, J., Liu, J., Zhou, L. & He, Y. 2023. HMGB family proteins: Potential biomarkers and mechanistic factors in cardiovascular diseases. *Biomed Pharmacother,* 165**,** 115118. 10.1016/j.biopha.2023.115118

Zhu, Z., Fan, H. & Fodor, E. 2023a. Defining the minimal components of the influenza A virus replication machinery via an in vitro reconstitution system. *PLoS Biol,* 21**,** e3002370. 10.1371/journal.pbio.3002370

Zhu, Z., Fodor, E. & Keown, J. R. 2023b. A structural understanding of influenza virus genome replication. *Trends Microbiol,* 31**,** 308-319. 10.1016/j.tim.2022.09.015

Zimmermann, P., Manz, B., Haller, O., Schwemmle, M. & Kochs, G. 2011. The viral nucleoprotein determines Mx sensitivity of influenza A viruses. *J Virol,* 85**,** 8133-40. 10.1128/JVI.00712-11

Zou, J., Tian, S., Zhu, Y., Cheng, Y., Jiang, M., Tu, S., Jin, M., Chen, H. & Zhou, H. 2023. Prohibitin1 facilitates viral replication by impairing the RIG-I-like receptor signaling pathway. *J Virol,* 97**,** e0092623. 10.1128/jvi.00926-23

Zurcher, T., Pavlovic, J. & Staeheli, P. 1992. Mechanism of human MxA protein action: variants with changed antiviral properties. *EMBO J,* 11**,** 1657-61. 10.1002/j.1460-2075.1992.tb05212.x

Appendices

Appendix A.

Proteins co-precipitating from WT cells and ANP32-KO cells infected with PR8 PB2-FLAG or PR8 WT (negative background control). Proteins were identified by mass spectrometry. Raw values are shown as label-free quantification (LFQ) intensities, which gives a normalised estimate of the protein abundance in each sample. Statistical analysis was performed using Perseus software v2.0.11. The LFQ intensities were used to calculate the significance of the protein enrichment in PR8 PB2-FLAG-infected cells versus in PR8 WT-infected cells (negative background control) for each cell type using a *t* test (two-sided, equal variance, S_0=0.2) and corrected for multiple hypotheses using the false discovery rate (FDR=0.05). Proteins enriched in PR8 PB2-FLAG-infected samples (hits) are shown by black plus sign. Proteins enriched in PR8 WT-infected samples (negative background control) are shown by grey plus sign.

	LFQ intensity																	
	WT cells																	
	PR8 PB2-FLAG									PR8 PB2-WT								
Gene names	**Exp 1.1**	**Exp 1.2**	**Exp 1.3**	**Exp 2.1**	**Exp 2.2**	**Exp 2.3**	**Exp 3.1**	**Exp 3.2**	**Exp 3.3**	**Exp 1.1**	**Exp 1.2**	**Exp 1.3**	**Exp 2.1**	**Exp 2.2**	**Exp 2.3**	**Exp 3.1**	**Exp 3.2**	**Exp 3.3**
PDCD6	20.4907	21.0319	20.8252	21.7538	21.0473	21.2128	19.9558	19.997	19.3234	18.8429	19.015	18.858	18.9557	19.0484	19.0304	20.9469	20.5396	20.5326
PSMA2	20.8011	20.9476	19.5492	21.98	22.0555	21.5195	22.1334	21.843	22.2989	18.4176	18.5928	18.4327	21.1157	21.4149	21.1739	18.8529	18.8465	20.795
NP	28.9951	29.0079	29.0655	29.8657	29.8574	29.9287	30.0312	29.9176	29.909	24.8494	24.98	24.8516	26.0048	26.0661	26.0997	25.65	25.5857	25.6461
M1	23.7266	23.6867	23.7748	24.8121	24.9163	24.7783	24.6654	24.7207	24.6605	22.0703	22.3703	22.1366	23.6856	23.7139	23.6438	23.5997	23.8145	23.5591
PB2	27.9877	27.9863	28.0824	29.0991	29.0708	29.1008	28.8084	28.8018	28.7467	19.3866	20.0124	19.5867	21.9357	22.0973	22.2071	21.6814	21.5893	21.5822
MYEF2	22.026	21.8458	21.8538	22.0395	22.2084	22.0719	22.0704	22.0263	21.815	21.4912	21.6393	21.4167	21.5581	21.5792	21.5735	21.4991	21.6474	21.4133
ZC3H8	22.4658	21.9292	21.9345	22.0786	22.1641	22.0358	22.0548	19.9239	20.2145	17.6942	19.9464	21.9252	19.8166	19.9526	19.9358	19.7629	21.9789	19.8322
HSPA1B	23.8168	23.7839	23.9186	24.4244	24.4578	24.4281	24.6277	24.6739	24.5902	23.4978	23.5566	23.5168	23.5497	23.7348	23.6998	23.296	23.3164	23.5101
C4	22.8233	22.9223	21.958	23.0502	22.7982	22.8539	22.7953	23.0455	22.7488	22.7073	23.0051	23.1791	19.0462	19.7698	22.4446	22.6654	19.3597	18.9263
ME2	19.2493	19.988	20.1207	20.1127	19.9573	20.6116	21.633	21.3657	21.6557	18.4825	19.1079	19.2029	18.052	20.3076	19.8952	19.6386	19.8189	19.9419
SMARCE1	22.7304	18.5281	22.704	22.8963	22.8431	22.6575	22.841	18.3996	19.556	22.5824	19.2581	17.784	18.8365	19.9146	18.6824	19.0906	17.9875	18.9757
KIF23	20.9363	20.8654	20.4561	19.4831	18.9232	20.8686	19.7488	19.6256	20.8615	18.0691	19.0242	17.9238	18.6745	18.768	18.2833	18.102	19.7166	18.9286
SSR1	18.6614	18.7463	18.1243	22.8697	22.7051	23.1327	22.6359	22.3394	19.3782	18.7196	18.9585	19.7561	18.5521	18.9935	19.7733	19.5995	18.097	18.6365
CLUH	21.7614	21.4887	21.889	22.4123	22.4211	22.4889	22.4163	22.5486	22.0363	21.449	21.1578	21.2382	21.6186	21.2423	21.5316	21.3844	21.2896	21.0562
SDF4	19.5063	19.5755	18.7978	22.3165	22.3193	22.093	19.1868	22.0318	18.927	19.1286	18.1574	18.4408	19.4136	19.2632	18.8547	19.0691	19.156	18.0788
AMD1	19.0309	20.3536	20.2673	20.5583	19.8813	20.3485	19.925	20.0088	20.0832	19.875	19.716	17.9301	18.1202	19.0098	19.3062	18.8141	20.2974	18.1328
ACAT1	20.8032	21.1241	21.1166	21.6441	21.7383	21.7433	22.511	22.4995	22.269	20.356	20.4643	20.6009	20.4652	20.6912	20.6215	21.0838	20.9886	20.9709
PB1	27.221	27.295	27.1821	28.1466	28.321	28.1758	28.0169	28.0324	27.9653	19.6356	19.2433	18.9986	21.9466	22.0629	21.3396	21.2908	21.5391	21.5373
HARS	19.4409	20.4443	18.3553	21.085	20.7317	20.929	21.3831	21.0688	21.3621	18.4798	19.1861	20.0343	19.2906	19.024	18.6798	20.329	18.0098	20.4199
AIFM1	20.9188	21.0538	21.45	21.5488	21.8712	21.3446	21.9474	22.0874	21.9916	18.2467	21.0322	21.7301	21.4279	20.9756	21.6682	18.5005	18.0635	19.2566
POLR2A	26.605	26.6176	26.7317	27.6124	27.5281	27.6044	27.5923	27.5862	27.3459	24.6173	24.9819	24.9942	24.7737	25.1074	24.8473	24.315	24.7868	24.8418
HSPB1	22.7405	22.8242	22.8147	23.1561	23.1501	23.0545	24.2677	24.0719	24.1348	22.5207	22.8202	22.6265	22.0882	22.5297	22.4576	22.1722	22.261	22.2642
ACO2	19.5367	19.6116	19.5017	21.6581	18.952	21.4611	22.4625	22.8271	22.2663	19.558	19.1531	18.8686	20.1428	19.2145	18.0665	19.1889	18.8568	20.1142

MACF1	26.9692	27.065	26.9473	26.8254	26.3807	26.9651	26.9827	26.8856	26.9319	26.5935	26.8673	26.8638	19.0318	26.9714	26.7252	20.0441	19.0134	18.777
VRK1	21.7538	21.42	21.416	21.6436	21.1709	21.3731	21.5364	21.5171	21.6693	20.9207	20.1324	20.5427	20.7518	21.0474	20.968	20.739	20.9938	20.6456
AKAP8	21.0355	20.9299	20.9803	21.2319	22.0249	21.397	21.0445	20.9533	20.9993	18.6965	19.011	19.5728	19.3553	19.1243	18.6676	18.7108	20.2875	18.76
P4HB	21.7567	21.6791	21.6651	22.4625	22.3297	22.5231	23.5053	23.4661	23.3691	21.2667	21.0882	21.2087	21.2892	21.7598	21.6333	21.7586	21.6954	21.7446
AKAP8L	23.3584	23.0755	23.3273	23.9355	23.679	24.1645	23.6821	23.9422	23.6981	21.6855	21.9636	22.4331	21.7606	20.4719	20.85	18.9879	18.4825	20.316
HA	22.2009	22.2151	22.4117	23.3218	23.6582	23.3225	23.4432	23.6208	23.6301	19.7399	20.5351	19.9742	22.2979	22.201	21.9631	22.0738	21.8969	22.432
CNN2	20.6235	20.4283	20.5772	21.3162	20.9166	21.1948	22.093	22.1823	22.2339	18.46	20.9479	18.5604	18.5854	21.1057	19.0289	20.7971	21.0032	20.9426
CS	21.0852	20.1446	21.0806	23.0124	22.9942	23.0896	24.4512	24.3932	24.2145	18.8075	19.7305	18.4752	18.4905	18.6791	19.5552	21.7903	21.2534	22.2085
HSPE1	21.221	21.3988	21.6265	22.8849	22.5583	22.7867	23.941	24.3435	24.2105	18.8251	18.9998	18.6065	20.4835	20.829	20.0707	20.6316	20.7536	20.4604
PTMA	22.3403	22.4607	22.3378	20.7864	22.7317	20.9583	24.0096	23.816	24.0811	18.3984	18.4911	18.8401	18.7125	19.8697	18.9816	19.8153	22.3267	22.4791
POLR2B	23.5085	23.3886	23.4594	24.0697	24.1021	24.1037	24.0255	23.985	23.8372	21.9453	22.0835	22.0709	21.9718	22.1269	22.1347	21.9268	21.9815	21.9958
CYCS	19.9033	18.5038	20.652	21.7033	20.8932	21.0682	22.0545	22.3439	21.8589	19.2619	19.5204	18.9137	19.6527	19.5961	19.7263	20.3477	20.4707	20.0595
POLR2H	23.2501	23.3671	23.6069	24.1259	24.0654	23.7723	24.0573	24.1895	24.1739	22.3422	22.4658	22.4896	22.4966	23.0191	22.9386	22.2263	22.6566	22.118
EIF4G2	19.9191	20.5891	20.1502	20.7403	21.0461	21.3044	21.6438	21.4548	21.4208	18.3152	19.2223	18.8426	20.3346	20.2551	20.1157	20.5894	20.3939	20.891
HSPA9	24.7023	24.6543	24.8088	25.5309	25.5949	25.5367	25.5816	25.6479	25.529	23.9771	24.071	23.9547	24.1733	24.3254	24.3024	24.18	24.1308	24.1361
NDUFV2	19.661	19.4738	19.0577	20.4494	20.2087	18.7894	18.934	20.4255	20.7778	19.0517	19.1934	17.877	17.878	17.9738	19.5872	17.7715	18.3354	19.415
STAU2	21.1966	21.1854	21.1075	21.3038	20.8257	21.2617	21.7445	21.4724	21.479	20.9857	20.8936	20.753	20.7135	20.8377	20.7381	20.6665	20.4977	20.2952
CSTF3	18.8471	23.1172	23.1605	22.8263	18.9379	23.4732	23.0007	23.1417	23.4473	18.6977	19.101	19.8119	22.5089	19.0866	18.1506	19.0273	19.3832	18.9581
ZC3H11A	21.0331	20.6998	20.7819	20.8644	21.0144	21.0736	21.3243	21.4587	20.9133	20.2022	20.4567	20.3513	19.6635	20.4741	19.5654	20.3333	20.8519	20.6562
PHF8	23.1823	19.2808	22.7686	23.6238	19.6533	22.9199	21.6577	19.2072	21.2625	18.4892	17.33	18.0293	21.1759	19.7588	18.6677	21.2545	18.9281	21.3988
ESD	18.7701	18.5629	19.4142	19.2885	20.0233	20.2026	21.25	21.3479	21.3105	18.6096	18.7284	18.6875	18.7712	18.8177	19.7417	18.5166	18.9852	18.5822
SF1	19.1147	20.5268	19.1977	19.2362	20.6046	19.5211	18.9688	20.9452	19.7004	19.2574	18.8881	18.6247	17.9412	17.4117	18.6958	18.0485	18.6616	18.1128
PHKG2	19.8847	18.8309	19.9685	20.3386	20.9796	21.4201	19.5612	19.2043	19.1372	18.8622	18.0098	18.5693	18.1541	18.884	18.6889	19.7057	19.2715	17.6863
CALR	20.5829	20.3764	20.8094	22.2636	22.4361	22.5048	24.7871	24.6416	24.7838	19.1734	18.3484	19.2732	19.9703	19.7556	20.0304	20.9552	20.0021	21.5957
PRKCSH	18.747	19.6529	19.6564	19.2947	20.513	19.2015	22.8466	22.9703	23.1027	18.7713	18.999	19.3077	19.8057	18.1183	17.3916	18.2931	19.7703	20.8126
SARS2	22.2065	22.0269	22.2105	22.285	22.0929	22.1828	22.1915	22.0368	22.1077	21.662	21.8739	21.8316	21.4985	21.7894	21.817	21.51	21.4769	21.5622
HAX1	21.7491	22.1423	22.3397	23.0312	23.8769	23.1384	23.0588	23.4584	23.594	18.455	20.4138	18.1867	18.6866	19.6374	19.4263	19.2551	20.1068	18.6924
SUPT5H	20.7784	21.3301	21.4214	22.1435	22.3168	21.865	19.7244	21.7034	21.3724	18.7114	19.3008	18.8418	18.357	18.072	19.4306	18.5727	18.744	17.9808
CLIC1	21.9063	21.1777	21.3135	21.8889	21.6328	21.4937	22.3216	22.9617	22.8153	21.0478	20.8436	20.1239	21.2882	21.3779	21.5715	21.2158	21.251	21.3156
KPNA3	23.0177	23.0673	23.1447	23.8082	23.658	23.7921	23.7396	23.7137	23.4566	22.1275	22.4452	22.3275	22.4379	22.5588	22.618	22.6098	22.5196	22.5055
AURKA	21.0135	21.1601	21.7411	20.9705	20.2915	21.0787	21.1335	21.0943	21.3054	19.6549	19.136	19.8432	18.832	19.4057	19.6202	19.1736	17.9123	18.7951
PPM1G	21.4727	21.0792	21.4124	21.8864	22.0004	22.1001	22.3221	22.2921	21.9859	21.036	21.0489	21.1555	21.2496	21.2846	21.048	21.4815	21.2685	21.2004
IPO8	20.1181	19.2079	18.6356	19.7704	19.9708	19.6519	19.9012	19.9093	19.1421	19.6285	19.1218	18.29	19.3574	18.4009	17.2886	18.2013	18.7226	19.2412
POLR2D	20.7464	21.1426	21.003	22.1548	22.0969	22.1474	21.5763	21.9767	21.606	18.9505	18.3706	19.6697	19.3908	19.0328	19.0812	18.8372	18.8651	18.8498
PJA2	21.9382	21.8	21.9976	23.0212	23.0078	23.0304	22.512	22.551	22.3621	18.1938	18.2322	19.1351	19.5465	18.4528	19.3882	18.6607	19.2822	17.1638
PAPSS1	20.5053	19.8895	18.6644	19.6065	19.9904	19.6566	19.5725	19.856	20.0231	18.0544	19.3917	19.3135	17.9764	18.8574	18.3821	18.4765	19.4381	19.7765
TIMM44	20.3163	20.5688	19.9875	21.5713	20.7651	21.4716	21.199	21.3699	20.8815	19.5252	19.6921	19.9217	17.211	19.8316	18.8392	20.0269	19.9156	19.963
GTPBP6	21.1042	21.1218	21.1489	21.0433	21.3356	21.3774	19.7544	19.6163	18.536	20.4738	19.7139	18.209	18.3063	19.6081	19.9819	20.2202	17.0992	18.3183
CALU	22.4557	22.4018	22.4057	23.4697	23.5458	23.6685	23.2521	23.6225	23.3163	21.6197	21.7245	21.7322	21.7069	21.8011	21.8778	21.5241	21.5453	21.2161
SNX2	20.1146	20.1779	19.2112	20.141	19.9958	19.9248	20.6042	20.6202	20.6621	18.6171	18.5249	19.5618	19.9713	19.4877	19.7193	20.051	18.4708	19.1997
DNAJA2	23.0654	23.0427	23.2492	23.8344	23.6776	23.7279	23.5629	23.6354	23.4838	22.3219	22.451	22.4053	22.5235	22.7127	22.794	22.5614	22.5104	22.6326
PMPCB	21.3157	21.263	21.2959	21.8257	21.807	21.8682	22.024	21.7446	21.8932	20.9052	21.2578	21.101	21.2016	21.3833	20.9929	20.923	21.1341	21.027
GPC4	21.161	20.9459	20.4373	22.4857	22.2112	22.3975	21.8864	21.8141	21.9171	21.0064	20.5468	20.156	19.3964	20.7604	20.1686	18.9573	19.1253	20.1535
HSBP1	21.0011	20.8756	21.1287	21.724	21.2264	21.9033	21.5253	21.6152	21.8517	18.9393	21.2222	21.0447	21.3967	18.288	21.277	18.2229	19.6329	19.6841
ERAL1	21.1472	21.1131	21.4144	21.3565	21.234	21.5832	21.3393	21.2129	21.237	20.7535	20.682	20.7129	20.737	20.8523	20.9344	20.681	20.4885	20.6048
CLPX	21.1538	20.9358	20.9829	21.3064	21.3893	21.4925	21.5845	21.3422	21.6295	19.8427	18.9497	20.192	20.3295	20.709	18.5546	20.4539	20.2493	21.0235

UBR5	21.9497	21.9294	21.8773	23.506	23.4737	23.6401	22.9151	22.7553	22.8695	19.7039	20.0743	19.5737	20.5349	20.9759	20.7868	20.756	20.705	20.7762
BAG2	21.6398	21.6066	21.8705	23.5785	23.7395	23.7168	23.1516	23.184	23.1612	20.6503	20.594	20.6952	18.5505	19.9441	21.5752	18.4463	21.2929	21.3032
LDHA	21.8696	21.5401	21.7262	22.8839	22.8637	22.8757	24.9396	24.7964	24.7038	20.6309	20.8036	20.4095	21.9427	21.9128	21.798	22.034	22.0063	22.0729
GLUD1	21.1353	20.5605	20.6802	21.3294	21.4	21.313	21.9263	22.0687	22.1414	19.7894	18.7032	20.0629	19.6366	20.0409	20.6467	19.5361	19.1848	18.5117
PGK1	21.7123	21.9554	21.6613	22.666	22.7301	22.7842	24.6079	24.8038	24.6802	17.6672	18.7671	19.4006	20.9523	20.7191	21.42	21.2752	21.7617	21.6407
TFRC	19.5126	19.7724	18.4495	20.7969	20.8872	20.6605	22.5344	22.4853	22.4777	17.5967	19.2654	17.8712	19.8027	18.5723	18.6109	20.1187	21.0171	20.5409
OAT	18.2969	20.3529	19.596	21.9253	21.1217	21.417	21.9294	22.4779	21.6322	18.7566	18.6813	18.0761	18.4515	19.1413	18.5537	21.2081	21.0062	21.362
TP53	20.4452	21.1172	21.2243	21.8179	21.899	21.5263	21.6874	21.6325	21.4833	20.3171	20.2062	20.6019	20.4118	20.4488	18.8756	20.716	20.7319	20.6419
HIST2H2B	23.2743	22.9522	22.9197	23.4454	23.3605	23.2605	23.6145	23.3941	23.3661	22.7842	23.0004	22.8851	22.7524	22.9068	22.8835	18.9464	20.091	17.9756
PFN1	20.2914	19.8623	19.7575	22.3021	22.2059	22.2107	24.6298	25.0658	24.7519	19.5786	18.9437	19.9868	20.2611	20.217	20.0774	20.9642	20.5278	19.4031
HSP90AA1	22.8533	22.7989	22.9948	23.8878	23.7785	23.8286	25.1784	25.1567	25.0564	22.3875	22.6514	22.5164	22.8109	22.9723	22.8657	23.1287	23.0678	23.2255
SNRPB2	20.7051	21.0335	21.2595	21.6542	21.6825	21.6671	21.7263	21.6539	21.6816	20.6286	20.5193	20.2268	21.0188	20.6371	21.1789	20.1594	20.4227	19.0133
ANXA5	19.2526	19.4032	18.5428	19.5428	18.7159	19.2728	21.93	22.1654	22.1144	19.0951	18.473	18.6083	18.0202	19.9985	18.0943	19.2559	18.3416	18.7668
GSTP1	23.3856	23.3628	23.539	23.9507	23.7645	23.911	25.5805	25.608	25.5656	23.083	23.3254	23.1874	22.873	23.3681	23.1846	22.9721	23.0523	23.0949
HMGB1	22.7945	22.4961	22.9138	22.7338	23.3625	23.1289	24.2681	24.7066	24.9175	22.4839	22.53	22.5477	19.8057	21.1401	20.6593	23.0506	23.2797	23.284
CALM	23.4796	23.2169	23.5599	24.5838	24.2723	24.3477	25.2314	25.1897	25.2736	22.9668	23.3631	23.287	23.3008	23.273	23.2144	22.9305	22.9835	23.176
HSPD1	25.9004	25.8936	25.9477	26.6857	26.7094	26.6237	27.1999	27.2415	27.1606	25.6069	25.7752	25.6798	25.8602	26.0025	26.0706	25.7936	25.847	25.9079
HSPA8	26.2636	26.2168	26.3261	27.2838	27.186	27.2945	27.3654	27.3973	27.3224	25.9421	25.9782	25.8806	26.156	26.2942	26.2429	26.0155	26.061	26.0455
PDHB	22.8226	22.6142	22.4347	22.967	22.8976	22.9553	23.1154	23.0885	23.0797	22.1773	22.5285	22.2061	22.2626	22.4502	22.1904	22.3515	22.2239	22.4685
RALA	19.2205	18.9398	19.7829	20.7934	20.5085	20.4655	20.5971	18.2166	19.6373	18.2472	18.5768	18.7861	18.754	18.9651	18.3181	18.6505	18.8981	17.8248
ETFA	20.7843	20.8551	20.2154	21.2277	21.208	21.1953	21.8937	21.8357	21.7766	18.9958	19.7316	18.2624	20.2334	20.1024	20.3074	20.6748	20.4756	20.6054
PGAM1	18.5129	19.445	19.018	21.3987	20.7582	21.9656	24.218	24.1125	23.5695	19.1979	17.9247	19.105	19.6672	18.8076	18.8146	18.8365	17.757	19.232
HK1	19.316	20.0165	20.0917	19.6172	19.0789	20.1107	20.8526	21.0952	20.7146	19.4893	18.8387	19.026	18.7395	19.2916	18.468	19.1644	18.1319	20.1486
POLR2C	24.6393	24.7988	24.7728	25.5577	25.4571	25.432	25.2866	25.1013	25.1932	23.0419	23.4751	23.2476	23.6078	23.5323	23.7184	23.5722	23.4125	23.6175
POLR2E	23.0636	22.9051	23.0306	23.7063	23.8035	23.8046	23.8473	23.7714	23.8174	22.2196	22.2323	22.4149	22.0598	22.1701	22.0028	22.0549	21.9906	22.2338
PSMB1	18.4762	19.2476	18.5952	21.4287	21.2636	20.3408	23.5377	22.5551	21.9977	18.4521	18.4706	19.2128	19.1996	18.7242	18.1382	18.5481	18.7628	18.702
PSMA1	21.6277	20.9884	21.4843	21.4912	22.0021	21.7932	22.6473	22.2991	22.2849	18.9885	18.1942	21.1492	21.1472	21.3918	21.1882	21.2575	19.1574	18.3526
PSMA3	18.491	19.5223	18.9397	21.556	21.2441	21.416	22.1251	22.3697	22.2908	20.881	18.655	18.9886	17.8546	18.9791	18.9611	18.2876	20.431	19.165
HMGB2	23.173	23.0426	23.1013	23.0237	23.0924	23.3496	24.5593	24.5581	24.3827	22.4255	22.8074	22.4558	21.9758	22.2896	22.062	23.4094	23.0941	23.2414
PSMB4	19.5457	18.9728	18.176	21.2601	18.9163	21.3598	22.2162	22.0703	22.1366	19.1111	18.5934	18.4673	19.3555	19.8205	19.8036	18.2033	19.559	18.0201
PSMB5	20.828	19.8121	20.3477	21.6359	21.392	21.1548	22.883	22.6506	22.6638	20.6109	18.9288	19.5183	19.8277	20.3056	18.4553	20.4273	20.0445	20.4165
ECHS1	21.0146	21.717	21.6595	22.1686	22.247	21.8867	23.1577	23.1359	22.8928	20.778	19.5691	17.76	21.9527	19.1217	21.4129	21.8968	21.2827	21.9014
PEBP1	20.4242	18.8131	18.6282	20.2878	18.9283	20.224	23.4878	23.2488	23.3464	18.2945	19.1153	19.6781	18.0619	18.5219	19.3525	19.4539	18.6046	19.0736
PDIA3	23.079	22.9777	23.036	23.8752	23.9347	23.9398	24.4728	24.4732	24.2281	22.9681	23.1304	23.0513	23.0376	23.0444	23.0278	22.8262	22.7968	22.9375
ALDH1B1	21.2542	21.0137	20.9433	21.6076	21.7243	21.7228	22.0142	21.8697	22.1667	20.4185	20.7524	20.4519	20.2016	20.6966	20.8825	20.4296	20.9266	20.7714
DNAJA1	23.8135	23.8031	23.8577	24.4052	24.4118	24.5134	24.5666	24.573	24.6451	23.383	23.5416	23.494	23.472	23.7533	23.7678	23.3951	23.4599	23.4821
UQCRC1	19.9463	19.1428	20.8281	21.5175	21.3001	21.03	21.1591	20.4447	21.3366	20.1751	19.3936	18.3097	18.4277	19.2434	19.1927	19.0065	19.0907	18.3398
ATIC	19.8031	19.3952	20.0301	19.0659	19.7053	18.8956	21.7874	21.6945	21.5605	17.2981	19.2732	18.3611	19.2784	19.2104	19.5772	19.63	18.1981	18.02
PYCR1	20.5403	20.5071	20.7735	21.1512	20.7521	20.9765	21.7182	21.1732	21.3425	18.0161	18.8008	20.1897	19.1947	19.5944	19.3731	18.2748	17.9514	18.9924
HSPA4	21.6865	21.1582	21.8193	22.1161	21.8033	21.8799	22.6522	22.6431	22.5774	21.0314	21.2943	21.2402	21.2926	21.5542	21.5076	21.0635	21.1642	21.2804
PHB1	22.6577	22.6463	22.8048	22.7668	22.7736	22.6672	23.0569	23.1101	23.1365	22.1659	22.3458	22.1316	21.9292	22.1647	22.2229	22.1096	22.195	22.3219
POLR2I	22.8765	22.9714	23.0656	23.6711	23.5339	23.7716	23.3955	23.4839	23.5658	21.4021	21.6158	21.6039	21.5287	19.3906	21.4145	21.1719	21.2201	21.373
TALDO1	19.9855	18.7803	20.0694	19.6539	19.2071	18.7977	20.6927	20.9582	20.9743	18.4182	19.0562	18.4954	19.1183	18.4462	19.6545	18.9255	17.7438	18.3882
MDH2	20.8564	20.4147	21.3643	22.6338	22.581	22.5915	24.589	24.3274	24.3905	19.5415	18.7222	20.1213	19.299	18.8285	19.1389	20.3397	20.9238	20.0003
MAP1B	23.1893	23.1904	23.2087	23.9095	23.8984	23.9276	23.7127	23.7212	23.6698	22.8075	22.9666	22.8302	22.8212	22.8763	22.8815	22.7834	22.7445	22.7743
NES	21.5985	21.481	21.7764	21.925	22.207	21.657	22.0427	22.0653	22.0395	21.2912	21.3215	21.4075	21.104	20.4025	21.4973	21.2008	21.4086	20.543

TUFM	24.9124	24.9114	24.9346	25.4582	25.4738	25.4815	25.3648	25.4016	25.3827	24.2221	24.2684	24.2415	24.2007	24.2756	24.2536	24.112	24.1199	24.2367
EMD	23.2023	23.3317	23.2329	23.9615	23.9894	24.1356	23.802	23.7607	23.8009	22.5576	22.583	22.5753	22.8691	22.6984	22.6573	22.6589	22.5544	22.636
HDGF	18.7001	21.0156	21.3168	20.4472	21.446	20.9434	22.6984	22.29	22.4122	20.6579	19.3641	19.2685	20.244	20.7561	17.5389	20.8738	19.3949	20.6792
POLR2J	22.1631	22.34	22.2595	23.1661	23.2307	23.0551	23.2145	23.5539	23.3903	21.3302	21.4068	19.0118	21.5887	21.5261	20.9274	21.5935	22.0706	21.8286
SMS	19.3137	19.8891	18.3784	21.9201	21.8398	19.2826	21.9038	21.9776	22.0036	17.707	19.5919	18.4911	17.4617	18.8771	18.2321	21.3762	19.1902	19.5624
BLVRA	19.1243	18.6419	19.6435	19.6556	19.3621	19.5816	21.6799	21.1798	19.4392	18.2938	17.7842	18.2475	18.156	17.7723	18.6803	19.4939	18.2417	19.1591
SLC16A1	21.4185	21.4591	21.0769	22.3318	21.8509	22.2405	21.6243	22.1138	22.2118	20.7994	21.0079	20.9049	21.3259	21.0355	21.2144	17.7871	20.9095	21.3417
RAD23B	17.9608	19.9527	18.0253	20.0889	21.0478	19.1446	20.4569	22.5974	22.1259	18.5067	19.2815	18.4782	19.6313	18.2511	17.8536	17.5687	18.8455	19.718
ALDH18A1	21.6437	21.663	21.7549	22.1302	22.1604	22.5305	22.4522	22.4365	22.762	21.7401	21.3953	21.6035	21.2966	21.2931	21.5689	21.2482	21.6731	21.3306
HADHB	20.9629	20.9276	21.6748	21.9482	22.3565	22.0153	22.1564	22.2614	21.9038	21.1477	21.4004	20.4019	20.7949	21.0255	20.8554	20.9805	20.936	20.7526
MAZ	23.1058	22.7117	23.0735	22.4672	23.2084	22.8269	23.2681	23.0764	23.1498	19.0921	18.9745	23.2448	22.5983	22.4643	21.9102	22.9204	18.9874	18.3858
SEC61B	22.9198	23	22.7738	23.5835	23.5222	23.2099	23.1437	23.0145	23.1703	22.6956	22.4744	22.2405	22.3754	22.3012	22.8264	22.1874	22.0782	22.4052
RAB2	21.3655	21.0929	20.263	21.5765	21.6916	21.8344	22.7717	21.7231	21.45	19.1946	18.2449	19.1705	19.3245	20.5787	19.3986	20.7619	21.2364	21.5517
UBE2N	21.2769	21.4359	21.4366	22.0131	21.5958	21.6068	22.7431	22.6797	22.5627	21.1071	21.3698	20.7808	19.2072	20.2668	21.1977	21.2528	21.021	21.6288
POLR2G	20.6714	20.2505	20.4385	21.3472	21.573	21.6814	21.266	21.3512	20.7407	18.9296	18.7346	18.9082	18.9876	17.8731	19.0705	18.7915	18.6744	18.835
POLR2L	22.789	22.8906	22.5971	23.5951	23.5411	23.6374	23.6935	23.7985	23.5878	21.8546	22.4359	21.3195	22.1852	22.5609	22.4194	22.0843	21.8356	22.073
SARNP	21.2713	21.0612	21.318	21.4301	21.6302	21.5601	22.6111	22.7907	22.5382	19.2643	20.1474	19.8945	19.3166	19.9412	19.8055	21.6939	21.3691	21.5517
FKBP3	21.2958	21.1888	21.2329	21.2668	21.7836	21.6799	22.3304	22.5126	22.4444	18.8085	19.635	18.03	18.4246	18.9312	17.9337	21.5777	21.7178	21.4183
CAP1	19.391	20.7067	19.9844	20.2513	19.0477	20.4892	22.2118	22.0337	21.651	20.0748	18.8006	19.729	18.4613	19.0802	19.7645	18.7863	19.9813	19.6818
FKBP4	19.1832	20.1735	19.3095	20.7475	20.6231	20.2901	22.6285	22.9844	23.1314	18.5604	19.9417	19.1547	19.258	19.4443	18.5369	18.6435	17.666	18.3253
AHNAK	22.7347	22.3806	22.7117	23.3608	23.3054	23.4628	24.2224	24.2738	24.2823	22.2314	21.4845	22.0726	22.4807	22.6726	22.5662	22.5963	22.7867	22.8237
DHRS2	20.2243	19.3545	20.7291	21.3032	19.978	18.7879	18.9285	19.463	20.7443	18.9935	19.405	19.2108	17.7566	19.3498	19.3791	18.2603	18.5608	17.7513
LBR	22.4634	22.439	22.7925	22.8639	22.4838	23.269	22.4473	22.769	22.7675	19.2064	22.2571	22.6957	18.2054	22.2089	19.317	22.1523	22.4395	22.419
EIF4H	21.0987	21.1284	20.982	21.6943	21.9705	21.7999	23.8532	23.6583	23.2912	19.1859	19.412	19.7653	18.9224	19.7008	18.2814	21.9112	21.9597	21.8302
RCN1	20.7792	20.9498	20.7431	19.0193	21.3418	19.3475	22.711	22.4855	22.2229	19.0308	17.1989	18.7441	20.1471	18.2498	18.6949	19.0947	20.3912	19.1808
TRIP13	20.4522	20.9483	17.8229	20.6837	20.2468	19.4281	20.9863	21.1863	21.0128	19.4407	18.897	18.095	19.3105	20.7151	18.9971	18.1134	19.0877	18.8798
NSDHL	21.2131	20.6895	20.3944	21.3602	21.1944	21.6529	21.5309	21.4995	21.4106	18.5594	21.035	19.8522	21.2206	19.3346	20.2198	18.9016	17.9776	20.9924
MLF2	18.6076	20.7393	19.7187	21.3261	21.6498	21.3978	21.5156	21.494	21.6458	17.4051	20.0844	19.2214	18.6825	18.5212	19.3846	19.2034	18.8951	18.3875
NDUFA9	20.6994	20.7444	20.5894	21.6635	20.7807	21.2875	21.1003	21.2809	21.1465	20.588	18.3254	20.5855	19.4155	20.1186	20.7398	20.4608	20.761	18.6446
PDS5A	20.3497	20.3514	20.2177	21.1269	21.1004	21.1082	21.4195	21.1647	21.056	19.9898	19.9708	17.6644	19.1013	19.2803	20.7122	20.6701	20.5727	20.4248
NME1	22.6354	22.8146	22.9897	23.7321	23.8334	23.829	24.6057	24.5909	24.4775	22.7828	22.654	22.5779	22.7915	22.7187	22.62	22.8351	22.7258	22.8175
MAGED2	21.1102	20.7794	21.1608	21.5344	21.7064	21.4707	21.3696	21.4417	21.3824	20.7859	18.909	19.1059	21.2848	21.1707	21.0018	20.6665	20.8245	18.278
RNF219	20.998	21.461	21.2885	22.56	22.6656	22.9141	22.2347	22.4174	22.4304	17.8434	19.2363	19.021	19.0015	19.6506	18.9204	18.5157	18.8859	19.0769
RPAP2	19.4711	20.5616	20.5524	21.4545	21.6914	22.2525	22.0035	21.8433	21.6929	18.7215	18.2101	18.4924	18.425	18.4684	18.9383	17.6814	18.9828	18.3222
ENAH	19.3965	18.9689	19.2323	20.5515	19.7043	19.0145	21.2478	21.2814	21.1338	18.5998	18.4486	18.8949	19.2717	18.7976	18.7626	18.6311	19.4513	18.8267
HJURP	19.8507	20.6895	20.3948	20.4174	21.3282	20.3858	20.7083	20.9649	20.2469	19.5321	20.5265	19.0411	17.1864	20.007	18.5007	19.5328	19.7255	17.5201
RB1CC1	24.9837	25.2083	25.3341	26.227	26.2043	26.1225	26.487	26.7471	26.8158	18.9598	24.0763	19.8989	24.647	24.9046	25.0445	25.6347	25.466	25.5034
ZNF622	20.767	20.6617	21.0525	21.1913	21.1179	21.3667	21.5607	21.1884	21.0033	18.6107	18.5316	17.8857	20.3075	20.3767	20.7683	19.433	19.0284	19.3087
FUBP1	21.5298	21.845	21.7634	22.4431	22.033	22.3135	22.9573	23.3407	23.4805	19.7336	18.5375	20.0068	20.8889	21.2569	18.0654	22.2554	21.9757	22.5274
THAP11	19.3817	20.2858	19.0822	21.0512	19.9067	20.2767	20.7892	20.5853	20.6301	18.018	19.2195	19.5187	18.9561	17.7878	20.5839	20.0258	18.5719	18.8038
DNAJA3	22.9935	23.4117	23.4394	23.5867	23.772	23.7679	23.6773	23.871	23.7262	22.9285	23.0878	22.6612	22.6374	22.9227	22.9456	22.6872	22.7564	22.5209
CDKN2AIPNL	20.2187	19.1361	18.8413	22.1153	22.6176	22.377	19.8037	21.1386	18.9789	18.4933	18.1669	18.5353	19.1589	20.7104	18.3597	20.811	18.5778	18.7032
CNDP2	19.0556	18.5872	20.3029	19.8123	20.1794	20.4864	20.2601	20.388	19.2409	17.9645	18.8664	18.6781	20.1096	19.9767	18.2721	18.6094	17.4628	18.5637
RBM14	23.3321	23.4076	23.5101	24.1162	24.0807	24.0741	24.037	24.0491	23.8746	22.5981	22.8035	22.7779	22.5091	22.6376	22.6152	22.4811	22.6031	22.5588
PHB2	22.9329	22.9694	23.092	23.2421	23.3305	23.1584	23.6125	23.6685	23.4221	22.4209	22.7293	22.5775	22.3603	22.452	22.4587	22.5576	22.5433	22.5767
CLPB	21.815	21.7432	21.7237	23.0797	22.967	22.607	22.4291	22.1525	22.0801	20.2764	19.8686	20.0395	20.4745	19.118	20.1236	20.2246	20.2484	20.2227

RAB1	23.2842	23.5217	23.6422	23.8065	23.9807	23.8943	24.3322	24.0596	24.2299	22.7355	23.0086	22.6485	22.8908	23.242	22.9351	23.3683	23.5691	23.5063
NOL6	19.1765	19.9703	19.2595	20.4566	20.1541	18.5536	21.0825	20.242	19.6664	17.9028	20.2825	18.9535	18.732	18.7371	18.234	19.0692	18.5129	18.3643
CACYBP	19.3987	18.9161	19.9734	18.5462	21.2041	21.016	21.5069	22.2136	21.3225	18.6125	18.9908	18.5616	18.7582	18.8749	19.1314	20.0946	17.9045	20.1277
SPC25	20.036	19.718	18.8494	20.9524	20.4831	20.692	19.4539	19.8912	19.966	19.7208	19.3656	19.0146	19.5389	18.8537	19.547	18.9663	18.9164	18.7231
RTN4	19.8995	21.5523	19.0368	21.8058	21.8396	22.0914	22.2406	22.0474	21.6693	19.8021	19.4999	17.4793	17.361	19.1492	18.8332	21.3085	21.1401	21.5769
TECR	22.1374	22.0955	22.3223	22.24	22.4784	22.3389	22.1694	22.1527	22.0692	21.9323	19.4929	22.0941	22.0983	18.6395	21.9232	21.6994	18.0476	20.1316
SAE1	19.6222	20.3045	18.7575	19.41	20.5938	18.5149	21.8344	21.3771	21.1813	19.0863	19.5586	18.5266	18.0465	19.2449	18.3859	19.4934	20.4715	17.3147
DNAJB11	21.0782	21.287	21.1618	22.2325	21.9707	22.1289	22.3069	22.1088	22.1532	21.2861	21.3808	21.2893	21.0725	21.2207	20.9088	20.4087	20.7729	20.6766
SEC63	20.9742	21.2626	21.1144	21.4614	21.1233	20.9544	19.2036	18.5008	21.1557	20.2939	19.7405	19.0486	20.1828	18.2246	19.1817	20.5047	18.1972	18.4827
Septin-9	20.5877	20.6712	20.5538	21.505	21.4403	21.65	21.9868	21.8458	22.0348	19.727	20.2351	20.1909	20.7702	20.9408	20.6794	20.7994	20.5287	21.0055
GPN3	20.8308	20.7441	20.6521	21.224	19.7442	21.4546	21.5171	21.0447	19.4664	18.4773	18.1706	18.8643	19.4729	21.024	18.295	17.8545	18.7849	18.6804
STOML2	20.8628	20.9616	20.7933	21.598	21.5242	21.4595	21.2907	21.3227	21.3621	20.6386	20.8262	20.7769	20.347	18.9041	19.0206	20.2781	20.1691	20.1664
UBQLN1	20.0295	19.8801	19.0944	20.5927	18.9843	19.4178	21.0117	21.0915	21.071	19.5041	18.5803	17.8979	19.8833	19.482	19.1416	18.7913	18.5594	19.4408
RUVBL2	23.4021	23.3704	23.5798	23.9308	24.0209	24.023	24.1048	24.1324	24.0539	23.3994	23.4453	23.3661	23.2203	23.4434	23.348	23.1108	22.9804	23.1348
PIN4	20.3434	20.7245	20.0194	20.82	21.2844	21.2385	21.7816	21.5209	21.5148	18.7659	18.8123	19.9194	19.2649	18.7625	19.5467	20.7379	20.6812	20.8095
RUVBL1	23.5135	23.5341	23.5765	24.116	24.0267	24.0771	24.0539	24.0412	23.8586	23.2633	23.4711	23.2557	23.3272	23.4456	23.4087	23.1472	23.1697	23.278
TLN1	20.1405	20.2521	20.6061	21.3425	21.349	21.3939	22.2345	22.3099	22.1866	19.1866	20.0926	19.5929	20.2703	20.0262	19.506	20.7576	20.9334	21.054
AP4S1	20.989	20.9479	18.2259	21.8934	22.0309	21.4261	21.3675	21.518	20.9158	18.6554	18.6632	19.5548	18.027	18.2318	18.8399	18.0239	21.1465	21.1573
YTHDF2	21.7172	21.6495	21.8935	22.692	22.6533	22.8768	22.1792	23.1086	22.7331	21.5618	21.4362	21.5573	21.5478	21.1703	21.8987	21.6324	21.6371	21.8068
MAGED1	22.2723	22.215	22.7047	23.1896	23.3885	23.4966	22.5385	22.7029	22.917	20.4137	19.0516	20.4867	18.5326	20.2537	18.6877	20.402	20.6498	18.9726
PSAT1	19.3306	19.8295	18.7818	19.6918	19.9212	19.5793	22.5813	22.3559	22.1908	18.6388	18.5615	18.8346	19.4281	18.1419	19.2145	18.6145	19.022	19.44
PA	26.9692	26.9619	27.0929	28.0912	28.0384	28.082	27.6391	27.5849	27.5696	18.1378	18.8651	18.0659	21.8587	21.3559	21.8804	21.083	20.8981	21.6436
NS1	25.8833	25.7949	25.9349	26.5401	26.5493	26.5976	26.7783	26.6495	26.651	22.9691	23.0762	23.1986	25.2622	25.4484	25.4049	25.1801	25.1688	25.1544
SNRPG	18.72281	23.13634	18.85147	23.9898	19.21407	18.66891	23.59263	23.40561	23.63334	22.84276	19.86057	22.91599	23.37146	23.45663	23.39008	23.16045	23.41145	23.44088
NDUFAB1	18.54382	21.25153	18.56209	19.68942	21.97183	19.07592	20.23875	21.52855	19.40563	19.601	19.29023	21.29334	21.26299	21.31041	18.90695	19.25592	18.57696	18.63851
CSTB	21.41307	21.00635	21.35089	18.97725	20.22683	19.71989	21.35536	21.22488	21.6465	21.41761	22.24792	22.06329	21.1354	21.46553	21.17956	21.39346	20.80845	20.81722
HIST1H2A	23.21818	23.23383	23.22957	22.9096	22.83304	23.13507	23.3672	20.09858	23.1942	23.25175	23.08821	22.89425	22.6091	22.65556	22.46039	18.34702	22.73329	22.63659
MYL1	18.39118	18.38889	18.03551	19.00521	19.16519	18.00398	19.2473	18.8221	19.34162	19.19921	17.88477	18.77163	18.53545	18.89707	19.12347	17.91166	19.52833	19.4075
GOLGA3	19.74832	19.23853	19.26623	19.63409	19.3606	19.82764	20.03471	18.97671	20.54392	19.34047	18.26399	23.23367	22.13849	22.48662	18.7058	22.52009	18.94429	18.70034
MYO5B	17.4924	19.16754	18.73311	17.87123	18.97939	19.11439	17.92138	18.67659	18.1429	19.19044	18.91263	18.60986	18.02567	18.36726	18.803	18.00044	17.50168	18.11304
RPL26L1	19.17639	23.77042	24.03246	23.87793	23.8347	23.61032	24.2967	24.27156	23.9649	24.05747	24.06702	23.89069	23.57623	23.72879	23.61358	24.13649	23.65807	23.77092

	LFQ intensity																	
	KO cells																	
	PR8 PB2-FLAG									**PR8 PB2-WT**								
Gene names	**Exp 1.1**	**Exp 1.2**	**Exp 1.3**	**Exp 2.1**	**Exp 2.2**	**Exp 2.3**	**Exp 3.1**	**Exp 3.2**	**Exp 3.3**	**Exp 1.1**	**Exp 1.2**	**Exp 1.3**	**Exp 2.1**	**Exp 2.2**	**Exp 2.3**	**Exp 3.1**	**Exp 3.2**	**Exp 3.3**
PDCD6	22.1989	21.4457	19.632	18.7736	18.8694	18.8017	18.9311	20.8348	18.9404	21.0117	18.3205	21.1675	22.6084	22.8585	22.9914	22.2039	22.3985	22.4762
PSMA2	21.4998	19.7034	19.2119	18.3625	18.4621	18.3923	18.5227	21.537	20.4858	19.0966	21.3124	18.3064	22.9063	23.0966	23.3244	22.3158	22.9207	22.3487
NP	25.2776	25.1227	25.2536	24.3735	24.4792	24.4573	24.6893	24.9347	24.6834	23.2656	23.374	23.267	24.0161	24.1604	23.9167	23.9618	24.2619	24.0324
M1	22.653	22.6362	22.7613	21.7808	21.832	21.7393	21.8228	22.1488	22.0841	21.7364	21.2838	21.8168	22.7878	22.7923	22.5923	22.1902	22.3975	21.0289
PB2	28.014	27.9821	27.9872	26.5709	26.5563	26.5284	27.1924	27.294	27.1721	18.6859	18.6107	18.5998	14.9813	19.2083	19.2185	19.2954	19.047	15.9392
MYEF2	22.2323	22.3689	22.1538	21.1978	21.0295	20.9609	21.1992	21.2948	20.7175	21.4277	21.6223	21.6697	22.1926	21.9619	22.3621	22.156	21.5678	21.4306
ZC3H8	22.6954	22.4366	22.5904	19.6801	19.1806	19.1146	22.1825	19.987	21.8668	18.6437	22.1229	22.5496	19.6728	20.6098	20.2986	23.0008	22.3627	22.3715
HSPA1B	25.3002	25.251	25.1593	23.9638	23.9837	23.8932	24.2531	24.2876	24.3138	24.3936	24.3913	24.4071	25.2768	25.2148	25.2813	25.1732	25.2725	25.2047
C4	23.5841	23.2207	23.7323	22.9512	22.6713	22.7489	22.9993	19.905	23.0321	20.0022	23.1097	23.3553	20.0505	19.501	20.0757	23.5037	23.4377	19.2964

ME2	18.6051	19.5821	20.371	18.864	18.5243	18.8917	18.9377	19.0102	18.6096	17.9873	18.6188	19.6583	21.3515	22.3001	22.1011	20.4272	20.4864	20.6082
SMARCE1	19.7423	23.2835	23.0575	22.8639	19.7294	19.0374	18.585	19.0934	22.3104	18.9777	22.8724	18.9637	23.5213	22.8766	22.9301	23.0402	22.8827	22.7709
KIF23	21.7516	21.8858	18.5709	20.9913	18.8782	18.057	18.9865	19.2388	20.8632	18.7486	18.9706	19.1844	20.5128	20.8884	20.9776	20.954	19.702	20.7415
SSR1	23.0996	23.4108	22.7162	19.642	18.8148	21.9162	22.0081	21.7236	18.8222	19.3331	22.1998	22.5845	24.0985	23.6707	23.4051	24.1456	20.2081	19.8789
CLUH	22.4595	22.4595	22.6638	21.2147	21.1242	21.2663	21.5749	21.7051	21.5797	21.57	21.3808	21.601	22.4463	22.6875	22.9115	22.5864	22.6293	22.7372
SDF4	19.6141	19.5242	20.392	17.8764	18.0954	19.0766	18.7564	18.9488	19.6786	19.0417	18.8117	20.4218	20.0456	21.2608	19.7007	19.3805	19.7059	19.155
AMD1	21.0978	20.6581	20.6632	18.5977	19.7668	19.844	20.5316	20.6835	20.5634	20.1982	20.3379	20.0352	20.9226	19.3652	19.5986	20.1684	20.35	20.9285
ACAT1	21.5918	21.7009	21.4887	20.9555	20.5299	20.5687	20.7031	21.1729	20.782	21.21	21.0722	21.0659	22.8743	22.8538	22.8359	21.9824	22.0508	22.1466
PB1	27.5039	27.4084	27.3775	26.009	25.7489	25.9688	26.7013	26.6369	26.6316	18.9209	20.4124	19.3795	15.959	15.3088	19.3717	18.7797	19.3219	16.3001
HARS	19.3248	20.7321	19.2198	19.1663	17.9135	18.7774	19.3856	20.3083	20.4684	19.3725	19.3817	19.9787	21.4285	21.1788	21.0597	19.7938	18.6146	21.2308
AIFM1	22.4994	22.0358	20.9456	21.3256	21.1315	20.9535	20.985	21.6309	20.9128	21.5179	20.6523	20.5067	22.5627	22.3879	22.2529	21.7686	21.9209	22.402
POLR2A	27.6631	27.6224	27.5968	26.2819	26.3482	26.26	26.5982	26.683	26.6603	25.0642	25.0598	24.9682	25.9434	25.7935	26.0994	25.887	25.9223	26.0499
HSPB1	23.7635	23.5793	23.3396	22.3845	22.3167	22.3241	22.5825	22.4839	22.0345	22.9885	22.8984	22.6774	24.7787	24.7714	24.7764	23.9926	23.9876	24.2292
ACO2	20.2013	22.662	19.852	22.9108	22.0795	19.4898	18.3587	18.2268	18.9021	21.4262	21.1534	21.7258	22.9314	22.7127	23.1143	19.3937	21.9594	18.553
MACF1	26.9358	19.7138	26.6422	19.1083	26.8059	26.9865	17.9727	26.7158	26.7677	26.7884	18.9235	19.3789	19.566	27.122	27.5431	26.9897	27.4883	27.4184
VRK1	21.6893	18.7205	21.1906	20.5461	19.0025	20.5436	20.9037	20.7931	20.8709	18.316	20.4973	20.6701	21.6063	21.6406	21.6037	21.5566	21.8902	21.4527
AKAP8	21.1667	20.4074	21.2043	19.4648	19.8544	20.7291	19.0965	20.4219	20.548	19.0723	20.2987	20.4047	19.3394	18.7873	20.8418	19.6637	20.012	19.9703
P4HB	22.8397	22.9537	22.8518	21.5401	21.6912	21.6407	21.9923	21.9689	22.056	22.0419	22.0194	22.1743	24.3286	24.1703	24.2319	23.2359	23.346	23.1866
AKAP8L	23.5289	23.16	23.3246	22.3651	22.1401	22.2624	22.4129	22.4881	22.4925	22.046	19.3811	22.1243	21.9168	21.4117	21.8193	22.1608	22.0154	22.0887
HA	19.1488	19.5592	19.0431	18.6321	18.5811	19.7919	18.7905	20.1829	19.1058	19.4832	19.1817	18.2757	19.8319	19.7999	19.8898	18.5671	20.1156	19.6177
CNN2	21.6956	21.9676	22.2722	20.54	20.5351	18.7676	20.902	21.2357	21.2729	21.1813	21.1554	21.1551	22.6166	22.8865	22.8781	22.2555	22.3845	22.3356
CS	20.749	19.2266	19.199	18.6553	18.6285	18.8483	21.1129	20.9929	20.8895	19.5508	18.3026	20.1705	24.5624	24.3745	24.4684	22.4004	22.8519	22.7615
HSPE1	19.5914	20.2385	19.4701	20.2537	19.5593	18.3738	20.1962	19.8869	18.6516	20.4865	19.5636	20.2361	23.1895	23.2131	23.3277	22.7837	22.3706	22.4248
PTMA	20.1419	21.2109	20.6483	19.0363	19.4131	19.6568	19.681	19.7937	19.4298	22.1997	18.993	22.2071	22.9635	24.0471	24.3957	23.0282	23.0075	23.0625
POLR2B	24.3574	24.253	24.2386	22.835	22.924	22.8735	23.2862	23.3458	23.2956	22.3003	22.1998	22.2637	23.2058	23.0406	23.1715	23.071	23.1613	23.1084
CYCS	20.8429	20.542	19.1537	20.8624	19.4214	18.8553	19.9653	20.9401	20.3671	19.9357	20.5707	19.9302	22.826	23.0192	23.2345	21.4491	21.0499	19.6788
POLR2H	24.5643	24.1948	24.4118	23.1918	23.0597	23.2653	23.3602	23.7919	23.3069	22.8786	22.9162	22.8976	23.1456	23.065	23.2575	23.2045	23.3279	23.2843
EIF4G2	21.2416	21.1421	20.8172	20.3152	18.078	20.3144	20.4922	20.9506	20.4408	20.3937	17.818	21.117	22.2757	22.4113	21.9593	21.8321	22.0616	21.9922
HSPA9	25.4861	25.4425	25.3926	23.9876	24.1056	24.0136	24.5635	24.5999	24.5305	24.4074	24.3604	24.4111	25.7233	25.6777	25.7181	25.5336	25.5771	25.5468
NDUFV2	20.377	20.2788	19.2538	19.1786	17.9969	19.7724	19.3332	19.8219	18.5139	18.9922	20.2923	19.9858	19.9865	19.7487	19.0173	20.2791	18.5407	19.7528
STAU2	21.6775	21.6554	21.4867	20.357	19.3999	20.2308	20.8508	20.4832	20.1205	20.864	20.3562	20.8039	21.1138	20.6453	21.3655	21.1449	21.185	21.3076
CSTF3	23.7116	23.792	23.1601	18.4228	19.4157	18.8398	21.2493	22.3047	23.0921	19.0818	18.252	18.8096	22.7701	24.1218	24.4503	24.5869	23.9271	23.6904
ZC3H11A	21.3455	18.7373	21.1198	17.8928	20.1417	20.2192	18.7394	20.7498	18.1474	18.587	20.101	20.7679	19.7291	20.9456	20.8331	20.6123	20.8351	20.6871
PHF8	22.5276	20.963	20.0241	21.587	19.7825	18.885	20.2987	19.9203	20.7035	22.0277	22.1361	23.0307	22.1256	21.1561	20.0775	21.7373	20.324	20.7713
ESD	21.1847	19.8444	20.0627	19.4924	18.768	19.224	19.0686	17.9199	18.3446	18.9564	18.8566	18.526	22.0111	21.8532	21.8353	20.2849	20.1957	20.1566
SF1	21.5569	19.5155	19.7153	18.433	18.2767	18.4613	18.5928	18.665	21.0024	19.5177	18.5378	18.2859	19.5759	20.1345	20.0007	18.6148	19.0181	18.9622
PHKG2	21.7332	18.8873	21.1296	18.4386	21.1642	18.5714	20.3183	19.4251	21.0431	19.1781	18.9776	19.5276	20.9297	18.8335	20.9412	21.2255	21.4976	19.4608
CALR	20.297	18.9491	17.8376	18.1407	18.0485	18.2465	20.7647	18.1183	20.8024	20.6076	20.4373	20.0858	25.29	24.922	25.2728	23.2636	23.0832	23.2357
PRKCSH	19.8184	18.0322	18.518	19.6956	19.3	19.2261	18.5915	17.7861	18.6024	19.1803	19.0799	18.7078	22.8397	22.8373	23.0088	21.7014	21.8959	21.5342
SARS2	22.7908	22.6503	22.4811	21.4479	21.3329	21.6242	21.5233	21.5137	21.2843	21.9044	21.7678	21.9157	22.4388	22.4797	22.3243	22.4022	22.4222	22.2989
HAX1	18.6257	21.9079	21.8557	20.0315	20.6587	19.1963	21.6739	21.3644	21.5431	20.3583	20.9369	19.8104	18.407	21.696	18.4575	21.8193	21.3919	20.1048
SUPT5H	21.7295	22.0517	22.4174	18.6713	20.7348	19.2006	21.3653	21.3417	21.1346	18.7564	19.7321	19.7256	19.8252	21.5785	21.7758	20.3927	19.135	21.8208
CLIC1	21.8229	21.932	20.0654	20.7142	21.221	21.2873	21.1982	21.4377	21.8752	21.6449	21.4315	21.5429	23.1374	23.4317	23.0709	22.6937	22.791	23.049
KPNA3	23.628	23.5853	23.4356	22.3623	22.4121	22.5238	22.7044	22.9028	23.0547	22.6755	22.6409	22.6546	23.6536	23.3492	23.6608	23.5493	23.6239	23.6085
AURKA	19.5477	21.6869	22.1159	18.4945	20.4127	19.2014	20.7364	20.659	18.7109	21.0365	19.724	19.6662	21.1074	20.5563	20.5671	20.2898	21.9266	20.2258
PPM1G	22.7447	22.6261	22.5023	21.1436	21.3914	21.315	21.6405	21.8146	21.7529	21.6168	21.6737	21.4816	22.6888	22.2861	22.4952	22.6305	22.5731	22.9479

IPO8	18.7033	19.7223	20.4969	18.7922	18.7434	19.3895	18.7674	18.0768	19.3636	20.0177	18.1719	19.2384	19.2018	20.1836	19.24	18.981	19.8122	19.7677
POLR2D	21.7653	22.0638	22.0653	20.6765	20.4969	17.8272	21.4276	20.867	21.0093	20.6725	20.3215	18.7337	20.4483	19.2297	20.4673	21.3982	19.447	19.3973
PJA2	23.5478	23.5627	23.4294	22.0313	22.1357	21.9744	22.9627	23.0879	22.8676	17.873	20.8734	19.4686	20.5062	20.4566	20.5243	20.3061	20.0965	21.9805
PAPSS1	21.7473	20.1123	20.7242	20.3964	19.6318	20.7113	20.6775	19.3975	19.9599	20.7612	20.0847	18.5179	22.071	21.883	21.6652	20.5232	20.779	20.056
TIMM44	20.8399	20.5598	20.447	19.4856	19.5951	17.0655	18.7071	20.4203	19.808	20.1385	20.2738	20.122	21.9339	19.7342	19.3042	21.5205	21.5356	19.5669
GTPBP6	19.3874	20.0288	20.9174	19.0931	18.3254	18.1554	19.3247	19.022	18.6735	18.5396	19.6652	19.0147	19.7144	19.2939	19.4318	19.6669	19.9229	19.8799
CALU	22.9561	22.9274	23.0877	22.0188	22.1208	22.1244	21.8191	22.248	22.1618	22.3277	22.3265	21.9564	23.5168	23.1822	23.5477	22.98	22.8305	23.0796
SNX2	18.0653	21.0037	19.0206	19.5378	19.8928	19.7501	19.9073	20.1926	18.015	18.932	18.5297	19.9685	21.9659	21.4965	21.8647	20.5871	21.4632	21.3101
DNAJA2	24.0762	23.873	23.9495	22.5658	22.5791	22.556	22.9747	22.9969	22.9312	23.0368	22.8286	22.8498	23.9567	23.9942	23.6688	23.8846	23.7821	23.9993
PMPCB	22.725	22.6991	22.5898	21.1705	21.2446	20.878	21.6533	21.6304	21.6434	21.723	21.7995	21.6357	22.7268	22.7955	22.6136	22.4939	22.6765	22.2526
GPC4	22.3018	22.0692	21.6952	21.4368	21.4592	21.2706	21.3486	21.2642	21.2678	20.3007	20.3607	20.535	21.5148	21.839	22.008	21.3803	21.5106	21.5406
HSBP1	22.3189	22.5241	19.3468	21.2741	19.4634	21.4332	21.4249	22.12	21.54	19.4969	18.7149	19.849	19.5758	20.2302	19.964	19.6106	19.4281	18.8397
ERAL1	21.8233	21.9876	21.6307	20.8859	20.2499	20.4714	20.6891	20.8534	21.0789	20.7332	20.7331	21.0184	21.5221	21.6627	21.3897	21.8703	21.8845	21.8435
CLPX	21.676	21.6181	21.8932	20.5492	20.6655	20.6483	20.5364	20.8244	20.5797	20.6455	20.7551	20.7903	21.5826	21.7303	21.8649	21.6686	21.8732	21.8628
UBR5	22.607	22.5657	22.2739	21.2015	21.1375	21.1572	21.6062	21.7574	21.5976	20.5779	20.7397	19.9746	22.1374	21.8902	21.926	21.8254	21.9377	21.7798
BAG2	23.059	22.548	22.9061	20.8966	21.0025	21.2856	22.3558	22.6896	22.0128	21.8524	21.9173	18.8676	22.8526	22.6311	22.459	22.657	22.6949	23.2026
LDHA	22.0227	21.9084	21.8278	21.7813	21.784	21.5109	21.8603	21.7442	21.721	21.7016	21.9164	22.0588	25.6563	25.6299	25.6219	23.4689	23.4296	23.5544
GLUD1	21.1726	19.144	21.3879	21.1423	18.7191	20.4129	20.3828	20.0998	20.1663	20.5848	20.5692	20.9212	22.3038	22.4595	22.5031	21.8231	21.2578	21.8323
PGK1	21.2529	21.2963	21.4513	21.3329	21.198	20.8057	21.4473	21.4145	21.5107	21.1715	21.4274	21.2371	25.606	25.5333	25.5621	23.1377	23.4454	23.6402
TFRC	19.665	20.152	19.0219	18.2973	18.9204	19.4581	20.4983	19.6592	19.7938	18.1189	20.114	18.8097	23.009	22.8781	22.9235	21.1793	19.4728	20.9611
OAT	21.0932	21.7107	21.308	21.4045	18.236	18.3984	21.0538	21.114	21.3401	21.6688	20.4882	21.4577	22.9774	22.861	22.9975	22.6616	21.6483	22.0568
TP53	20.5396	20.611	20.4235	18.9547	19.8568	19.4792	20.0739	20.0678	19.4974	19.9693	20.2774	19.4122	20.2226	20.6676	20.5961	18.1184	21.0839	19.7074
HIST2H2B	24.419	24.5521	24.7396	22.4919	22.6378	22.6622	24.4262	24.3307	24.276	23.5247	23.1787	23.5452	25.0344	24.8543	24.984	25.2994	25.3774	25.2245
PFN1	19.7196	19.0643	18.6018	19.5996	20.4215	19.7156	20.2722	17.4932	17.9793	18.4482	17.5747	18.3366	25.6198	25.5779	25.6351	22.7673	23.0459	22.7236
HSP90AA1	23.7314	23.8346	23.866	22.7815	22.7516	22.6948	23.1828	23.1876	23.0232	23.4634	23.2946	23.2765	26.0659	26.0028	25.972	24.9252	25.1003	25.0777
SNRPB2	21.2783	21.4511	21.6556	20.2167	17.7925	19.8075	21.0355	20.6841	19.2064	20.3259	20.8962	20.7487	23.264	22.5707	22.9171	20.1653	20.9466	20.8643
ANXA5	19.3538	19.2182	21.0237	19.2583	18.163	18.3	19.2074	19.1207	19.0574	18.5001	18.7097	19.7123	22.7603	22.89	22.7689	19.2134	19.4247	19.8334
GSTP1	24.8658	24.8763	24.8209	23.6126	23.8279	23.732	23.7915	24.0171	23.8659	24.2667	24.2656	24.4447	26.7605	26.6818	26.8142	25.3268	25.3685	25.4023
HMGB1	21.1219	20.3142	21.6592	22.0989	21.7318	22.18	22.4614	22.3878	22.4006	22.0008	22.2523	20.5161	25.3944	25.6841	25.0445	23.6934	23.54	23.6563
CALM	24.6412	24.4938	24.3705	25.1973	25.1923	25.2731	23.9829	23.875	23.8354	24.3766	24.2598	24.4156	25.7988	25.7307	25.7215	24.6169	24.7027	24.7788
HSPD1	27.242	27.1998	27.1239	25.8753	25.9373	25.8861	26.2684	26.3958	26.3229	26.4485	26.4192	26.4823	27.8582	27.8389	27.831	27.5538	27.5938	27.5356
HSPA8	27.751	27.7414	27.6335	26.0224	26.1157	26.0516	26.8329	26.9444	26.8542	26.5298	26.4797	26.542	27.6331	27.5659	27.5393	27.5271	27.5552	27.5898
PDHB	23.1646	23.0309	23.0429	22.1082	22.2455	21.8662	21.6591	21.9959	21.9979	22.5157	22.4307	22.51	23.4405	23.0733	23.4476	23.428	23.103	23.412
RALA	19.1764	20.197	19.7383	18.8251	18.6303	17.8707	18.3079	19.1835	19.2756	20.4573	18.7575	19.4304	18.3105	21.4841	21.0253	21.0082	19.1128	20.7632
ETFA	21.6445	20.6854	19.7896	19.7176	19.522	20.275	20.2475	19.6856	20.4081	20.3156	20.0471	20.1908	22.6703	22.7425	22.6347	21.0672	21.4521	21.551
PGAM1	19.0967	18.751	19.2181	18.0176	18.299	17.8518	19.1108	20.2382	19.2512	19.2348	18.9555	20.0739	25.1804	25.2606	25.2062	22.4616	21.9926	22.0582
HK1	20.1088	19.7558	21.3182	19.118	17.9845	17.6024	20.0581	20.6534	20.2017	19.8552	20.1444	20.3011	20.0663	20.336	22.1871	19.6438	21.2538	21.131
POLR2C	25.5156	25.4896	25.3628	24.2052	24.2506	24.3374	24.5646	24.6873	24.4765	23.6599	23.724	23.5182	24.6169	24.4931	24.4441	24.426	24.7072	24.5972
POLR2E	24.0189	24.0087	23.952	22.5259	22.7355	22.7794	23.3307	23.2096	23.1495	22.4962	22.2545	21.8648	23.3113	23.2741	23.2334	23.2232	23.2235	23.246
PSMB1	21.6	19.052	21.3971	19.4848	18.9422	19.1445	21.23	18.5027	21.3693	21.1642	21.0955	18.6581	23.1032	22.8476	22.7829	22.0617	21.9243	19.8024
PSMA1	22.3182	21.7874	22.191	20.9471	19.0303	20.7172	21.3494	21.509	21.6235	21.5566	21.3432	21.4804	22.5407	22.3273	23.273	22.0322	22.1124	23.1107
PSMA3	21.5093	21.6612	20.1272	20.938	19.4115	19.9267	20.9599	21.0663	18.4403	18.6208	19.8546	21.0887	23.1823	22.1914	23.0027	22.3318	21.8568	18.8312
HMGB2	21.7624	19.6386	21.5078	22.52	22.3176	22.5231	22.4313	21.8522	22.4669	22.6051	22.4838	22.5843	24.544	24.4886	24.388	23.7715	23.5012	23.807
PSMB4	21.2493	21.1965	19.2028	18.2105	19.4882	18.4994	20.1646	20.8773	18.0099	19.2775	19.8722	19.6149	22.6224	23.1528	22.3927	22.0131	21.6734	22.2631
PSMB5	21.0141	20.8854	21.0481	20.6094	19.3508	19.7611	20.4232	20.4247	20.3806	20.6571	20.4435	20.2208	23.1051	22.9092	23.2656	22.1	22.6366	21.3286
ECHS1	22.3039	21.9177	21.7269	20.5991	21.5378	21.6141	21.3237	21.5904	21.2699	19.7765	22.1595	21.067	23.6793	23.6984	23.6287	23.0716	23.0534	22.8625

PEBP1	20.3459	19.6183	19.7272	18.4487	19.105	19.0444	18.5139	19.4025	18.7899	19.4095	18.9534	19.4648	24.3475	24.2914	24.5577	20.5902	20.7007	19.9117
PDIA3	24.8568	24.878	24.7438	23.2898	23.3744	23.2842	23.8939	23.9767	23.7657	23.8968	23.6832	23.8095	25.3752	25.2857	25.3451	24.9046	24.7338	24.8643
ALDH1B1	20.4281	22.299	22.3962	19.9948	19.126	21.2259	21.1359	21.3755	20.9972	21.0555	20.844	21.0691	22.6875	22.8322	22.5758	21.9869	22.3451	22.4968
DNAJA1	24.7542	24.5879	24.5814	23.4983	23.4322	23.5487	23.7701	23.8883	23.6455	23.7085	23.5886	23.6643	24.8633	24.7642	24.8463	24.5991	24.8125	24.7362
UQCRC1	20.0542	20.0194	19.477	20.8188	20.7687	17.9123	20.5429	19.0547	20.7429	20.3375	18.6683	21.1255	21.3001	19.5953	19.6414	19.3956	20.263	19.8939
ATIC	19.5132	20.8151	20.0422	19.1732	19.9384	18.4782	18.4571	18.072	18.9916	19.5808	18.1579	19.4431	21.7689	22.2258	21.9402	19.5635	19.8465	19.6518
PYCR1	20.9998	21.0961	18.6765	18.7042	17.8179	17.706	18.7771	18.3679	18.0102	18.677	18.4913	18.9671	21.073	20.3433	21.8568	18.8427	20.6278	20.912
HSPA4	22.5548	22.7358	22.536	21.4937	21.4537	21.1638	21.746	21.6898	21.7363	21.8689	21.7367	21.7716	23.4851	23.4187	23.1819	22.9095	23.1455	22.941
PHB1	21.5047	21.9065	21.668	21.3015	21.5459	21.3036	20.8297	21.1533	20.9776	21.9436	22.08	21.9148	22.899	23.087	23.1618	22.5315	22.4908	22.7804
POLR2I	23.8571	23.805	23.8045	22.6324	22.5529	22.8523	22.5763	22.7242	22.7957	22.2729	21.4645	21.9109	22.0819	21.8385	20.1688	22.7841	22.5927	22.7266
TALDO1	20.2288	20.4277	19.6846	18.9266	19.6548	20.0175	19.0236	19.9503	18.3057	18.16	19.7891	19.1477	22.5653	22.362	22.4696	20.8193	19.6062	19.4381
MDH2	19.3079	19.4833	18.6744	18.1978	18.7436	17.252	18.7804	20.4994	19.9391	18.6198	20.818	18.6376	25.7736	25.4633	25.5803	22.2303	22.0646	22.592
MAP1B	24.3689	24.3446	24.3171	23.0609	23.0455	23.0437	23.4118	23.4795	23.4809	23.4276	23.3196	23.273	23.8279	23.7566	23.817	24.1029	24.1131	24.1931
NES	22.1786	22.7744	22.59	21.5749	21.4975	21.6157	21.1727	21.3684	21.4915	21.5414	21.5876	21.5928	22.3524	21.7045	22.5561	22.6014	22.1697	22.4795
TUFM	25.6977	25.5674	25.5441	24.3378	24.3369	24.3262	24.5185	24.601	24.465	24.6544	24.4825	24.5748	25.3602	25.3075	25.3057	25.2876	25.2925	25.3622
EMD	24.1265	24.025	24.2307	23.056	22.9369	22.9758	23.1623	23.1459	23.0987	23.2988	23.003	23.1099	23.9395	23.8652	24.0786	24.1378	24.0789	24.1517
HDGF	21.5919	21.9086	21.5011	19.4121	19.9291	18.3768	20.9604	20.9352	20.9508	20.6194	20.4956	18.9724	23.5737	22.9933	23.3986	22.1546	23.3882	22.1342
POLR2J	23.5121	23.5106	23.6206	22.012	21.986	22.0962	22.286	22.7534	22.8365	20.0482	17.8966	18.3538	22.3768	22.5866	23.3977	19.734	20.1128	22.369
SMS	20.705	19.1658	19.9491	19.0115	19.3892	18.9275	19.2392	18.7887	18.726	19.558	19.5803	19.113	22.8337	22.8119	22.6758	21.5162	21.8167	21.9296
BLVRA	21.3492	20.0318	20.7473	20.9929	19.4037	18.4256	20.015	18.7636	18.7008	19.0331	19.1938	19.3883	20.0012	21.6866	21.808	19.4457	20.4479	21.2261
SLC16A1	21.9071	21.7209	21.6406	21.3468	20.8121	21.1017	21.2155	20.9708	20.7921	21.2733	21.2864	21.4808	22.6637	22.2843	21.3463	22.489	22.4807	22.6967
RAD23B	21.6504	20.3397	19.0566	18.6019	18.9091	19.8763	18.6913	21.4266	17.8481	19.0132	19.5034	18.8602	22.7882	22.5226	23.0749	19.6445	19.6868	19.2129
ALDH18A1	23.1819	23.0209	22.659	21.6233	21.9096	21.557	22.3366	21.9463	21.9543	21.9317	22.1812	21.5796	23.432	23.7165	23.5976	22.9716	23.2341	22.9074
HADHB	22.2525	22.1978	21.9433	20.6706	21.3997	20.9739	21.3231	21.5733	21.0554	19.4067	21.2542	21.6371	23.066	23.2277	23.3619	22.5533	22.88	22.7717
MAZ	23.8624	24.0257	23.9893	22.8692	19.2625	22.8648	23.4933	23.1013	23.1135	23.1015	22.7602	23.1172	23.0406	19.7528	23.3774	18.799	18.8454	24.2439
SEC61B	24.1768	24.2553	24.4324	22.4622	22.324	22.4555	22.5848	22.5739	22.4682	22.7388	22.9506	22.8895	20.7008	19.0543	20.5591	20.127	20.167	20.5593
RAB2	20.086	19.3186	18.9708	21.6069	20.8526	20.7113	20.5353	21.0532	20.2558	18.8555	21.2989	21.7622	22.384	22.7596	22.8528	22.2084	22.4851	22.0845
UBE2N	22.8839	22.3424	22.3601	21.56	21.5403	21.5266	21.2425	21.8017	21.2023	22.2971	21.8111	21.8698	23.2353	23.2846	23.0683	21.9921	22.3822	22.4339
POLR2G	21.2198	21.3753	21.0831	19.9951	19.9237	19.6799	20.1188	20.7398	20.3209	18.2042	18.7566	20.2624	21.0115	19.5358	20.4031	20.5549	20.5927	20.7968
POLR2L	24.0039	23.4444	23.5959	22.2961	22.6156	22.4558	23.3151	23.0264	23.6012	22.346	19.1269	22.4479	23.0382	23.2884	23.1603	23.2714	22.9181	22.8404
SARNP	18.6152	19.3463	20.6781	19.8034	19.7449	19.6169	21.0059	20.4331	20.5592	20.2092	20.0466	20.0111	22.883	22.7658	22.663	22.2685	22.176	22.3963
FKBP3	19.6648	19.6411	19.8318	19.025	18.9174	17.6287	19.1682	18.4035	18.3413	18.5214	18.8354	18.1574	22.2822	22.2785	21.5101	21.4591	21.3388	20.3139
CAP1	20.1071	19.9772	20.1913	18.9011	19.5759	19.3243	19.7316	18.9903	18.5169	20.0329	20.0642	20.3651	22.7425	22.4194	23.0813	21.2153	21.6802	21.211
FKBP4	18.8261	18.5034	20.2705	18.8055	19.4257	18.8989	19.0924	19.1291	18.9395	19.1689	20.0971	18.0674	22.5207	22.6398	22.5382	20.4886	20.7068	21.7975
AHNAK	23.3499	23.3913	22.5745	22.0456	21.9144	22.2822	22.602	22.7475	22.7067	21.6889	21.6069	22.6314	23.831	23.7067	23.9357	23.4336	23.7194	23.8272
DHRS2	25.4387	25.3816	25.3819	24.329	24.4339	24.0654	25.2576	25.2969	25.6112	24.8745	25.3161	24.8542	26.1069	26.4846	26.0837	26.1443	26.1084	26.1752
LBR	22.0629	19.8549	19.0903	21.9444	22.3637	22.2597	19.0708	21.9315	21.8566	22.5499	22.4851	22.1377	22.7632	23.0954	22.6876	22.654	22.434	20.3314
EIF4H	18.6548	19.5109	18.8153	19.8437	19.0997	18.85	21.0765	20.5353	18.8571	18.5671	19.7337	19.5732	23.1815	23.1756	23.1985	22.5033	22.2836	21.9812
RCN1	21.6261	21.3688	21.2153	19.4277	21.8175	20.6302	21.0204	21.0607	20.9339	20.842	18.7446	20.7054	22.3308	22.5813	22.3794	22.0023	21.5408	21.5247
TRIP13	20.6518	19.3294	20.8801	19.7521	19.3457	20.0281	18.454	20.6275	20.6581	20.5098	18.8263	19.8992	22.0269	21.8085	21.1221	21.7216	21.9105	22.0315
NSDHL	21.6015	21.2443	21.4448	21.0666	20.7163	19.7758	20.5	20.83	21.0525	21.0457	18.1933	21.2002	22.1713	21.909	22.067	22.0201	22.0962	22.1936
MLF2	21.2886	21.4308	19.2125	20.2354	20.057	18.9917	17.4481	19.5253	19.8301	20.3169	20.5193	18.3621	19.3959	19.7986	19.6952	20.3291	19.1698	19.16
NDUFA9	21.2131	20.8551	21.1258	20.2175	20.3959	18.8409	20.5332	20.3993	20.6351	20.5053	20.822	18.7894	19.8434	21.2787	21.8511	21.5624	20.9073	19.6647
PDS5A	21.274	21.9758	21.2645	18.0237	20.1697	20.4014	20.5069	20.6349	20.2505	20.2283	20.7316	21.2353	22.0832	21.7353	22.0064	21.9735	21.5627	21.8801
NME1	24.2526	24.0694	24.0724	22.7553	22.5308	22.5963	22.909	22.9192	22.9903	23.1003	22.9922	23.2023	25.6087	25.6232	25.5455	24.5581	24.5991	24.6296
MAGED2	22.2821	22.4797	21.7065	20.8973	20.9079	20.5581	21.5388	21.4978	21.1739	21.3165	21.2598	21.6756	22.1523	21.6066	21.9943	22.2173	22.1368	22.231

RNF219	22.2393	22.1967	22.4399	21.4386	18.9147	20.6153	21.3538	21.7137	21.0424	21.5966	21.139	19.7015	20.2235	19.9294	19.8717	19.8092	19.2131	20.4455
RPAP2	21.856	22.337	21.9017	20.5632	20.2697	20.7664	20.6918	20.6907	20.867	18.772	19.0214	18.4993	19.3015	19.6362	20.3429	20.5783	20.3722	20.4358
ENAH	20.3072	20.1932	20.206	19.125	18.8232	19.1798	18.6083	18.2078	19.1299	19.4362	19.3955	18.1171	21.3856	21.4252	19.5401	18.8524	21.5444	19.4249
HJURP	20.9099	21.0766	21.2676	19.1051	17.6177	18.5288	19.9901	19.7036	19.198	17.8994	20.246	18.6521	20.2512	20.8242	18.8025	19.5753	19.6134	20.1726
RB1CC1	27.3026	27.2344	27.2874	19.1534	24.7499	24.8037	25.8696	26.0112	25.6943	25.5548	25.1513	24.777	26.2907	26.1088	26.2976	26.4134	26.4778	26.4244
ZNF622	21.5163	20.0613	20.8488	20.6584	20.6433	20.828	18.4062	19.4816	21.1851	21.1774	20.7253	18.594	22.0234	21.9232	21.2779	22.17	21.7374	22.3013
FUBP1	19.9721	20.041	21.5183	20.9416	19.7935	19.8383	21.4999	21.3394	21.2579	20.4278	18.1334	21.1331	23.635	22.9893	23.3381	23.0836	22.9659	23.1351
THAP11	20.0354	19.8883	20.8709	18.6587	19.9173	18.1029	18.898	20.565	19.1169	19.4509	18.9942	19.6336	20.3423	20.7653	21.2737	19.4863	20.5872	20.2718
DNAJA3	24.1264	23.6007	23.8488	22.4071	22.779	22.4529	23.0391	22.6752	22.5321	22.4933	22.7863	22.403	24.1528	23.9633	24.1448	23.7492	23.8454	24.228
CDKN2AIPNL	20.2032	19.4242	20.1234	20.2877	17.7375	19.7282	18.6599	19.6036	18.7212	19.5771	19.0167	19.4645	20.219	20.4987	19.6611	19.022	19.1313	19.0478
CNDP2	19.523	19.4623	18.4396	19.1039	18.0931	18.0458	19.2237	19.8756	18.8311	19.2326	19.5986	20.5348	21.2383	21.378	20.7627	20.27	20.3093	18.7009
RBM14	24.2575	24.1363	24.3494	22.7438	22.7835	22.6834	23.2842	23.264	23.1674	22.7483	22.4779	22.4491	23.7593	23.3669	23.4651	23.4007	23.4338	23.5164
PHB2	22.6995	22.6002	22.7774	21.7942	21.6396	21.9104	21.8306	21.6536	21.6796	22.2106	22.2864	22.1787	23.2995	23.3258	23.4635	22.838	22.9683	22.8921
CLPB	22.1014	21.9252	21.6694	19.8798	20.5053	20.4241	20.9393	21.0562	21.1803	20.583	20.3451	20.4182	21.6986	21.9852	22.1769	19.9974	21.2067	21.4542
RAB1	23.8894	23.9959	23.8722	23.2362	23.2038	23.0685	23.0563	23.0662	22.7307	23.5062	23.46	23.0151	24.5447	24.4161	23.9696	24.3837	24.4649	24.1359
NOL6	20.3662	19.8837	18.2209	18.7212	19.3716	18.4652	20.2268	17.7474	18.804	19.264	18.3482	20.0677	19.8595	19.5838	20.0469	19.5022	20.1301	20.6237
CACYBP	19.6169	20.7284	17.825	19.0488	20.0996	20.2775	20.7055	21.1286	21.109	20.1444	20.2933	19.598	22.8816	22.7827	22.9541	19.1947	21.6924	21.7917
SPC25	20.9538	19.9228	19.5844	18.1251	18.4846	17.9563	20.6053	20.5684	18.8248	19.4828	19.7463	18.1946	19.497	20.0323	19.6885	19.8044	19.9738	19.7698
RTN4	21.9821	20.2825	21.6914	18.7834	19.3822	20.0002	21.5257	18.3361	20.8947	20.8718	21.2462	17.954	23.1513	22.9334	22.7762	22.8908	22.933	23.2777
TECR	22.6052	23.0566	22.8141	22.1733	22.1703	22.1877	22.1943	21.8061	21.9152	22.3184	19.8443	20.0377	22.2064	22.3341	22.1716	22.4961	22.4897	22.2276
SAE1	19.4962	20.7829	19.8129	18.6289	20.0789	18.9525	19.1684	20.4595	18.7071	18.9936	20.7773	19.4136	22.329	22.3187	22.3367	20.9929	21.3699	18.6638
DNAJB11	22.3005	22.3617	22.4651	20.8195	21.0874	20.5269	21.1368	21.453	21.6642	21.3622	21.0884	21.2557	22.3338	22.0575	22.1158	22.1359	22.681	22.1584
SEC63	19.0632	19.3856	20.6604	19.2914	20.7645	18.8884	18.8446	19.6657	18.2849	19.1323	18.996	19.0701	21.6316	21.3951	22.0519	21.8348	20.3348	21.5435
Septin-9	21.9825	21.6927	21.2971	20.7185	20.7081	20.4019	20.992	21.022	21.282	21.2691	20.8291	21.1436	22.2855	21.9339	22.3725	22.0913	22.4157	22.2304
GPN3	21.5883	21.4213	21.5195	20.6404	20.1805	17.9867	20.8736	20.9967	20.6319	19.7775	17.9721	19.6115	20.7911	19.9862	21.1501	21.366	18.8469	19.4141
STOML2	18.5121	20.8015	20.7132	20.4739	20.3027	20.6425	18.8145	20.0748	19.4674	20.8805	20.6414	20.5342	21.2802	21.4942	21.0826	20.9758	21.181	20.78
UBQLN1	18.9377	19.5046	19.2919	17.955	19.5627	19.6465	19.145	17.809	18.1625	18.2399	19.2605	18.1906	21.1624	21.295	21.2497	18.6768	20.4604	20.165
RUVBL2	24.5867	24.5298	24.5742	23.0906	23.2276	23.183	23.5976	23.5552	23.5613	23.7719	23.5926	23.5945	24.4102	24.348	24.3648	24.4281	24.4111	24.5619
PIN4	20.7962	19.9837	19.5373	19.2905	19.2075	20.0175	18.6976	18.0691	19.5745	19.6647	18.4644	19.4037	19.9516	19.5438	19.8635	19.4202	19.7766	19.3718
RUVBL1	24.3875	24.4125	24.2938	23.2005	23.3059	23.4127	23.5634	23.6423	23.5673	23.7523	23.6826	23.7141	24.5452	24.4954	24.5812	24.6901	24.6168	24.6449
TLN1	22.2028	21.4398	21.4277	20.162	20.3161	19.7975	21.0024	21.0234	20.8703	20.9356	20.7001	21.1067	22.6954	22.7648	22.8312	22.8274	22.4361	22.7573
AP4S1	22.4913	22.3434	22.1878	21.3222	21.2017	21.2377	21.5394	21.8881	21.2708	22.0828	19.7783	22.2636	22.6801	22.5613	22.6018	22.8232	22.4202	22.8078
YTHDF2	23.3652	23.269	23.5348	21.7891	21.9253	21.1486	22.3475	22.4152	22.249	22.0042	21.5732	21.7862	22.9398	23.4838	23.0743	23.0577	22.9588	22.9229
MAGED1	23.2902	23.4094	23.4428	22.2158	22.0042	22.0065	23.0015	23.0191	22.9763	20.996	20.8249	20.4881	21.5776	21.8158	21.9889	21.3193	22.0716	21.5833
PSAT1	20.466	18.8385	19.5785	19.0991	19.5367	19.1258	19.966	18.8307	18.2968	20.517	19.2977	19.0275	22.7999	22.8712	22.1323	20.253	20.1667	20.0563
PA	27.1721	27.1047	27.11	25.8974	25.9746	25.8636	26.5071	26.6169	26.4297	19.1037	19.0757	18.9114	16.0544	17.5563	20.5878	16.5876	17.7632	19.355
NS1	19.494	20.3218	19.4283	18.5202	19.3302	16.7739	20.4837	19.8409	20.8513	20.0921	18.1122	19.6612	18.7365	17.8718	18.9728	18.6692	20.1796	19.621
SNRPG	23.64768	23.55766	23.48738	22.89946	23.29404	23.08678	19.91879	23.06567	23.21312	23.37836	23.32649	23.37518	19.86173	20.24891	20.15859	19.81373	19.21971	19.13498
NDUFAB1	22.01676	22.12161	21.82981	18.54806	21.01311	21.22075	21.47402	21.61558	21.51196	18.08361	21.5265	21.07084	19.15137	19.18011	19.11119	20.00811	19.02657	18.97083
CSTB	22.22829	22.28675	22.26665	21.40374	21.40385	21.10335	21.25003	20.98905	21.05219	21.64614	21.66839	21.57085	19.77965	20.23441	20.67839	19.38451	21.05338	19.10456
HIST1H2A	23.84995	23.52205	23.58669	22.3584	22.27736	22.6437	23.48321	19.73188	23.31299	22.92396	22.84111	22.92816	20.66271	20.58533	19.10578	19.90175	20.20505	19.98095
MYL1	24.37206	24.39519	24.12747	23.93292	23.8839	24.25472	23.14638	19.28012	19.66774	17.35454	18.56996	19.21689	20.57914	19.06245	19.07266	20.36317	24.03313	24.28496
GOLGA3	20.06368	19.80281	22.92111	19.17054	22.33109	22.35008	22.50809	19.14336	19.08006	18.5694	19.49664	19.1488	19.6762	20.57242	19.0645	19.94946	19.99025	19.04786
MYO5B	23.12707	22.84228	22.99955	22.8043	23.03596	23.10079	21.83823	22.27222	22.377	21.35251	22.19313	22.97533	20.67805	21.22459	20.92658	21.75336	22.05252	21.71335
RPL26L1	24.78052	24.66758	24.39231	23.71534	23.41635	19.12327	23.28475	23.2103	23.27284	23.86155	23.88344	23.83335	20.23853	19.02464	20.18391	20.6799	20.21555	18.92235

	Data processing					
	eHAP WT cells - PR8-FLAG vs PR8-WT			eHAP ANP32-KO cells - PR8-FLAG vs PR8-WT		
Gene names	-Log(p value)	t-test Difference	Hit	-Log(p value)	t-test Difference	Hit
PDCD6	1.94428	1.09647	+	2.04375	-1.95656	+
PSMA2	2.27571	1.72071	+	1.96416	-2.16114	+
NP	11.3203	4.09386	+	4.48939	1.00173	+
M1	3.06218	1.23862	+	0.141603	0.092485	
PB2	11.4704	7.51169	+	10.5451	9.07904	+
MYEF2	6.8253	0.459935	+	0.826789	-0.359572	
ZC3H8	2.04558	1.55072	+	0.110892	-0.210931	
HSPA1B	4.76989	0.782596	+	1.16537	-0.467707	
C4	1.5586	1.54356	+	1.1119	1.39031	
ME2	2.09854	1.13852	+	1.69113	-1.34924	+
SMARCE1	1.8281	2.22714	+	0.741521	-1.23698	
KIF23	3.87748	1.58652	+	0.106913	-0.161838	
SSR1	1.73354	1.94521	+	0.442944	-0.81897	
CLUH	4.67747	0.832765	+	1.03765	-0.500234	
SDF4	2.09704	1.68797	+	0.946181	-0.617908	
AMD1	2.27484	1.02836	+	0.066685	0.0557132	
ACAT1	3.47859	1.02296	+	2.30418	-0.95537	+
PB1	10.6633	6.97361	+	9.2234	8.47025	+
HARS	1.96325	1.26076	+	0.931733	-0.749201	
AIFM1	1.84836	1.47914	+	0.642362	-0.394625	
POLR2A	9.80575	2.43981	+	3.7005	1.21402	+
HSPB1	3.21855	0.941576	+	2.29663	-1.14351	+
ACO2	2.13601	1.67931	+	0.76398	-1.14298	
MACF1	1.69217	3.45171	+	0.0783603	-0.396609	
VRK1	5.2676	0.750962	+	0.550578	-0.552566	
AKAP8	7.28391	2.04563	+	0.83429	0.500333	
P4HB	2.83262	1.0347	+	1.88999	-1.02228	+
AKAP8L	4.8713	2.87905	+	2.07681	1.02337	+
HA	2.96198	1.63447	+	0.346623	-0.214138	
CNN2	1.93108	1.34828	+	1.65993	-1.07334	+
CS	2.89617	2.83059	+	1.85782	-2.34899	+
HSPE1	4.42247	2.81235	+	3.38622	-2.37489	+
PTMA	3.24071	2.84525	+	3.79252	-2.76583	+
POLR2B	11.1819	1.80471	+	1.68556	0.654103	
CYCS	1.99085	1.27025	+	1.37521	-1.19377	
POLR2H	6.53451	1.31727	+	1.95615	0.574389	
EIF4G2	1.98826	1.03432	+	0.851756	-0.896561	
HSPA9	6.05849	1.14839	+	1.07398	-0.537071	
NDUFV2	2.44605	1.18826	+	0.301186	-0.22989	
STAU2	4.04417	0.577285	+	0.470959	-0.2805	
CSTF3	2.71863	2.80297	+	0.23171	-0.63353	
ZC3H11A	3.43141	0.734322	+	0.683724	-0.667269	

PHF8	1.76711	2.0582	+	1.20225	-0.966055	
ESD	2.16102	1.19221	+	1.00077	-0.974078	
SF1	3.30129	1.35263	+	0.150245	0.174593	
PHKG2	2.59753	1.27705	+	0.00968081	0.0154686	
CALR	2.91814	2.67571	+	3.70304	-3.88814	+
PRKCSH	1.51171	1.63506	+	2.76604	-2.35722	+
SARS2	6.15743	0.479926	+	0.930108	-0.367258	
HAX1	7.98543	3.7254	+	0.323002	0.430579	
SUPT5H	6.85157	2.73825	+	0.574246	0.656108	
CLIC1	2.31213	0.830691	+	2.81864	-1.24878	+
KPNA3	6.61669	1.02758	+	0.721218	-0.31196	
AURKA	6.46267	1.93505	+	0.365081	-0.392703	
PPM1G	3.24301	0.642035	+	0.767647	-0.384746	
IPO8	2.12138	0.895004	+	0.421702	-0.284337	
POLR2D	8.70093	2.60026	+	0.994879	0.89816	
PJA2	9.01653	3.79613	+	4.8161	2.61271	+
PAPSS1	2.3206	0.899766	+	0.337752	-0.331452	
TIMM44	3.11893	1.4672	+	0.874085	-0.800148	
GTPBP6	1.94377	1.45634	+	0.338392	-0.244626	
CALU	6.04543	1.48783	+	1.17242	-0.475919	
SNX2	2.44701	0.872027	+	1.39541	-1.19249	
DNAJA2	6.63493	0.929604	+	0.780665	-0.388737	
PMPCB	3.96077	0.567912	+	1.0252	-0.498129	
GPC4	3.8549	1.66505	+	0.733894	0.347091	
HSBP1	2.27671	1.46038	+	3.17696	1.74846	+
ERAL1	6.82934	0.576804	+	0.668165	-0.331914	
CLPX	3.49546	1.27919	+	0.92001	-0.420276	
UBR5	6.26334	2.33662	+	0.52114	0.346144	
BAG2	4.03715	2.51075	+	0.0289091	-0.042052	
LDHA	2.2464	1.62093	+	2.47188	-1.87524	+
GLUD1	4.88553	1.82696	+	2.29766	-1.29191	+
PGK1	3.09704	2.66634	+	2.42507	-2.11677	+
TFRC	1.63875	1.57563	+	1.2332	-1.33338	
OAT	1.53791	1.50139	+	1.87177	-1.46207	+
TP53	3.46491	1.098	+	0.0649411	-0.0612276	
HIST2H2B	1.65943	1.70689	+	0.950257	-0.72076	
PFN1	2.26115	2.34641	+	1.71539	-2.98468	+
HSP90AA1	2.28763	1.10078	+	2.73687	-1.56943	+
SNRPB2	3.22324	1.02873	+	1.09024	-1.06348	
ANXA5	1.6307	1.36512	+	1.07701	-1.2345	
GSTP1	2.53487	1.16965	+	2.39719	-1.32456	+
HMGB1	1.80479	1.3934	+	1.86424	-1.71401	+
CALM	3.32763	1.18445	+	0.724965	-0.393332	
HSPD1	2.91274	0.75763	+	1.93364	-0.812227	+
HSPA8	3.83848	0.893308	+	0.561964	-0.334973	
PDHB	5.04572	0.568452	+	1.96361	-0.694427	

RALA	2.89609	1.23789	+	1.41615	-1.01606	
ETFA	2.92394	1.28924	+	1.88475	-1.18844	+
PGAM1	2.48984	2.62845	+	2.86644	-3.39882	+
HK1	2.54201	1.06617	+	1.08418	-0.901971	
POLR2C	9.04877	1.66818	+	1.3622	0.522543	
POLR2E	7.40351	1.37457	+	0.815818	0.398131	
PSMB1	2.5508	2.1369	+	1.33309	-1.41304	
PSMA1	2.60064	1.75464	+	1.44792	-0.922594	
PSMA3	2.02626	1.75018	+	0.564983	-0.768823	
HMGB2	2.32439	0.946871	+	3.02597	-1.68371	+
PSMB4	1.73143	1.52443	+	1.85621	-1.77598	+
PSMB5	2.7773	1.6481	+	2.2399	-1.41878	+
ECHS1	1.9425	1.57827	+	1.31347	-1.01261	
PEBP1	1.83993	1.9147	+	1.75065	-2.13678	+
PDIA3	2.90775	0.799615	+	1.235	-0.648315	
ALDH1B1	4.64003	0.976161	+	1.43118	-0.990458	
DNAJA1	4.70193	0.760083	+	0.94575	-0.430692	
UQCRC1	4.12626	1.7251	+	0.0798273	-0.0921792	
ATIC	2.15042	1.45458	+	1.00704	-0.96642	
PYCR1	5.72453	2.06081	+	1.04478	-1.07059	
HSPA4	3.24046	0.767518	+	1.78575	-0.816546	
PHB1	6.65688	0.670352	+	4.79189	-1.18867	+
POLR2I	6.64576	2.1794	+	2.32266	1.08438	+
TALDO1	2.5605	1.2081	+	0.833772	-0.904212	
MDH2	4.04014	2.98148	+	2.52618	-3.43352	+
MAP1B	5.59701	0.771321	+	0.27183	-0.142024	
NES	3.66345	0.73512	+	0.519587	-0.25796	
TUFM	8.61197	1.04339	+	0.513737	-0.248087	
EMD	6.73262	1.04746	+	0.712787	-0.322853	
HDGF	1.66842	1.38803	+	1.24066	-1.35154	
POLR2J	3.72974	1.67662	+	1.90975	1.97089	+
SMS	1.90571	1.77988	+	2.68235	-1.99257	+
BLVRA	2.66627	1.38656	+	0.377623	-0.422317	
SLC16A1	1.88295	1.11125	+	1.96242	-0.721517	
RAD23B	1.5971	1.47397	+	0.604851	-0.878497	
ALDH18A1	3.64937	0.709319	+	1.07633	-0.595853	
HADHB	3.38731	0.879132	+	0.903545	-0.752103	
MAZ	2.05914	2.03442	+	0.628454	1.06042	
SEC61B	4.96674	0.750357	+	2.58339	1.99852	+
RAB2	2.67473	1.58966	+	2.06845	-1.47784	+
UBE2N	2.41673	1.05761	+	1.55609	-0.657161	
POLR2G	8.0881	2.27947	+	0.641845	0.482044	
POLR2L	5.03848	1.2624	+	0.727569	0.657422	
SARNP	2.81306	1.46963	+	2.60615	-1.73518	+
FKBP3	2.8823	2.1398	+	1.7417	-1.56388	+
CAP1	2.0596	1.26742	+	3.46309	-1.94403	+

FKBP4	2.88905	2.17115	+	2.22316	-1.79268	+
AHNAK	2.60374	1.00217	+	0.805591	-0.529637	
DHRS2	2.3072	1.20505	+	1.85655	-0.772405	
LBR	1.63106	1.48823	+	1.38604	-1.18928	
EIF4H	2.43526	2.05638	+	2.23439	-2.10605	+
RCN1	2.90143	2.09644	+	0.392476	-0.394525	
TRIP13	1.90998	1.24789	+	1.5557	-1.12552	+
NSDHL	2.47307	1.42803	+	0.548544	-0.518284	
MLF2	3.62195	2.03441	+	0.116164	0.141397	
NDUFA9	2.26864	1.0726	+	0.10527	-0.112053	
PDS5A	1.98597	1.05646	+	1.48446	-0.992775	
NME1	2.88754	0.998311	+	1.8742	-1.19596	+
MAGED2	1.92717	1.10317	+	0.87212	-0.394222	
RNF219	8.35468	3.20202	+	1.6609	1.11385	+
RPAP2	6.64931	2.80899	+	2.9966	1.44264	+
ENAH	2.50596	1.20518	+	0.621754	-0.593448	
HJURP	2.72341	1.49049	+	0.111284	0.151211	
RB1CC1	1.66397	2.22162	+	0.301224	-0.598814	
ZNF622	4.05516	1.73986	+	1.08425	-0.922319	
FUBP1	2.18747	1.82875	+	1.30241	-1.40436	
THAP11	2.20128	1.16704	+	0.702699	-0.527997	
DNAJA3	5.70802	0.788662	+	0.778614	-0.478295	
CDKN2AIPNL	1.63547	1.52341	+	0.148425	-0.127707	
CNDP2	2.0462	1.08991	+	2.47091	-1.26969	+
RBM14	7.97695	1.21079	+	0.375989	0.227983	
PHB2	6.19169	0.750214	+	2.35271	-0.764217	+
CLPB	7.74608	2.22234	+	0.0198648	-0.0204595	
RAB1	3.71148	0.760797	+	1.82235	-0.641882	
NOL6	2.24419	1.08591	+	0.934158	-0.62433	
CACYBP	2.03268	1.44904	+	1.17249	-1.19929	
SPC25	2.37269	0.821711	+	0.117378	-0.12933	
RTN4	1.87958	1.78139	+	1.46795	-1.68402	+
TECR	1.94654	1.54944	+	0.749611	0.532995	
SAE1	1.66095	1.27413	+	1.40113	-1.23423	
DNAJB11	3.10265	0.823484	+	0.644599	-0.374842	
SEC63	1.9628	1.3215	+	1.55996	-1.23794	+
Septin-9	2.3999	0.822031	+	1.86033	-0.719375	
GPN3	3.72652	1.89488	+	0.802356	0.769262	
STOML2	3.33563	1.11645	+	2.37435	-1.00525	+
UBQLN1	2.19162	1.09914	+	1.16702	-0.965047	
RUVBL2	3.81984	0.574411	+	0.903115	-0.397446	
PIN4	2.79071	1.32746	+	0.0375094	-0.0318186	
RUVBL1	4.73698	0.559029	+	1.64452	-0.548506	
TLN1	2.29819	1.15507	+	2.12621	-1.2014	+
AP4S1	2.43586	1.89053	+	0.743445	-0.504067	
YTHDF2	3.15354	0.806068	+	0.234016	-0.19524	

MAGED1	7.19387	3.10829	+	4.13955	1.41114	+
PSAT1	2.18748	1.59629	+	1.89546	-1.48708	+
PA	9.13263	7.13784	+	10.5088	8.18677	+
NS1	3.63666	1.83513	+	0.3085	0.347558	
SNRPG	0.842572619	-1.403921763		1.806887244	1.961436166	+
NDUFAB1	0.162109457	0.236803691		2.340798197	1.691394594	+
CSTB	1.035598766	-0.623046239		1.715494297	0.984848658	+
HIST1H2A	0.379193301	0.504790624		1.777463827	1.736826791	+
MYL1	0.140962419	-0.095344967		1.713768352	2.724843343	+
GOLGA3	0.621781571	-0.855890698		1.395696314	1.317256504	+
MYO5B	0.088061959	0.063877318		2.808654926	1.058664534	+
RPL26L1	0.334703636	-0.40709877		1.513315764	2.113335503	+

Appendix B.

Proteins co-precipitating from PR8 WT-infected and mock-infected ANP32-KO cells transfected with ANP32B-FLAG or GFP-FLAG (negative background control). Proteins were identified by mass spectrometry. Raw values are shown as label-free quantification (LFQ) intensities, which gives a normalised estimate of the protein abundance in each sample. Statistical analysis was performed using R v.4.2.2. The LFQ intensities were used to calculate the fold change (FC) between the protein abundance in ANP32B-FLAG-transfected cells and GFP-FLAG-transfected cells for each infected/uninfected conditions. The significance of the protein enrichment was determined using a *t* test (two-sided, equal variance). Proteins were classified as hits based on their enrichment (FC=2, p-value=0.2) over negative background control. Proteins enriched in ANP32-FLAG transfected samples (hits) are shown by black plus sign.

	LFQ intentsity												Data processing					
	Infected cells						Mock-infected cells						Infected cells			Mock-infected cells		
	ANP32B-FLAG			GFP-FLAG			ANP32B-FLAG			GFP-FLAG			ANP32B-FLAG vs GFP-FLAG			ANP32B-FLAG vs GFP-FLAG		
Gene names	**Exp 1**	**Exp 2**	**Exp 3**	**Exp 1**	**Exp 2**	**Exp 3**	**Exp 1**	**Exp 2**	**Exp 3**	**Exp 1**	**Exp 2**	**Exp 3**	**P-value**	**Fold change (FC)**	**Hit**	**P-value**	**Fold change (FC)**	**Hit**
PP2AA	24.7207	24.6148	24.5480	0.0000	0.0000	0.0000	24.7999	0.0000	0.0000	0.0000	0.0000	0.0000	4.16737E-06	24.62784259	+	0.422649731	8.26662	
AN32B	32.6059	32.4569	32.8327	0.0000	0.0000	0.0000	32.7703	33.3124	33.0881	0.0000	0.0000	0.0000	1.12133E-05	32.63181178	+	2.2635E-05	33.05694834	+
CCD86	26.2983	26.8351	25.6701	0.0000	0.0000	0.0000	26.6720	25.5195	0.0000	0.0000	0.0000	0.0000	0.000164203	26.26782227	+	0.18370239	17.39716339	+
TMOD2	23.5811	23.4538	24.4165	0.0000	0.0000	0.0000	0.0000	0.0000	0.0000	0.0000	0.0000	0.0000	0.000160674	23.81709989	+	0	0	
U3IP2	0.0000	25.7535	24.8365	0.0000	0.0000	0.0000	0.0000	0.0000	0.0000	0.0000	0.0000	0.0000	0.18363751	16.86331495	+	0	0	
IMA7	0.0000	23.6426	24.3441	0.0000	0.0000	0.0000	0.0000	0.0000	0.0000	0.0000	0.0000	0.0000	0.183590655	15.99558957	+	0	0	
OXSR1	0.0000	23.8083	23.8756	0.0000	0.0000	0.0000	0.0000	23.9615	23.9234	0.0000	0.0000	24.0794	0.183504231	15.89463806	+	0.426421026	1.988621231	
LMNA	0.0000	26.3353	26.4476	0.0000	0.0000	0.0000	0.0000	27.0480	26.7407	0.0000	0.0000	0.0000	0.183505266	17.59429932	+	0.183516743	17.92958069	+
TPM2	24.3697	23.7210	0.0000	0.0000	0.0000	0.0000	0.0000	0.0000	24.4707	0.0000	0.0000	24.8413	0.183577687	16.03021558	+	0.422649731	0.985082684	
RU2A	24.5865	25.2074	0.0000	0.0000	0.0000	0.0000	0.0000	24.6425	0.0000	0.0000	0.0000	0.0000	0.183566903	16.5979646	+	0.422649731	8.214152654	
TPR	0.0000	27.7744	23.9110	0.0000	0.0000	0.0000	0.0000	23.6896	23.7703	0.0000	24.7628	24.6947	0.185775001	17.2284584	+	0.185762083	0.959610176	
SPEE	0.0000	23.7273	23.6678	0.0000	0.0000	0.0000	0.0000	0.0000	0.0000	0.0000	24.0637	0.0000	0.183504062	15.79839452	+	0.422649731	0	
PHB	0.0000	28.0414	23.0647	0.0000	0.0000	0.0000	0.0000	0.0000	0.0000	23.8527	0.0000	23.8600	0.187347382	17.03537877	+	0.183503429	0	
VDAC2	0.0000	27.3804	26.1029	0.0000	0.0000	0.0000	0.0000	26.6295	26.2328	25.7282	25.5642	26.4382	0.183736223	17.82777405	+	0.442442001	0.680070754	
MSH6	0.0000	24.8255	24.3985	0.0000	0.0000	0.0000	0.0000	0.0000	0.0000	0.0000	0.0000	0.0000	0.183534137	16.40801175	+	0	0	
NU107	0.0000	27.3180	22.3119	0.0000	0.0000	0.0000	0.0000	0.0000	0.0000	0.0000	0.0000	0.0000	0.187625835	16.54329681	+	0	0	
ARP2	25.6728	0.0000	25.8739	0.0000	0.0000	0.0000	0.0000	25.8849	25.7532	25.6193	0.0000	26.1743	0.183509637	17.18223572	+	0.997534775	0.996997361	
GBB2	0.0000	25.2835	25.0553	0.0000	0.0000	0.0000	0.0000	24.7987	24.7101	25.2700	0.0000	25.8919	0.183511811	16.77959696	+	0.973058316	0.967688946	
KIF23	0.0000	24.4703	24.1219	0.0000	0.0000	0.0000	0.0000	23.9423	24.3729	0.0000	0.0000	0.0000	0.183524399	16.19741313	+	0.183535853	16.10505931	+
NU160	0.0000	26.2941	24.5538	0.0000	0.0000	0.0000	0.0000	0.0000	0.0000	0.0000	0.0000	0.0000	0.183981206	16.94928996	+	0	0	
MYO1E	0.0000	24.1395	24.5136	0.0000	0.0000	0.0000	0.0000	0.0000	0.0000	0.0000	0.0000	0.0000	0.183527547	16.21770732	+	0	0	
ACOX1	0.0000	23.2260	23.4288	0.0000	0.0000	0.0000	0.0000	23.1911	0.0000	0.0000	0.0000	0.0000	0.183511131	15.55160332	+	0.422649731	7.730360667	
PLEC	0.0000	24.0075	24.3299	0.0000	0.0000	0.0000	0.0000	24.1007	24.8430	24.0761	24.1200	24.2915	0.183521579	16.11248271	+	0.435559154	0.675200588	
PCM1	24.3469	0.0000	25.3867	0.0000	0.0000	0.0000	0.0000	25.4449	24.9471	0.0000	0.0000	24.7759	0.183681841	16.57786179	+	0.418777763	2.033911614	
PCKGM	0.0000	23.6926	23.5544	0.0000	0.0000	0.0000	0.0000	23.3680	0.0000	0.0000	23.4135	0.0000	0.183506915	15.74900754	+	0.422649731	0.998055953	
ALKB5	0.0000	23.2282	23.0889	0.0000	0.0000	0.0000	0.0000	22.8035	23.1079	0.0000	0.0000	0.0000	0.183507111	15.4390405	+	0.183521373	15.30379168	+
ATAD2	0.0000	27.2421	21.7984	0.0000	0.0000	0.0000	0.0000	0.0000	0.0000	0.0000	0.0000	0.0000	0.188487879	16.34681575	+	0	0	

FA98A	24.1714	24.4591	0.0000	0.0000	0.0000	0.0000	0.0000	0.0000	0.0000	0.0000	0.0000	0.0000	0.183517702	16.21016693	+	0	0	
KI18A	25.1566	0.0000	24.5385	0.0000	0.0000	0.0000	25.1441	24.8276	25.5219	24.7225	24.5616	24.6127	0.183566566	16.56501961	+	0.110874378	1.02160834	
NU205	0.0000	27.2183	26.2474	0.0000	0.0000	0.0000	0.0000	0.0000	0.0000	0.0000	0.0000	0.0000	0.183638004	17.82188479	+	0	0	
EXOS8	0.0000	23.3468	23.1882	0.0000	0.0000	0.0000	0.0000	0.0000	0.0000	0.0000	0.0000	0.0000	0.183508159	15.51166789	+	0	0	
NUD11	25.5321	24.9776	0.0000	0.0000	0.0000	0.0000	0.0000	0.0000	25.1902	0.0000	25.0357	25.3379	0.183552621	16.83656184	+	0.419253686	0.500067531	
TRIM9	24.3904	0.0000	24.3494	0.0000	0.0000	0.0000	0.0000	0.0000	24.5694	0.0000	0.0000	0.0000	0.183503708	16.24661001	+	0.422649731	8.189784368	
UN45A	0.0000	23.4344	24.1932	0.0000	0.0000	0.0000	0.0000	0.0000	22.6596	0.0000	0.0000	0.0000	0.183607014	15.87586085	+	0.422649731	7.553192139	
HEAT1	0.0000	26.6674	25.9299	0.0000	0.0000	0.0000	0.0000	0.0000	0.0000	0.0000	0.0000	0.0000	0.183583658	17.53242811	+	0	0	
RPR1B	0.0000	24.8270	24.0488	0.0000	0.0000	0.0000	0.0000	0.0000	0.0000	0.0000	0.0000	0.0000	0.183606908	16.29192734	+	0	0	
MDN1	0.0000	23.4666	23.2669	0.0000	0.0000	0.0000	0.0000	0.0000	0.0000	0.0000	0.0000	23.1864	0.183510879	15.57782555	+	0.422649731	0	
MIC19	0.0000	25.3100	25.4572	0.0000	0.0000	0.0000	0.0000	0.0000	25.0532	0.0000	0.0000	25.2264	0.183506854	16.92240206	+	0.422649731	0.993130914	
AATF	0.0000	24.1972	24.0521	0.0000	0.0000	0.0000	0.0000	22.2104	0.0000	0.0000	0.0000	0.0000	0.18350711	16.08308029	+	0.422649731	7.403471629	
STML2	0.0000	24.5390	23.7013	0.0000	0.0000	0.0000	0.0000	0.0000	0.0000	0.0000	0.0000	0.0000	0.183626474	16.08009911	+	0	0	
WDR3	0.0000	26.2343	22.9326	0.0000	0.0000	0.0000	0.0000	0.0000	0.0000	0.0000	0.0000	0.0000	0.185338184	16.38899167	+	0	0	
SAM50	0.0000	23.5367	23.7419	0.0000	0.0000	0.0000	0.0000	0.0000	0.0000	0.0000	0.0000	0.0000	0.18351111	15.75953865	+	0	0	
IMA5	24.8903	25.4113	25.4740	0.0000	23.7961	0.0000	24.6832	24.9465	24.7992	0.0000	0.0000	0.0000	0.1582401	3.184366556	+	9.42401E-06	24.80962435	+
ARC1A	26.5823	25.9741	26.6382	0.0000	25.6421	0.0000	0.0000	26.9383	26.8782	26.2689	25.9259	27.1390	0.17844266	3.088462043	+	0.439612462	0.678355402	
GBB1	26.0586	26.0949	25.8406	0.0000	0.0000	25.2606	25.8130	25.8941	25.9472	25.7528	25.8568	26.4301	0.174524501	3.087583259	+	0.544052442	0.995060574	
CND3	23.8414	24.7231	24.2011	0.0000	23.6392	0.0000	23.5862	23.8291	24.4042	24.2800	24.0121	24.1395	0.16553081	3.078176171	+	0.537975558	0.991550464	
CKAP4	24.2772	24.9573	24.2915	24.0074	0.0000	0.0000	23.8180	0.0000	24.6266	24.2911	0.0000	24.2914	0.179129965	3.062634272	+	0.86276224	0.99716311	
SOX2	25.9273	26.0475	25.4493	25.4313	0.0000	0.0000	26.3674	0.0000	25.5593	0.0000	0.0000	0.0000	0.175769817	3.044444879	+	0.183602259	17.30889448	+
EPIPL	23.8616	24.1938	24.5875	24.0889	0.0000	0.0000	22.6594	23.9112	24.3551	23.9415	24.0733	24.0189	0.187351943	3.015615533	+	0.520908459	0.984618372	
SYTC	24.3855	24.5144	24.3540	24.3043	0.0000	0.0000	24.6741	24.4032	24.1344	24.3307	24.4241	24.6117	0.182153903	3.014029396	+	0.848001689	0.997888897	
KIFA3	21.9947	21.9608	22.5751	22.1032	0.0000	0.0000	0.0000	22.2797	0.0000	0.0000	0.0000	0.0000	0.185575523	3.010001952	+	0.422649731	7.426562627	
ADT3	25.3429	25.5312	25.3652	0.0000	25.3571	0.0000	26.0273	25.6300	25.7273	0.0000	26.1745	0.0000	0.180709525	3.006624659	+	0.192195616	2.956493583	+
SYNE2	24.2105	25.5864	24.4536	24.7455	0.0000	0.0000	24.3846	24.9639	24.8887	24.6877	24.7245	0.0000	0.192531826	3.000567221	+	0.424197171	1.502406603	
CWC15	24.4246	24.2592	23.9049	24.2767	0.0000	0.0000	0.0000	0.0000	24.5838	0.0000	0.0000	0.0000	0.18102614	2.990057019	+	0.422649731	8.194589615	
UBC9	24.3444	25.3143	25.1760	0.0000	0.0000	25.1045	0.0000	25.4427	0.0000	0.0000	0.0000	0.0000	0.182484072	2.980933926	+	0.422649731	8.480885824	
PSB2	21.8501	22.2360	22.2968	0.0000	22.6213	0.0000	0.0000	0.0000	0.0000	0.0000	0.0000	0.0000	0.190731139	2.934537099	+	0	0	
AROS	0.0000	24.8262	0.0000	25.3499	24.8841	0.0000	25.8524	25.1344	24.8522	0.0000	0.0000	0.0000	0.42133265	0.494211464		0.000138674	25.27966626	+
H2AY	0.0000	30.5844	24.5742	24.9078	23.7117	0.0000	23.1093	24.4944	24.0469	0.0000	0.0000	0.0000	0.894125276	1.134494545		0.000291813	23.88354556	+
OPA1	0.0000	0.0000	0.0000	0.0000	0.0000	0.0000	0.0000	24.7052	24.0206	0.0000	0.0000	0.0000	0	0		0.183583998	16.2419637	+
THIL	0.0000	0.0000	0.0000	0.0000	0.0000	0.0000	25.0722	0.0000	24.7855	0.0000	0.0000	0.0000	0	0		0.183516915	16.61923281	+
S61A1	0.0000	0.0000	0.0000	0.0000	0.0000	0.0000	0.0000	23.1181	23.0352	0.0000	0.0000	0.0000	0	0		0.183504735	15.38441213	+
LTOR1	0.0000	0.0000	0.0000	0.0000	0.0000	0.0000	0.0000	23.7627	24.0061	0.0000	0.0000	0.0000	0	0		0.183514013	15.92293739	+
USP9X	0.0000	0.0000	0.0000	0.0000	0.0000	0.0000	0.0000	23.6006	23.8867	0.0000	0.0000	0.0000	0	0		0.183518237	15.82909711	+
MIB1	0.0000	0.0000	24.2515	0.0000	0.0000	0.0000	0.0000	24.2389	24.1759	0.0000	0.0000	0.0000	0.422649731	8.083848953		0.183504109	16.13825798	+
CSN4	0.0000	0.0000	21.3548	0.0000	0.0000	0.0000	0.0000	20.6240	20.6187	0.0000	0.0000	0.0000	0.422649731	7.118256887		0.183503426	13.74757131	+
EIF3L	0.0000	0.0000	24.5270	0.0000	0.0000	0.0000	0.0000	24.6342	24.6612	0.0000	0.0000	0.0000	0.422649731	8.175670624		0.183503542	16.43181864	+
CDK1	0.0000	24.7363	24.3905	0.0000	0.0000	24.5962	0.0000	24.4622	24.3560	0.0000	0.0000	0.0000	0.4274688	1.997339299		0.18350535	16.27274068	+
HCFC1	0.0000	23.0800	22.8243	22.9931	0.0000	0.0000	23.4685	23.0279	0.0000	0.0000	0.0000	0.0000	0.667462494	1.996438996		0.183540077	15.49879138	+
EWS	0.0000	26.7506	0.0000	0.0000	26.2159	26.0950	26.3614	26.0355	0.0000	0.0000	0.0000	0.0000	0.434599466	0.511377077		0.183519218	17.46562831	+
PABP2	24.3707	0.0000	0.0000	24.2940	0.0000	23.6033	0.0000	24.4649	23.9631	0.0000	0.0000	0.0000	0.424526933	0.508810128		0.183547264	16.14266586	+
PELP1	0.0000	24.6766	23.1848	0.0000	22.9890	0.0000	0.0000	22.5784	22.8405	0.0000	0.0000	0.0000	0.382260005	2.081925985		0.183517016	15.13963826	+
RPAC1	23.5158	23.8342	0.0000	23.4396	23.5976	0.0000	0.0000	22.8699	23.1457	0.0000	0.0000	0.0000	0.27345749	1.006649427		0.183518081	15.33852959	+
ZN207	25.5303	24.6839	0.0000	25.2597	25.2711	0.0000	0.0000	25.2102	25.3653	0.0000	0.0000	0.0000	0.717367947	0.993736866		0.183507259	16.85851733	+

LYRIC	0.0000	0.0000	23.9806	23.9406	23.9564	23.7203	0.0000	23.7520	23.4847	0.0000	0.0000	0.0000	0.18796534	0.334843414		0.183516488	15.74554507	+
ZC3HF	0.0000	23.8955	0.0000	24.6959	24.4937	24.3675	0.0000	24.2307	24.3512	0.0000	0.0000	0.0000	0.173689007	0.324856332		0.183505934	16.19396973	+
RTF2	0.0000	0.0000	24.1923	23.9586	23.6299	24.0678	0.0000	23.8650	24.1548	0.0000	0.0000	0.0000	0.185666006	0.337616501		0.183518278	16.00660197	+
DPY30	0.0000	24.0976	24.6478	22.6563	23.7852	0.0000	0.0000	23.1994	23.2048	0.0000	0.0000	0.0000	0.960267541	1.049612127		0.183503425	15.46808306	+
KAP2	23.3195	23.4568	24.1227	23.2072	0.0000	23.4839	0.0000	23.4376	23.0427	0.0000	0.0000	0.0000	0.404392816	1.518465614		0.183532887	15.49342283	+
ECHA	22.8052	23.4085	22.7287	22.9388	0.0000	22.9757	22.9121	0.0000	22.5005	0.0000	0.0000	0.0000	0.432078966	1.501536612		0.183536962	15.13753382	+
SC23A	22.4809	22.6008	22.7036	22.7918	0.0000	22.3763	22.6527	21.9207	0.0000	0.0000	0.0000	0.0000	0.422346451	1.500734404		0.183613472	14.85780017	+
RIOX2	23.9281	23.3765	23.9183	23.6093	0.0000	23.9482	0.0000	23.5416	23.6300	0.0000	0.0000	0.0000	0.415568441	1.497616874		0.183504854	15.72385597	+
BTF3	24.8296	24.2047	24.9578	24.9421	24.7469	25.0531	0.0000	23.7402	24.2779	0.0000	0.0000	0.0000	0.229421347	0.989966036		0.183554611	16.00601578	+
RS29	27.4829	27.9693	27.8428	28.2101	28.1952	28.5003	0.0000	27.9954	27.6096	0.0000	0.0000	0.0000	0.07572838	0.981030714		0.183523079	18.53500621	+
SMC4	25.0542	25.3042	25.1018	24.7279	24.9801	24.7182	25.2955	0.0000	24.7737	0.0000	0.0000	0.0000	0.003181062	1.013894103		0.183547752	16.6897227	+
PLK1	25.3271	25.5221	25.2501	25.1257	24.9518	25.1948	26.2004	24.9931	25.2587	0.0000	0.0000	24.9666	0.213745951	1.010989167		0.179098953	3.062180531	+
EIF3I	25.7977	25.4569	25.5574	25.7951	25.7290	25.8218	26.0704	25.7133	25.9455	25.5317	0.0000	0.0000	0.187486309	0.993096808		0.175087391	3.044416246	+
MA7D1	24.5761	0.0000	24.5543	24.4799	24.3322	24.5827	24.7206	24.4865	24.9231	24.3551	0.0000	0.0000	0.424263923	0.669399291		0.177539982	3.043726265	+
SRS10	0.0000	0.0000	0.0000	0.0000	25.4748	0.0000	26.0463	26.0019	26.1362	0.0000	25.9406	0.0000	0.422649731	0		0.182547075	3.013974559	+
SKP1	25.6860	25.4289	25.7458	25.2869	25.3884	25.4724	25.8011	25.4919	25.4004	0.0000	0.0000	25.4801	0.152065598	1.009364098		0.184788655	3.009935242	+
MA7D3	26.0001	25.1642	25.8354	25.5892	25.5416	25.8499	25.6484	25.5497	26.0647	0.0000	0.0000	25.7070	0.980435693	1.000245713		0.177840138	3.005519785	+
GTPB1	24.7491	24.7065	24.9724	25.0994	24.9962	25.2102	25.2741	24.7022	24.8207	0.0000	0.0000	24.9053	0.012121799	0.988343957		0.184940795	3.003258808	+
LA	23.6662	23.7055	23.6104	23.7845	23.9416	0.0000	23.3185	23.9557	23.7687	0.0000	0.0000	23.6859	0.431351861	1.487280905		0.1821504	2.999373986	+
RUXE	25.2184	25.0836	24.9547	25.1010	24.9084	24.9888	25.0005	24.5534	24.8427	0.0000	0.0000	24.8085	0.301548502	1.003446534		0.18297267	2.99883999	+
NHP2	24.1803	25.4458	0.0000	24.6818	24.5796	24.2226	24.5554	24.3957	23.9470	0.0000	0.0000	24.3354	0.431827346	0.675332099		0.190038091	2.995551222	+
NOLC1	0.0000	26.8646	26.7053	24.2384	24.8695	0.0000	24.2910	23.5560	23.2245	0.0000	24.3374	0.0000	0.928679743	1.090859323		0.197348848	2.920265265	+

Appendix C.

Alignment of single guide RNA (sgRNA) sequences (sgRNA1-3) to the RUVBL2 (A), HMGB2 (B), and RPAP2 (C) genes. The sgRNAs were designed by and obtained from Synthego. The alignments were performed in Geneious Prime v.2019.2.3 software.

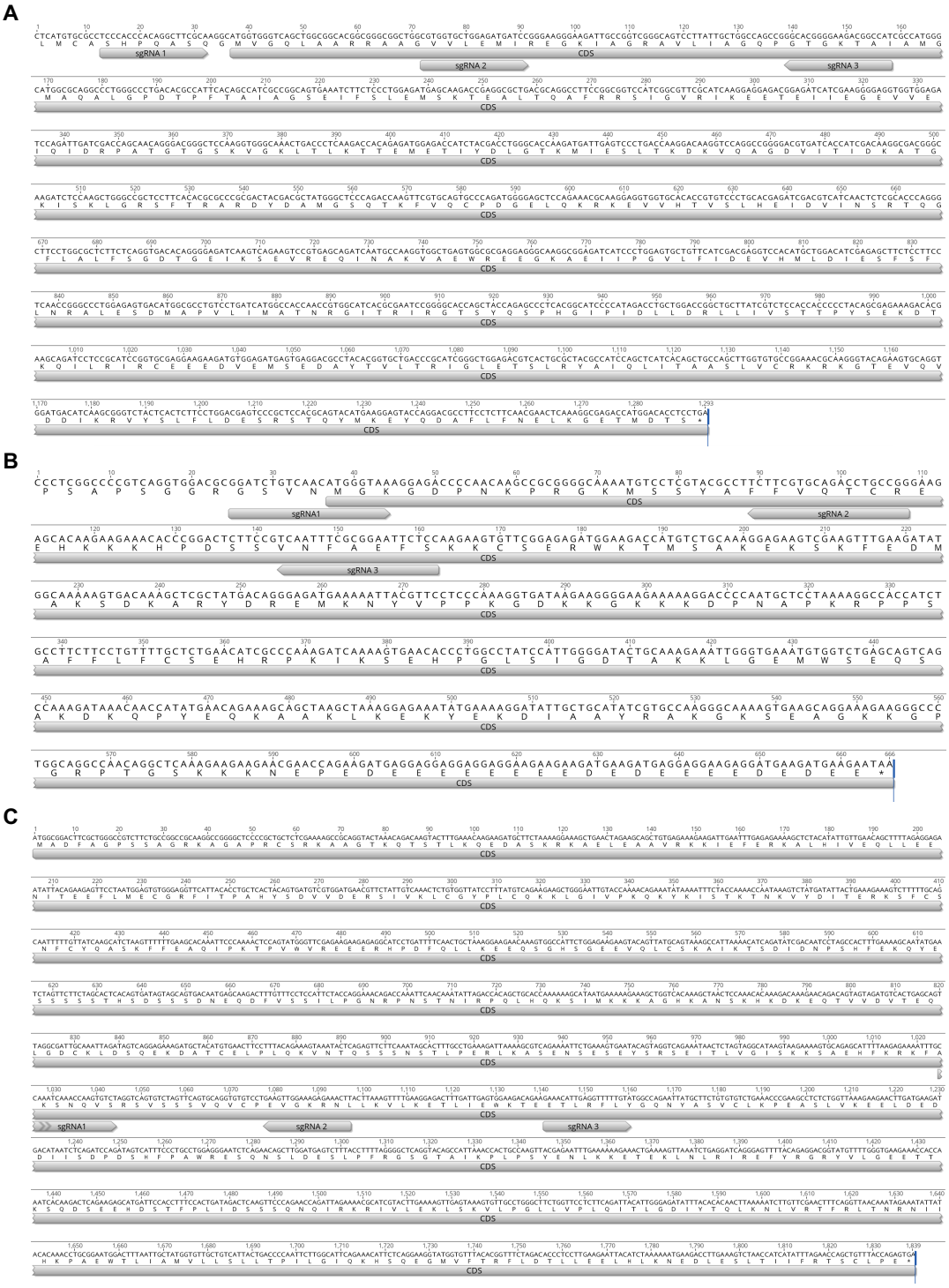

Appendix D.

Western blots testing two RPAP2 antibodies, PA5-61244 (Invitrogen) (A) and 17401-AP (Proteintech) (B). Neither antibody was able to detect RPAP2 protein expression in A549 WT cells despite tubulin (cellular control) protein expression.

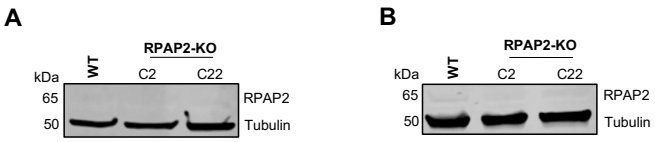

Appendix E.

Type of work	Legend	Source	Copyright holder	Permission requested	Permission obtained	License number
Figure	Figure 1. The ecology of influenza viruses.	Long et al., 2019	© Springer Nature	05/08/2025	Yes	6082400284159
Tomogram	Figure 2A and B. Structrue of an IAV virion.	Peterl et al., 2025	Licensed with a Creative Commons Attribution 4.0 International (CC BY) license, which permits reuse when correctly cited.	Not required	Not required	N/A
Electron micrograph	Figure 2D. Structrue of an IAV virion.	Noda et al., 2006	© Springer Nature	01/09/25	Yes	6100370344547
Electron micrograph	Figure 3B. Structure of a vRNP.	Peng et al., 2025	© American Association for the Advancement of Science (AAAS)	19/08/25	Yes	N/A
Figure	Figure 8. Overview of the mechanism of viral transcription.	Wandzik et al., 2020	© Elsevier	07/08/2025	Yes	6083560497361
Figure	Figure 9. Overview of the mechanism of viral RNA replication.	Te Velthuis et al., 2021	© Springer Nature	07/08/25	Yes	6083560832085
Figure	Figure 12. The temporal dynamics of vRNA, cRNA, and mRNA synthesis during infection.	Phan 2021	Licensed with a Creative Commons Attribution 4.0 International (CC BY) license, which permits reuse when correctly cited.	Not required	Not required	N/A
Figure	Figure 14. Cumulative host range barriers that AIVs must overcome to initiate a pandemic in the human population.	Long et al., 2019	© Springer Nature	05/08/2025	Yes	6082400284159
Figure	Figure 32. Schematic demonstrating CRISPR-Cas9 genome editing.	Ran et al., 2013	© Springer Nature	05/08/2025	Yes	6082490933630
Figure	Figure 51. Cartoon representations of the hexameric structure of RUVBL2.	Silva et al., 2018	Licensed with a Creative Commons Attribution 4.0 International (CC BY) license, which permits reuse when correctly cited.	Not required	Not required	N/A